NORTHWEST GEOLOGY

The Journal of The Tobacco Root Geological Society

Volume 44, July–August 2015

40th Annual Field Conference

Geology of the Elliston Area, Montana
and other papers

Rhyolite tuff exposed at the summit of
Crater Mountain in the Nevada Mountains.

The Tobacco Root Geological Society, Inc.

P.O. Box 118
Butte, Montana 59703

Geology of the Elliston Area, Montana and other papers

TABLE OF CONTENTS

FIELD GUIDES

TRGS CHARTER MEMBERS

Stanley W. Anderson
Clyde Cody
William S. Cordua
Lanny H. Fisk
Richard I. Gibson†
Thomas Hanley
Stephen W. Henderson
Thomas E. Hendrix
Mac R. Hooton
Inda Immega
Steven W. Koehler
Marian Millen Lankston†
Robert W. Lankston†
J. David Lazor
Joe J. Liteheiser, Jr.
Judson Mead*
Marvin R. Miller
Vicki M. Miller
Allen H. Nelson
Alfred H. Pekarek
Patricia Price*
Donald L. Rasmussen
Raymond M. Rene

TRGS LIFETIME MEMBERS

John Childs
Rob Foster
Joan (Mrs. Jack) Harrison*
Karen Keefer
Layaka Mann
Chris Pool

† = co-founder
* = deceased

TRGS HAMMER AWARD RECIPIENTS

Awarded for distinguished achievement in the study of the geology of the Northern Rocky Mountains

1993: Ed Ruppel*
1994: Dick Berg
2003: Don Winston
2004: Dean Kleinkopf
2009: Betty Skipp
2010: Jim Sears
2011: John Childs
2012: J. Michael O'Neill
2013: Paul Karl Link
2014: Reed Lewis
2015: Jeff Lonn

TRGS HONORARY MEMBERS

1980: Charles J. Vitaliano*
2008: Elizabeth Younggren
  (also honorary Board member)
2010: Dick Berg
2010: Bruce Cox
2010: Dean Kleinkopf
2010: Dave Lageson
2011: Marie Marshall Garsjo
2011: Paul Link
2011: Rob Thomas
2012: Jeff Lonn
2012: Mitch Reynolds
2013: Reed Lewis

DEDICATION TO DAVID ALT

Volume 44 of Northwest Geology is dedicated to David Alt, one of this publication's early editors and an inspirational and imaginative geologist. David Alt held court at the University of Montana Geology Department for several decades where he taught introductory geology courses. His mesmerizing approach to teaching geologic processes is legendary—no one dozed off during Doctor Alt's lectures. During and after his tenure at U of M, Dave co-authored (with Don Hyndman) several volumes of the Roadside Geology series, which continue to captivate anyone inclined toward geologic study.

One of Dave's great contributions to modern geology was his understanding of the sometimes passive, sometimes cataclysmic processes associated with Glacial Lake Missoula (GLM). Through his own research and that of his graduate students, Dave unraveled an astounding story expressed in the distinctively layered GLM silts. His theory of ice-dam thinning and rupture continues to be the accepted mechanism for the catastrophic floods that formed many of the GLM features we can see today. Dave summarized these ideas in his book "Glacial Lake Missoula and its Humongous Floods." The Preface to the book provides an enduring perspective on how any scientific investigation should be conducted.

Dave was also a leading proponent of the idea that meteorites were significant players in Earth's geologic evolution. His published papers produced Hurrahs and Boos in the geologic community—such ideas bring energy to geologic study. Dave's ideas may have been Far Out, but they may also prove to be correct.

He was Older than Dirt and left us in the Spring of 2015.

Dave Alt and Don Winston. Cartoon by former UM graduate student's fater.

2015 HAMMER AWARD: JEFF LONN

Jeff Lonn received his Master's Degree in Geology from the University of Montana in 1985. It was there that he was introduced to Mesoproterozoic Belt rocks and the challenges of mapping this extraordinarily thick package of rocks that underlie most of western Montana. Jeff started his career as an exploration and engineering geologist but found his niche–mapping Mesoproterozoic Belt rocks in physically challenging, remote areas of Montana–when he went to work for the Montana Bureau of Mines and Geology (MBMG) in 1992. In his 23 years at the MBMG, Jeff has published over 30 geologic maps and related reports, mentored students, directed the MBMG's bedrock mapping program in western Montana, and jointly established ongoing, collaborative mapping projects with the Idaho Geologic Survey.

Jeff has distinguished himself with his research on Belt rocks in Montana and Idaho. In recent years, Jeff and his colleagues at the Idaho Geological Survey have focused on the ambitious task of resolving stratigraphic and structural relations between the Belt Supergroup rocks in Montana and similar rocks of the Lemhi Group in Idaho. This research and mapping has resulted in significant revision of many of the regional stratigraphic and structural concepts of these rocks that span the mutual state border.

Jeff's accomplishments as a field mapper go well beyond his work on the Belt. He was involved in recognizing and mapping the Anaconda Metamorphic Complex and has completed maps along a large part of the Lewis and Clark Line. This work significantly contributes to understanding the tectonic history of western Montana. Jeff has also mapped surficial deposits in the rapidly developing Bitterroot and Gallatin valleys, maps that will have enduring practical value as these areas continue to grow.

Jeff is a long-time supporter of TRGS. Since 1984, he has contributed over 20 papers, talks, and field trip guides, including his unique float-trip logs for sections of the Yellowstone and Clark Fork Rivers. In 2013, he was co-organizer of the joint Belt Symposium–TRGS meeting. Jeff also serves on the board of directors of the Belt Association.

2015 SCHOLARSHIP RECIPIENTS ($8,500)

- Alexandra Adams (TRGS Scholarship), University of Idaho, *Isotopic fractionation of light elements—Reconstructing past elevations in east Idaho and southwest Montana*

- Cody Bodman (TRGS Scholarship), Montana State University, *Effects of hanging-wall anticline growth on a Lare Cretaceous marine alluvial fan-delta system, Cordilleran Thrust Belt front, SW Wyoming*

- Kyle Eastman (Michael Thompson Foster Scholarship), Montana Tech, *Understanding the geology and geochemistry of the bedrock source of acidic streams at Mt. Evans, Anaconda Range, western Montana*

- Sara Edinberg (TRGS Scholarship), Montana Tech, *Natural acid rock drainage chemistry related to geology of the alkaline intrusions of the Judith Mountains of central Montana*

- G. Graham Ellsworth (TRGS Scholarship), University of Memphis, *Fracture relationships and the timing of the Heart Mountain allochthon*

- Nicholas Fox (Harrison Scholarship), Montana State University, *The Mesoproterozoic LaHood Formation: Provenance and tectonic environment of deposition*

- Nicholas Krohe (TRGS Scholarship), Idaho State University, *Neoproterozoic to Ordovician sandstone provenance west of the Lemhi Arch: Implication for rift geometry of the Laurentian passive margin*

- Robert McDermott (TRGS Scholarship), Utah State University, *A multichronometer approach to documenting ancient seismicity along the Wasatch Fault Zone, Utah*

- Joshua Messenger (Michael Thompson Foster Scholarship), Montana Tech, *Skarn paragenesis and the temporal relationship of scheelite mineralization at Calvert Mine, Pioneer Mountains, MT*

- Stuart Parker (TRGS Scholarship), University of Montana, *Deformed river gravel of the southern Beaverhead Mountains; Neotectonic implications*

- Luke Schwab (TRGS Scholarship), University of Idaho, *Reservoir characterization of the Logan Gulch Member of the Three Forks Formation in western Montana*

- Charles Shobe (TRGS Scholarship), University of Colorado, *Mapping rockfalls and understanding canyon evolution on the Clarks Fork Yellowstone River, Northern Wyoming*

- Daphne Tuzlac (TRGS Scholarship), Utah State University, *Mapping, correlating, and dating terraces to understand incision and uplift resulting from the Yellowstone Hotspot—Snake River Canyon, Wyoming*

- Michael Vineyard (TRGS Scholarship), Montana Tech, *Sequence stratigraphic correlation of the Bow Island Formation using surface outcrop and subsurface data, Glacier and Toole Counties, north-central Montana*

ABSTRACTS AND PAPERS

TAXONOMY AND BIOSTRATIGRAPHY OF THE MAMMALIAN FAUNA FROM THE CABBAGE PATCH BEDS (RENOVA FORMATION): AFFINITIES WITH ARIKAREEAN FAUNAS OF THE GREAT PLAINS AND OREGON

Johnathan J. Calede

University of Washington Department of Biology, Seattle, WA 98195

ABSTRACT

The mammalian fossil record of the Arikareean North American Land Mammal "age" is well known from the rich fossil assemblages of the Great Plains (Arikaree Group, MacFadden and Hunt, 1998) and Oregon (John Day Formation, Albright and others, 2008). Little work has comparatively been undertaken on the fossil record of the Rocky Mountains. Yet, a rich mammalian fauna is preserved in the Cabbage Patch beds (upper Renova Formation) cropping out in western Montana (Rasmussen and Prothero, 2003). It offers a window into the composition of the mammalian fauna from the region and the opportunity to investigate faunal affinities across western North America at a time of global climatic change and regional environmental perturbations (Strömberg, 2005; Zachos and others, 2008).

The study of over 900 mammalian specimens from the Cabbage Patch beds broadly supports an Arikareean age for the beds and the division of the beds in three biostratigraphic units (fig. 1, following page) suggested by previous work and the molluscan fauna (Pierce, 1993; Rasmussen and Prothero, 2003). The lower unit of the Cabbage Patch beds is characterized by the presence of the rabbits *Palaeolagus* and *Megalagus*, the leptomerycid *Pronodens* and two sciurids previously unknown in the area: *Miosciurus* and *Petauristodon*. The beaver fauna from the lower Cabbage Patch beds is also unique in including two new taxa of anchitheriomyine beaver in addition to the well-known palaeocastorine *Palaeocastor* and the basal castorid *Agnotocastor*. Several new taxa of aplodontids, including two species of *Niglarodon*, are also characteristic of this unit of the beds. The middle Cabbage Patch can be differentiated by the presence of a very abundant and species-rich fauna of entoptychine gophers. Indeed, the genus *Pleurolicus* is represented by three different species. The upper unit of the beds also hosts a unique set of mammalian taxa including another genus of entoptychine gopher, *Gregorymys*, the basal heteromyid *Mookomys*, and the little known gopher *Tenudomys* as well as the cricetid *Leidymys montanus*.

A comparison of the Cabbage Patch faunas with contemporary faunas from Oregon and the Great Plains suggests complex biogeographical affinities across the western Unites States. The carnivore fauna, and specifically the presence of *Archaeocyon leptodus* and *Cynodesmus thooides*, suggests affinities between Cabbage Patch and the Gering and Sharps formations of the Great Plains (Wang and others, 1999). The rodent fauna from Cabbage Patch, however, suggests a more complex pattern with some affinities with the John Day Formation (e.g., aplodontid and entoptychine rodents, *Miosciurus*, *Palaeocastor peninsulatus*, Tedford and others, 2004). A quantitative analysis of the composition of mammalian assemblages across the western United States supports an east to west faunal gradient from the Great Plains to Oregon. The geographically intermediate Rocky Mountains appear to correspond to a zone of faunal mixing between Oregon and the Great Plains. The Cabbage Patch beds are found to be most similar to the assemblages from the Fort Logan Formation of central Montana (Koerner, 1940; Black, 1961; Calede, 2014). Nevertheless, the many unique taxa found in the Cabbage Patch beds suggest a high degree of endemism with the diversification of taxa rare elsewhere during the Arikareean. Future work combining radiometric dating of select horizons throughout the beds and the ecological characterization of the small mammals will help understand the tempo and mode of faunal change throughout the Cabbage Patch beds and the possible drivers of faunal turnover through time in this unique region during the rise of modern mammalian communities (Webb and Opdyke, 1995; Woodburne, 2004).
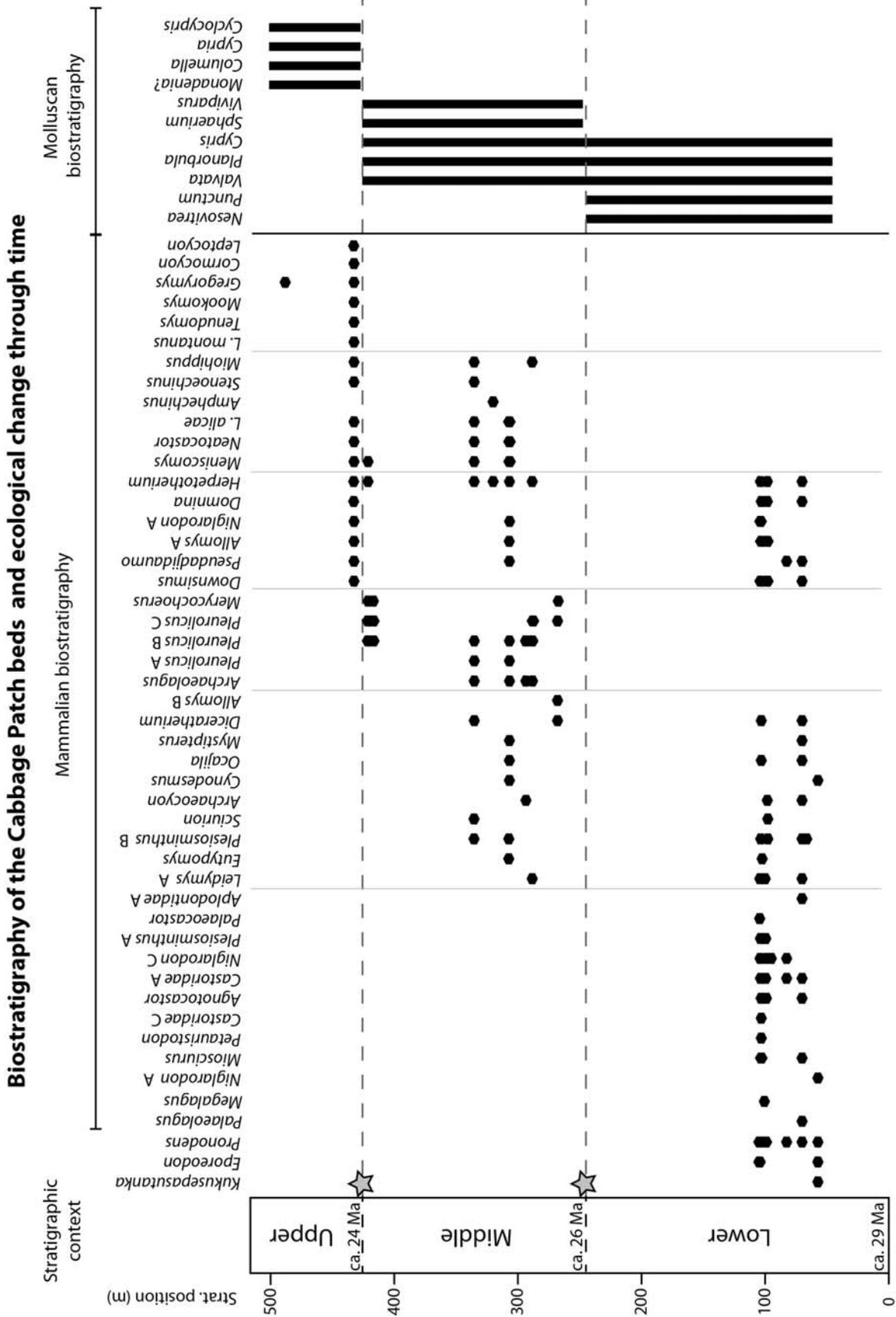
Figure 1. Summary of the mammalian biostratigraphy of the Cabbage Patch beds. Select fossil occurrences are indicated by dots (drawn from data modified and updated from Rasmussen, 1977; Rasmussen and Prothero, 2003). Species are indicated only when several from the same genus are present. Stars indicate faunal turnover events. They correspond to the boundaries between the lower, middle, and upper units of the beds.

REFERENCES

Albright, L.B., Woodburne, M.O., Fremd, T.J., Swisher III, C.C., MacFadden, B.J., and Scott, G.R., 2008, Revised chronostratigraphy and biostratigraphy of the John Day Formation (Turtle Cove and Kimberly members), Oregon, with implications for updated calibration of the Arikareean North American Land Mammal Age: The Journal of Geology, v. 119, p. 211–237.

Black, C.C., 1961, Rodents and lagomorphs from the Miocene Fort Logan and Deep River formations of Montana: Postilla, v. 48, p. 1–20.

Calede, J., 2014, Skeletal morphology of *Palaeocastor peninsulatus* (Rodentia, Castoridae) from the Fort Logan Formation of Montana (Early Arikareean): ontogenetic and paleoecological interpretations: Journal of Mammalian Evolution, v. 21, p. 223–241.

Koerner, H.E., 1940, The geology and vertebrate paleontology of the Fort Logan and Deep River formations of Montana: American Journal of Science, v. 238, p. 837–862.

MacFadden, B.J., and Hunt, R.M., 1998, Magnetic polarity stratigraphy and correlation of the Arikaree Group, Arikareean (late Oligocene-early Miocene) of northwestern Nebraska *in* Terry, D.O., Jr., LaGarry, H.E., and Hunt, R.M., eds. Depositional Environments, Lithostratigraphy, and Biostratigraphy of the White River and Arikaree Groups (Late Eocene to Early Miocene, North America). Geological Society of America Special Paper v. 325, p. 143–165.

Pierce, H.G., 1993, The nonmarine mollusks of the late Oligocene-early Miocene Cabbage Patch fauna of western Montana III. Aquatic mollusks and conclusions: Journal of Paleontology v. 67, p. 980–993.

Rasmussen, D.L., 1977, Geology and mammalian paleontology of the Oligocene–Miocene Cabbage Patch Formation, central-western Montana. Unpublished Ph.D. dissertation, University of Kansas, Lawrence, 794 p.

Rasmussen, D.L., and Prothero, D.R., 2003, Lithostratigraphy, biostratigraphy, and magnetostratigraphy of the Arikareean strata west of the Continental Divide in Montana in Raynolds, R.G., and Flores, R.M. eds. Cenozoic Systems of the Rocky Mountain Region: Rocky Mountain Section SEPM. p. 479–499.

Strömberg, C.A.E., 2005, Decoupled taxonomic radiation and ecological expansion of open-habitat grasses in the Cenozoic of North America: Proceedings of the National Academy of Sciences, v. 102, p. 11980–11984.

Tedford, R.H., L.B., Albright III, A.D., Barnosky, I., Ferrusquia-Villafranca, R.M., Hunt Jr., J.E., Storer, C.C., Swisher III, M.R., Voorhies, S.D., Webb, and Whistler, D.P., 2004, Mammalian biochronology of the Arikareean through Hemphillian interval (Late Oligocene through Early Pliocene epochs) in Woodburne, M.O. eds. Late Cretaceous and Cenozoic Mammals of North America: Biostratigraphy and geochronology. Columbia University Press. p. 315–343.

Wang, X., Tedford, R.H., and Taylor, B.E., 1999, Phylogenetic systematics of the Borophaginae (Carnivora, Canidae): Bulletin of the American Museum of Natural History, v. 243, p. 1–391.

Webb, S.D., and Opdyke, N.D., 1995, Global climatic influence on Cenozoic land mammal faunas. In Stanley, S.M., A.H., Knoll, and Kennett, J.P. eds. Effects of past global change on life: Washington, D.C., National Academies Press. p. 184–208.

Woodburne, M.O., 2004, Global events and the North American mammalian biochronology in Woodburne, M.O. eds. Late Cretaceous and Cenozoic Mammals of North America: Biostratigraphy and geochronology. Columbia University Press. p. 315–343.

Zachos, J.C., Dickens, G.R., and Zeebe., R.E., 2008, An early Cenozoic perspective on greenhouse warming and carbon-cycle dynamics: Nature, v. 451, p. 279–283.

USING GRAVITY DATA TO DECIPHER THE STRUCTURAL SETTING OF THE AVON VALLEY IN WEST-CENTRAL MONTANA

Leif K. Knatterud,[1] Marvin A. Speece,[2] Jesse G. Mosolf,[3] Catherine McDonald,[4] and Xiaobing Zhou[5]

[1]Montana Tech, Butte, MT, USA, lkknatterud@mtech.edu; [2]Montana Tech, Butte, MT, USA, mspeece@mtech.edu; [3]Montana Bureau of Mines and Geology, Butte, MT, USA, jmosolf@mtech.edu; [4]Montana Bureau of Mines and Geology, Butte, MT, USA, kmcdonald@mtech.edu; [5]Montana Tech, Butte, MT, USA, xzhou@mtech.edu

ABSTRACT

The Avon Valley and adjacent mountains are located in west-central Montana and lie within the Lewis and Clark Line. The Lewis and Clark Line is a major system of WNW-striking faults and folds that transect the more northerly structural grain of the northern Rocky Mountains (Wallace and others, 1990; Sears and Hendrix, 2004). The structure of the northwest-trending Avon Valley has most recently been interpreted as an extensional half graben filled with Tertiary sedimentary and volcanic deposits (Schmidt and others, 1994). Earlier interpretations show faults on both sides of the valley, consistent with a full graben (Pardee, 1950; Reynolds, 1979). Recent geologic mapping by the Montana Bureau of Mines and Geology has identified a system of high-angle, northwest- and northeast-striking faults occurring along the margins of the Avon Valley, consistent with the interpretations of Pardee and Reynolds (McDonald and others, in prep). No focused geophysical investigation or borehole data have been previously reported for the Avon Valley area, making structural interpretations in this region tenuous at best. In this study, the structural architecture of the Avon Valley and the thickness of its Tertiary basin fill are investigated through geophysical techniques including gravity and seismic reflection profiling.

The geologic setting of the Avon area is complex, consisting of Mesoproterozoic through Cenozoic rocks, Cretaceous intrusions, and unconsolidated deposits that record a prolonged history of tectonism (McDonald and others, in prep). The eastern Garnet Range defines the southwest margin of the Avon Valley where Tertiary volcanic and sedimentary deposits rest on an unconformity truncating faulted and folded Mesoproterozoic–Mesozoic sedimentary sequences. These shortening structures are overprinted by a system of steeply dipping, northwest- and northeast-striking faults. A major southwest-dipping normal fault or system of faults bounds the northeast side of the Avon Valley, placing Tertiary–Quaternary sedimentary deposits against folded and faulted Mesoproterozoic–Mesozoic sequences. Elevated areas of Tertiary volcanic and sedimentary deposits unconformably overlying Proterozoic–Mesozoic sequences border the northwest and southeast margins of the Avon Valley and are possibly displaced by northeast-striking faults.

New geophysical data collected in this study suggest the structural architecture of the Avon Valley is more complex than originally interpreted. Steep gradients within the gravity data (fig. 1) highlight two structural domains. The domains are separated by a high-angle, northeast-striking fault or system of faults that bisect the valley. The northern domain is characterized by a full-graben geometry (fig. 2). Here, a previously unrecognized northeast-dipping fault with significant normal displacement bounds the southwest margin of the basin, generally following the orientation of the Avon Valley. The northeast-margin of this basin has been reinterpreted in this study as a series of southwest dipping normal or oblique-slip faults. The southern structural domain is more consistent with a half-graben geometry (fig. 3). A northwest-striking fault bounds the northeast margin of the basin and continues into the northern structural domain. Unlike the northern domain, however, no valley bounding fault is apparent on the western side of the basin. Preliminary forward models show Tertiary fill within the valley to reach depths up to 2 kilometers in the northern structural domain (fig. 2).

Normal and/or oblique-slip faults characterizing the Avon Valley's structural domains presumably formed during regional transtensive shear within the Lewis and Clark Line following Cretaceous–-Paleocene transpressive shortening (Sears and Hendrix, 2004), and are tentatively interpreted to be guided by or localized on shortening structures.
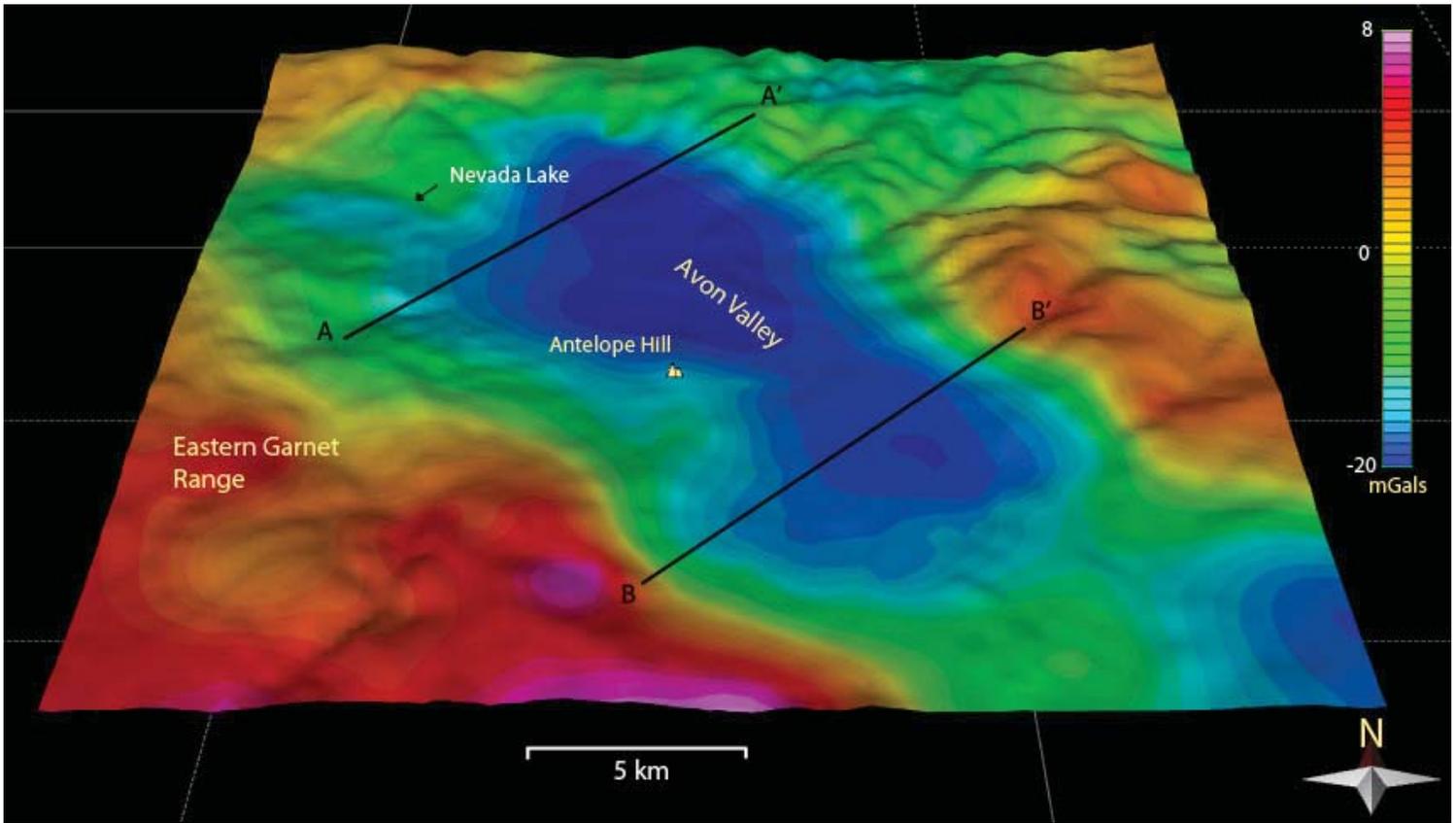
Figure 1. Gravity contour map of the Avon Valley and adjacent mountains showing the modeled depth-to-bedrock. Lows are shown by the negative gravity anomaly (blue).
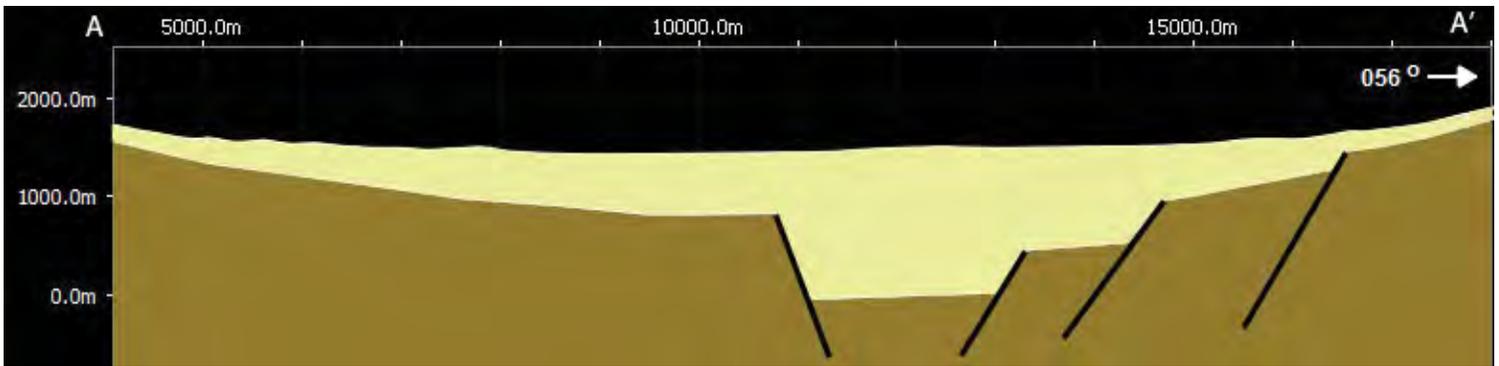
Figure 2. Interpretive cross section A-A'.
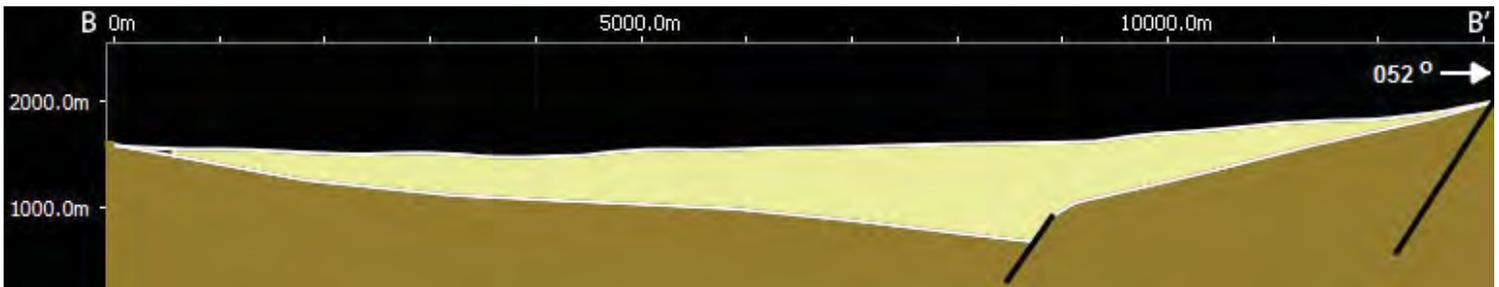
Figure 3. Interpretive cross section B-B'.

REFERENCES

McDonald, C., Mosolf, J.G., Vuke, S.M., and Lonn, J.D., in preparation, Preliminary geologic map of the Elliston 30' x 60' quadrangle, west-central Montana: Montana Bureau of Mines and Geology Open-File Report, 1 sheet, scale 1:100,000.

Pardee, J.T., 1950, Late Cenozoic block faulting in western Montana: Geological Society of America Bulletin, v. 61, p. 359-406.

Reynolds, M.W., 1979, Character and extent of basin-range faulting, western Montana and east-central Idaho, *in* Newman, G.W., and Goode, H.D., eds., Basin and Range Symposium: Rocky Mountain Association of Geologists, p. 185-193.

Schmidt, R.G., Loen, J.S., Wallace, C.A., and Mehnert, H.H., 1994, Geology of the Elliston region, Powell, and Lewis and Clark Counties, Montana: U.S. Geological Survey Bulletin 2045, 25 p., scale 1:48,000.

Sears, J.W., and Hendrix, M., 2004, Lewis and Clark line and the rotational origin of the Alberta and Helena salients, North American Cordillera, *in* Sussman, A.J., and Weil, A.B., eds., Orogenic curvature: integrating paleomagnetic and structural analyses: Geological Society of America Special Paper 383, p. 173-186.

Wallace, C.A., Lidke, D.J., and Schmidt, R.G., 1990, Faults of the central part of the Lewis and Clark line and fragmentation of the Late Cretaceous foreland basin in west-central Montana: Geological Society of America Bulletin, v. 102, p. 1021-1037.

GEOLOGIC SUMMARY OF THE ELLISTON 30′ X 60′ QUADRANGLE, WEST-CENTRAL MONTANA

Catherine McDonald, Jesse G. Mosolf, Susan M. Vuke, and Jeffrey D. Lonn

Montana Bureau of Mines and Geology, 1300 W. Park St, Butte, MT 59701, kmcdonald@mtech.edu

INTRODUCTION

The Montana Bureau of Mines and Geology recently completed the *Geologic Map of the Elliston 30' x 60' Quadrangle* (McDonald and others, in prep). The quadrangle encompasses a geologically complex and seismically active part of west-central Montana. It is located within the eastern part of the Lewis and Clark Line and is within the Montana Thrust-and-Fold belt (fig. 1). The quadrangle is underlain by Mesoproterozoic through Cretaceous sedimentary rocks, extensive Cretaceous and Tertiary volcanic rocks, the northern edge of the Cretaceous Boulder Batholith, numerous smaller Cretaceous and Tertiary intrusions, and Tertiary and Quaternary deposits. The map is the result of six years of 1:24,000-scale mapping by MBMG and compilation of numerous existing maps. This paper provides a brief summary of the geology of the quadrangle.

MESOPROTEROZOIC METASEDIMENTARY ROCKS

Mesoproterozoic metasedimentary rocks of the Belt Supergroup are the oldest exposed rocks in the Elliston quadrangle. The thick (about 8,000 m) Belt strata are widespread in the north half of the quadrangle (fig. 2) and include nearly the entire Belt Supergroup section (fig. 3). The Greyson Formation of the lower Belt (Prichard Formation correlative) is the oldest unit exposed and records deep-water sedimentation. It consists of siltite, argillite, and interbedded
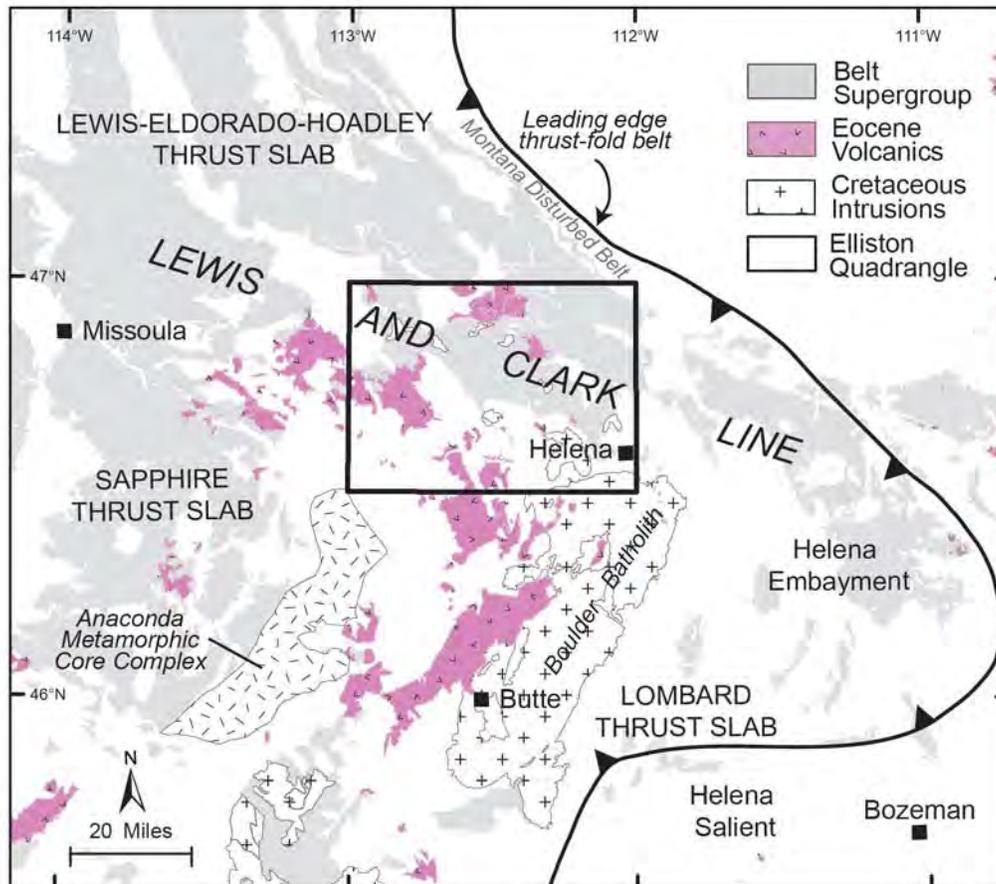
Figure 1. Regional setting of the Elliston 30′ x 60′ quadrangle.
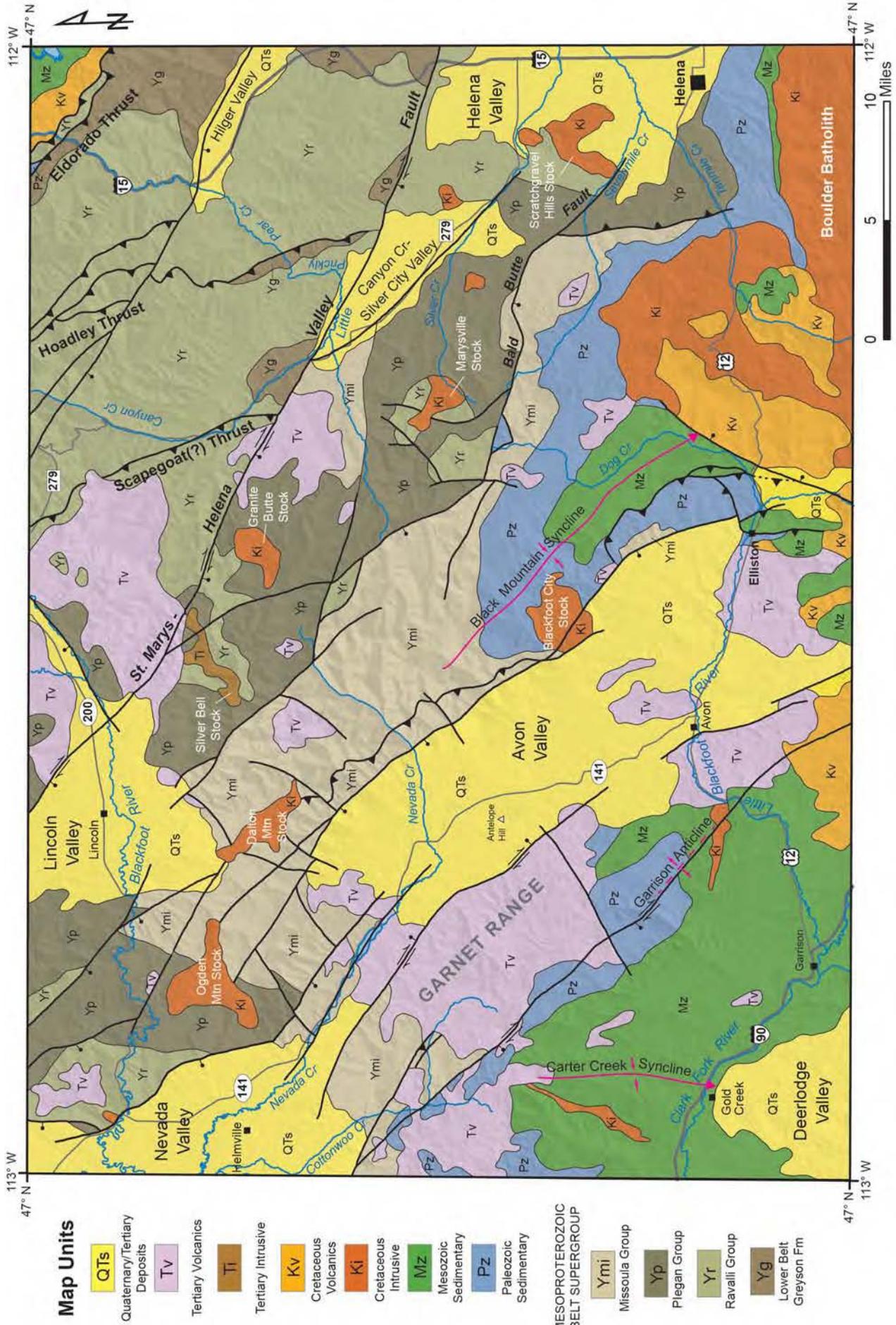
Figure 2. Simplified geologic map of the Elliston 30' x 60' quadrangle (modified from McDonald and others, in prep).

Map Units

- QTs — Quaternary/Tertiary Deposits
- Tv — Tertiary Volcanics
- Ti — Tertiary Intrusive
- Kv — Cretaceous Volcanics
- Ki — Cretaceous Intrusive
- Mz — Mesozoic Sedimentary
- Pz — Paleozoic Sedimentary

MESOPROTEROZOIC BELT SUPERGROUP

- Ymi — Missoula Group
- Yp — Piegan Group
- Yr — Ravalli Group
- Yg — Lower Belt Greyson Fm
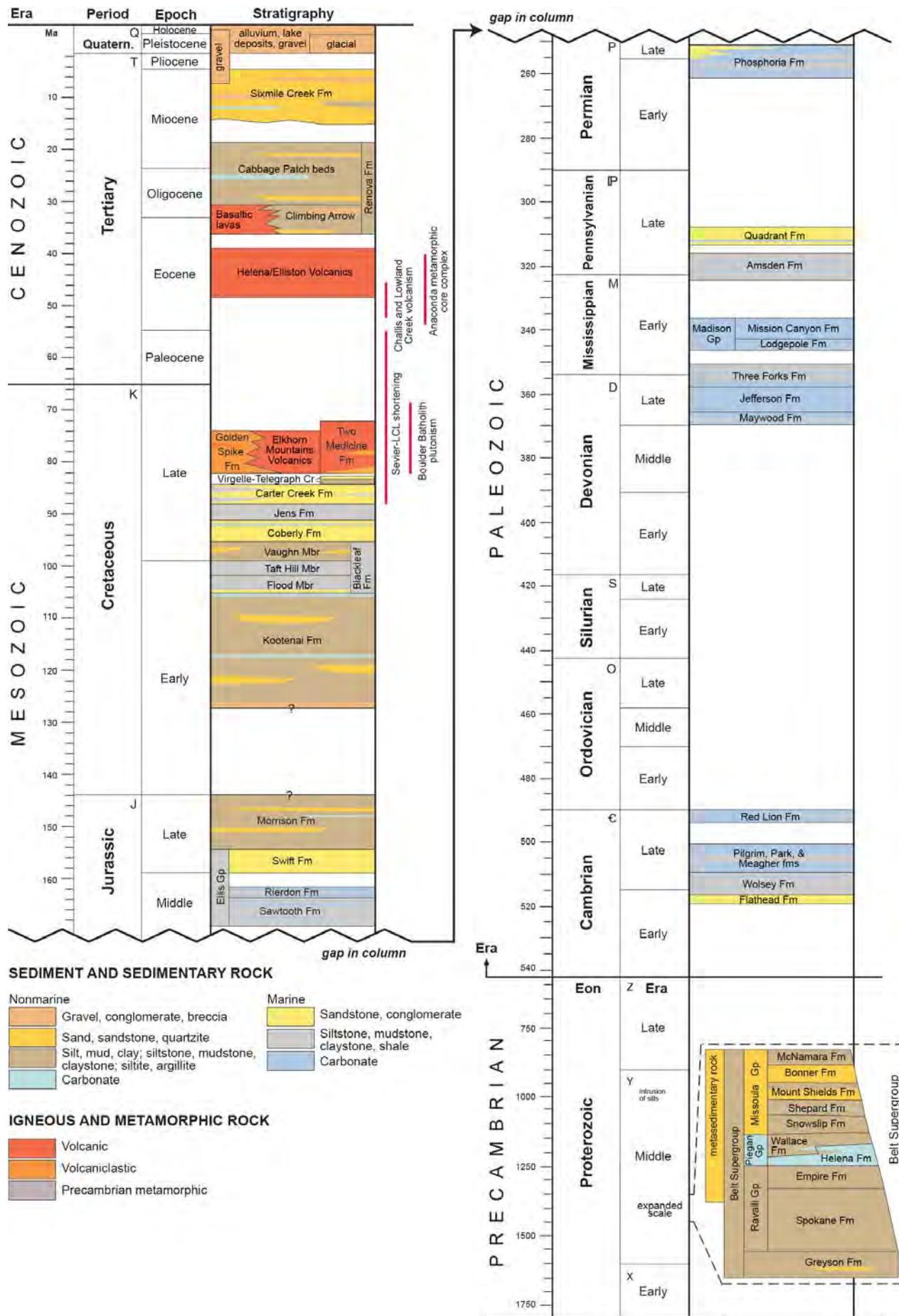
Figure 3. Simplified stratigraphic column of the Elliston 30′ x 60′ quadrangle (modified from Vuke and others, 2007).

quartzite. The overlying Spokane and Empire Formations (Ravalli Group) are dominantly fine-grained, thin-bedded argillites and siltites most likely deposited on periodically exposed mudflats near where distal margins of huge eastward-sloping alluvial megafans encountered the Belt Sea (Winston and Link, 1993; Winston, 2013). During subsequent deposition of the Piegan Group, the Belt Sea expanded and deepened, although it was still shallow enough that storm waves could rework the bottom sediments (Winston, 1986a). The Piegan Group includes the carbonate-rich shallowing-upward depositional cycles of the Helena and Wallace Formations, but mappers have not recognized the Wallace Formation in the Elliston quadrangle. The Missoula Group tops the Belt succession with alternating sandy (deposited on vast northward-sloping alluvial megafans and flats) and muddy (deposited in a shallow ephemeral sea distal to the megafans) formations (Winston and Sears, 2013).

The Belt strata in the Elliston quadrangle preserve evidence of Mesoproterozoic to possibly Early Cambrian deformation. The Middle Cambrian Flathead Formation unconformably overlies the McNamara Formation (upper Missoula Group) in the western part of the quadrangle, but overlies the Snowslip Formation (lower Missoula Group) in the southeastern part, and the Spokane Formation (Ravalli Group) in the northeastern part. This unconformity documents regional-scale deformation of the Belt prior to the Middle Cambrian. In the northeast part of the quadrangle, mafic sills that intruded the Belt sediments from 780 to 750 Ma (Mudge and others, 1982; Burtis and others, 2007) may have accompanied this deformation. In the southeast part of the quadrangle, Mesoproterozoic deformation is suggested by abrupt thickness changes in Missoula Group strata. Winston (1986b) proposed that an east-west striking, down-to-the-north Mesoproterozoic growth fault, the Garnet Line, resulted in a thickened section to the north. The proposed Garnet Line crosses the Elliston quadrangle and will be examined on a 2015 TRGS field trip (Lonn, this volume).

PALEOZOIC AND MESOZOIC SEDIMENTARY ROCKS

Paleozoic and Mesozoic sedimentary rocks are widely exposed in the southern part of the Elliston quadrangle and are deformed by north-northwest

trending folds (fig. 2). Mesozoic rocks are also found in the footwall of the Eldorado Thrust in the northeast corner of the quadrangle. The Paleozoic sedimentary section includes Cambrian, and Devonian through Permian rocks (fig. 3); Silurian and Ordovician strata are missing. The upper Cambrian, Devonian, and Mississippian strata are mainly marine carbonates; the other Paleozoic units are dominantly terrigenous sediments.

Mesozoic rocks include Jurassic and Cretaceous marine and non-marine sedimentary rocks deposited in the foreland of the Rocky Mountain Thrust-and-Fold belt. In the southwestern part of the quadrangle, Cretaceous sediments of the Colorado Group (Blackleaf through Carter Creek Formations, fig. 3) were deposited in the Garrison Depression, a deep basin that has the thickest accumulation (from 3,000 to 4,500 m) of Colorado Group strata in Montana (Gwinn, 1960; O'Brien, 2000). The Colorado Group thins to the east to about 410 m in the northeast corner of the quadrangle (Bregman, 1981).

The youngest Mesozoic sedimentary rocks in the quadrangle are Cretaceous volcaniclastic sediments of the Golden Spike Formation, in the southwest corner of the quadrangle, and the Two Medicine Formation in the northeast corner.

INTRUSIVE ROCKS

The oldest intrusive rocks are Neoproterozoic diorite and gabbro sills in Belt Supergroup rocks. The mafic sills are thought to be a component of the Gunbarrel Large Igneous Province (Harlan and others, 2003). A sill from the Lewis and Clark Range north of the Elliston quadrangle yielded a K-Ar age of 750 ± 25 Ma (Mudge and others, 1968).

The most widespread intrusive rocks are Late Cretaceous plutonic rocks of the Boulder Batholith (fig.2) that were emplaced from 82-74 Ma (see du Bray and others, 2012 and references therein) into folded and faulted Mesoproterozoic to Mesozoic sedimentary rocks and into the cogenetic Late Cretaceous Elkhorn Mountains Volcanics. The Butte Granite, which forms the main body of the Boulder Batholith, was emplaced from ~76 to 74 Ma (du Bray and others, 2012). The Unionville Granodiorite, located along the north margin of the Boulder Batholith, is an older pluton

emplaced about 78 Ma (du Bray and others, 2012). Farther north, several granodiorite satellite stocks, including the Marysville, Scratchgravel Hills, Black-foot City, Granite Butte, Dalton Mountain, and Og-den Mountain Stocks, with reported ages of 81 to 76 Ma, also preceded emplacement of the Butte Granite (Schmidt and others, 1994; du Bray and others, 2012). Several small gabbroic intrusions of undetermined age are located near the head of Washington Creek east of the Avon Valley.

Tertiary sills, dikes, and small intrusive bod-ies with compositions ranging from trachydacite to rhyolite are common throughout the quadrangle where they intrude the Eocene-Oligocene volcanics and older underlying rocks. The Silver Bell Stock, located south of Lincoln, has reported K-Ar dates on biotite of 48.1±1.8 Ma (Daniel and Berg, 1981) and 52.0±1.8 Ma (Schmidt and others, 1994). The stock is adjacent to the Crater Mountain Volcanic field (Melson, 1964; Parker, 1995) and may have been a precursor to that eruptive cycle.

Gold, silver, lead, zinc, and other mineral deposits are associated with many of the Tertiary and Creta-ceous intrusive bodies in the quadrangle.

EXTRUSIVE VOLCANIC ROCKS

Extrusive volcanic deposits and associated hyp-abyssal intrusions occur throughout the Elliston quad-rangle (fig. 2) and record significant intervals of Late Cretaceous, Eocene, and Oligocene volcanism (fig. 3). These pulses of volcanism spanned major changes in the Elliston region's tectonic setting as Late Creta-ceous-Paleocene transpressive shortening ceased and transtensional deformation began as discussed below.

The Late Cretaceous Golden Spike Formation, Elkhorn Mountains Volcanics, and Two Medicine Formation (Kv on fig. 2) contain the oldest extrusive rocks exposed in the quadrangle. The Elkhorn Moun-tains Volcanics and Golden Spike Formation are the most extensively exposed Cretaceous volcanic units and occur only in the southern part of the quadrangle where they rest unconformably on Paleozoic through Late Cretaceous sedimentary and igneous rocks. The volcanism recorded by these units was comagmatic with the Boulder Batholith (Smedes, 1966), and largely occurred during Late Cretaceous-Paleocene

crustal shortening (Sears and Hendrix, 2004). The Golden Spike Formation near Garrison is composed of alternating andesitic flows and tuffs; volcaniclas-tic sandstone and diamictite; and non-volcaniclastic pebble conglomerate, siltstone, and mudstone (Gwinn, 1961; Gwinn and Mutch, 1965). Intervals of the Golden Spike Formation intertongue with the Elkhorn Mountains Volcanics east of Garrison. The base of the Elkhorn Mountains Volcanics is characterized by andesitic lava flows with minor volcaniclastic intervals (Peterson, 1985), whereas the overlying stratigraphy is dominated by crystal-rich ash-flows intercalated with minor andesite lavas (Berg, 2009; Derkey and others, 2004). Radiometric age data are sparse for Cretaceous volcanic and volcaniclastic deposits in the Elliston quadrangle, but a suite of U-Pb ages obtained from the Elkhorn Mountains Volcanics outside the Elliston quadrangle range from 82-74 Ma (Ihinger and others, 2011). A distinctive set of Late Cretaceous potassic pyroxene andesite and/or diorite dikes and sills (Ki on fig. 2) locally intrude the Golden Spike Formation, Elkhorn Mountains Volcanics, and underlying Pha-nerozoic formations (Sears and others, 1998).

Tertiary volcanic and volcaniclastic rocks exposed throughout the Elliston quadrangle rest on a regional unconformity that truncates faulted and folded Me-soproterozoic through Late Cretaceous rocks (Tv on fig. 2). Tertiary volcanic rocks are locally tilted and displaced by oblique-slip faults presumably formed during regional transtensive deformation as discussed below. The most geographically widespread outcrops of Tertiary volcanic rock occur in the Avon, Garnet Range, and Crater Mountain volcanic fields (Call-meyer, 1984; Parker, 1995; Trombetta, 1987). Each of these volcanic fields shares a strikingly similar vol-canic stratigraphy that can be mapped and correlated throughout the Elliston quadrangle (McDonald and others, in prep). A series of aphanitic and porphyritic trachydacite flows interlayered with minor dacitic tuff deposits and rhyolite lava are the oldest units exposed and yielded U-Pb zircon ages spanning 47.55 to 46.01 Ma (McDonald and others, in prep). Rhyolite lavas and ash flow deposits (40.8 to 39.24 Ma) overlie the older Eocene volcanic units in the Avon and Crater Mountain volcanic fields. Isolated exposures of basal-tic andesite lavas (37.3 to 29.95 Ma) are the youngest extrusive rocks exposed in the Elliston quadrangle. These flows are locally intercalated with the Climbing Arrow Member of the Renova Formation.

TERTIARY SEDIMENTARY ROCKS

Tertiary sedimentary rocks underlie the major valleys in the Elliston quadrangle (fig. 1) and occur as isolated deposits (not shown on the simplified geologic map) in the Garnet Range and in the Mullan Pass area north of Elliston. The stratigraphy of the Tertiary deposits is similar to that in other western Montana valleys with Paleogene/early Neogene Renova Formation unconformably overlain by Neogene Sixmile Creek Formation. Vertebrate fossils (Konizeski, 1961, 1965; Rasmussen, 1977; Trombetta and Berg, 2012) and stratigraphic position of the deposits relative to newly dated volcanic rocks in the quadrangle (McDonald and others, in prep.) indicate age equivalence to similar Tertiary units in other western Montana valleys.

The Eocene Climbing Arrow Member of the Renova Formation is equivalent to the Douglass Creek beds, named for Douglas Creek in the Helmville area (Konizeski, 1961, 1965) and to the Blackfoot City beds in the Avon area (Loen, 1990). It is dominantly bentonitic mudstone and pebble beds, with subordinate carbonaceous shale, and lignite.

The Miocene/Oligocene Cabbage Patch beds (Konizeski and Donahoe, 1958) of the upper Renova Formation (Rasmussen, 1989) are best exposed on Antelope Hill in the central Avon Valley where they overlie the Climbing Arrow Member (McDonald and others, in prep.) and in the Gold Creek area where they are overlain by Sixmile Creek Formation equivalents (Loen, 1986). The Cabbage Patch beds consist primarily of siltstone with sandstone lenses, marlstone, limestone, local gastropod coquina, ash, and porcellanite.

Isolated exposures of lacustrine Cabbage Patch beds in the Garnet Range are similar to deposits in the adjacent Avon/Nevada Valleys. Likewise, lignitic Climbing Arrow Member is preserved at Mullan Pass and in the Avon Valley. The similarity of these lowland deposits in the present-day mountains and valleys suggests that the ranges were not positive elements at the time of deposition.

A widespread middle Miocene unconformity, recognized in other western Montana valleys, separates the Renova Formation from overlying Sixmile Creek Formation. The Sixmile Creek is composed of tuffaceous siltstone with abundant local to laterally persistent, mostly matrix-supported, granule to boulder lenses. It is lithologically similar to the Sixmile Creek Formation in the Drummond and Townsend Valleys, southwest and southeast, respectively, of the Elliston quadrangle.

An extensive, matrix-supported gravel with abundant subangular to subrounded boulders is preserved along range-front faults on the northeast side of the Avon Valley, the southwest side of the Nevada Valley, and as higher remnants. Loen (l990) suggested a late Miocene(?) age for the deposits in the Blackfoot City area and interpreted them as alluvial fans. Channel deposits within these fans have been mined for placer gold.

QUATERNARY DEPOSITS

Most Quaternary deposits in the Elliston quadrangle are in the Cenozoic valleys. Surficial deposits in the eastern valleys are dominantly silt, sand, and gravel deposited on alluvial plains and pediments, and as alluvial fans. Glacial deposits associated with Pinedale and Bull Lake(?) ice caps, located primarily north and south of the quadrangle, extend into the Lincoln and northern Nevada Valleys, and the upper Little Blackfoot River drainage (Witkind and Weber, 1982; Ruppel, 1963; Wittkop, 2009). Remnants of mountain glacial deposits occur along the Continental Divide between MacDonald Pass and the Lincoln Valley. A dissected outwash fan covers a large area of the central Avon Valley, and glacial outwash underlies part of the Tenmile Creek drainage. Glacial deposits are also present in the Gold Creek Valley in the southwestern corner of the quadrangle.

Pediments are well developed on Tertiary deposits in the Avon, southern Nevada, and Gold Creek Valleys and are mantled with gravel, lag, and regolith deposits. In the western part of the quadrangle numerous landslide deposits occur, mostly in the Renova Formation and volcanic rock.

STRUCTURAL GEOLOGY AND TECTONICS

The dominantly WNW-striking structural grain in the Elliston quadrangle records a complex tectonic history associated with the long-lived Lewis and Clark Line (LCL), a major WNW-striking crustal-scale shear

zone transecting the more northerly oriented structural grain of the northern Rockies (Sears and Hendrix, 2004). Deformation along and adjacent to the LCL has been varied and episodic from the Mesoproterozoic (discussed earlier) to Holocene, involving intermittent periods of extensional, transpressive, and transtensive faulting (Wallace and others, 1990; Sears and Hendrix, 2004; Foster and others, 2007). The St. Mary's-Helena Valley fault zone in the northeast part of the quadrangle forms the northern boundary the LCL, whereas the southern LCL boundary lies south of the quadrangle. The northwest- and northeast-striking oblique-slip faults, and north- to northwest-trending folds (fig. 2) are interpreted to record at least two major deformational cycles associated with LCL tectonism (Sears and Hendrix, 2004): early (Late Cretaceous-late Paleocene) sinistral, transpressive shortening followed by later (post-middle Eocene) dextral, transtensive deformation.

Transpressive structures in the Elliston quadrangle are characterized by northwest-trending, oblique-slip thrust and reverse faults, and north-northwest trending (south-southeast plunging) upright folds (e.g. the Black Mountain and Carter Creek Synclines, and Garrison Anticline; fig. 2). A set of progressive unconformities underlying and within the early Campanian Golden Spike Formation suggest shortening was underway by ca. 88 to 83 Ma (Sears and Hendrix, 2004). The Black Mountain and Carter Creek Synclines are cored by Late Cretaceous sedimentary rocks intruded by a distinctive set of folded mafic dikes and sills (~75.9 Ma; Sears and others, 1998), suggesting transpressive deformation continued after 76 Ma. Transpressive structures are interpreted to represent a rotational shear zone developed within the LCL during Late Cretaceous-Paleocene(?) shortening, which accommodated differential rotation between the Lewis-Eldorado-Hoadley (LEH) thrust slab to the north (fig. 1) and the Sapphire-Lombard thrust slab to the south (Sears and Hendrix, 2004; Mudge and Earhart, 1983).

The Eldorado, Hoadley, and Scapegoat (?) Thrust Faults and associated folds mapped in the northeast corner of the quadrangle are part of the LEH thrust slab (fig. 2). The Eldorado Thrust Fault carries relatively undeformed Mesoproterozoic rocks of the Greyson and Spokane Formations eastward over folds and imbricate thrust faults in the Upper Cretaceous Two Medicine Formation of the Montana Disturbed belt

(Mudge, 1970). West of the Eldorado Thrust Fault, the Scapegoat (?) and Hoadley thrusts place Greyson Formation over Spokane Formation. The Hoadley Thrust Fault is cut by the Hilger Valley Normal Fault. Both faults terminate against the St. Mary's-Helena Valley Fault, one of the major right-lateral, high-angle faults of the LCL.

The major transtensive structures mapped in the Elliston quadrangle include dominantly northwest- and northeast-striking normal, oblique-slip, and strike-slip faults that overprint the older transpressive structures. While the timing of transtensive deformation in the Elliston area is somewhat uncertain, faulting likely initiated during mid-Eocene volcanism and rapid exhumation of the nearby Anaconda metamorphic core complex (53-39 Ma; Foster and others, 2010). Following Eocene volcanism, a broad depositional basin with minor internal faulting developed in the Elliston region and accommodated fine-grained basin deposits of the Renova Formation and intercalated basaltic lava flows. A regional mid-Miocene unconformity separating the Renova Formation from the overlying Sixmile Creek Formation records segmentation of the Renova basin into major fault-bounded valleys including the Avon, Nevada, Canyon Creek-Silver City, Helena, and Lincoln Valleys in the Elliston quadrangle. These valleys are interpreted as grabens associated with pull-apart basins formed during Miocene and younger transtensive deformation (after Reynolds, 1979).

Recent seismicity indicates that many faults in the Elliston area are still active, with more than half of all fault plane solutions showing right-lateral offset (Stickney, 2015, this volume). The seismicity data also suggest that the LCL may function as the northern boundary of the middle Tertiary to Holocene Basin and Range province (Stickney, 2015, this volume; Reynolds, 1979).

REFERENCES

Berg, R.B., 2009, Geologic map of the Black Mountain 7.5′ quadrangle, southwestern Montana: Montana Bureau of Mines and Geology Open-File Report MBMG 587, scale 1:24,000.

Bregman, M.L., 1981, Structural geology of the Sheep Creek and Rattlesnake Mountain quadrangles, Lewis and Clark County, Montana: Montana Bureau of Mines and Geology Geologic Map GM

26, scale 1:24,000.

Burtis, E., Sears, J.W., and Chamberlain, K.R., 2007, Age and petrology of Neoproterozoic intrusions in the northern Rocky Mountains, U.S.A., *in* Link, P.K., and Lewis, R.S., eds., Proterozoic geology of western North America and Siberia: SEPM (Society for Sedimentary Geology) Special Publication 86, p. 175-192.

Callmeyer, T.J., 1984, The structural, volcanic, and hydrothermal geology of the Warm Springs Creek area, eastern Garnet Range, Powell County, Montana: Bozeman, Montana State University, M.S. thesis, 79 p.

Daniel, F., and Berg, R.B., 1981, Radiometric dates of rocks in Montana: Montana Bureau of Mines and Geology Bulletin 114, 144 p.

Derkey, R.E., Watson, S.M., Bartholomew, M.J., Stickney, M.C. and Downey, P.J., 2004, Geologic map of the Deer Lodge 15′ quadrangle, southwestern Montana: Montana Bureau of Mines and Geology Open-File Report MBMG 271, scale 1:48,000.

du Bray, E.A., Aleinikoff, J.N., and Lund, K., 2012, Synthesis of petrographic, geochemical, and isotopic data for the Boulder Batholith, southwest Montana: U.S. Geological Survey Professional Paper 1793, 39 p.

Foster, D.A., Doughty, P.T., Kalakay, T.J., Fanning, C.M., Coyner, S., Grice, W.C., and Vogl, J. 2007, Kinematics and timing of exhumation of metamorphic core complexes along the Lewis and Clark fault zone, northern Rocky Mountains, USA, *in* Till, A.B., Roeske, S.M., Sample, J.C., and Foster, D.A., eds., Exhumation associated with continental strike–slip fault systems: Geological Society of America Special Paper 434, p. 207–232.

Foster, D.A., Grice, W.C., Kalakay, T.J., 2010, Extension of the Anaconda metamorphic core complex: ^{40}Ar/^{39}Ar thermochronology and implications for Eocene tectonics of the northern Rocky Mountains and the Boulder Batholith: Lithosphere, v. 2, no. 4, p. 232-246.

Gwinn, V.E., 1960, Cretaceous and Tertiary stratigraphy and structural geology of the Drummond area, western Montana: Princeton, New Jersey, Princeton University, Ph.D. dissertation, 153 p.

Gwinn, V.E., 1961, Geology of the Drummond area, central-western Montana: Montana Bureau of Mines and Geology Geologic Map GM 4, 1 sheet, scale 1:62,500.

Gwinn, V.E., and Mutch, T.A., 1965, Intertongued Upper Cretaceous volcanic and nonvolcanic rocks, central-western Montana: Geological Society of America Bulletin, v. 76, p. 1125-1144.

Harlan, S.S., Heaman, L., LeCheminant, A.N., and Premo, W.R., 2003, Gunbarrel mafic magmatic event: A key 780 Ma time marker for Rodinia plate reconstructions: Geology, v. 31, p. 1053-1056.

Ihinger, P., Mahoney, J.B., Johnson, B.R., Kohel, C., Guy, A.K., Kinbrough, D.L., and Friedman, R.M., 2011, Late Cretaceous magmatism in southwest Montana: the Boulder Batholith and Elkhorn Mountains Volcanics, Geological Society of America, Abstracts with Programs, v. 43, no. 5, p. 647.

Konizeski, R.L., 1961, Paleoecology of an early Oligocene biota from Douglass Creek basin, Montana: Geological Society of America Bulletin, v. 72, p. 1633-1642.

Konizeski, R.L., 1965, Tertiary deposits in basins marginal to the Flint Creek Range: Billings Geological Society Sixteenth Annual Field Conference Guidebook, p. 10-18.

Konizeski, R.L., and Donohoe, J.C., 1958, Faunal and stratigraphic relationships of the Cabbage Patch beds, Granite County, Montana: Society of Vertebrate Paleontology, Eighth Annual Field Conference, p. 45-49.

Loen, J.S., 1986, Origin of gold placers in the Pioneer District, Powell County, Montana: Fort Collins, Colorado State University, M.S. thesis, 164 p.

Loen, J.S., 1990, Lode and placer gold deposits in the Ophir District, Powell, and Lewis and Clark Counties, Montana: Fort Collins, Colorado State University, Ph.D. dissertation, 268 p.

McDonald, C., Mosolf, J.G., Vuke, S.M., and Lonn, J.D., in preparation, Geologic map of the Elliston 30′ x 60′ quadrangle, west-central Montana: Montana Bureau of Mines and Geology Open-File Report, 1 sheet, scale 1:100,000.

Melson, W.G., 1964, Geology of the Lincoln area, Montana and contact metamorphism of the

impure carbonate rocks: Princeton, New Jersey, Princeton University, Ph.D. dissertation, 153 p., 4 pls., scale 1:31,680.

Mudge, M.R., Erickson, R. L., and Kleinkopf, M.D., 1968, Reconnaissance geology, geophysics, and geochemistry of the southern part of the Lewis and Clark Range, Montana: U.S. Geological Survey Bulletin 1252-E, 35 p.

Mudge, M.R., 1970, Origin of the Disturbed belt in northwestern Montana: Geological Society of American Bulletin, v. 81, p. 377-392.

Mudge, M.R., Earhart, R.L., Whipple, J.W., and Harrison, J.E., 1982, Geologic and structure map of the Choteau 1° x 2° quadrangle, western Montana: U.S. Geological Survey Miscellaneous Investigations Map I-1300, 2 sheets, scale 1:250,000.

Mudge, M.R., and Earhart, R.L., 1983, Bedrock geologic map of part of the northern Disturbed belt, Lewis and Clark, Teton, Pondera, Glacier, Flathead, Cascade, and Powell Counties, Montana: U.S. Geological Survey Miscellaneous Investigations Map I-1375, 2 sheets, scale 1:250,000.

O'Brien, M.W., 2000, Stratigraphic analysis of the Albian through Campanian Colorado Group within the Garrison Depression, west-central Montana: Missoula, University of Montana, M.S. thesis, 122 p.

Parker, D.B., 1995, The geology, petrology, and volcanic history of the Crater Mountain Volcanic Complex, Lewis and Clark County Montana: Missoula, University of Montana, M.S. thesis, 240 p.

Portner, R.A., Hendrix, M.S., Stalker, J.C., Miggins, D.P., Sheriff, S.D., 2011, Sedimentary response to orogenic exhumation in the northern Rocky Mountain Basin and Range province, Flint Creek basin, west-central Montana: Canadian Journal of Earth Sciences, v. 48, p. 1131-1153.

Peterson, M.P., 1985, The geology of the southwest quarter of the Avon 15-minute quadrangle, Powell County, Montana: Butte, Montana College of Mineral Science and Technology, M.S. thesis, 78 p.

Rasmussen, D.L., 1977, Geology and mammalian paleontology of the Oligocene-Miocene Cabbage Patch Formation, central-western Montana: Lawrence, University of Kansas, Ph.D. dissertation, 794 p.

Rasmussen, D.L., 1989, Depositional environments, paleoecology, and biostratigraphy of Arikareean Bozeman Group strata west of the Continental Divide in Montana: *in* French, D.E. and Grabb, R.F., eds., Geological Resources of Montana v. 1, Montana Geological Society, Montana Centennial Edition, 1989 Field Conference, Guidebook, p. 205-215.

Reynolds, M.W., 1979, Character and extent of basin-range faulting, western Montana and east-central Idaho, *in* Newman, G.W., and Goode, H.D., eds., Basin and Range Symposium: Rocky Mountain Association of Geologists, p. 185-193.

Ruppel, E.T., 1963, Geology of the Basin quadrangle, Jefferson, Lewis and Clark, and Powell Counties, Montana: U.S. Geological Survey Bulletin 1151, 121 p.

Schmidt, R.G., Loen, J.S., Wallace, C.A., and Mehnert, H.H., 1994, Geology of the Elliston region, Powell, and Lewis and Clark Counties, Montana: U.S. Geological Survey Bulletin 2045, 25 p., scale 1:48,000.

Sears, J.W., and Hendrix, M., 2004, Lewis and Clark line and the rotational origin of the Alberta and Helena Salients, North American Cordillera, *in* Sussman, A.J., and Weil, A.B., eds., Orogenic curvature: integrating paleomagnetic and structural analyses: Geological Society of America Special Paper 383, p. 173-186.

Sears, J.W., Hendrix, M., Webb, B., and Archibald, D., 1998, Constraints on deformation of the northern Rocky Mountain fold-thrust belt in Montana from $^{40}Ar/^{39}Ar$ geochronology of andesite sills: American Association of Petroleum Geologists Annual Convention, Salt Lake City, Utah, Abstract 587.

Smedes, H.W., 1966, Geology and igneous petrology of the northern Elkhorn Mountains, Jefferson and Broadwater Counties, Montana: U.S. Geological Survey Professional Paper 510, 116 p.

Stickney, M., 2015, Seismicity within and adjacent to the eastern Lewis and Clark Line, west-central Montana: Northwest Geology, v. 44.

Trombetta, M.J., 1987, Evolution of the Eocene Avon Volcanic Complex, Powell County, Montana: Bozeman, Montana State University, M.S. thesis, 112 p.

Trombetta, M.J., and Berg, R.B., 2012, Geologic map of the Avon 7.5′ quadrangle, Powell County, Montana: Montana Bureau of Mines and Geology GM 63, scale 1:24,000.

Vuke, S.M., Porter, K.W., Lonn, J.D., and Lopez, D.A., 2007, Geologic Map of Montana: Montana Bureau of Mines and Geology Geologic Map 62A, 73 p., 2 sheets, scale 1:500,000.

Wallace, C.A., Lidke, D.J., and Schmidt, R.G., 1990, Faults of the Lewis and Clark line and fragmentation of the Late Cretaceous foreland basin in west-central Montana: Geological Society of America Bulletin, v. 102, p. 1021-1037.

Winston, D., 1986a, Sedimentology of the Ravalli Group, middle Belt carbonate, and Missoula Group, Middle Proterozoic Belt Supergroup, Montana, Idaho, and Washington, *in* Roberts, S.M., ed., Belt Supergroup: A guide to Proterozoic rocks of western Montana and adjacent areas: Montana Bureau of Mines and Geology Special Publication 94, p. 85-124.

Winston, D., 1986b, Sedimentation and tectonics of the Middle Proterozoic Belt Basin, and their influence on Phanerozoic compression and extension in western Montana and northern Idaho, *in* Peterson, J.A., ed., Paleotectonics and sedimentation in the Rocky Mountain region, United States: American Association of Petroleum Geologists Memoir 41, p. 87-118.

Winston, D., 2013, Analysis of sheetflood fluvial systems in the Middle Proterozoic Belt Supergroup, northern Idaho and northwestern Montana: Northwest Geology, v. 42, p. 71-74.

Winston, D., and Link, P.K., 1993, Middle Proterozoic rocks of Montana, Idaho, and eastern Washington: Belt Supergroup, *in* Reed, J.C., Bickford, M.E., Houston, R.S., Link, P.K., and Ranking, D., eds., The Geology of North America: Precambrian, Conterminous U.S.: Boulder, Colorado, Geological Society of America, the Geology of North America, the Decade of North American Geology (DNAG) v. C-2, p. 487-517.

Winston, D., and Sears, J.W., 2013, Stratigraphy of the Proterozoic Belt Supergroup and structure of the Belt Basin: Glacier National Park and Blackfoot River Canyon, Montana: Northwest Geology, v. 42, p. 237-256.

Witkind, I.J., and Weber, W.M., 1982, Reconnaissance geologic map of the Big Fork-Avon environmental study area, Flathead, Lake, Lewis and Clark, Missoula, and Powell Counties, Montana: U.S. Geological Survey Miscellaneous Investigations Series Map I-1380, scale 1:125,000.

Wittkop, C., 2009, Glacial sediments of the Little Blackfoot River Valley, Montana: revisiting the Pleistocene Boulder Mountains ice cap: Geological Society of America Rocky Mountain Section Abstracts with Programs, v. 41, no. 6, p. 13.

SEISMICITY WITHIN AND ADJACENT TO THE EASTERN LEWIS AND CLARK LINE, WEST-CENTRAL MONTANA

Michael Stickney

Montana Bureau of Mines and Geology, 1300 W. Park Street, Butte, MT 59701, mstickney@mtech.edu

INTRODUCTION

The Intermountain Seismic Belt (ISB) transects western Montana, extending from Yellowstone National Park northwestward to northwestern Montana (fig. 1). The ISB is defined by a 100 km-wide general pattern of shallow diffuse seismicity with embedded clusters of dense activity and some areas of low seismicity. Recent seismicity does not sharply define the margins of the ISB except in an area just south of Helena where the ISB's western edge makes a sharp right-angle bend from NNE to WNW coincident with the southern edge of the Lewis and Clark Line (LCL), suggesting that faults within this structural feature accommodate recent earthquakes. This paper discusses the distribution of more than 13,000 earthquake locations and 157 well-determined fault plane solutions with respect to post-Laramide faults in the eastern part of the LCL, and Quaternary faults north and south of the LCL.

The LCL is a WNW-trending, 80 km-wide fault and fold zone that extends 400 km ESE from near the Montana-Idaho border to east of Helena, MT. The LCL includes at least a dozen major faults with a long history of movement. Variations in Belt Basin sedimentation indicate displacement along some LCL faults during the middle Proterozoic (Harrison and others, 1974). Some faults accommodated sinistral transpression during Cretaceous to Paleocene crustal shortening, which resulted in a "flower structure" between the large thrust plates north and south of the LCL (Sears and Hendrix, 2004). Regional crustal extension that began in the middle Tertiary and that continues today reactivated LCL faults with dextral and normal offsets (Wallace and others, 1990; and Reynolds, 1979).

Pardee (1950) recognized that the youngest movement on many western Montana faults was normal slip along mountain range fronts in response to the extensional tectonic forces that succeeded Laramide compression. Witkind (1975) compiled the first western Montana Quaternary fault map based on information from colleagues. This map contained inconsistencies because Witkind did not specify the field relationships that define Quaternary offset. Stickney and Bartholomew (1987) visited most of western Montana's Quaternary faults and applied more uniform criteria to classify the ages of last movements. Their data, although in many cases still reconnaissance level, were incorporated into the Quaternary Fault and Fold database (USGS, 2015a) that remains the authoritative source on Quaternary faults in Montana. Faults with identified late Quaternary surface offset extend southward from the Helena area and northward from the LCL but a prominent gap in recognized Quaternary faults exists between Missoula and Helena (fig. 1).

MONTANA REGIONAL SEISMIC NETWORK

Although Montana has a long history of destructive and deadly earthquakes (Qamar and Stickney, 1979), continuous monitoring by a permanent regional seismograph network did not begin until l980, when the Montana Bureau of Mines and Geology (MBMG) upgraded an antiquated seismograph station in Butte. As resources permitted, the MBMG expanded seismic monitoring coverage to most of western Montana. By 1982, the Montana regional seismic network included enough stations to determine earthquake locations and magnitudes and begin publishing an earthquake catalog. Major network improvements occurred in 1995 when a cooperative effort with the Confederated Salish and Kootenai Tribes established six new stations on the Flathead Reservation to provide approximately 5,500 km2 of coverage in the Mission Valley-southern Flathead Lake region, and in 1996 when a U.S. Geological Survey (USGS) grant provided funding to deploy nine stations to cover 11,500 km2 of the LCL from Helena to the Montana-Idaho border.

Prior to 1990, seismic data were recorded exclusively on paper seismograms. In August 1990,

MBMG implemented triggered digital recording. In 1999, the MBMG established continuous digital recording and real-time seismic-data exchange with networks in surrounding states and provinces. The capability to exchange data in real time dramatically increased the number and quality of earthquake hypocenter locations in the Montana earthquake catalog. A significant, though temporary, improvement to the regional monitoring accompanied the deployment of the EarthScope Transportable Array stations in Montana from 2006 to 2009 (IRIS, 2015). EarthScope deployed 400 high-quality seismograph stations on a grid with an average spacing of approximately 70 km for about two years at each recording site. Transportable Array data, from 83 stations deployed in Montana, combined with data from the Montana regional seismograph network provided some of the most robust hypocenter locations and fault plane solutions ever generated in Montana.
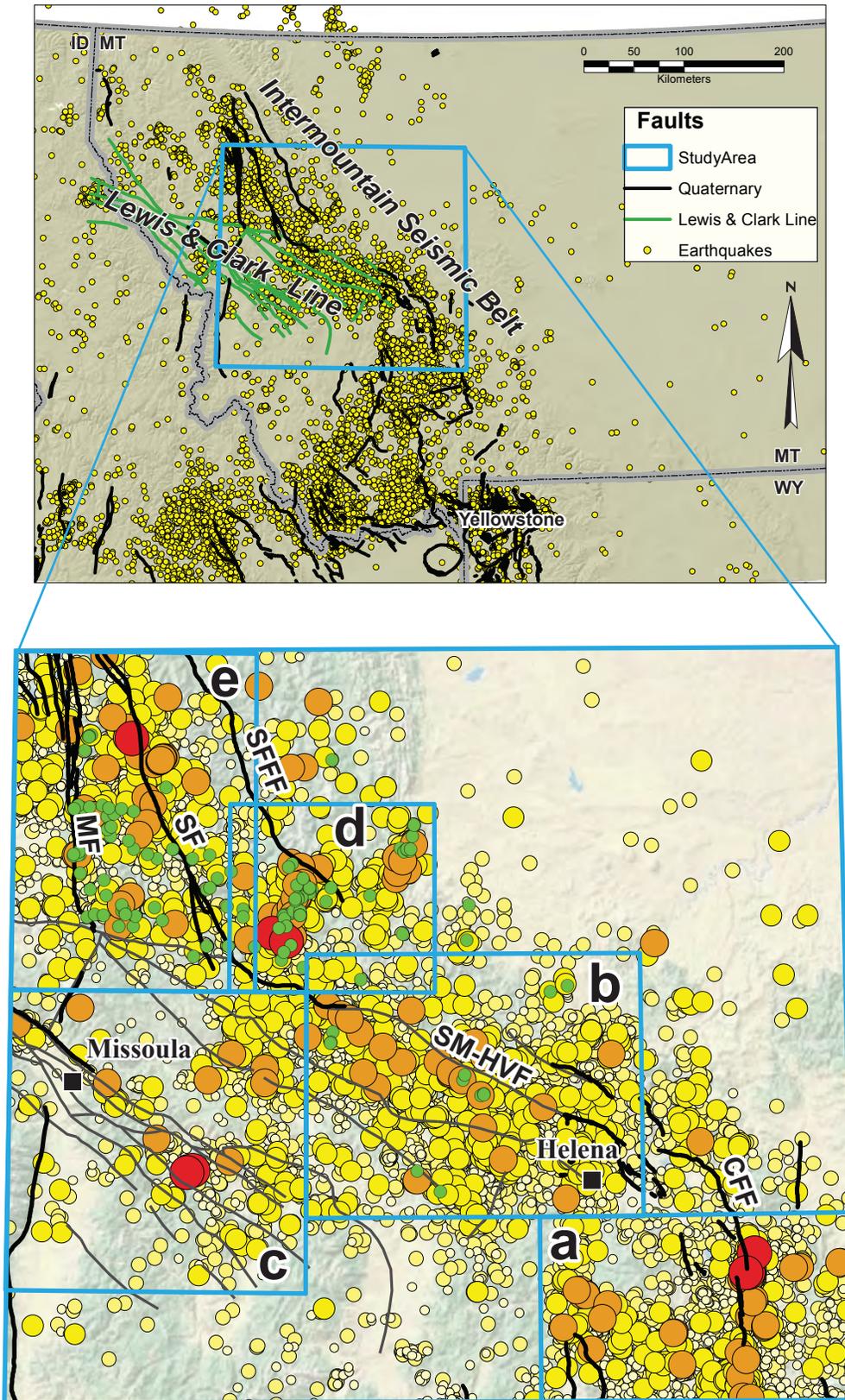
Figure 1. Upper panel: epicenter locations for earthquakes of magnitude 1.5 and larger that occurred from January 1982 through March 2015 define the Intermountain Seismic Belt. Black lines show Quaternary faults, green lines show LCL faults. Blue rectangle shows the study region. Lower panel: Over 13,000 earthquake epicenters scaled by magnitude; red dots show earthquakes with magnitudes of 4.0 to 4.9. Green dots show well-located earthquakes with hypocenter depths of 20 km or more. Black lines show Quaternary faults; grey lines show older LCL faults. Rectangles delineate areas of Figures 2-6: a-Townsend, b-Helena, c-Missoula, d-Southern Swan, and e-Swan-Mission. Labeled faults are: CFF-Canyon Ferry Fault, SM-HVF-St. Mary's-Helena Valley Fault, SFFF-South Fork Flathead Fault, SF-Swan Fault, and MF-Mission Fault.

TOWNSEND REGION

The Townsend region includes the ISB that extends along the Missouri River Valley from just north of Three Forks to the midpoint of Canyon Ferry Reservoir and west to about Boulder (fig. 2). Quaternary faults include the Lower Duck Creek Fault; and the southern and Toston segments of the Canyon Ferry fault, which flank the west side of the Big Belt Mountains. West of Canyon Ferry Reservoir along the east flank of the Elkhorn Mountains is the Beaver Creek Fault. These faults form a broad, north-trending graben, along the axis of which the Missouri River flows northward into Canyon Ferry Reservoir.

In the southwest corner of the Townsend region, the Bull Mountain western border fault and the Boulder River Valley western border fault flank the Bull Mountain horst. In the extreme southeast corner, the northernmost end of the Bridger Fault flanks the west side of the Bridger Range. These Quaternary faults form a discontinuous network of north-trending structures typical of the northern Basin and Range Province.

Three areas of dense seismicity occur in the Townsend region: the Clarkston Valley-Toston area, the Sixmile Creek area, and an area east of Townsend (fig. 2; areas a, b, and c). A diffuse band of seismicity extends from the Clarkston Valley northwestward to Boulder where there is a fourth area of elevated seismicity (fig. 2d). The Elkhorn Mountains to the northeast of Boulder exhibit little to no seismicity and this relatively quiet zone extends east-northeastward across the southern half of Canyon Ferry reservoir into the central Big Belt Mountains. The quiet zone includes the Missouri River Valley which is flanked by Quaternary faults on both sides.

The Clarkston Valley seismicity cluster coincides with the 1925 Clarkston Valley earthquake (Montana's second largest historic quake) which had a magnitude of 6.6; caused significant damage to brick buildings in Three Forks, Manhattan, and White Sulphur Springs; triggered numerous rockfalls from railroad cuts in the epicentral region; and was felt throughout an area of 800,000 km2 at a maximum of 10 on the Rossi-Forel intensity scale (Pardee, 1926) (equivalent to intensity 8 on the now-widely used Modified Mercalli Intensity scale). Using historic seismograms recorded at tele-

seismic distances, Doser (1989) determined a fault plane solution for the 1925 earthquake that indicates oblique-normal slip. The west-dipping Clarkston Valley Fault cuts late Tertiary sediments and bounds the eastern margin of the Clarkston Valley but is not recognized as a Quaternary fault (Pardee, 1926; Vuke and Stickney, 2013).The nodal planes from Doser's (1989) fault plane solution are incompatible with potential slip on the Clarkston Valley Fault. Qamar and Hawley (1979) reported fault plane solutions from the Clarkston Valley that show both normal and strike-slip faulting.

The Clarkston Valley seismicity cluster (fig. 2; a) is by far the most active source zone in the Townsend region. Since routine reporting of earthquakes began in 1982, the MBMG has located over 1,300 earthquakes in the Clarkston Valley. The largest modern earthquake occurred on January 1, 1984, had a magnitude of 3.8, and was part of a swarm of 137 earthquakes that began December 3, 1983 and continued through January 8, 1984. A second, swarm occurred April 4 through 20, 2012 that included 21 earthquakes, the largest of which was a magnitude 3.2 on April 7. Despite the high number of earthquakes in the Clarkston Valley cluster, only four earthquakes have exceeded magnitude 3.0 and only 18 have magnitudes from 2.5 to 2.9. Three of four fault plane solutions from the Clarkston Valley (fig. 2a) indicate normal faulting along north-trending faults and one fault plane solution indicates strike-slip faulting.

The Sixmile Creek seismicity cluster is compact group of epicenters lying about 20 km NNE of the Clarkston Valley (fig. 2b) that includes 90 events. This small source area produced only seven earthquakes prior to 2008 and only one earthquake since 2010. An earthquake swarm began August 20, 2008 that included 43 earthquakes, one with a magnitude of 3.5, during eight days. Another 19 earthquakes occurred during September, 2008. Three of four fault plane solutions from this cluster indicate strike-slip movement and one fault plane solution indicates normal slip along a northwest-trending fault (fig. 2; b).

A cluster of earthquakes centered 10 km NE of Townsend includes over 400 events (fig. 2; c). This cluster lies near the right-hand step-over between the southern end of the Canyon Ferry Fault's southern section and the northern end of the Canyon Ferry Fault's
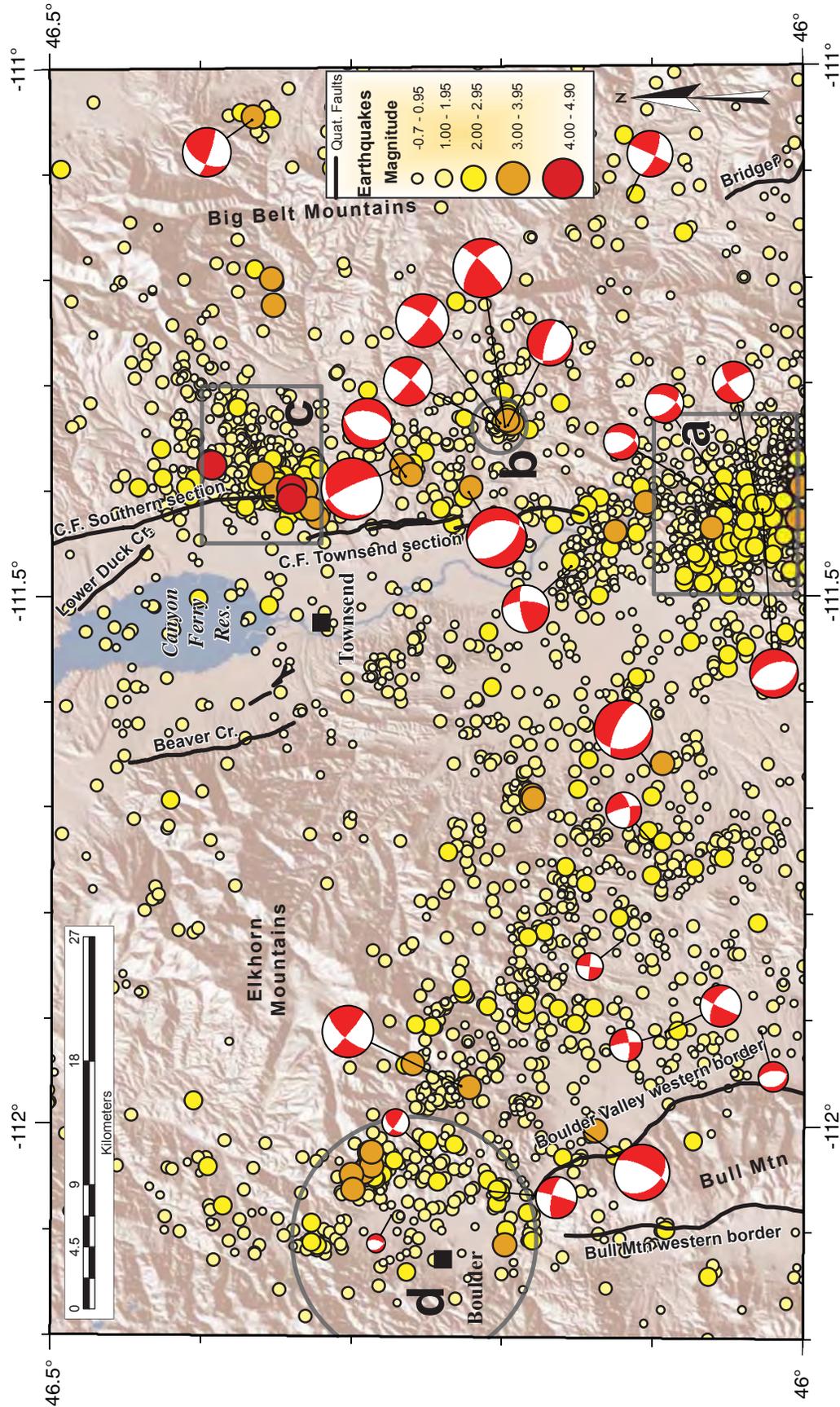
Figure 2. Epicenter locations for 3,724 earthquakes located within the Townsend region from January 1982 through March 2015. Faults from the Quaternary Fault and Fold Database (USGS 2015a) are shown as bold black lines. Fault sections labeled "C.F." indicate Canyon Ferry. Rectangles and circles indicate source zones discussed in text: a-Clarkston Valley; b-Sixmile Creek; c-east of Townsend; and d-Boulder.

Toston section. The Townsend cluster is dominated by a swarm of 75 earthquakes that occurred from March 22 through July 29, 2000 and includes two earthquakes of magnitude 4.0 as well as six earthquakes with magnitudes from 3.0 to 3.4. From August 2000 through mid-January 2001, an additional 45 earthquakes occurred in this source area including a magnitude 4.0 earthquake on November 10, 2000 that occurred in the footwall block of the Canyon Ferry Fault, six km NNE of the earlier magnitude 4.0 events. Local residents reported feeling 24 of the earthquakes in this swarm. Because the Townsend cluster lies near the edge of the Montana regional seismic network, insufficient data are available from which to calculate reliable fault plane solutions, but most of these hypocenters occurred in the footwall block of the Canyon Ferry Fault.

Seismicity occurs along the north, east, and southern margins of the Boulder Valley, but diminishes south of the northern tips of the faults bounding Bull Mountain (fig. 2d). The most significant seismicity occurred as two swarms, the first included 18 earthquakes from July 7 through July 22, 1986, with two earthquakes of magnitude 3.4. The second swarm, from October 18 through November 12, 1986, included 40 additional earthquakes with five events ranging from magnitude 3.2 to 3.5. Six of the seven magnitude 3+ earthquakes occurred at the northeastern corner of Boulder Valley but the September 9, 1986, M 3.3 earthquake occurred at the southern edge of Boulder Valley. Two of three Boulder Valley fault plane solutions indicate strike-slip faulting; one solution indicates normal faulting (fig. 2d).

Two fault plane solutions from the Big Belt Mountains, east of the Missouri River Valley, indicate strike-slip faulting (fig. 2). Three of four fault plane solutions along the Missouri River Valley, between the Clarkston and Townsend clusters, indicate normal faulting on north-trending faults and one solution indicates strike-slip faulting. Within the band of seismicity extending northwestward between the Clarkston Valley and Boulder, three fault plane solutions indicate normal faulting on north-to-northwest-trending faults and five solutions indicate strike-slip faulting.

HELENA REGION

In 1935, the western Helena Valley hosted an energetic swarm that produced a magnitude 6.3 earthquake on October 18 and a magnitude 6.0 on October 31 (Qamar and Stickney, 1983). In Helena, these earthquakes caused structural damage to 60 percent of the buildings and falling building debris killed four people. From October 3, 1935 to April 30, 1936, local observers reported feeling 1,880 earthquakes (Scott, 1936). Data from a strong motion seismograph installed in the Lewis and Clark County courthouse just before the October 31 event showed that earthquakes occurred within the southwest Helena Valley only 5 to 7 km from downtown Helena.

Doser (1989) constructed fault plane solutions for the October 18 and October 31, 1935 earthquakes that indicate strike-slip faulting, right-lateral motion if the east-west nodal planes represent the fault planes. Freidline and others (1976) operated a temporary seismograph network northwest of Helena and determined three composite fault plane solutions; two solutions indicated normal slip on northwest-trending fault and one solution indicated strike-slip faulting. Stickney (1978) reported two composite fault plane solutions from the Scratchgravel Hills area just north of Helena; one solution indicated northwest-trending normal faulting and one solution indicated strike-slip faulting.

Since 1982, diffuse seismicity occurred throughout the western Helena Valley, similar to areas farther west along the LCL (fig. 3). Western Helena Valley seismicity includes 226 earthquakes (fig. 3a), none of which have magnitudes over 3.0 and none as swarms. Since 2000, only two earthquakes have had magnitudes over 2.0 but 24 earthquakes from 1982 through 1999 had magnitudes ranging from 2.0 to 2.7, indicating low seismicity levels for this area during the past 15 years. Local residents reported feeling or hearing most earthquakes with magnitudes greater than 2.5, which suggests that Scott's (1936) 1935-36 earthquake compilation probably includes earthquakes down to about magnitude 2.5. A fault plane solution for one earthquake from the northern part of this area indicates strike-slip faulting (fig. 3a), right-lateral if the WNW-trending nodal plane represents the fault.
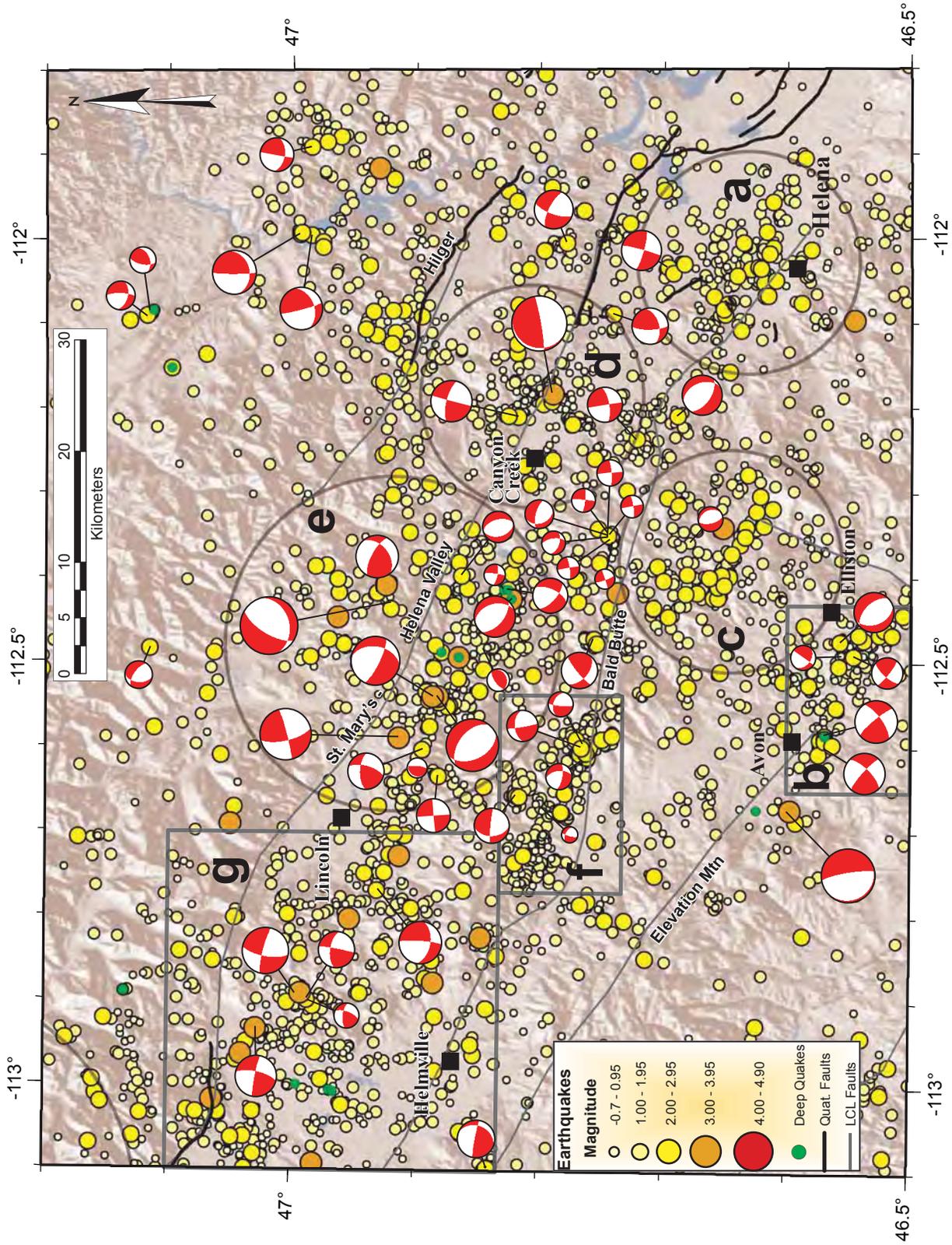
Figure 3. Epicenter locations for 3,372 earthquakes located within the region northwest of Helena from January 1982 through March 2015. Green dots show well-located earthquakes with hypocenter depths 20 km or more. Faults from the Quaternary Fault and Fold Database (USGS 2015a) shown as bold black lines. LCL faults from Wallace et al. (1990) are shown as thin grey lines. Rectangles and circles highlight source zones discussed in text: a-Helena; b-Avon-Elliston; c- Mullan Pass; d- Canyon Creek; e-Lincoln; f-Nevada Creek; g-Kleinschmidt.

The cluster of seismicity in the Avon-Elliston area (fig. 3b) includes 174 earthquakes that have occurred since 1982 in sporadic bursts with intervening quiescent periods lasting up to two years. The largest earthquake, a magnitude 3.0 that occurred September 28, 2009, was followed by 15 earthquakes over the next 16 hours and is characteristic of a main shock-aftershock sequence. This source area has produced 22 earthquakes with well-determined hypocenter depths ranging from 18 to 24 km, significantly deeper than typical ISB earthquakes, which typically originate from 3 to 16 km below the surface. Three fault plane solutions for this cluster (fig. 3b) indicate strike-slip faulting and two solutions indicate normal faulting.

Although the majority of seismicity northwest of Helena is concentrated between the St. Mary's-Helena Valley and the Bald Butte faults, an exception is the concentration of seismicity located between the Bald Butte Fault and Elliston near Mullan Pass, which includes 222 earthquakes (fig. 3c). A swarm of 45 earthquakes occurred from June 27 through July 9, 1993; the largest was magnitude 2.7. The largest recorded earthquake in this source area had a magnitude of 3.1 on October 31, 1995 but had no other associated seismicity. Only three earthquakes since 2000 have had magnitudes of 2.0 or larger, but 23 earthquakes during the previous 18 years had magnitudes of 2.0 or larger. This pattern of relatively low seismicity since 2000 resembles the temporal seismicity pattern observed in the western Helena Valley. A fault plane solution from the Mullan Pass area indicates normal slip on a NNW-trending fault (fig. 3c).

Prior to 2010, a seismicity cluster that straddles the St. Mary's-Helena Valley Fault near Canyon Creek (fig. 3d) included sporadic earthquake activity of magnitudes less than 2.2. From November 30, 2010 through January 25, 2011 a swarm of 40 earthquakes, the largest of which occurred on January 16, 2011 with a magnitude of 3.7, was felt by local residents. Collapse of an abandoned mine stope beneath a ski run on Mount Belmont was attributed to shaking from this earthquake. Seismicity following the swarm in 2010-2011 is significantly elevated compared to the pre-swarm rate. One of two fault plane solutions from this cluster indicates strike-slip faulting with a nodal plane parallel to the St. Mary's-Helena Valley Fault indicating dextral slip and the other solution indicates oblique-normal slip with a vertical nodal plane trending ENE-WSW (fig. 3d).

The area southeast of Lincoln (fig. 3e) has produced 390 earthquakes since 1982, the majority of which lie south of the St. Mary's-Helena Valley Fault. Nine earthquakes have magnitudes from 3.0 to 3.9; the largest occurred 15 km ESE of Lincoln on April 1, 1993, but had no other associated seismicity. Despite the relatively high level of recent seismicity, no swarms or aftershock sequences occurred in this area. Following an earthquake of magnitude 3.5 on April 23, 2014, the Stemple Pass area, 15 km southeast of Lincoln, experienced a magnitude 3.6 earthquake on September 28 and a magnitude 3.3 on October 15. In addition, 28 small earthquakes occurred between September and the end of 2014. Thirteen earthquakes have well-determined hypocenters 18 to 22 km below the land surface. Three fault plane solutions indicate strike-slip faulting, five normal faulting, one oblique-normal faulting, two reverse faulting, and two oblique-reverse faulting (fig. 3e). In contrast to most other areas, one of the normal fault plane solutions indicates slip on a north-east trending fault. The presence of reverse and oblique-reverse fault plane solutions indicate local areas of compressional stress.

Seismicity near Nevada Creek (fig. 3f) is mainly north of the Bald Butte Fault near the north end of the Avon Valley where more than 430 earthquakes have occurred since 1982. Prior to 2005, seismicity occurred as intermittent bursts of activity with magnitudes up to 2.5 interspersed with quiet periods lasting up to two years. From 2005 through 2007, nearly 60 percent of the earthquakes occurred in three swarms: February 3-March 17, 2005—32 events with maximum magnitude 2.6 on February 8; March 1-May 29, 2006—75 events with maximum magnitude 2.7 on April 25; and December 22, 2006-May 3, 2007—74 events with maximum magnitude 2.1 on December 24, 2006. The majority of the swarm events occurred in a tight 2-km-diameter cluster about one km east of where Nevada Creek enters the Avon Valley and apparently originated within the footwall block of the valley-bounding fault on the northeast side of the Avon Valley. Two small clusters of seismicity located 6 and 8.5 km northwest of the primary swarm cluster were active during these swarms. Recent seismicity levels are low, with only three earthquakes since

2013. Five fault plane solutions from this area indicate oblique-normal faulting (fig. 3f).

Seismicity west of Lincoln and north of Helmville in the Kleinschmidt Flat area (fig. 3g) occurs primarily between the St. Mary's-Helena Valley and Bald Butte faults. This area has experienced 564 earthquakes since 1982 but none of them occurred as swarms. The largest earthquake was a magnitude 3.7 on September 15, 1998 that occurred 10 km northeast of Ovando, but had no aftershocks. Prior to 1999, nine earthquakes of magnitude 3.0 or larger occurred in the region, but only one earthquake of magnitude 3.0 has occurred since. Four fault plane solutions from this area (fig. 3g) indicate strike-slip faulting and a fifth solution indicates oblique normal faulting.

Nineteen fault plane solutions have been computed for Helena region earthquakes but from outside the source zones discussed above (fig. 3). Seven solutions indicate strike-slip faulting, five indicate normal faulting, five indicate oblique-normal faulting, and two indicate oblique-reverse faulting.

MISSOULA REGION

Since 1982, the largest earthquakes along the LCL between Missoula and Helena occurred in the Rock Creek area 30 km west of Drummond (fig. 4a). From 1982 to 2000, only one small earthquake had been recorded in this area, but on June 28-29, 2000, a magnitude 4.5 earthquake was followed by 11 aftershocks. Only 24 earthquakes, none larger than magnitude 2.1, occurred during the following 11.4 years. On November 11, 2011 a magnitude 4.1 earthquake was followed by 14 aftershocks during a 10-day period. Another 18 events—including two earthquakes of magnitude 3.5 and 3.4—were recorded during the next year. No earthquakes larger than magnitude 1.0 have occurred since 2013. This source area is characterized by main shock-aftershock sequences separated by periods of low seismicity. Of four fault plane solutions from the Rock Creek cluster (fig. 4; a), two indicate strike-slip faulting, one indicates oblique-normal faulting, and one indicates oblique-reverse faulting. All four fault plane solutions have a nodal plane nearly parallel to nearby LCL faults.

The Clearwater Junction area (fig. 4b), about 50

km ENE of Missoula, has had a steady rate of seismicity since 1982 that lacks swarms or main shock-aftershock sequences. A quiet period occurred in this area from mid-1994 through mid-1996 when there were no locatable earthquakes. Only four earthquakes have exceeded magnitude 3.0, the largest was a magnitude 3.2 event on July 6, 1991. Two fault plane solutions indicate normal slip along north or northwest-trending faults, one solution indicates strike-slip faulting, and three solutions indicate oblique-normal faulting (fig. 4b). A magnitude 4.9 earthquake occurred in this area on April 28, 1978 with a fault plane solution that is consistent with right-lateral strike slip movement on a N65°W-striking fault (Qamar and Stickney, 1983).

The Frenchtown area (fig. 4c), about 20 km northwest of Missoula, includes a 10-km-diameter cluster of 82 earthquakes located south of the Ninemile Fault. The MBMG located a single magnitude 2.2 earthquake in this are from 1982 through 1998, at a time when seismic monitoring coverage was minimal. A magnitude 3.2 earthquake, followed by two small aftershocks on September 5, 1999, is the area's largest earthquake to date. Since seismic monitoring coverage improved in the late 1990s, the MBMG locates an average of about 5 events with magnitudes less than 2.0 annually in this area. Fault plane solutions for three earthquakes indicate strike slip faulting with a right-lateral sense of slip, if the west-to-northwest-trending nodal planes—which parallel nearby LCL faults—represent the fault plane (fig. 4c). Stickney (2011) reported on seismicity in the Alberton-Frenchtown area west of this map, and determined an average T-axis orientation of S88°W, dipping 10° based on 13 fault plane solutions.

Of three fault plane solutions for earthquakes near Drummond (fig. 4d), two indicate north-south normal faulting and one indicates strike-slip faulting. The northwest-trending nodal plane of the strike-slip solution is parallel to nearby LCL faults and is consistent with right-lateral faulting. One fault plane solution for an earthquake north of Missoula indicates normal faulting on a northwest-trending fault and two solutions for earthquakes southeast of Missoula indicate and oblique normal faulting.
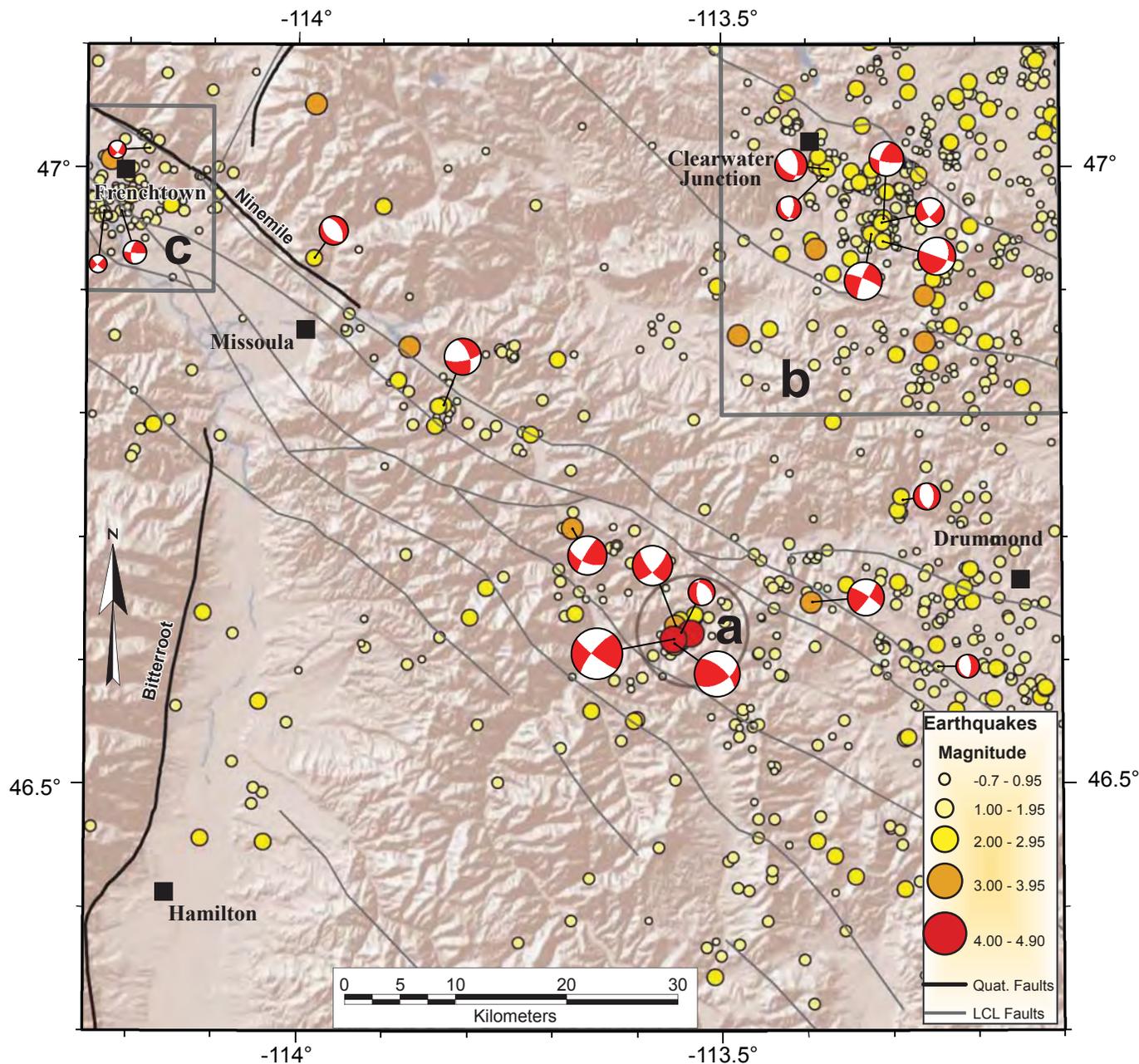
Figure 4. Epicenter locations for 922 earthquakes located within the Missoula region from January 1982 through March 2015. Bold black and thin grey lines show Quaternary and LCL faults, respectively. Rectangles and circles indicate source zones discussed in text: a-Rock Creek; b-Clearwater; c-Frenchtown.

SOUTHERN SWAN REGION

The southern Swan region (fig. 5) covers the southern Swan Mountains and part of the Lewis and Clark Range, north of the WNW-trending St. Mary's-Helena Valley Fault that locally defines the northern edge of the LCL. From its southern tip in the Monture Creek region (fig. 5a), the South Fork Flathead Fault trends N45°W for 25 km to where it bends to about N25°W. The trace of the St. Mary's-Helena Valley Fault similarly changes from WNW to NW where it intersects the Swan Fault near the southwestern edge of this area.

Extending for about 40 km between the St. Mary's-Helena Valley and South Fork Flathead faults with a trend of about N30°E, is a zone of more than 600 earthquakes (fig. 5a). Since 1982, the Monture Creek zone has produced three earthquakes with magnitudes ranging from 4.0 to 4.9, and 16 earthquakes with magnitudes ranging from 3.0 to 3.9. The magnitude 4.9 earthquake occurred on April 1, 1985 and was followed by 12 aftershocks during four days. All of the other large earthquakes in this source zone had minimal aftershock sequences. The Monture Creek zone has produced no notable swarms.
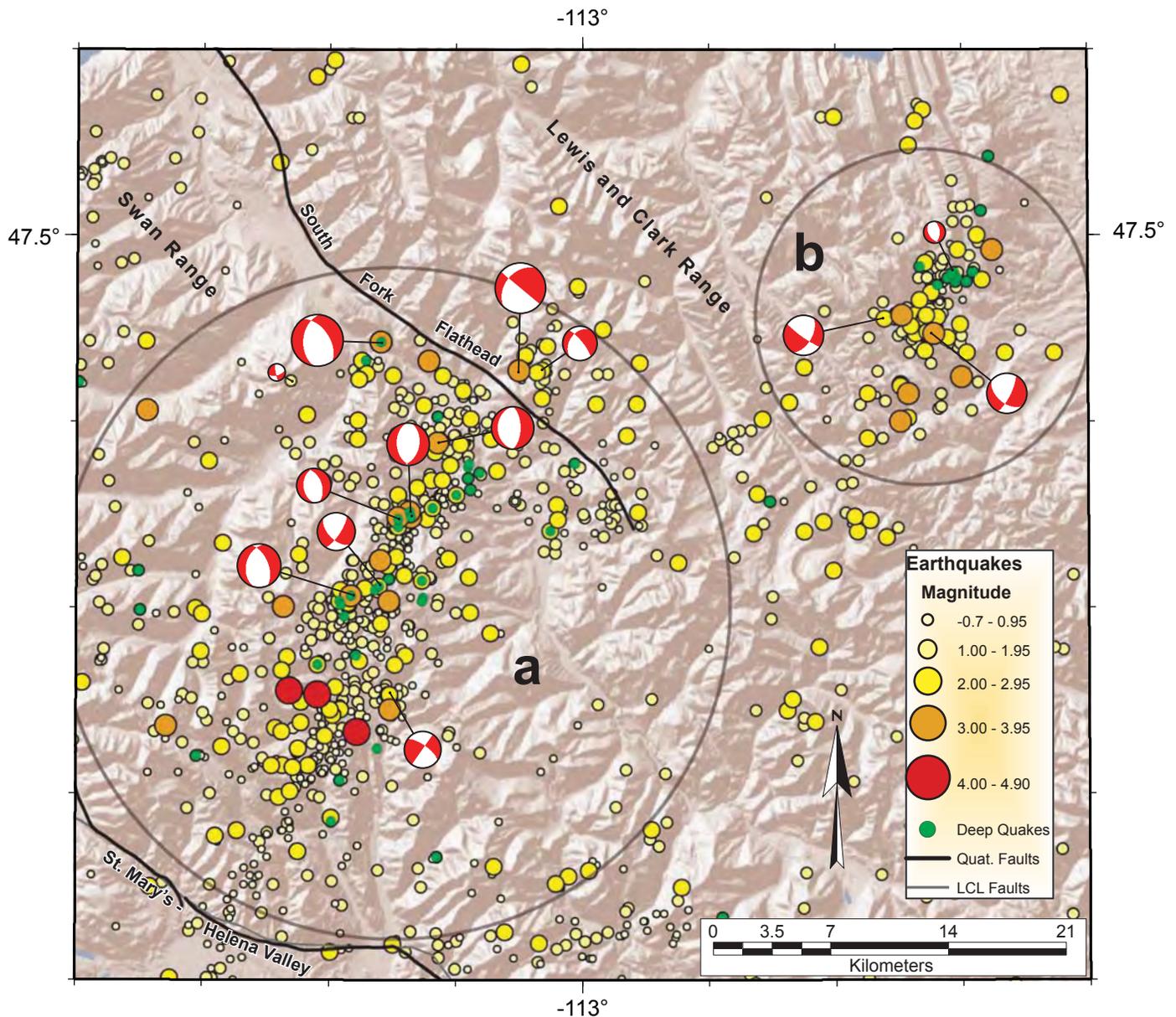
Figure 5. Epicenter locations for 1,091 earthquakes located within the southern Swan Mountains region from January 1982 through March 2015. Green dots show well-located earthquakes with hypocenter depths 20 km or more. Bold black and thin grey lines show Quaternary and LCL faults, respectively. Circles indicate source zones discussed in text: a-Monture Creek; b-Ford Creek. Solid black lines show Quaternary faults, dashed lines show LCL faults.

For earthquakes in the Monture Creek area prior to 1996, seismic monitoring was inadequate to provide reliable hypocenter control. Much of the Monture Creek zone lies within roadless and wilderness areas where seismograph stations have not been operated. However, since expansion of the Montana regional seismograph network into the LCL in 1996, adequate data exist with which to reliably constrain hypocenter depths for many events in the Monture Creek area. More than 50 percent of the earthquakes with adequate data have calculated hypocenter depths greater than or equal to 18 km, which is deeper than usual for ISB seismicity.

Eleven earthquakes in the Monture Creek source zone have fault plane solutions (fig. 5a). Five earthquakes located to the southwest of the South Fork Flathead Fault have fault plane solutions that indicate normal slip on north-trending faults; three solutions indicate strike-slip faulting. If these fault plane solutions adequately characterize fault movement, then the Monture Creek source zone may result from slip on a series of short, north-trending, en echelon normal faults oblique to the south end of the South Fork Flathead Fault. The strike-slip solutions may represent earthquakes that transfer extension between normal faults. The two earthquakes with fault plane solutions located in the footwall block immediately northeast of the South Fork Flathead Fault, exhibit oblique-normal

slip with a near-vertical nodal plane that parallels the nearby fault. All 10 fault plane solutions in this source zone are consistent with east-west extension despite the northwest strikes of nearby Quaternary faults.

The Ford Creek source zone (fig. 5b) is a modest cluster of seismicity in the southern Lewis and Clark Range just west of the Rocky Mountain Front. This source zone includes 150 earthquakes, the largest of which had a magnitude of 3.9 on March 17, 1983, that was followed by four aftershocks during seven days. Six other earthquakes had magnitudes ranging from 3.0 and 3.4 but there have been no earthquake swarms. Eighty percent of these earthquakes have computed hypocenter depths of 18 km or greater, however, the Ford Creek zone is too distant from the Montana regional seismic network coverage to reliably determine hypocenter depths. However, from 2007 to 2009, EarthScope Transportable Array data (IRIS, 2015) supplemented the Montana network data for 12 earthquakes in the Ford Creek source zone. Hypocenter depths for all 12 earthquakes during this period of improved monitoring coverage were from 18 to 31 km below the surface, lending credibility to the occurrence of unusually deep seismicity in this source zone. Two fault plane solutions indicate oblique-normal slip and the other indicates normal slip. All three are consistent with east-west extension (fig. 5b).

SWAN–MISSION REGION

The Swan-Mission region is mostly north of the LCL and includes the north- to NNW-trending late Quaternary Mission, Swan, and South Fork Flathead normal faults (fig. 6). All three of the faults dip to the west. At their southern ends, the Mission and Swan faults either terminate against or merge with the St. Mary's-Helena Valley Fault, which marks the northern margin of the LCL. The southern-most eight km of the Mission Fault bends to the southeast before intersecting the St. Mary's-Helena Valley Fault. Ostenaa and others (1995) reported a combination of normal and right lateral displacements of young glacial moraines along this section of the Mission Fault. To the north, where the Mission Fault trends north-south, displacement is normal. Ostenaa and others (1995) divided the Mission fault into two sections based on age of last surface rupture. To the north, the Flathead Lake segment has not produced surface rupture since the retreat of the Flathead Lobe of the Cordilleran ice sheet from the Polson moraine about 15 ka. Paleoseismic data from six trenches indicate that the southern 45 km-long Mission Valley segment last ruptured 7.7±0.2 ka with a previous event from 19 to 15 ka. These two segments meet immediately east of Pablo.

Relatively few earthquakes were detected and located in the Swan-Mission region until expansion of the Montana regional seismic network into the Flathead Valley in 1995 and along the LCL in 1996. Recent seismicity is widely distributed throughout the area east of the Mission Fault and north of Pablo and includes two significant seismicity clusters.

The Squeezer Creek cluster (fig. 6a) includes 1,008 earthquakes located in the hanging and footwall blocks of the Swan Fault. The cluster's largest earthquake had a magnitude of 4.3 and occurred April 1, 1992. Fifteen other earthquakes had magnitudes of 3.0 to 3.8. Nine of the magnitude 3+ earthquakes occurred during a period of accelerated seismicity that began in February 2005 and continued through March 2006, which included over 214 earthquakes. While significantly more active than the preceding or following intervals, this period of accelerated seismicity does not resemble a typical earthquake swarm because of its 13-month duration and low average rate of about 0.5 earthquakes daily. During its peak from June 27 through July 21, 2005 activity was more swarm-like with 67 earthquakes and included three events with magnitudes of 3.0 to 3.5.

Six fault plane solutions from the Squeezer Creek Cluster indicate strike-slip faulting and two others indicate oblique-normal faulting (fig. 6a). One oblique-normal fault plane solution lies west (down-dip) of the Swan Fault but is not consistent with normal-slip at depth on the Swan Fault because the nodal plane that most closely matches the fault's local strike dips to the east, opposite of the Swan Fault dip.

The North Crow Creek cluster (fig. 6b) lies just east of the Mission Fault and about 2-3 km south of the boundary between the Flathead Lake and Mission Valley segments. This cluster is elongated east-west with dimensions of approximately 5 by 2 km. A period of high seismicity that occurred from June 15 through December 31, 2000 includes 47 earthquakes; the maximum magnitude was 3.1. None of these earthquakes has a fault plane solution, but because they occurred
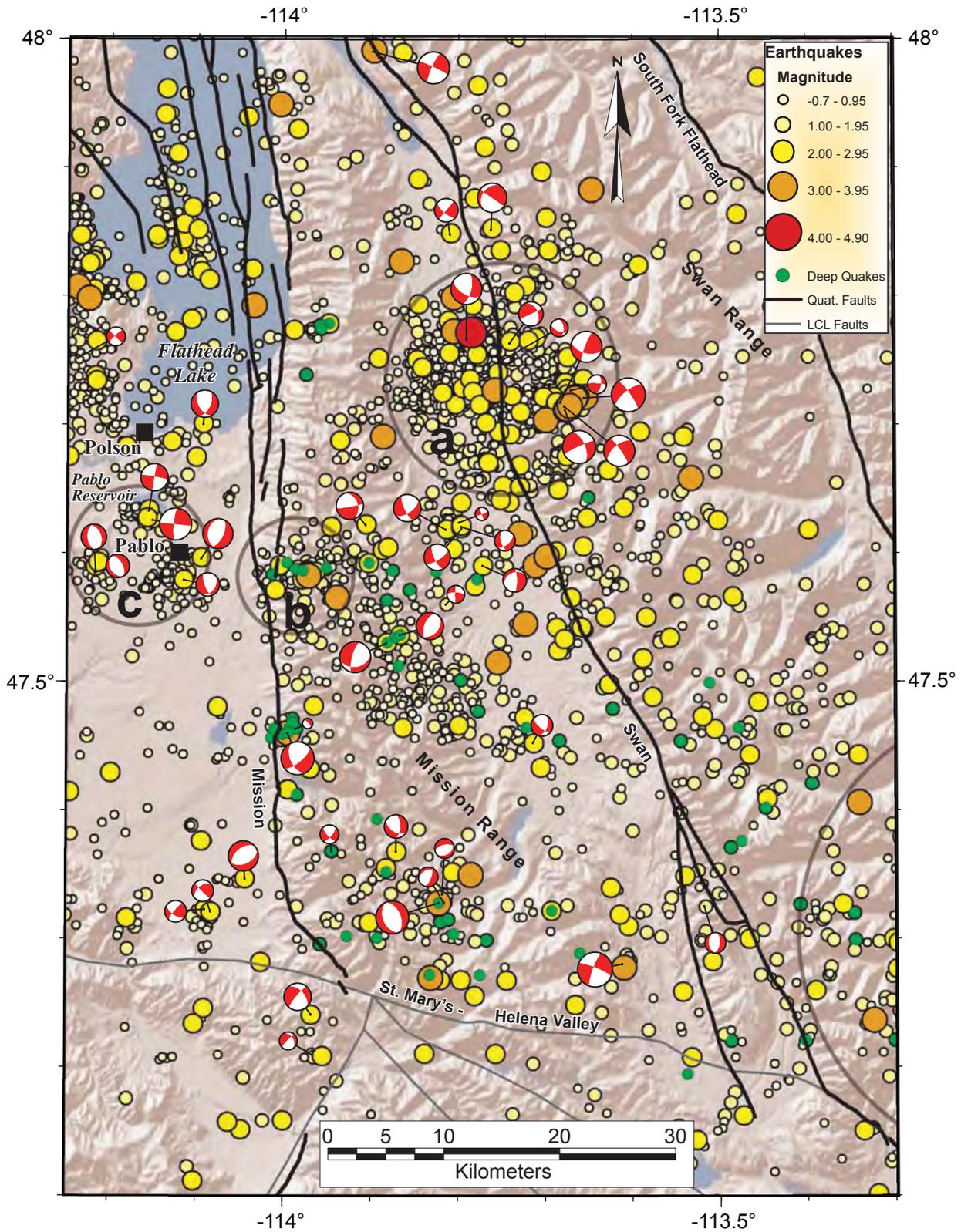
Figure 6. Epicenter locations for 3,012 earthquakes located within the southern Swan-Mission region from January 1982 through March 2015. Green dots show well-located earthquakes with hypocenter depths 20 km or more. Bold black and thin grey lines show Quaternary and LCL faults, respectively. Circles indicate source zones discussed in text: a-Squeezer Creek; b-North Crow Creek; c-Pablo.

within the footwall block of the Mission Fault, cannot be associated with the fault.

The Pablo cluster (fig. 6c) consists of three small groups of epicenters: 1) within two km of the town of Pablo; 2) eight km west of Pablo; and 3) northwest of Pablo beneath Pablo Reservoir. The centroid of the Pablo cluster lies 10 km west of where the Mission Fault's Flathead Lake and Mission Valley segments meet. Two fault plane solutions for earthquakes on March 18 and May 20, 2003 from the group nearest Pablo indicate normal slip along north-trending normal faults. The March 18, 2003 earthquake was 4.5 km west of the trace of the Mission Fault and the hypocenter has a well-determined focal depth of 19.9 ± 0.6 km. This hypocenter is too deep to lie on the plane of the Mission Fault based on reasonable estimates of fault dip (55° ± 15°). The May 20, 2003 earthquake was 6.3 km west of the Mission Fault at a depth of 13.3 ± 0.8 km, consistent with slip at depth on a 65° west-dipping Mission Fault.

Two fault plane solutions for earthquakes in the group centered eight km west of Pablo also indicate normal slip on north-trending normal faults. The April 5 and April 6, 2014 earthquakes were 13.8 and 13.6 km, respectively, west of the Mission Fault at depths of 16.0 ± 0.8 and 16.5 ± 1.2 km. The hypocenter depths and fault plane solutions are compatible with slip at depth along a 50° west-dipping Mission Fault.

The Pablo Reservoir group has two fault plane solutions that both indicate strike-slip faulting, either on north-south-trending, left-lateral or east-west-trending, right-lateral faults. Neither solution is consistent with movement on the Mission Fault at depth but the east-west nodal planes could perhaps represent a fault that accommodates differential slip between the Mission Valley and Flathead Lake segments of the Mission Fault.

South of the Pablo cluster, sparse seismicity is located west of the Mission Fault (fig. 6). This region down-dip of the Mission Fault is noticeably lacking in seismicity when compared to most other areas north of the LCL, indicating quiescence along the most recently active segment of the Mission Fault. The MBMG has located 30 earthquakes from 3-15 km west of the bend near the southern end of the Mission Fault. Two

fault plane solutions indicate strike-slip faulting and one indicates normal faulting on an ENE-trending fault—nearly perpendicular to the strike of the Mission Fault (fig. 6). Perhaps this slightly more active area in the otherwise low seismicity region west of the Mission Valley segment is related to space accommodation issues near the Mission Fault's 45° bend to the southeast.

North of the Pablo cluster, a north-trending band of seismicity coincides with the long axis of Flathead Lake and a second north-trending band of seismicity extends north from Polson along the west shore of Flathead Lake for about 20 km (fig. 6). One fault plane solution for recent Flathead Lake area seismicity indicates normal slip on a north-trending fault just east of Polson and a second solution indicates strike-slip motion for an earthquake about 10 km northwest of Polson (fig. 6).

Within the Mission Mountains and the Swan Valley, seismicity is wide spread and includes the previously discussed Squeezer Creek and North Crow Creek clusters. Relatively few earthquakes have been located in a 10 by 20 km area in the southern Mission Mountains near latitude 47.4° N as compared to areas immediately to the north and south (fig. 6). North and south of the quiet area, 45 earthquakes with well-determined hypocenters have depths ranging from 20.0 to 23.6 km. Twenty-one fault plane solutions from the Mission Mountains-Swan Valley (south of the Squeezer Creek and North Crow Creek clusters) area indicate both normal and strike-slip motions (fig. 6). Approximately one-third of these fault plane solutions indicate strike-slip movement, one-third normal slip, and the remainder oblique-normal faulting. The normal faults are predominately north-south, but two fault plane solutions east of the Mission Fault bend and two others at about 47.5°N latitude in the Mission Mountains trend northeast-southwest. Seven earthquakes with depths of 20 km or greater have fault plane solutions indicating normal slip, including the two northeast-trending normal faulting solutions near 47.5°N latitude. With the exception of the portion of the Squeezer Creek cluster that extends into the Swan Range, seismicity in the Swan Range is uniformly distributed along the length of the range within about 20 km of the Swan Fault (fig. 6).

T-AXIS ORIENTATIONS

The Montana regional seismograph network, adjacent permanent seismic networks, and the temporary Transportable Array have recorded adequate data from 157 earthquakes near or within the eastern LCL since 1990 to generate well-determined fault plane solutions. These solutions exhibit a variety of movements, but mostly describe strike-slip and normal faulting. The variety of types and orientations of faulting likely reflect the region's long tectonic history and many pre-existing planes of weakness available to the current stress field. The common factor for the majority of these fault plane solutions is an east-to-northeast, nearly horizontal, axis of minimum compressive stress (T-axes) and an orthogonal belt of maximum compressive stress (P-axes) trending north-south to NNW-SSE.

North of the LCL (marked by the St. Mary's-Helena Valley Fault), 62 fault plane solutions have an average T-axis orientation of N87°E and an average plunge of 4° (fig. 7a). The half apical angle is ± 32°. For 92 fault plane solutions within and south of the LCL, the average T-axis orientation is N68°E, the plunge is 2° (fig. 7c). The half apical angle is ± 31°. Although there is overlap in the uncertainty of these two data sets, they suggest a 19° clockwise rotation in the extensional direction from south to north across the northern boundary of the LCL. The nearly east-west extension direction to the north is consistent with the long northerly trending Quaternary faults and the ENE extension direction within and south of the LCL is similar to the S45°W±15° extension direction Stickney and Bar-
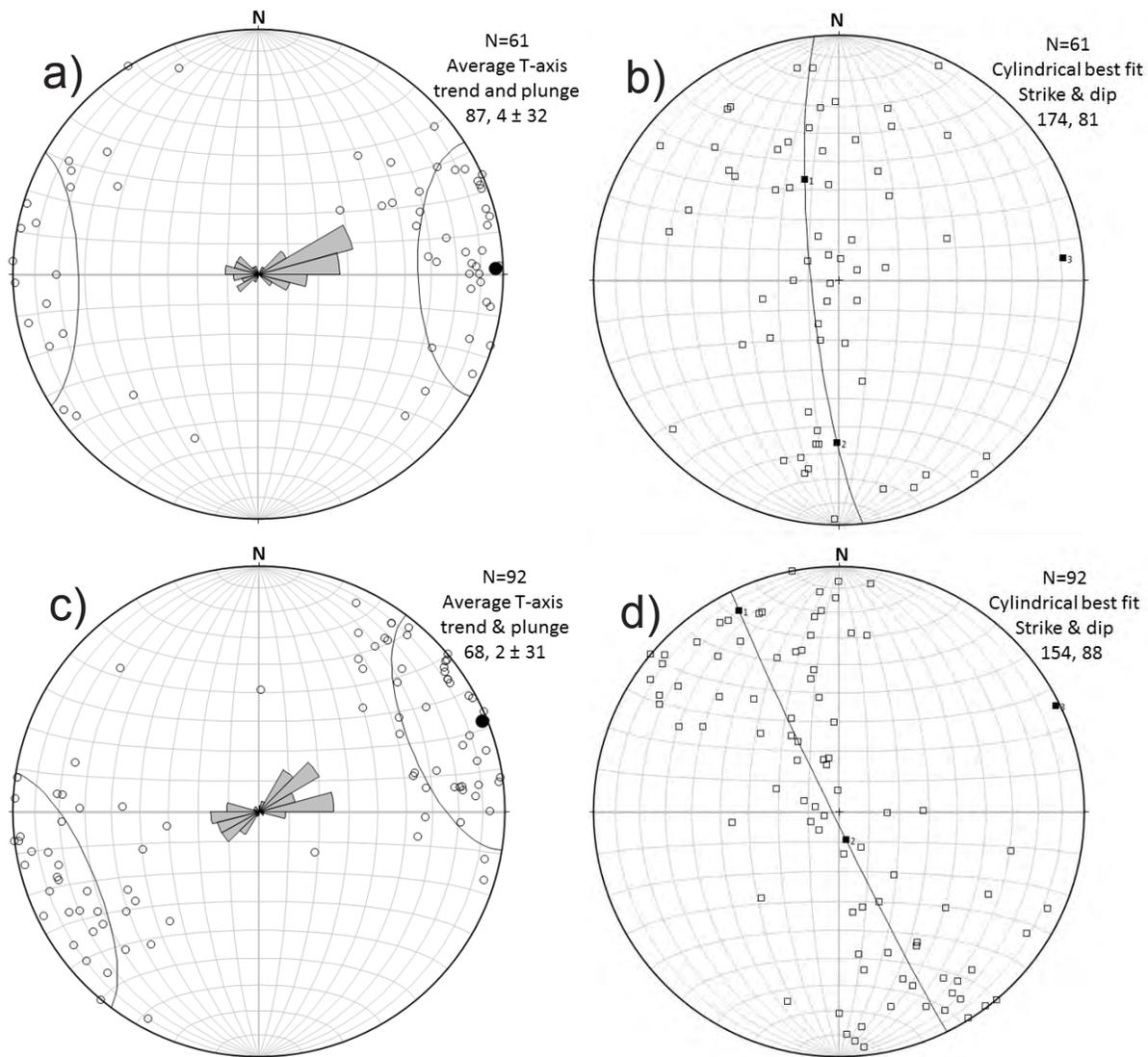
Figure 7. T-axes and P-axes from earthquake fault plane solutions. a) T-axes from 61 earthquakes north of the LCL with conical best fit (black dot), apical half angle (measure of scatter) shown as small circle, and rose diagram. b) P-axes from 61 events north of the LCL with cylindrical best fit (great circle) and computed principle stress axes (small black squares). c) T-axes from 92 earthquakes within and south of the LCL. Other symbols explained in a) above. d) P-axes from 92 earthquakes within and south of the LCL. Other symbols explained in b) above.

tholomew (1987) reported for fault plane solutions and fault trends in the northern Basin and Range Province of southwestern Montana and east-central Idaho.

DISCUSSION

Recent earthquakes in the ISB between the Clarkston Valley and Flathead Lake have a patchy distribution that is not clearly associated with mapped Quaternary faults. Numerous seismic clusters occur in areas that lack Quaternary faults; examples include the Clarkston Valley, Rock Creek, Monture Creek, and the region between Helmville and Helena. Other seismicity concentrations occur near the mapped ends of Quaternary faults, or fault segments, within the footwall blocks; examples include east of Townsend, south of Boulder, and North Crow Creek. Areas of relative seismic quiescence include the down-dip projection of Quaternary faults that are apparently locked during the 33-year reporting period of the MBMG earthquake catalog. Examples of currently quiescent Quaternary faults include the Canyon Ferry Fault, Beaver Creek Fault, and Mission Valley segment of the Mission Fault. Late Quaternary fault scarps—documenting magnitude 6.5 or larger paleoearthquakes—indicate that these faults are not always quiet. Just over one percent of the earthquakes in this study have fault plane solutions, so it is impossible to demonstrate how much seismicity occurring down-dip near Quaternary faults actually represents slip on those faults at depth. The only fault plane solutions consistent with slip at depth on a mapped Quaternary fault are for three earthquakes on the Mission Fault near Pablo which occurred near the northern boundary of the apparently locked Mission Valley segment of the Mission Fault.

Earthquake hypocenters deeper than 20 km are atypical in the northern Intermountain Seismic Belt. However, this data set includes 127 earthquakes with reliably determined hypocenter depths of 20 to 32 km below the surface, almost half of which occurred from 2006 through 2009 when data from the EarthScope Transportable Array (IRIS, 2015) were available to supplement the permanent seismic network. Only six of these reliably determined deep earthquakes occurred within the LCL, the majority occurred within a 40-km wide belt to the north of the LCL and east of the Mission Fault (green dots in fig. 1). Seventeen of these deep earthquakes have fault plane solutions. Within the LCL, two fault plane solutions indicate

strike-slip faulting, one indicates oblique-normal faulting, and one indicates normal faulting. Of the 12 fault plane solutions for deep events north of the LCL, 10 indicate normal faulting and two indicate oblique-normal faulting. The style of faulting for these deep earthquakes is similar to that of nearby shallow earthquakes.

The depth of brittle failure in the earth's crust depends on temperature, rheology, and strain rates. The spatial distribution of the deep earthquakes suggests that the Mission and St Mary's-Helena Valley faults penetrate the brittle upper crust and juxtapose middle crustal rocks with different properties and/or strain rates. The proximity of deep seismicity in the footwall blocks adjacent to the southern parts of the Mission, Swan, and South Fork Flathead faults and perhaps the St. Mary's-Helena Valley Fault, suggests the possibility that these faults may be capable of storing elastic energy to depths of at least 20 km. Lacking evidence to the contrary, the base of the seismogenic zone for most faults in the ISB is thought to be about 15 km. If these faults with nearby deep seismicity can in fact store elastic energy to depths of 20 km, then the fault rupture areas may be up to 25 percent larger than assumed for major earthquakes along these faults, with corresponding greater maximum probable earthquake magnitudes.

The Quaternary Fault and Fold Database (USGS, 2015) shows only normal faults for the eastern LCL and adjacent areas. According to this database, the 60-km long part of the LCL extending from the eastern end of the unnamed fault north of Ovando to the western end of the Helena Valley Fault has no faults with Quaternary displacement. However, the seismicity that defines the ISB is continuous along this part of the LCL, indicating continuing tectonic deformation. Furthermore, 53 percent of the fault plane solutions indicate strike-slip faulting and the majority are consistent with right-lateral slip on WNW-trending fault planes. Therefore, it seems likely that there are faults in the eastern LCL with unrecognized Quaternary displacement. Field evidence for Quaternary displacement on strike slip faults with low slip rates (perhaps one surface-rupturing earthquake every 5,000 to 30,000 years) is difficult to recognize. Compared to normal faults, scarps produced by strike-slip earthquakes are much smaller and discontinuous. Forests and dense vegetation cover much of the area, and gla-

ciers and post-glacial alluviation also have modified significant areas of the land surface, further obscuring evidence of young strike-slip faulting. Perhaps the best chance of identifying evidence of late Quaternary strike-slip displacement will require detailed mapping with the aid of high-resolution elevation data such as LiDAR. The lack of identified Quaternary faults in this part of the LCL contributes to lower predicted shaking levels portrayed on the National Seismic Hazard Maps (USGS, 2015b), in this part of the northern ISB, perhaps under reporting the true seismic hazard levels.

The sharp westward bend in the western border of the ISB where it intersects the LCL near Helena suggests that LCL structures control the locations of modern seismicity. Also, the change in character of Quaternary faults from several, long, continuous faults to the north, to numerous, short, discontinuous faults to the south suggests a fundamental influence of the LCL. The ENE-trending average extension direction for fault plane solutions within and south of the LCL and abundance of strike-slip fault plane solutions are compatible with the concept that strike-slip movement on faults within the LCL accommodate basin and range extension to the south, as proposed by Reynolds (1979). From this perspective, the LCL may be considered as the functional northern boundary of the Basin and Range Province.

CONCLUSIONS

- With few exceptions, seismic data suggest that recent earthquakes are not occurring at depth along mapped Quaternary faults.

- Strike-slip fault plane solutions are consistent with dextral slip on LCL faults, even though Quaternary strike-slip offsets have not been recognized on these faults.

- The distribution of deep seismicity and T-axis rotation suggest that the LCL is an important structural feature that influences crustal properties and may function as the northern boundary of the Basin and Range Province.

- Possible unrecognized active strike-slip faults and potentially seismogenic fault planes extending to depths of at least 20 km on normal faults north of the LCL may contribute to under-estimated seismic hazards on the National Seismic Hazard maps for west-central Montana.

REFERENCES

Allmendinger, R.W., Cardozo, N., and Fisher, D., 2012, Structural Geology Algorithms: Vectors and Tensors in Structural Geology: Cambridge University Press, 289 p.

Doser, D.I., 1989, Source Parameters of Montana Earthquakes (1925-1964) and Tectonic Deformation in the Northern Intermountain Seismic Belt: Bulletin of the Seismological Society of America, v. 79, p. 31-50.

Freidline, R.A., Smith, R.B., and Blackwell, D.D., 1976, Seismicity and Contemporary Tectonics of the Helena, Montana area: Bulletin of the Seismological Society of America, v. 66, pp. 81-95.

IRIS, 2015, Incorporated Research Institutions for Seismology website http://ds.iris.edu/ds/nodes/dmc/earthscope/usarray/#_, last accessed 4/22/15.

Ostenaa, D.A., Levish, D.R., and Klinger, R.E., 1995, Mission Fault Study: U.S. Bureau of Reclamation Seismotectonic Report 94-8, Denver, CO, 94-8, 170 p.

Pardee, J.T., 1926, The Montana Earthquake of June 27, 1925: U.S. Geological Survey Professional Paper 147-B, 23 p.

Qamar, A. and Hawley, B., 1979, Seismic Activity near the Three Forks Basin, Montana: Bulletin of the Seismological Society of America, v. 69, p. 1917-1929.

Qamar, A.I. and Stickney, M.C., 1983, Montana Earthquakes 1869-1979, Historical Seismicity and Earthquake Hazard: Montana Bureau of Mines and Geology Memoir 51, 80 p.

Reynolds, M.W., 1979, Character and Extent of Basin-

Range Faulting, Western Montana and East-Central Idaho: in 1979 Basin and Range Symposium, Rocky Mountain Association of Geology and Utah Geological Association, p. 185-193.

Scott, H.W., 1936, The Montana Earthquakes of 1935: Montana Bureau of Mines and Geology Memoir 16, 47 p.

Stickney, M.C., 1978, Seismicity and Faulting of Central Western Montana: Northwest Geology, v.7, p. 1-9.

Stickney, M., 2011, The Alberton-Frenchtown Seismic Zone: Northwest Geology, v. 40, p. 71-79.

Stickney, M.C. and Bartholomew, M.J., 1987, Seismicity and Late Quaternary Faulting of the Northern Basin and Range Province, Montana and Idaho: Bulletin of the Seismological Society of America, v. 77, p. 1602-1625.

USGSa, 2015, U.S. Geological Survey Quaternary Fault and Fold Database for the United States, accessed April 23, 2015, from USGS web site: http://earthquake.usgs.gov/hazards/qfaults/.

USGSb, 2015, U.S. Geological Survey National Seismic Hazard Maps Showing Peak Ground Acceleration with 2% Probability of Exceedance in 50 Years, Western U.S., last accessed 4/23/2015: http://earthquake.usgs.gov/hazards/products/conterminous/2002/maps/wus/pga.wus.2pc50.gif.

Vuke, S.M. and Stickney, M.C., 2013, Geologic map of the Clarkston Valley, Broadwater and Gallatin Counties, West-Central Montana: Montana Bureau of Mines and Geology Open-File Report 642, 16 p., 1 sheet, scale 1:24,000.

Wallace, C.A., Lidke, D.J., and Schmidt, R.G., 1990, Faults of the Central Part of the Lewis and Clark Line and Fragmentation of the Late Cretaceous Foreland Basin in West-Central Montana: Geological Society of America Bulletin, v. 102, p. 1021-1037.

Wessel, P., and W. H. F. Smith 1995, New Version of the Generic Mapping Tools: Eos Transactions of the American Geophysical Union, v. 76, no 33, p. 329–329, doi:10.1029/95EO00198.

Witkind, I.J., 1975, Preliminary Map showing Known and Suspected Active Faults in Western Montana: U.S. Geological Survey Open-File Report 75-285, 37 p.
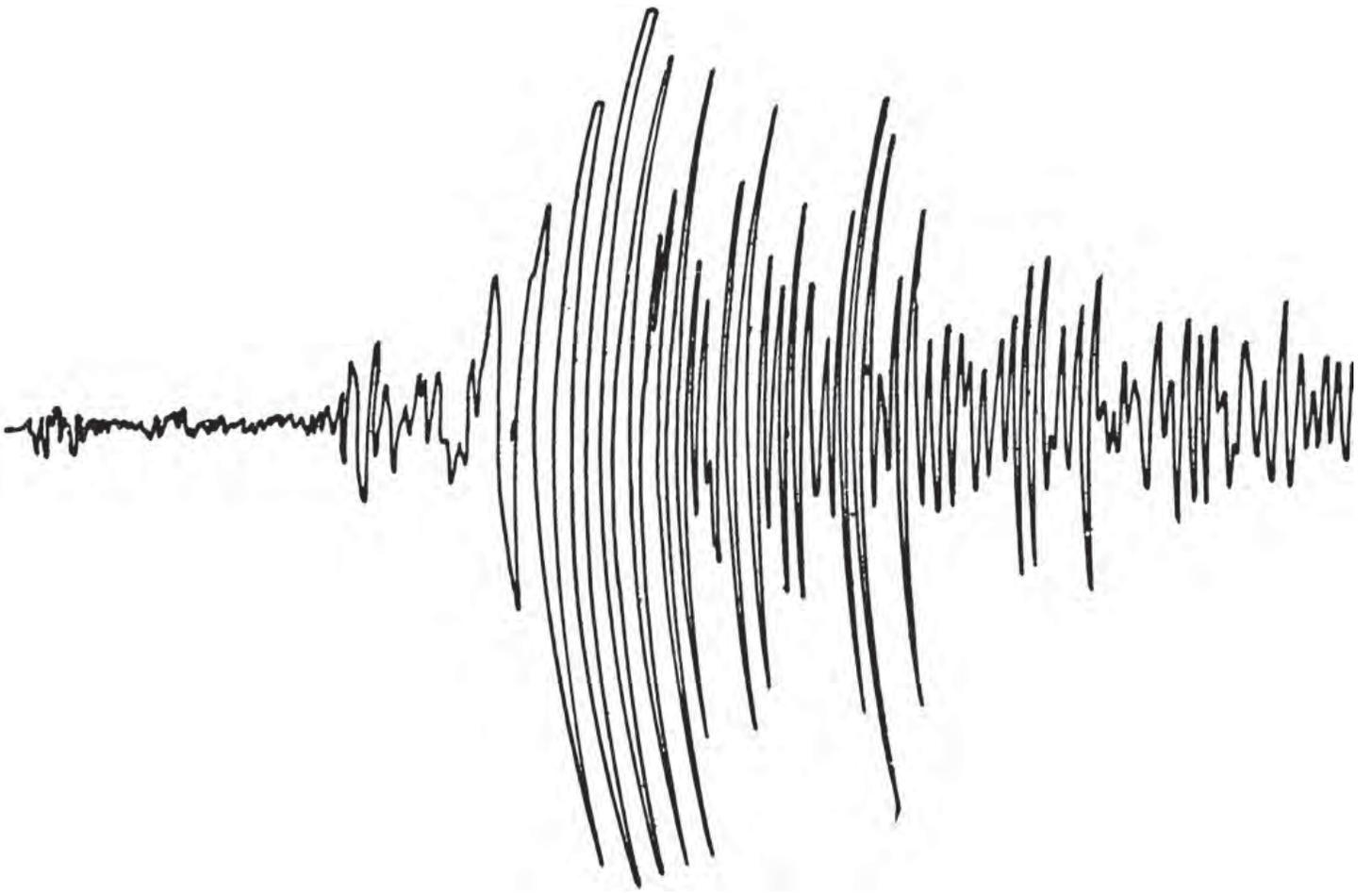
MINERAL PARAGENESIS OF EPITHERMAL GOLD-SILVER VEINS AT THE DRUMLUMMON MINE, MARYSVILLE, MONTANA

A. Griffith* and C.H. Gammons[1]

*Montana Resources, Inc., Butte, MT, 59701; [1]Department of Geological Engineering, Montana Tech of The University of Montana, 1300 W. Park Street, Butte, MT 59701

INTRODUCTION

The Drumlummon Mine is located in the Marysville mining district (fig. 1), about 17 miles northwest of Helena, Montana. Early reports of the economic geology of the mine are given in Barrell (1907), Knopf (1913), Pardee and Schrader (1933), McClernan (1982) and Walker (1992). Between the 1870s and the 1950s, the mine produced approximately 1 million oz. of Au and 12 million oz. Ag. RX Gold & Silver began renewed exploration in 2007, and underground drilling discovered the rich Charly vein to the east of the historic mine workings (fig. 2). In 2010 a decline was driven to access the Charly vein as well as unmined portions of the adjacent veins. Underground mining took place between 2010 and early 2013, with the ore processed at a mill in Philipsburg, Montana. A drop in
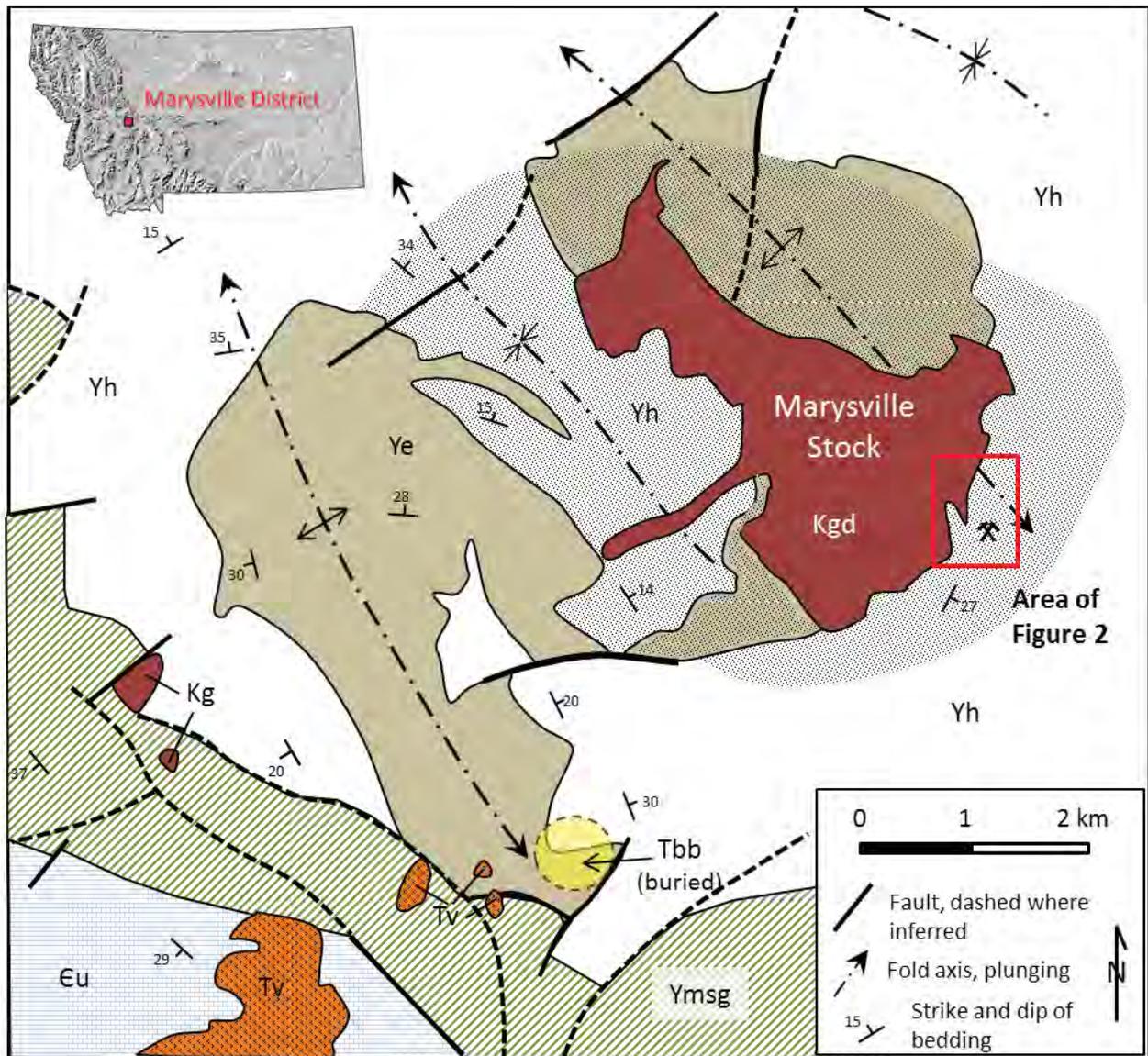

Figure 1. Simplified geologic map of the region surrounding the Drumlummon Mine. Ye = Empire Fm., Yh = Helena Fm., Ymsg = Spokane and Greyson Fms., Єu = Cambrian sediments, undivided, Kgd = Marysville Pluton, Tv = Tertiary volcanic rocks, Tbb = Bald Butte stock. Shaded region in center indicates contact-metamorphic aureole of the Marysville Pluton. Modified from Blackwell et al. (1974).

Figure 2. Map of the Drumlummon Mine showing the location and attitude of individual veins. (Courtesy U.S. Silver and Gold).

Mesoproterozoic Belt Supergroup. The metamorphic petrology of this contact aureole has been the subject of several classic papers (Melson, 1971; Rice, 1977; Ferry, 1994). Although the veins are located in the hornfels, the Au-Ag mineralization is thought to be much younger (Blackwell and others, 1974). Two buried granite porphyry stocks are found just to the west of the Marysville stock, the 47.8 ± 2 Ma Bald Butte and 40 Ma Empire Creek stocks. Several quartz porphyry dikes above the plutons have been dated at 37 Ma (Blackwell and others, 1974). The Bald Butte stock contains a molybdenum deposit which has been explored several times since the late 1960s. The hydrothermal event that mineralized the Drumlummon veins may be related to the emplacement of these Eocene stocks, although dates have not been obtained.

Regionally, the Drumlummon Mine is located near the intersection of the northern borders of the Great Falls Tectonic Zone (GFTZ) and the Lewis and Clark Fault Zone (LCFZ). The GFTZ, as interpreted by Sims et al. (2004), is a northeast-trending, 1.85 Ga suture zone between the Archean Medicine Hat Terrain to the north and the Archean Wyoming Terrain to the southeast. The LCFZ is a group of WNW-striking faults cutting across western Montana and the Idaho panhandle. The LCFZ has a long and very complex geologic history, beginning in the Proterozoic and continuing through the Tertiary (Berger and others, 2011). The intersection of the GFSZ and LCFZ may have played a role in the emplacement of the younger intrusive stocks and the hydrothermal mineralization in the Marysville district. The brittle nature of the hornfels in the contact aureole surrounding the Marysville Stock may also have helped to localize the veins. Interestingly, geothermal activity continues today in the Marysville District, roughly 5 km west of the Drumlummon mine, and is possibly fueled by recent magmatic activity (Blackwell and others, 1974).

metals prices in the spring of 2013 resulted in a suspension of mining and exploration at Drumlummon.

The Drumlummon mine follows several veins that run parallel to the SE margin of the Marysville pluton, a late Cretaceous (78 Ma; Daniel and Berg, 1981) granodiorite stock that is a satellite pluton to the larger Boulder Batholith. Important veins include the Drumlummon (the biggest historic producer), the Empire, the Frankie, the Castletown, the North Star, and the newly discovered Charly vein. With the exception of the Frankie vein, which dips towards the pluton, the veins strike ENE to NNE and dip steeply to the SE (fig. 2). Emplacement of the Marysville stock resulted in a concentric aureole of contact metamorphism (hornfels) of the Empire and Helena Formations of the

Although early workers described the mining geology of the Marysville district, until recently there had been no detailed studies using modern methods of ore deposit research. The objective of the present study, which constituted the M.S. thesis of the first author (Griffith, 2013), was to combine ore petrography with fluid inclusion analysis to formulate an updated geochemical model for the origin of the mineralization at Drumlummon. The renewed activity at the mine provided an excellent opportunity to collect new vein and wallrock specimens.

METHODS

Approximately 50 standard petrographic thin sections and 30 polished slabs were examined in this study. Samples were collected from diamond drill core, ore piles at the mine, and from exposures of veins and altered wallrock underground. All of the major veins in the mine complex were sampled, with a greater number taken from the newly discovered Charly vein. Polished slabs were examined by reflected light microscopy and scanning-electron microscopy (SEM). The LEO 1430VP SEM at the Center for Advanced Mineral Processing (CAMP), Montana Tech, was used. Mineral compositions were determined via energy dispersive X-ray analysis (SEM-EDX), and photographs were taken in back-scattered electron (BSE) mode. Approximately 12 doubly polished sections were examined using a fluid inclusion heating/freezing stage. Details of the fluid inclusion results, as well as a complete listing of SEM-EDX data, can be found in Griffith (2013). Some of the fluid inclusion findings are summarized near the end of this paper.

RESULTS

Hornfels Mineralogy

The country rock hosting most of the vein mineralization at the Drumlummon mine is a fine-grained calc-silicate hornfels which typically shows cm-scale banding of light and dark layers (fig. 3). This unit has been mapped as the Helena Formation (Blackwell and others, 1974), a siliceous dolomite. Based on SEM results, the light layers are almost equal parts quartz, diopside, and plagioclase and the dark layers almost equal parts quartz, actinolite, and potassium feldspar with up to 10% muscovite. The diopside from the light layer has an Fe/(Fe+Mg) mole ratio of 0.17 to

0.28, whereas the actinolite has an Fe/(Fe+Mg) ratio of 0.22. Plagioclase from the light layer has a Ca/(Na+Ca) mole ratio of 0.62, which corresponds to labradorite.

Hydrothermal Alteration

The emplacement of the veins resulted in relatively little alteration of the hornfels wallrock, suggesting that the flow of hydrothermal solutions through the vein-forming structures was relatively short-lived. At most, a small seam (<3-5 cm wide, sometimes absent) of chlorite ± muscovite was found at the boundary between the vein and the hornfels. A single SEM analysis from the Charly vein revealed chlorite to be Mg-rich, with a calculated Fe/(Fe+Mg) atomic ratio of 0.15. This ratio is slightly less than that of the pre-
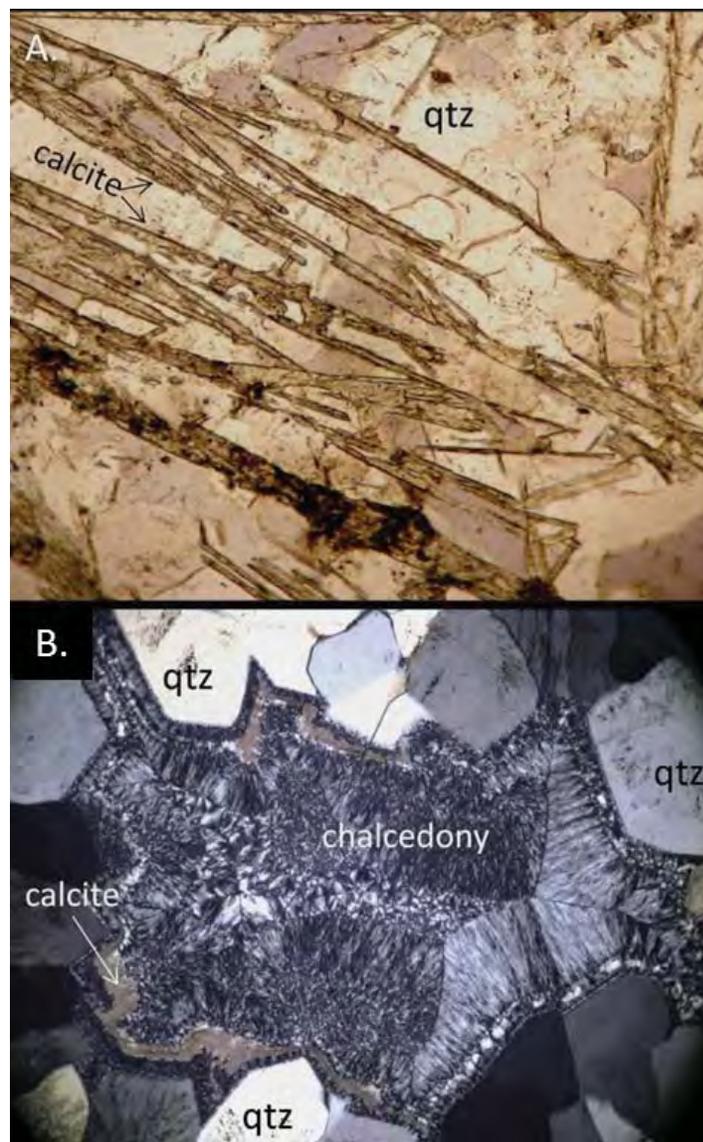

Figure 3. A) Hand sample of typical hornfels country rock. Specimen is about 5" wide. B) SEM-BSE image of a dark band in the hornfels. C) SEM-BSE image of a light band in the hornfels.

cursor actinolite and diopside in the hornfels, which had $Fe/(Fe+Mg)$ ratios of 0.22 and 0.28, respectively. Therefore some Fe in the hornfels minerals may have been scavenged to form Fe-bearing sulfide minerals. The few mafic dikes that were found in the mine are propylitically altered to epidote and chlorite. It is not known whether this alteration was associated with the main mineralizing event, or was simply a result of the dikes heating up and reacting with the surrounding groundwaters as they cooled.

VEIN MINERALOGY

Gangue Minerals

Veins in the Drumlummon Mine are primarily quartz and carbonate, the latter being calcite, dolomite, or a combination of the two (table 1). Quartz and calcite locally occur as coarse, bladed intergrowths (fig. 4A), a texture that is diagnostic of boiling epithermal fluids (Simmons and Christenson, 1994, White and Hedenquist, 1995). Coarse, euhedral quartz is also found in proximity to chalcedony (fig. 4B), indicating fluctuations in temperature and/or rates of silica precipitation that are typical of epithermal systems. The quartz is mostly milky or clear, although minor amounts of amethyst were noted, including at surface outcrops of the Drumlummon vein. Calcite and dolomite locally form fine masses filling pore space that are intergrown with fine-grained ore minerals. When viewed under SEM-BSE, the distribution of ore minerals in the carbonate masses resembles a constellation of stars (fig. 5A).

Although adularia was reported by the mine operators as a common vein mineral at Drumlummon, only trace amounts of adularia were found in this study. Hand samples of quartz-rich vein material with a pinkish hue were tested with HF/Na-cobaltinitrite K-feldspar staining, and almost all of these samples tested negative. Nonetheless, a few small grains of adularia were identified in this study by SEM from high-grade ore in the Pixley vein where they occurred intergrown with quartz, sulfides, and electrum. Based on SEM-EDS analyses, the adularia grains are close to pure $KAlSi_3O_8$.

Ore Minerals

Two stages of ore minerals are present in the veins of the Drumlummon Mine, the first being primary

Table 1. Paragenesis of ore and gangue minerals of the Drumlummon Mine.

Ore Minerals	Primary	Secondary
Electrum, Au-rich	trace	
Electrum, Ag-rich		trace
Silver		common
Stromeyerite		common
Argentite	common	trace
Argentopyrite	trace	
Ag-tetrahedrite	common	
Pearceite	common	
Proustite	trace	
Pyrargyrite	common	
Other sulfides		
Pyrite	common	
Galena	abundant	common
Low-Fe sphalerite	abundant	common
Chalcopyrite	abundant	common
Bornite		trace
Gangue Minerals		
Quartz	abundant	
Calcite	common	
Dolomite	common	
Aragonite		trace
Barite	trace	
Adularia	trace	
Alteration Minerals		
Chlorite	abundant	
Sericite	common	

(hypogene), and the other inferred by mineral textures and compositional trends as being secondary (table 1). Some minerals are common to both groups (sphalerite, galena, chalcopyrite), whereas others (e.g., silver, stromeyerite) are only found in secondary ore.

Whereas sphalerite, galena, and chalcopyrite are ubiquitous in the veins of Drumlummon, pyrite is a minor constituent, sometimes completely absent. Sphalerite is pale brown to white in color, indicating a very low FeS content. Based on SEM-EDX, sphalerite grains near pyrite have slightly higher iron content ($X_{FeS} = 0.013$, n = 10) compared to sphalerite from veins with no pyrite ($X_{FeS} = 0.008$, n = 13). Despite the abundance of chalcopyrite in the veins, none of the sphalerite show "chalcopyrite disease" (i.e., small rounded inclusions of chalcopyrite). The sphalerite contains significant cadmium, with typical values in the range 0.5 to 1.5 at% Cd (Griffith, 2013).
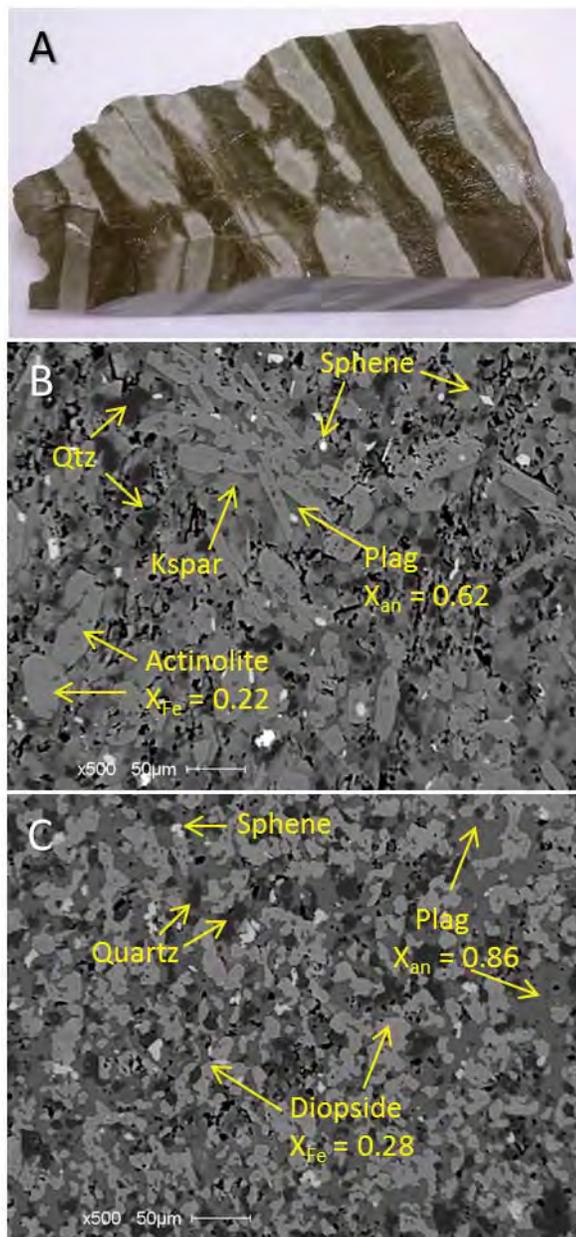
Figure 4. A) Thin section of bladed calcite intergrown with quartz. B) Thin section (crossed polars) of intergrown quartz, calcite and chalcedony. Field of view in both photos is about 1 cm.

The so-called "ruby silver" minerals pearceite/polybasite $(Ag,Cu)_6(As,Sb)_2S_7(Ag_9CuS_4)$ and pyrargyrite/proustite $Ag_3(Sb,As)S_3$ are fairly common ore minerals in the primary mineral assemblage at Drumlummon (fig. 5B), but are absent from the secondary ore. Based on SEM-EDX analysis, pearceite (the As-rich endmember) is much more common than polybasite, whereas pyrargyrite (the Sb-rich endmember) is much more common than proustite. It is interesting to note that the Drumlummon mine was one of the first recorded occurrences of pearceite, and excellent specimens collected from the mine were used to help determine the mineral's crystallographic properties (Penfield, 1896).

Silver-rich tetrahedrite $(Ag_{>0.4}Cu_{<0.6})_6Cu_4(Fe,Zn)_2(Sb,As)_4S_{13}$ is a fairly common ore mineral in the primary assemblage, but is absent from secondary ore (table 1). The Ag content of the tetrahedrite grains ranged between 9 to 15 mol% (Griffith, 2013). A few samples from the Charly vein had enough Ag to be considered freibergite, i.e., at least 4 Ag atoms per 13 S atoms in the calculated formula (Johnson and others, 1986). The Ag content of tetrahedrite tends to vary inversely with Zn, whereas Sb is always more abundant than As. A few grains of As-rich tennantite were found in a single sample from the Charly vein that was rich in native silver and stromeyerite. Based on this mineral association, tennantite probably belongs in the "late/shallow" column of the paragenesis (table 1). Compared to tetrahedrite, the Ag-content of tennantite is very low.

Argentite/acanthite (Ag_2S) occurs throughout the veins in trace to minor amounts, and was often found in close proximity to the Ag-sulfosalts and electrum. The argentite grains contain low amounts of Cu, with Ag/(Ag+Cu) atomic ratios ranging from 0.88 to 1.00. A single grain of argentopyrite $(AgFe_2S_3)$ was found in a sample from the Frankie vein that also contained abundant argentite.

Electrum was the only gold-bearing phase found in this study. The electrum occurs as amorphous grains anywhere from 1 μm to 1 mm in diameter, the latter being visible in hand sample. Electrum can be found associated with any of the common ore and gangue minerals, but is especially common near Ag-tetrahedrite or Ag-sulfosalts. In the deeper veins, electrum has a mole fraction of gold (X_{Au}) of 0.4 to 0.6 (Griffith, 2013). In contrast, some of the shallower veins have more Ag-rich electrum, or electrum grains that show a wider range in Au:Ag ratio.

Stromeyerite, AgCuS, was found as irregular-shaped grains occupying void space between quartz, carbonate and other ore minerals, and generally appears to be late in the paragenesis. Some samples of high-grade ore from the Charly vein contained masses of stromeyerite up to 0.5 cm in diameter. In reflected light, the stromeyerite was found to exist as oriented intergrowths with chalcopyrite and native silver, sometimes with a few small grains of bornite (figs. 5D, 5E). All stromeyerite grains analyzed in this study were
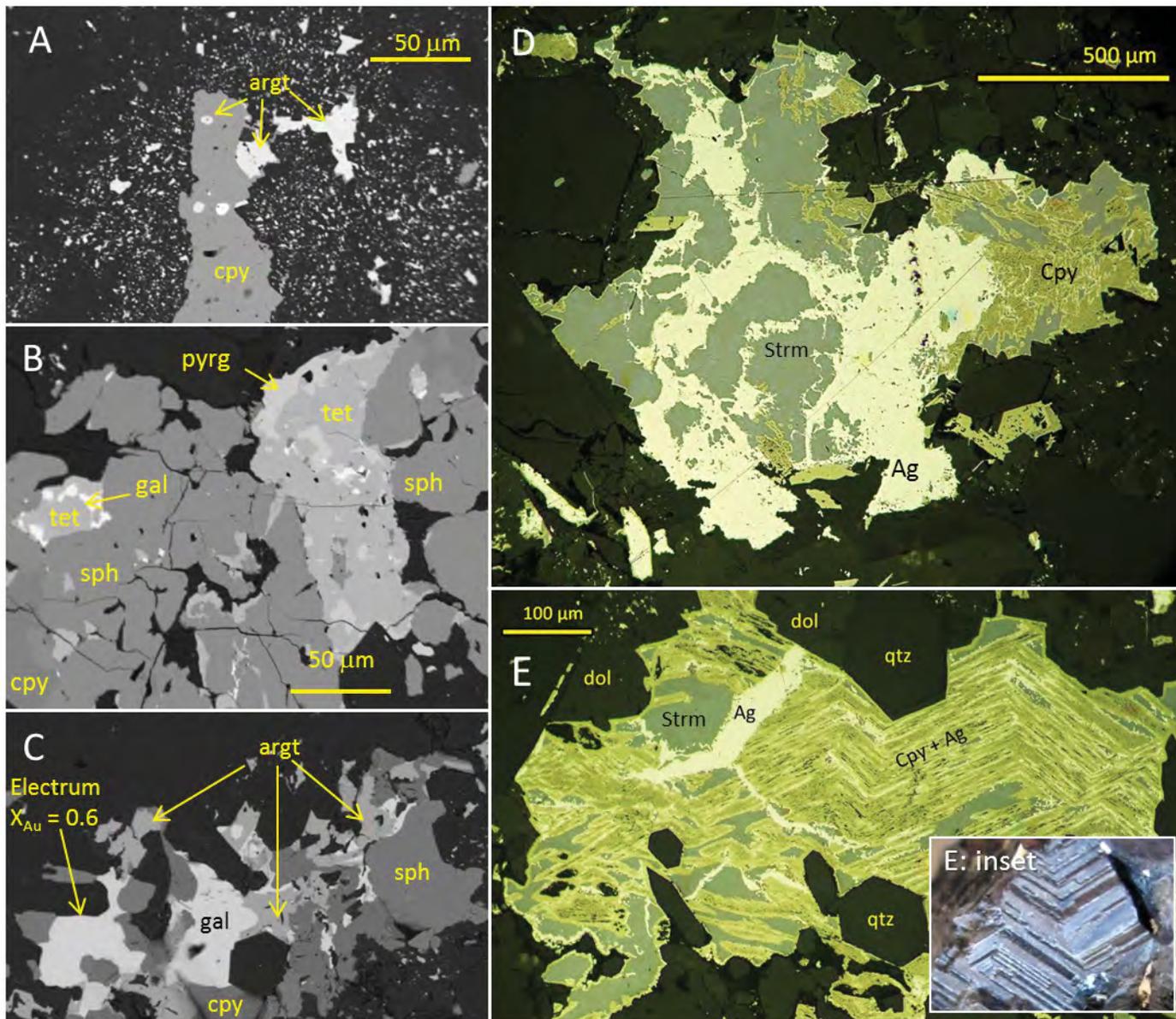
Figure 5. A) SEM-BSE image of dolomite (black) with abundant inclusions metal sulfides (bright), including chalcopyrite (cpy) and argentite (argt). B and C) SEM-BSE images of primary ore, showing sphalerite (sph), tetrahedrite (tet), pyrargyrite (pyrg), galena (gal), chalcopyrite (cpy), argentite (argt) and electrum. D and E) Reflected light photographs of intergrowths of stromeyerite (strm), native silver (Ag) and chalcopyrite. E-inset shows a photograph of a tetrahedrite crystal taken from mindat.org.

very close to the ideal 1:1:1 stoichiometry of AgCuS. Ideas on the possible origin of this texture are given below.

Native silver is abundant in some of the high-grade ore from Charly 500 and 600 levels, and was rarely found in samples unless stromeyerite was nearby. Besides the intergrowths with stromeyerite and chalcopyrite, native silver also occurs as narrow rims bounding the more common sulfides, and as irregular veinlets cutting across all other minerals. None of these textures resemble the geometry of primary electrum grains, which tend to occur as individual grains that are more or less equant in dimension. Whereas elec-

trum showed a wide range in Au:Ag ratio, all analyses of native silver were pure Ag with no detectable Au or Cu. Native silver ± stromeyerite are rarely found in the same sample as Ag-rich tetrahedrite or the Ag-sulfosalts. These relationships suggest that stromeyerite and native silver formed as a lower-temperature replacement of pre-existing Ag-rich tetrahedrite, and/or Ag-sulfosalts.

DISCUSSION

Mineralogical Constraints on Temperatures of Vein Formation

The ore mineral assemblage at Drumlummon can be used to place constraints on the temperature and fugacity of $S_2(g)$ (f_{S2}, bars) of the hydrothermal fluids. An f_{S2}-T diagram was constructed (fig. 6) using thermodynamic data for metal sulfides (Barton and Skinner, 1979) and electrum (White and others, 1957). The upper and lower pairs of sphalerite curves in figure 6 correspond to the minimum and maximum value of the mole fraction of FeS (X_{FeS}) for sphalerites analyzed in this study where pyrite was nearby. Barton and Skinner (1979) give two equations based on different thermodynamic data sources for computing fS2 based on sphalerite compositions. These are shown in figure 6 by solid or dashed lines. The Au/Ag ratio of electrum coexisting with argentite is also a sensitive indicator of f_{S2} (Gammons and Williams-Jones, 1995). Electrum compositions of 40 to 60 atomic% Ag repre-

sent the primary mineralization. To draw the electrum/ Ag_2S stability curves in figure 6, thermodynamic data from White et al. (1957) were used and substituted into the acanthite/argentite equations from Barton and Skinner (1979).

Based on the thermodynamic constraints imposed by the sphalerite and electrum compositional fields, figure 6 shows that the primary mineral assemblage at Drumlummon most likely formed at a temperature between 190 to 340°C. This temperature range overlaps with the homogenization temperatures of fluid inclusions in quartz measured by Griffith (2013), which ranged from 120 to 360°C. Figure 6 also shows the inferred conditions for the secondary mineral assemblage that contains pure silver coexisting with Fe-poor sphalerite. Temperatures below 100°C are indicated by this assemblage, which agrees with previous experimental work that has shown that stromeyerite is only stable at temperatures less than 90°C (Skinner, 1966).
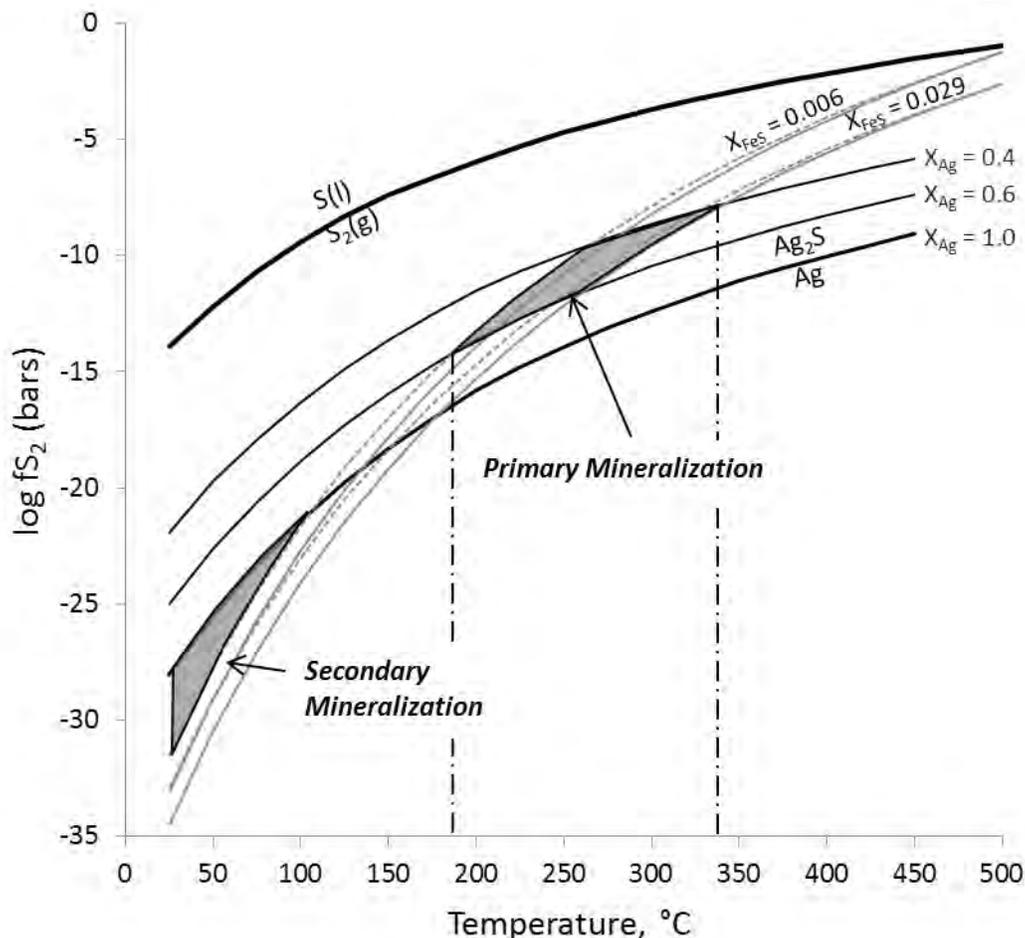
Figure 6. f_{S2}-temperature diagram summarizing conditions of formation of primary and secondary mineralization at Drumlummon. The "X_{Ag}" curves show equilibrium between argentite and electrum with differing mole fraction of Ag. The "X_{FeS}" curves show equilibrium between pyrite and sphalerite with differing mole fraction of FeS.

Origin of Stromeyerite/Silver/Chalcopyrite Intergrowths

We hypothesize that the fascinating intergrowths of stromeyerite+silver+chalcopyrite described earlier (fig. 5E) owe their origin to a late, low-temperature replacement of primary Ag-rich tetrahedrite. The following equation shows how an oxidizing fluid could have leached antimony and sulfate out of Ag-rich tetrahedrite (idealized formula of $Cu_5Ag_5Fe_2Sb_4S_{13}$), forming stromeyerite, chalcopyrite, and silver:

$$Cu_5Ag_5Fe_2Sb_4S_{13}(s) + 12H_2O + 12O_2 \rightarrow$$
$$3CuAgS(s) + 2CuFeS_2(s) + 2Ag(s) +$$
$$4Sb(OH)_3(aq) + 6SO_4^{2-} + 12H^+$$
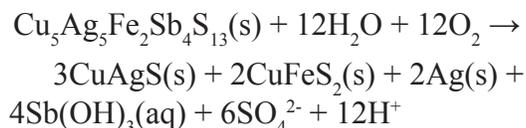
The interesting "zigzag" intergrowth of stromeyerite, chalcopyrite, and native silver mimics the geometric faces of what could have been a pre-existing euhedral crystal of tetrahedrite (see inset to fig. 5E). Furthermore, the proportions of stromeyerite, chalcopyrite, and silver in the secondary intergrowths are close to the 3:2:2 stoichiometry of the above equation.

Depth of Mineralization

Hydrothermal fluid pressure (P, in bars) was estimated from the boiling curve for water (fig. 7). A range of temperatures between 250 and 340°C was used, based on the homogenization temperatures of fluid inclusions that showed evidence of boiling (i.e., paired liquid-rich and vapor-rich inclusions; Griffith, 2013). The range in pressures corresponding to the L-V curve for this temperature range is 40 to 150 bars. The depth of formation was estimated from: depth (m) = P(bars)*10/ density(g/cm³). To approximate hydrostatic conditions, an average water density value of 0.85 kg/cm³ was used, which is midway between the density of a 260°C fluid and a 100°C fluid. This assumes that the water column extended upwards to a near-surface boiling hot spring.

The computed depth values at hydrostatic conditions range from 470 to 1760 m. To determine the depth under lithostatic conditions, the same equation was used with a rock density of 2.8 kg/cm³ (appropriate for hornfels). This gave a depth range of 140 to 540 m. In reality, the pressure regime probably fluctuated between hydrostatic and lithostatic pressure, as cracks were periodically opened and sealed. Using either set of depth estimates, the results of this study are consistent with a near-surface, epithermal origin for the veins at Drumlummon. Additional evidence supporting the conclusion that the veins are epithermal is the fact that most the fluid inclusions had low salinity, falling in the range of 0 to 3 wt% NaCleq, and showed no evidence of high CO_2 concentrations (Griffith, 2013).

CONCLUSIONS

Based on the results of this study, the veins of the Drumlummon mine are most likely of relatively shallow, epithermal origin. The primary mineral assem-
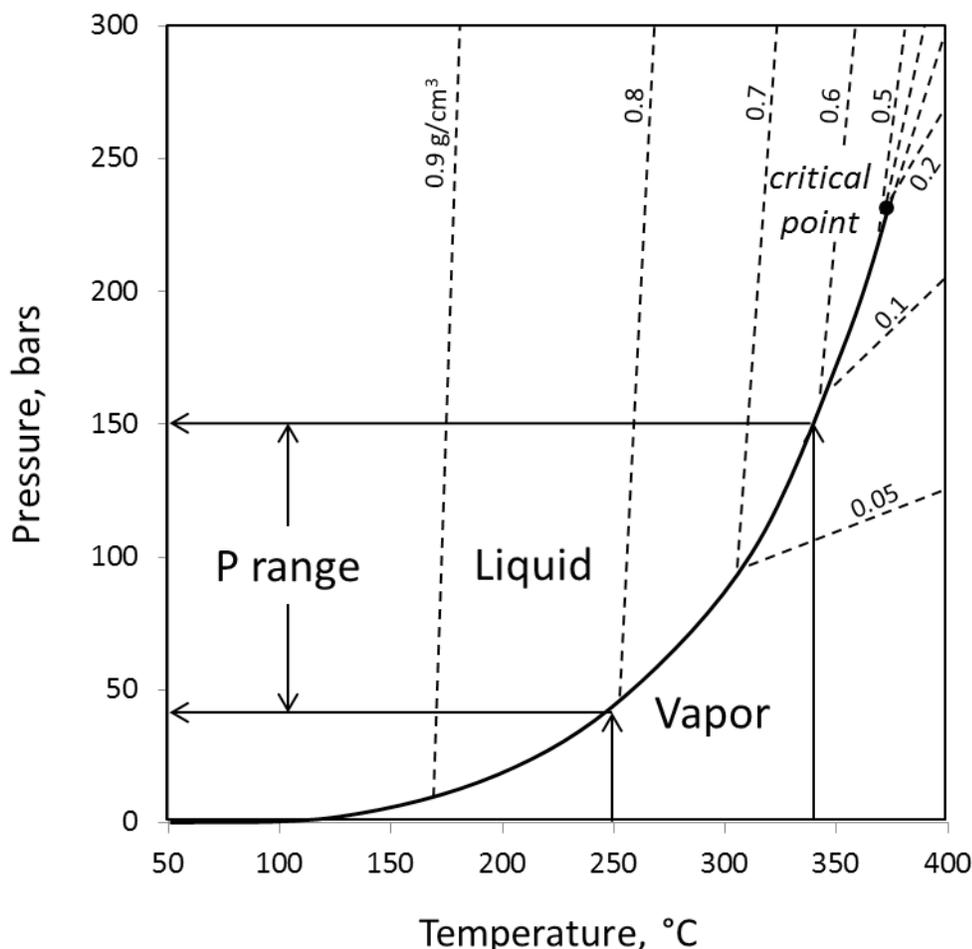
Figure 7. Phase diagram for water showing the inferred conditions of primary vein mineralization at Drumlummon.

blage contains abundant base metals (galena, sphalerite, chalcopyrite), electrum, Ag-rich tetrahedrite, and Ag-sulfosalt minerals, and most likely formed at temperatures between 140 and 350°C, with episodic boiling being a major control on ore and gangue mineral deposition. Secondary ore includes locally abundant native silver and stromeyerite, and most likely formed from more oxidized fluids at a temperature <100°C. Although dates are lacking, the main episode of mineralization at Drumlummon is speculated to be roughly the same age as the intrusion of nearby Eocene granitoid stocks, including the Bald Butte porphyry, a known Mo deposit. The age of later oxidation and silver enrichment is less well constrained.

The epithermal quartz-carbonate veins of the Drumlummon mine are somewhat unique in southwest Montana, as most other hydrothermal deposits in the region are inferred to be of relatively deep origin, such as the porphyry-lode deposits of Butte (Rusk and others, 2008), the polymetallic veins of the Emery district (Zimmerman and others, 2015) and the skarn/replacement/vein deposits of Philipsburg (Holser, 1950). Although the large Au-Ag mines at Montana Tunnels (Sillitoe and others, 1985) and Golden Sunlight (Porter and Ripley, 1985) were probably epithermal, these deposits occur in the form of large breccia pipes, not discrete veins. More exploration in the Marysville district and surrounding region may yet uncover more precious metal "bonanza" veins.

ACKNOWLEDGMENTS

REFERENCES

Barrell, J., 1907, Geology of the Marysville mining district: U.S. Geol. Survey. Professional Paper 57, 178p.

Barton, P.B. Jr., and Skinner, B.J., 1979, Sulfide mineral stabilities: Ch. 7 in Barnes, H.L. (ed.) Geochemistry of Hydrothermal Ore Deposits, 2nd ed., J. Wiley, New York.

Berger, B.R., Hildenbrand, T.G., O'Neill, J.M., 2011, Control of Precambrian basement deformation zones on emplacement of the Laramide Boulder Batholith and Butte mining district, Montana, United States: U.S. Geological Survey, Scientific Investigations Report 5016.

Blackwell, D. D., Brott, C. A., Goforth, T. T., and 7 others, 1974, Geological and geophysical exploration at Marysville geothermal area: 1973 results: NSF-RANN Grant No. GI 38972, Technical Report. 104pp.

Daniel, F., and Berg, R.B., 1981, Radiometric dates of rocks in Montana: Montana Bureau of Mines and Geology, Bulletin 114, 144p.

Ferry, J. M., 1994, Role of fluid flow in the contact metamorphism of siliceous dolomitic limestones: American Mineralogy, v.79, p. 719-736.

Gammons, C. H., and Williams-Jones, A. E., 1995, Hydrothermal geochemistry of electrum: Thermodynamic constraints: Economic Geology, v. 90, p. 420-432.

Griffith, A., 2013, Paragenesis and fluid inclusion study of epithermal Au-Ag veins at the Drumlummon Mine, Marysville, Montana: M.S. Thesis, Montana Tech, Butte, MT.

Holser, W. T., 1950, Metamorphism and associated mineralization in the Philipsburg region, Montana: Geological Society of America Bulletin, v. 61, p. 1053-1090.

Johnson, N. E., Craig, J. R., Rimstidt, J. D., 1986, Compositional trends in tetrahedrite: Canadian Mineralogist, v. 24, p. 385-397.

Knopf, A., 1913, Ore deposits of the Helena mining region: U.S. Geological Survey Bulletin 527, 143 pp.

McClernan, H. G., 1982, Metallic mineral deposits of Lewis and Clark County, Montana: Montana Bureau of Mines and Geology Memoir 52, 49 pp.

Melson, W. G., 1966, Phase equilibria in calc-silicate hornfels, Lewis and Clark County, Montana: American Mineralogist, v. 51, p. 402-421.

Pardee, P. and Schrader, F.C., 1933, Metalliferous deposits of the greater Helena mining region, Montana: U.S. Geological Survey Bulletin 842.

Penfield, S. L., 1896, On pearceite, a sulpharsenite of silver and on the crystallization of polybasite:

American J. Science, 4th Series, Vol. II (no. 1), p. 17-29.

Porter, E. W., and Ripley, E. M., 1985, Petrologic and stable isotope study of the gold-bearing breccia pipe at the Golden Sunlight deposit, Montana: Economic Geology, v. 80, p. 1689-1706.

Rice, J. M., 1977, Progressive metamorphism of impure dolomitic limestone in the Marysville aureole, Montana: American Journal of Science, v. 277, p. 1-24.

Rusk, B.G., Reed, M. H., Dilles, J. H., 2008, Fluid inclusion evidence for magmatic-hydrothermal fluid evolution in the porphyry copper-molybdenum deposit at Butte, Montana: Economic Geology, v.103, p. 307-334.

Sillitoe, R. H., Grauberger, G. L., Elliott, J. E., 1985, A diatreme-hosted gold deposit at Montana Tunnels, Montana: Economic Geology, v. 80, p. 1707-1721.

Simmons, S. F., and Christenson, B. W., 1994, Origins of calcite in a boiling geothermal system: American Journal of Science, v. 294, p. 361-400.

Sims, P. K., O'Neill, J. M., Bankey, V., Anderson, E., 2004, Precambrian basement geologic map of Montana – An interpretation of aeromagnetic anomalies: U.S. Geological Survey, Scientific Investigations Map 2829.

Skinner, B. J., 1966, The system Cu-Ag-S: Economic Geology, v. 61, p. 1-26.

Walker, G. E., 1992, Geology and history of the Marysville mining district and the Drumlummon Mine, Lewis and Clark County, Montana: Montana Bureau of Mines and Geology, Open-File Report 254, 27 pp.

White, J. L., Ore, R. L., Hultgren, R., 1957, The thermodynamic properties of silver-gold alloys: Acta Metallurgica, v. 5, p. 747-760.

White, N. C., and Hedenquist, J. W., 1995, Epithermal gold deposits: Styles, characteristics, and exploration: SEG Newsletter, no. 23, p. 1 and 9-13.

Zimmerman, J., Gammons, C. H., Korzeb, S., 2015, Fluid inclusion and petrographic analysis of the Emery mining district, southwest Montana, [abstr.] Geological Society of America, Rocky Mountain Section, Casper, WY, May, 2015.

GLACIAL GEOLOGY AND GEOMORPHOLOGICAL FEATURES OF THE LINCOLN AREA, LEWIS AND CLARK AND POWELL COUNTIES, MONTANA

M. Vineyard, A. Sherimkulova, E. Welk, K. Eastman, T. Hagan, C. Thomson, L.N. Smith, M. Chambers, M. Machinal, A. Mack, and N. Hofland

Department of Geological Engineering, Montana Tech of the University of Montana, Butte, MT, 59701, lsmith@mtech.edu

ABSTRACT

The Lincoln, Montana area has undergone several episodes of glaciation, with each episode showing multiple cycles of glacial advance and retreat. Evidence of glaciation observed in field investigations and photogeologic mapping include: trimlines, moraines (lateral, medial, recessional, and terminal), eskers, drumlins, glacial meltwater channels, and ice marginal channels. Existing maps of the Lincoln area showed geologic contacts and glacial extent. Aerial photographs and field investigations were used to refine the mapping of glacial features in the Lincoln area. Ice marginal channels showed greater glacial extent than previously mapped by Locke and Smith in the Blackfoot River drainage area.

INTRODUCTION

Repeated glacial cycles during the Pleistocene Epoch (2.6-0.12 Ma) shaped the landscape of the northern Rocky Mountains of western Montana (Pierce, 2003). The region north of Lincoln, Montana was dominated by continental valley glaciers. Most glacial activity in this area has been dated to the Bull Lake and Pinedale glaciations.

The extensive Bull Lake glaciation, 200 ka-130 ka, extended from northwestern Montana to the Southern Rockies of New Mexico, concurrent with the Illinoian Stage of the Quaternary Ice Age (Pierce, 2003; Fullerton and others, 2004). The Bull Lake glaciation was followed by a warm interglacial period which lasted approximately 60,000 years. The Pinedale glaciation occurred after this warm period, approximately 30 ka-10 ka, and primarily consisted of valley glaciers.

The objective of this project was to map the Quaternary glacial deposits and landforms near Lincoln, Montana (fig. 1) and to determine the extent of glacial ice in the area. The Lincoln area was chosen because previous work had not been conducted on the glacial extent in the area specifically and the stereo photos were readily available. The data provide a better understanding of the glacial history of the area, the extent of glacial ice, and give insight to past climatic and geologic events by showing the sequence of when they occurred.

METHODS

Preliminary geologic mapping of the Elliston (McDonald and others, in prep.) and Dearborn River (Vuke, 2014) 30' x 60' quadrangles provided a base for glacial features observed in the field, and mapped from stereo images. Glacial landforms were mapped using color stereo images, taken along several flight lines during the summer of 2003 (USDA-BLM 16 MT 100). The photos selected for this study cover an area of approximately 300 square miles centered at a point northwest of Lincoln, Montana. To increase coverage of features on the northern edge of the study area, a set of grayscale stereo images taken in 1977 (GS-VELB Choteau Quad) was also investigated. Due to the large area covered, group participants mapped individual north-south flight lines and worked together to create an overview map. A field trip to the study area confirmed locations and lithology of numerous glacial features.

Features were mapped on acetate overlays of aerial photos, then compiled on mylar, scanned, and digitized using ArcGIS. FGDC (Federal Geographic Data Committee) glacial and glaciofluvial symbols were used to map glacial features and geologic contacts. The mylar map was georeferenced to the 1:24,000 map of the quadrangles in Montana. Suspected glacial landforms and deposits were compared to known examples throughout western Montana (Smith and others, 2010).
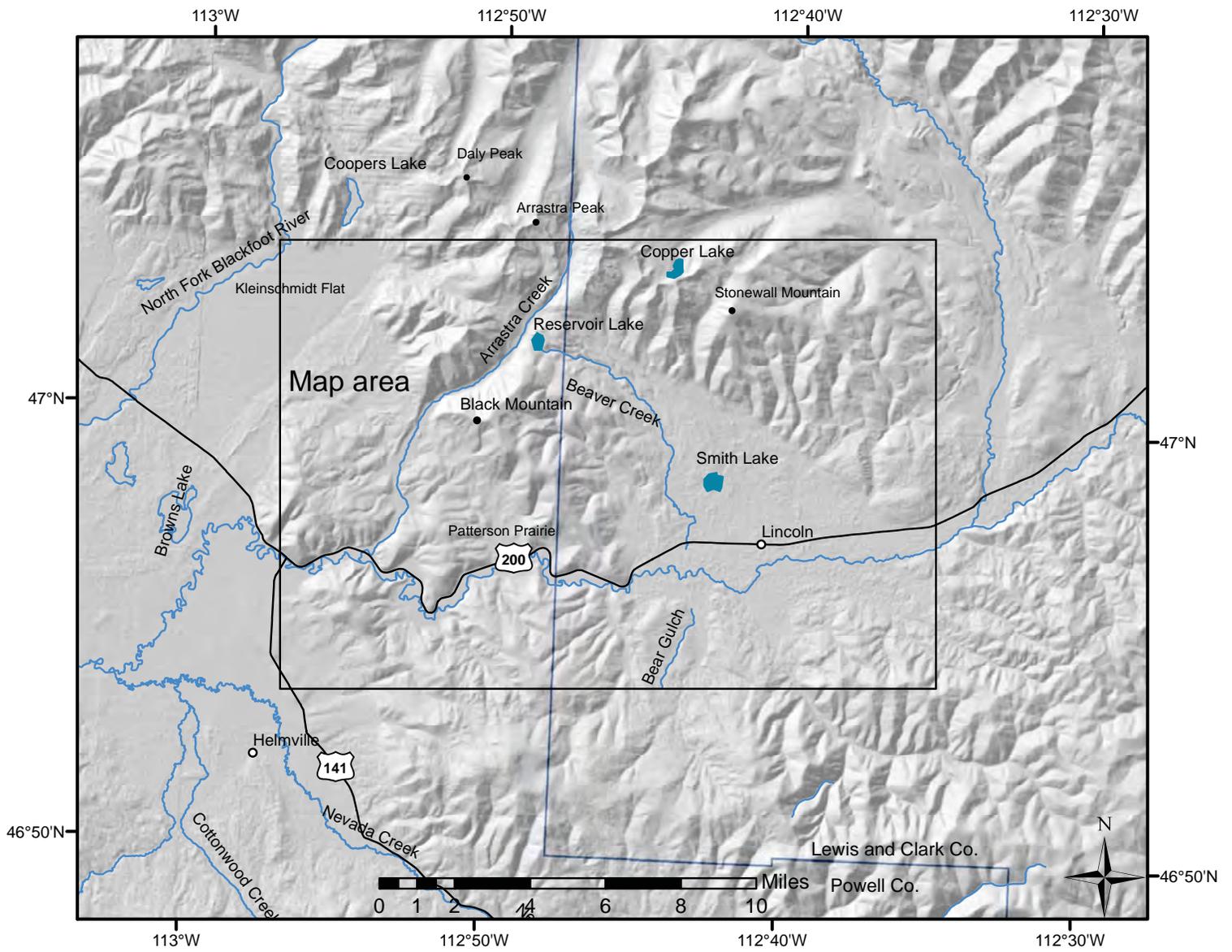
Figure 1. Location map of the Lincoln area. Black rectangle labeled "Map Area" is the area shown in figures 2 and 3.
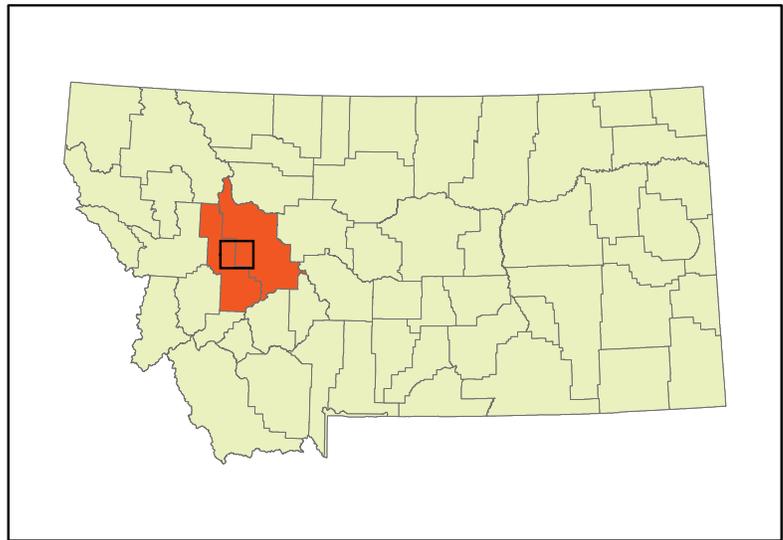
DESCRIPTION OF MAPPED GLACIAL LANDFORMS

Mapped glacial landforms (fig. 2) include: lateral, terminal, and recessional moraine crests, trimlines, glacial stream channels, kettles (within kame and kettle topography), modern fault scarps, and landslide headwall scarps. Associated glacial, alluvial, and colluvial deposits were mapped separately from landforms, and include: till, outwash, terraces, drumlins, landslide/slump deposits, and modern alluvium.

Moraines/Moraine Crests

Moraines are sharp-crested landforms composed of till that are formed alongside the ablation zone of a glacier during movement and melting. Moraine crests are linear features on top of the moraine deposits, and define the maximum height of the glacial ice through periods of glacial advance and retreat. Lateral moraines consist of sediment that has been pushed to the sides; these typically indicate the lateral extent of the glacier and are parallel to the direction of flow.

Terminal moraines amass at the toe of the glacier and are perpendicular to the direction of flow; these indicate maximum extent of glacial movement into the valley. Recessional moraines are terminal moraines that formed during a previous standstill or advance of a glacier, and were subsequently overridden by another glacial advance in which another terminal moraine was deposited. These landforms can be completely eroded by secondary advances, and may provide geomorphological evidence as to the amount and pattern of glacial advances/retreats in the area. Medial moraines form at the junction of two glaciers; these deposits are often scoured away by later glacial movement or eroded by the melting of glacial ice.

Lateral moraines are visible in many locations in the map area, including along the sides of Beaver Creek (fig. 2). Medial moraines are present in the upper Arrastra Creek and Beaver Creek Valleys. Terminal moraines were mapped south of Smith Lake as well as in the valley south of Lincoln (fig. 2), along with multiple recessional moraines.
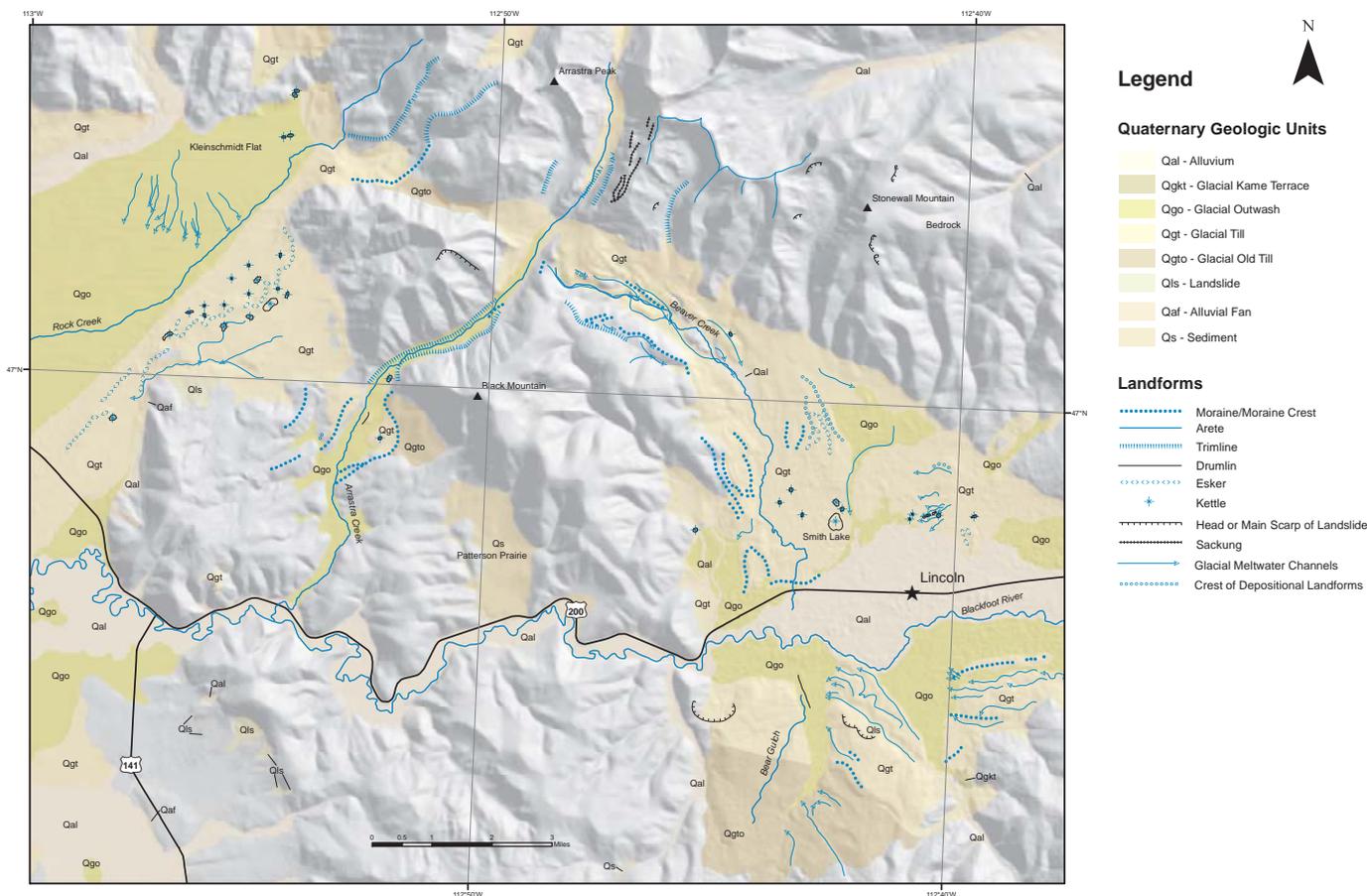
Figure 2. Geologic and geomorphic map of the Lincoln area. Geologic contacts are modified from McDonald and others (in prep.) and Vuke (2014).

Arêtes

Arêtes are sharp, prominent ridges formed by bedrock erosion between two or more glacial valleys. Arêtes are along the divide south of Copper Lake (fig. 1).

Trimlines

Trimlines are linear features following the edge of a glacial valley or cirque that define the highest point of glacial erosion, and where bedrock erosion occurred. These features are evident south of Copper Lake on the east side of the glaciated valley, east of Coopers Lake between Daly Peak and Arrastra Mountain, along the valley starting at Reservoir Lake, and extend southwest past Black Mountain (fig. 2). Trimlines were mapped by tracing the tops of talus slopes and extending linear features down-valley.

Eskers

Eskers are elongated sinuous ridges composed of stratified glacial till that represent channels formed within or below glaciers. These channels accumulate sediment that is left behind after the glacier retreats. Eskers are noticeable along the western edge of the map area near Kleinschmidt Flat, in the glacial till east of Smith Lake, and in the valley north of Lincoln (fig. 2).

Kame and Kettle Topography

Kame and kettle topography is irregular topography representing sediment and ice left behind by the retreat of glaciers. Ice blocks can become stranded in the sediment, melt, and form depressions known as kettles. Kettles are completely or partially filled with water. Kames form when depressions in glacial ice accumulate sediment and leave behind positive topographic features. This topography is evident east and southeast of Kleinschmidt Flat and throughout most of the glaciated valleys where till is present (fig. 2). Only large kettles, such as Smith Lake, are shown on the map to indicate where this topography exists (fig. 2).

Landslides and Sackungen

Landslides are slope failures that result in ground movement from higher to lower elevation. Landslide deposits consist of rock debris, with coarse cobble size, angular rock fragments in a silt or clay matrix, which forms hummocky topography. Rock fall and rockslide avalanches, slumps, and earthflows can produce similar types of landforms. We mapped landslide headscarps, not deposits.

These features were mapped at the base of either side of the north-south trending glacial valley to the north of Reservoir Lake as well as west of Stonewall Mountain. Additional landslides were mapped south of the arête near Copper Lake, and between Arrastra Peak and Black Mountain and southwest of Lincoln (fig. 2).

Sackungen are linear trenches found on the top of ridges and as anti-slope scarps along the sides of steep valleys. These features are believed to form by large-scale gravitational spreading and movement along existing fracture planes. The sackungen in this area may have formed from unloading by glacial melting, which caused subsequent steepening of the valley (Savage and others, 1987). The ridge-top troughs resulted from falling of bedrock from each side of the ridge. The vertical offset in the anti-slope scarps was a result of the tilt of the bedding and uphill erosion (Hippolyte and others, 2006). Sackungen are present along the crest and the west-facing slope of the north-south trending glacial valley north of Reservoir Lake.

Glacial Meltwater Channels and Ice Marginal Channels

Glacial meltwater channels are inactive stream channels that were formed by glacial activity. In the mapped area, meltwater channels accord with ice-marginal channels. The meltwater channels are typically located in the center of a valley, whereas the ice-marginal channels are located near the sides of the glacial valley and are not as preserved as meltwater channels. Both forms of these channels are mapped extensively in the valley south of Lincoln and Beaver Creek valley (fig. 2). In the Kleinschmidt Flat area, the glacial meltwater channels join with underfit streams. Underfit streams represent channels that previously hosted greater glacial discharge, and now are occupied by streams of greatly diminished flow.

Crests of Depositional Landforms

Crests of depositional landforms are undifferentiated constructional features such as lateral or medial moraines, drumlins, and eskers. In most cases these

features are linear, irregularly-shaped, and parallel to glacial flow. These features were mapped north of Lincoln in the glacial till and in Arrastra Creek valley (fig. 2).

Drumlins are small depositional landforms of streamlined till that form within a retreating glacier and record the final direction of glacial flow. We mapped these features north of Bear Gulch and in the southern end of the glacial outwash in Arrastra Creek valley (fig. 2).

DESCRIPTION OF MAPPED GLACIAL DEPOSITS

Glacial Till (fig. 2 map units Qgt & Qgto)

Till is composed of gravel and poorly-sorted sediment deposited by glaciers. It is commonly associated with areas of hummocky kame and kettle topography, eskers, and moraines. Till contacts were modified from preliminary mapping done in Beaver Creek valley by McDonald and others (in prep.). Till was differentiated as younger (Qgt) and older (Qgto) to delineate different periods of glaciation.

Glacial Outwash (fig. 2 map unit Qgo)

Glacial outwash deposits are lower elevation plains formed by deposition of glacial sediments from meltwater at the terminus of a glacier. These deposits contain well-sorted, flat-lying sediments in the bottoms of valleys. They are usually related to kame and kettle topography and glacial till deposits. Typically, till is deposited when the glacier is advancing, and outwash is deposited when the glacier is retreating. Outwash deposits are found in Patterson Prairie and in Arrastra Creek valley (fig. 2). In an area northeast from Lincoln, the amount of outwash deposits was reduced from preliminary mapping by McDonald and others (in prep).

Alluvium (fig. 2 map unit Qal)

Alluvium is loose unconsolidated sediments reworked by recent stream and fluvial activity. We remapped a large part of the Blackfoot River plain shown as glacial outwash (Qgo) on McDonald and others (in prep) to younger alluvial sediments (Qal).

DISCUSSION

Repeated glaciations efficiently removed bedrock from the mountains north of Lincoln that formed extensive glacial deposits to the south. In the Lincoln valley, lateral moraines, recessional moraines, and streamlined depositional landforms represent small-scale glacial advances, retreats, and associated sediment deposition.

McDonald and others (in prep.) mapped several deposits such as Quaternary glacial till (Qgt), Quaternary glacial outwash (Qgo), and Quaternary alluvium (Qal). Photogeologic mapping and field investigations of the area showed that the contact locations of the deposits needed to be reevaluated and relocated. The Qal boundary was changed considerably to map the meander scars of the Blackfoot River. The boundary for Qgt was extended to include the kame and kettle topography. Older Quaternary glacial till was mapped as Qgto. The classification of this unit was necessary to explain the differences between the till to the north and south of Lincoln valley.

Peripheral to the main valley glaciers were glacial meltwater channels that likely migrated throughout the areas affected in response to glacial advances and retreats. The Blackfoot River was forced to the south during major glacial advances. Moraines, streamlined depositional landforms, and ice-marginal channels in the valley provide evidence of glacial advance from the north-northeast into the valley south of Lincoln (fig. 3). Older glacial till south of these channels was from previous glaciations but is not verified by this study. Extensive alluvium fills much of the valley surrounding Lincoln (fig. 2).

Glaciers left behind trimlines and distinct lateral moraines along the sides of the valley. Terminal or recessional moraines are not readily visible; any terminus was likely later eroded by outwash flow. Drumlins were mapped in the Arrastra Creek valley and north of Bear Gulch. These landforms were denoted as till and glacial outwash in mapping by McDonald and others (in prep.).

Kleinschmidt Flat is the major low-lying region along the western edge of the mapped area. The surface of the flat is marked by a very shallow fan of glacial outwash that radiates from the valley containing
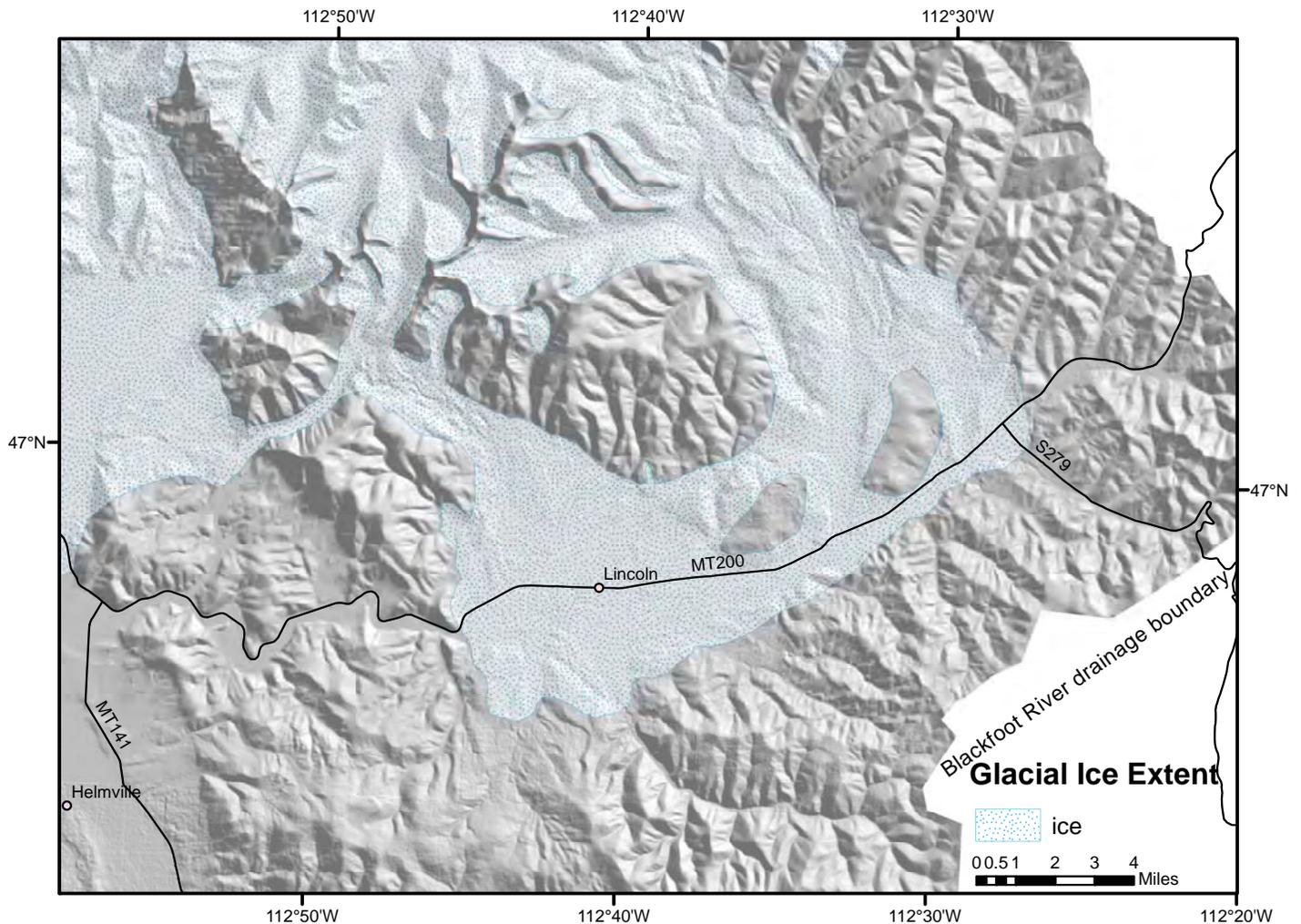
Figure 3. Ice extent map during the last glacial period of the Blackfoot River drainage. Modified from Locke and Smith (2004).

the North Fork of the Blackfoot River. Kleinschmidt Flat is unlike any other landforms in the area. It is a distinctly smooth feature, bordered on the northwest and southeast by hummocky kame and kettle topography and eskers. The present courses of the North Fork of the Blackfoot River and the Rock Creek drainages surround the Kleinschmidt Flat (fig. 1). These streams are both underfit, indicating their channels contained greater flow in the past. A possible explanation is that Kleinschmidt Flat area was the result of an outburst flood, additional work would be needed to investigate this possibility.

Landslides have modified the glacial terrain throughout the mapped area. The majority of the landslides within the study area lack vegetation, which indicates that they are recent and not related to deglaciation of the area. The majority of the landslides are on north-facing slopes, and some may be related to logging activity. Landslides are also present on east and west facing slopes, and may be associated with gravitational spreading.

CONCLUSIONS

- Distribution of ice and ice flow directions were more accurately mapped.

- We refined the contacts between till, outwash, and alluvium.

- We mapped a variety of landforms and depositional features.

- Older till and trimlines are indications of multiple glaciations for the area. The valley east of Kleinschmidt Flat may have been filled with ice during the Bull Lake glaciation as indicated by the presence of trimlines and moraines.

- Ice marginal channels south of Lincoln show the Blackfoot River may have flowed continually during glaciation but may have been dammed by the glacier in the Beaver Creek valley.

ACKNOWLEDGMENTS

REFERENCES

Fullerton, D. S., Colton, R. B., and Bush, C. A., 2004, Limits of mountain and continental glaciations in northern Montana and north-western North Dakota, U.S.A.: *in* Ehlers, J., and Gibbard, P.L., eds., Quaternary Glaciations: Extent and Chronology, Part II: Elsevier, Amsterdam, p. 131-150.

Hippolyte, J.C., Brocard, G., Tardy, M., Nicoud, G., Bourles, D., Braucher, R., Menard, G., Souffache, B., 2006, The recent fault scarps of the Western Alps (France): tectonic surface ruptures or gravitational sackung scarps? A combined mapping, geomorphic, levelling, and ^{10}Be dating approach: Tectonophysics, v. 418, p. 255-276.

Locke, W.W., 1995, Modelling of icecap glaciation of the northern Rocky Mountains of Montana: Geomorphology, v. 14, p. 123-130.

McDonald, C., Mosolf, J.G, Vuke, S.M., and Lonn, J.D., in preparation, Preliminary geologic map of the Elliston 30' x 60' quadrangle, west-central Montana: Montana Bureau of Mines and Geology Open-File Report XXX, 1 sheet, scale 1:100,000.

Pierce, K.L., 2003, Pleistocene glaciations of the Rocky Mountains: Development in Quaternary Science, v. 1, p. 63-76.

Savage, W. Z., Varnes, D.J., 1987, Mechanics of gravitational spreading of steep-sided ridges (sackung): Bulletin of the International Association of Engineering Geology, v. 35, p. 31-36.

Smith, L.N., Smith, M.G.A., Croft, T.O., Dutton, A.D., Gordon, L.M., Wright, J.R., and Dresser, H.W., 2010, Quaternary mapping and glaciation of the northern Anaconda Range and the southern Flint Creek Range, Deer Lodge, Granite, and Powell Counties, Montana: Northwest Geology, v. 39, p. 1-14.

Vuke, S.M., 2014, Preliminary geologic map of the Dearborn River 30' x 60' quadrangle, west-central Montana: Montana Bureau of Mines and Geology Open-File Report 649, 9 p., 1 sheet, scale 1:100,000.

Locke, W.,Smith, L.N., 2004. Pleistocene mountain glaciation in Montana, USA. In: Ehlers, J., Gibbard, P.L. (Eds.), Extent and Chronology of Glaciations. Elsevier, Amsterdam, pp. 117–121.

IRON MINERALOGY AND REDOX CHEMISTRY OF THE MESOPROTEROZOIC NEWLAND FORMATION IN THE HELENA EMBAYMENT, BELT SUPERGROUP, MONTANA

Sarah P. Slotznick,[1*] Jerry Zieg,[2] Samuel M. Webb,[3] Joseph L. Kirschvink,[1,4] and Woodward W. Fischer[1]

[1]*Division of Geological and Planetary Sciences, California Institute of Technology, 1200 East California Boulevard, Pasadena, CA 91125, USA; [2]Tintina Resources Inc., 17 E. Main Street, P.O. Box 431, White Sulphur Springs, MT, 59645, USA;[3]Stanford Synchrotron Radiation Lightsource, Menlo Park, CA 94025, USA;[4]Earth-Life Science Institute, Tokyo Institute of Technology, Meguro-ku, Toyko 152-8550, Japan;*sslotz@caltech.edu*

INTRODUCTION

The Mesoproterozoic era falls in the period between 1.85 to 0.85 Ga called "the boring billion", sandwiched between the rise of multi-cellularity and animals in the Neoproterozoic and the Great Oxygenation Event and rise of oxygen in the Paleoproterozoic (Holland, 2006). However, important evolutionary developments occurred over the period with the rise of eukaryotes and macroscopic organisms (Knoll and others, 2006). The Belt Supergroup contains some of the early micro- and macrofossils that have been attributed to eukaryotes (Horodyski and others, 1989). One particularly well-studied example is found in the Greyson Shale of the Helena Embayment region in southwestern Montana (fig. 1a). First identified by Charles Doolittle Walcott (1899) and later renamed (Walter and others, 1976), Grypania spiralis is a curved or coiled ribbon, 0.2 to 1.7 mm wide, and 6 to 14 mm in coiled diameter, and has been interpreted as eukaryotic algae as well consortia of several microscopic organisms (Horodyski and others, 1989; Knoll and others, 2006; Walter and others, 1976).

Due to our understanding of eukaryotic phylogeny, the fact that most modern eukaryotes are aerobic, and the requirement of oxygen in making certain biological compounds (sterols) contained in eukaryotes, eukaryotes have been tied to oxygenic conditions (e.g. Brocks and others, 2003; Embley and Martin, 2006; Raymond and Blankenship, 2004). Therefore, there is a need to understand more about the environmental conditions in which early macroscopic organisms lived to understand the pacing of eukaryotic evolution and how it might have been aided, frustrated, or unaffected by changing environmental conditions during the Proterozoic.However, understanding the redox state of ancient oceans has been a longstanding problem since a good oxygen barometer has not yet been developed.

In general, geologists and geochemists have looked at iron, sulfur, and other redox sensitive elements as records of oxygen levels, but these approaches often give discordant answers. Some studies have suggested a fully oxygenated mid-Proterozoic ocean (Cloud, 1968; Holland, 1984, 2006), while others have suggested a stratified system with anoxic and/or euxinic deep oceans (Canfield, 1998; Poulton and Canfield, 2011). Aerobic/oxic environments are defined as having >80 μM O2, anoxic/ferruginous have <5 μM O2, and euxinic environments are anoxic with H2S also present (Raiswell & Canfield 1998).

Even within the subset of studies focused on samples of the Belt Supergroup, there have been conflicting hypotheses about redox conditions. Due to their preservation and low metamorphic grade (Duke and Lewis, 2010), the strata contained in the Helena Embayment, specifically the shale-dominated Newland Formation, have been the main target for understanding the ancient redox character and geochemistry of the Belt Basin. Sulfate concentrations and sulfur isotopes (Gellatly and Lyons, 2005; Luepke and Lyons, 2001; Lyons and others, 2000) as well as presence of basin-wide sedimentary laminations in the shales of the Newland and Prichard Formations similar to those found in the Black Sea (Lyons and others, 2000) were initially argued as evidence of a chemically stratified euxinic basin during deposition of the lower Belt Supergroup. Bottom water suboxic to euxinic conditions were also suggested by the high (several wt.%) organic content observed in shales (Lyons and others, 2000), and the syndepositional to early diagenetic abundant pyrite and sulfide-hosted base metal deposits of Cu, Co, and Ag (Graham and others, 2012; White and others, 2014). Others suggested the euxinic conditions forming early diagenetic pyrite were restricted to pore waters (Schieber, 1989c).

In sharp contrast, iron speciation results indicate anoxic and ferruginous conditions for basinal waters of the lower Belt Supergroup (Planavsky and others, 2011). Iron speciation is a recently-developed bulk geochemical technique that uses sequential extraction to estimate proportions of different reactive iron minerals within a given rock sample (Poulton and Canfield, 2005), which are then mapped to redox conditions based on empirical calibrations from modern sediment samples. Additionally, recent nitrogen isotope measurements of samples from the Chamberlain, Greyson and Newland formations suggest oxygenated portions of the water column (Stüeken, 2013).

In this study, we focus on samples of the Newland Formation from the Black Butte Deposit in the Helena Embayment since previous workers investigating mid-Proterozoic redox conditions used drill core specimens from this deposit to avoid complications of recent surface oxidation (Gellatly and Lyons, 2005; Luepke and Lyons, 2001; Lyons and others, 2000; Planavsky and others, 2011). To help reconcile the different redox interpretations and test the iron speciation results, we investigated the iron mineralogy of the Newland Formation using a range of petrographic, spectroscopic, and rock magnetic techniques that help shed light on both the paleoenvironmental processes of iron deposition in the sediments as well as post-depositional modifications to those phases.

Bulk rock magnetism experiments provide sensitive techniques to identify ferromagnetic minerals, including magnetic iron sulfide phases. Magnetic iron sulfides such as pyrrhotite have not previously been identified in materials collected from the Newland Formation, but have been widely observed throughout correlative units elsewhere in the lower Belt Supergroup (e.g. Luepke, 1999; Luepke and Lyons, 2001; Slotznick and others, in review). Much of the pyrrhotite in the rock record is interpreted to be due to the metamorphic alteration of pyrite or precipitation from high temperature fluids (Craig and Vokes, 1993; Hall, 1986); and pyrrhotite observed in Belt strata reflects both of these post-depositional processes (Luepke, 1999). Pyrite can transform to pyrrhotite beginning at 200°C (Hall, 1986) if a suitable reducing environment or organic matter is present, although some experiments suggest even lower temperature transitions are possible (Moreau and others, 2005; Raub and others, 2012). Thus the presence of pyrrhotite can provide a

tool for understanding metamorphic temperatures and metasomatic conditions of the Newland Formation at the Black Butte Deposit, aiding us in recognizing if bulk geochemical proxies have been compromised by post-depositional alteration.

Additionally, synchrotron-based X-ray spectroscopy provided a complimentary tool to discover and image a wide range of non-magnetic iron minerals such as chalcopyrite and pyrite while confirming the presence or absence of pyrrhotite. By applying these paired magnetic and spectroscopic techniques to the Belt Supergroup, we should be able to improve upon previous bulk geochemical studies in deducing how iron was being deposited and transformed in the environment to reconstruct ancient redox conditions.

GEOLOGIC SETTING

The Helena Embayment is an E-W trending limb of the larger Belt Basin, with strata broadly correlative to three of the four stratigraphic groups recognized elsewhere in the basin: lower Belt Group, Ravalli Group, Middle Belt Carbonate Group (fig. 1a; Graham and others, 2012; Winston and Link, 1993). Fine-grained siliciclastics and carbonates dominate the lower Belt in the northern part of the Helena Embayment near the Black Butte Deposit (fig. 1b). The Neihart Quartzite is a basal quartz arenite sandstone with planar and trough cross-bedding, parallel lamination, and lenses of pebbles lying unconformably on early Proterozoic gneiss basement (Schieber, 1989b; Walcott, 1899). Overlying the Neihart quartzite, the Chamberlain Formation is a wavy laminated to bedded black shale, siltstone and sandstone with lenses of molar tooth hash near the top (Zieg, 1986). The Chamberlain Formation grades into the Newland Formation. The Newland Formation varies considerably in thickness across the Embayment from 610 m to over 3000 m, but is approximately 1,100 m in the region of the Black Butte Cu-Co-Ag deposit near the northern margin of the Helena Embayment (Nelson, 1963; Walcott, 1899; Zieg, 1986).

The Newland Formation is subdivided into two informal members: a lower parallel-laminated shale interbedded with debris flows, turbidites, and carbonates and an upper shale with more abundant carbonate beds (Zieg, 1986). Conformably overlying the Newland Formation is the Greyson Formation of wavy
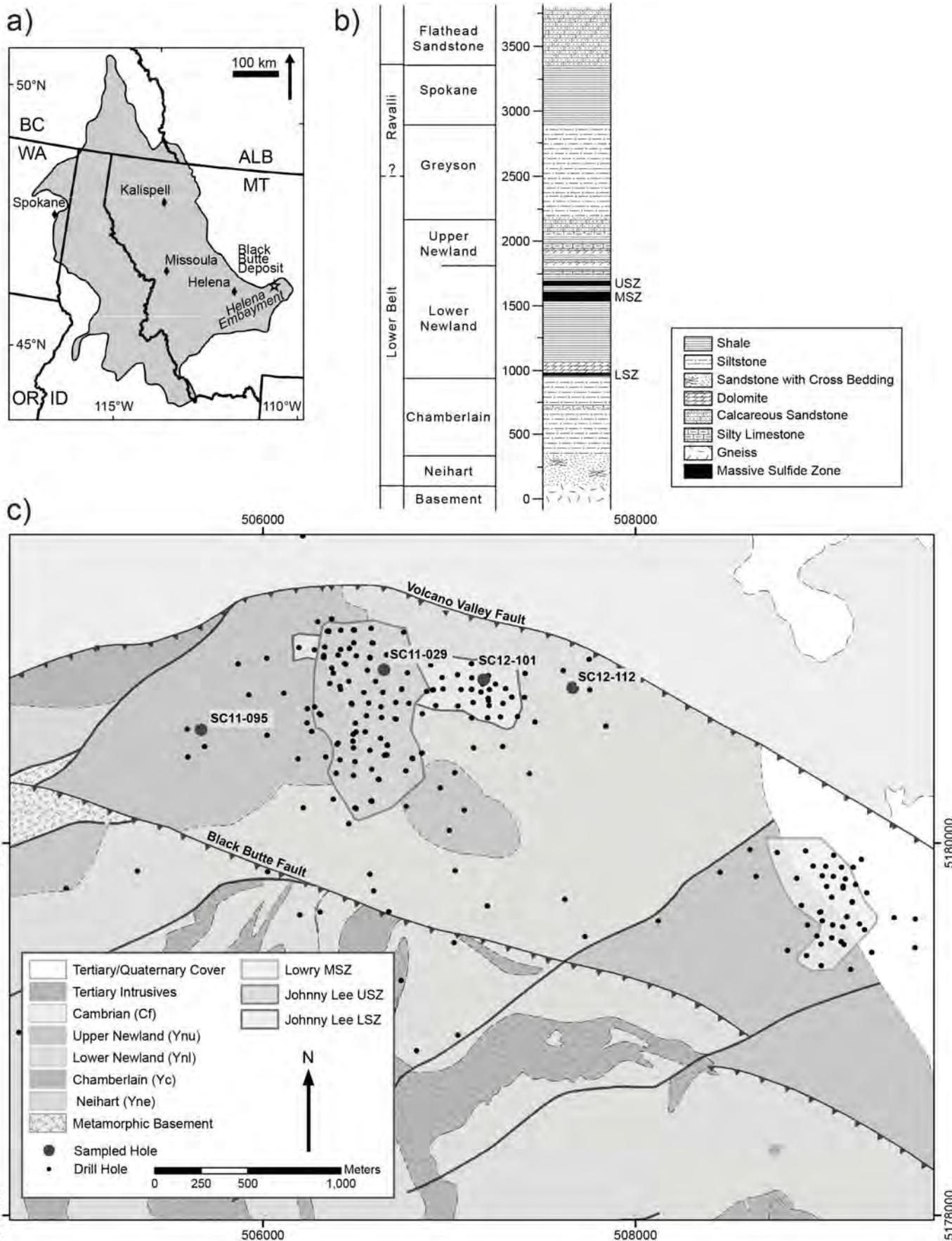
Figure 1. a) Map showing the extent of Belt Supergroup outcrops and the location of the Black Butte Deposit within the Helena Embayment. b) General stratigraphic column of Belt Supergroup strata in the Black Butte Deposit region of the Helena Embayment with height in meters. Note: USZ = Upper Sulfide Zone, MSZ = Middle Sulfide Zone, LSZ = Lower Sulfide Zone. c) Geologic Map of the Black Butte Deposit region with locations of all drill cores drilled by Tintina Resources Inc. and Cominco American Inc. and labels for the drill cores that were sampled in this study.

laminated siltstone and dark shale, which as been assigned by some to the lower Belt Group (Graham and others, 2012; Ross and Villeneuve, 2003; Winston and Link, 1993) and by others to the Ravalli Group (Harrison, 1972; Mudge and others, 1968). The red siltstone and claystone Spokane Formation overlies the Greyson Formation as part of the Ravalli Group. The Empire Formation (Ravalli Group) and the Helena Formation (Middle Belt Carbonate) are also exposed in the Helena Embayment, but these two units are not present in the Black Butte region. Instead, the Spokane is uncomfortably overlain by the Cambrian Flathead Sandstone (fig. 1b; Deiss, 1935).

BLACK BUTTE DEPOSIT

The strata-bound Black Butte Cu-Co-Ag Deposit occurs in the Newland Formation associated with spectacular synsedimentary pyrite-rich horizons that extend over a 25 km by 8 km area, although the main ore mineralization is localized to a fault-bounded block 8 km by 4 km (fig. 1c). Three mineralized zones occur in the lower member, which are separated stratigraphically by approximately 600 m and divided by the Volcano Valley Fault (VVF). They have been named the Johnny Lee Upper Sulfide Zone (USZ), the Lowry Middle Sulfide Zone (MSZ) and the Johnny Lee Lower Sulfide Zone (LSZ) (fig. 1b, 2; Zieg and others, 2013). The MSZ is still being studied and explored, and no samples were collected from it: this study focuses on the relatively well-characterized Johnny Lee deposits.

Petrographic analyses have shown that the mineralization within the USZ and LSZ zones is distinct texturally and mineralogically although both contain abundant early and late diagenetic pyrite and early diagenetic barite (Graham and others, 2012). Much of the early diagenetic pyrite is framboidal or occurs in small fine-grained aggregates including small circular tubes proposed to reflect pyritized microbial filaments (McGoldrick and Zieg, 2004) and chimneys (Present and others, in prep). The early diagenetic pyrite is interpreted to form from fault controlled iron-rich fluids moving through the sedimentary pile and venting at or just below the sediment surface at low temperatures (Graham and others, 2012; White and others, 2014), or from diagenetic transformations of detrital iron oxides under conditions of microbial sulfate reduction in shallow pore fluids (Schieber, 1989c). Based on framboi-

dal textures, a general lack of base metal enrichments, and S isotopes, several authors have extended these arguments to suggest water-column precipitation of pyrite from euxinic bottom waters (Lyons and others, 2000; White and others, 2014).

A secondary diagenetic phase, especially prevalent in the USZ, formed overgrowth rims and coarse cements of pyrite. Sulfur isotope data implies the sulfur for these secondary pyrites was sourced from seawater (Zieg and Leitch, 1999). Some galena and sphalerite phases occurring in the USZ are tied to diagenetic fluids, but these minerals are not prevalent especially when compared to surrounding non-mineralized strata; Pb and Zn are not yet recognized in economic concentrations (Graham and others, 2012; White and others, 2014).

Although many Co-Ni-As-Cu rich sulfides formed relatively early during diagenesis in the USZ, a third mineralization event prior to lithification in both zones created most of the chalcopyrite as well as some chalcocite, bornite, tennenite, cobaltite, and chlorite (LSZ only) while remobilized base metals in the USZ formed siegenite (White and others, 2014). The LSZ contains a higher percentage of chalcopyrite than the USZ, although more mineralization results in a higher tonnage for the USZ. Thermodynamic calculations suggest these hydrothermal fluids were between 125°C and 225°C (White and others, 2014). In late post-lithification events, dolomite and ankerite (USZ only) precipitated within the mineralized zones (Graham and others, 2012).

METHODS

Samples from near both the USZ and LSZ were collected and analyzed to understand the richness in iron mineralization processes in the Newland Formation in this part of the Belt basin (fig 2). Twenty-five quarter-core block samples were collected in July 2013 from 4 different cores housed in the Tintina Resources, Inc. core shed, White Sulphur Springs, MT. Samples were cut using a non-magnetic brass blade into 3 cm by 2 cm billets, and made into polished thin or thick sections for further analyses. Table 1 summarizes the sample data for the 11 samples from 10 quarter-cores that were analyzed in detail.

Non-destructive rock magnetic experiments were
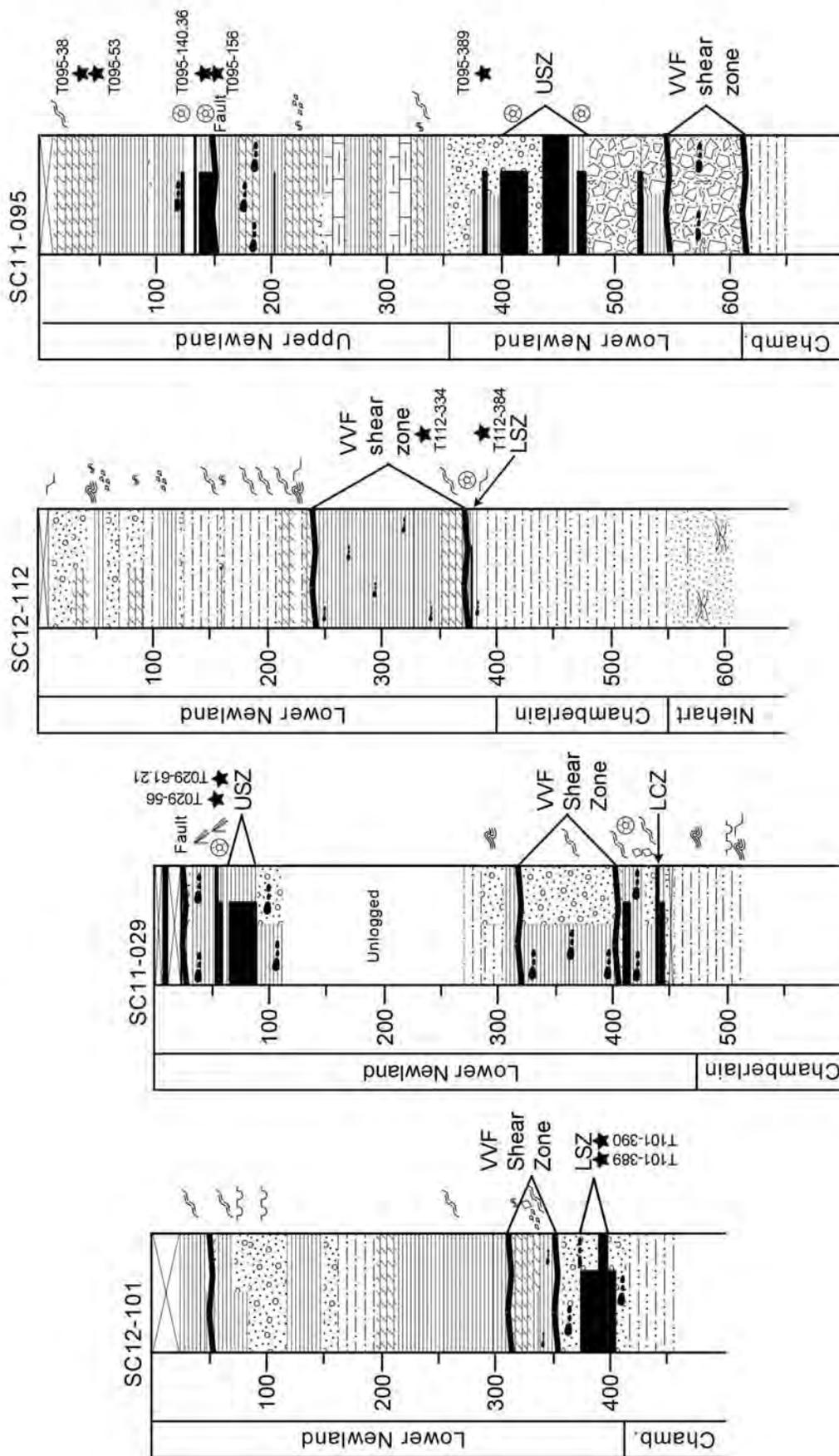
Figure 2. Lithostratigraphic columns of the drill cores from the Black Butte Deposit area examined in this study. Labeled black stars mark the stratigraphic positions of samples analyzed. Cores are not aligned by stratigraphic datum, and core depth is in meters.

59

Table 1: Detailed Sample Data

Sample Name	Drill Core	GPS of Drill Core Collar	Sulfide Zones	Depth of Billet (m)	Stratigraphy	Description
T029-56	SC11-029	N 46° 46' 54.8" W 110° 54' 46.33"	USZ, LSZ	56.475-56.50	Upper Newland right above USZ	Early unfilled circular tube network of iron sulfides 1-4mm in diameter with .5mm thick walls in larger massive sulfide zone
T029-61.21	SC11-029	N 46° 46' 54.8" W 110° 54' 46.33"	USZ, LSZ	61.205-61.235	Upper Newland right above USZ	Early diagenetic barite laths with differential compaction of laminated dolomitic shale with intergrown sub-parallel iron sulfide blebs rimmed with altered barite
T095-38	SC11-095	N 46° 46' 44.76" W 110° 55' 32.7"	USZ	38.70-38.76	Upper Newland far above USZ	Grey laminated silty dolomitic shale with abundant dolomite veins and iron oxide along fracture surfaces
T095-53	SC11-095	N 46° 46' 44.76" W 110° 55' 32.7"	USZ	53.50-53.56	Upper Newland far above USZ	Black laminated dolomitic shale with disseminated iron sulfides
T095-140.36	SC11-095	N 46° 46' 44.76" W 110° 55' 32.7"	USZ	140.375-140.405	Upper Newland	Early diagenetic iron sulfide nodules with differential compaction, laminae, and wavy laminae in larger massive sulfide zone, minor altered barite
T095-156	SC11-095	N 46° 46' 44.76" W 110° 55' 32.7"	USZ	156.815-156.845	Upper Newland	Large iron sulfide bleb within cross-cutting late iron sulfide band in micro-faulted grey laminated dolomitic shale
T095-389	SC11-095	N 46° 46' 44.76" W 110° 55' 32.7"	USZ	389.22-389.255	Upper Newland right above USZ	Grey laminated dolomitic shale with small debris flows and early iron sulfide broken tubes, complete to disaggregated framboids, and fine-grained laminations
T101-389	SC12-101	N 46° 46' 53.15" W 110° 54' 21.17"	LSZ	389.935-389.96	Lower Newland in LSZ	Multiple generations of cross-cutting sulfides (up to 3mm blebs) in heavily recrystallized dolomite and shale within larger massive sulfide zone
T101-390	SC12-101	N 46° 46' 53.15" W 110° 54' 21.17"	LSZ	390.085-390.11	Lower Newland in LSZ	Multiple generations of cross-cutting sulfides in heavily recrystallized dolomite and shale within larger massive sulfide zone
T112-334	SC12-112	N 46° 46' 51.53" W 110° 53' 58.67"	LSZ	334.62-334.64	Lower Newland in Volcano Valley Fault Shear Zone	Black laminated shale with disseminated iron sulfides
T112-384	SC12-112	N 46° 46' 51.53" W 110° 53' 58.67"	LSZ	384.43-334.49	Lower Newland right below LSZ	Sheared black and grey silty shale with intergrown iron sulfide blebs (<1mm) and disseminated iron sulfides

performed on thick sections or billets returned from thin sections for all 11 samples using a 2G Enterprises SQuID magnetometer following the RAPID protocols, and analyzed using the RAPID Matlab (The Mathworks, Inc.) scripts (Kirschvink and others, 2008). The RAPID protocol used here includes measurements of alternating field (AF) demagnetization of the natural remanent magnetization (NRM), anhysteretic remanent magnetization (ARM) acquisition and demagnetization, isothermal remanent magnetization (IRM) acquisition and demagnetization, backfield IRM acquisition, and rotational remanent magnetization (RRM) acquisition and demagnetization. Combined, these measurements quantify fundamental properties that can be used to distinguish different ferromagnetic minerals present in the samples (e.g. Peters and Dekkers, 2003). The destructive rock magnetic technique of KappaBridge thermal susceptibility was measured

on neighboring specimens for one sample using an AGICO MFK1-FA KappaBridge and resulting data were analyzed in Matlab. Ultra-high resolution scanning SQuID Microscopy (UHRSSM) was performed on 5 of the sections with 100 μm pixels after giving them an IRM to locate and image ferromagnetic grains at the microscale.

Additional chemical imaging techniques were employed to study the non-magnetic iron- and sulfur-bearing mineral phases. Transmitted and reflected light microscopy was used to observe petrographic textures and preliminarily identify mineralogy. High-energy synchrotron-based microprobe X-ray ray fluorescence (XRF) at 13500 or 20200 eV was used to map elemental abundances with 35 μm pixels across regions in 10 representative sections at beamline 10-2 at the Stanford Synchrotron Radiation Lightsource. Additionally,

synchrotron-based X-ray near-edge absorption spectroscopy (XANES/XAS) at sulfur energies (2400-2500 eV) was paired with redox imaging at the S K-edge using a new lower energy X-ray microprobe (beamline 14-3) to collect both full spectra and multiple energy maps with 4 μm resolution and determine the mineral chemistry (oxidation state, orbital electronics, type and number of neighbors) while retaining textural information. Differences in the shape of these K-edge absorption spectra allow us to easily distinguish between a wide range of materials (Fleet, 2005; Mosselmans and others, 1995). Paired with end-member XANES spectra, the absorptions at multiple excitation energies in diagnostic regions of the XANES spectrum were collected and fit to create large maps of the mineralogy in samples. Principle component analysis of this multiple energy data was used to target and check for additional minerals. Chalcopyrite and pyrrhotite have similarities in their S K-edge spectra and thus the elemental maps made by high-energy XRF at 10-2 were used to evaluate the abundance of Cu. Synchrotron XANES and XRF analyses were performed at the Stanford Synchrotron Radiation Lightsource. Additional petrographic observations and mineral identifications were made using a ZEISS 1550VP FESEM, scanning electron microscope in the Caltech GPS Division Analytical Facility. This instrument is paired with an Oxford X-Max SDD X-ray Energy Dispersive Spectrometer (EDS) system and was used to determine X-ray spectra of elemental abundance at sub-micron sized spots on 3 thin sections to confirm the presence of chalcopyrite and galena implied from synchrotron data.

RESULTS

Rock magnetic techniques both confirmed previous observations (Graham and others, 2012; White and others, 2014) and highlighted the presence of iron mineralization not previously described in the Newland Formation shales at the Black Butte Deposit.

Rotational Remanent Magnetization (RRM)

The presence of RRM can be used to identify magnetic iron-sulfide phases like pyrrhotite, although the sensitivity limits are not well understood (Snowball, 1997; Thomson, 1990). RRM is acquired during the application of an alternating field of 90 mT (950 Hz) perpendicular to the spin axis of a sample while it is rotating at a given speed. Studies have shown that BRRM (normalized field strength of acquired RRM)

varies with speed and direction of rotation so the sample is rotated clockwise and counterclockwise from 0 to 20 revolutions per second, rps (e.g. Suzuki and others, 2006). Two samples, T029-56 and T095-140.36, indicated strong evidence for magnetic iron sulfides, BRRM $> \pm 20$ μT at 5 rps (Potter and Stephenson, 1986; Suzuki and others, 2006), while the rest of the samples showed no signs of RRM with BRRM ≈ 0 (fig. 3a). Importantly, UHRSSM imaging revealed the ferromagnetic grains in these two samples to be located in epoxy-filled holes (fig. 4cd) created either for standard emplacement of a pyrite grain for textural S isotope analyses (Present and others, in prep) or to fill porous textures when making thin sections, demonstrating that these grains are contaminants (metal alloys can produce strong RRM, Snowball, 1997). Thus, there is no evidence of magnetic iron sulfides in the Newland Formation, including the mineralized zones associated with the Black Butte Deposit.

Coercivity of Remanence Acquisition

The coercivity of remanence acquisition (Hcr'), defined as the magnetic field required to permanently flip half of the magnetic moments in a mineral, is a useful property to differentiate ferromagnetic minerals (Peters and Dekkers, 2003). Overall a measurement of how easily a mineral becomes magnetized, it is determined by taking the derivative of the acquisition of IRM curve and deconvolving the spectra into distinct peaks of different field strengths, which are the different coercivities of the mineral assemblage (Heslop and others, 2002; Robertson and France, 1994). Goethite is easily identified with coercivities over 1000 mT, and the range of 140-800 mT is unique for hematite. However, extensive data collection has shown that the coercivity ranges for hematite, magnetite, titanomagnetite, greigite and pyrrhotite overlap between 16-140 mT—though the averages of hematite (270 mT), pyrrhotite (53 mT), greigite (75 mT) are higher than those for magnetite and titanomagnetite (30 mT). Thus mineral identifications solely using Hcr' for identification have some margin of error and benefit from additional analyses (table 2).

Notably, three groups of ferromagnetic mineralogy can be separated based on Hcr' and stratigraphic/lithologic information (fig. 3b). All of the samples collected far outside the strongly mineralized sulfide zones (T095-38, T095-53, T112-334, T112-384) primarily
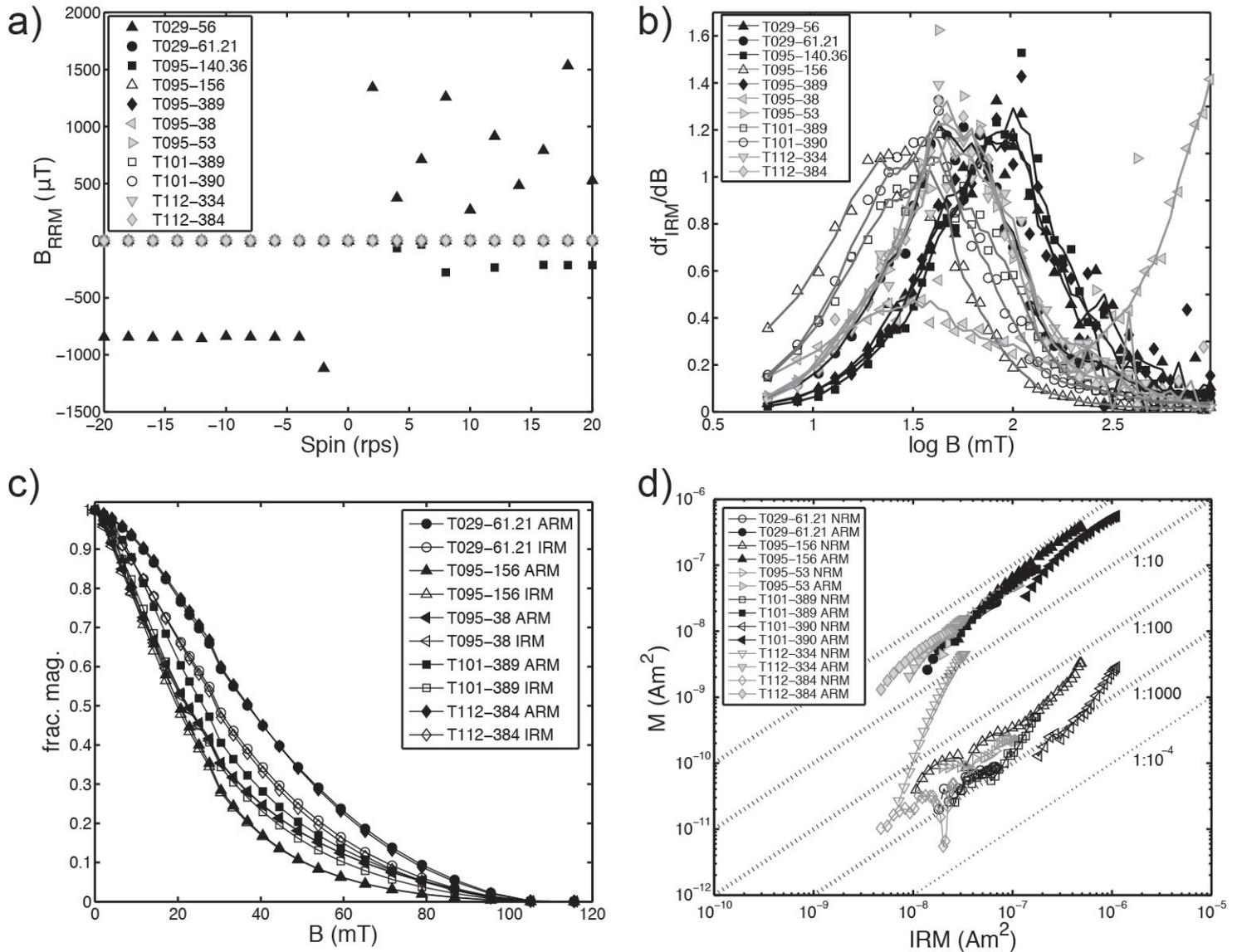
Figure 3. Rock magnetic data from shale samples of the Newland Formation. a) Rotational remanent magnetization (RRM) data to assess the presence or absence of magnetic iron sulfide phases. Negative spin speed indicated counter-clockwise rotation around the spin axis when the perpendicular alternating field is applied. All 11 samples are plotted, but only 2 of the samples are clearly visible since most of the samples have BRRM ≈ 0 at all spin speeds. b) Data showing the derivative of the isothermal remanent magnetization (IRM) of all samples to determine the coercivity of remanence (Hcr') and from this information the ferromagnetic mineralogy. The applied field (B, x-axis) at the peaks of the spectra is the Hcr'. c) Results of representative samples from the Lowrie-Fuller test to inform domain state and grain size based on the relative strength of the IRM vs. the ARM curves as measured by the fraction of total magnetization (frac. mag., Y-axis) when a specific demagnetizing field is applied (B, x-axis). d) Results from the Fuller test to provide insight into the origins (detrital, chemical, thermal) of magnetization based on the ratio of the NRM (y-axis) to IRM (x-axis). The ratio of ARM:IRM is also plotted using the same axes.

contain finely disseminated pyrite and show very similar mid-coercivity peaks interpreted to be magnetite. Sample T095-38 also shows a striking high-coercivity goethite peak; this sample contains fractures mineralized with oxides seen in hand sample and described in the core log for this stratigraphic height. Sample T029-61.21 has early diagenetic pyrite textures with minimal secondary recrystallization and contains the same magnetite mid-coercivity peak as the four samples described above. The other three samples exhibiting early diagenetic textures (T029-56, T029-140.36,

T095-389), including the two samples with known ferromagnetic contamination, have slightly higher coercivity spectra. While T095-389 did not show RRM, it does have an epoxied hole with a standard, which could be contaminated by a ferromagnetic mineral/ alloy similar to samples T029-140.36 and T095-389. Therefore we interpret the characteristic slightly higher Hcr' peak of these three samples to be due to contamination and not representative of early textures. Lastly, three samples display multiple generations of sulfide-bearing minerals including late displacive and

Table 2: Mineralogical Identifications from Samples of Newland Formation from Black Butte Deposit

Sample name	Bulk Techniques				S XANES and EDS							High-Energy XRF			
	Mag	Goe	Pyr	Cont	Py	Pyr	FerS	CuPy	Cov	Gal	SO4	AsPb	Cu	Zn	Ni
T029-56				X	X*			X*	X*	X*		X	X	t	
T029-61.21	X				X						X	t	X	X	
T095-38	X	X										X	X	X	t
T095-53	X				X						X	X	X	X	t
T095-140.36				X								X			
T095-156	X				X							t			
T095-389				X	X*			X*	X*	X	X	X			
T101-389	X				X		X	X				X	X	X	
T101-390	X											X	X	t	
T112-334	X				X						X	X	X	X	t
T112-384	X											t	t		t

Abbreviations: XANES = X-ray Absoption Near Edge Spectroscopy, EDS = X-ray Energy Dispersive Spectroscopy, XRF = X-ray Fluorescence, Mag = Magnetite, Goe = Goethite, Pyr = Pyrrhotite, Cont = Contamination, Py = Pyrite, FerS =Ferric Disulfide, CuPy = Chalcopyrite, Cov = Covellite, Gal = Galena, SO4 = Sulfate often Barite, AsPb = Arsenic and/or Lead

For XRF, t=trace, X = important mineral constituent

* Data from Present et al., in prep based on reflected light petrography

replacive textures (T095-156, T101-389, T101-390). These samples show a range of mid- to low-coercivity spectra suggesting larger grain size and/or multi-domain magnetite (Peters and Dekkers, 2003).

Lowrie-Fuller Test

To further examine the grain size and magnetic domain state, we employed a rock magnetic technique called the Lowrie-Fuller test—a measure of ferromagnetic grain size based on the relative stability of IRM versus ARM to applied demagnetizing AF (Lowrie and Fuller, 1971; Xu and Dunlop, 1995). In single domain grains, ARM is more stable and less easily demagnetized than IRM, while in larger multidomain grains, IRM is more stable and less easily demagnetized using AF than ARM. Although the exact physics are poorly understood, if the ARM is consistently stronger than the IRM then single domain or pseudo single domain (<10 μm) particles probably represent the majority of the magnetized minerals in a sample. While most of the samples appear to contain single-domain or pseudo-single domain particles, T095-156 (which had low coercivity spectra) does contain multi-domain grains (fig. 3c). T095-38 also is shown to contain multi-domain grains, but this sample contains goethite, which would bias the Lowrie-Fuller test toward multi-domain results. From this data, multi-domain magnetite is more common in samples with replacive textures

suggesting it could have formed from recrystallization or authigenic precipitation—this can be tested if it shows a chemical remanent magnetization.

Fuller Test of NRM

Magnetite appears to be the primary ferromagnetic component in the majority of the Newland Formation shale samples. As a result, we can apply a useful rock magnetic experiment called the Fuller Test of NRM to determine if the magnetization carried by the magnetite is detrital or chemical in origin. This test uses the ratio of the NRM:IRM compared to empirical calibrations and synthetic ARM:IRM relationships of a given sample (Fuller and others, 1988; Fuller and others, 2002). Empirical calibrations on rocks with magnetite as the primary ferromagnetic mineral suggest that the weak NRM:IRM ratios of 1:1000 occur in sedimentary rocks with detrital remanent magnetization formed during primary deposition and ratios of 1:10 represents chemical remanent magnetization when magnetite has grown in situ or authigenically in a sample (Fuller and others, 2002). The ARM:IRM curve is used for comparison to demonstrate which changes in the shape of the curve are characteristic of the sample. Most samples of the Newland Formation show an NRM:IRM ratio of 1:1000, which is consistent with weak detrital remanent magnetization (fig. 3d). T112-334 shows indication of chemical remanent magneti-
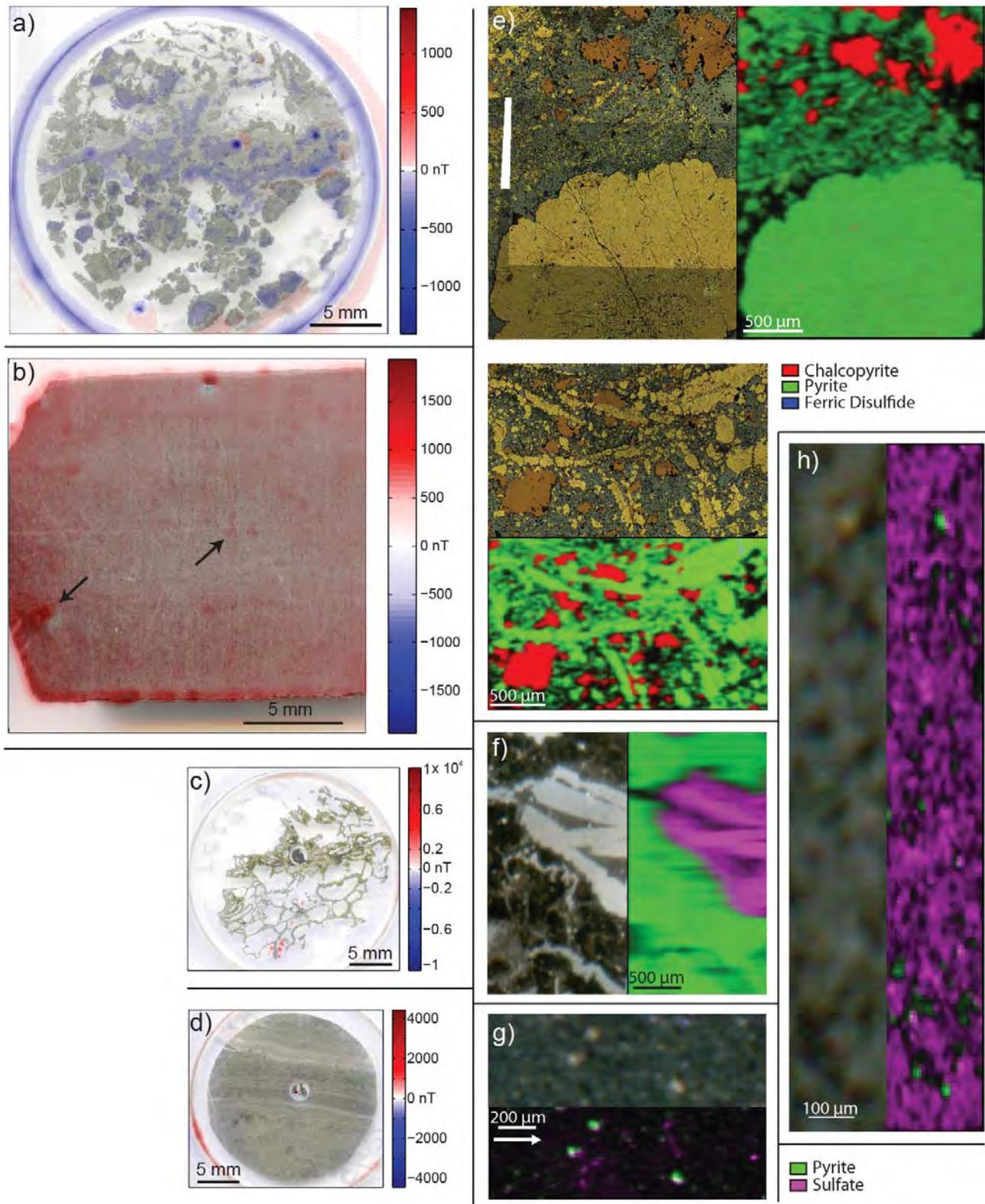
Figure 4. Parts a-d show UHRSSM magnetic microscopy images of ferromagnetic minerals. Hot and cool colors reflect magnetic vectors out of and into the page, respectively. e) Map of T101-389 showing scattered dipoles focused in fine-grained regions. f) Scattered dipoles including some that trend with post-depositional crosscutting features, such as pointed out by arrows, in T112-334. g) Image of T029-56 showing dipoles in epoxied holes around iron sulfide tube network that reflect contaminant phases introduced via standard preparation. h) Map of T095-140.36 showing single strong dipole in epoxied drill hole with pyrite standard that reflect contaminant phases introduced during preparation. Parts e-h show paired reflected light microscopy or photograph on the left-top and multiple-energy maps fit to minerals using end-member S XANES spectra on the right-bottom. Samples are oriented with correct up direction; an arrow marks the up direction for part c a) Two mapped regions of T101-389 contain multiple generations of sulfide phases including chalcopyrite, pyrite, and a unique ferric disulfide. b) Map of T026-61.21 with barite laths surrounded by early diagenetic pyrite in layers. c) Disseminated pyrite grains with associated sulfate and distinct sulfate domains in T095-53. d) Disseminated pyrite with low abundance sulfur in matrix in T112-334. Scale bar provided for each image or image pair.

zation, in which magnetite is an authigenic phase that either grew during early diagenesis or during a later diagenetic mineralization. UHRSSM maps showed the locations of disperse dipoles of ferromagnetic grains throughout samples in fine-grained material, located close to and far from secondary cross-cutting textures, consistent with a detrital origin (fig. 4a,b). However, due to the sub-micron size of these grains, the ferromagnetic minerals in the regions with dipoles could not be visualized via petrography.

KappaBridge Thermal Susceptibility

To further study the magnetite, a neighboring sample from T101-389 was used for destructive thermal susceptibility experiments using a KappaBridge. Powdered rock was slowly heated from -190°C to 700°C and then cooled to 40°C while the susceptibility from a weak induced field was measured at 20 second intervals. Susceptibility measures the ability of a sample to be magnetized in the presence of an applied field. Thus it is a magnetic measurement that integrates the entire assemblage of minerals in a sample, although ferromagnetic minerals usually dominate the signal. Changes in susceptibility during heating and cooling are produced by mineralogical transformations within the sample. A drop in susceptibility at 580°C indicates the presence of magnetite as it becomes paramagnetic at its Curie temperature (fig. 5a). The low-temperature Verwey transition typical for magnetite at -150°C as it transforms from weakly magnetic monoclinic magnetic structure and to ferromagnetic cubic structure was

not observed in this sample; either it was suppressed due to low abundance with other phases dominating the signal, or the magnetite contains a small weight percent titanium (Kozłowski and others, 1996; Moskowitz and others, 1998). A slight drop in susceptibility at 80°C is suggestive of goethite decomposing and reacting with sulfur to form pyrite or decomposition of titanomagnetite (Charilaou and others, 2011; Minyuk and others, 2013). Although the typical pyrite/chalcopyrite decomposition peak to magnetite is not seen (Li and Zhang, 2005; Minyuk and others, 2013), some new magnetite and a substantial amount of pyrrhotite were formed after heating to 700°C in an argon atmosphere based on the fact that the cooling curves increase in susceptibility during cooling with distinct peaks at 580°C and at 320°C the respective Curie temperatures for those minerals (fig. 5b). The creation of these minerals suggests there were non-magnetic iron sulfides in these samples that transformed into magnetic minerals during the heating process.

X-Ray Spectroscopy

Iron sulfide phases were visually identified in all of the samples using light microscopy. We used X-ray spectroscopy, specifically XANES and XRF, to evaluate the exact chemical composition and crystal structure of these phases (table 2). Ferrous disulfide was identified as the major sulfide-bearing phase in all the samples (fig. 6). The ferrous disulfide minerals marcasite and pyrite have similar S K-edge spectra
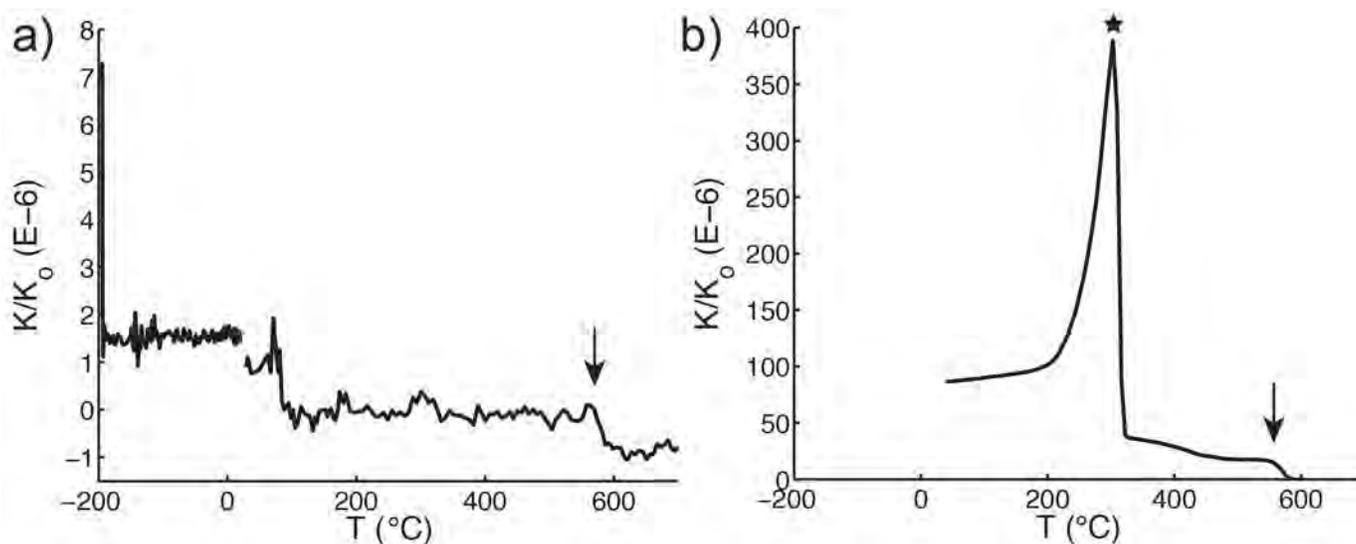
Figure 5. KappaBridge results for a representative shale sample, T101-389. a) Magnetic susceptibility during heating from -190°C to 700°C. b) Magnetic susceptibility during cooling from 700°C to 23°C. Note the different y-axis scale as there is increased susceptibility during this cooling phase. Data are normalized to the blank, an empty specimen holder measurement. Arrows mark the Curie temperature of magnetite (580°C) while the star marks the Curie temperature of pyrrhotite (320°C).

Figure 6. Synchrotron S K-edge XANES spectra for phases identified in all samples. An unnamed unique mineral, a ferric disulfide not previously found in natural samples, is identified based off its K-edge spectra, which shows Fe+3 bonding with di-sulfide valence sulfur.

highlight interesting patterns in base metal mineralization. Some replacive pyrite grains contain greater amounts of As, Pb, Zn, or Cu (fig. 7 d,e,g), while other regions hosted chalcophile metals as dominant cations in sulfide phases like Cu in chalcopyrite (fig. 7a-f,h). Microprobe X-ray spectroscopy paired mapping capabilities, coupled with traditional petrographic and bulk chemical techniques, provide an exciting new tool for mineral analysis opening new avenues for inquiry into trace metal abundances, redox states and gradients, and mineral phase identification.

DISCUSSION AND CONCLUSIONS

Bulk rock magnetic techniques employed in this study confirm the absence of pyrrhotite in shales of the Newland Formation near the Black Butte Deposit, in contrast to its ubiquitous presence in correlative units at higher metamorphic grades to the northwest (Slotznick and others, in review). This result confirms that these rocks have not been heated to very high temperatures, and while hydrothermal fluids did cause overprinting and recrystallization of sulfide phases, no pyrrhotite was formed with this mineralization. This is important for bulk geochemical studies such as iron speciation (Planavsky and others, 2011) because pyrrhotite may be misplaced in sequential chemical extraction with the magnetite fraction and/or result in incorrect iron calculations due to its unique chemistry during the pyrite extraction—both could make a basin appear more ferruginous than it was by incorrectly identifying the iron mineralogy (Asael and others, 2013; Schumann and others, 2012)). Samples collected far outside the massive sulfide mineralization zones contain early diagenetic disseminated pyrite grains (Schieber, 1989a); copper, zinc, and lead sulfides are rare in these areas but their presence still signals some mineralization extends beyond the regions of economic interest. Sulfide phases tied to these hydrothermal fluids should be taken into account when using Belt strata to interpret the ancient redox conditions and processes operating in the Belt Basin, because these phases show iron was mobile and likely advected from elsewhere in the sediment pile. The hydrothermal fluids could have also sourced iron for some of the magnetite present in the samples and/or been responsible for recrystallization processes.

The identification of magnetite in Newland Formation shales provides important insights into the redox

using XANES and can only be readily distinguished by the Fe L-edge (Mosselmans and others, 1995) or X-ray diffraction, which were not measured here. However, petrography shows that the disulfides phases present in these samples are pyrite. Chalcopyrite was observed as a major component of T101-389 (fig. 4e, 6). Sulfate salts were also identified in many of the samples including laths of barite that show differential compaction of sedimentary laminae (fig. 4f, 6). However, in the samples with disseminated pyrite, small domains of sulfate (10-20 μm in size) were found both alone and associated with pyrite, suggesting some of the sulfate minerals could be iron sulfates instead of barite (fig. 4g,h, 6). EDS and high-energy XRF maps were used to confirm the presence of chalcopyrite (as opposed to pyrrhotite); however, the XRF maps also

Figure 7. High-Energy XRF maps of metal abundances (right-bottom) shown alongside a light scan of a given sample in thick or thin section (left-top). Samples are oriented with correct up direction; an arrow marks the up direction for part e. a) Unfilled tubular network of iron sulfide cements with small inclusions of Pb- and Cu-bearing minerals in T029-56. b) Early diagenetic and recrystallized barite containing trace Sr with sub-parallel pyrite blebs and small Cu-bearing minerals in T029-61.21. c) Disseminated pyrite with distinct Zn and Cu minerals that show mineralization associated both along lamination and crosscutting features in T112-334. d) Multiple generations of sulfides including pyrite and chalcopyrite with As- and Pb-rich grains, zones of finely disseminated grains, and zones within euhedral grains in T101-389 e) Closer look at multiple generations of iron sulfides and chalcopyrite with As- and Pb-rich grains and zones in larger grains in T101-390. f) Dolomite vein containing iron oxide with As-, Pb-, and Zn-rich minerals associated with smaller non-dolomitized fractures and/or laminations in T095-38. g) Vertical dolomitic veins cut Pb-rich pyrite bleb within a crosscutting pyrite aggregate in a laminated dolomitic shale in T095-156. h) Intraformational detrital iron sulfides parallel to, and deforming shale laminates with small amounts of galena in T095-389.

character and mode of iron delivery in this part of the Belt Basin. Rock magnetic experiments indicate that magnetite is primarily detrital in origin, with limited evidence for authigenic magnetite in some samples. Though pyrite is commonly the most abundant iron-bearing mineral present in these diagenetically stabilized lithologies, detrital magnetite represents an important sedimentary vector for iron delivery to this basin that is not a direct measure of redox conditions in seawater. Furthermore, detrital iron oxides might bias iron speciation data toward compositions that appear more anoxic and ferruginous (Planavsky and others, 2011); during deposition Belt Basin waters could have either been more oxic or more euxinic depending on the relative abundances of these oxides and other iron-bearing minerals. Petrography and X-ray imaging reveal that pyrite is ever-present as small framboids and disseminated grains exhibiting textures that are consistent with the formation of much of this pyrite in the water column or in sediments during early diagenesis (Graham and others, 2012; Schieber, 1989a; Wilkin and others, 1996). We speculate that detrital iron oxides were an important source of reactive iron for early pyrite formation (e.g. Canfield and Berner, 1987; Reynolds and others, 2000; Schieber, 1989c). Many samples (not just limited to economically meaningful sulfide mineralization zones) show additional sulfide phases in late diagenetic textures that mark iron sourced by hydrothermal fluids. If iron sources did not limit early pyrite formation more broadly, perhaps this was limited by the abundance of H2S in the bottom water, bacterial sulfate reduction/sulfur oxidation rates, and/or sedimentation rates. More work is needed to better understand the interplay between these factors (Present and others, in prep), but what is clear at present is that we do not see clear evidence for the ferruginous water column conditions during the depositional of Newland Formation shales put forward on the basis of iron speciation data (Planavsky and others, 2011).

Based on our observations, we hypothesize that bottom waters in Helena Embayment during the deposition of the Newland Formation were suboxic or possibly euxinic (Gellatly and Lyons, 2005; Lyons and others, 2000), and that detrital fluxes played an important role in delivery of iron into the Helena Embayment, much of which was transformed into pyrite during sulfate reduction associated with early diagenesis of these organic-rich sediments (Lyons and others, 2000; Strauss and Schieber, 1990). This is a similar mode of iron deposition and pyrite production today in modern euxinic basins and anoxic pore waters in marine sediments (e.g. Berner, 1984), and implies a degree of continuity of redox conditions and processes operating in large sedimentary basins over the past one and a half billion years.

ACKNOWLEDGMENTS

REFERENCES

Asael, D., Tissot, F. L., Reinhard, C. T., Rouxel, O., Dauphas, N., Lyons, T. W., Ponzevera, E., Liorzou, C., and Chéron, S., 2013, Coupled molybdenum, iron and uranium stable isotopes as oceanic paleoredox proxies during the Paleoproterozoic Shunga Event: Chemical Geology, v. 362, p. 193-210.

Berner, R. A., 1984, Sedimentary pyrite formation: an update: Geochimica et Cosmochimica Acta, v. 48, no. 4, p. 605-615.

Brocks, J. J., Buick, R., Summons, R. E., and Logan, G. A., 2003, A reconstruction of Archean biological diversity based on molecular fossils from the 2.78 to 2.45 billion-year-old Mount Bruce Supergroup, Hamersley Basin, Western Australia: Geochimica et Cosmochimica Acta, v. 67, no. 22, p. 4321-4335.

Canfield, D., 1998, A new model for Proterozoic ocean chemistry: Nature, v. 396, no. 6710, p. 450-453.

Canfield, D. E., and Berner, R. A., 1987, Dissolution and pyritization of magnetite in anoxie marine

sediments: Geochimica et Cosmochimica Acta, v. 51, no. 3, p. 645-659.

Charilaou, M., Löffler, J., and Gehring, A., 2011, Fe–Ti-O exchange at high temperature and thermal hysteresis: Geophysical Journal International, v. 185, no. 2, p. 647-652.

Cloud, P. E., 1968, Atmospheric and Hydrospheric Evolution on the Primitive Earth: Science, v. 160, no. 3829, p. 729-736.

Craig, J. R., and Vokes, F. M., 1993, The metamorphism of pyrite and pyritic ores: an overview: Mineralogical Magazine, v. 57, no. 1, p. 3-18.

Deiss, C., 1935, Cambrian-Algonkian unconformity in western Montana: Geological Society of America Bulletin, v. 46, no. 1, p. 95-124.

Duke, E. F., and Lewis, R. S., 2010, Near infrared spectra of white mica in the Belt Supergroup and implications for metamorphism: American Mineralogist, v. 95, no. 7, p. 908-920.

Embley, T. M., and Martin, W., 2006, Eukaryotic evolution, changes and challenges: Nature, v. 440, no. 7084, p. 623-630.

Fleet, M. E., 2005, XANES spectroscopy of sulfur in earth materials: The Canadian Mineralogist, v. 43, no. 6, p. 1811-1838.

Fuller, M., Kidane, T., and Ali, J., 2002, AF demagnetization characteristics of NRM, compared with anhysteretic and saturation isothermal remanence: an aid in the interpretation of NRM: Physics and Chemistry of the Earth, v. 27, no. 25-31, p. 1169-1177.

Gellatly, A. M., and Lyons, T. W., 2005, Trace sulfate in mid-Proterozoic carbonates and the sulfur isotope record of biospheric evolution: Geochimica et Cosmochimica Acta, v. 69, no. 15, p. 3813-3829.

Graham, G., Hitzman, M. W., and Zieg, J., 2012, Geologic Setting, Sedimentary Architecture, and Paragenesis of the Mesoproterozoic Sediment-Hosted Sheep Creek Cu-Co-Ag Deposit, Helena Embayment, Montana: Economic Geology, v. 107, no. 6, p. 1115-1141.

Hall, A. J., 1986, Pyrite-pyrrhotine redox reactions in nature: Mineralogical Magazine, v. 50, p. 223-229.

Harrison, J. E., 1972, Precambrian Belt basin of north-western United States: Its geometry, sedimentation, and copper occurrences: Geological Society of America Bulletin, v. 83, no. 5, p. 1215-1240.

Heslop, D., Dekkers, M., Kruiver, P., and Van Oorschot, I., 2002, Analysis of isothermal remanent magnetization acquisition curves using the expectation-maximization algorithm: Geophysical Journal International, v. 148, no. 1, p. 58-64.

Holland, H. D., 1984, The chemical evolution of the atmosphere and oceans, Princeton University Press.

Holland, H.D., 2006, The oxygenation of the atmosphere and oceans: Philosophical Transactions of the Royal Society B: Biological Sciences, v. 361, no. 1470, p. 903-915.

Horodyski, R. J., Winston, D., and Whipple, J. W., 1989, Paleontology of the middle Proterozoic belt supergroup, *in* Winston, D., Horodyski, R. J., and Whipple, J. W., eds., Middle Proterozoic Belt Supergroup, Western Montana: Great Falls, Montana to Spokane, Washington: 28th International Geological Congress, Field Trip Guidebook T334, p. 7-26.

Kirschvink, J. L., Kopp, R. E., Raub, T. D., Baumgartner, C. T., and Holt, J. W., 2008, Rapid, precise, and high-sensitivity acquisition of paleomagnetic and rock-magnetic data: Development of a low-noise automatic sample changing system for superconducting rock magnetometers: Geochemistry Geophysics Geosystems, v. 9, no. 5.

Knoll, A. H., Javaux, E. J., Hewitt, D., and Cohen, P., 2006, Eukaryotic organisms in Proterozoic oceans: Philosophical Transactions of the Royal Society B: Biological Sciences, v. 361, no. 1470, p. 1023-1038.

Kozłowski, A., Kakol, Z., Kim, D., Zalecki, R., and Honig, J., 1996, Heat capacity of Fe 3-α M α O 4 (M= Zn, Ti, $0 \leqslant \alpha \leqslant 0.04$): Physical Review B, v. 54, no. 17, p. 12093.

Li, H. Y., and Zhang, S. H., 2005, Detection of Mineralogical Changes in Pyrite Using Measurements of Temperature-Dependence Susceptibilities: Chinese Journal of Geophysics, v. 48, no. 6, p. 1454-1461.

Lowrie, W., and Fuller, M., 1971, Alternating field demagnetization characteristics of multidomain thermoremanent magnetization in magnetite:

Journal of Geophysical Research, v. 76, no. 26, p. 6339-&.

Luepke, J. J., 1999, Goechemical trends in shales of the Belt Supergroup, Northwestern US: a marine model for the evolution of the Mesoproterozoic weatern Laurentian Margin [M.S. thesis: University Missouri-Columbia, 133 p.

Luepke, J. J., and Lyons, T. W., 2001, Pre-Rodinian (Mesoproterozoic) supercontinental rifting along the western margin of Laurentia: geochemical evidence from the Belt-Purcell Supergroup: Precambrian Research, v. 111, no. 1, p. 79-90.

Lyons, T. W., Luepke, J. J., Schreiber, M. E., and Zieg, G. A., 2000, Sulfur geochemical constraints on Mesoproterozoic restricted marine deposition: lower Belt Supergroup, northwestern United States: Geochimica et Cosmochimica Acta, v. 64, no. 3, p. 427-437.

McGoldrick, P., and Zieg, J., Massive microbes from the Mesoproterozoic of Montana, *in* Proceedings 17th Australia Geological Geological Convention Hobart, Australia, 2004, Volume 73, p. 100.

Minyuk, P., Tyukova, E., Subbotnikova, T., Kazansky, A. Y., and Fedotov, A., 2013, Thermal magnetic susceptibility data on natural iron sulfides of northeastern Russia: Russian Geology and Geophysics, v. 54, no. 4, p. 464-474.

Moreau, M., Ader, M., and Enkin, R., 2005, The magnetization of clay-rich rocks in sedimentary basins: low-temperature experimental formation of magnetic carriers in natural samples: Earth and Planetary Science Letters, v. 230, no. 1, p. 193-210.

Moskowitz, B. M., Jackson, M., and Kissel, C., 1998, Low-temperature magnetic behavior of titanomagnetites: Earth and Planetary Science Letters, v. 157, no. 3, p. 141-149.

Mosselmans, J., Pattrick, R., Van der Laan, G., Charnock, J., Vaughan, D., Henderson, C., and Garner, C., 1995, X-ray absorption near-edge spectra of transition metal disulfides FeS2 (pyrite and marcasite), CoS2, NiS2 and CuS2, and their isomorphs FeAsS and CoAsS: Physics and Chemistry of Minerals, v. 22, no. 5, p. 311-317.

Mudge, M. R., Erickson, R. L., Kleinkopf, M. D., and Zartman, R. E., 1968, Reconnaissance geology, geophysics, and geochemistry of the southeastern

part of the Lewis and Clark Range, Montana.

Nelson, W. H., 1963, Geology of the Duck Creek Pass quadrangle, Montana, U.S. Geological Survey Bulletin, Volume 1121-J, p. 56.

Peters, C., and Dekkers, M., 2003, Selected room temperature magnetic parameters as a function of mineralogy, concentration and grain size: Physics and Chemistry of the Earth, Parts A/B/C, v. 28, no. 16, p. 659-667.

Planavsky, N. J., McGoldrick, P., Scott, C. T., Li, C., Reinhard, C. T., Kelly, A. E., Chu, X., Bekker, A., Love, G. D., and Lyons, T. W., 2011, Widespread iron-rich conditions in the mid-Proterozoic ocean: Nature, v. 477, no. 7365, p. 448-451.

Potter, D., and Stephenson, A., 1986, The detection of fine particles of magnetite using anhysteretic and rotational remanent magnetizations: Geophysical Journal International, v. 87, no. 2, p. 569-582.

Poulton, S. W., and Canfield, D. E., 2005, Development of a sequential extraction procedure for iron: implications for iron partitioning in continentally derived particulates: Chemical Geology, v. 214, no. 3, p. 209-221.

Poulton, S.W., and Canfield, D.E., 2011, Ferruginous conditions: a dominant feature of the ocean through Earth's history: Elements, v. 7, no. 2, p. 107-112.

Present, T. M., Slotznick, S. P., Creveling, J. R., Bergmann, K. D., Meyers, C. E., Williford, K. H., Fischer, W. W., Knoll, A. H., Grotzinger, J. P., and A., Z. G., in prep, Porous macroscopic pyrite networks in a Mesoproterozoic SEDEX massive sulfide deposit.

Raub, T., Johnson, S. C., and Raub, T. D., 2012, Rock magnetic detection of the pyrite-to-pyrrhotite reduction: applications to hydrocarbon maturity, mineral resources, and biogeochemistry, American Geophysical Union, Fall Meeting: San Francisco, CA, p. GP34A-08.

Raymond, J., and Blankenship, R. E., 2004, Biosynthetic pathways, gene replacement and the antiquity of life: Geobiology, v. 2, no. 4, p. 199-203.

Reynolds, R. L., Rosenbaum, J. G., Sweetkind, D. S., Lanphere, M. A., Roberts, A. P., and Verosub, K. L., 2000, Recognition of primary and diagenetic magnetizations to determine the magnetic polarity record and timing of deposition of the moat-fill

rocks of the Oligocene Creede Caldera, Colorado: Geological Society of America Special Papers, v. 346, p. 77-93.

Robertson, D., and France, D., 1994, Discrimination of remanence-carrying minerals in mixtures, using isothermal remanent magnetisation acquisition curves: Physics of the Earth and Planetary Interiors, v. 82, no. 3, p. 223-234.

Ross, G. M., and Villeneuve, M., 2003, Provenance of the Mesoproterozoic (1.45 Ga) Belt basin (western North America): Another piece in the pre-Rodinia paleogeographic puzzle: Geological Society of America Bulletin, v. 115, no. 10, p. 1191-1217.

Schieber, J., 1989a, Facies and origin of shales from the mid-Proterozoic Newland Formation, Belt Basin, Montana, USA: Sedimentology, v. 36, no. 2, p. 203-219.

Schieber, J., 1989b, The origin of the Neihart Quartzite, a basal deposit of the Mid-Proterozoic Belt Supergroup, Montana, USA: Geological Magazine, v. 126, no. 03, p. 271-281.

Schieber, J., 1989c, Pyrite mineralization in microbial mats from the mid-Proterozoic Newland Formation, Belt Supergroup, Montana, USA: Sedimentary geology, v. 64, no. 1, p. 79-90.

Schumann, R., Stewart, W., Miller, S., Kawashima, N., Li, J., and Smart, R., 2012, Acid–base accounting assessment of mine wastes using the chromium reducible sulfur method: Science of the Total Environment, v. 424, p. 289-296.

Slotznick, S. P., Winston, D., Webb, S. M., Kirschvink, J. L., and Fischer, W. W., in review, Iron mineralogy and redox conditions during deposition of the Mesoproterozoic Appekunny Formation, Belt Supergroup, Glacier National Park Geological Society of America Special Paper.

Snowball, I. F., 1997, The detection of single-domain greigite (Fe3S4) using rotational remanent magnetization (RRM) and the effective gyro field (Bg): mineral magnetic and palaeomagnetic applications: Geophysical Journal International, v. 130, no. 3, p. 704-716.

Strauss, H., and Schieber, J., 1990, A sulfur isotope study of pyrite genesis: the Mid-Proterozoic Newland Formation, Belt Supergroup, Montana: Geochimica et Cosmochimica Acta, v. 54, no. 1, p. 197-204.

Stüeken, E. E., 2013, A test of the nitrogen-limitation hypothesis for retarded eukaryote radiation: nitrogen isotopes across a Mesoproterozoic basinal profile: Geochimica et Cosmochimica Acta, v. 120, p. 121-139.

Suzuki, Y., Kopp, R. E., Kogure, T., Suga, A., Takai, K., Tsuchida, S., Ozaki, N., Endo, K., Hashimoto, J., and Kato, Y., 2006, Sclerite formation in the hydrothermal-vent "scaly-foot" gastropod—possible control of iron sulfide biomineralization by the animal: Earth and Planetary Science Letters, v. 242, no. 1, p. 39-50.

Thomson, G. F., 1990, The anomalous demagnetization of pyrrhotite: Geophysical Journal International, v. 103, no. 2, p. 425-430.

Walcott, C. D., 1899, Pre-Cambrian fossiliferous formations: Geological Society of America Bulletin, v. 10, no. 1, p. 199-244.

Walter, M., Oehler, J. H., and Oehler, D. Z., 1976, Megascopic algae 1300 million years old from the Belt Supergroup, Montana: a reinterpretation of Walcott's Helminthoidichnites: Journal of Paleontology, p. 872-881.

White, J., Gammons, C. H., and Zieg, G., 2014, Paragenesis of cobalt and nickel in the Black Butte shale-hosted copper deposit, Belt Basin, Montana, USA: Mineralium Deposita, v. 49, no. 3, p. 335-351.

Wilkin, R., Barnes, H., and Brantley, S., 1996, The size distribution of framboidal pyrite in modern sediments: an indicator of redox conditions: Geochimica et Cosmochimica Acta, v. 60, no. 20, p. 3897-3912.

Winston, D., and Link, P., 1993, Middle Proterozoic rocks of Montana, Idaho and eastern Washington: the Belt Supergroup: Precambrian: Conterminous US: The Geology of North America, v. 2, p. 487-517.

Xu, S., and Dunlop, D. J., 1995, Toward a better understanding of the Lowrie-Fuller test: Journal of Geophysical Research: Solid Earth (1978–2012), v. 100, no. B11, p. 22533-22542.

Zieg, G., and Leitch, C., The geology of the Sheep Creek copper deposit, Meagher County, Montana, *in* Proceedings Belt Symposium III Abstracts, 1993: Montana Bureau of Mines and Geology1999, Volume 381.

Zieg, G., Scartozzi, V., Chutas, N., Albers, D., Gostomski, K., and Jones, J., 2013, Black Butte copper deposits, lower Belt Supergroup, Montana: Northwest Geology, v. 42, p. 131-147.

Zieg, G. A., 1986, Stratigraphy and sedimentology of the Middle Proterozoic Newland Limestone: Montana Bureau of Mines and Geology Special Publication, v. 94, p. 125-141.

THE HOODOO IS THE SWAUGER AND OTHER HERESIES: LEMHI SUBBASIN CORRELATIONS AND STRUCTURES, EAST-CENTRAL IDAHO

Russell F. Burmester,[1,3] Reed S. Lewis,[1] Jeffrey D. Lonn,[2] and Mark D. McFaddan[1,4]

[1]*Idaho Geological Survey, University of Idaho, Moscow, Idaho 83844-3014; [2]Montana Bureau of Mines and Geology, Montana Tech, Butte, Montana 59701; [3]Geology, Western Washington University, Bellingham, Washington 98225-9080, russb@wwu.edu; [4]Natural Sciences Division, North Idaho College, Coeur d'Alene, Idaho 83814*

ABSTRACT

Recent stratigraphic study of Mesoproterozoic rocks in east-central Idaho has resulted in new correlations of strata in the Lemhi and Beaverhead ranges, with speculation of correlations of those strata with rocks in the Salmon River Mountains. At least part of the Hoodoo Formation exposed over Taylor Mountain, and some strata mapped as Gunsight Formation southeast of there, can be shown to correlate with the Swauger Formation of the Lemhi Group, and by reason of proximity and similarity, at least part of the type Hoodoo Formation is or includes strata of the Swauger Formation. The upper part of the Swauger Formation of Taylor Mountain is interbedded with and overlain by rocks with characteristics of the Lawson Creek Formation, above which are thick sequences of thinly laminated siltite, pinch and swell quartzite, siltite and argillite couplets and couples, hummocky cross laminated very fine-grained feldspathic quartzite and a finer and biotitic quartzite interval. Map units for these strata are, in ascending order, the coarse siltite, banded siltite, Lake Mountain, and Trapper Gulch members of the Apple Creek Formation. Thus, the Hoodoo Formation cannot correlate with the Big Creek Formation in the Lemhi Group, which is well below the Lawson Creek and Swauger formations. Also, detrital zircon ages from the Apple Creek strata are too young to support previous correlations with Piegan or Ravalli group units of the Belt Supergroup. Instead, all the Mesoproterozoic strata of the Salmon River Mountains, Lemhi Range and Beaverhead Mountains are equivalent to strata of the Missoula Group. Correlation of the thick strata of the Lemhi subbasin with the thinner units of the upper part of the Belt Supergroup requires fundamentally different depositional rates and histories, consistent with the Salmon River Mountains hosting the latest depocenter of Belt Supergroup strata. The late and rapid subsidence of this region may be intimately related to the genesis and localization of the 1380–1370 Ma mafic and A-type granitic magmas that intruded these rocks.

INTRODUCTION AND ORGANIZATION

The area around Salmon, Idaho (fig. 1), including parts of the Beaverhead Mountains to the east, Lemhi Range to the south, and Salmon River Mountains to the west, hosts extensive exposures of mostly fine-grained feldspathic quartzite, siltite and argillite that are part of the Mesoproterozoic Belt-Purcell Supergroup. Nomenclature and correlation of their stratigraphy has been somewhat of a random walk, resulting in a confusing array of stratigraphic and structural configurations. The history of mapping and stratigraphic studies that led to the present confusion in correlation of units in the mountains around Salmon, Idaho, was eloquently and humorously summarized at the end of the 20th century in Winston and others (1999). A major improvement at the time was recognition that the Hoodoo Formation was not within the Yellowjacket Formation, which left the type Yellowjacket below the Hoodoo and the units above renamed members of the "Cobalt Yellowjacket" (fig. 2a). The next breakthrough was recognition that some of the supra-Hoodoo units were correlative with members of the type Apple Creek Formation developed by Tysdal (Tysdal, 1996a, b; Tysdal and Moye, 1996) in the Lemhi Range. Extending those members into the Salmon River Mountains (Tysdal and others, 2000) was the first step in tearing down the walls between ranges. A remaining obstacle was that the type Apple Creek Formation had been miscorrelated with strata below the Gunsight Formation farther south. That mix-up shuffled the deck, making it appear that the Hoodoo Formation was in the same stratigraphic position as the Big Creek Formation. Reinterpretation of unit relationships without that miscorrelation raised the type Apple Creek Formation above the Swauger and overlying Lawson Creek formations, and greatly simplified stratigraphic
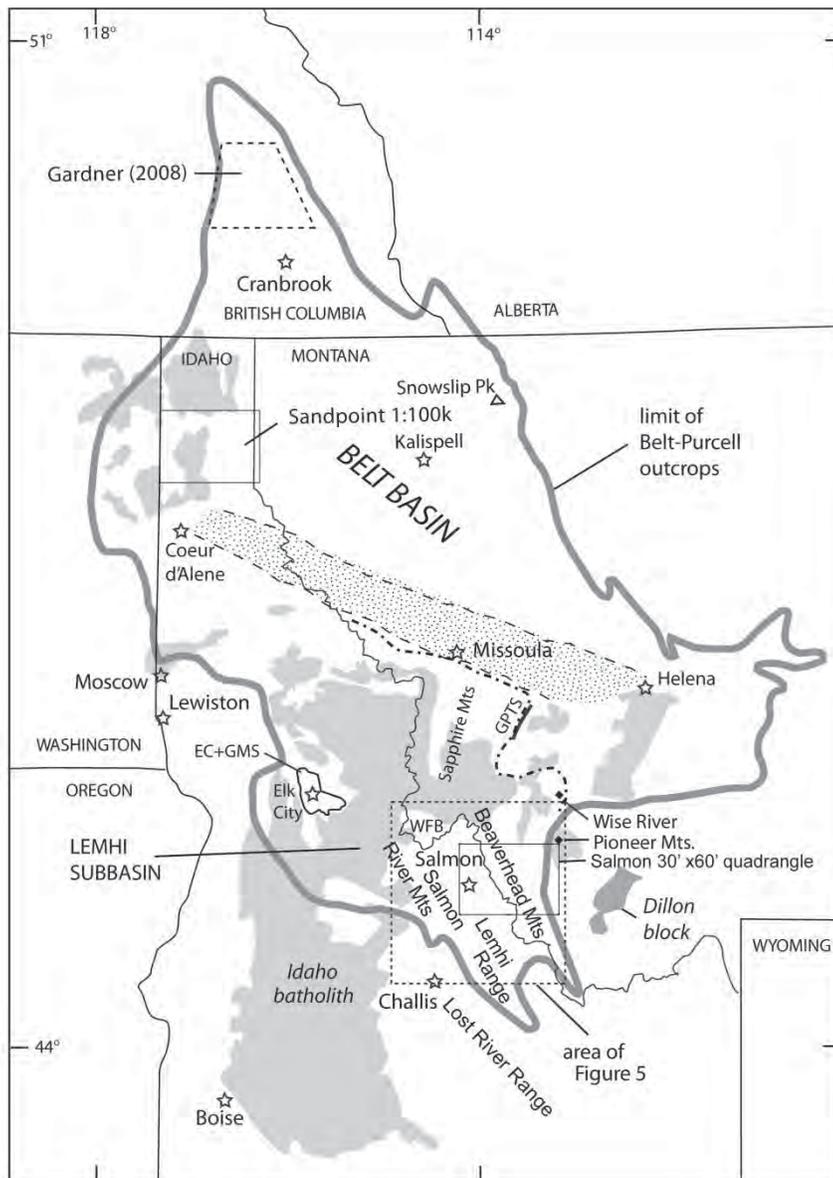
Figure 1. Location map showing areal limit of present outcrops of Belt-Purcell Supergroup strata and the boundary between Belt basin and Lemhi subbasin deposits (dash-dot line). Speckled pattern approximates the Lewis and Clark fault zone. Lighter shaded areas are Cretaceous through Eocene plutonic rocks; darker shaded Dillon block is Archean basement. EC-GMS—Elk City-Golden metamorphic sequence; GPTS—Georgetown-Phillipsburg thrust system; MCMS—Meadow Creek metamorphic sequence; WFB—West Fork Bitterroot River. Missoula Group type sections are near Snowslip Peak for lower units, east of Missoula for upper ones. The Salmon and Sandpoint 1:100k quadrangles and the area studied by Gardner (2008) referred to in the text are outlined.

cession through the stratigraphic column, Winston and others (1999) offered correlations among strata of the Lemhi Range, Salmon River Mountains, and the main Belt basin. Our paper is an oblique tribute to Winston's contributions, especially the 1999 paper. It is a tribute because our work would not have been possible without his. It is oblique because it refutes some of the 1999 conclusions. We see this as a continuation of the work that Winston pursued, with our new view of the stratigraphy allowing re-interpretation of the geology in a way that further simplifies the structural picture, which was one of his goals.

This complex story, however, is more convoluted than the field relations of the rocks themselves indicate. Although we had encroached on the area from the north in the early 1990s, our work started in 2006 with a look at the thorium-REE district around Lemhi Pass in the Beaverhead Mountains on the Idaho-Montana state line. We were confused by the rocks, but pressed ahead mapping the Salmon 1:100,000 quadrangle as a StateMap cooperative project between the Idaho Geological Survey and the Montana Bureau of Mines and Geology. Field work for this effort ran through 2014. Only by going out of bounds on reconnaissance trips to the Lemhi Range were we able to get a grip on the nature of the beast – relatively simple geology complicated by faults that were invoked to reconcile miscorrelations and misidentification of units. That is not to say that the geology is entirely simple, and one big challenge remained: the Salmon Mountains. Fueled by our perverse compulsion to understand the whole Lemhi subbasin, we jumped west and found the story there also was much simpler than advertised. Although our incursion west was only reconnaissance, we did look carefully at several transects, using the Salmon Forest map (Evans and Green, 2003), as well as prior maps and reports (Connor and Evans, 1986; Evans and Connor, 1993; Ekren, 1988, Tysdal and others, 2000).

This report starts with a review of Mesoproterozoic strata of the Lemhi subbasin as recently redefined

correlations between the Lemhi Range and Beaverhead Mountains (fig. 3c, d; Burmester and others, 2013) and the structures within them (Lonn and others, 2013).

Winston and others (1999) tried to impose order on the confusion by measuring critically selected sections and describing the strata using Winston's (Winston, 1986; Link and others, 1993; Winston, 2007) sediment types. Based on sediment types present and their suc-

Group	Formation	a) SRM unit	b) Lemhi Group	c) Tysdal (2000a, b)	d) Tysdal (2003)	e) Salmon River Mts	f) Lemhi Range	g) age control ages in Ma
	main Belt basin	a) Winston et al. (1999)		Lemhi subbasin		this effort		
Missoula	Ypi Pilcher / Ygr Garnet Range / Ymc McNamara	Ylc		Ylc		Ygm / Yatg / Yalm / Yab / Yac ... Ylc = Yaq	Yab / Yac / Yad / Yaf / Yalp / Ylc	1377 ± 4 Big Deer Creek [4] pluton / 1410 (1) Yalm [2] / 1409±10 (9) Yab [4] / 1365 (4) Yro [3]
Missoula	Ybo Bonner / Yms Mount Shields	Ys		Ys	Ys	Ys / Yy	Ys / Yg	1386 (4) Yph [3] / 1401 ± 06 Ybo [0] / 1454 ± 09 Yg [2]
Missoula	Ysh Shepard / Ysn Snowslip	Cobalt Yye	Yg	Yg	Yg		Yyl / Ybc / Ywf+Yic	1429 ± 08 Ysh [1] / 1443±07 top Ysn [0]
Piegan	Yw Wallace	Cobalt Yyd / Cobalt Yyc	Ya	Yac / Yad	Yab / Yac			1454± 09 top Yw [0]
Piegan	Yhe Helena	Cobalt Yyb / Cobalt Yya			Yad / Yaf			
				Yaf				
Ravalli	Ysr St Regis	Yho	Ybc					
Ravalli	Yr Revett / Ybu Burke	Yy	Ywf+Yic	Ywf+Yic				1505 Yr [1]

(Belt-Purcell Supergroup)

Figure 2. Correlation chart for Belt Supergroup units in the main Belt basin (left columns) and Lemhi subbasin strata in the Salmon River Mountains and Lemhi Range according to previous studies and our interpretations. a) Winston et al. (1999) separation of the Yellowjacket Formation into type Yellowjacket below the Hoodoo Formation and "Cobalt Yellowjacket" units above it, and b) correlative units in the Lemhi Group, Lemhi Range; c and d) Tysdal's (2000a, b; 2003) Apple Creek Formation unit names; e) and f) our shuffling of those Apple Creek units in the Salmon River Mountains and Lemhi Range to rectify miscorrelation of the type Apple Creek with the unit below the Gunsight Formation; g) youngest radiometric ages for units from sources in square brackets: 0—Evans et al. (2000); 1—Ross and Villeneuve (2003), 2—Link et al. (2007); 3—Gardner (2008); 4—Aleinikoff et al. (2012). Ages in Ma are U-Pb on zircons. Number of grains averaged are in parentheses. Units are Ylc—Lawson Creek; Ys—Swauger; Yya-Yye— "Yellowjacket" units above the Hoodoo; Yho—Hoodoo; Yy—type Yellowjacket; Yg—Gunsight; Ya—Apple Creek undivided; Ybc—Big Creek; Ywf + Yic—West Fork and Inyo Creek. Members of the Apple Creek are Yatg—Trapper Gulch; Yalm—Lake Mountain; Yab—banded siltite; Yac—coarse siltite; Yad—diamictite; Yaf—fine siltite; Yalp—Lem Peak. Plutonic megacrystic granite is Ygm. Roosville and Phillips formations, correlatives of McNamara and Bonner in Canada, are Yro and Yph.

(Burmester and others, 2013) and of the Salmon River Mountains. It segues to recent observations, including age control of rocks in and near the Salmon River Mountains, proposes correlations, and speculates about some faults. Lest we seem authoritarian, consider this quote:

"We have not succeeded in answering all our problems—indeed we sometimes feel we have not completely answered any of them. The answers we have found have only served to raise a whole set of new questions. In some ways we feel that we are as confused as ever, but we think we are confused on a higher level, and about more important things. So this report does not purport to give final answers, or to claim that we now 'know how to do it.' We see more need for revision than ever. But we are doing better than we did. And this is a progress report, rendered with humility because of the unsolved problems we see now which we could not see before." (p. 2; Kelley, 1951).

MESOPROTEROZOIC ROCKS OF EAST-CENTRAL IDAHO

Units Common to the Lemhi Subbasin

Figure 3 shows the Lemhi-Beaverhead stratigraphy as of 2014. The lowest three units (Ybc, Ywf, & Yic) do not appear in the Salmon River Mountains, so we start with the unit below the Gunsight Formation in Ruppel's (1975) reference section, which is now the Yellow Lake Formation. Histograms for feldspar content and ratios in some of the units are in figure 4. Feldspar content is from visual estimates on stained slabs of quartzite samples. Quartz comprises most of the rest, with generally less than 5 percent other grains and matrix but as much as 10 percent in some finer-grained and more feldspathic samples. High feldspar content reflects lack of weathering during rapid uplift and erosion of source rocks common to most Lemhi subbasin units (see Link and others 2015 this volume).
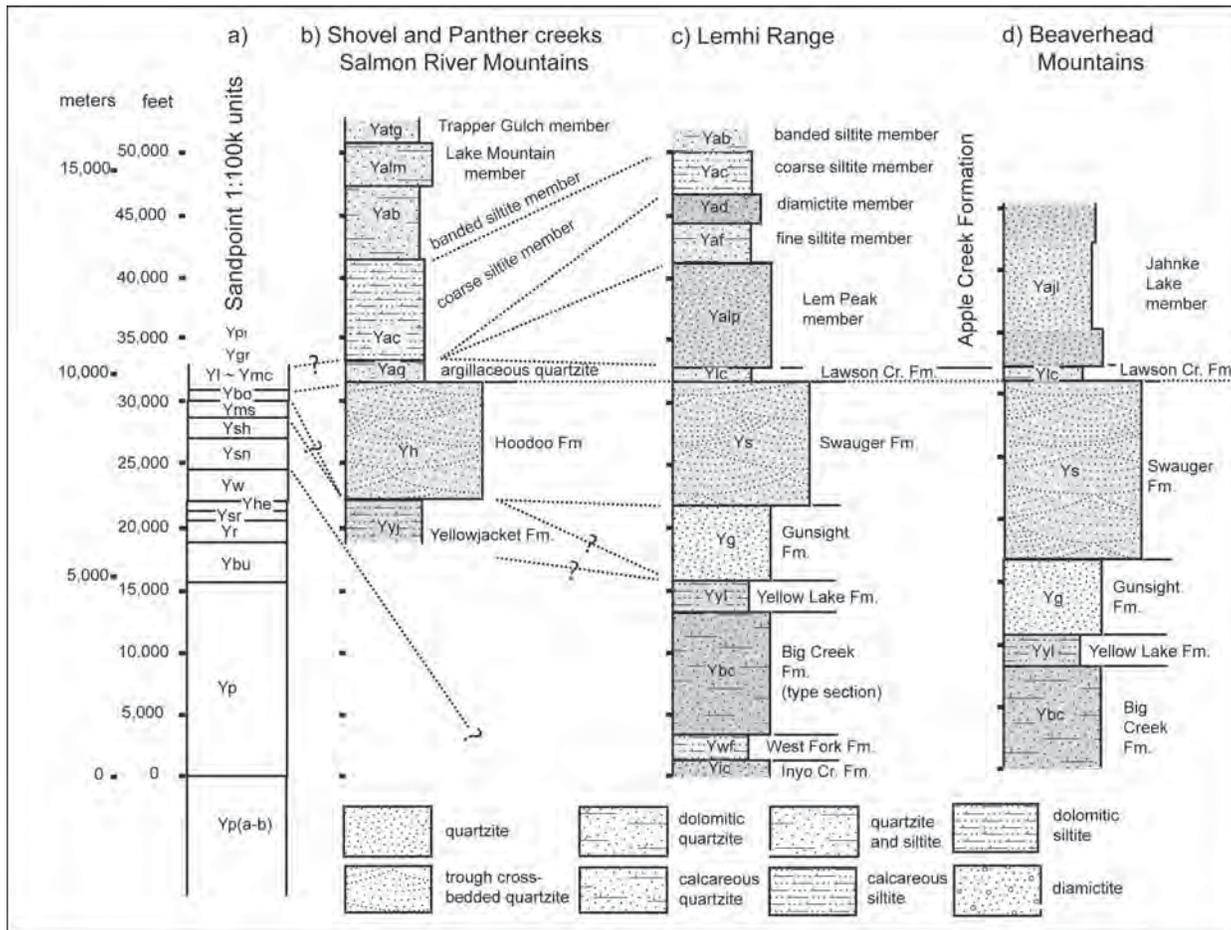
Figure 3. Stratigraphic columns for Belt Supergroup section in the Sandpoint 1:100k quadrangle (Lewis et al., 2008), b) Salmon River Mountains, c) Lemhi Range, and d) Beaverhead Mountains. For (a) abbreviations are as in fig. 2 with the addition of: Yl—Libby Formation correlative with McNamara; Yp—Prichard Formation members c up through h and t; Yp(a-b)—lowest members base not exposed but estimated to extend at least to the bottom of the lines. For (b), backsliding on the Iron Lake fault is assumed to make net stratigraphic throw negligible. Lack of lateral continuity of the fine siltite and diamictite members (c) may reflect locally restricted environments of deposition.
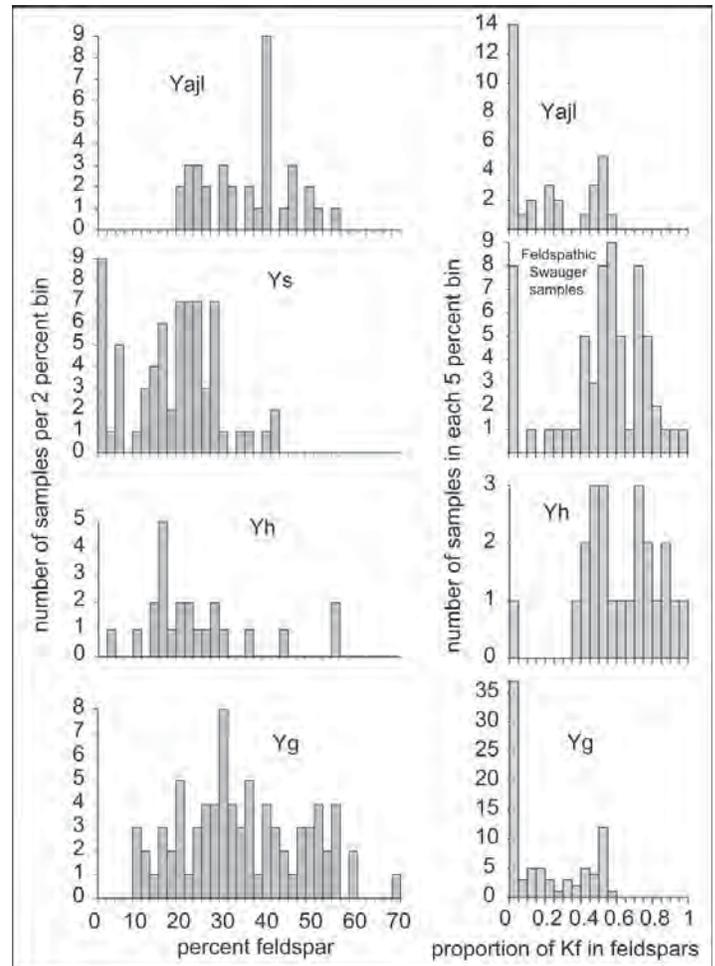
Figure 4. Histograms of feldspar content and ratio of potassium feldspar to total feldspar for the Apple Creek Formation Jahnke Lake member in the Beaverhead Mountains (Yajl, 32 samples), Swauger Formation (Ys, 68 samples), Hoodoo Formation (Yh, 23 samples) and Gunsight Formation (Yg, 81 samples). Five samples of Ys had no feldspar. Most of the samples have less than 5 percent other grains and matrix, with quartz making up the rest. Low feldspar content reflects attrition from weathering or transport (Link et al. 2015 this volume). Proportions of feldspar reflect source composition.

Proportions of feldspar reflect source composition. Low feldspar content dominated by potassium feldspar, commonly angular, for the Hoodoo and Swauger formations reflects dilution by additional sources from mature sand stored on a pediment (Sears, 2007) and the nearby Dillon block of Archean bedrock.

Yellow Lake Formation

The Yellow Lake Formation is thinly bedded siltite and argillite with even and mudcracked couplets toward the bottom, very fine-grained quartzite to argillite non-cracked, lenticular and even couplets in the middle, and pinch and swell sediment type with some carbonate toward the top (Winston and others, 1999). It grades upward into the Gunsight Formation with increasing concentration of thicker and coarser quartzite beds. In the same manner that the Yellowjacket name could not be applied to units both above and below the Hoodoo Formation (Winston and others, 1999; Tysdal, 2000b), Apple Creek Formation nomenclature cannot be applied to units both above and below the Swauger Formation. Keeping the name with the type section established by Anderson (1961) near Hayden Creek (HC, fig. 5) follows the reasoning of Winston and others (1999) that the name should stay with the type section. This choice allows the name Apple Creek Formation to continue to apply to the Salmon River Mountains (Tysdal, 2003; Evans and Greene, 2003). The unit below the Gunsight Formation that Ruppel (1975) had correlated with the Apple Creek became Tysdal's (2000a) Yellow Lake unit, now renamed the Yellow Lake Formation. It grades upward into the Gunsight Formation with increasing concentration of thicker and coarser quartzite beds.

Gunsight Formation

The Gunsight Formation is well sorted, fine-grained feldspathic quartzite, typically with 20-50 percent feldspar (fig. 4). Overall, quartz and potassium feldspar increase up section while plagioclase, micas, and matrix decrease (McBean, 1983). Quartz grains are subrounded; some toward the base and into the underlying Yellow Lake unit are medium grained. Lamination is typically planar, but includes ripple, ripple-drift, and trough cross-lamination. Some contortion of internal lamination is attributed to soft sediment deformation. West of Gunsight Peak in the Lemhi Range (GP, fig. 5) on the ridge above the reference section, it grades up into coarser strata of the Swauger Formation. The contact is distinguished by large (cm-thick) mudchips and cracks as well as lower feldspar content and larger, well-rounded quartz grains. Winston and others (1999) described the upper contact as "where beds of the discontinuous-layer sediment type disappear upward into flat-laminated and trough-crossbedded medium-grained arenite of the Swauger Formation". The contact is gradational elsewhere in the Lemhi Range as well (Ross, 1947; Anderson, 1961; Ruppel, 1975). Our recent work in the western part of the Salmon 30′ x 60′ quadrangle suggests that the Gunsight becomes thicker, finer-grained, and thinner-bedded north of the type section.

Swauger Formation

The Swauger Formation is a varicolored, mostly pure quartzite with argillite interbeds at several horizons (Ross, 1947) to the south of Patterson (fig. 5), but is mostly white or white weathering elsewhere. Distinct tabular beds are commonly trough cross bedded and flat laminated. Sorting is poor with quartz grains up to coarse size, but most are medium to fine and generally well rounded. Some samples from the head of Kadletz Creek, south of Lem Peak in the Lemhi Range (KC and KP, fig. 5), are dominated by coarse, dark, well-rounded quartz grains. Pebbles and small red chert (?) grains are distributed locally, not uniformly. Feldspar content of 68 samples, primarily from the Beaverhead Mountains with a smaller number from the Lemhi Range, varies widely (fig. 4). Some samples have no feldspar. Most but not all of those are from the Lemhi Range. Highest feldspar content is 45 percent. Most of the more feldspathic samples are from the Beaverhead Mountains in the northern part of the Salmon 1:100k quadrangle in Idaho. We interpret this disparity to reflect local variation of sediment distributary systems. The ratio of potassium feldspar to total feldspar also ranges widely, but only 13 samples have more plagioclase than potassium feldspar. Perhaps a clearer picture is shown by statistics: average and median values for feldspar content are 18 and 20 percent, and for potassium to total feldspar are 64 and 60 percent. The upper part of the Swauger contains Lawson Creek-like strata in several places (e.g., Tysdal, 1996b; Tysdal, 2000a).
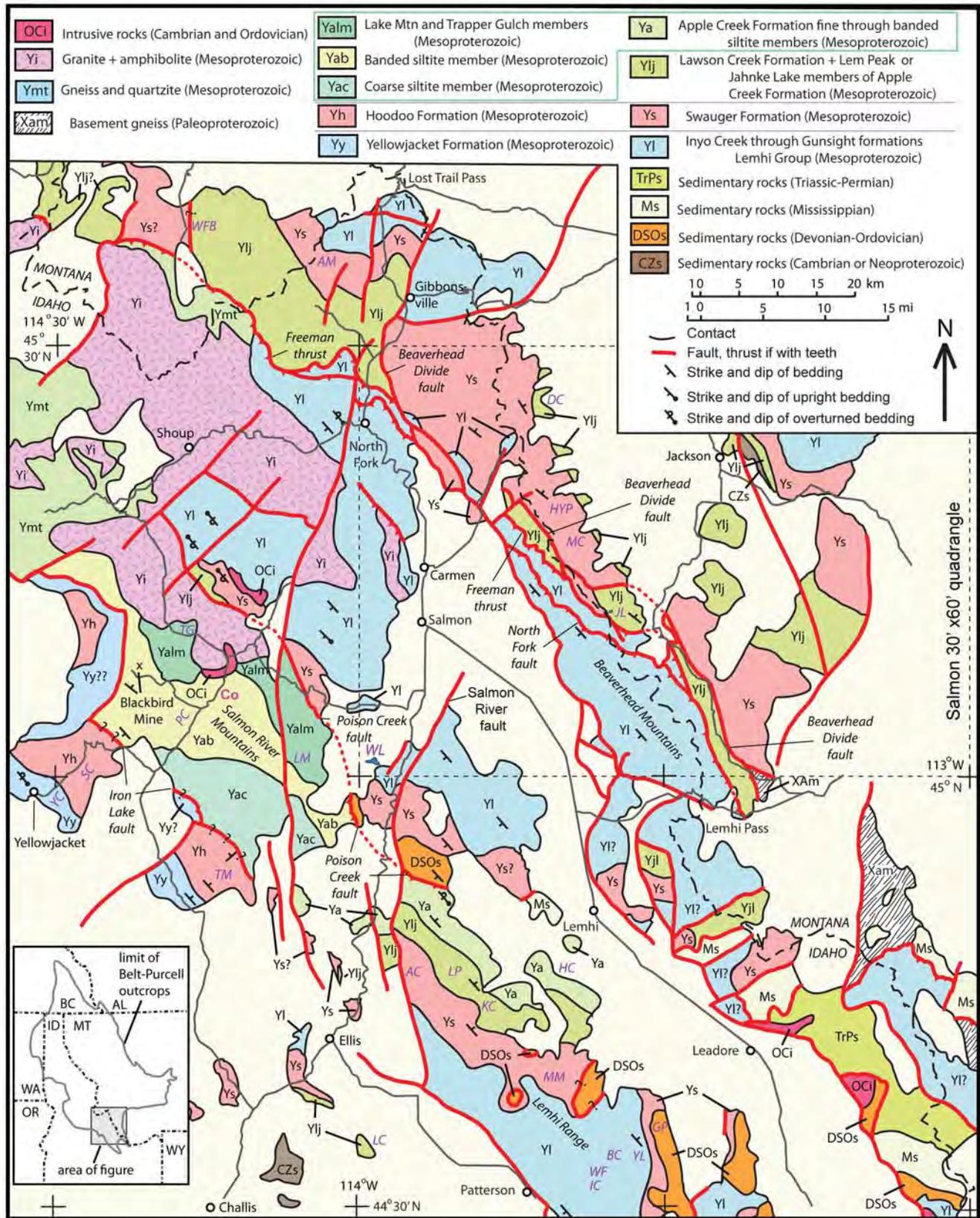
Figure 5. Generalized geologic map of the greater Salmon area showing locations of type and reference sections and other points of interest. Initials in color: BC—Big Creek; Co—Cobalt; DC—Dry Creek; GP—Gunsight Peak; HC—Hayden Creek; HYP—Homer Youngs Peak; IC—Inyo Creek; JL—Jahnke Lake; KC—Kadletz Creek; LC—Lawson Creek; LM—Lake Mountain; LP—Lem Peak; MC—Miner Creek; MM—Mogg Mountain; PC—Panther Creek; SC—Shovel Creek; WF—West Fork Big Creek; WL—Williams Lake; YC—Yellowjacket Creek; YL—Yellow Lake. Freeman thrust and North Fork fault are from Lonn et al. (2013b); other named faults from Evans and Green (2003). Thin solid gray lines are roads; the one from Ellis through Salmon, North Fork and Shoup follows the Salmon River.

Lawson Creek Formation

The Lawson Creek Formation was named for a locally carbonate bearing heterogeneous succession of purple-hued quartzite, highly feldspathic quartzite, siltite, and argillite that gradationally overlies the Swauger Formation in the northeastern foothills of the Lost River Range (Hobbs, 1980) south and southwest of Ellis (fig. 5). Where exposed farther north, the colors are lost and most of the argillite is black. Bedding is characteristically thin, with couplet-scale quartzite, siltite, and argillite. Lenticular and flaser bedding are common and characteristic. The Lawson Creek Formation contains abundant desiccation cracks and mud rip-up clasts; much less common are chert beds and cherty rip-ups. Carbonate cement is non-uniformly distributed. The Lawson Creek grades upward to pale green to gray, fine-grained, very feldspathic quartzite in meter-thick beds with few or very thin argillite or siltite interbeds.

Apple Creek Formation

Tysdal (1996a, b) refined the Apple Creek Phyllite (Anderson, 1961) into fine siltite, diamictite, and coarse siltite units in the greater Hayden Creek area of the northern Lemhi Range (HC, fig. 5). The fine siltite unit is thinly planar laminated and ripple cross-laminated fine-grained siltite and argillaceous siltite. The diamictite unit is argillite, argillaceous siltite, and fine- to medium-grained siltite distinguished by zones of matrix-supported pebbles. Most pebbles are similarly fine material but some are fine-grained quartzite, lithologies similar to Lemhi Group strata (Tietbohl. 1986). The coarse siltite unit includes beds with erosional bases of fine-grained quartzite that grade up to medium-grained siltite. However, because of the miscorrelation between the Yellow Lake and Apple Creek formations, Tysdal mapped the Lem Peak fault between the Lawson Creek and type Apple Creek, including a thick section of "Big Creek Formation" underneath the type Apple Creek. After work in the Lem Peak area (LP, fig. 5), we reinterpreted the Lem Peak fault as a stratigraphic contact, placing the type Apple Creek above the Swauger and Lawson Creek, and adding Tysdal's "Big Creek" to the bottom of the Apple Creek as the Lem Peak member (figs. 2, 3c). The correlative of this unit in the Beaverhead Mountains, the Jahnke Lake member (fig. 3d), has high feldspar content and plagioclase in excess of potassium feldspar (fig. 4).

Just to the northwest of the type section, Tysdal and Moye (1996) included a fault slice of the banded siltite unit in the Lemhi Range. They did not include it in the Apple Creek Formation but suggested that it may be the middle part of Conner and Evans' (1986) Yellowjacket. It is predominantly uneven to undulating couplets and couples of lighter siltite grading to dark argillite tops. Our examination of this fault slice showed the banded siltite to be in stratigraphic contact with the underlying Apple Creek units described by Tysdal (1996a, b). The fine siltite and diamictite units were mapped northwest across the Salmon River fault and Salmon River, but not far (Evans, 1998; Tysdal, 2000b, 2003). Farther northwest are units that were originally interpreted as Yellowjacket Formation above the Hoodoo (Connor and Evans, 1986; Connor, 1990; Evans and Connor, 1993) and later termed the "Cobalt Yellowjacket" by Winston and others (1999). Tysdal (2000b, 2002, 2003; Tysdal and others, 2000) applied the name "coarse siltite unit" to the lower part of this succession and renamed the middle part the "banded siltite unit" reviewing Sobel's (1982) description of it near the Blackbird mine. Above the banded siltite in the Salmon River Mountains we added the Lake Mountain member of hummocky crossbedded fine-grained feldspathic quartzite and the Trapper Gulch member of very fine-grained quartzite and siltite and anomalously biotite-rich rocks ("biotitite") above that (fig. 3b). The Lake Mountain member had been mapped as Gunsight Formation and the Trapper Gulch member had been included in the banded siltite,

Units Unique to the Salmon River Mountains

Despite inroads that the Lemhi Range names have made into the Salmon River Mountains, there are still unit names used nowhere else. These are the type Yellowjacket and Hoodoo formations of Ross (1934) and the informal argillaceous quartzite unit of Ekren (1988).

Yellowjacket Formation

Defined originally by Ross (1934) for only strata below the Hoodoo Quartzite near the Yellowjacket mine, the Yellowjacket Formation is 520 m (700 ft) of "banded and variegated gray, white, and green, more or less calcareous rocks" overlain by 2,158 m (7,080 ft) of readily-weathered dark-gray argillaceous quartzite. Thicknesses are suspect because the measured

section is complicated by folds and locally overturned beds (Ekren, 1988). In sediment type terminology, the section is interbedded discontinuous layer and uncracked and mudcracked lenticular and even couplets above tabular beds of flat-laminated and trough crossbedded and ripple marked sand (Winston and others, 1999). Scapolitic rocks rich in sodium were interpreted as metaevaporites by Tysdal and Desborough (1997). The base of the Yellowjacket Formation is not exposed; the upper contact is gradational into the overlying Hoodoo Formation (Ross, 1934; Ekren, 1988). It is not as widespread as Ruppel (1975, 1980) mapped based on using dark color from biotite content. Winston and others (1999) and Tysdal (2000b) rightly pointed out that the biotite was metamorphic and could not be used for lithostratigraphic correlation.

Hoodoo Formation

The Hoodoo Formation also was defined by Ross (1934), who measured 1,085 m (3,560 ft) of quartzite strata along Yellowjacket Creek (YC, fig. 5) northeast of the Yellowjacket mine. The quartzite there it has about 85 percent well-rounded quartz grains, 5-15 percent feldspar, and 0-10 percent biotite and sericite from upper greenschist facies metamorphism (Ekren, 1988). Sedimentary structures on bedding surfaces and within massive quartzite beds include cross-bedding, and oscillatory and current ripples (Ekren, 1988). Farther northeast, it is tightly cemented light gray to white quartzite and orthoquartzite with minor feldspar, biotite and sericite, and steep cross-lamination of dunes, oscillatory current and locally linguoid ripples (Tysdal and others, 2000). At Taylor Mountain (TM, fig 5) it contains 85-94 percent quartz grains ranging in size from 0.2 to 1.5 mm, similar to the Hoodoo Formation along Yellowjacket Creek (Ekren, 1988). The Hoodoo Formation grades upward through several hundred meters from clean quartzite into argillaceous quartzite and siltite (Ekren, 1988) of the informal argillaceous quartzite unit.

Argillaceous Quartzite Unit

This package of rock is described as greenschist facies, distinctly banded, gray, slightly calcareous quartzite (Ross, 1934), or bluish-gray to gray, argillaceous, fine-grained quartzite and siltite (Ekren, 1988). Beds of fine-grained quartzite and quartz-rich metasandstone are interlayered with beds of fine- to medium-grained argillaceous siltite and show abundant cross-beds, ripple cross-laminations, and local rip-up clasts (Tysdal, 2000b). In more detail northeast of the area mapped by Ross, Tysdal and others (2000) noted that this unit is medium-gray to gray-green biotitic siltite with interbeds of fine-grained quartzite and quartz-rich metasandstone, metamorphosed to biotite-grade greenschist facies. Siltite is thin bedded and planar laminated to ripple cross-laminated; quartzite and quartz-rich metasandstone beds are most abundant in lower strata of the unit where flaser and lenticular bedding are most common. Total thickness could be greater than 400 m (Tysdal and others, 2000).

NEW OBSERVATIONS AND CORRELATIONS

Age Control—Current or Recent Radiometric Dating

In the decade and a half since Winston and others (1999) there has been a vast increase in age control of the rocks in question. Most new ages are U-Pb LA-ICPMS or SHRIMP dates on detrital zircons in the metasedimentary rocks, but the age of the Mesoproterozoic granite (Yi, fig. 5) also has been nailed down (Ygm, fig.2). Logically, a sedimentary unit can be no older than the minimum age of detrital zircons in it, but analytical or other error may cause a few grains to appear younger than they are. However, a cluster of young ages may accurately record input from a juvenile source close to the age of deposition. Available data from Ross and Villeneuve (2003), Link and others (2007), Gardner (2008), and Aleinikoff and others (2012) are provided in Figure 2g. Ross and Villeneuve used about 30 grains, so minimum ages are not as well defined as are those from later sources that have about 100 grains per sample. Ages on volcanic rock within the Belt-Purcell Supergroup are from Evans and others (2000). The 1409 age from banded siltite (Yab) is an average of 9 grains, and approximates or is older than the age of deposition of sediment near the top of the Apple Creek Formation in the Salmon River Mountains.

Our Perspective and Entangling Association with the Past (EAP)

We boldly put our necks in the nooses of critics when we proposed a revised stratigraphy for the

Lemhi Range, Beaverhead Mountains, and east and northeast of there (Burmester and others, 2013) much as Winston and others (1999) stretched their necks across the chopping block to see whether their heretical correlations were borne out by the rocks. Armed with our new stratigraphic information, we visited selected areas where major faults had been invoked to accommodate miscorrelations. Results of our investigation are described below; our simplified correlations and regional map are shown in Figures 3 and 5.

Sedimentary structures are locally spectacular and useful attributes for describing and characterizing the fossil-free Mesoproterozoic rocks of the Belt-Purcell Supergroup. Sedimentary structures, along with grain size, mineral composition and color, have been combined by Winston (Winston, 1986; Winston, 1998; Link and others, 1993; Winston, 2007) into a classification scheme of sediment types that are found throughout the Belt stratigraphic pile in recurrent patterns. Winston and others (1999) used these to describe units within the Lemhi subbasin and correlate them with units of the main Belt basin. Although we acknowledge that sediment types are very useful, we do not place as much trust in them to brand units as Winston does. One of us recalls the late experimental petrologist Hatton S. Yoder warning about EAP. His acronym EAP, for Entangling Association with the Past, was to remind us that our prejudices, conceptions and thoughts are conditioned by what we have seen before. Most of the us have seen fewer Belt rocks than has Winston, and many of those rocks are in Idaho. Although Winston's pinch and swell sediment type with ptygmatically folded dikelets of light silt in black argillite is best developed in the Wallace Formation, we've seen it in the Sandpoint area (fig. 1; fig 3a) in the top member of the Prichard Formation, top member of the Mount Shields Formation, and bottom member of the Libby Formation (McNamara correlative) (Lewis and others, 2006b; McFaddan and others, 2006). We have also seen atypically coarse and well-rounded quartz grains scattered through the section in Prichard Formation members c and e (Lewis and others, 2006a), Snowslip Formation (Lonn and others, 2010), middle of the Mt Shields and base of the Bonner formations (Burmester and others, 2006), so we don't expect that such grains should identify a unit. Nevertheless, only the Bonner is young enough to be correlative with the Swauger, so we are happy to pursue the hypothesis that the large round quartz, angular feldspar, and other exotic grains in the Bonner

and Swauger are a product of the Bonner disturbance (Elston, 1991, Elston and others, 2002). The anomalously large and spherical quartz grains may have been stored on a pediment to the east (Sears, 2007) and been shed into the Belt basin during other events where they became minor components in other units.

The Yellowjacket-Hoodoo-Argillaceous Quartzite Stack

A couple of us walked across the Yellowjacket-Hoodoo contact between Yellowjacket Creek and its West Fork. The contact appears gradational with no evidence for faulting, consistent with previous observations (Ross, 1934; Ekren, 1988). We visited the Taylor Mountain block of quartzite mapped as Hoodoo Formation (TM, fig. 5; Evans and Green, 2003; Tysdal, 2003). Most remarkable to us were the well-rounded medium and coarse quartz grains and low feldspar content common to many Hoodoo beds. Also common were trough cross lamination; less common were ripples, and rare were very large (1-2 dm) mud cracks, thick mud chunks, and black mud chips in foresets. Those are all features that we have found in the Swauger Formation of the Beaverhead Mountains (Burmester and others, 2011). Furthermore, both the Hoodoo and Swauger are the only units in the Lemhi subbasin that typically have potassium feldspar in excess of plagioclase (fig. 4). Twenty-three samples from outcrops mapped as Hoodoo, and 68 samples from outcrops mapped as Swauger, mostly from the Salmon 1:100 k quadrangle, have identical median feldspar content of 20 percent. Potassium feldspar to plagioclase ratios for the same samples are indistinguishable at about 3:2. Also in the Taylor Mountain block are several intervals of dark, fine-grained, thin-bedded strata with characteristics of the Lawson Creek Formation. These intervals are similar to intervals Tysdal (1996b; 2000a) found in the Lemhi Range, so are not evidence against correlation. We also visited the section that spans Yellowjacket Creek. Most impressive were very dark, well-rounded coarse quartz grains in the upper part of the Hoodoo Formation (or lower part of the argillaceous quartzite unit) mapped there. These grains appear very similar to some in the Taylor Mountain block, the Swauger at the head of Kadletz Creek in the Lemhi Range, and grains Tysdal (2000a) described as glassy.

Apple Creek Formation in the Salmon River Mountains

We took closer looks at the Apple Creek Formation in the Salmon River Mountains and are happy to report that it is alive and well. The lower members from the Lemhi Range do not persist far to the northwest but two new members appear on top. Missing, except near the Salmon River, are the lowest quartzite mapped across Lem Peak, which we rebranded as the Lem Peak member, the fine siltite unit (Yaf) of Tysdal (1996-2002), and the diamictite member (Yad). The diamictite unit continues across the Salmon River fault and Salmon River as a 300 m (985 ft) stack of 5 m (16 ft) thick beds of diamictite, but it thins abruptly to the west (Evans, 1998). Curiously, there also are diamictite interbeds in the coarse siltite, banded siltite and the new Lake Mountain member as previously reported by Conner and Evans (1986) for units of their Yellowjacket Formation.

Winston and others (1999) interpreted the Apple Creek diamictite to be debris-flow deposits on periodically exposed mudflats, perhaps adjacent to an unidentified uplifted basin block. If true, perhaps the nearly exclusive restriction of the diamictite unit to the northern Lemhi Range reflects localization of the source or mud flats. Individual diamictite beds there as well as higher in the Apple Creek Formation could be from debris flows triggered by severe storms or earthquakes. In contrast, Tietbohl (1986) suggested the beds could result from subaqueous slumping off a relatively upfaulted paleotopgraphic high.

The lowest member farther northwest in the Salmon River Mountains is the coarse siltite member. It is mapped northeast of the argillaceous quartzite across the Iron Lake fault (Tysdal, 2003). Along Panther Creek (PC, fig. 5) as well as along the Dugan Mountain road south of Lake Mountain (LM, fig. 5) it grades up into the banded siltite (Connor and Evans, 1986; Tysdal and others, 2000; Tysdal, 2003). Gradational above the banded siltite is the Lake Mountain member, consisting of hummocky crossbedded very-fine feldspathic quartzite. It is well described and illustrated by Tysdal (2003) as the Gunsight Formation in the Salmon River Mountains. All of these members occupy broader swaths across the map to the west. Some of this pattern may be structural repetition, but some is from adding beds (Conner and or Evans, 1986). Highest is a new unit, the Trapper Gulch member of finer grained, more biotite rich quartzite. It was previously included in the banded siltite.

Hoodoo-Swauger Correlation and Implications

Lopez (1981) interpreted the Hoodoo Quartzite as Swauger Formation. Tysdal (2000b) considered the possibility that both were lithic and time equivalents, but appears to have rejected the conclusion that they were the same unit because strata under and over each were not lithic equivalents. On our initial visit to the Yellowjacket area in 2011, we also rejected the correlation for similar reasons. However, in completing mapping on the Salmon 30′ x 60′ quadrangle and examining the Swauger-Gunsight sections to the east and northeast of the Yellowjacket area, we observed that the Gunsight grades laterally from its type section in the Lemhi Range into a finer-grained and thinner-bedded rock. We now also consider that the type Yellowjacket could be a facies of the Gunsight, changing across a dynamic sedimentary basin. There is much less difference among the Lawson Creek exposures we have seen and the strata overlying the Hoodoo, at least the Taylor Mountain, so we accept their correlation and consider it likely that the argillaceous quartzite also correlates with the Lawson Creek.

A composite section northeast from Yellowjacket, Idaho, up Yellowjacket, Shovel and Panther creeks past the Blackbird mine (fig. 5) consists of Yellowjacket, Hoodoo, and the argillaceous quartzite in a conformable sequence (Tysdal, 2000b), and the Apple Creek Formation's coarse siltite and banded siltite units (Evans and Green, 2003) plus the new Lake Mountain and Trapper Gulch members. Since the banded siltite near the Blackbird mine is young (1409 Ma maximum age, Aleinikoff and others, 2012), this composite section is likely the upper part of the Lemhi Group through the Swauger Formation and into the overlying Lawson Creek Formation and members of the Apple Creek Formation (fig. 3b, c). Given this nearly continuous stratigraphic section, the role of the Iron Lake fault becomes omission of the Lawson Creek, top of the Swauger, and (or) base of the-Apple Creek formations in different places, not juxtaposition of disparate sections.

SALMON RIVER MOUNTAINS STRUCTURES REINTERPRETED

Iron Lake Fault

The Iron Lake fault is shown on the Salmon Forest map (Evans and Green, 2003) as a backslid thrust. Along the lower Moyer Creek road, carbonate and scapolitic siltite may be pieces of type Yellowjacket Formation caught between non-coplanar thrust and normal fault surfaces. However, near Iron Lake, there is no similar evidence. Quartzite mapped as Hoodoo over Taylor Mountain includes only minor tourmalinite (?) breccia near the contact with the coarse siltite member of the Apple Creek Formation. To the north, the only evidence of faulting is increased foliation in fine-grained dark rocks that are probably Lawson Creek Formation. Furthermore, correlating the Hoodoo with Swauger greatly reduces the need for displacement on the Iron Lake fault where mapped between Hoodoo and Gunsight southeast of Taylor Mountain. Our conclusion is that there is no structural evidence comparable to that along the Poison Creek fault to support major displacement on the Iron Lake fault.

Poison Creek Fault

The Poison Creek fault turns out to be the big fault in the area. See Tysdal (2002) for history of naming and interpretations. East of the Salmon River, it places Apple Creek Formation banded siltite, coarse siltite, and diamictite over Paleozoic carbonate (Tysdal, 2002). Near the fault, those rocks are highly foliated, and demonstrably overturned while still facing northeast. The fault continues northwest across the Salmon River (fig. 5) where the banded siltite is clearly in the hanging wall against the Ordovician strata, which, at least for the Kinnikinic, are depositional on the Swauger Formation. The footwall block northeast of the fault continues to the northwest with southwest facing Swauger and older rocks to at least the Hot Springs fault, near which the youngest strata are overturned, southwest facing Lawson Creek Formation. Contrast in depth of pre-Ordovician erosion along this block is evidence for earlier block tilting. The hanging wall block to the southwest carries the northeast facing Apple Creek strata into the Blackbird-Cobalt mining area. This difference in depth of erosion of the two blocks documents considerable pre-Ordovician

stratigraphic displacement on the fault. Its history may include synsedimentary movement as a growth fault, intrusion by mafic and A-type granitic magmas about 1380-1370 Ma (Aleinikoff et al, 2012), and normal displacement during Neoproterozoic to early Paleozoic as well as after reverse motion during Cretaceous contraction. Details still need to be worked out.

REGIONAL TECTONIC IMPLICATIONS

The Apple Creek Formation displays extreme and rapid lateral changes in continuity, lithology and thicknesses of its members, at least compared to usual Belt variations. Diamictite beds in some of the higher strata also may record local effects of syndepositional tectonic activity. For example, they might be the result of debris flows or slumps triggered by earthquakes on local growth faults. Hahn and Hughes (1984) suggested that active northwest striking growth faults caused deformation in what we consider upper Apple Creek strata southwest of the Poison Creek fault in the Salmon River Mountains. It is plausible that those faults existed before deposition of the Swauger as well, so environments for Gunsight and Yellowjacket could have been adjacent across such faults or topography they controlled. Maybe not coincidentally, the southern end of the anorogenic Mesoproterozoic(?) granite intrusions is where the youngest Lemhi subbasin strata, especially the Apple Creek members, are thickest. Thick and young supports the idea that this also was the locus of the most recent and rapid subsidence or extension. Gardner's (2008) evidence in the upper Purcell Supergroup strata for growth faulting north of the international border (fig. 1) suggests that extension during Missoula Group time affected the northern part of the Belt-Purcell basin as well. Perhaps the 1380 Ma magmatic event in the Salmon River Mountains, and northwest toward Moscow where similar age granites exist (Lewis and others, 2005), are part of the East Kootenay orogeny as previously proposed, but magmatism was during extension or transtension, and not due to burial depth and conductive heating as proposed by Doughty and Chamberlain (1996) when the Yellowjacket was still considered to be the Prichard Formation at the bottom of a thick accumulation of Belt Supergroup strata (fig. 3a).

Summary

The Yellowjacket Formation is not the Prichard Formation statement of 1999 (Winston, 1999) is still true (fig. 3) and no longer heretical. This year's heresy is that the type Yellowjacket Formation does not correspond to the flat-laminated sand of the Inyo Creek Formation and the rippled, mudcracked West Fork Formation of the Lemhi Group, nor does it correlate with the Burke Formation of the Belt Supergroup. Rather it is the top of the Lemhi Group and a lateral facies of the type Gunsight and possibly Yellow Lake formations. Also heretical in some eyes is that the overlying trough-crossbedded and flat-laminated, medium-grained quartzite mapped as the Hoodoo Formation *is* the Swauger Formation, and correlates with the Bonner and perhaps Mount Shields formations, not the Big Creek Formation of the Lemhi Group or the Revett Formation of the Belt. The argillaceous quartzite unit where mapped separately, and the top of the Hoodoo Formation where the argillaceous quartzite is not recognized, probably are or include the Lawson Creek Formation above the Swauger Formation. Mudcracked even couplets, microlaminae, and pinch-and-swell couples in the coarse siltite and banded siltite members of the type Apple Creek Formation are much too young to correlate with the Helena and Wallace formations of the Belt Supergroup. The hummocky cross-laminated and flat-laminated quartzite unit that overlies the banded siltite but was previously mapped as Gunsight or upper unit (or E) of the "Yellowjacket" is even younger than the banded siltite, so cannot correlate with the Snowslip Formation of the Belt Supergroup. In an odd way, Ruppel (1975) was correct in correlating widespread occurrences of biotite-grade strata with the Yellowjacket. Many of those units are part of the Gunsight Formation, which, like the Yellowjacket Formation, is below the Swauger Formation and therefore correlative. Based on Ruppel's (1975) definition of the Lemhi Group to be all of Ross's (1947) Lemhi quartzite below the Swauger Formation, the Yellowjacket Formation is the only unit of the Lemhi Group in the Salmon River Mountains; all higher units are without a group, at least for now. The bottom line is that we think we are confused on a higher level now, and the Salmon River Mountains rocks are at higher stratigraphic levels. At least that part of the story is more accurate and in more detail than written on a monument at Iron Creek (fig. 6).

SCULPTURE OF THE LAND

THIS FORMATION OF QUARTZITE ROCK BEGAN AS PARTICLES OF SAND AND SILT IN THE PRECAMBRIAN AGE ABOUT 570 MILLION YEARS AGO. SANDY SEDIMENTS, THOUSANDS OF FEET THICK, WERE DEPOSITED IN AN INLAND SEA UP TO 300 MILES WIDE STRETCHING FROM CANADA TO ARIZONA. OVER TIME, THE EFFECTS OF HEAT AND PRESSURE CHANGED THE SEDIMENTS TO QUARTZITE ROCK. OTHER CHANGES OCCURRED AS AN ANCIENT GROUND RUPTURE (FAULT) TILTED THE FORMATION AND WATER RUN-OFF CARVED THE IRON CREEK VALLEY. WATER SEEPING INTO SMALL CRACKS AND JOINTS CAUSED LARGER CRACKS THROUGH FREEZING AND THAWING. EVENTUALLY, THE PRESENT ROCK BLOCKS WERE FORMED AND VEGETATION WAS ABLE TO SURVIVE IN THE DEEPER CRACKS.

Figure 6. Geologic history monument, confluence of Iron Creek and its North Fork (44.9213N, 114.1097 W WGS 84); a) setting, b) closeup.

ACKNOWLEDGMENTS

REFERENCES

Aleinikoff, J.N., Slack, J.F., Lund, K., Evans, K.V., Fanning, C.M., Mazdab, F.K., Wooden, J.L., and Pillers, R.M., 2012, Constraints on the timing of Co-Cu ± Au mineralization in the Blackbird District, Idaho, using SHRIMP U-Pb ages of monazite and xenotime plus zircon ages of related Mesoproterozoic orthogneisses and metasedimentary rocks: Economic Geology, v. 107, p. 1143–1175.

Anderson, A.L., 1961, Geology and mineral resources of the Lemhi quadrangle, Lemhi County, Idaho: Idaho Bureau of Mines and Geology Pamphlet 124, 111 p.

Burmester, R.F., Breckenridge, R.M., McFaddan, M.D., and Lewis, R.S., 2006, Geologic Map of the Derr Point Quadrangle, Bonner and Shoshone Counties, Idaho: Idaho Geologic Survey Digital Web Map 59, scale 1:24,000.

Burmester, R.F., Lewis, R.S., Othberg, K.L., Lonn, J.D., Stanford, L.R., and McFaddan, M.D., 2011, Geologic Map of the Badger Spring Gulch Quadrangle, Lemhi County, Idaho: Idaho Geologic Survey Digital Web Map 132, scale 1:24,000.

Burmester, R.F., Lonn, J.D., Lewis, R.S., and McFaddan, M.D., 2013, Toward a Grand Unified Theory for Stratigraphy of the Lemhi Subbasin of the Belt Supergroup: Northwest Geology, v. 42, p. 187-1-19.

Connor, J.J., 1990, Geochemical stratigraphy of the Yellowjacket Formation (Middle Proterozoic) in the area of the Idaho Cobalt Belt, Lemhi County, Idaho: U.S. Geological Survey Open-File Report 90-0234, 30 p.

Connor, J.J., and Evans, K.V., 1986, Geologic map of the Leesburg quadrangle, Idaho: U.S. Geological Survey Miscellaneous Field Studies Map MF-1880, scale 1:62,500.

Doughty, P.T., and Chamberlain, K.R., 1996, Salmon River Arch revisited: new evidence for 1370 Ma rifting near the end of deposition in the Middle Proterozoic Belt basin: Canadian Journal of Earth Sciences: v. 33, p. 1037-1052.

Ekren, E.B., 1988, Stratigraphic and structural relations of the Hoodoo Quartzite and Yellowjacket formation of Middle Proterozoic age from Hoodoo Creek eastward to Mount Taylor, central Idaho: U.S. Geological Survey Bulletin 1570, 17 p.

Elston, D.P., 1991, Geologic and paleomagnetic evidence for a ~1,300 Ma tectonic event in the Missoula Group, Belt Supergroup (~1,450-1,250 Ma), Montana and Idaho: Geological Society of America Abstracts with Programs, v. 23, no. 4, p. 423-433.

Elston, D.P., Enkin, R.J., Baker, J., and Kisilevsky, D.K., 2002, Tightening the Belt: Paleomagnetic–stratigraphic constraints on deposition, correlation, and deformation of the Middle Proterozoic (ca. 1.4 Ga) Belt–Purcell Supergroup, United States and Canada: Geological Society of America, Bulletin, v. 114, p. 619–638.

Evans, K.V., 1986, Middle Proterozoic deformation and plutonism in Idaho, Montana and British Colombia: *in* Roberts, S.M., ed., Belt Supergroup: A guide to Proterozoic rocks of western Montana and adjacent areas: Montana Bureau of Mines and Geology Special Publication 94, p. 237-244.

Evans, K.V., 1998, The Yellowjacket Formation of east-central Idaho, *in* Berg, R.B., ed., Proceedings of Belt Symposium III-1993: Montana Bureau of Mines and Geology Special Publication 112, p. 17-30.

Evans, K.V., and Connor, J.J., 1993, Geologic map of the Blackbird Mountain 15-minute quadrangle, Lemhi County, Idaho: U.S. Geological Survey Miscellaneous Field Studies Map MF-2234, scale 1:62,500.

Evans, K.V., and Green, G.N., 2003, Geologic map of the Salmon National Forest and vicinity, east-central Idaho: U.S. Geological Survey Geologic Investigations Series Map I-2765, scale 1:100,000,

2 sheets, 19 p. text.

Evans, K.V., Aleinikoff, J.N., Obradovich, J.D., and Fanning, C.M., 2000, SHRIMP U-Pb geochronology of volcanic rocks, Belt Supergroup, western Montana; evidence for rapid deposition of sedimentary strata: Canadian Journal of Earth Sciences, v. 37, no. 9, p. 1287-1300.

Gardner, D.W., 2008, Sedimentology, stratigraphy, and provenance of the upper Purcell Supergroup, southeastern British Columbia, Canada: implications for syn-depositional tectonism, basin models, and paleogeographic reconstructions: University of Victoria, BC, M.S. thesis, 76p, http://hdl.handle.net/1828/911

Hahn, G.A., and Hughes, G.J., Jr., 1984, Sedimentation, tectonism, and associated magmatism of the Yellowjacket Formation in the Idaho Cobalt Belt, Lemhi County, Idaho, *in* S.W. Hobbs, ed., The Belt: Abstracts with Summaries, Belt Symposium II, 1983: Montana Bureau of Mines and Geology Special Publication 90, p. 65-67.

Hobbs, S.W., 1980, The Lawson Creek Formation of middle Proterozoic age in east-central Idaho: U.S. Geological Survey Bulletin 1482-E, 12 p.

Kelley, E.C., 1951, Workshop way of learning: Harper & Brothers, New York, 169 p.

Lewis, R.S., Bush, J.H., Burmester, R.F., Kauffman, J.D., Garwood, D.L., Myers, P.E., and Othberg, K.L., 2005, Geologic map of the Potlatch 30 x 60 minute quadrangle, Idaho: Idaho Geological Survey Geologic Map GM41, scale 1:100,000, 30 p.

Lewis, R.S., Breckenridge, R.M., McFaddan, M.D., and Burmester, R.F., 2006a, Geologic Map of the Trout Peak Quadrangle, Bonner County, Idaho: Idaho Geologic Survey Digital Web Map 58, scale 1:24,000.

Lewis, R.S., Burmester, R.F., Breckenridge, R.M., McFaddan, M.D., Miller, F.K., and Miller, D.M, 2006b, Geologic Map of the Sagle Quadrangle, Bonner County, Idaho: Idaho Geologic Survey Digital Web Map 74, scale 1:24,000.

Lewis, R.S., Burmester, R.F., Breckenridge, R.M., McFaddan M.D., and Phillips W.M., 2008, Preliminary Geologic Map of the Sandpoint 30 x 60 Minute Quadrangle, Idaho and Montana, and the Idaho Part of the Chewelah 30 x 60 Minute Quadrangle: Idaho Geologic Survey Digital Web Map DWM-94.

Link, P.K., Christie-Blick, N., Devlin, W.J., Elston, D.P., Horodyski, R.J., Levy, Marjorie, Miller, J.M.G., Pearson, R.C., Prave, Anthony, Stewart, J.H., Winston, Don, Wright, L.A., Wrucke, C.T., 1993, Middle and Late Proterozoic stratified rocks of the western U.S. Cordillera, Colorado Plateau, and Basin and Range province, *in* Reed, Jr., J.C., Bickford, M.E., Houston, R.S., Link, P.K., Rankin, R.W., Sims, P. K., and VanSchmus W.R., eds., Precambrian: Conterminous U.S. The Geology of North America volume C-2: Decade of North American Geology: Geological Society of America, p. 463-595.

Link, P.K., Fanning, C.M., Lund, K.I., and Aleinikoff, J.N., 2007, Detrital-zircon populations and provenance of Mesoproterozoic strata of east-central Idaho, U.S.A.: SEPM Special Publication no. 86, p. 101–128.

Lonn, J.D., McDonald, C., Sears, J.W., and Smith, L.N., 2010, Geologic map of the Missoula East 30' x 60' quadrangle, western Montana: Montana Bureau of Mines and Geology Open-File Report 593, 2 sheets, scale 1:100,000.

Lonn, J.D., Lewis, R.S., Burmester, R.F., and McFaddan, M.D., 2013, The complex structural geology of the northern Beaverhead Mountains, Montana and Idaho: Northwest Geology, v. 42, p. 111-130.

Lopez, D.A., 1981, Stratigraphy of the Yellowjacket Formation of east-central Idaho: U.S. Geological Survey Open-File Report 81-1088, 219 p.

McBean, A.J., II, 1983. The Proterozoic Gunsight Formation, Idaho-Montana: Stratigraphy, sedimentology, and paleotectonic setting: M.S. thesis, The Pennsylvania State University, 235 p.

McFaddan, M.D., Breckenridge, R.M., Burmester, R.F., and Lewis, R.S., 2006, Geologic Map of the Cabinet Quadrangle, Bonner and Shoshone Counties, Idaho: Idaho Geologic Survey Digital Web Map 60, scale 1:24,000.

Ross, C.P., 1934, Geology and ore deposits of the Casto quadrangle, Idaho: U.S. Geological Survey Bulletin 854, 135 p.

Ross, C.P., 1947, Geology of the Borah Peak Quadrangle, Idaho: Geological Society of America Bulletin, v. 58, p. 1085-1160.

Ross, G.M., and Villeneuve, M., 2003, Provenance of

the Mesoproterozoic (1.45 Ga) Belt basin (western North America): another piece in the pre-Rodinia paleogeographic puzzle: Geological Society of America Bulletin, v. 115, p. 1191-1217.

Ruppel, E.T., 1975, Precambrian Y sedimentary rocks in east-central Idaho: U.S. Geological Survey Professional Paper 889-A, 23 p.

Ruppel, E.T., 1980, Geologic map of the Patterson Quadrangle, Lemhi County, Idaho: U.S. Geological Survey Geologic Quadrangle Map GQ-1529, scale 1:62,500.

Sears. J.W., 2007; Rift destabilization of a Proterozoic epicontinental pediment: a model for the Belt-Purcell basin, North America, *in* Link, P.K., and Lewis, R.S., eds., Proterozoic Geology of Western North America and Siberia: SEPM Special Publication No. 86, ISBN 978-1-56576-126-1, p. 55–64.

Sobel, L.S., 1982, Sedimentology of the Blackbird mining district, Lemhi County, Idaho: Cincinnati, Ohio, University of Cincinnati M.S. thesis, 235 p.

Tietbohl, D., 1986, Middle Proterozoic diamictite beds in the Lemhi Range, east-central Idaho, *in* Roberts, S.M., ed., Belt Supergroup; A guide to Proterozoic rocks of western Montana and adjacent areas: Montana Bureau of Mines and Geology Special Publication 94, p. 197-207.

Tysdal, R.G., 1996a, Geologic map of the Lem Peak quadrangle, Lemhi County, Idaho: U.S. Geological Survey Geologic Quadrangle Map GQ-1777, scale 1:24,000.

Tysdal, R.G., 1996b, Geologic map of parts of the Hayden Creek and Mogg Mountain quadrangles, Lemhi County, Idaho: U.S. Geological Survey Miscellaneous Investigations Series I-2563, scale 1:24,000.

Tysdal, R.G., 2000a, Stratigraphy and depositional environments of Middle Proterozoic rocks, northern part of the Lemhi Range, Lemhi County, Idaho: U.S. Geological Survey Professional Paper 1600, 40 p.

Tysdal, R.G., 2000b, Revision of Middle Proterozoic Yellowjacket Formation, central Idaho: U.S. Geological Survey Professional Paper 1601–A, 14 p.

Tysdal, R.G., 2002, Structural Geology of western part of Lemhi Range, east-central Idaho: U.S. Geological Survey Professional Paper 1659, 33p.

Tysdal, R.G., 2003, Correlation, sedimentology, and structural setting, upper strata of Mesoproterozoic Apple Creek Formation and lower strata of Gunsight Formation, Lemhi Range to Salmon River Mountains, east-central Idaho, *in* Tysdal, R.G., Lindsey, D.A., and Taggart, J.E., Jr., eds., Correlation, sedimentology, structural setting, chemical composition, and provenance of selected formations in Mesoproterozoic Lemhi Group, central Idaho: U.S. Geological Survey Professional Paper 1668-A, p. 1-22.

Tysdal, R.G., and Desborough, G.A., 1997, Scapolitic metaevaporite and carbonate rocks of Proterozoic Yellowjacket Formation, Moyer Creek, Salmon River Mountains, central Idaho: U.S. Geological Survey Open-File Report 97-268, 26 p.

Tysdal, R.G. and Moye, Falma, 1996, Geologic map of the Allison Creek quadrangle, Lemhi County, Idaho: U.S. Geological Survey Geologic Quadrangle Map GQ-1778, scale 1:24,000.

Tysdal, R.G., Evans, K.V., and Lund, K.I, 2000, Geologic map of the Blackbird Mountain quadrangle, Lemhi County, Idaho: U.S. Geological Survey Geological Investigation Series I-2728, scale 1:24,000.

Winston, Don, 1986, Sedimentology of the Ravalli Group, Middle Belt Carbonate and Missoula Group, Middle Proterozoic Belt Supergroup, Montana, Idaho and Washington, *in* Roberts, S.M., ed., Belt Supergroup: A guide to Proterozoic rocks of western Montana and adjacent areas: Montana Bureau of Mines and Geology Special Publication 94, p. 85-124.

Winston, Don, 1993, Carbonate and siliciclastic facies in cycles of the Helena and Wallace formations, Middle Proterozoic Belt Supergroup, *in* Berg, R., ed., Proceedings of Belt Symposium III: Montana Bureau of Mines and Geology Special Publication 112, p. 70–86.

Winston, Don., 2007, Revised Stratigraphy and Depositional History of the Helena and Wallace Formations, Mid-Proterozoic Piegan Group, Belt Supergroup Montana and Idaho, *in* Link, P.K., and Lewis, R.S., eds., Proterozoic Geology of Western North America and Siberia: SEPM Special Publication No. 86, ISBN 978-1-56576-126-1, p. 65–100.

Winston, Don, Link, P.K., and Hathaway, Nathan, 1999, The Yellowjacket is not the Prichard and other heresies–Belt Supergroup correlations, structure, and paleogeography, east-central Idaho, *in* S.S. Hughes, and G.D. Thackray, eds., Guidebook to the Geology of Eastern Idaho: Pocatello, Idaho, Idaho Museum of Natural History, p. 3-20.

PROVENANCE OF THE PLEISTOCENE AND HOLOCENE ST. ANTHONY DUNE FIELD, EASTERN SNAKE RIVER PLAIN, IDAHO: INSIGHTS FROM U/PB DETRITAL ZIRCON GEOCHRONOLOGY

David R. Gaylord,[1] Paul K. Link,[2] and Justin T. McKoon[2]

[1]*School of the Environment, Washington State University, Pullman, WA 99164-2812, gaylordd@wsu.edu;*
[2]*Department of Geosciences, Idaho State University, Pocatello, ID 83209, linkpaul@isu.edu*

ABSTRACT

U/Pb detrital zircon analyses of surface and shallow subsurface Holocene and Late Pleistocene St. Anthony sand dune and alluvial sediment provide new insight into the provenance of paleoclimatically significant eolian deposits on the eastern Snake River Plain, Idaho. Our new detrital zircon geochronologic provenance data suggest that zircons from the Holocene, eastern side of the dune field were derived primarily from the Henry's Fork of the Snake River whereas zircons from buried Late Pleistocene dune sands were derived primarily from the Yellowstone volcanic plateau. On the western side of the dune field, Holocene dune sediment was recycled from Pleistocene Lake Terreton deposits and the Big Lost Trough. These provenance results are consistent with, but also augment, previous sedimentary petrologic and geochemical analyses. The detrital zircon analyses reported here suggest that while the alluvial patterns of the Henry's Fork channel system were largely stable during the Late Pleistocene and Holocene, the landscape and sediment transport patterns of dune sand across the area nevertheless changed. This changing landscape influenced surface and subsurface hydrologic conditions, vegetation types and densities, airflow patterns, and wind strengths, all factors that are commonly inferred from eolian sedimentary deposits. The detrital zircon record presented here: 1) improves understanding of the provenance of the St. Anthony dune field and evolution of the surrounding landscape, and 2) lays the groundwork for interpreting paleoclimate fluctuations from buried eolian, alluvial, and lacustrine deposits that are interstratified with older Pleistocene and Pliocene Snake River Plain basalt flows.

INTRODUCTION

The St. Anthony dune field of eastern Idaho mantles >20,000 km2 of the eastern Snake River Plain with up to 40 m of active and stabilized sand dune and sand sheet deposits that preserve a proxy record of Quaternary landscape evolution and paleoclimate change (Coughlin, 2000; Gaylord and others, 2000; Coleman, 2002; Forman and Pierson, 2003; Hoover, 2014; Rich and others, 2015) (fig. 1). Active dunes in this field consist of >400 km2 of simple and compound barchan, barchanoid ridge, and parabolic dunes in three large dune complexes along a ~35 km long trend that largely parallels the prevailing SW-NE wind direction (figs. 1 and 2). These sand dune and sand sheet deposits cap Pliocene to Holocene basaltic lava flows, alluvium, lake sediment, and loess (Scott, 1982). Thin section point counts and XRF bulk chemical analyses from previous dune-field studies suggest that St. Anthony dune sands originated primarily from Snake River alluvium derived from northeastern sources and secondarily from western Big and Little Lost River alluvium and glacial Lake Terreton sediment (Coughlin, 2000; Gaylord and others, 2000).

In this paper, we report primarily on the U/Pb detrital-zircon geochronology of surface and shallow subsurface sedimentary eolian and alluvial deposits within and near the St. Anthony dune field. The primary goal of this paper is to establish a detrital zircon framework for Late Pleistocene to Holocene eolian and alluvial deposition on the eastern Snake River Plain. Using this depositional framework will also help improve understanding of the influence that airflow-terrain interactions can have on eolian morphology and sedimentology (e.g., Gaylord and Dawson, 1987; Gaylord and Stetler, 1994).

GEOLOGIC SETTING

The eastern Snake River Plain upon which the St. Anthony dune field (fig. 1) and other Quaternary sedimentary deposits reside is an elongate and relatively low-relief volcano-tectonic basin that cuts across the dominant north-south fabric of the northern Basin and Range province (Pierce and Morgan, 1992; Mor-
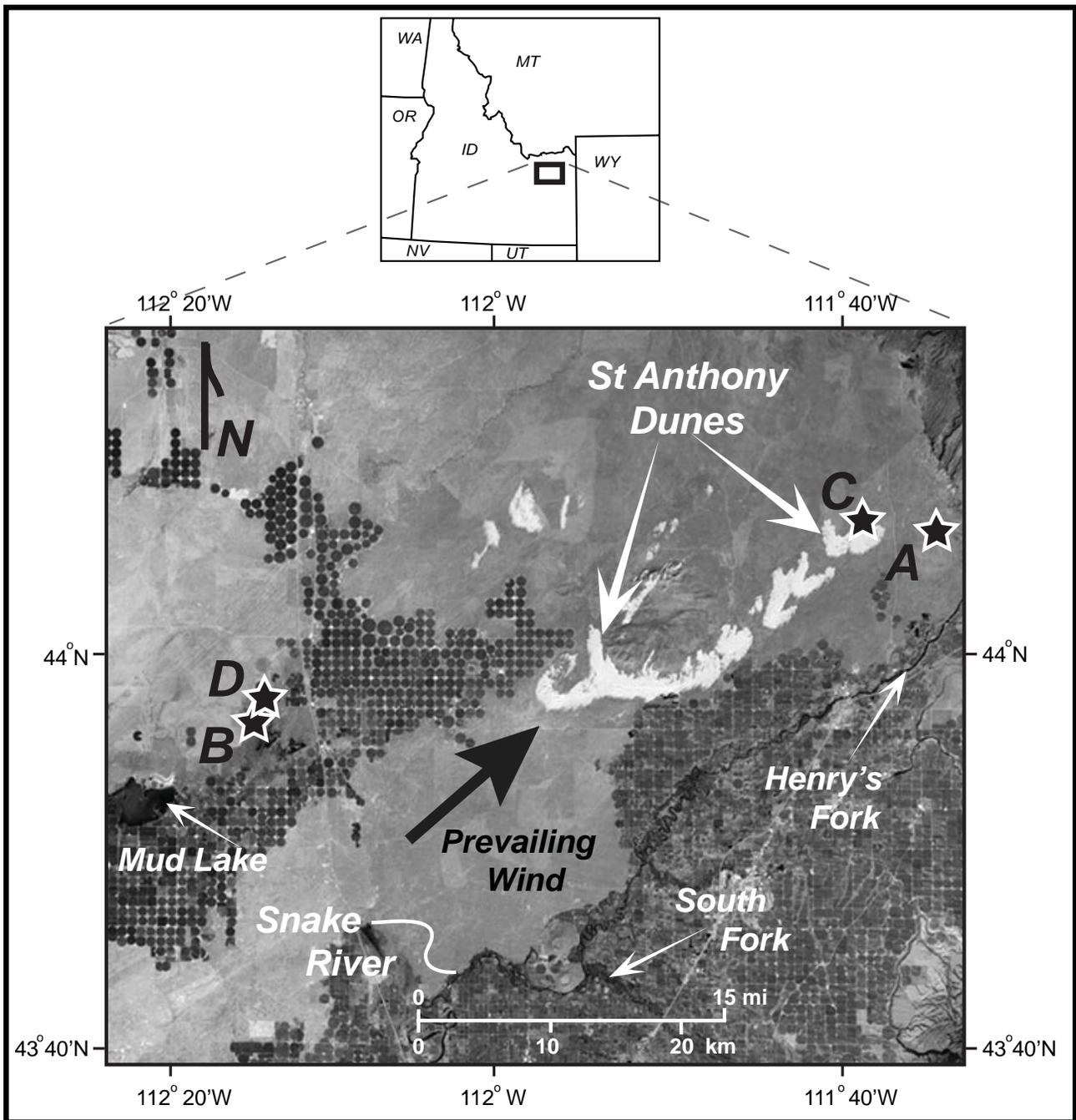
Figure 1. Map showing sample locations (A, B, C, and D) and spatial relations between the St. Anthony dune field, eastern Snake River Plain, Basin and Range uplands (to the north), and the broader Snake River (including the Henrys Fork and South Fork). The Yellowstone Plateau and Tetons are just out of view to the east whereas Mud Lake is visible to the west of sample sites A and D. The eastern boundary of the 10-15 km wide, SW-NE trending, Big Lost Trough is just out of view and ~20 km west of Mud Lake. Image courtesy of Google Earth.
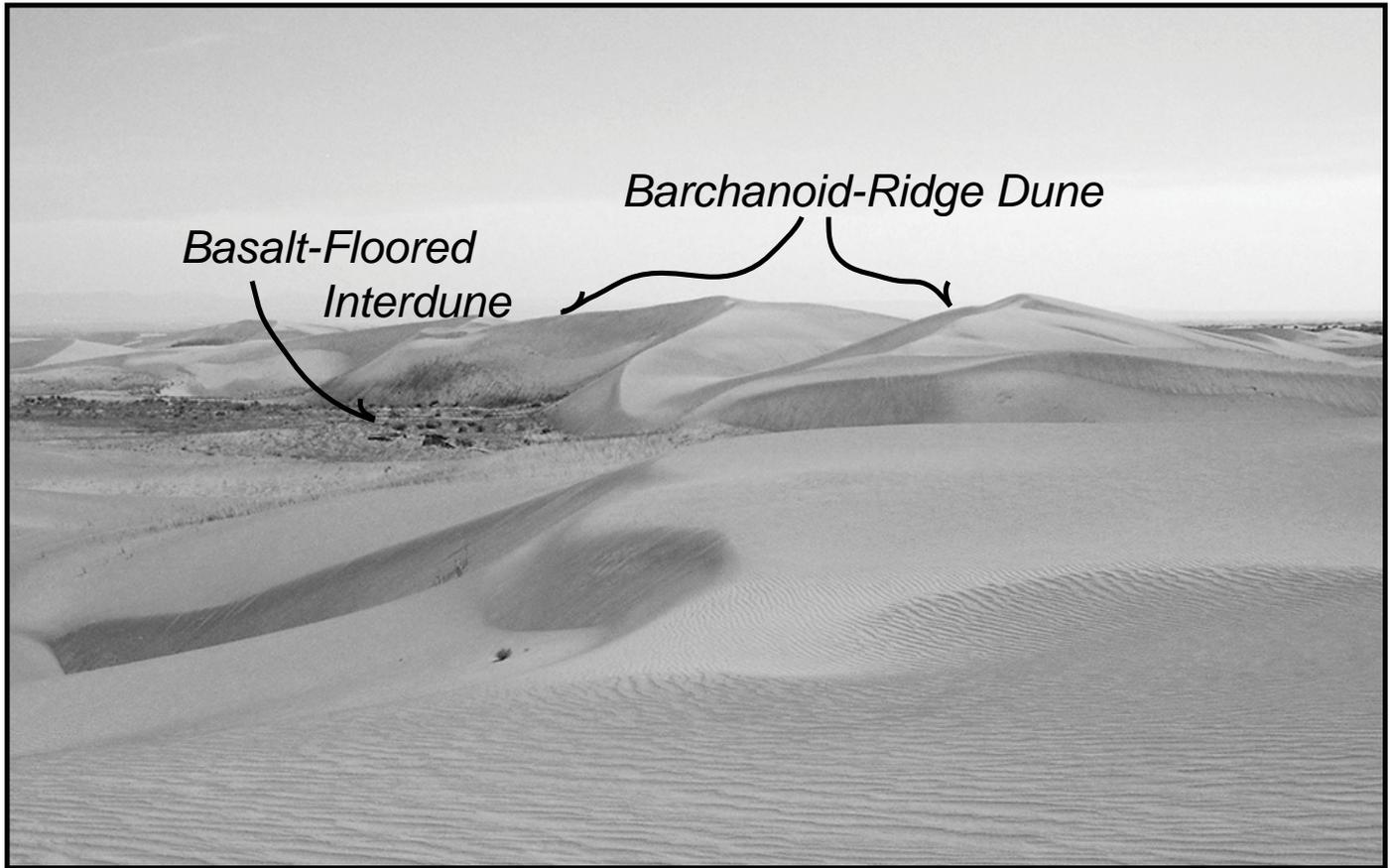
Figure 2. Actively migrating 5-15 m-high barchanoid ridge sand dune within northeastern complex of the St. Anthony dune field. View in this image is to the south from center of Section 25, Township 9N, Range 40E. Migration of this large, sinuous-crested, transversely oriented barchanoid-ridge dune has been from SW to NE (from upper right to lower left of image). Note encroachment of slip face over a dark, sparsely vegetated, basalt-floored interdune.

gan and McIntosh, 2005). The Miocene to Holocene volcanic rocks that dominate the plain resulted from the passage of the North American plate over a mantle hotspot (Pierce and Morgan, 1992; Christiansen, 2001). Volcanism associated with the passage of this hotspot produced a series of caldera complexes that young to the northeast. These complexes are characterized by large-volume rhyolitic eruptive centers that were subsequently buried beneath smaller volume, yet still widespread, basalt flows.

Extensive drill core-based exploration of basaltic strata beneath the Idaho National Laboratory ~40 km west of the St. Anthony dune field revealed a record of Pliocene and Pleistocene lacustrine, fluvial and eolian sedimentation in the Big Lost Trough (Bestland and others, 2002; Gianniny and others, 2002). Quaternary Big Lost Trough sedimentary deposits are closely analogous to those observed at and near the surface of the St. Anthony dune area. The eolian sediment supplies for both were generated primarily during peak glacial episodes in the surrounding Rocky Mountains (Allison, 2001; Gianniny and others, 2002), when

meltwater fed an abundant supply of loose sediment to lower-lying river valleys and lakes. When basin-water levels dropped during interglacial episodes, unconsolidated lake and river sediment was exposed to eolian reworking that produced the sand dunes, sand sheets, and loess deposits that blanket much of the modern landscape of the eastern Snake River Plain (Scott, 1982). The detrital zircon provenance spectra of these sediments and the distribution of their source areas are presented in Link and others (2005, fig. 2). Inferences about source areas for the several detrital zircon age-populations are discussed in greater detail there.

METHODS

A limited number of samples (four) were collected and analyzed to document the broad geochronologic character of the detrital zircon spectra from (three) dune sand accumulations (each with a different estimated age) and from a single alluvial source. This limited dataset was deemed sufficiently representative to provide a foundation upon which to begin documenting the detrital zircon evolution of Holocene and Pleis-

tocene dune sands on the eastern Snake River Plain. We extended sampling of the St. Anthony dune sands into the shallow subsurface (~3.5 m depth) as a first step in bridging the gap in detrital zircon knowledge between these putatively Late Pleistocene dune sands and older Middle to Late Pleistocene sedimentary deposits documented in the Big Lost Trough (Geslin and others, 1999, 2002; Bestland and others, 2002).

Detrital zircon grains were extracted from the four sand-dominated samples by traditional methods that utilized a Wilfley table, heavy-liquid, and magnetic separation. Representative splits of heavy mineral fractions were incorporated into 2.5-cm epoxy mounts, along with fragments of zircon standards. The mounts were ground to a depth of ~20 μm, polished, and imaged optically prior to isotopic analysis. U-Pb analyses were completed for 100 to 300 grains using laser ablation-multicollector-inductively coupled plasma mass spectrometry (LA-MC-ICPMS) at the University of Arizona LaserChron Center, Tucson. Analyses followed procedures established by Gehrels and others (2006, 2008). Age uncertainties, based only on measurement errors, using this method are typically less than ±1% at a 1-sigma level (i.e. ±20 m.y. for a 2000 Ma grain). U-Pb data were plotted on Concordia and age-probability diagrams using the software package Isoplot (Ludwig, 2008). The 206 Pb/207 Pb age is used for grains >1000 Ma and the 206 Pb/238U age is used for younger grains. Analyses >10% discordant or >5% reverse discordant (based on comparison of 206Pb/238U and 206Pb/207Pb ages) were discarded.

More than 300 analyses were acquired from Samples A and C; however, mineral separation difficulties permitted only 102 analyses to be acquired from Samples B and 159 analyses from Sample D (figs. 3, 4, and 5). Nevertheless, in spite of the lower number of total analyses, significant detrital zircon populations are obvious in Samples B and D. In this case, size (number of analyses) does not really matter. Accuracy (i.e., equated here to the content of the primary populations) is evident with 60 analyses (Link and others 2005; Beranek and others, 2006). Precision (population size and peak age) is enhanced by obtaining more analyses.

RESULTS

A schematic chronostratigraphic section compiled from field mapping and subsurface data (fig. 3) reveals the general architecture of the upper, eastern Snake River Plain stratigraphy as well as the approximate locations of the detrital-zircon samples. The interstratified nature of dune sand, alluvial, lake-pond, loess and basalt deposits depicted in this figure captures the breadth of sedimentary and volcanic activity on the modern landscape and provides a basis for estimating the spatial relations between these strata in the subsurface. Though not drawn to scale, the beds are generally from a few meters to <5 m thick; field relations demonstrate that basalt flows and eolian deposits (including loess) are more laterally continuous and traceable than ponded and alluvial sedimentary deposits. Paleosols are common in the subsurface and often correlate with plant rootlet concentrations. The basalt that underlies or is interstratified with sand dune deposition ranges in age from Pliocene to Holocene. In Holocene dunes, samples were collected from upwind and downwind sites (Samples B and C, respectively). Sample A was collected from a Pleistocene dune sand whereas sample D was collected from Pleistocene alluvium that underlies the western margins of the dune field.

Detrital zircon spectra are presented in Figures 4 and 5 originated from: 1) Sample A, an isolated late Pleistocene sand dune deposit that was surrounded by and partially buried beneath a Late Pleistocene basalt with an estimated age >50 ka (Kuntz and others, 1994, 2003). The Pleistocene sand dune deposits depicted near the middle of the schematic section (fig. 3) are analogous to Sample A; 2) Samples B and C, Holocene dune sand collected from the proximal-to-source (southwest) and distal (northeast) sides, respectively, of the modern St. Anthony dune field. These samples are analogous to those depicted in the upper, Holocene part of Figure 3; and 3) Sample D, Late Pleistocene alluvial deposits of the Henry's Fork of the Snake River at a site located upwind from the most active Holocene dune sands. Analogous Pleistocene alluvium is depicted near the center of Figure 3. Comparing these detrital zircon data with those from sands in the Big and Little Lost River system to the west (Geslin and others, 1999, 2002) and Pleistocene and Holocene loess deposited elsewhere on the Snake River Plain (Link and others, 2005) facilitates interpretation of

Depositional Processes and Deposits

Eolian: Active & Stabilized Sand Dunes & Sand Sheets **[Samples B and C]**

Subaqueous & Subaerial Suspension Settling: Pond & Loess Clayey Silt

Eolian: Active & Stabilized Sand Dunes & Sand Sheets **[Sample A (>50 ka)]**

Lava Flows: Basalt

Eolian: Active & Stabilized Sand Dunes & Sand Sheets

Alluvial: Channel Sand & Gravel **[Sample D]**

Lava Flows: Basalt
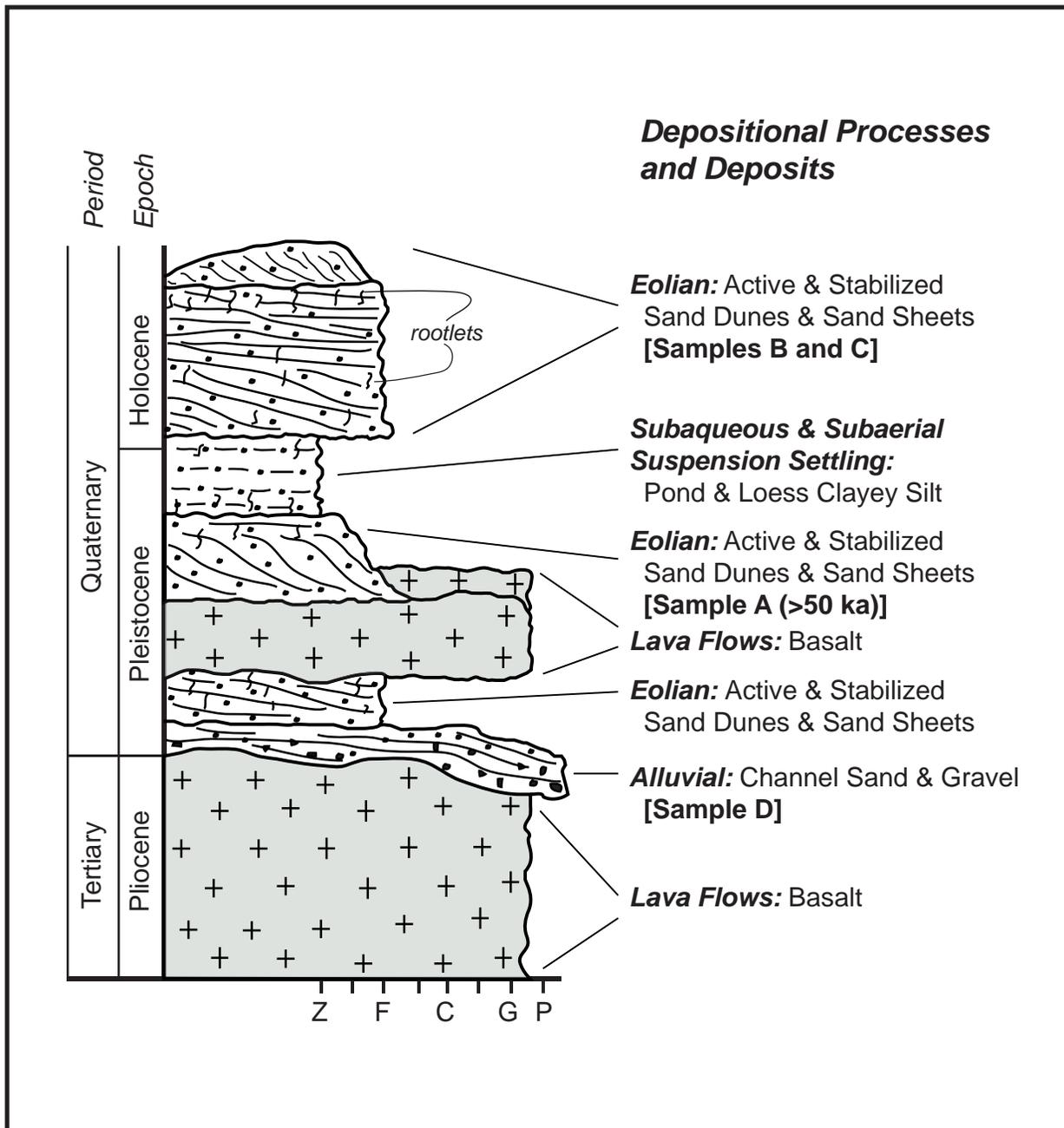
Figure 3. Schematic chronostratigraphic section of the eastern Snake River Plain, Idaho illustrating the range of depositional processes and deposits of interstratified sedimentary and volcanic deposits. Approximate sample locations are identified in text to right of section. Though the section is not to scale the depicted beds commonly are from a few to < 5 m thick. Symbol Explanation: Z=Silt; F=Fine Sand; C=Coarse Sand; G=Granule; P=Pebble. Rootlets occur in all sedimentary deposits. Where densely concentrated, rootlets commonly coincide with carbonate- and gypsum-cemented paleosols.

sand transport directions and source-sediment relations. Figure 4 contains full plots of all the grains in each sample. Figure 5 displays only Mesozoic and Tertiary grains; however, these young <120 Ma grains reveal the most geologically significant relations.

Figure 4 shows intermediate to small populations of Precambrian detrital zircons found in Sample D (Henry's Fork alluvium). These populations include recycled Grenville (~950 to 1300 Ma), Paleoprotero-

zoic 1600-1800 Ma grains, likely recycled from upper Belt Supergroup strata (peak at 1735 Ma), and sparse Archean grains. These populations also are consistent with those of detrital zircons identified in fluvial and eolian sedimentary deposits from the upper to middle Snake River depositional system (Link and others, 2005).

The three significant Mesozoic and Tertiary U/ Pb detrital zircon grain-populations recognized in the
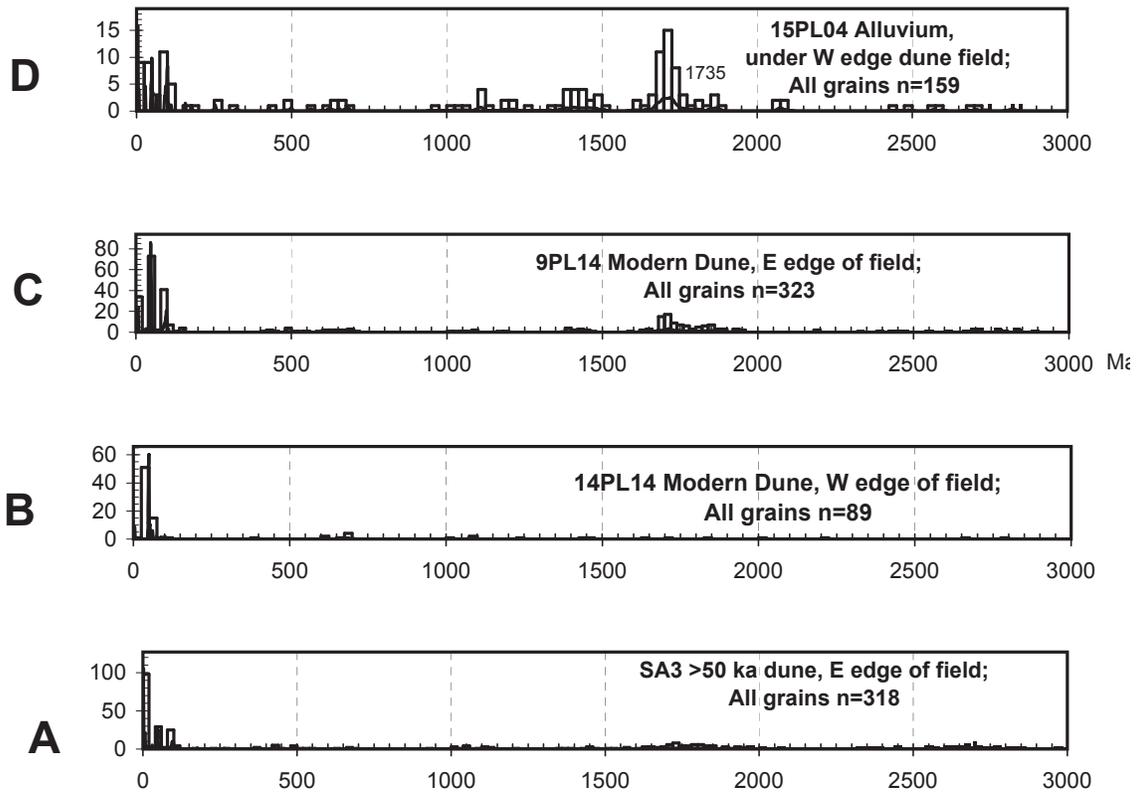
All grains are plotted;
small number is estimated 1735 Ma age-peak

Figure 4. Probability-density curves for all grains from four samples collected from the St. Anthony dune area. Histograms (25 m.y. wide) show binned ages. Graph shows probability-density curve, which takes one sigma standard deviation into account. Peak ages are shown for the 1735 Ma Paleoproterozoic group in Sample D, Henry's Fork alluvium.

samples analyzed in this study are obvious in Figure 5. The figure also shows (in the small font) the age peaks of the probability distributions, which gives a reasonable estimate of the age distribution of that source population. The youngest grain-population includes grains <10 Ma with provenance from the Yellowstone-Snake River Plain magmatic system (Pierce and Morgan, 1992; Link and others, 2005). This provenance includes 4 to 7 Ma grains from the Heise volcanic field and 0 to 2 Ma grains from the Yellowstone volcanic field (major eruptions at 0.6, 1.2 and 2.0 Ma). The precision of the U/Pb detrital zircon age analyses for these very young (<2 Ma) grains, however, is low (perhaps 5%). The second largest age group is Eocene (45 to 50 Ma), derived from Challis magmatic rocks exposed in central Idaho. The third group is Late Cretaceous (80 to 100 Ma) grains ultimately derived from the Idaho batholith of central Idaho. As discussed in Link and others (2005) these Cretaceous grains were likely recycled through Late Cretaceous sandstones from the Montana-Wyoming thrust belt. Their ultimate source was the Idaho batholith and their proximate

source was the Henry's Fork of the Snake River.

Sample A, collected from a depth of ~3.5 m within a Late Pleistocene sand dune, is estimated to be older than 50 ka based on ages discerned from field relations and preliminary $^{40}Ar/^{39}Ar$ dates (Creighton, 1987; Ferdock, 1987; Kuntz and others, 2003; M.A. Kuntz, personal communication, 2014). This sample contains a far greater percentage of grains derived from the Yellowstone volcanic field (peaks at 0.6 and 2.0 Ma) than any other sample. It also has the fewest Challis magmatic grains (peak at 49 Ma).

Sample B, a Holocene dune sand from the upwind, western side of the dune field contains no Yellowstone grains, abundant Eocene grains (peak at 49 Ma), and no 80-100 Ma grains. This detrital-zircon content is consistent with its derivation from the Lake Terreton area and the Big Lost Trough.

Sample C is a Holocene sand from the distal, downwind side of the St. Anthony dune field. It contains abundant Eocene grains (peak at 48 Ma) as well
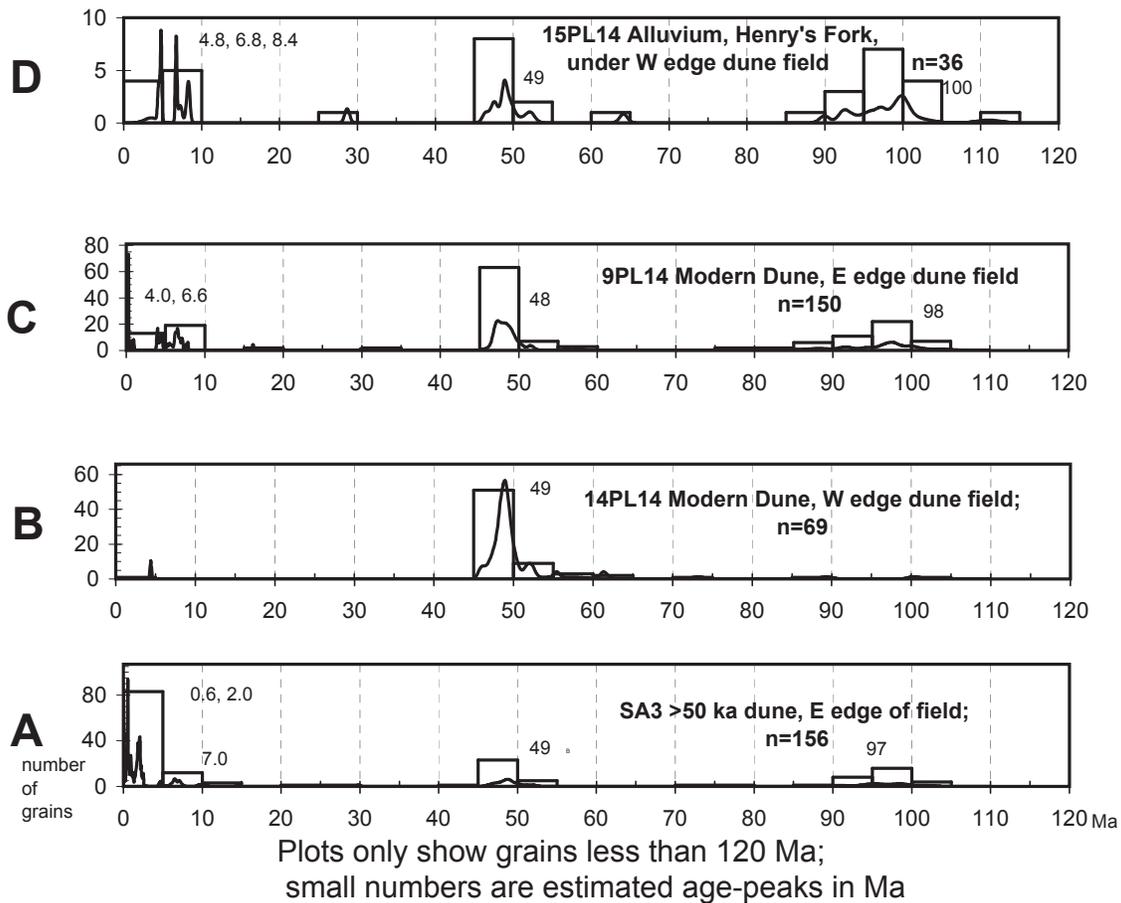
Figure 5. Probability-density curves from the four samples for grains <120 Ma. Histograms (5 m.y. wide) show binned ages. Graph shows probability-density curve, which takes one sigma standard deviation into account. Peak ages are shown, and represent, from older to younger, reworked Idaho batholith, direct and reworked Challis magmatic, and Yellowstone-Snake River Plain grains (Yellowstone field is 0 to 2 Ma and Heise field is 4 to 7 Ma). This figure only shows ages (and number of analyses) for grains <120 Ma. These are the age groupings that show significant variation between samples.

as Heise volcanic field (peaks at 4.0 and 6.6 Ma) and recycled Idaho batholith grains (dispersed ages that peak at 98 Ma).

Sample D, which was collected from Pleistocene Henry's Fork alluvium (as mapped by Scott, 1982) is exposed near Camas National Wildlife Refuge. It contains all three Mesozoic to Tertiary grain groups described previously. The Snake River Plain-Yellowstone grains in this alluvium are largely >5 Ma (peaks at 6.7 and 8.3 Ma). This sample contains more than 50% pre-Mesozoic grains that are interpreted to have been transported by the Henry's Fork from sources in the Montana-Wyoming thrust belt.

INTERPRETATION AND DISCUSSION

The older age distribution of Snake River Plain-Yellowstone grains in Henry's Fork alluvium (Sample D) is similar to Sample C, from the eastern Holocene dune field, and contrasts with that of Sample A, the

Late Pleistocene dune sand. The detrital zircon grain-populations in Sample D are similar to those reported in previous studies of the Henry's Fork (Link and others, 2005); this similarity suggests a relatively stable and long-standing alluvial system (Coughlin, 2000; Gaylord and others, 2000).

Sample B, from the western edge of the dune field demonstrates clastic sedimentary input from western and northern sediment sources including the Big and Little Lost River system, and smaller northern drainages including Birch Creek and Camas Creek. We hypothesize that sediment from these western and northern sources was mixed in glacial Lake Terreton and, following drops in lake levels, exposed, and subsequently reworked by the wind. Many questions, however, remain regarding the timing and nature of Quaternary eolian activity in this region.

SUMMARY AND CONCLUSIONS

Investigation of detrital zircon populations from a broadly representative but limited set of Quaternary eolian and alluvial sedimentary samples within and surrounding the St. Anthony dune field reveals that the modern landscape and associated sediment-transport pathways have experienced elements of both stability and change since the Late Pleistocene. A relatively stable Henry's Fork of the Snake River alluvial system is suggested by the similarities between the detrital zircon grain-populations of the Late Pleistocene alluvial deposits analyzed in this study and those from the Big Lost Trough to the west. The Challis-aged detrital content of the upwind, western Holocene dune sand suggests it was sourced from the Lake Terreton–Mud Lake area to the west but not from eastern sources. In contrast, the Holocene and Late Pleistocene dune sands from the eastern side of the dune field contain abundant Yellowstone-Snake River Plain magmatic grains that were primarily derived from the Heise volcanic field.

The older, partially basalt-encased Late Pleistocene dune sand (Sample A) contains far more very young Yellowstone volcanic field-derived grains than Sample C (distal Holocene dune sand), perhaps because sediment was transported there via strong west- and south-directed winds that originated from ice-covered portions of the nearby Yellowstone Plateau and the Teton Range during glacial maxima.

In sum, this study suggests both a relatively stable Henry's Fork alluvial system and an evolving eolian system in which landscape- and climatically induced changes periodically modified eolian sedimentary transport and depositional patterns. A more comprehensive sampling program of Quaternary source sediment and dune sand in this region will improve understanding of the landscape evolution and provide the insight necessary to interpret the influence of paleoclimate fluctuations on the eolian proxy depositional record preserved in the St. Anthony area.

ACKNOWLEDGMENTS

REFERENCES

Allison, R. R., 2001, Climatic, volcanic, and tectonic influences on Late Pleistocene sedimentation along the Snake River and in Market Lake: Bonneville, Jefferson, and Madison Counties, Idaho: Pocatello, Idaho State University, M.S. Unpublished Thesis, 116 pp.

Beranek, L.P., Link, P.K., and Fanning, C.M, 2006, Miocene to Holocene landscape evolution of the western Snake River Plain region, Idaho: Using the SHRIMP detrital zircon provenance record to track eastward migration of the Yellowstone hotspot: Geological Society of America Bulletin, v. 118, p. 1027-1050.

Bestland, E.A., Link, P.K., Lanphere, M.A., and Champion, D.E., 2002, Paleoenvironments of sedimentary interbeds in the Pliocene and Quaternary Big Lost Trough, eastern Snake River Plain, Idaho, *in* Link, P.K., and Mink, L.L., eds., Geology, Hydrogeology, and Environmental Remediation: Idaho National Engineering and Environmental Laboratory, Eastern Snake River Plain, Idaho:, Geological Society of America Special Paper 353, p. 27-44.

Christiansen, R.L., 2001, The Quaternary and Pliocene Yellowstone Plateau Volcanic Field of Wyoming, Idaho, and Montana: U.S. Geological Survey Professional Paper 729G, 145 pp.

Coleman, A. J., 2002, Mid-to-late Holocene eolian, alluvial and lacustrine deposits and paleoclimate fluctuations from the eastern St. Anthony dune field, southeastern Idaho; Pullman, Washington St. University, Unpublished M.S. Thesis, 103 pp.

Coughlin, J., 2000, Sedimentary and geomorphic development and climatic implications of the St. Anthony dune field, Fremont County, southeastern Idaho: Pullman, Washington State University, Unpublished M.S. Thesis, 83 pp.

Creighton, D.N., 1987, Menan Buttes, southeastern

Idaho, *in* Beus, S.S., ed., Centennial Field Guide, volume 2, Rocky Mountain Section of the Geological Society of America, p. 109-111.

Ferdock, G.C., 1987, Geology of the Menan volcanic complex and related volcanic features, northeastern Snake River Plain, Idaho; Pocatello, Idaho St. University, Unpublished M.S. Thesis, 171 pp.

Forman, S. L., and Pierson, J., 2003, Formation of linear and parabolic dunes on the eastern Snake River Plain, Idaho in the nineteenth century: Geomorphology, v. 56, p. 189–200.

Gaylord, D.R., and Dawson, P.J., 1987, Airflow-terrains interactions through a mountain gap - with an example of eolian activity beneath an atmospheric hydraulic jump: Geology, v. 15, p. 789-792.

Gaylord, D.R., and Stetler, L.D., 1994, Eolian-climatic thresholds and sand dunes at the Hanford Site, south-central Washington, USA: Journal of Arid Environments, v. 28, p. 95-116

Gaylord, D. R., Coughlin, J., Coleman, A., Sweeney, M., and Rutford, R.H., 2000, Holocene sand dune activity and paleoclimate from Sand Creek, St. Anthony dune field, Idaho: Geological Society of America, Abstracts with Programs, Rocky Mountain Section Meeting, (April 17-19), University of Montana, Missoula, Montana, v. 32, no 5, p.10.

Gehrels, G., Valencia, V., and Pullen, 2006, Detrital zircon geochronology by laser-ablation multicollector ICPMS at the Arizona LaserChron Center: Paleontological Society Papers, v. 12, 67 pp.

Gehrels, G.E., Valencia, V.A., and Ruiz, VJ., 2008, Enhanced precision, accuracy, efficiency, and spatial resolution of U-Pb ages by laser ablation–multicollector–inductively coupled plasma–mass spectrometry, Geochemistry, Geophysics, Geosystems, v. 9, Q03017, doi:10.1029/2007GC001805.

Geslin, J.K., Link, P.K, and Fanning, C.M., 1999, High-precision provenance determination using detrital-zircon ages and petrography of Quaternary sands on the eastern Snake River Plain, Idaho: Geology, v. 27, p. 295-298.

Geslin, J.K., Link, P.K., Riesterer, J.W., Kuntz, M.A., and Fanning, C.M., 2002, Pliocene and Quaternary stratigraphic architecture and drainage systems of the Big Lost Trough, northeastern Snake River Plain, Idaho, *in* Link, P.K., and Mink, L.L., eds.,

Geology, Hydrogeology, and Environmental Remediation: Idaho National Engineering and Environmental Laboratory, Eastern Snake River Plain, Idaho: Geological Society of America Special Paper 353, p. 11-26.

Gianniny, G.L., Thackray, G.D., Kaufman, D.S., Forman, S.L., Sherbondy, M.J., Findeisen, D., 2002, Late Quaternary highlands in the Mud Lake and Big Lost Trough sub basins of Lake Terreton, Idaho, *in* Link, P.K., and Mink, L.L., eds., Geology, Hydrogeology, and Environmental Remediation: Idaho National Engineering and Environmental Laboratory, Eastern Snake River Plain, Idaho: Boulder Colorado, Geological Society of America Special Paper 353, p. 77-90.

Hoover, R.H., 2014, Investigation of the influences of meteorology and topographic features on the mobility of the NE portion of the St. Anthony dune field, Idaho: Pullman, Washington State University, Unpublished M.S. Thesis, 98 pp.

Kuntz, M.A., Skipp, B., Lanphere, M.A., Scott, W.E., Pierce, K.L., Dalrymple, G.B., Champion, D.E., Embree, G.F., Page, W.R., Morgan, L.A., Smith, R.P., Hackett, W.R., and Rodgers, D.W., 1994, Geological map of the Idaho National Engineering Laboratory and adjoining areas, eastern Idaho: U.S. Geological Survey Miscellaneous Investigations Series Map I-2330, scale 1:100,000.

Kuntz, M.A., Geslin, J.K., Mark, L.E, Hodges, M.K.V., Kauffman, M.E., Champion, D.E., Lanphere, M.R., Rodgers, D.W., Anders, M.H., Link, P.K., and Boyack, D.L., 2003, Geologic Map of the northern and central parts of the Idaho National Engineering and Environmental Laboratory, Eastern Idaho: Idaho Geological Survey Geologic Map 35, scale 1:50,000.

Link, P.K., Fanning, C.M., and Beranek, L.P., 2005, Reliability and longitudinal change of detrital-zircon age spectra in the Snake River system, Idaho and Wyoming: An example of reproducing the bumpy barcode: Sedimentary Geology, v. 182, p. 101-142.

Ludwig, K. R., 2008, User's manual for Isoplot 3.6: a Geochronological Toolkit for Microsoft Excel. Berkeley Geochronology Center Special Publication, Berkeley, CA.

Morgan, L.A., and McIntosh, W.C., 2005, Timing and development of the Heise volcanic field: Geologi-

cal Society of America Bulletin, v. 117, p. 288-306.

Pierce, K.L., and Morgan, L. A., 1992, The track of the Yellowstone hot spot : Volcanism, faulting, and uplift, *in* Link, P.K., Kuntz, M.A., and Platt, L.B., (eds.), Regional Geology of Eastern Idaho and Western Wyoming: Geological Society of America Memoir 179, p. 1-54.

Rich, J., Rittenour, T.M., Nelson, M.S., and Owen, J., 2015, OSL chronology of middle to late Holocene aeolian activity in the St. Anthony dune field, southeastern Idaho, USA: Quaternary International, v. 362, p. 1-10.

Scott, W. D., 1982, Surficial geologic map of the eastern Snake River Plain and adjacent areas, 111°-115°W, Idaho and Wyoming: U.S. Geological Survey Miscellaneous Series Map I-1372. Scale 1:250,000.

FIELD GUIDES

EXPLORATION OF THE COPPER CLIFF MINING DISTRICT: PRE-MEETING FIELD TRIP

Clinton Roberts[1] and Whitney Bausch[2]

[1]*Project Manager, Kennecott Exploration;* [2]*Geologist, Childs Geoscience Inc.*

INTRODUCTION

The Copper Cliff district is located within the Garnet Range approximately 57 km (35 mi) east of Missoula in Missoula and Granite Counties. Ore was discovered in 1891 by W.P. Shipler (Irving, 1963), and the district has been prospected for over 100 years. Past production was fairly insignificant, probably amounting to only a few thousand tons from which recorded smelter returns show recoveries of 110,898 lbs. of Cu, 259 oz. of Au, and 567 oz. of Ag, primarily from siliceous breccia ores from the Copper Cliff and Leonard mines. Anaconda Copper Mining Company first recognized the potential for deep porphyry copper mineralization over 30 years ago and ran an IP (induced polarization) survey across the property including a long line up the Union Creek drainage that yielded positive results.

The Copper Cliff district is underlain by a thick sequence of Proterozoic Belt Supergroup clastic metasediments and overlying Cambrian carbonates and shales that occupy the southern flank of a broad SE-plunging anticline (fig. 1). A series of intermediate composition Tertiary high level dikes and plugs intrude these strata along distinct linear belts that trend northeast, northwest, and east-northeast. Coeval Tertiary volcanics are exposed a short distance to the south of the property.

Advanced argillic alteration, characterized by variable development of quartz, alunite, kaolinite, dickite, pyrophyllite and diaspore is the predominant alteration type in the central part of the property and shows moderate to strong spatial correlation with anomalous Cu and Au in soil and rock samples. Siliceous breccia dikes cut both sediments and intrusive rock and locally contain high grades of Cu-Au in the form of interstitial sulfosalts, sulfides, and oxides and are flanked by quartz-alunite alteration in the intrusive wall rocks. This alteration is flanked by argillic, intermediate argillic, and lesser propylitic alteration assemblages and all are within a broad envelope of bleached and variably pyritized metasediments of the Belt Supergroup.

The current target being explored by Kennecott Exploration is a deep Cu-Au porphyry system related to the high sulfidation assemblage and advanced argillic alteration at Copper Cliff. Coincident geochemical, magnetic, and IP (induced polarization) anomalies help to guide the exploration.

FIELD TRIP ITINERARY

The tour of the Copper Cliff project will begin at the Kennecot core shed (fig. 1). We will then travel about 8 miles to Union Creek to the Copper Cliff mine area for subsequent stops (figs. 2 and 3).

STOP 1 | Potomac Core Shed

The Kennecott core shed is located at 124 Morrison Lane, Building A in Potomac, MT. This stop will begin with a Safety Induction to familiarize everyone with hazards and safety procedures.

Once everyone has been inducted, there will be a tour of the core logging area and the core cutting facility followed by an introduction to the geology of the Copper Cliff project. Kennecott uses a fully-automated NTT core saw (fig. 4), which greatly increases core cutting efficiency and quality.
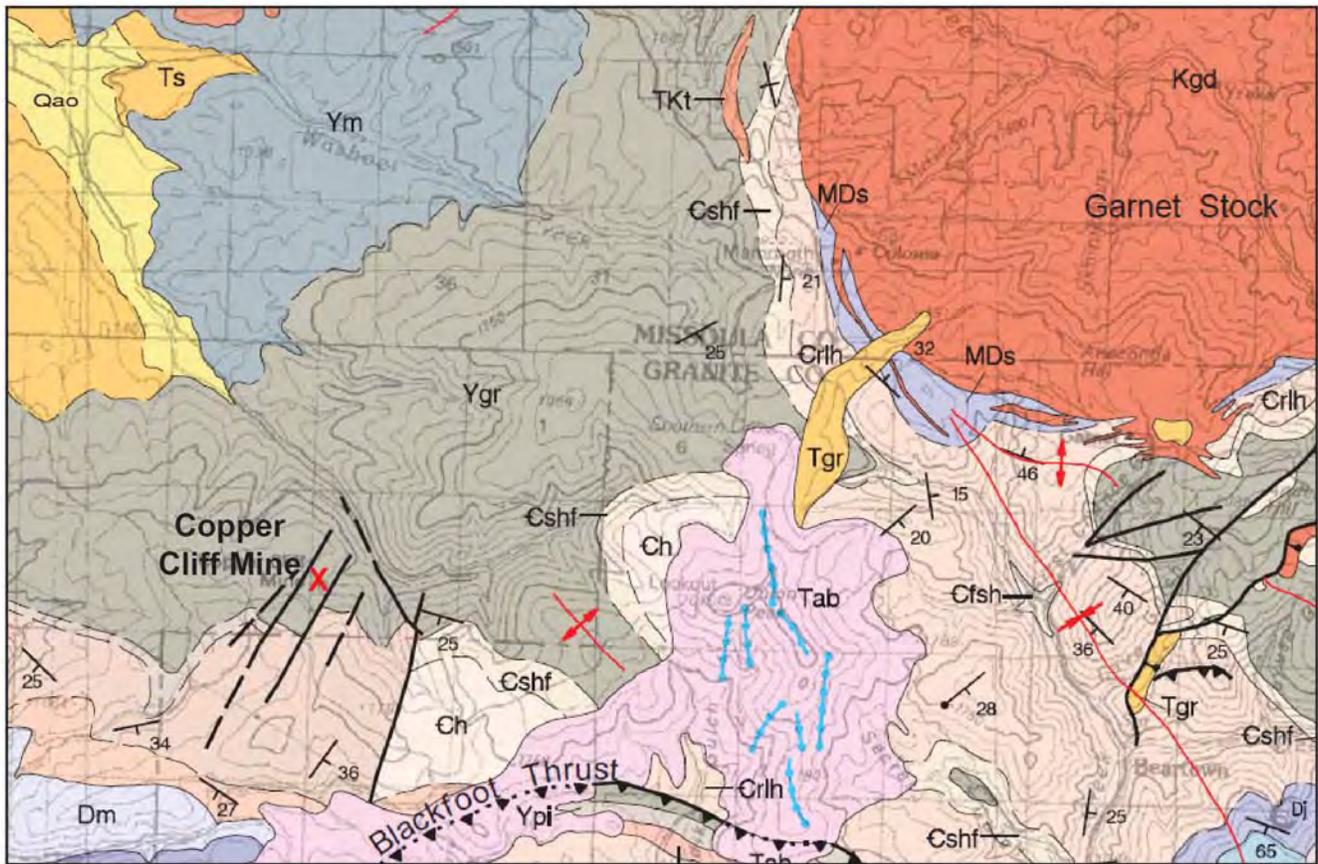
MAP UNITS

Ts	Tertiary sediments	
Tab	Andesite and basalt	
TKt	Trachyte	
Kgd	Granodiorite	
MDs	Three Forks, Jefferson, Maywood Fms, undivided	
Dj	Jefferson Fm	
Dm	Maywood Fm	
Crlh	Red Lion and Hasmark Fms	
Ch	Hasmark Fm	
Cshf	Silver Hill and Flathead Fms	
Ypi	Pilcher Fm	
Ygr	Garnet Fm	
Ym	McNamara Fm	
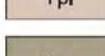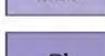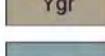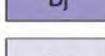
Figure 1. Regional geologic map of the area around the Copper Cliff project.
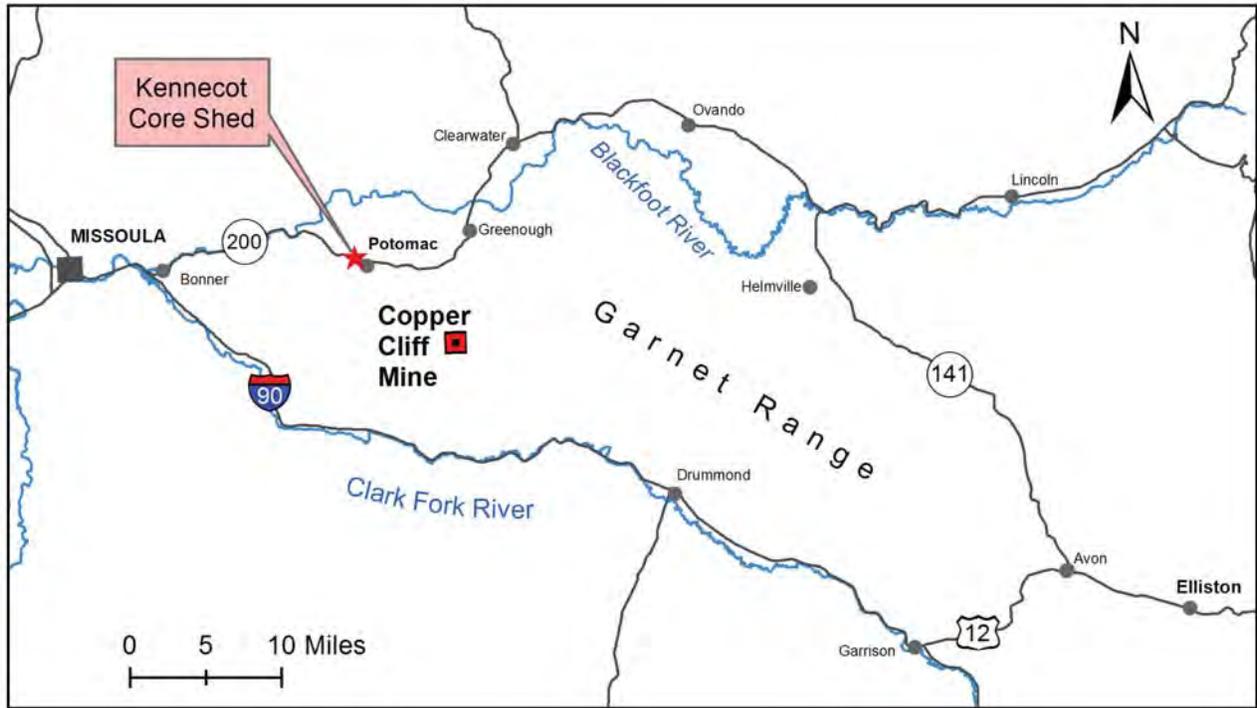
Figure 2. Location of Stop 1 (Potomac warehouse) and Copper Cliff project in relation to Missoula and Elliston.
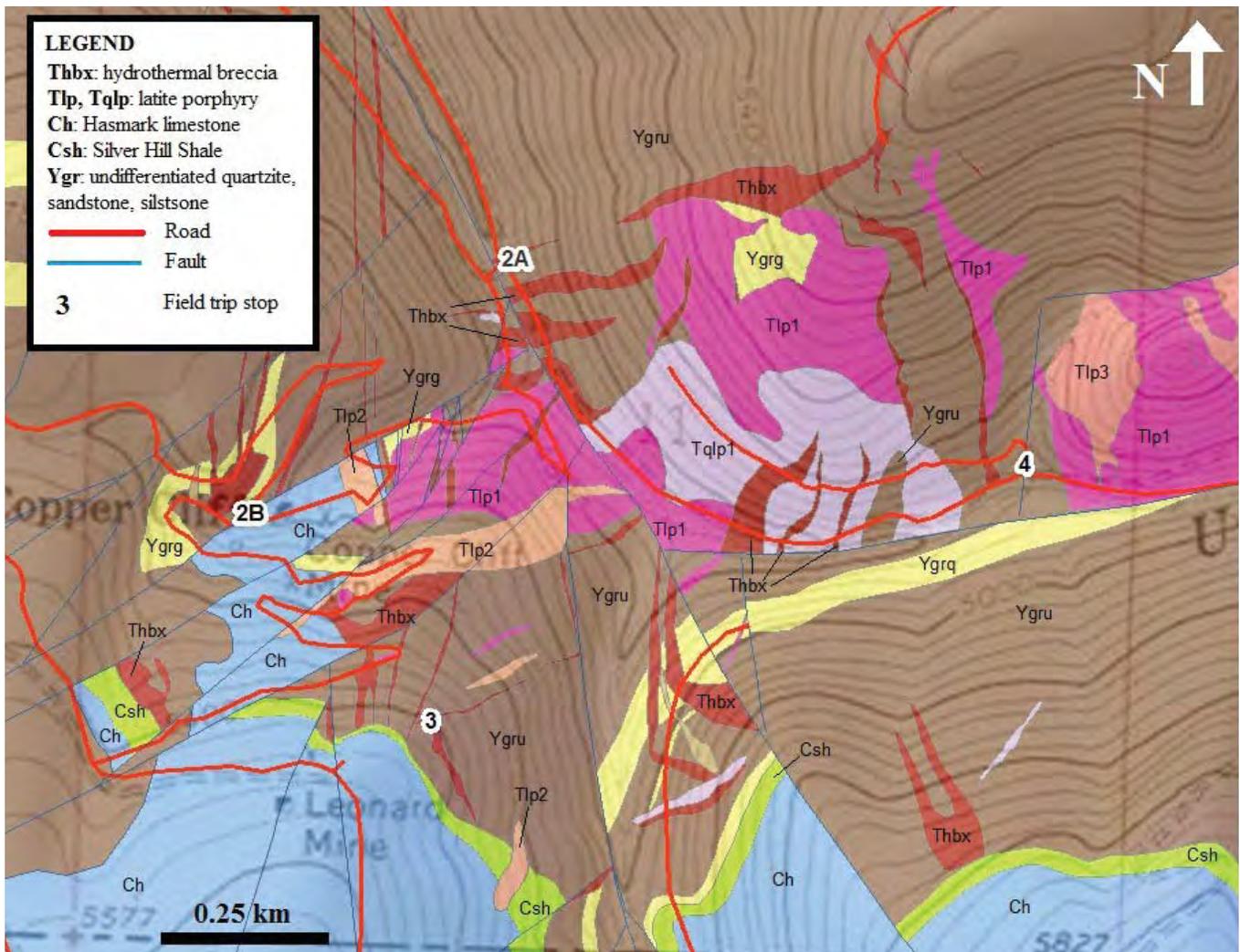
Figure 3. Field trip stops on geologic map of Copper Cliff.

Figure 4. NTT Automated Core Saw (located against back wall) used on the Copper Cliff project

STOP 2A | Frog's Diner Adit

A quick stop will take place at Frog's Diner Adit (fig. 3). This collapsed adit has been developed into a spring in accordance with state regulations and provides water for diamond drilling. Water consumption at Copper Cliff is minimized with the use of a centrifuge, thus keeping the average overall water consumption at 1 gallon per minute for the duration of the drilling program.

STOP 2B | Copper Cliff

We will visit the Copper Cliff hydrothermal breccia exposure and look at the copper mineralization (fig. 5). This stop highlights one of the most interesting features in the area as there are very few outcrops of the breccia. The breccia is within the Mesoproterozoic Garnet Range Formation.

Figure 5. Copper staining on exposed hydrothermal breccia pipe at Copper Cliff.

STOP 3 | Klenzie Mine

The contact separating the Garnet Range and Silver Hill formations, which is present where the Silver Hill Formation is not underlain by the Flathead quartzite, is exposed at the Klenzie mine portal. The exposure is aligned along a northeast trending fault within the Cambrian Silver Hill Formation. Gold and copper mineralization is present within silicified carbonates and breccias. Here, jasperoidal breccia cuts the Garnet Range Formation (fig. 3). The breccia is similar to the hydrothermal breccia exposed at Copper Cliff, but contains predominately silicified limestone clasts (Ellsworth, 1993).

STOP 4 | Drill Sites

We will travel to one of the active drill sites (fig. 6) to observe the drilling process. There we will see drillers obtaining core, review the diamond drilling equipment, discuss the benefits of the centrifuge, and learn about Rio Tinto HSEC requirements. All participants will be required to wear the appropriate PPE while visiting the drill rig. If time allows, the group will visit a reclaimed drill site.

Figure 6. Active drill pad.

REFERENCES

Ellsworth, Peter C., 1993, Alteration and Mineralization of the Copper Cliff Prospect, Garnet Range, Montana, M.S. thesis, University of Montana, Missoula.

Irving, J.G., 1963, Report on Copper Cliff mining district, Missoula and Granite Counties, Montana: In-house consultant Report to the American Mining Company, 54 p.

Lonn, J.D., McDonald, Catherine, Sears, J.W., and Smith, L.N., 2010, Geologic map of the Missoula East 30′ x 60′ quadrangle, western Montana: Montana Bureau of Mines and Geology Open-File Report 593, scale 1:100,000.

Pederson, R.J., 1988, Preliminary evaluation report on the Copper Cliff and Garnet prospects, Missoula and Granite Counties, Montana: Western Energy Company unpublished in-house report, 29 p.

Sillitoe, R.H., 1988, Gold and silver deposits in porphyry systems, in Shafer, R.W. Cooper, J.J., and Vikre, P.G., eds., Bulk minable precious metal deposits of the western United States, Symposium Proceedings: Reno, Geologic Society of Nevada, p. 233-257.
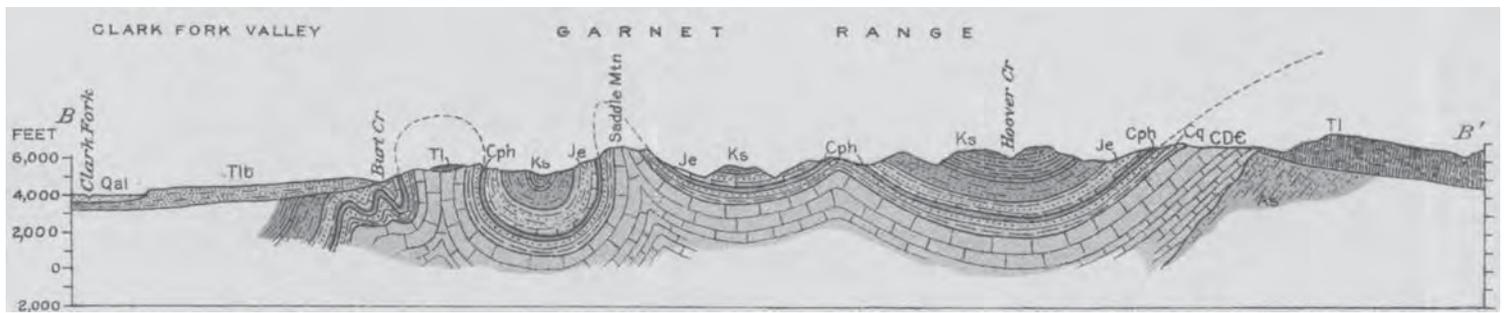
CLARK FORK VALLEY   G A R N E T   R A N G E

GEOLOGIC RELATIONSHIPS IN THE NORTHERN HELENA SALIENT, MONTANA: GEOLOGY OF THE ELLISTON REGION

J.B. Mahoney,[1] G.S. Pignotta,[1] P.D. Ihinger,[1] C. Wittkop,[2] E.A. Balgord,[3] J.J. Potter,[4] and A. Leistikow[1]

[1]*Department of Geology, University of Wisconsin-Eau Claire;* [2]*Department of Chemistry and Geology, Minnesota State University-Mankato;* [3]*Department of Geosciences, University of Arizona;*[4]*Call & Nicholas, Inc., Tucson, Arizona*

INTRODUCTION

The Elliston region is located in the northern portion of the Helena Salient, a broad, convex-eastward protrusion of the Montana Disturbed Belt (fig. 1). The Helena Salient is unique within the Cordilleran fold and thrust belt, as it encompasses both the Helena embayment, a pronounced eastward projection of the Mesoproterozoic Belt-Purcell basin (Sears, 2007) and the entire Boulder Batholith, a major Late Cretaceous intrusive complex emplaced within the orogenic wedge far east of the main axis of the magmatic arc (Lageson and others, 2001). The origin of the Helena Salient and the relationship between thrust belt development and magmatism is a matter of debate (Schmidt and others, 1990; Kalakay and others, 2001; Lageson and others, 2001).

The tectonic evolution of the Helena Salient is complex, characterized by Late Cretaceous folding and thrust fault imbrication of Mesoproterozoic to Cretaceous strata during the Sevier orogenic event, pre-, syn- and post-deformational emplacement of the Boulder Batholith magmatic system, and Paleocene to Eocene extensional deformation and volcanism (Robinson and others, 1968; Ruppel and others, 1981; Smedes and others, 1988; Schmidt and others, 1994; Foster and others, 2010). Geologic investigations in
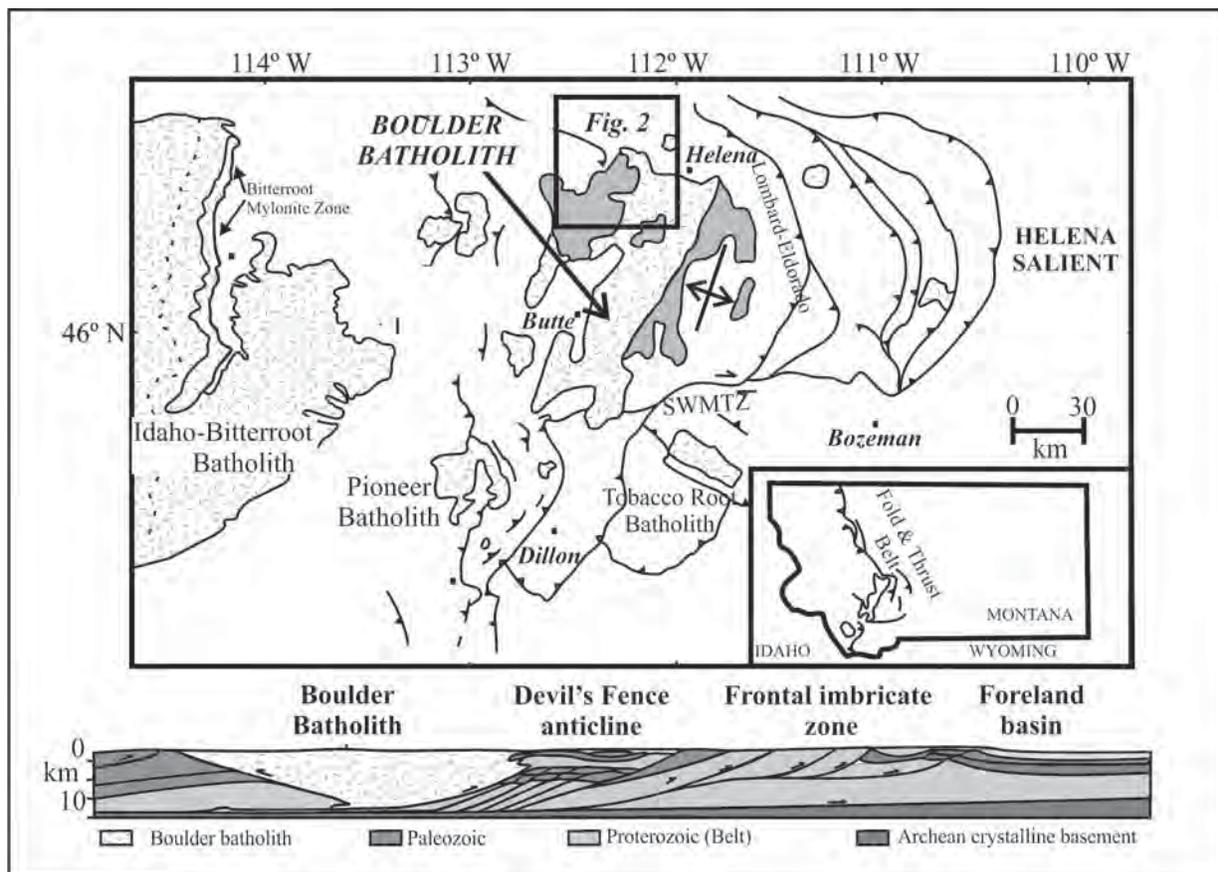

Figure 1. Schematic map and cross-section of pertinent geologic features in the northern U.S. Rocky Mountains (modified from Lageson and others, 2001). Note location of Elliston region area within the Helena salient of the Montana Disturbed Belt. Note close spatial relationship between the Boulder Batholith and contractional features associated with the Lombard-Eldorado thrust system.

the Elliston region seek to constrain the evolution of the Helena Salient by documenting the relationship between folded and faulted Mesoproterozoic to Mesozoic strata and magmatic rocks associated with the Boulder Batholith (Balgord and others, 2010; Ihinger and others, submitted). This region is the focus of ongoing STATEMAP investigations by the Montana Bureau of Mines and Geology, and mapping and analytical work in the area have been supported by the USGS EDMAP program.

REGIONAL GEOLOGY

The Elliston region lies at the junction of several important geologic provinces, including: 1) the southern portion of the Mesoproterozoic Belt-Purcell basin (Sears, 2007); 2) the northwestern margin of the Boulder Batholith (Smedes and others, 1988; du Bray and others, 2012); 3) the northern edge of the Helena Salient, along the eastern edge of the Sapphire thrust plate, which contains complexly folded and faulted Mesoproterozoic to Cretaceous strata (Ruppel and others, 1981; Schmidt and others, 1994); 4) the eastern edge of Tertiary extension related to core complex development (Foster and others, 2010); and 5) the northeastern portion of Eocene volcanic rocks, including the Lowland Creek and Avon volcanic complexes (Trombetta, 1987; Schmidt and others, 1994)(figs. 2, 3).

The geology of the Elliston region was first documented by Knopf (1963), who mapped the area west of Helena at a scale of 1:48,000, and by Bierwagen (1964), who mapped the area north of Elliston at a scale of 1:125,000. The Tertiary Avon Volcanic field was mapped and described in a M.Sc. thesis by Trombetta (1987). The surficial deposits north and northwest of Elliston were mapped as part of a M.Sc. thesis by Loen (1990). The first detailed structural and stratigraphic descriptions of the Elliston region were provided by Schmidt and others (1994), whose 1:62,500 mapping focused on the area flanking the Little Blackfoot River drainage area in Lewis and Clark and Powell counties. Lewis and others (1998) compiled the geology of the Elliston area within the Butte 1° x 2° quadrangle (fig. 2). Faculty and students from the University of Wisconsin-Eau Claire and Minnesota State University-Mankato have focused on geologic mapping and associated geologic studies within four 1:24,000 quadrangles in the Elliston area,

including the Esmeralda Hill, Greenhorn Mountain, Elliston, and MacDonald Pass 7.5' quadrangles (fig. 3). Recent geologic mapping by K. McDonald, J. Mosolf and others from the Montana Bureau of Mines and Geology will be released as the 1:100,000 Elliston quadrangle in 2015.

STRATIGRAPHY

Mesoproterozoic Belt Supergroup

The oldest strata in the Elliston area are rocks of the Mesoproterozoic Belt Supergroup, which are primarily exposed north of the Little Blackfoot River on the north side of the continental divide (figs. 2, 3). Most of the Belt Supergroup is exposed in the area, including the Empire Formation of the Ravalli Group, the Helena Formation of the Piegan Group (Middle Belt Carbonate) and the entire Missoula Group, which comprises the vast majority of the Mesoproterozoic strata in the region.

The Empire Formation is the lowest unit of the Belt Supergroup exposed in the area, and consists of thin-bedded, fine-grained greenish-grey, locally calcareous, argillite and siltite with lesser fine-grained quartzite interbeds. The unit is generally recessive and poorly exposed. In the Greenhorn Mountain quadrangle (fig. 3), the Empire Formation is exposed in a northeast-dipping structural panel in fault contact with the Helena Formation, where it is metamorphosed to lower greenschist facies by intrusion of an Eocene (38.6+1.5 Ma K-Ar age) quartz feldspar porphyry (Gearity, 2013). This intrusion produced gold-silver-lead- molybdenum vein mineralization of the Bald Butte mine (Walker, 1992).

The Helena Formation is widely exposed along the continental divide, and is the host rock for the Marysville Mining District. The unit consists of thin- to medium bedded, light to medium blue grey, microlaminated dolomitic siltstone, fine-grained sandstone and dolomicrite with abundant sedimentary structures, including ripple marks and mud rip-up clasts. The unit commonly displays cyclic bedding, and stromatolites occur locally (Schmidt and others, 1994). Gold and silver mineralization within the Helena Formation in the Marysville Mining District was initially assumed to be associated with the Cretaceous Marysville Stock, but subsequent work has demonstrated that the min-

Figure 2. Regional geologic map of a portion of the 1:250,000 scale compilation map of the Butte 1x2 degree map area, modified from Lewis and others (1998). Quadrangles mapped under the auspices of USGS EDMAP program by faculty and students at University of Wisconsin-Eau Claire are outlined.

Geologic Units (abbreviated)

Magmatic Rocks

Tertiary
- Trv — Avon Volcanics

Cretaceous
- Kg — Granite
- Kgd — Granodiorite
- Kem — Elkhorn Mountain volcanics

Stratified Rocks

Cenozoic
- Ts — Tertiary strata

Mesozoic
- KJs — JuraCretacous strata

Paleozoic
- PDs — Dev-Permian strata
- Cs — Cambrian clastic strata

Mesoproterozoic
- Ym
- Ybo
- Yms
- Yss — Belt Supergroup
- Ysh
- Ysn
- Yc

Lithologic Units

Cenozoic

Qs	Quaternary sediments (undivided)
Ts	Eocene to Oligocene sedimentary rocks
Tv	Eocene volcanic rocks

Mesozoic

Kib	Cretaceous intrusive rocks (undivided)
Kem	Cretaceous Elkhorn Mountain Volcanics
Kb	Cretaceous Blackleaf Formation
Kk	Cretaceous Kootenai Formation
Jem	Jurassic Ellis and Morrison Formations

Paleozoic

Pp	Permian Phosphoria Formation
Pq	Pennsylvanian Quadrant Formation
MPa	Mississippian to Pennsylvania Amsden Formation
Mmc	Mississippian Mission Canyon Formation
Mlp	Mississippian Lodgepole Formation
Dtf	Devonian Three Forks Formation
Dj	Devonian Jefferson Formation
Cmr	Cambrian Maywood and Red Lion Formation
Cpi	Cambrian Pilgrim Formation
Cp	Cambrian Park Formation
Cm	Cambrian Meagher Formation
Cw	Cambrian Wolsey Formation
Cf	Cambrian Flathead Formation

PreCambrian

Ym	Neoproterozoic McNamara Formation
Yb	Neoproterozoic Bonner Formation
Yms	Neoproterozoic Mount Shields Formation
Ysn	Neoproterozoic Snowslip Formation
Ye	Neoproterozoic Helena Formation
Yh	Neoproterozoic Empire Formation

Structure

/	Contacts
//	Strike-slip fault; arrows show displacement direction; dashed where approximate
⤳	Normal fault; dashed where approximate
⤴	Thrust fault; dashed where approximate
⤢	Anticline; arrow indicates direction of plunge*
⤡	Syncline; arrow indicates direction of plunge* *folds on map indicated by white lines for clarity
④	Field trip stop location

Figure 3. Schematic geological map of 1:24,000 scale quadrangles mapped in the Elliston area. (Field trip stop numbers are shown in white polygons).

eralization is primarily Eocene in age, associated with small stocks and sills intruding the Helena Formation (Walker, 1992; Gearity, 2013).

The Missoula Group is the most widespread component of the Belt Supergroup in the region. The strata primarily consist of fine-grained clastic rocks that are recessive and poorly exposed along the continental divide. The basal unit of the Missoula Group is the Snowslip Formation, which overlies the Helena Formation southeast of the Marysville Mining District. The unit consists of thin-bedded reddish siltstone and argillite with lesser thin-bedded fine-grained quartzite intercalated with thin-bedded, thin-laminated green siltstone. The Snowslip Formation is conformably overlain by the Shepard Formation, which is characterized by a basal stromatolitic zone overlain by light tan to green thin-bedded siltstone, argillite and argillaceous dolomicrite (Schmidt and others, 1994). The Shepard Formation is primarily exposed north of the Bald Butte fault.

The Mount Shields Formation consists of medium red to light tan, thin- to medium bedded, parallel and trough cross-laminated, fine to medium-grained subfeldspathic arenite intercalated with thin-bedded reddish argillite. Cyclic variations in sand content allow the formation to be subdivided into six members regionally, and result in laterally significant changes in unit thickness (Wallace and others, 1984; Schmidt and others, 1994). The Mount Shields Formation is conformably overlain by the Bonner Formation, which consist of distinctly cliff forming, medium red to whitish tan, thickly bedded, moderately to poorly sorted, subangular-angular, trough cross-stratified, feldspathic arenite. The Bonner Formation is prominently cross-stratified, and is locally conglomeratic with arkose and quartz pebbles and locally abundant mud rip-up clasts. The Bonner Formation is conformably overlain by the McNamara Formation, which is a largely recessive, purple-red, thin-bedded, fine-grained, well sorted, interbedded arkosic arenite interbedded with red argillaceous shale and siltstone. The unit displays abundant sedimentary structures, including low angle cross-stratification, climbing ripple cross-stratification and abundant rip-up clasts (see Stop 3 in accompanying road log).

Nature of the Proterozoic/Cambrian Boundary

The basal Paleozoic strata in the Elliston region, and throughout the Intermontane West, is the Middle Cambrian Flathead Sandstone. In the Elliston region, the Flathead Sandstone was deposited across a low angle angular unconformity that bevels the underlying west-dipping panel of the Missoula Group progressively from east to west (fig. 3). Schmidt and others (1994) estimate that a minimum of 2500 m of Mesoproterozoic strata have been eroded over a lateral distance of about 30 km, requiring a regional angular discordance of about 5 degrees.

North of the Helena Salient, near Lewis and Clark Pass, the Flathead Sandstone unconformably overlies both the Ravalli (lower Belt) and Missoula (upper Belt) groups, which requires substantial pre-middle Cambrian uplift (>5 km) and erosion of the Belt Supergroup. South of the Helena Salient, near Ermont, MT, a boulder fanglomerate within the Flathead Sandstone immediately above an unconformity over probable pre-Belt "Argenta" strata suggests structurally-controlled sedimentation (Sears and others, 2010). In central Idaho, where Cambrian strata are absent, rapid uplift and erosion of Neoproterozoic plutons yields 500 Ma zircon within the ca. 500 Ma Worm Creek quartzite of SE Idaho (Todt and others, 2013). In contrast, within the Helena Salient, the mapped contact between coarse-grained Flathead Sandstone and rocks mapped as fine-grained strata of the Ravalli Group appears to be a conformable transition, suggesting the existence of previously unrecognized Neoproterozoic to Middle Cambrian strata conformably below the Flathead Sandstone. This relationship is supported by the intercalation of two distinct zircon populations (Balgord and others, 2009). The highly variable nature of the basal Cambrian contact (locally an angular unconformity, a disconformity above crystalline basement, and an apparent conformable contact), the coarse-grained nature of basal Cambrian strata, and evidence for uplift of both Belt Supergroup strata (>5 km) and Neoproterozoic plutonic rocks suggests the continental margin was tectonically active in Neoproterozoic to Cambrian time, in marked contrast to the traditional interpretation of a passive margin setting.

Detrital zircon geochronology of the Mesoproterozoic Missoula Group and the Middle Cambrian Flathead Sandstone constrain the provenance of each succession, and the Proterozoic/Cambrian transition

was characterized by a major shift in provenance (fig. 5a, b). The upper Belt Supergroup (Missoula and Lemhi Groups) is characterized by a major age peak at ~1720 Ma (1620-1800 Ma), with lesser Mesoproterozoic (~1450) Ma and Archean peaks (fig. 5b). Stewart and others (2010) use detrital zircon signatures and isotopic data to suggest that the provenance of the upper Belt Supergroup was non-North American, involving sediment derivation from both syn-depositional Belt sources and from an East Antarctic/Australian source. In contrast, the overlying Flathead Sandstone has a significantly different detrital zircon signature, strongly dominated by an unidentified ~1779 Ma source and lesser, broadly distributed Paleoproterozoic and Archean peaks (fig. 5b). Note the lack of distinctly Missoula Group detritus in the overlying Flathead sandstone, and the complete absence of any grains younger than ~1745 Ma (fig. 5a). These data provide a cautionary tale with respect to the use of the youngest detrital zircon age populations to constrain true depositional ages.

Paleozoic Strata

The Middle Cambrian Flathead Sandstone forms the base of the Paleozoic section in the Elliston region (fig. 4). The Flathead Sandstone is progressively overlain by recessive calcareous brown shale of the Wolsey Formation, bioturbated, locally oolitic limestone of the Meagher Formation, and recessive green shale of the Park Formation. Balgord and others (2010) mapped thin bedded intercalated micrite and micritic quartz arenite overlain by distinct medium to thick bedded, bioturbated dolomicrite to dolowackestone overlying the Park shale as the Pilgrim Formation. Conversely, Schmidt and others (1994), apply nomenclature from north and west of the Elliston area, and point out that the area is in a transition zone wherein Middle to Late Cambrian rocks form a transgressive sequence that becomes younger to the east. As such, rocks that Balgord and others (2010) recognized as Pilgrim Formation are mapped in earlier reports as the Upper Cambrian Hasmark Formation.

Cambrian strata are overlain by Middle to Late Paleozoic strata across an unconformity contained within a recessive, fine-grained succession known as the Red Lion/Maywood Formations (Upper Cambrian-Upper Devonian; fig. 4). The Devonian Jefferson Formation forms scalloped cliffs of medium to thick bedded dark grey sucrosic dolomicrite to dolowackestone, over-

lain by a recessive succession of thin-bedded, locally calcareous fine-grained sandstone, siltstone and shale of the Devonian Three Forks Formation. The most well-exposed Paleozoic carbonate in the Elliston region is the Mississippian Madison Group, which forms prominent cliffs in the hills west of Dog Creek (figs. 3, 4). The Mississippian Lodgepole Formation contains medium to thick bedded, cyclically bedded bioclastic (crinoid, brachiopod, bryozoan) wackestone, packstone, floatstone, and rudstone that was exploited in the lime quarries west of Dog Creek (see Stop 5). The Lodgepole Formation is overlain by the thick bedded to massive Mission Canyon Formation, with forms distinct, low rounded outcrops with indeterminate bedding.

Mississippian carbonate strata are overlain by a recessive package of red, locally calcareous, siltstone and shale which forms conspicuous red regolith. These rocks have been mapped near Elliston as the Amsden Formation (Balgord and others, 2010). Schmidt and others (1994) assigned these strata to the Snowcrest Range Group. These rocks are overlain by prominent cliffs of the Pennsylvanian Quadrant Formation, which consists of tan, fine to medium-grained, well sorted quartz arenite. The formation is a very resistant cliff forming unit that is locally strongly silicified. The Quadrant Formation is overlain by a very thin (1-5 m) succession of black shale, oolitic phosphorite, lithic sandstone and conglomerate and black chert assigned to the Permian Phosphoria Formation (see Stop 7).

Mesozoic Strata

Mesozoic rocks in the Elliston region consist of predominantly recessive, fine-grained Jurassic and Cretaceous clastic strata that are relatively poorly exposed. Schmidt and others (1994) recognized that Jurassic and Cretaceous strata become thicker and coarser-grained to the west, where the strata are subdivided into a number of formations that are absent or indistinguishable in the Elliston area.

Jurassic strata of the combined Jurassic Ellis and Morrison formations (Jem) unconformably overlie the Permian Phosphoria Formation. These strata are recessive, and consist of poorly exposed red to orange, thick bedded fine-grained sandstone, siltstone, and shale (fig. 4). Jurassic strata are unconformably overlain by the distinct, brown-weathering, medium bedded, medium to coarse-grained chert lithic arenite

Renova Fm. (Ts; >100 m?): Conglomerate, sandstone, siltstone and shale.

Avon Volcanic Complex (Tr; ~0-300 m): Rhyolitic volcanic rocks, minor dacite and andesite.

Elkhorn Mountains Volcanics (Kem; >1000 m): Andesitic to rhyolitic flows, breccias, lapilli tuff, tuff and intercalated sediments

Black Leaf Fm. (Kbl; >100 m): Sandstone, siltstone and shale.

Kootenai Fm. (Kk; 120 m): Chert lithic feldspathic arenite.

Ellis Gp - Morrison Fm. (Jem; 90 m): Recessive thin bedded quartz arenite, siltstone, shale and sandy micrite

Phosphoria Fm. (Pp; 2-3 m): Black-dark grey bedded chert, cherty limestone, and oolitic phosphatic shale.

Quadrant Fm. (Pq; 100 m): Quartz arenite.

Amsden Fm. (MPa; 30-50 m): Quartz arenite, siltstone, shale and silty micrite.

Mission Canyon Fm (Mmc; 275 m): Wacke to packstone, locally rudstone.

Lodgepole Fm. (Ml; 125 m): Turbiditic micrite to packstone.

Three Forks Fm. (MDt; 50-75 m): Calcareous micaceous shale to silty micrite.

Jefferson Fm. (Dj; 250 m): Fossiliferous sandy dolomitic wackestone with thin sand laminations.

Maywood and Red Lion Fm. (ЄDmr; 60 m): Quartz arenite, siltstone and shale.

Pilgrim Fm. (Єpi; 150 m): Lower portion consists of micrite; upper portion consists of bioturbated dolomitic wackestone.

Park Fm. (Єp; 50 m): Micaceous shale.

Meagher Fm. (Єm; 100 m): Fossiliferous sandy micrite to packstone.

Wolsey Fm. (Єw; 90 m): Micaceous sandy shale/siltstone

Flathead Fm. (Єf;15-30 m): Subfeldspathic arenite to quartz pebble conglomerate.

MesoProterozoic Belt Supergroup (Yb; >3000 m): Siltstone, shale and thin bedded carbonate interbedded with micaceous subfeldspathic arenite. Includes Ravalli (Ybr), Piegan (Ybh) and Missoula (Ybm) Groups

thicknesses are approximate

Figure 4. Schematic stratigraphic column of Mesoproterozoic to Tertiary units in the Elliston area.
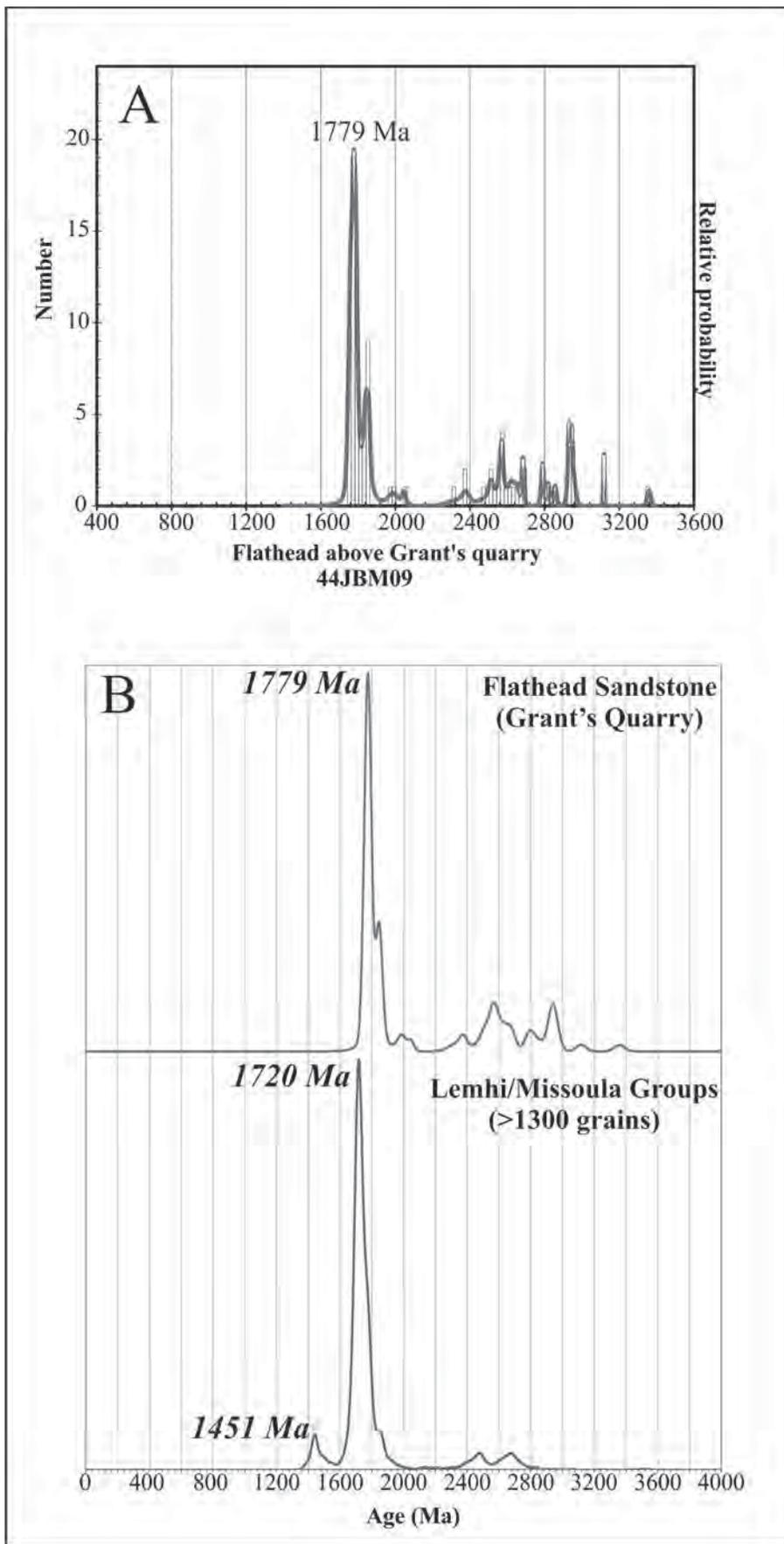
Figure 5. A: Detrital zircon probability plot of the Flathead Sandstone above Grant's quarry; B: Normalized age probability plots comparing the Flathead Sandstone with a cumulative plot of the Missoula and Lemhi Groups. Note that the Flathead peak is distinctly older, and that the Flathead contains no grains younger that ca. 1745 Ma.

of the Cretaceous Kootenai Formation. The Kootenai Formation thickens dramatically from southeast to northwest; south of Helena in the Devil's Fence anticlinorium the unit is ~100 m thick (Mahoney and others, 2008), whereas west of Avon in the Garnet Range, this unit is 520 m thick (Schmidt and others, 1994). The Kootenai Formation is subsequently overlain by relatively poorly-exposed thin to medium bedded tan, brown, and green fine-grained sandstone, siltstone, and shale of the Cretaceous Blackleaf Formation. The coarser units tend to form thin ribs of sandstone that stand in bold relief to the recessive finer-grained interbeds.

The Cretaceous Elkhorn Mountains Volcanics are part of the Boulder Batholith magmatic system, and represent the volcanic carapace to the Boulder Batholith (Rutland and others, 1989). The succession is widely exposed along the northwestern margin of the Boulder Batholith, where it is intruded by the Butte Granite (formerly the Butte Quartz Monzonite). The Elkhorn Mountains Volcanics consists of a heterogeneous, laterally variable succession of andesitic to rhyolitic flows, breccias, lapilli tuff, tuff, and intercalated sediments that aggregate to more than 1000 m. The geochronology and geochemistry of the Elkhorn Mountains Volcanics are discussed under the Boulder Batholith magmatic system.

Cenozoic Strata

The Avon Volcanic Complex is overlain by a widespread, poorly exposed succession of thin-bedded to massive buff-yellow to reddish tuffaceous siltstone, fine-grained sandstone and shale with minor conglomerate referred to herein as the Avon Basin sequence (Eocene-Oligocene?). Small landslides and slope failures are common in this unit. These rocks apparently represent deposition in a restricted terrestrial/lacustrine basin developed on top of the Eocene Avon Volcanic Complex.

MAGMATIC ROCKS

The Boulder Batholith Magmatic System

Three phases of magmatic activity constitute the calc-alkaline Boulder Magmatic Suite (BMS). They include the eruption of the Elkhorn Mountains Volcanics (EMV), emplacement of the large plutons of the Boulder Batholith, and intrusion of numerous small-volume satellite stocks, dikes and sills into the adjacent folded Paleozoic rocks. Detailed geochronology and geochemistry on each phase of magmatism outline a coherent story for the origin and evolution of the magmatic system (figs. 6-8). Here we summarize the results of Ihinger and others (2015), wherein the temporal and chemical evolution of the BMS is described in detail.

Initiation of the BMS was marked by the Crow Creek andesite flow at 85 Ma. Magmas with widely varying composition continued to erupt for at least the next 6 Ma. These magmas span the compositional range from basalt to rhyolite and include several large-volume ignimbrite sheets. The plutons of the batholith intrude the volcanic carapace (Klepper and others, 1974; Rutland and others, 1989). The oldest pluton intruded at 82 Ma and overlapped with the tail end of volcanic activity. Plutonism spanned a ten million-year interval and continued well after the cessation of voluminous volcanism. Precision geochronology on four satellite intrusions show crystallization ages between 80 and 75 Ma, indicating that magmatism peripheral to the batholith was coeval with BMS plutonism.

Summaries of the major and trace element geochemistry for rocks associated with each phase of the BMS are presented in figures 8A-D. The compositions define a distinct calc-alkaline trend on an AFM diagram (fig. 8B), and the characteristic depletion in Nb and Ti (fig. 8D) indicate clearly that magmas from each phase of the BMS have origins linked to subduction zone processes. Both the EMV and Boulder Batholith satellite intrusions have widely scattered and variable compositions with silica contents that range between 47 to 74 wt% SiO_2 (fig. 8A, C). Both major and trace element concentrations vary by more than factors of two for any given silica concentration. These differences persist across the spectrum of silica contents for both volcanic and satellite samples.

Boulder Magmatic System
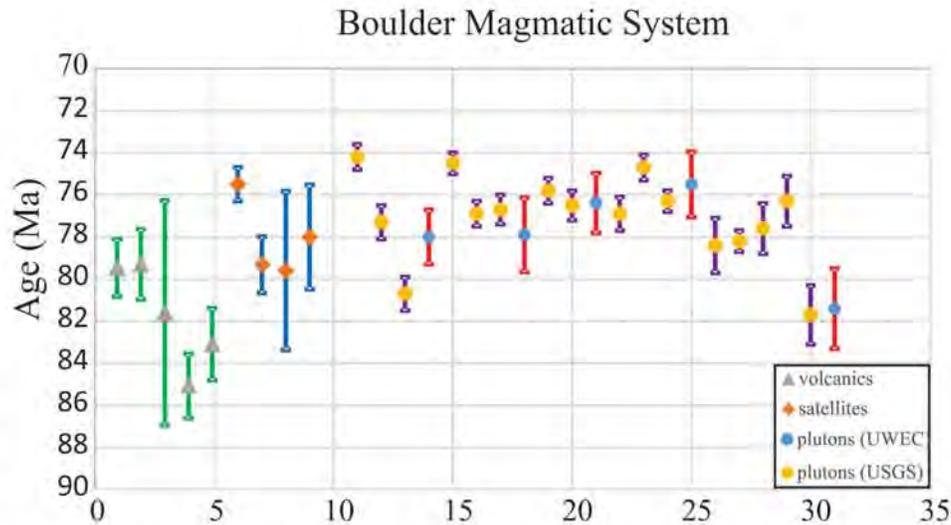
	UNIT		AGE	ERROR
Volcanics	1	**Hadley Park/N. Bull Mtn**	79.5	1.4
	2	**Watertank Gulch**	79.3	1.7
	3	**Crow Peak**	81.6	5.4
	4	**Crow Creek**	85.1	1.5
	5	**MacDonald Pass spring**	83.1	1.7
Satellites	6	**Doherty Mtn**	75.5	0.8
	7	**Sagebrush Park Stock**	79.3	1.3
	8	**Cabin Creek Stock**	79.6	3.8
	9	**Rustler's Gulch**	78.0	2.5
Plutons	10	Monzogranite of Hell Canyon	73.7	0.6
	11	Monzogranite of Moose Creek	74.2	0.6
	12	Granodiorite of Burton Park	77.3	0.8
	13	Rader Creek Granodiorite	80.7	0.8
	14	**Rader Creek Pluton**	**78.0**	**1.3**
	15	Granodiorite of Donald	74.5	0.5
	16	Granophyre of Deer Creek	76.9	0.6
	17	Granodiorite of Climax Gulch	76.7	0.7
	18	**Pipestone Pass**	**77.9**	**1.8**
	19	Monzogranite of Homestake	75.8	0.6
	20	Butte Granite (at Homestake Pass)	76.5	0.7
	21	**Continental Divide**	**76.4**	**1.4**
	22	Butte Granite (in Butte mining district)	76.9	0.8
	23	Butte Granite (at Bison Creek)	74.7	0.6
	24	Monzogranite of Pulpit Rock	76.3	0.5
	25	**Priest Pass Pluton**	**75.5**	**1.6**
	26	Granodiorite of Crystal Creek	78.4	1.3
	27	Unionville Granodiorite	78.2	0.5
	28	Granodiorite of Little Butte	77.6	1.2
	29	Granodiorite of Colorado Gulch	76.3	1.2
	30	Monzogranite of Camp Thunderbird	81.7	1.4
	31	**MacDonald Pass**	**81.4**	**1.9**

Figure 6. Geochronology of Boulder Magmatic System. Compilation includes geochronologic samples from plutons of the Boulder Batholith by the U.S. Geological Survey (du Pray and others, 2012) and from plutons, satellite bodies and the Elkhorn Mountain Volcanics completed by the University of Wisconsin-Eau Claire (Ihinger and others, 2015). Samples are arranged as volcanics, satellites and plutons, with each category arranged from south-to-north view left-to-right.
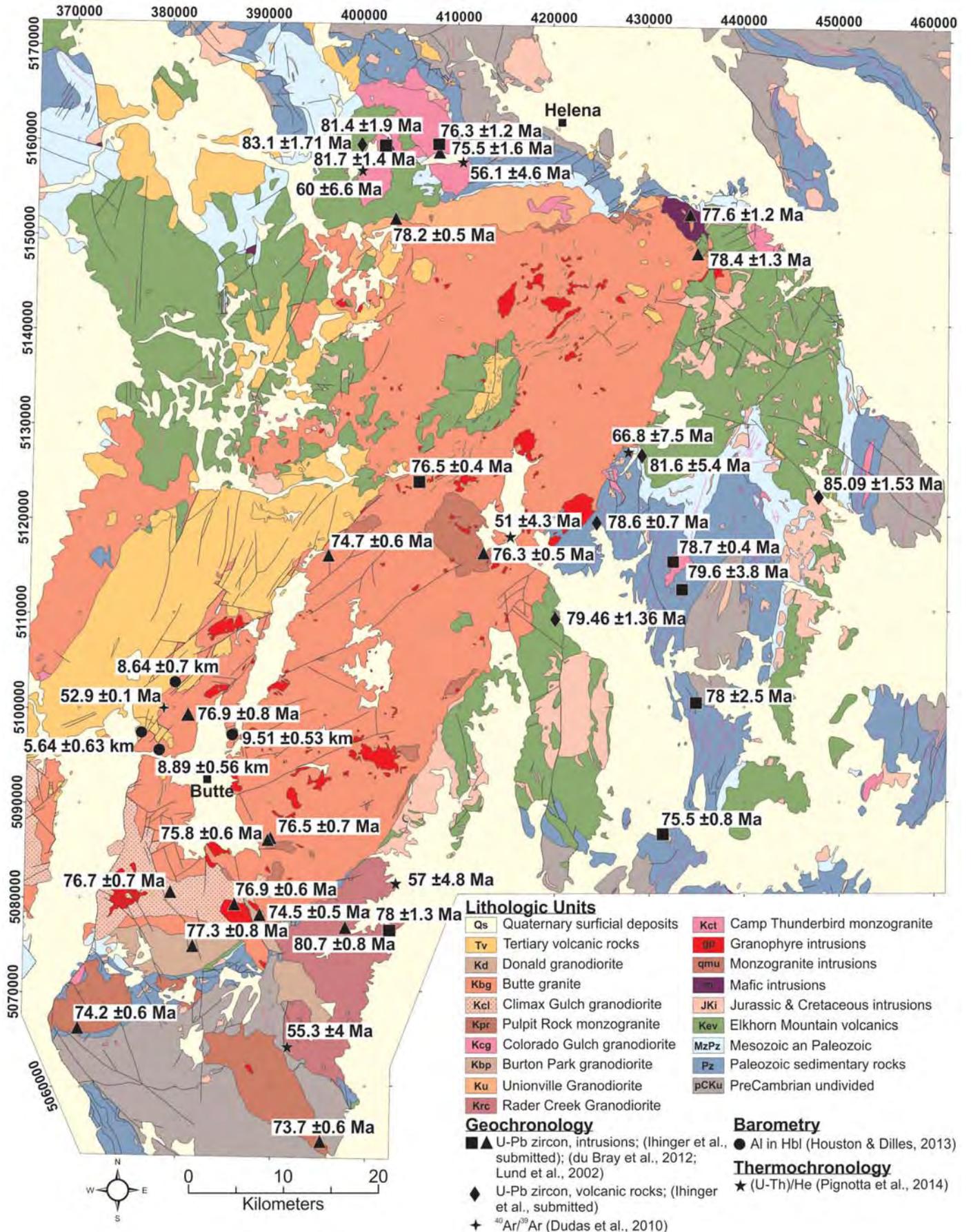
Figure 7. Summary map showing U-Pb ziron geochronology, ^{40}Ar/^{39}Ar geochronology, Al-in-hbl barometry, and (U-Th)/He thermochronology for the Boulder Batholith, its satellite plutons, and the Elkhorn Mountain Volcanics. Map modified from du Bray and others, 2009.
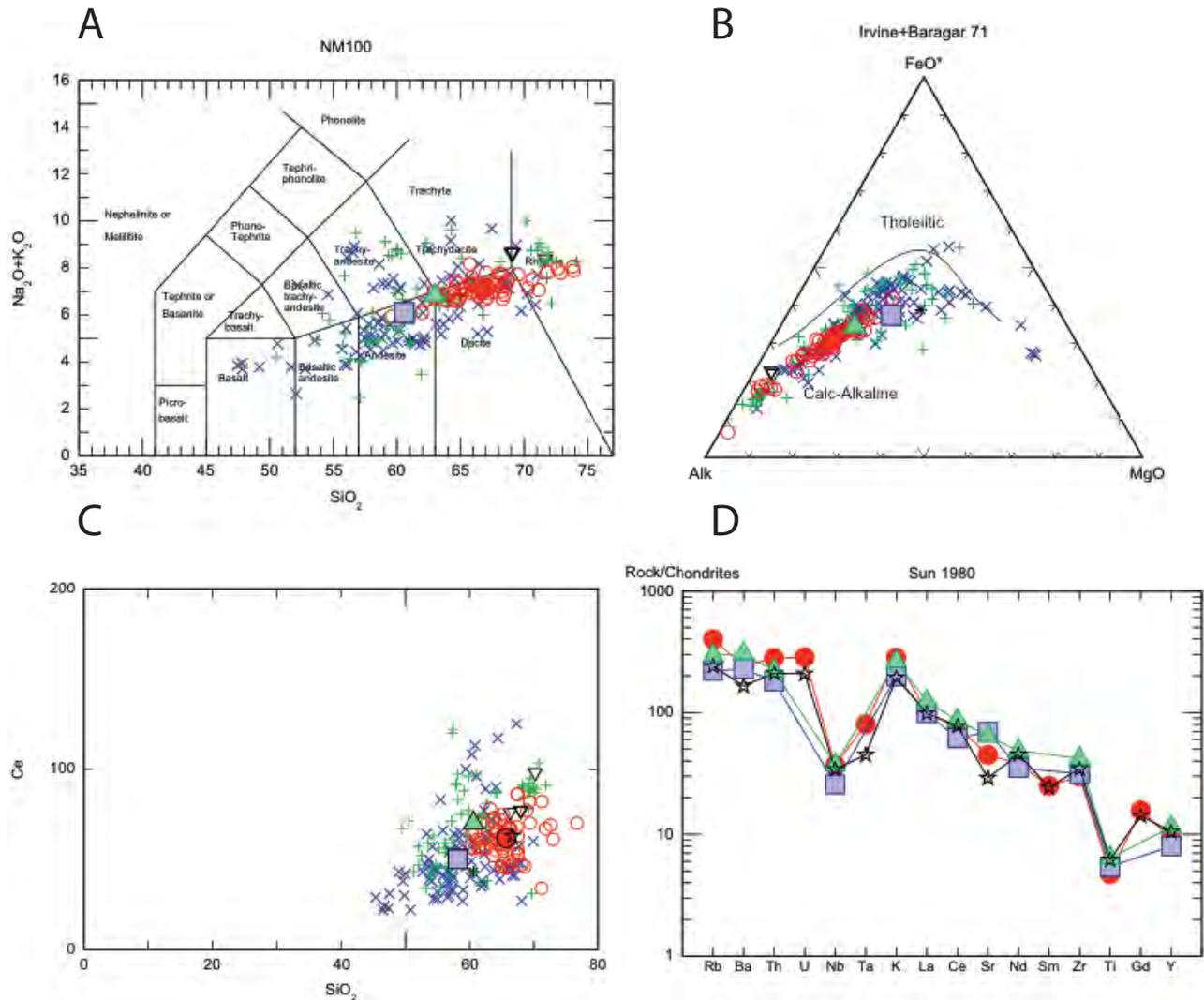
Figure 8. Geochemistry of magmatic rocks of the Boulder Magmatic Suite (all data from Ihinger and others, 2015). Key for symbols: + = EMV; x = satellite dikes, sills, and stocks; o = Boulder Batholith plutons; inverted triangle = ignimbrite flows within EMV; solid triangle = average of all EMV analyses (n= 90); solid box= average of all EMV analyses (n= 73); solid circle = average of all Boulder Batholith plutons (n= 60). A: silica vs. total alkalis; B: Alkali-FeO-MgO (AFM) plot; C: representative trace element (Ce) vs. silica; D: trace element spider diagram showing average abundances in the three phases of the BMS; star = average upper continental crust (Rudnick and Gao, 2004).

In contrast, Harker diagrams for Boulder Batholith plutons define narrow bands that trend through the middle of the scatter observed for every major element in the associated EMV and satellite samples. These observations suggest that the Boulder Batholith plutons represent amalgamations of multiple batches of smaller volume magmas inside homogenizing storage chambers. Calc-alkaline magmas at continental margins have long been understood to accumulate and evolve within crustal chambers whereby constituent magmas experience MASH (Mixing, Assimilation, Storage, and Hybridization) processes (Hildreth and Moorbath, 1988). The radiogenic Sr and Nd isotopic compositions of the Boulder Batholith plutons are consistent with MASH-style assimilation and mixing of crustal material in such chambers (Du Bray and others, 2012; Ihinger and others, 2015).

The dominant felsic character of the Boulder Batholith plutons indicates that they represent felsic extractions from deeper homogenizing chambers that were formed from a collection of magmas with EMV/satellite composition. Every pluton is more silica-rich than the average silica content for both the EMV and satellite rocks. As crystallization proceeded inside the chambers, a dense crystalline framework formed at the expense of the evolving interstitial liquid. Predominantly driven by iron removal, a critical threshold in density difference was eventually reached, and the remaining buoyant interstitial liquid migrated up and out of the compacting crystalline residue (e.g., Philpotts and others, 1996; Bachmann and Bergantz, 2004). The

bulk composition of the extracted magma is dependent on the amount of crystalline network entrained into the segregating viscous liquid. The range in chemistry observed across the suite of Boulder Batholith plutons offers insights into the dynamics of this extraction process. The large-volume ignimbrite tuffs found in the upper layers of the volcanic pile lay on the felsic end of the Boulder Batholith pluton compositional trends (figs. 8A-C) and likely represent the extrusive equivalent of these silica-rich melt segregations. The additional 'plutonic' component (in the form of ignimbrite tuffs) thus supplements the average EMV composition and provides an explanation for its slightly more felsic character when compared to the average composition of the suite of satellite rocks.

In summary, the BMS is comprised of a series of calc-alkaline magmas of widely variable composition that formed between 85 and 74 Ma. The compositions of these magmas are reflected in the chemistries of the satellite intrusions and small-volume flows of the EMV. After ~3 million years, the magma production rate was high enough to generate significantly large reservoirs beneath the volcanic carapace to collect and amalgamate subsequent rising magmas. The cross-sectional areas of the developing storage chambers were sufficiently large to effectively choke off overlying volcanism. To the east, where the production rate was lower, minor volumes of magmas continued to penetrate the overlying Paleozoic sedimentary rocks throughout the duration of BMS activity. Meanwhile, the large chambers allowed for mixing and homogenization of magmas with widely disparate composition. Upon cooling and crystallization, buoyant felsic bodies segregated from their host MASH reservoirs to form the individual Boulder Batholith plutons and large extrusive ignimbrite tuffs. By 74 Ma, magmatism in the region had ceased, and remained dormant until commencement of the Tertiary Lowland Creek and Avon volcanics.

Tertiary Avon Volcanic Complex

The Avon Volcanic Complex is exposed in an apparent fault-bounded basin across approximately 90 km2 to the east and south of Elliston (figs. 2, 3). It is a part of an extensive Eocene-Oligocene volcanic province exposed throughout large areas of the northern Rocky Mountains that includes the Challis, Absaroka-Gallatin, Garnet Range, and Lowland Creek volcanics. Trombetta (1987) divided the volcanic complex into

seven map units and supplied basic structural interpretation, and provided limited geochemical analyses. The Avon Volcanic Complex appears to contain very little pyroclastic material and is dominated by quite voluminous, crystal-rich lava flows and volcanic domes, which is unusual for such highly siliceous rocks. Geochemical and geochronologic analyses of the Avon Volcanic Complex conducted in conjunction with mapping by faculty and students of the University of Wisconsin-Eau Claire provides constraints on the age and composition of the Avon Volcanic Complex.

Trombetta (1987) describes the Avon Volcanic Complex as predominately rhyolite porphyry, with lesser rhyolite tuff, lapilli tuff and breccia, with lesser andesite flows. Geochemical samples were collected from the lateral and vertical extent of the Avon Volcanic Complex, and the rocks form three distinct geochemical groups. The first occurs as dacitic flows and domes. The other two groups are rhyolitic in composition but are divided based upon significant differences in elemental abundance. One of the rhyolite groups is enriched in NaO_2, Nb, Pb and Rb and depleted in Hf, La, Nd and Zr relative to the other (fig. 9). Geochemistry suggests the Avon Volcanic Complex represents a highly evolved, subduction-related magma system. The geochemical signature, including high LIL/HFSE ratios suggest interaction with an evolved crustal source during magma genesis.

Geochronologic data for the Avon Volcanic Complex is limited. A K-Ar sanidine analysis from a rhyolite porphyry exposed 2.9 km (1.8 miles) west of Avon along U.S. Highway 12 yields an age of 39.4 ± 1.6 Ma (Chadwick, 1981). A sample of the rhyolite porphyry collected in the Elliston 1:24,000 quadrangle in the southeastern portion of the Avon Volcanic Complex yielded a U/Pb zircon age of 40.98 ± 0.44 Ma (fig. 10). These Late Eocene dates suggest the Avon Volcanic Complex may be slightly younger than both the Lowland Creek Volcanics to the south (Dudas and others, 2010) and to volcanic strata in the Garnet Range to the west (Callmeyer, 1984).
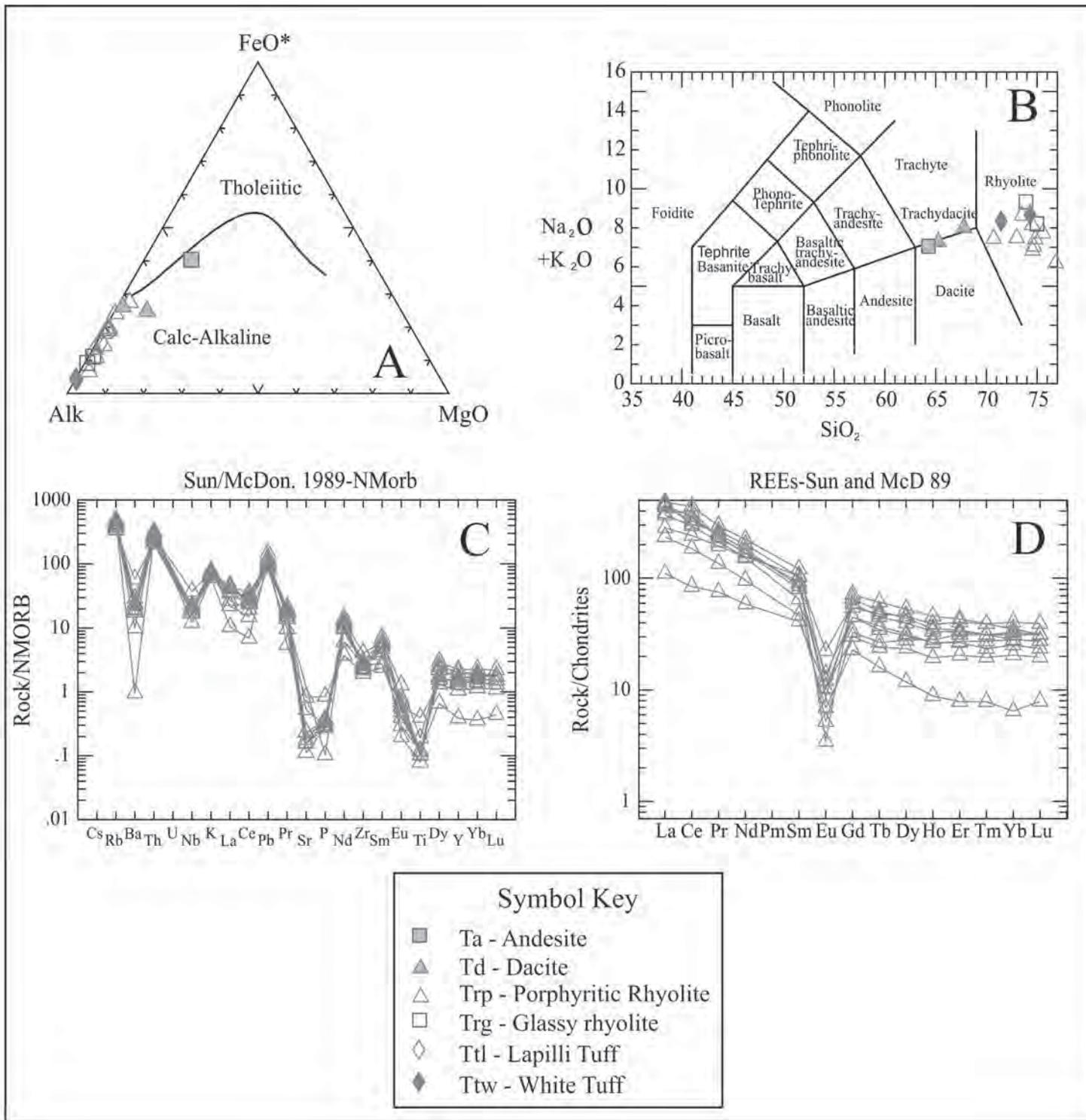
Figure 9. Geochemical diagrams from the Avon Volcanic Complex. A: Rocks have a calc-alkaline affinity with extremely low Magnesium content suggestive of highly evolved magmas; B: Note strongly rhyolitic nature of the AVC; C: Spider diagrams of the rhyolite porphyry, the most volumetrically important unit in the AVC. Note the strongly spiked nature of the spider diagram with depletion in Nb and Ti and LILE enrichment indicative of subduction-related magmatism; D: Rare earth element patterns from the rhyolite porphyry, with a strong Eu anomoly suggesting significant fractionation of plagioclase and a high La/Yb ratio also suggests significant magmatic fractionation.
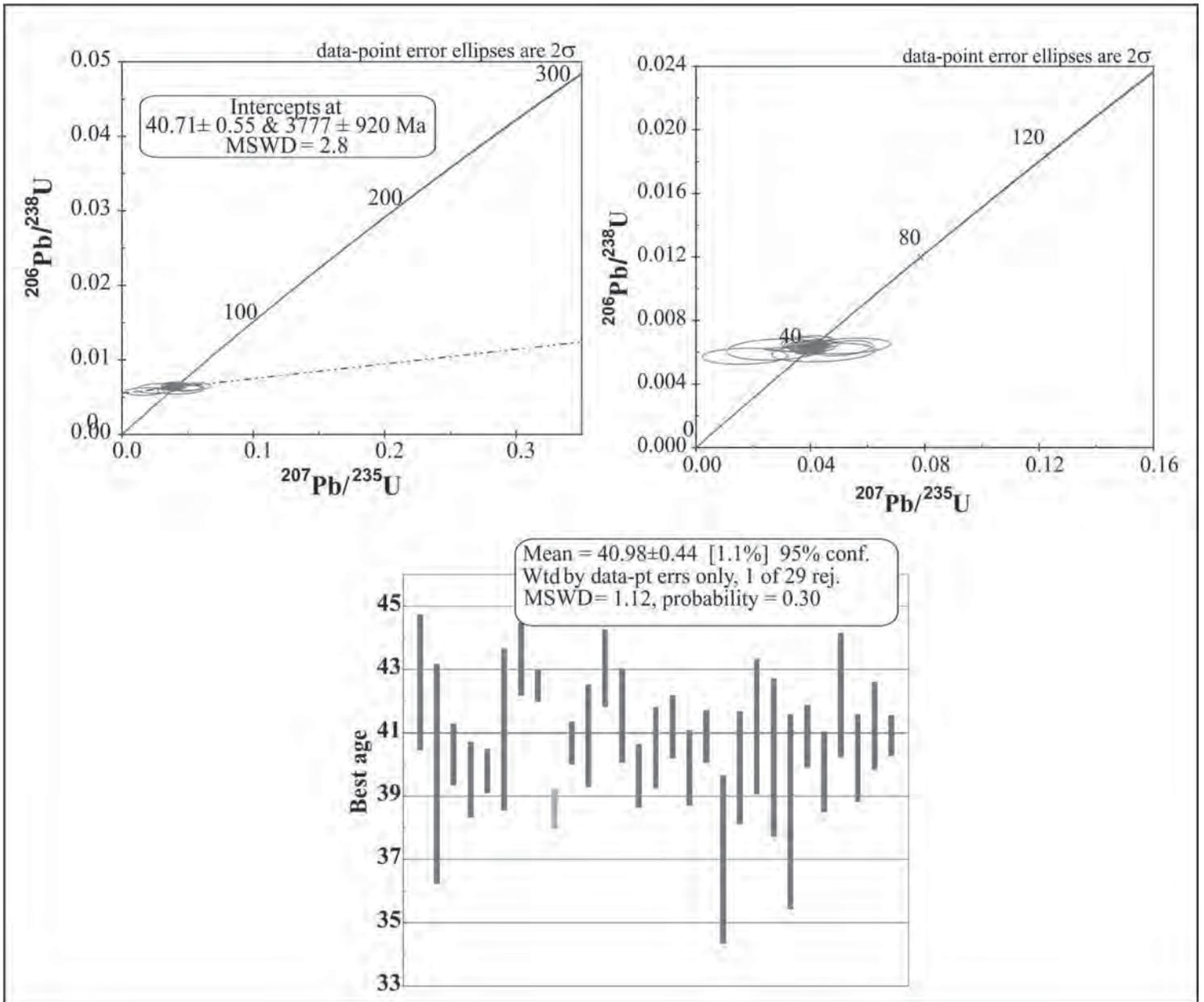
Figure 10. Geochronologic diagrams from zircon derived from the rhyolite porphyry in the southeastern portion of the Avon Volcanic Complex.

STRUCTURAL GEOLOGY

Fold and Thrust Belt

The Elliston region contains a complex succession of Mesoproterozoic to Cretaceous strata imbricated along a series of primarily west-dipping thrust faults developed along the southeast portion of the Sapphire thrust plate (Ruppel and others, 1981; Schmidt and others, 1994). Schmidt and others (1994) describe significant differences in stratigraphic thickness within the Cambrian Silver Hill Formation (thicker to the west), the Devonian Three Forks Formation (thinner to the west), and the Jurassic Ellis and Cretaceous Kootenai formations (thicker to the west). In the Elliston area, the primary representation of these thrust faults is the juxtaposition of thin sheets of folded Mesoproterozoic to Paleozoic strata over Mesoproterozoic to Cretaceous strata folded within the Black Mountain Syncline. The youngest rocks clearly involved in the thrusting are from the Cretaceous Blackleaf Formation. However, folds within the Elkhorn Mountains Volcanics and steep dips within these strata along the intrusive contact with the Boulder Batholith suggest that the Elkhorn Mountains Volcanics may be deformed immediately prior to the emplacement of the Boulder Batholith. Intrusive relationships between folded and faulted Mesoproterozoic to Cretaceous strata, the Elkhorn Mountains Volcanics, and both satellite intrusions and plutons of the Boulder Batholith indicate that magmatism was pre-, syn- and post-deformational (i.e. ca. 85-74 Ma). Recent (U-Th)/He in apatite thermochronology from the Boulder Batholith suggests that cooling/exhumation through 70°C/~2 km could have occurred as early as 66.8 ± 7.5 Ma for parts of the batholith (Pignotta and McCann, 2014)(fig. 7).

Strike-Slip Faults

The Bald Butte fault has been mapped as a regional strike-slip fault with a dextral offset of 28 km that extends from Helena, Montana to east of Ravalli, Montana, where it intersects the regional St Mary's-Helena Valley Fault (Wallace and others, 1990). Schmidt and others (1994) map the structure as a dextral oblique slip normal fault, down on the south. In the Greenhorn Mountain quadrangle, the fault appears to dip shallowly to the north, and juxtaposes the Mesoproterozoic Empire and Helena Formations (lower Belt Supergroup) over the Mesoproterozoic Missoula

Group (upper Belt Supergroup) and overlying Paleozoic strata, and is therefore mapped as a thrust fault (Mahoney and others, unpublished mapping). The fault cuts Late Cretaceous rocks of the Black Mountain Syncline, and is apparently overlain by Eocene volcanic rocks, restricting the age of the structure to Late Cretaceous to Paleocene (Wallace and others, 1990; Schmidt and others, 1994).

Normal Faults

Prominent high angle normal faults within the Elliston area occur along the eastern edge of the Avon Valley and along Dog Creek, but are common to the west and south (figs. 2, 3). Many of these faults cut both Cretaceous and Eocene rocks, and must post-date these units, but a younger limit on extension is difficult to pinpoint. Along the east side the Avon Valley, a north-northwest trending fault (the Illinois Ridge fault of Schmidt and others (1994)) cuts rhyolitic rocks of the Avon Volcanic Complex and forms the eastern edge of the Eocene-Oligocene(?) Avon basin strata, which suggests a structural control on deposition of Avon basin strata. The Dog Creek fault drops Elkhorn Mountains Volcanics down to the east against folded Paleozoic and Mesozoic rocks, requiring post-Late Cretaceous movement. Schmidt and others (1994) show the Dog Creek fault overlain by rhyolite of the Avon Volcanic Complex, suggesting post-Late Cretaceous, pre-Eocene displacement.

QUATERNARY AND GLACIAL GEOLOGY

Alden (1953) provided the first detailed descriptions of glacial deposits in the region, and attributed them to a pre-Wisconsinan and a Wisconsinan glacial advance. Ruppel (1962) performed detailed mapping of glacial erosional and depositional features in the northern Boulder Mountains. The bedrock-focused work of Schmidt and others (1994) also mapped extensive undifferentiated glacial deposits in the Elliston area. Locke and Smith (2004) compiled data from above sources supplemented with additional mapping and provided the first comprehensive overview of Pleistocene ice extent in western Montana including the Boulder Mountains.

New Mapping and Beryllium-10 Dating

Beginning in 2008, new 1:24,000-scale mapping of glacial deposits in the Elliston area was supported

by Minnesota State University, University of Wisconsin-Eau Claire, and USGS EDMAP. This new mapping identified a broader extent of glaciation than described by previous investigations, and differentiated glacial tills from glaciofluvial landforms in the Little Blackfoot River valley just below the confluence with Telegraph Creek. Extensive lateral moraine sets can be traced throughout the study area, and complimentary ice-marginal features such as lateral meltwater channels incised into bedrock were also identified. New mapping also clarified the extent of cirque glaciers in the vicinity of Nevada Mountain (fig. 11).

Cosmogenic nuclide dating of boulders from the maximum extent of the Elliston moraine from a location just north of Elliston village was conducted at the PRIME Isotope Lab at Purdue University. Boulders were sampled and processed following standard procedures (Gosse and Phillips, 2001). A mean age of 16.7 ka BP (thousands of calendar years before present; Table 1) from four boulders is consistent with many "Pinedale" aged mountain glaciers in the northern Rockies that appeared to reach maximum extent between the global Last Glacial Maximum of ~21 ka and the onset of the Bolling-Allerod interstadial after 15 ka (fig. 12).

Ice Source(s)

Pleistocene glacial deposits of the Elliston region have two sources: a large ice cap system centered on the northern Boulder Mountains, and isolated cirque glaciers in the general vicinity of Nevada Mountain (fig. 11).

Deposits of the Little Blackfoot River drainage represent the northernmost extent of a Pleistocene ice cap that developed on the Boulder Mountains, first described by Ruppel (1962). This system developed from a series of coalescing cirque glaciers, and reached a maximum area of approximately 500 km^2. Only the highest peaks of the Boulder Mountains, such as Red and Thunderbolt mountains, would have risen from the ice mass as nunataks. The most prominent terminal deposits of the ice cap can be found in the Boulder River and Little Blackfoot River valleys. In the Elliston area, valley outlet glaciers occupying the Telegraph Creek and Little Blackfoot River drainages coalesced and created the suite of glaciogenic features evident in the vicinity of the village.

To the north, Pleistocene cirque glaciers developed in a number of drainages along a low range of primarily Missoula Group sediments now forming the continental divide centered around Nevada Mountain. Cirques are well developed in the headwaters of the Little Prickly Pear and Threemile Creek watersheds, though well-preserved moraines are not consistently associated with erosional landforms. Equilibrium-line-altitude analysis of cirques in this area suggest that mean summer temperatures in the region were 12-13°C colder during maximum Pleistocene ice extent relative to today (Wittkop and others, 2011).

Glacial Tills

Unconsolidated ice-deposited polymicts (tills) in the Elliston region consist of a silty, buff colored matrix supporting clasts of igneous and sedimentary rocks including prominent Elkhorn Mountains Volcanic and Boulder Batholith lithologies. These polymicts often contrast strongly with monolithic regoliths of unglaciated terrain. In situ clasts may show evidence of glacial polish and striations and can include large boulders a meter or more in size. The till preserves hummocky surfaces in many areas, most prominently in the floor of the Little Blackfoot River valley. Lateral moraines are also prominent on the valley margins up to the maximum extent of late Pleistocene ice.

Glaciofluvial Deposits

Glaciofluvial deposits are prominent locally in the Little Blackfoot River valley, particularly in the vicinity of Elliston village and upstream to the confluence with Telegraph Creek. The valley-floor deposits visible from the wayside at the base of MacDonald Pass include prominent recessional moraines surrounded by large flats of glaciofluvial sands and gravels. Smaller, higher-elevation glaciofluvial terraces are also present and can be observed along the Little Blackfoot River Road south of US 12. These deposits are less prominent west of Elliston village.

Erosional Landforms

Well-developed, presumably late Pleistocene cirques are evident in Nevada Mountain vicinity. Ruppel (1962) provides detailed descriptions of glacial erosional landforms in the Boulder Mountains. Lateral meltwater channels incised into Elkhorn Mountains Volcanic bedrock can be found on the east side of Telegraph Creek just prior to its confluence with the Little Blackfoot River.
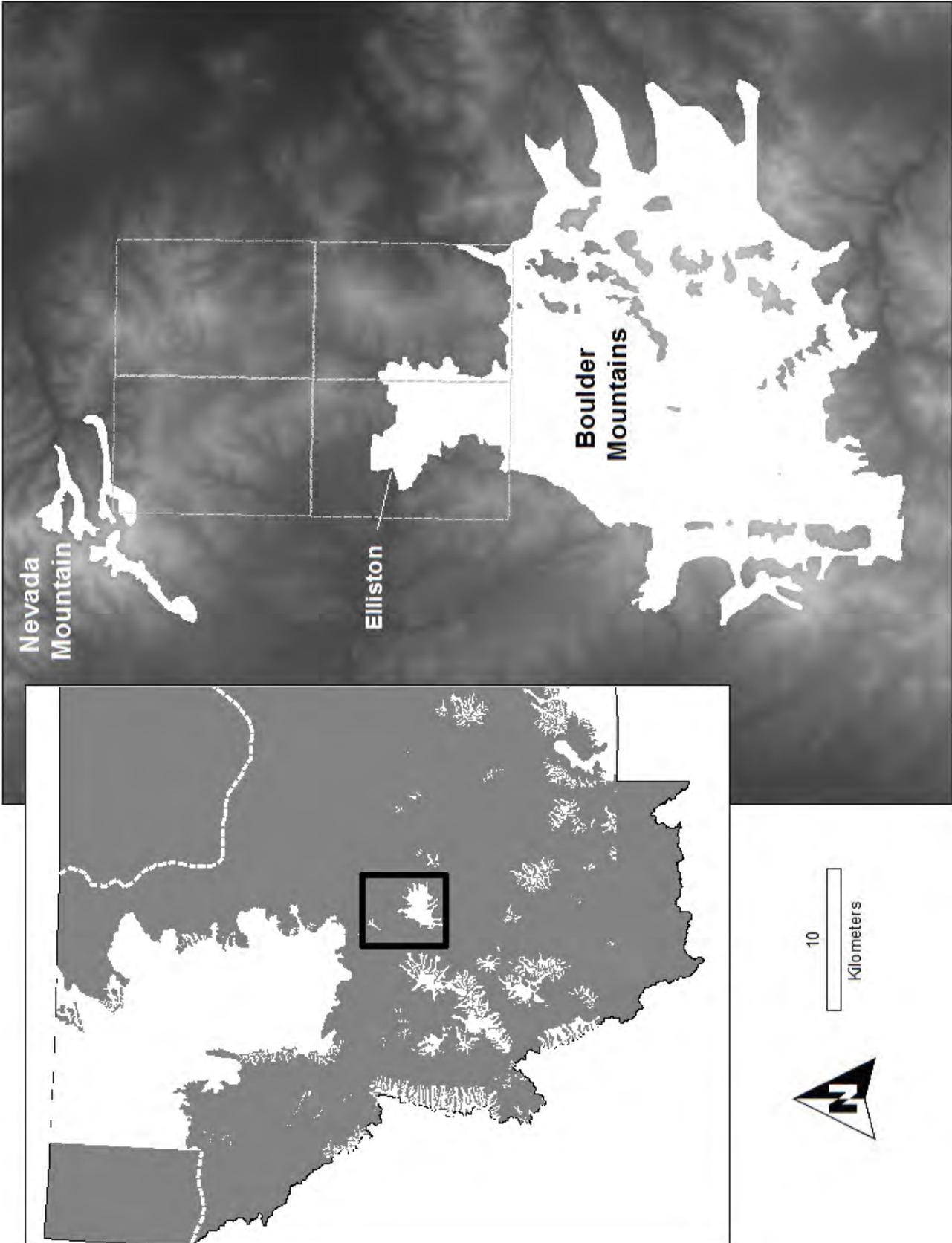
Figure 11. Maps showing late Pleistocene ice extents in western Montana region (inset) and study area (showing extent of 1:24,000 quads, clockwise from upper left, Esmeralda Hill, Greenhorn Mountain, MacDonald Pass, and Elliston). Solid white areas are mountain glaciers and ice caps. Dashed lines represent approximate extents of continental ice sheets. Ice extents in inset map from Locke and Smith (2004). Ice extent of Boulder Mountains redrawn from Locke and Smith (2004) and Derkey and others (1993), supplemented with new mapping.

Table 1. Beryllium-10 data from Elliston moraine boulders. Exposure ages calculated with constant production rate model using Cronus-Earth exposure age calculator wrapper script 2.2, main calculator 2.1, constants 2.2.1, muons 1.1.

| Sample ID	UTM 12 E	UTM 12 N	Elevation (masl)	Lithology	Height	Thickness (cm)	Density	g Quartz	10Be atoms g-1	uncertainty atoms g-1	Exposure age (yr)	Error (internal)
cw0901	389944	5159448	1618.0	Rhyolite	30 cm	1.0	2.7	9.4985	298983	15294	17385	893
cw0902	390162	5159595	1620.0	Quartz monzonite	45 cm	1.5	2.7	6.9257	288123	16759	16796	981
cw0903	390286	5159645	1621.0	Quartz monzonite	90 cm	1.5	2.7	11.785	282956	16211	16480	948
cw0904	390388	5159661	1621.0	Quartz monzonite	50 cm	1.5	2.7	25.273	467569	18811	27307	1106
cw0905	390388	5159551	1635.0	Quartzite	25 cm	0.5	2.6	20.466	475470	20429	27246	1179
cw0906	390453	5159462	1651.0	Quartzite	20 cm	0.5	2.6	28.906	287683	8758	16246	497
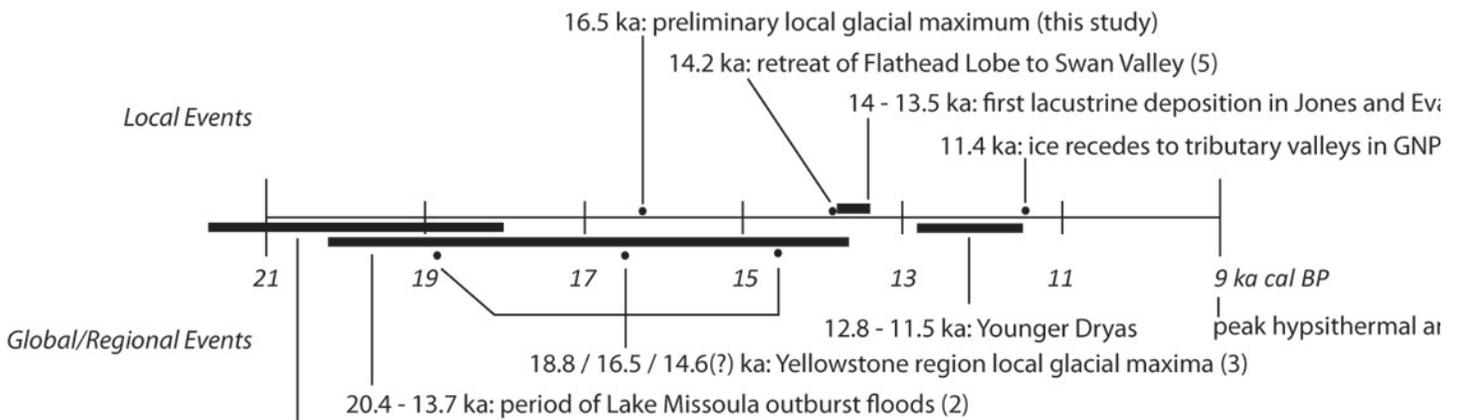
Figure 12. Timeline of major regional and global late Pleistocene events relevant to this study. Data sources as follows: 1. Davis and others, 2006. 2. Clauge and others, 2003. 3. Licciardi and Pierce, 2008. 4. Carrara, 1989. 5. Hoffman and Hendrix, 2010. Jones Lake chronology (Ovando Valley) from Shapley and others, 2009.

Periglacial Features

Schmidt and others, (1994) mapped undifferentiated deposits on the high flanks of the Continental Divide which do not appear to be glacial in origin but may represent periglacial features. Openwork boulder fields are noted in the vicinity, including in cirques of the Deadman Creek watershed and on the eastern slope of the Continental Divide just south of MacDonald Pass. These features have not been subjected to detailed investigations, but potentially represent rock glacier and/or felsenmeer type deposits.

ROAD LOG
(STOPS SHOWN ON FIGURE 3)

MILEAGE

0.0   Lions International Sunshine Camp.

The Sunshine Camp is on Little Blackfoot River,

just north of its confluence with Slate Creek. The ridges above the Camp are Cretaceous Elkhorn Mountains Volcanics (Kem) in fault contact with Paleozoic and Mesozoic sediments to the north (fig. 3).

1.2   Junction of Little Blackfoot River road (FS 227) and the Telegraph Creek road (FS 495).

The Little Blackfoot River Valley broadens at this point, revealing abundant Quaternary deposits of the Little Blackfoot River. Cliffs to west are the Cretaceous Elkhorn Mountains Volcanics. The Continental Divide is visible to the east. The hills on the west side of the continental divide are andesite flows and volcaniclastic sediments of Elkhorn Mountains Volcanics. The Butte Granite of the Boulder Batholith forms the continental divide, with the instrusive contact with Kem just below the ridge line. Drainage visible to north is Dog Creek. Grassy slopes on the east side of Dog Creek are Kem andesite and sediments.

1.5   Cross Little Blackfoot River.

3.0   STOP 1   Regional Overview

Roadside stop along the wide valley of the upper Little Blackfoot River. View to the northeast into the Dog Creek drainage toward Mullan Pass. Note hummocky Quaternary deposits in foreground. Andesitic volcanic rocks and volcaniclastic sediments of the Elkhorn Mountains Volcanics are exposed east of Dog Creek. Ridges to west of Dog Creek are underlain by folded and thrust faulted Paleozoic and Mesozoic sediments along the southeast edge of the Sapphire thrust plate. Quarry visible in the middle foreground is a limestone quarry in the Mississippian Lodgepole Formation (see Stop 5).

3.5   Borrow pit on Little Blackfoot River Road (short stop if time).

Glaciofluvial terrace developed during recession of the Telegraph Creek and Little Blackfoot River glaciers. Similar glaciofluvial deposits form a series of terraces along the west side of the Little Blackfoot River road. Some exposures contain steeply dipping foresets and other soft sediment deformation features consistent with deposition in a dynamic, ice-contact environment.

4.2   Junction of the Little Blackfoot River road and Montana Highway 12. Turn west on Highway 12.

Prominent cliffs to north and cliffs at the intersection are west dipping Pennsylvanian Quadrant Formation within a west dipping panel of Paleozoic and Mesozoic rocks in the footwall of the Sapphire thrust plate.

4.7   Elliston Montana.

Elliston began as a trade center for nearby mining districts in the early 1880's. The Northern Pacific Railway built a line through Elliston for its line from Logan, Montana, to Garrison, Montana in 1883. Elliston was likely named for the Northern Pacific Railroad's director, John Ellis. The town reached its peak in population and activity during the first half of the 1890s, when the town's primary economic base was woodcutting. Cutting cord wood for the Anaconda Copper Mining Company's smelter at Anaconda em-

ployed more than one hundred wood cutters. The town was destroyed by fire in 1894 and again in 1895.

5.0   Spotted Dog Creek forest service road. LawDog's Saloon.

Spotted Dog Creek road runs to south and leads to westernmost exposures of the Eocene Avon Volcanic Complex unconformably overlying Cretaceous Kootenai Formation and sediments of the Elkhorn Mountains Volcanics.

5.7   Road cut in rhyolite of Avon Volcanic Complex.

7.6   Columnar jointed rhyolite plug within Avon Volcanic Complex (see Stop 4).

Cliffs exposed along north side of Little Blackfoot River for next three miles are rhyolitic volcanic rocks of the Avon Volcanic Complex capped by Tertiary lacustrine and fluvial sedimentary rocks.

10.4   Turn south onto Snowshoe Creek road.

10.6   Cross Little Blackfoot River.

11.2   Note view to west. Forested ridges to the north and south of Avon, MT are underlain by rhyolitic rocks of the Avon volcanic complex. Ridges on the western skyline are primarily composed of Cretaceous sedimentary rocks in the upper plate of the Sapphire thrust fault.

14.3   Junction of Snowshoe Creek road (FS 100) and Clark Canyon road (FS 192). Bear right onto Clark Canyon Road.

The Snowshoe Creek drainage, visible to the north, runs along the eastern intrusive contact between Cretaceous plutonic rock of the Blackfoot City Stock and folded Paleozoic and Mesozoic rock in the Black Mountain Syncline (Schmidt and others, 1994). Rolling grassy hills to the north and east are underlain by fine-grained Eocene sedimentary rocks deposited in a fluvial and lacustrine basin overlying the Avon Volcanic complex. The fine-grained red sandstone, siltstone and clay is exposed in the slope failure visible on the hillside to the north. Rotational slumps and slope failures are common in the grassy hills to the east.

16.7 [STOP 2] Mesoproterozoic Bonner Formation

Right angle bend to north in road at corral. Park vehicles and proceed across field to mouth of Gold Canyon Creek.

Mesoproterozoic Bonner Formation of the Missoula Group is exposed at the mouth of Gold Canyon Creek. Medium to thick bedded, cross-stratified medium to coarse-grained moderately sorted feldspathic arenite that represents the coarsest unit within the Missoula Group. These rocks are contained in a west dipping thrust plate that places Mesoproterozoic and lower Paleozoic sedimentary rocks over the Paleozoic and Mesozoic rocks of the Black Mountain Syncline.

18.5 [STOP 3] Mesoproterozoic/Cambrian Unconformity

Grant's Quarry. Approximately 100 meters west of the National Forest boundary.

Angular unconformity between the Mesoproterozoic McNamara Formation of the Missoula Group and the overlying Cambrian Flathead Sandstone. McNamara Formation consists of thin to medium-bedded fine to medium-grained feldspathic arenite, siltone and shale. Beds are tabular and laterally continuous, and display ripple cross-lamination, parallel laminations, graded bedding and basal scour surfaces. Unit is deformed into a broad anticline and cut by a small normal fault. Contact with the overlying Flathead Sandstone is well exposed in the ridges to the north, but here is obscured by large boulders of medium to coarse-grained, planar to cross-stratified siliceously cemented quartz arenite of the Flathead Sandstone on the hillside on the east end of the quarry.

Return to Highway 12.

21.1   Cross North Trout Creek.

22.7   Junction of Snowshoe Creek road (FS 100) and Clark Canyon road (FS 192). Bear left toward Montana Highway 12.

26.7   Junction Snowshoe Creek Road and Montana Highway 12. Turn east toward Elliston.

29.3 [STOP 4] Columnar jointed rhyolite of the Avon Volcanic Complex

Columnar jointed rhyolite plug (volcanic neck?) within Avon Volcanic Complex. For the purposes of time management and safety, this stop is out of geochronologic order. The Avon volcanics are an Eocene volcanic complex strongly dominated by rhyolite flows. This stop examines spectacularly columnar jointed, flow-foliated primarily aphanitic rhyolite interpreted to be a volcanic plug which served as a conduit for the widespread rhyolite flows and volcanic breccias in the area.

31.8   Elliston, Montana.

32.8   Little Blackfoot Road turnoff. Continue east on Highway 12.

33.0   Cross Little Blackfoot River.

34.3   Mullen Road Historic Point.

34.4   Turn left onto quarry road, keep left.

34.8 [STOP 5] Mississippian Lodgepole Formation and Quaternary overview

The Bear Town Sign Company. Chainsaw art by Ern Johnson. Mr. Johnson is very interested in geology, and is happy to host our trip. Park in the lot, and be sure to tour the gift shop!

The Bear Town is built on the old workings of a lime quarry that was an important industry of the district in the 1890s. The quarry and lime plant were operated by the Elliston Lime Company, who mined Madison limestone from these prominent outcrops. The limestone was then roasted in kilns that lined the right-of-way of the Northern Pacific Railway. The lime kilns were continuous kilns, which were essentially vertical furnaces made of mortar, brick, wire cable and wood poles. The square-shaped kilns had openings at the top and at the base. Alternate layers of wood fuel and quarried limestone cobbles were stacked inside the kiln, and fired at a high temperature. Wood and limestone was continuously fed into the top of the

kiln while the resulting and powdery quicklime was shoveled from the bottom kiln mouth into wood barrels. The chemistry of lime-burning process is simple. Limestone is mostly calcium carbonate ($CaCO_3$). When heated at 700°C (1650°F), it decomposes to yield calcium oxide (CaO or quicklime) and carbon dioxide gas. Historically, kilns were fired for 48 to 72 hours, with additional time allowed for cooling. The kilns here produced about 5000 tons of lime/year (Knopf 1913).

The quarry was developed in the upper portion of the Lodgepole Formation, very close to the contact with the overlying Mission Canyon Formation. The Lodgepole Formation consists of medium to thick bedded, laterally continuous fossiliferous packstone to rudstone containing abundant crinoidal fossil hash. The beds are organized into fining upward couplets characterized by basal crudely laminated bioclastic packstone to rudstone that grades upward to wackestone and micrite, indicative of mass sediment gravity flows. The Lodgepole forms the core of a north-plunging anticline in the footwall of the Sapphire thrust plate. The prominent west dipping strata on the ridges north of Elliston represent the western limb of this anticline.

The prominent Quaternary deposits in the Little Blackfoot valley floor between the confluences of Telegraph and Dog creeks represent an assemblage of recessional moraines and glaciofluvial deposits that formed during deglaciation of the Pleistocene Boulder Mountains ice cap. Large valley glaciers occupying the drainages of Telegraph Creek, the Little Blackfoot River, and Tenmile Creek were the primary outlets on the north side of the ice cap.

The highest relief features in the valley floor are recessional moraines which locally contain large boulders and small kettle ponds. Low relief features are braided fluvial deposits of meltwater streams, which form two prominent terrace levels above the Holocene alluvial plain. Braid plains are evident in aerial photos on well-preserved surfaces of the largest terraces.

The maximum extent of Pleistocene ice in the vicinity is much higher than suggested by first glance at the valley floor. The highest hummocks on recessional moraines in the valley floor approach 5300 feet in elevation, while the maximum extent of ice due west

of Camp Child was mapped to an elevation of over 5900 feet. Glaciated hillslopes can be identified by the presence of lateral moraine sets and cobbles and boulders of Elkhorn Mountains Volcanics and Boulder Batholith phases. Exposures of glaciofluvial sediments and glacial tills can also be observed as US 12 climbs the west side of MacDonald Pass.

Coalescing ice from the Telegraph Creek and Little Blackfoot outlet glaciers crossed the valley in the vicinity of the Lodgepole Formation quarry at Bear Town and pushed up the hillside to an elevation of approximately 5900 feet, or about 300 feet above the quarry. This configuration would have created an ice dam on Dog Creek to the northeast, leading to the development of a glacial lake, though the buried glaciolacustrine sediments observed in the valley in fresh road cuts during the 1931 field season by Alden (1953) could not be relocated in recent mapping. Four boulders sampled for cosmogenic 10Be dating near the terminal moraine margin north of Elliston returned a mean age of 16.7 ka BP (thousands of years before present), suggesting that the deposits of the Little Blackfoot valley floor formed after this time.

35.4   Junction Lime Quarry Road and Highway 12. Turn left (east).

35.9   Dog Creek Road turn off to Mullan Pass on left.

Continue on toward MacDonald Pass. Road cuts along highway consist of volcaniclastic sediments of the Elkhorn Mountains Volcanics.

37.6   Artesian spring set in road monument on left.

38.6   Helena National Forest Boundary.

39.4   MacDonald Pass Recreation Area. Turn right. Proceed to MacDonald Pass Vista.

40.0 | STOP 6 | **Boulder Magmatic Suite/ MacDonald Pass Vista**

MacDonald Pass is on the Continental Divide, and this vista provides an excellent overview of the Boulder Batholith. View to east into the Helena Valley and the Missouri River drainage. Mountains on the eastern skyline are the Big Belt Mountains, which

contain a thick succession of folded Proterozoic to Mesozoic sedimentary strata. Highway 12 to the east parallels Ten Mile Creek, which is flanked on both sides in the foreground by the Colorado Gulch grano-diorite, and towards Helena by metasedimentary rocks along the northern edge of the Unionville granodiorite. The northern edge of the batholith roughly parallels the Helena Valley, extending from Helena northwest to just north of Priest Pass, the next pass to the north along the continental divide. The Butte Granite, the most volumetrically significant component of the Boulder Batholith, underlies the forested topography to the south of the viewpoint. The western margin of the batholith forms an irregular intrusive boundary with the Elkhorn Mountains Volcanics to the west and south of the viewpoint. The contact between the Camp Thunderbird Monzogranite, an early pluton in the Boulder Batholith and the Elkhorn Mountains Volcanics is exposed on the viewpoint, where coarse-grained biotite quartz monzonite intrudes andesitic tuffs, volcaniclastic sedimentary rocks and minor andesite lava.

Return to Highway 12

40.6   Highway 12, head west to Elliston.

42.4   Artesian Spring. Artesian spring emanates from Elkhorn Mountains volcaniclastic sedimentary rocks. Sedimentary rocks of the Elkhorn Mountains Volcanics dip steeply to the north at this point. Along the western edge of the batholith, volcaniclastic rocks tend to dip steeply with a strike at a high angle to the intrusive boundary, suggesting that the Elkhorn Mountains Volcanics were folded prior to being intruded by the Boulder Batholith.

This artesian spring was apparently discovered when the MacDonald Pass road was originally built as a toll road in 1867. The monument was built when the road was widened to four lanes in the 1970s. The spring flows at an impressive rate, and yields excellent quality water. Be sure to fill up your water jugs prior to returning to Elliston!!

45.9   Little Blackfoot River.

46.1   Little Blackfoot River Road.

46.7   Elliston.

47.0   Turn north into scenic downtown Elliston.

47.4   STOP 7   **Little Blackfoot River/ Pennsylvanian Quadrant/ Permian Phosphoria Contact**

Abandoned quarry at the contact between Penn-syvlanian Quadrant Formation and the overlying Permian Phosphoria Formation. The boundary is indi-cated by beds of phosphatic oolites, lithic sandstone, and minor conglomerate. The thin bedded chert that characterizes the formation elsewhere in the area is not exposed at this outcrop. Grassy slopes to west are underlain by Jurassic sedimentary rocks. Cliffs visible to the west are rhyolite of the Avon Volcanic Complex.

End of field trip. Return to Elliston.

ACKNOWLEDGMENTS

REFERENCES

Alden, W.C., 1953, Physiography and Glacial Geology of Western Montana and Adjacent Areas: U.S: Geological Survey Professional Paper 231. 191 p (plus map).

Bachmann, O., and Bergantz, G.W., 2004, On the origin of crystal-pore rhyolites; extracted from batholithic crystal mushes: Journal of Petrology, v. 45, p. 1565-1582.

Balgord, E.A., Mahoney, J.B., and Gingras, M., 2009, Detrital zircon evidence requires revision of Belt stratigraphy in southwestern Montana: Geological Society of America Abstracts with Programs, v. 41, p. 590.

Balgord, E.A., Mahoney, J.B., Potter, J.J., Pignotta, G.S., Wittkop, C., King, N.E., Ihinger, P.D., Hardel, B.G., and Kadulski, B., 2010, Geologic Map of the Esmeralda Hill 7.5' quadrangle, Lewis and Clark County and Powell County, Montana: Montana Bureau of Mines and Geology EDMAP portion of the National Geologic Mapping Program 8, 1 sheet, scale 1:24,000.

Callmeyer, T.J., 1984, The structural, volcanic, and hydrothermal geology of the Warm Springs Creek area, eastern Garnet Range, Powell County, Montana: Bozeman, Montana State University, M.S. thesis, 84 p., 2 pls.

Carrara, P.E., 1989, Late Quaternary glacial and vegetative history of the Glacier National Park region, Montana: U.S. Geological Survey Bulletin 1902, 64 p.

Chadwick, R.A., 1981, Chronology and structural setting of volcanism in southwestern and central Montana: *in* Tucker, T.E. and others, eds., Montana Geological Society Field Conference and Symposium Guidebook to Southwestern Montana, p. 301–310.

Clauge, J.J., Barendregt, R., Enkin, R.J., and Foit, F.F. Jr., 2003, Paleomagnetic and tephra evidence for tens of Missoula floods in southern Washington: Geology, v. 31, p. 247-250.

Davis, N.K., Locke, W.W. III, Pierce, K.L., and Finkel, R.C., 2006, Glacial Lake Musselshell: Late Wisconsin slackwater on the Laurentide ice margin in central Montana, USA: Geomorphology, v. 75, p. 330-345.

Derkey, R.E., Watson, S.M., Bartholomew, M.J., Stickney, M.C., and Downey, P.J., 1993, Geologic Map of the Deer Lodge 15' quadrangle Southwest Montana: Montana Bureau of Mines and Geology Open-File Report MBMG 271, map scale 1:48,000.

Dudás, F.Ö., Ispolatov, V.O., Harlan, S.S., and Snee, L.W., 2010, $^{40}Ar/^{39}Ar$ geochronology and geochemical reconnaissance of the Eocene Lowland Creek volcanic field, west-central Montana: Journal of Geology, v. 118, p. 295–304.

du Bray, E.A., Aleinikoff, J.N., and Lund, K., 2012, Synthesis of Petrographic, Geochemical, and Isotopic data for the Boulder Batholith, southwest Montana: U. S. Geological Survey Professional Paper 1793, 39 pp.

Foster, D. A., Grice, Jr., W., and Kalakay, T., 2010, Extension of the Anaconda metamorphic core complex: $^{40}Ar/^{39}Ar$ thermochronology and implications for Eocene tectonics of the northern Rocky Mountains and the Boulder batholith: Lithosphere, v. 2, p. 232-246.

Gearity, E.C., 2013, Geology of the Marysville mining district, Montana: Two phases of mineralization: Bozeman, Montana State University, M.S. thesis, 123 p.

Gosse, J.C., and Phillips, F.M., 2001, Terrestrial in situ cosmogenic nuclides: Theory and application: Quaternary Science Reviews, v. 20, p. 1475-1560.

Hildreth, W., and Moorbath, S., 1988, Crustal contributions to arc magmatism in the Andes of central Chile: Contributions to Mineralogy and Petrology, v. 98, p. 455-489.

Hofmann, M.H., and Hendrix, M.S., 2010, Depositional processes and the inferred history of ice-margin retreat associated with the deglaciation of the Cordilleran Ice Sheet: The sedimentary record from Flathead Lake, northwest Montana, USA: Sedimentary Geology v. 223, p. 61-74.

Ihinger, P.D., Mahoney, J.B., Johnson, B.R., Kohel, C.A., Guy, A.K., Kimbrough, D.L., and Friedman, R.M., 2015, Origin and evolution of the Boulder Magmatic Suite: Constraining spatial and temporal relationships between plutonism, volcanism, and deformation, submitted to Lithosphere.

Kalakay, T.J., John, B.E., and Lageson, D.R., 2001, Fault-controlled pluton emplacement in the Sevier fold-and-thrust belt of southwest Montana, USA: Journal of Structural Geology, v. 23, no. 6–7, p. 1151-1165.

Klepper, M.R., Robinson, G.D., Smedes, H.W., Hamilton, W., and Myers, W.B., 1974, Nature of the Boulder Batholith of Montana [discussion and reply]: Geological Society of America Bulletin, v. 85, p. 1953-1960.

Knopf, Adolph, 1913, Ore Deposits of the Helena Mining Region, Montana: U. S. Geological Sur-

vey Bulletin 527, v. 1, p. 92.

Lageson, David R., Schmitt, James G., Horton, Brian K., Kalakay, Thomas J., Burton, Bradford R., 2001, Influence of Late Cretaceous magmatism on the Sevier orogenic wedge, Montana: Geology, v. 29, p. 723-726.

Lewis, R.S., compiler, 1998, Geologic map of the Butte 1 x 2 degree quadrangle: Montana Bureau of Mines and Geology Open File Report 363, 16 p., 1 sheet(s), 1:250,000.

Licciardi, J.M., and Pierce, K.L., 2008, Cosmogenic exposure-age chronologies of Pinedale and Bull Lake glaciations in greater Yellowstone and the Teton Range, USA: Quaternary Science Reviews, v. 27, p. 814-831.

Locke, W., and Smith, L.N., 2004, Pleistocene mountain glaciation in Montana, USA: *in* Ehlers, J., and Gibbard, P. L. (eds.), Extent and Chronology of Glaciations: Amsterdam, The Netherlands, Elsevier, p. 117–121.

Lund, Karen, Aleinkoff, J.N., Kunk, M.J., Unruh, D.M., Zeihen, G.D., Hodges, W.C., du Bray, E.A., and O'Neill, J.M., 2002, Shrimp U-Pb and ^{40}Ar/^{39}Ar age constraints for relating plutonism and mineralization in the Boulder batholith region, Montana: Economic Geology, v. 97, p. 241–267.

Mahoney, J.B., Nawikas, J., Kjos, A., Stolz, J., Maclaurin, K., and Kohel, C., 2008, Geologic map of Tacoma Park 7.5' quadrangle, west-central Montana: Montana Bureau of Mines and Geology Open-File Report 564, 11 p., 1 sheet, scale 1:24,000.

Philpotts A.R., Carroll, M., and Hill, J.M., 1996, Crystal-mush compaction and the origin of pegmatitic segregation sheets in a thick flood-basalt flow in the Mesozoic Hartford Basin, CT: Journal of Petrology, v. 37, pp. 811-836.

Pignotta, G.S. and McCann, Chaz, 2014, The Boulder batholith: A perplexing example of coeval magmatism, volcanism and deformation during Laramide fold and thrust belt evolution in southwest Montana: Geological Society of America Abstracts with Programs, v. 46, no. 6, p.571.

Robinson, G.D., Klepper, M.R., and Obradovich, J.D., 1968, Overlapping plutonism, volcanism and tectonism in the Boulder batholith region, western Montana, in Coats, R.R., Hay, R.L. and Anderson, C.A., eds., Studies in volcanology: Geological Society of America Memoir 116, p. 557-576.

Rudnick, R.L., and Gao, S., 2004, Composition of the continental crust, Elsevier, Oxford.

Ruppel, E.T., 1962, A Pleistocene Ice Sheet in the Northern Boulder Mountains Jefferson, Powell, and Lewis and Clark Counties, Montana: U.S. Geological Survey Bulletin 1141-G, 22 p (plus map).

Ruppel, E.T., Wallace, C.A., Schmidt, R.G., and Lopez, D.A., 1981, Preliminary interpretation of the thrust belt in southwest and west-central Montana and east-central Idaho: *in* Tucker, T.E., ed., Southwest Montana: Montana Geological Society Field Conference and Symposium Guidebook, p. 191-199, with map, scale 1:24,000.

Rutland, C., Smedes, H.W., Tilling, R.I., and Greenwood, W.R., 1989, Volcanism and plutonism at shallow crustal levels—The Elkhorn Mountains Volcanics and the Boulder batholith, southwestern Montana: International Geological Congress, 28th, Washington, D.C., Field Trip Guidebook T337, p. 16–31.

Scarberry, K.C., and Elliott, C.G., 2013, Geology of the Eocene Lowland Creek volcanic field: Butte North 30'x60' quadrangle, southwestern Montana: Geological Society of America Abstracts with Programs, v. 46, no. 5, p. 30.

Schmidt, R.G., Loen, J.S., Wallace, C.A., and Mehnert, H.H., 1994, Geology of the Elliston region, Powell and Lewis and Clark Counties, Montana: U.S. Geological Survey Bulletin 2045, scale 1:62,500.

Sears, J.W., 2007, Belt-Purcell basin: Keystone of the Rocky Mountain fold-and-thrust belt, United States and Canada, in Whence the Mountains? Inquiries into the Evolution of Orogenic Systems: A Volume in Honor of Raymond A. Price: GSA Special Paper 433, p. 147-166.

Sears, J.W., Link, P.K., Balgord, E.A., and Mahoney, J.B., 2010, Quartzite of Argenta, Beaverhead County, Montana, revisited; definitive evidence of Precambrian age indicates edge of Belt Basin: Northwest Geology, v. 39, p. 41-47.

Shapley, M.D., Ito, E., and Donovan, J.J., 2009, Late glacial and Holocene hydroclimate inferred from

a groundwater flow-through lake, Northern Rocky Mountains, USA: The Holocene, v. 19, p. 523-535.

Smedes, H.W., Klepper, M.R., and Tilling, R.I., 1988, Preliminary map of plutonic units of the Boulder batholith, southwestern Montana: U.S. Geological Survey Open-File Report 88–283, scale 1:200,000.

Stewart, E.D., Link, P.K., Fanning, C.M., Frost, C.D., and McCurry, M., 2010, Paleogeographic implications of non-North American sediment in the Mesoproterozoic upper Belt Supergroup and Lemhi Group, Idaho and Montana, USA: Geology, v. 38, p. 927-930.

Trombetta, M.J., 1987, Evolution of the Eocene Avon volcanic complex, Powell County, Montana: Bozeman, Montana State University, M.S. thesis, 112 p., 2 pls., map scale 1:24,000.

Trombetta, M.J., and Berg. R.B., 2012, Geologic map of the Avon 7.5' quadrangle, Powell County, Montana: Montana Bureau of Mines and Geology Geologic Map 63, 1 sheet, scale 1:24,000.

Todt, Mary K., Link, Paul K., Beal, Lakin K., Pearson, David, and McCurry, Michael, 2013, Sedimentary provenance of the Upper Cambrian Worm Creek quartzite, Idaho, using U-Pb and Lu-Hf isotopic analysis of zircon grains; Geological Society of America Abstracts with Programs, v. 46, no. 5, p.80.

Vuke, S.M., Lonn, J.D., Berg, R.B., and Schmidt, C.J., 2014, Geologic map of the Bozeman 30' x 60' quadrangle, southwestern Montana: Montana Bureau of Mines and Geology Open-File Report 648, 44 p., 1 sheet, scale 1:100,000.

Wallace, C.A., Harrison, J.E., Whipple, J.W., Ruppel, E.T., and Schmidt, R.G., 1984, A summary of stratigraphy of the Missoula Group of the Belt Supergroup and a preliminary interpretation of basin subsidence characteristics, western Montana, northern Idaho, and eastern Washington, *in* Hobbs, S.W., ed., The Belt: Montana Bureau of Mines and Geology Special Publication 90, p. 27-29.

Wallace, C.A., and 14 co-authors, 1986, Preliminary geologic map of the Butte 1x2 degree quadrangle, western Montana: U.S. Geological Survey Open File Report 86-292, 17 p., map scale 1:250,000.

Walker, G.E., 1992, Geology and history of the Marysville mining district and the Drumlummon mine, Lewis and Clark County, Montana: Montana Bureau of Mines and Geology Open-File Report 254, 27 p., 2 sheets.

Wittkop, C., Brugger, K.A., Boley, T.D., Bleess, R., and German, Q., 2011, Surface exposure dating and climatic interpretation of Pleistocene glaciers along the Continental Divide, Montana, USA: Geological Society of America Abstracts with Programs, v. 43, p. 475.

Photo by Phyllis Hargrave.

FIELD TRIP TO THE NEVADA LAKE BRECCIAS, POWELL COUNTY, MONTANA

C. McDonald, J.D. Lonn, S.M. Vuke, and J.G. Mosolf

Montana Bureau of Mines and Geology, Butte, MT 59701, kmcdonald@mtech.edu

This ½ day field trip to the Nevada Lake area requires a round-trip drive of about 70 miles from the Sunshine Camp south of Elliston, Montana, and a moderate off-trail hike of about 3 miles and less than 1,000 feet of elevation gain/loss. There are two stops, both near Nevada Lake (fig. 1). The accompanying road log begins near Elliston and ends at Nevada Lake.

INTRODUCTION

The Montana Bureau of Mines and Geology recently completed field work for the Geologic Map of the Elliston 30′ x 60′ quadrangle (McDonald and others, in prep). Near Nevada Lake at the northwestern end of the Avon Valley, an area of brecciated Mesoproterozoic Bonner and Mount Shields formations covers more than 2 square miles. The authors disagree on the origin of the breccia; Lonn interprets it as a Tertiary sedimentary deposit, whereas McDonald and Vuke suggest that it is mostly of tectonic origin.

Figure 2 shows the geology near Nevada Lake. The map shows two types of breccia. One is brecciated bedrock (designated by black triangle) and the other is a sedimentary breccia (map unit Tbr). Lonn suggests that much of the area with the black triangles is actually

sedimentary breccia and would include it in map unit Tbr. He believes the breccia's extensive distribution, position above the roadside Belt outcrops, contacts with Tertiary volcanic rocks, association with mapped landslides, and location on the downthrown side of the valley-bounding fault all suggest a sedimentary origin.

McDonald and Vuke believe the breccia in the areas shown by black triangle is tectonic. They interpret the corridor between the Avon and Nevada Creek valleys as a complex brittle fault zone marked by extensive brecciated and highly fractured bedrock. The brecciated rock consists of angular clasts with no obvious matrix that grades into highly fractured bed-
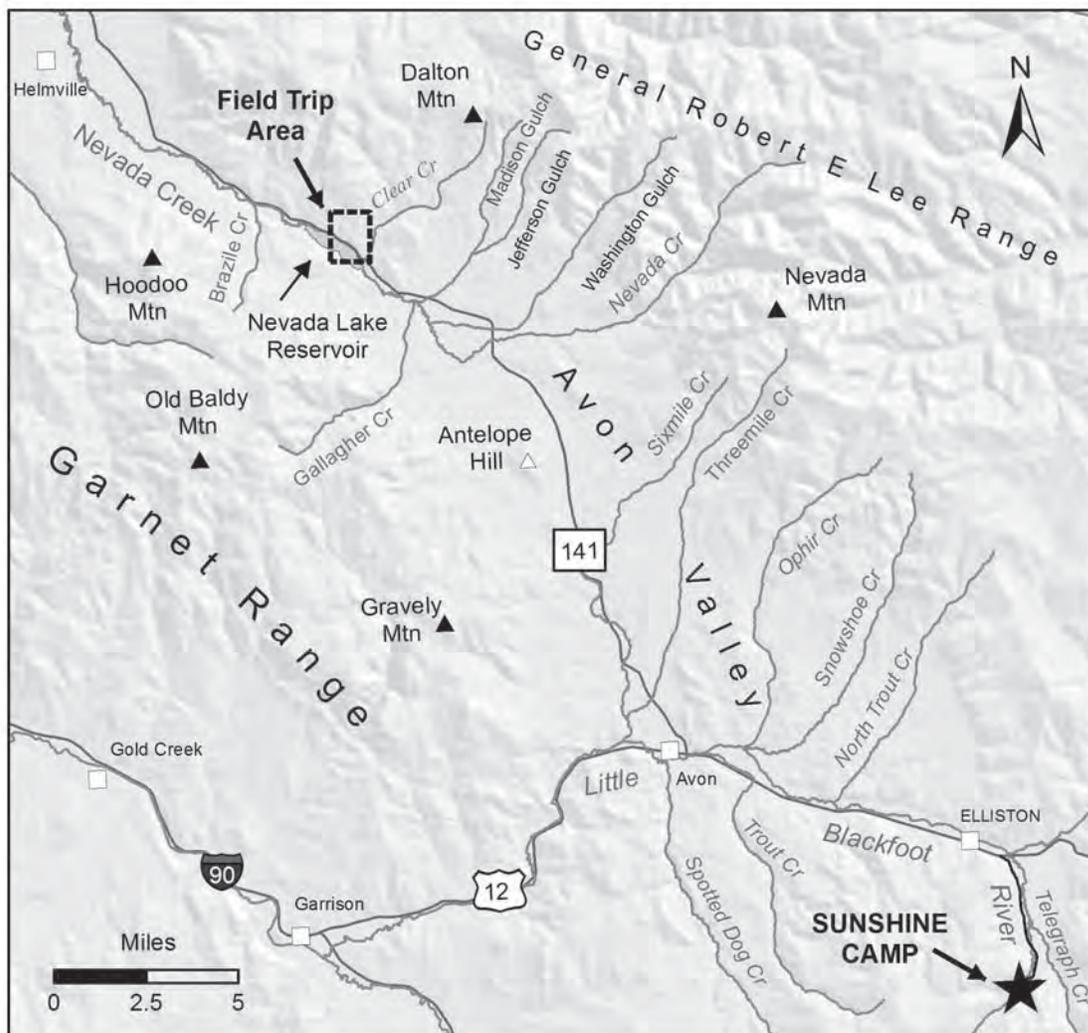

Figure 1. Location map showing field trip stops.
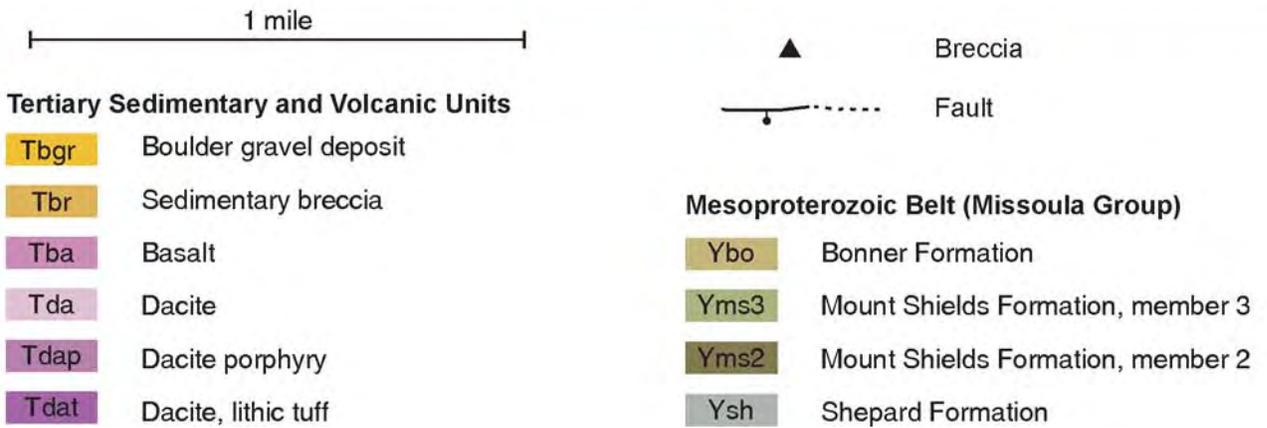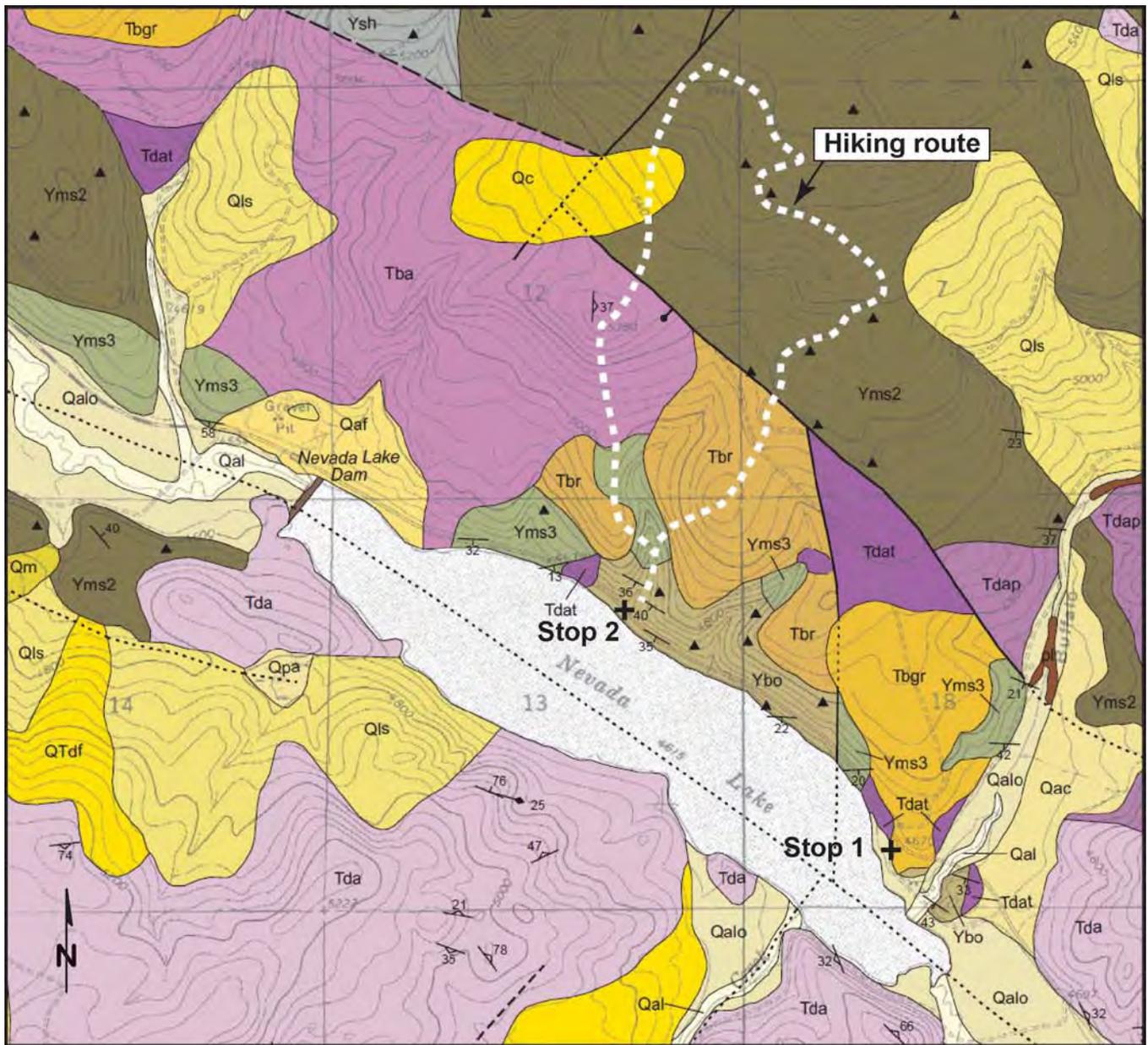
Figure 2. Geologic map of the Nevada Lake area (modified from McDonald and others, in review).

Legend:

1 mile

▲ Breccia

—•—······ Fault

Tertiary Sedimentary and Volcanic Units

Tbgr	Boulder gravel deposit
Tbr	Sedimentary breccia
Tba	Basalt
Tda	Dacite
Tdap	Dacite porphyry
Tdat	Dacite, lithic tuff

Mesoproterozoic Belt (Missoula Group)

Ybo	Bonner Formation
Yms3	Mount Shields Formation, member 3
Yms2	Mount Shields Formation, member 2
Ysh	Shepard Formation

rock (fig. 3). They do interpret the small area mapped as Tbr (fig. 2) as a sedimentary breccia, deposited as a colluvial-wedge on the downthrown side of a NW striking fault. The interpretation is based primarily on map pattern and lack of discernable bedding in outcrop (fig. 4). And, unlike the tectonic breccia, this sedimentary breccia appears to contain a clay infilling, as well as quartzite clasts.

Figure 3. Photograph of fractured and brecciated Bonner Formation exposed in quarry at Stop 2.

Figure 4. Photograph of outcrop of Tertiary sedimentary (?) breccia exposed on ridge above the quarry at Stop 2.

We hope field trip participants will, by examining the breccia and the nearby Belt and Tertiary volcanic rocks, contribute their own ideas.

ROAD LOG

The road log begins at the intersection of the Little Blackfoot Road and Highway 12.

MILEAGE

0.0   Little Blackfoot Road-Highway 12 Intersection. Hills to north and south of highway underlain by thrust faulted Paleozoic and Mesozoic sedimentary rock.

0.8   Town of Elliston. Continue west. For the next 3 miles, the timbered hills south of highway are underlain by Tertiary (Eocene) rhyolite and dacite of the Avon Volcanic field. North of the highway, beyond the Little Blackfoot River, the sparsely timbered low hills are underlain by mudstone and siltstone of the Climbing Arrow Member of the Tertiary Renova Formation and Tertiary porphyritic rhyolite.

3.5   Large cliff of dacite on south side of road.

6.2   U.S. Forest Service "Snowshoe Access" road to north. Renova Formation forms low hills on both sides of road.

7.4   Outcrop of Renova Formation on south side of road.

8.5   Rhyolite porphyry in road cut to south also underlies the timbered hills north of highway. A K-Ar date on sanidine from the porphyry yielded an age of 39.4±1.6 Ma (Chadwick, 1981) and a U-Pb zircon age of 40.8±0.17 Ma (McDonald and others, in prep).

8.7   Avon Cafe.

8.9   Cross Little Blackfoot River.

9.1   Turn right on Highway 141, pass through town of Avon. For the next 18 miles, the road traverses the Avon Valley, a northwest-trending graben lying between the Garnet Range to the west and the Nevada Mountains to the east.

9.3   Alluvial gravels in road cut on east.

9.7   Climbing Arrow Member of Renova Formation

in road cut to east.

10.3   Avon Cemetery.

10.9   Cross Threemile Creek. For the next mile, the road crosses Quaternary glacial outwash deposits that form a prominent apron south and southwest of the mountain front and that originated from the Threemile Creek drainage.

11.3   Quarry in rhyolite porphyry visible at base of hill to east.

11.7   Ophir Creek Road on right. Alluvium along Ophir Creek produced placer gold, as did many similar stream valleys that drain lode gold-mining districts. The Ophir Mining District is one of the largest and most productive gold districts in western Montana (Loen, 1990).

12.1   Cross Sixmile Creek. For the next several miles, pale olive green bentonitic mudstone and yellowish gray siltstone beds, typical of the Climbing Arrow Member of the Renova Formation, are visible in road cuts and low hills adjacent to road. The member is prone to landslides.

16.5   The top of the hill is the drainage divide between Little Blackfoot River to south and Blackfoot River to north. The divide coincides with a gravity high in the subsurface (Hanna and others, 1994; Knatterud and others, this volume) that bisects the Avon Valley. We suspect the gravity high marks an eastward continuation of a NE trending high-angle fault mapped by Mosolf (in review) in the Garnet Range.

17.3   Power station on left.

17.9   The timbered hill to the west is Antelope Butte, a northwest trending syncline underlain by the Renova Formation. The lower slopes are the Eocene Climbing Arrow Member. Antelope Hill is capped by beds of gastropod-bearing marlstone, limestone, tufa, travertine, and local gastropod coquina that in many places overlie coarse-grained sandstone with plant impressions, petrified wood, and associated shale. These beds are equivalent to the Miocene/Oligocene Cabbage Patch beds of the Renova Formation. In some places in the Garnet Range, this member

overlies volcanic rock that yielded a U-Pb zircon date of 29.95±0.17 Ma (Mosolf and Vuke, in review). The carbonate beds on Antelope Hill are locally silicified to white-weathering, gray porcellanite and variegated chert that was quarried by native peoples for projectile points. The "Avon Chert" has a distinctive chemical signature and has been found as distant as Illinois (Roll and others, 2005).

20.5   Climbing Arrow Member of Renova Formation to east of road.

21.4   Reddish dark brown Climbing Arrow Member with abundant plant fossils, dark brown paper shale, and sandy lenses is in road cut to east.

22.3   Cross Nevada Creek. To right (east) is the upper Nevada Creek Valley. The high mountains in the distance are underlain by Mesoproterozoic Belt rocks. The range front is defined by aligned faceted spurs that mark the location of the down-to-the-west normal fault on the east side of the Avon Valley. Immediately west of the fault are large Tertiary deposits. The low hills on either side are of the creek are underlain by Renova Formation.

22.6   Cross Washington Creek. Washington Creek, along with Nevada, Jefferson, and California Creeks were all placered for gold derived from lode deposits around the margins of the Dalton Mountain Stock. The stock intruded Mesoproterozoic Belt rocks and is located approximately 6 miles due north.

22.8   Nevada Creek road on right. For next several miles, Climbing Arrow Member of Renova Formation is exposed in road cuts. The high mountains to the east and north are underlain by Belt rock, to the west the mountains are predominantly Tertiary volcanic rock.

24.5   Dalton Mountain Road on right.

25.2   Tertiary (Eocene) dacite and volcaniclastic sediments in road cut on right. These rocks occur in road cuts for about next 1.5 miles.

26.7   Outcrop on left (south) is lithic tuff in contact with the Mesoproterozoic Bonner Formation.

26.9   Bridge over Clear Creek.

27.1   Clear Creek Road to right, Nevada Lake on

left is just coming into view. For the next five miles, the road travels through a narrow valley that separates the Avon and Nevada Creek Valleys. Most of the bedrock exposed on the north side of the road is the Mesoproterozoic Mount Shields Formation members 2 (quartzite) and 3 (grayish red argillite), and the Bonner Formation (quartzite). Several high angle northwest trending faults that parallel the road fractured and brecciated the Mesoproterozoic rocks.

27.2 STOP 1

Pull over and park on the gravel road on left (south) side of highway. Cross highway to road cut on north (Highway 141 is busy so use caution). The contact between Tertiary (Eocene) volcanics and Mount Shield Formation, member 3 (Mt Shields 3) is exposed in the road cut (best exposure is in terraced benches above the road).

The volcanic rock includes lithic ash flow tuff with angular and rounded Belt clasts, volcanic clasts, and plant fragments; thin dacite(?) flows; and possible volcaniclastic beds. We tentatively interpret this unit (fig. 2, map unit Tdat) as equivalent to ash flows found at the base of and intercalated with Eocene porphyritic dacite lava flows elsewhere in the eastern Garnet Range volcanic field (Mosolf, in review; Mosolf and Vuke, in review; McDonald and others, in prep). The porphyritic dacite (and associated ash flows) represent one of the older deposits in the Eastern Garnet Range volcanic field based on zircon separates that yielded U-Pb zircon ages spanning 46.2 to 48.1 Ma.

Walk northwest along the highway to an outcrop of gently south-dipping, grayish red quartzite-argillite with couples and couplets. There are abundant salt crystal casts on the argillite bedding planes. The outcrop is Mt Shields 3. Some bedding-parallel zones of breccia are apparent in this outcrop, lending support to the interpretation of McDonald and Vuke.

Return to the cars and continue west for 0.7 miles to a gravel track in a gully on the right that accesses a small quarry. Turn right and pull into quarry.

27.9 STOP 2

We will gather, discuss the geology of the quarry walls, and then begin our hike.

This small quarry is located in thick-bedded, poorly-sorted, fine- to coarse-grained feldspathic quartzite that we interpret as the Bonner Formation. The rock contains common granule-sized grains and abundant mud rip-ups and red argillite interbeds. The Bonner dips to the southwest, is highly fractured, has breccia zones, and rare surfaces with slickenlines. The "brecciation" we see here is typical of most quartzite outcrops along the corridor between the Avon and Nevada Creek valleys. One goal today is to determine if the tectonic breccia we see in the quarry differs from the other breccias we will observe.

According to our mapping (fig. 2), we have come downsection from the outcrop of Mount Shields 3 at Stop 1 yet we are stratigraphically above the Mt Shields 3, necessitating the fault shown in figure 2.

From the quarry, walk northeast through a gate and up the small valley. Although boulders of quartzite breccia litter the valley floor, by about 0.25 miles up-valley we see outcrops of red argillite with salt casts, indicating that we have gone down section from the Bonner into the underlying Mt Shields 3 Formation.

Turn to the northeast and ascend the steep forested slope to the knob near the section corner. At the knob are large outcrops of cemented quartzite breccia consisting of angular cobble- to boulder-sized clasts (Tbr, fig. 2), similar to the boulders we saw in the valley. Some of the float contains possible clay clasts. Bedding is not apparent. McDonald, Vuke, and Lonn agree this could be a sedimentary breccia. Note the abrupt tree line at the east edge of the Tbr outcrops; the trees appear to prefer the quartzite substrate over fine-grained Tertiary volcanics immediately to the northeast (fig. 2, map unit Tdat- lithic dacite tuff) which supports grass and sagebrush. The edge of the trees (and the edge of the breccia) is very straight and may mark the northwest striking fault that we crossed between stops 1 and 2.

From the knob, walk northeast into the grassy area. A lack of angular quartzite cobbles indicates we are out of the sedimentary breccia (Tbr) and into the fine grained volcanics (Tdat). Some digging produces brown soil that contains rare rounded pebbles and cobbles that appear to be weathered out of the lithic tuff. Keep walking northeast. Cross a saddle, an old road,

and proceed uphill to a well-established two-track road where angular quartzite boulders are encountered. Turn left (NW) on the road which ascends a hill of angular quartzite float and rare boulders of breccia.

The origin of the breccia in this area is where the authors disagree. McDonald and Vuke show a second fault along the base of the slope that juxtaposes volcanic deposits (Tdat) to the south against Mesoproterozoic Mt Shields 2 on the north (fig. 2). They interpret the brecciated Mt Shields outcrops (black triangles) north of the fault as tectonic breccia. Lonn interprets the breccia as sedimentary and thinks it overlies the volcanic deposits. We will examine the breccia in this area to try to determine which interpretation is correct. If it is a sedimentary breccia overlying fine-grained volcanics as Lonn suggests, it could explain the landslides mapped to the northeast (fig. 2).

Continue walking up the road for about 0.5 miles to where it splits. Take the left fork. Follow the road through more quartzite breccia float for another 0.5 miles until a switchback in an open (grassy) area is encountered.

Option 1: If time permits, continue up the road until another fork is reached, and again take the left fork. The left-hand road contours along the slope and crosses a NE-striking fault before the road turns south and heads downhill (fig. 2). Lonn interprets the fault as separating his Tertiary sedimentary breccia from Mt Shields 2 bedrock. McDonald and Vuke believe it is bedrock on both sides of the fault. If you continue down the road, you will go downsection into the underlying Shepard Formation. There is additional breccia exposed along the road that Lonn, McDonald, and Vuke all agree is tectonic and related to faulting.

Option 2: Most likely, time will be short, so near the switchback in the open area, leave the road and head southwest, down the hill to an open, flat saddle. The saddle marks the northwestward continuation of the NW-striking fault(s) observed earlier (fig. 2). At this location, basalt (Tba) is faulted against Mt Shields 2. The basalt is one of the youngest volcanic units in this area (Oligocene) with a K-Ar age date of 32.3±1.3Ma (Mitchell Reynolds, U.S. Geological Survey, written commun., 2015). Continue south along the ridge to a small knob. The basalt on the knob appears to dip gently northeast into the fault, suggesting

that movement on the nearby NW trending faults is younger than about 32 Ma.

Traverse down the steep south side of this knob, crossing basalt for several hundred vertical feet. If the flows really dip northeast, then they comprise a thick sequence that covers more than a square mile. As the terrain flattens, follow a fingerlike ridge straight south. When it steepens, descend left (west), where more quartzite breccia is encountered. It is impossible to determine the relationship between the breccia and the basalt; mapping shows only that they are in contact in several places. The breccia in this area is interpreted as a sedimentary breccia and appears to contain clay as clasts or possibly a later infilling. Contour back around the ridge to the east and descend into the gully. We eventually descending into bedrock, suggesting the quartzite breccia overlies the bedrock here.

Follow the gully back to the car.

REFERENCES

Chadwick, R. A., 1981, Chronology and structural setting of the volcanism in southwestern and central Montana, in Tucker, T.E. and others, eds., Montana Geological Society Field Conference and Symposium Guidebook to Southwestern Montana, p. 3013-310.

Hanna, W.F., Hassemer, J. H., Elliott, J.E., Wallace, C.A., and Snyder, S.L., 1994, Maps showing gravity and aeromagnetic anomalies in the Butte 1° x 2° quadrangle, Montana: U.S. Geological Survey Miscellaneous Investigations Series Map I-2050, 35p., 2 sheets, scale 1:250,000.

Knatterud, L.K., Speece, M.A., Mosolf, J.G., and Zhou, X., 2015, Using gravity and seismic reflection profiling to decipher the structural setting of the Avon Valley, west-central Montana: Northwest Geology, v. 44.

Loen, J.S., 1990, Lode and placer deposits of the Ophir district, Lewis and Clark and Powell Counties, Montana: Fort Collins, Colorado State University Ph.D. dissertation, 268 p.

McDonald, C., Mosolf, J.G., Vuke, S.M., and Lonn, J.D., (in preparation), Geologic map of the Elliston 30' x 60' quadrangle, west-central Montana: Montana Bureau of Mines and Geology Open-File Report xxx, 1 sheet, scale 1:100,000.

McDonald, C., Mosolf, J.G., and Lonn, J.D., in review, Geologic map of the Nevada Lake 7.5 quadrangle, Lewis and Clark and Powell Counties, west-central Montana: Montana Bureau of Mines and Geology Open-File Report xxxx, 1 sheet, scale: 1:24,000.

Mosolf, J.G., and Vuke, S. M., (in review), Geologic map of the Gravely Mountain 7.5' quadrangle, Lewis and Clark and Powell Counties, west-central Montana: Montana Bureau of Mines and Geology Open-File Report xxxx, 1 sheet, scale: 1:24,000.

Mosolf, J.G., 2014, (in review), Geologic map of the Windy Rock 7.5' quadrangle, Powell County, west-central Montana: Montana Bureau of Mines and Geology Open-File Report xxxx, 1 sheet, scale: 1:24,000.

Roll, T.E., Neeley, M.P., Speakman, R.J., and Glascock, M.D., 2005, Characterization of Montana Cherts by LA-ICP-MS, in Laser Ablation-ICP-MS in Archaeological Research, Speakman, R.J., and Heff, H., eds., University of New Mexico Press, Albuqueque, p. 58-76.

Photo by Katie McDonald.

GEOLOGY AND MINERALOGY OF THE EMERY MINING DISTRICT, POWELL COUNTY, MONTANA

Stanley Korzeb and Kaleb Scarberry

Montana Bureau of Mines and Geology, 1300 W. Park Street, Butte, MT 59701, skorzeb@mtech.edu

INTRODUCTION

The Emery or Zosell mining district is located about 6 miles east of Deer Lodge in Powell County and is one of several small gold-silver-lead-zinc producing districts associated with the Boulder batholith. Metal production was from a shallow dipping (5° to 35° W) north-south vein and a number of related steeply dipping east-west veins. Recent fluid inclusion and isotope data (unpublished data, Korzeb 2015) suggest the near surface veins could be related to a deep-seated porphyry system that supplied hydrothermal fluids to near surface fractures. This field trip will examine the district's key past-producing mines, the related geology, and the alteration mineralogy.

GEOLOGY

Veins are hosted by the Cretaceous age Elkhorn Mountains Volcanic suite (Derkey, 1986). Within the district these volcanic rocks are represented by tuffs, andesite, and basalt. Two types of basalt exposed in the district are described by Derkey (1986) as 1) dark-gray, porphyritic basalt with plagioclase phenocrysts and 2) medium green porphyritic basalt with pyroxene phenocrysts. Pardee and Schrader, (1933) described the basalts as andesite. Because the volcanic rocks hosting the veins are highly altered, they are difficult to accurately classify. South of the district, deuterically altered volcanic rocks mapped by Scarberry (2015) can be correlated with the basalts within the district. Whole rock analysis of these deuterically altered basalts indicates they should be re-classified as basaltic andesite. The basaltic andesite flows exposed in the Emery district are interpreted by Scarberry (2015) to be the oldest units of the Elkhorn Mountains Volcanic suite. The polymetallic veins in the district are hosted by these two basaltic andesite flows. The flows have amygdaloidal and vesicular equivalents throughout the district that formed beds or planes of structural weakness.

The entire region was subject to regional compressive deformation during the Laramide orogeny that lasted from approximately 75 to 55 Ma (Houston and Dilles, 2013). Two thrust faults that crop out along the east side of the district are likely evidence for this compression (Derkey, 1986). Thrusting was to the east.

When thrust faulting took place, there was a period of low angle and normal faulting (Derkey, 1986). Robertson (1953) described one mineralized low angle fault that formed in amygdaloidal zones or planes of weakness in basaltic andesite. The fault follows amygdaloidal zones, extends north-south for one mile and dips from 10° to 40° to the east. In its more steeply-dipping sections, it cuts amygdaloidal zones. A major vein extending from the Argus mine in the north to the Bonanza mine in the south now occupies this fault. Mineralized east-west normal faults up to a mile long and with dips from 80° to vertical have been interpreted to be tear faults that developed during the thrusting event that formed the low angle faults (Derkey, 1986).

After mineralization, two sets of non-mineralized normal faults offset the mineralized faults. Northeast trending faults do not offset the veins significantly and are described as tight shears by Robertson (1953). Northwest trending faults with large displacements offset some veins. The Black Rock fault (fig. 2) described by Robertson (1953) has a N 70° to 75° W strike and displaces the south side of the Emery vein horizontally to the west by 500 to 1,000 ft.

Figure 1 is a map showing our route and stops. Figure 2 is a geologic map from Derkey (1986) showing mine locations and veins. Figure 3 is a map from Robertson (1953) showing the geology, vein, and mines at the northern end of the north-south vein system. Figures 4 and 5 are underground mine maps of the Bonanza and Emery mines (from Robertson, 1953).
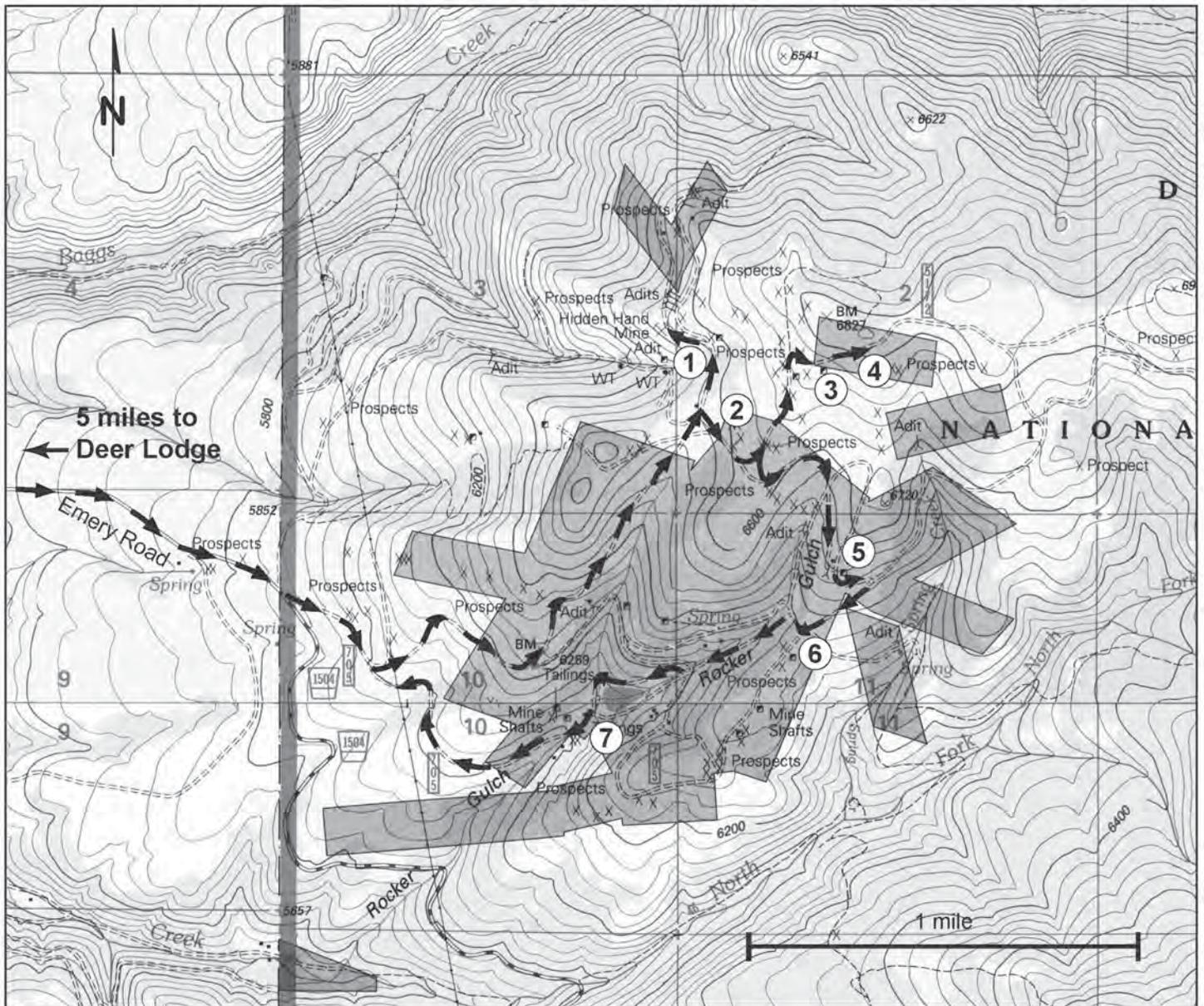
Figure 1. Road log index, Emery Mining District. Route marked with arrows, stops with numbers.

ROAD LOG

Travel west from Elliston 21 miles on Highway 12. At flashing traffic light, turn left (south) and follow signs to I-90 south. Travel south about 9 miles; take the first Deer Lodge exit (Exit 184). Turn left at bottom of off ramp, head east under (freeway) for about 0.2 miles and turn right (south) onto Boulder Road. Proceed south for 1 mile and turn east (left) onto Emery Road.

Set odometer to 0.0 at the Boulder Road-Emery Road intersection.

MILEAGE

0.0   Boulder Road-Emery Road Intersection. Head east on Emery Road.

4.1   Turn south, continuing on Emery Road. Emery Road becomes a gravel road at this point.

5.5   Emery Road curves to east.

6.9   Emery Road – USFS Road 1504 intersection. Turn left, continue east on Emery Road.

7.1   Intersection with FS 705 (may not be marked), turn left onto FS 705, passing under high-tension power lines.

7.7   FS 705 splits. Turn left and continue to the north for another 0.9 mile.
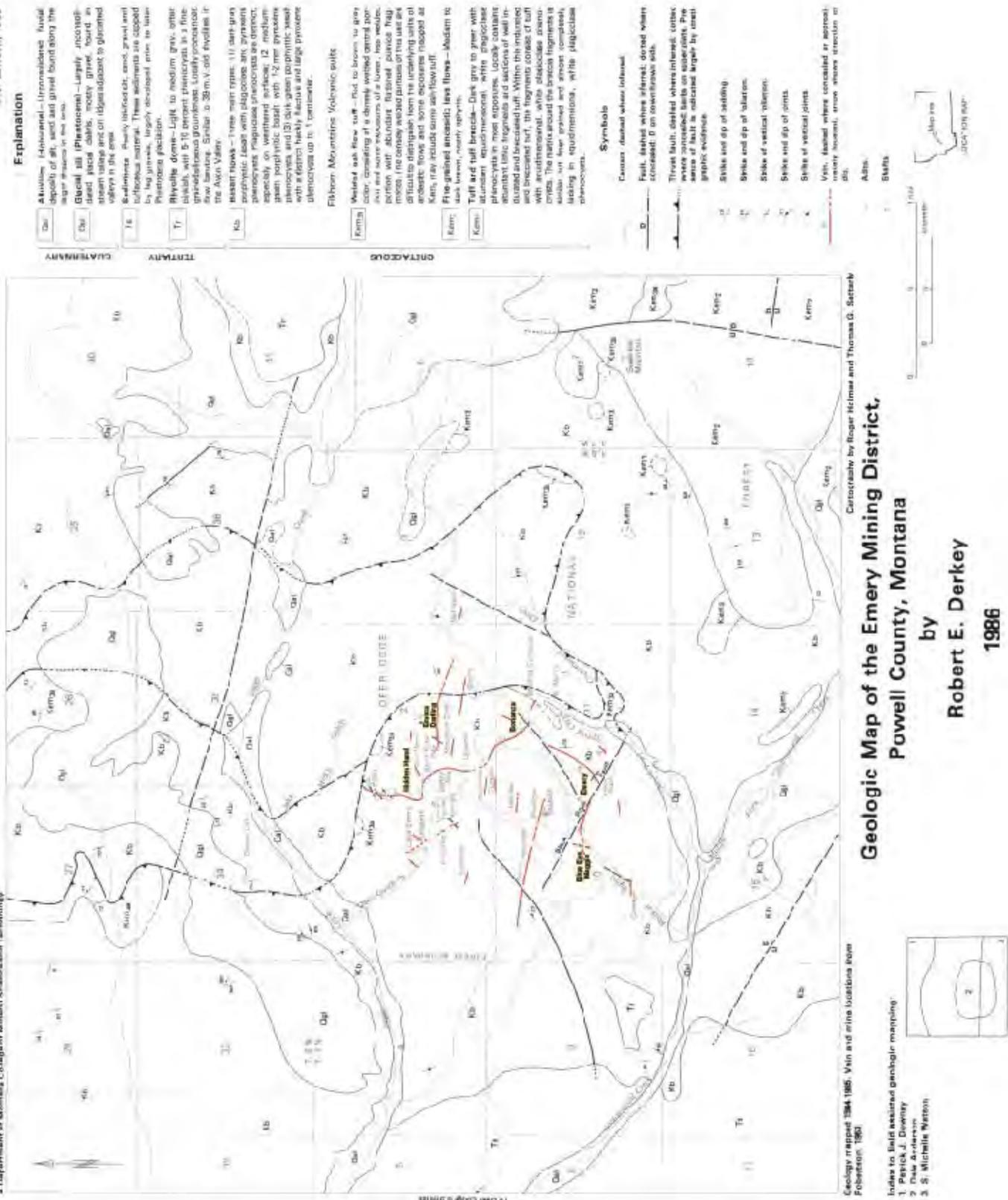
Figure 2. Geologic map of Emery District showing vein and mine locations (from Derkey, 1986).

B

SKETCH MAP OF THE ARGUS–HIDDEN HAND VEIN

Showing all known development. Compiled from field surveys
and maps made available by William Howard, 1949.
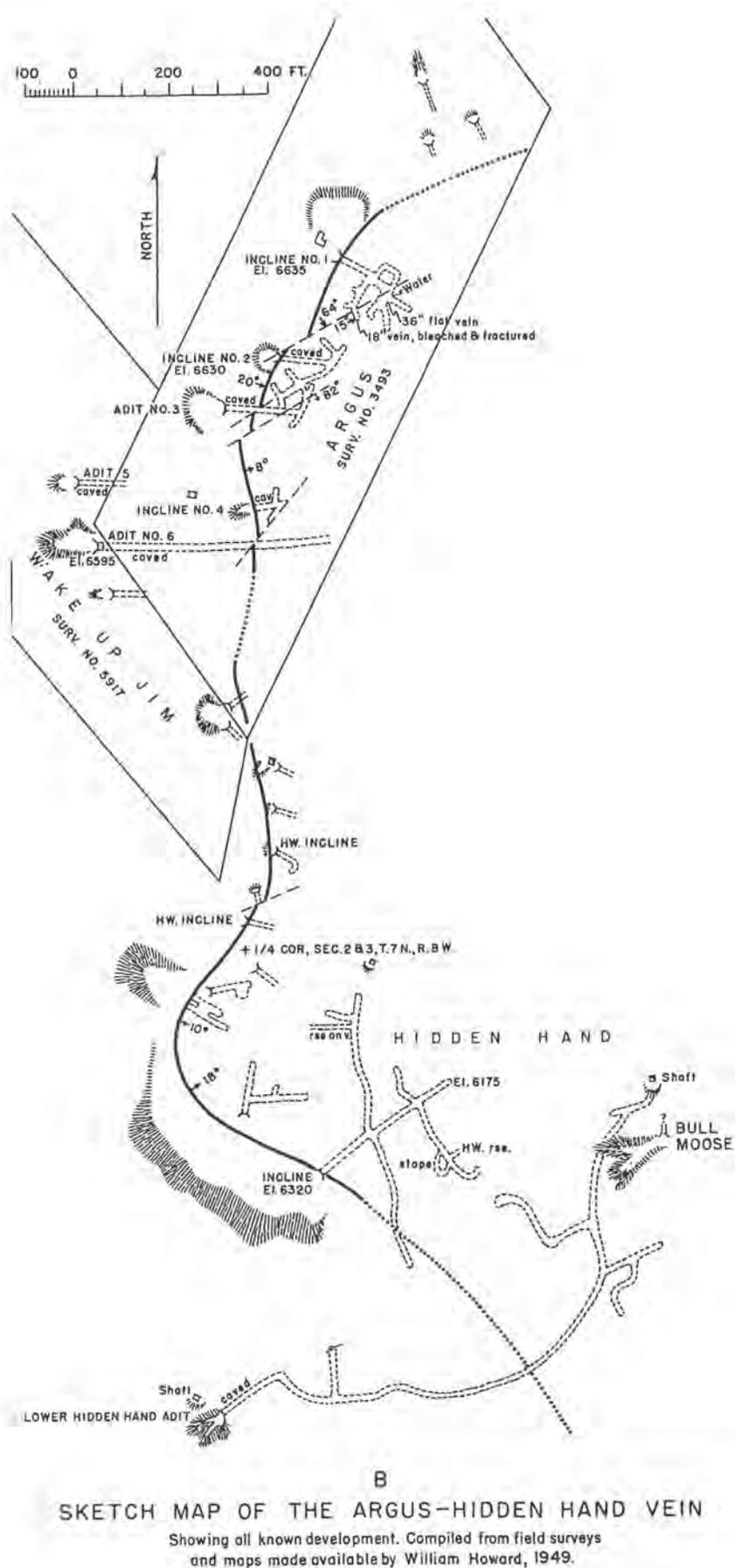
Figure 3. Map of the Argus-Hidden Hand vein and associated mines (from Robertson, 1953).

8.6 STOP 1 Hidden Hand Mine (46.387907 N, 112.578517 W).

The road passes over the dumps for the Hidden Hand Mine. An open cut will be on the right. Park on the mine dumps.

Hidden Hand Mine. At this site we will examine surface exposures and remains of the Hidden Hand Mine. The Hidden Hand produced gold, silver, and lead from quartz filled fissures cutting silicified and brecciated basaltic andesite host rock. The altered amygdaloidal-basaltic andesite host rock is visible in a cut to the east. The Hidden Hand's original portal is buried and no longer visible.

The Hidden Hand vein is part of a major north-south striking vein system (fig. 2) that extends through the Emery district. The Hidden Hand vein dips 18° east and follows "bedding" in the basaltic andesite host rock. The host rock is brecciated with quartz veining and alteration varying from propylitic to sericitic/argillic. Robertson (1953) describes the vein to be a brecciated shear zone cemented by quartz veining. The quartz stingers and veins contain galena, pyrite, arsenopyrite, sphalerite and traces of chalcopyrite. The oxidized portion of the vein contains sericite and clays with minor sulfide minerals remaining. The Argus Mine, to the north (figs. 2 and 3) is located at the northern end of the Hidden Hand vein.

The upper workings consisted of a 20° decline following the dip of the vein (Robertson, 1953). The decline extended for about 350 feet (ft.) and was driven into the oxidized portion of the vein. Most gold production came from the oxidized zone. In the ravine below, a 1,200 ft. long adit was driven to intersect the vein (Robertson, 1953). Most silver and lead production came from the un-oxidized portion of the vein. The dumps from this adit can be seen below.

The Hidden Hand vein was discovered in 1887 and the mine operated intermittently from 1887 to 1950 (Derkey, 1986). Early production is unknown but was estimated to be valued at $45,000 (Robertson, 1953). In 1928, the Harvey Creek Mining Company stripped silver-lead ore from a shallow flat lying vein. No production records for this operation exist. From 1928 to 1937, the property was idle. William Howard leased the property in 1937 and its important production

occurred from 1937 to 1947. Total production from this period was valued at $120,000. William Howard was the last operator and the mine remains idle. In the 1980's Lacana Corporation, Freeport-McMoran, and Exxon Corporation started exploration programs near the Hidden Hand Mine (Montana Bureau of Mines and Geology archives).

From STOP 1, reverse course for 0.2 miles and pull to the left side of the road to reach STOP 2.

9.0 STOP 2 Granodiorite intrusion (46.385346 N, 112.576759 W).

At this location a small granodiorite intrusion is exposed in a trench excavated by Freeport-McMoran in the 1980's. We will walk east across the meadow to examine the granodiorite found in piles lining the trench and discuss varying degrees of alteration ranging from propylitic to sericitic. Gulf Mineral Resources suspected this intrusion could be related to a deep-seated porphyry system.

In 1976, Gulf Mineral Resources drilled a hole to a depth of 2,903 ft. in search of the intrusion and possible related porphyry system. The drill hole, located adjacent to the remains of a log cabin in the meadow west of the trench, began in basaltic andesite and bottomed in andesite. The andesite near the bottom of the hole had quartz veining with anomalous copper and molybdenum values (Al-Khirbash, 1982). The drill results indicate that if there is an intrusion and porphyry system, it is deeper than 2,903 ft.

U-Pb zircon dating of the granodiorite from the trench yielded an age of 1.77 Ga±8 Ma (unpublished results from Korzeb, 2015) which is similar to dates obtained from other intrusions related to the porphyry system in the Butte district. In the Butte district, intrusions with Proterozoic dates are interpreted to have passed through and assimilated Belt Supergroup formations (Field and others, 2005). The granodiorite in the Emery district may have likewise assimilated Belt Supergroup rock preserving zircons with Proterozoic dates. Sulfur isotopes from the Emery district veins also show a possible Belt Supergroup influence with $\delta^{34}S$ values ranging from 1.0 to 8.7 permil. Pyrite that crystallized early in the veins has an average $\delta^{34}S$ value of 8.0 permil which is slightly higher than

average for diagenetic pyrite found in the lower Belt Supergroup (Lyons and others, 2000; Field and others, 2005).

9.03   Road splits, proceed left (the split is about 50 yards south of STOP 2).

9.2   The road splits again, go to the left, or north, and proceed another 0.4 miles, passing a cabin on the left and old mine working on right.

9.6   STOP 3   Emma Darling Mine (46.786454 N, 112.571015 W).

Emma Darling Mine (south side of road): At this stop we will examine the dump and surface workings of the Emma Darling Mine. Altered amygdaloidal-basaltic andesite host rock and sections of vein can be found on the dump and near the ore bin. The vein material consists of quartz and ankerite with arsenopyrite, pyrite, sphalerite, galena, and chalcopyrite.

The Emma Darling mine opened in 1908 and operated intermittently until 1942 (Robertson, 1953). The mine is developed by a vertical shaft reported to be 90 ft. deep (Pardee and Schrader, 1933). The Emma Darling vein is a near vertical east-west striking structure that extends for about a half a mile (fig. 2), is from 2 to 7 ft. thick (Robertson, 1953), and is exposed at the portal of a collapsed adit east of the mine. There are no production records.

The hill to the north of the mine has been explored by numerous prospect pits and was drilled by Freeport-McMoran, Exxon Corporation, Hecla Mining Corporation, and Lacana Corporation in the 1980's (Montana Bureau of Mines and Geology archives). These companies were searching for a near-surface disseminated gold resource. Drill holes averaged about 400 ft. deep, limiting exploration to the altered basaltic andesite. Freeport-McMoran defined an area with potential for a 150,000 oz. disseminated-gold resource.

From STOP 3, hike or drive 0.2 miles east to STOP 4, located on west side of Spring Creek drainage.

9.8   STOP 4   Emma Darling vein (46.386427 N, 112.567250 W)

Emma Darling Vein: At this stop, we will examine one of the few vein outcrops exposed in the district as well as the sheared and altered basaltic andesite hosting the Emma Darling vein. The vein consists of quartz stringers and veins of ankerite with disseminated pyrite. Pardee and Schrader (1933) reported the vein assayed 2.5 oz/t silver and gold worth $2.40 based on a $20.00 per ounce gold price.

In 1978, north of the adit, near the road intersection, Gulf Resources drilled to a depth of 1,965 ft. searching for a deep-seated porphyry system (Montana Bureau of Mines and Geology archives). The log for this hole has been lost.

From STOP 4 reverse course and drive about 0.5 mile southwest, to where the road splits (just south of cabin on the left).

10.3   Road splits, turn left (east) and proceed 0.5 miles east then south to Bonanza Mine. Road passes in front of the ore bin and over the dumps at the mine.

10.8   STOP 5   Bonanza Mine (46.379555 N, 112.570639 W).

Bonanza Mine. At this stop we will examine the remains and dumps of the Bonanza mine. The mine is presently owned by Montana Precision Mining. In 2014, they investigated the dumps for potential gold and silver ore.

The Bonanza vein was discovered in 1895 and the mine was opened the same year by W. T. Zosell. The main workings are an inclined shaft that follows the dip of the vein (fig. 4). The inclined shaft dipped 30° and extended to a depth of 340 ft. with short drifts extending into the vein at 100 ft. and 235 ft. levels (Pardee and Schrader, 1933). By 1949, the underground workings consisted of 640 ft. of inclined shaft and 3,500 ft. of drifts (Robertson, 1953). The vein was developed to a vertical depth of about 250 ft.

The Bonanza Mine was the second largest producer in the Emery district (Robertson, 1953). Gold, silver, and lead were the main metals produced.
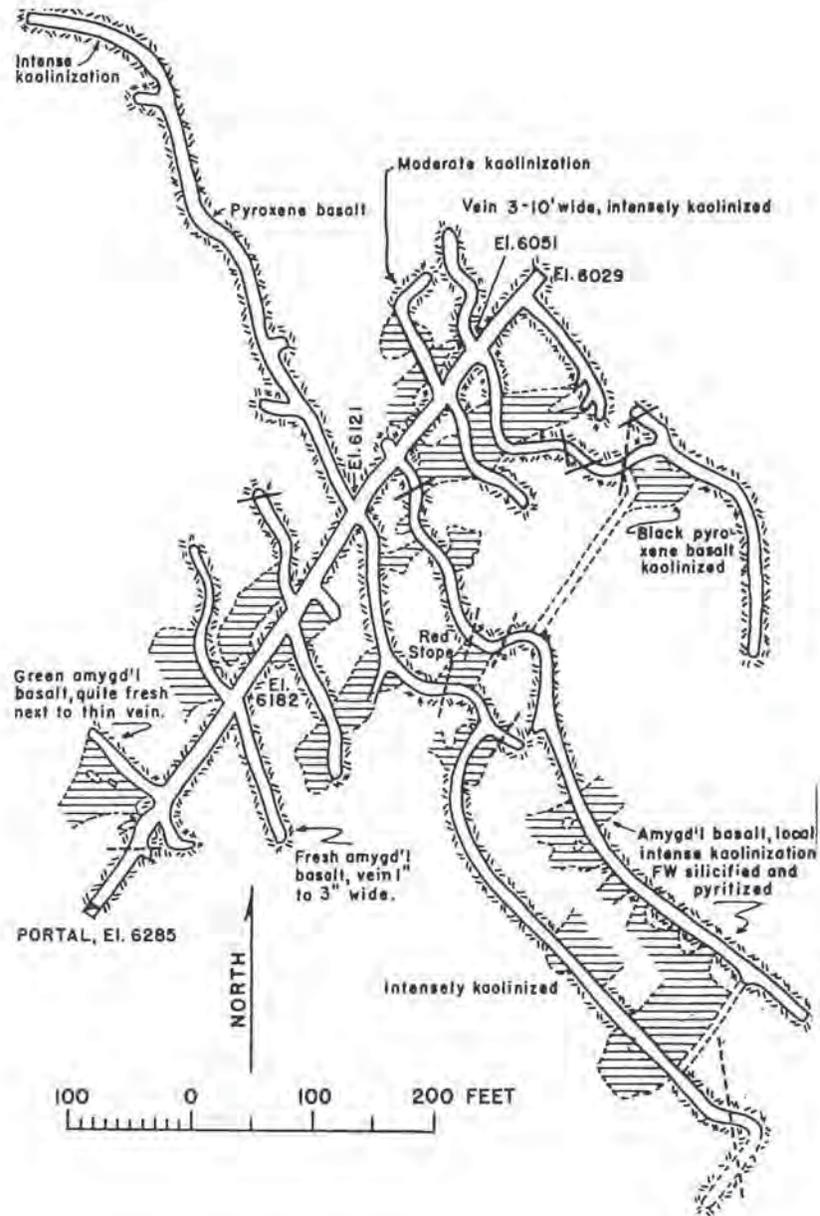
C. PLAN MAP OF BONANZA MINE
Revised from map by F. A. Stejer, 1949.

- - - - - Faults
———— Manganese veinlets
〰〰〰 Basalt
▭▭▭ Stopes

Figure 4. Map of Bonanza Mine underground workings (from Robertson, 1953).
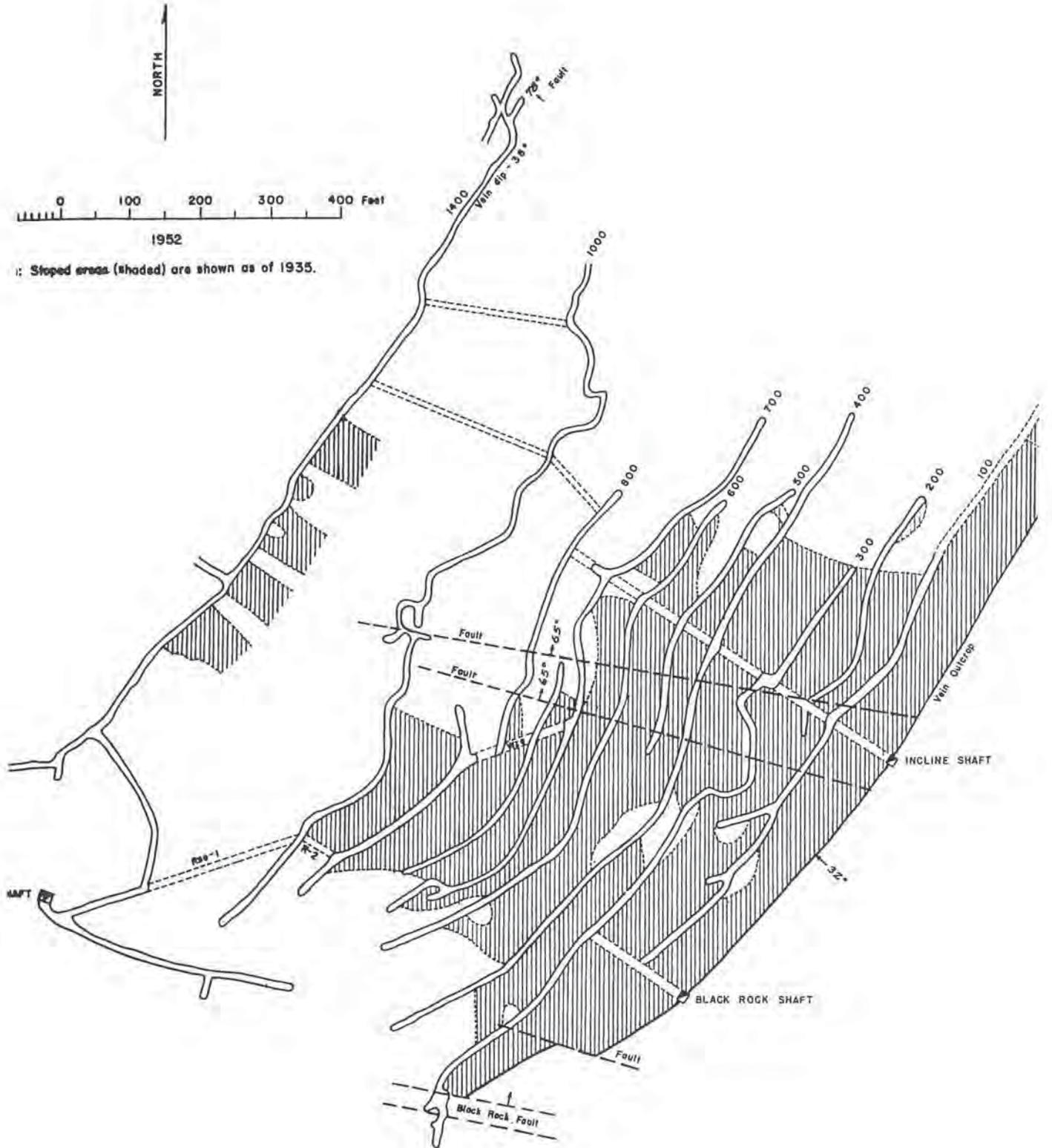
A. PLAN MAP OF EMERY MINE, ZOSELL (EMERY) DISTRICT, POWELL COUNTY, MONTANA

Prepared by Forbes Robertson from maps by J.E. Higgins, H.C. Elliott, and W. F. Criswell, representing development through 1949.

Figure 5. Map of Emery Mine underground workings (from Robertson, 1953).

The first recorded shipments from the mine were in 1911and consisted of 4.5 tons of hand sorted ore. The next shipment in 1911 to the East Helena smelter was 16 tons of ore. From 1919 to 1920, William Zosell produced some ore from the first and second levels. In 1924, the mine was leased to the Bonanza Mining Company and the shaft was sunk to the fourth level. Considerable drifting was done from this level but an inflow of water hampered the operation. The mine was reopened from 1936 to 1937 by W. Oliphant and T. Boatman and gold ore was mined from the top levels in the oxidized zone. Operations were taken over by the Bonanza Leasing Co. in 1938 and continued until 1950. During this time the shaft was sunk to the eighth level. Total value for shipped ore from 1938 to 1950 was over $125,000.

The Bonanza vein is the southern end of the north-south striking vein that extends across the district from the Argus and Hidden Hand Mines (fig. 2). Robertson (1953) described the vein as a bedding plane fissure striking N 30 W and dipping 10° to 25° NE, The width of the vein ranged from 3 ft. to 20 ft. and consisted of quartz veins with sulfides. Mineralogy of the vein is quartz, ankerite and rhodochrosite with arsenopyrite, pyrite, sphalerite, galena, chalcopyrite, and tetrahedrite. These minerals can be found on the dump in vein sections consisting of quartz veins with bands of disseminated sulfides.

In 1986, Freeport-McMoran and Exxon Corporation, in a joint venture, explored a potential disseminated gold resource on the hill east of the mine. The exploration effort demonstrated the potential for a shallow gold resource of 50,000 oz. By 1989, the exploration program was terminated because the resource was too small to be profitable (Montana Bureau of Mines and Geology archives).

From STOP 5 continue south about 0.1 mile to intersection.

10.9   Turn right and proceed south 0.2 mile on Emery road to 4-way intersection.

11.1 ☐STOP 6☐ Emery Vein (46.377342 N, 112.572070 W).

Northeast striking fault cutting off east end of Emery vein. Beyond the locked gate are three inclined shafts that develop the Emery vein. The shafts are currently owned by Montana Precision Mining and their dumps were investigated in 2014 for potential gold and silver ore. We cannot go beyond the locked gate without permission from Montana Precision Mining.

At the road intersection, a northeast striking fault mapped by Derkey (1986) extends southwest from the Bonanza vein to the Emery mill in Rocker Gulch (fig. 2). Rocker Gulch follows the strike of the fault. The northeast striking fault appears to have displaced the south end of the Bonanza vein and cuts off the east end of the Emery vein in the road intersection. Robertson (1953) suggested that post- mineralization, northeast striking faults produced minor displacement of the veins. Fault movement was most likely normal to the bedding with the south side of the fault up thrown. A number of prospect pits and trenches were excavated in the area searching for the extension of the Emery vein north of the fault.

The elongated hill or ridge hosting the Emery vein is known as Carbonate Hill. The Emery vein was discovered in 1888 by John Renault at a site past the locked gate. The first inclined shaft was sunk on the vein in the same year the vein was discovered. The Emery vein strikes along the top of Carbonate Hill near the southern edge of the crest. The dip of the Emery vein varies from 15° to 45° and averages 30° northwest (Robertson, 1953). Its width varies from a few inches to 2 ft. and averages several inches. Pardee and Schrader (1933) describe the vein as a persistent tabular body with a banded structure of sulfides, quartz, and carbonates. Mineralogy is characterized by quartz and ankerite with arsenopyrite, pyrite, sphalerite, galena, chalcopyrite, tetrahedrite, boulangerite, and chalcopyrite forming massive bands and disseminated grains.

From STOP 6, proceed west 0.6 mile along the Emery road, following Rocker Gulch. Drive past the Emery mine and mill (visible on south side of road) and park below the mine.

11.7 STOP 7 Emery Mine and mill (46.374620 N, 112.580560 W).

The mill is visible on the south side of Rocker Gulch. The main inclined shafts are located on Carbonate Hill above the mill site. The workings of the Emery Mine (fig. 5) consisted of three inclined shafts, a 500 ft vertical shaft, and 7,000 ft. of drifts, crosscuts, levels, and stopes (Pardee and Schrader, 1933). The vertical shaft was sunk in 1907 by the Deer Lodge Consolidated Mines Company to gain better access to the underground workings (Derkey, 1986).

The Emery vein was discovered in 1888 by John Renault and was staked by W. C. Emery. It was the largest producer in the district (Robertson, 1953). Emery developed the mine on a decline to 100 ft. and sold the claim to Conrad Kohrs in 1890. Kohrs successfully operated the mine until 1902 and sold the mine to the Emery Mining Company. Operations continued for the next five years producing gold, silver, and lead with a total reported value of $90,000. In 1907, Deer Lodge Consolidated Mines acquired the property and went bankrupt only a year later because of overspending and insufficient production. The property was idle from 1908 to 1910. In 1910 the old Emery Mining Company became the Emery Consolidated Mining Company, and took control of the mine. In 1923, electricity arrived and a 70 ton-per-day flotation mill was constructed. There was little production until 1935 when 12,000 tons of ore were processed. Mining activity was limited from 1936 to 1939 and ore was hand sorted for shipment. John B. White constructed a 100 ton-per-day flotation mill in 1945 which was run by the Deer Lodge Mining Company for 3 to 4 years. During a two year period, 8,968 tons of ore were processed. By 1950, the Emery Mine was closed because of high labor and material costs.

Derkey (1986) reported renewed activity at the Emery Mine in the late 1980's when the Emery Mining Association (renamed Montana Precision Mining Company) constructed a 200 ton-per-day mill at the vertical shaft. A test at the mill, using ore from the Emery Mine, produced approximately 100 tons of concentrate which was shipped to the East Helena smelter. After the test run, the mill closed for economic reasons.

On the south side of the road are the extensive dumps of the Blue Eye Maggie Mine. Like the Emery Mine, Robertson (1953) reports the Blue Eye Maggie produced gold, silver, and lead from a vein averaging 5 to 7 inches wide. The mine was developed by a 170 ft. long, 8° to 10° incline shaft with drifts extending 250 ft. east and 50 ft. west. The inclined shaft had four levels and a winze. Ore grades were 1 to 1.5 oz/t gold, 42 to 63 oz/t silver, 2 to 6% lead. Zinc occurred from trace to 6 percent.

Cutting across the road to the southwest of the Emery Mine and northeast of the Blue Eye Maggie Mine is the Black Rock fault (fig. 2). This fault strikes northwest and is steeply dipping. The Black Rock fault cuts off the Emery vein at its southern end and cuts the Blue Eye Maggie vein at its northern end. The fault has a strike-slip displacement up to 1,000 ft. with right lateral movement. Based on the right lateral movement, Robertson (1953) suggests that the Blue Eye Maggie vein is a displaced extension of the Emery Vein. Confirmation of Robertson's assessment is that the thickness and mineralogy of the Blue Eye Maggie vein is the same as that of the Emery vein.

End of Road Log (Continue west on Emery Road, back to Deer Lodge).

ACKNOWLEDGMENTS

REFERENCES

Al-Khirbash, S., 1982, Geology and mineral deposits of the Emery Mining District, Powell County, Montana: University of Montana, M.S. thesis, 60 p.

Derkey, R.E., 1986, The Emery mining district, Powell County, Montana: Montana Bureau of Mines and Geology Bulletin 124, p. 31-42. (geologic map of district at1:24,000 scale).

Field, C.W., Zhang, L., Dilles, J.H., Rye, R.O., and Reed, M.H., 2005, Sulfur and oxygen isotopic record in sulfate and sulfide minerals of early, deep, pre-main stage porphyry Cu-Mo and late

main stage base-metal mineral deposits, Butte district, Montana: Chemical Geology, volume 215, p. 61-93.

Houston, R.A., and Dilles, J.H., 2013, Structural geologic evolution of the Butte District, Montana: Economic Geology, volume 108, p.1397-1424.

Lyons, T.W., Luepke, J.J., Schreiber, M.E., and Zieg, G.A., 2000, Sulfur geochemical constraints on Mesoproterozoic restricted marine deposition: lower Belt Supergroup, northwestern United States: Geochimica et Cosmochimica Acta, volume 64, number 3, p. 427-437.

Pardee, J.T., and Schrader, 1933, Metalliferous deposits of the greater Helena mining region, Montana: U.S. Geological Survey Bulletin 842, 318 p.

Robertson, F., 1953, Geology and mineral deposits of the Zosell (Emery) Mining District, Powell County, Montana: Montana Bureau of Mines and Geology Memoir 34, 29 p.

Incorporated Under the Laws of the State of Washington

No. 96

50000 Shares

Ophir Gold and Copper Mining Co.

Non-Assessable | Capital Stock, $100,000 | 1,000,000 Shares | 300,000 Shares In Treasury

MINES LOCATED IN POWELL COUNTY, MONTANA

This Certifies that _____ is the owner of

_____ Shares of the Capital Stock of

OPHIR GOLD AND COPPER MINING COMPANY

transferable only on the books of the Corporation by the holder hereof in person or by Attorney, upon surrender of this Certificate properly endorsed.

In Witness Whereof, the said Corporation has caused this Certificate to be signed by its duly authorized officers and to be sealed with the Seal of the Corporation at Spokane, Washington, this _____ day of _____ A.D. 19____

Secretary

SHARES
10c
EACH

President

FIELD GUIDE TO THE GEOLOGY AND PALEONTOLOGY OF THE CABBAGE PATCH BEDS IN THE FLINT CREEK BASIN (RENOVA FORMATION, ARIKAREEAN)

Jonathan J. Calede[1,2] and Donald L. Rasmussen[3]

[1]University of Washington Department of Biology, 24 Kincaid Hall, Box 351800, Seattle, Washington 98195, USA, caledj@uw.edu; [2]Burke Museum of Natural History and Culture, Seattle, Washington 98105; [3]Plateau Exploration, Inc., 1450 Kay St., Longmont, CO 80501, plateau.expl@comcast.net

ABSTRACT

The Arikareean-aged Cabbage Patch beds were first described in the Flint Creek basin near Drummond and later traced to other nearby basins west of the Continental Divide in Montana. Within the beds, locally abundant invertebrate and vertebrate fossils are found mainly in fine-grained fluvial overbank, paludal (swamp), lacustrine, and lacustrine delta fill deposits; logs, branches, and other large pieces of wood are found in fluvial channel deposits; leaves, seeds, wood, fusain, and other plant fragments are common in paludal deposits; and root traces and burrows are very common in all fluvial and paludal deposits and some lacustrine deposits. In the Flint Creek basin, the Cabbage Patch strata are bounded by unconformities and have been subdivided into three biostratigraphic intervals using diagnostic mammalian and molluscan fossil assemblages. The lithostratigraphy and fossil assemblages indicate climatic conditions with mild winters and alternating humid and semiarid seasons. The beds host a diverse fossil fauna including mollusks, amphibians, and mammals. The mammalian fauna, in particular, has been studied for its potential to inform the age of the beds and their similarity with coeval faunas of the Great Plains and Oregon. During this field trip we examine select outcrops of the Cabbage Patch beds from the Flint Creek basin to introduce the rich molluscan and vertebrate fossil record of the Cabbage Patch beds and their depositional and paleoenvironmental context.

GENERALIZED GEOLOGY OF THE CABBAGE PATCH BEDS

The geological discussions below are summarized and updated from Pierce and Rasmussen (1992) and Rasmussen and Prothero (2003). Arikareean-aged strata mapped west of the Continental Divide in western Montana collectively called the Cabbage Patch beds (Konizeski and Donohoe 1958) are known from nu-merous contiguous and isolated outcrops of tuffaceous strata in the Blackfoot, Douglas Creek, Flint Creek, Deer Lodge, and Divide intermontane basins (fig. 1; Douglass, 1899, 1901, 1903, 1909; Konizeski, 1957, 1965; Gwinn, 1960, 1961; Rasmussen, 1969, 1973, 1977, 1989, 2003; Rich and Rasmussen, 1973; Rasmussen and Fields, 1980; Loen, 1986; McLeod, 1987; Pierce and Rasmussen, 1989, 1992; Pierce, 1992; Sears and others, 2000; Rasmussen, 2003; Rasmussen and Prothero, 2003: Vuke, 2004; Portner, 2005; Portner and Hendrix, 2005; McCune, 2008; McCune and Hendrix, 2009; Portner and others, 2011). The Cabbage Patch beds are time equivalent and similar in lithology and paleontology to strata assigned to the upper Renova Formation of the Bozeman Group in the intermontane basins east of the present Continental Divide in western Montana (fig. 2; Kuenzi and Fields, 1971; Fields and others, 1985; Rasmussen, 2003), and correspond to the "Sequence 3" (i.e. the upper part of the lower sequence for the Divide basin in fig. 2) of Hanneman and Wideman (1991, 2006) and Hanneman and others (2003).

Cabbage Patch strata in western Montana may be tilted, folded, faulted, and deeply eroded. They unconformably onlap an irregular topography of Precambrian to Mesozoic strata and, locally, onlap erosional remnants of older Cenozoic (Eocene and Oligocene) sedimentary deposits and volcanics (including the Eocene-aged Lowland Creek volcanics and a rhyolitic welded tuff in the Flint Creek basin). An angular unconformity ("middle Tertiary uncon-formity") is present between the Arikareean Cabbage Patch strata and the overlying Miocene (Barstovian) Flint Creek and Barnes Creek beds in the Flint Creek basin (Rasmussen, 1973, 1977, 1989; Rasmussen and Prothero, 2003). This "middle Tertiary unconformity" is recognized elsewhere in western Montana and has been dated to approximately 17 Ma at nearby outcrops (Robinson, 1960, 1963, 1967; Kuenzi, 1966; Kuenzi and Richard, 1969; Kuenzi and Fields, 1971; Petke-
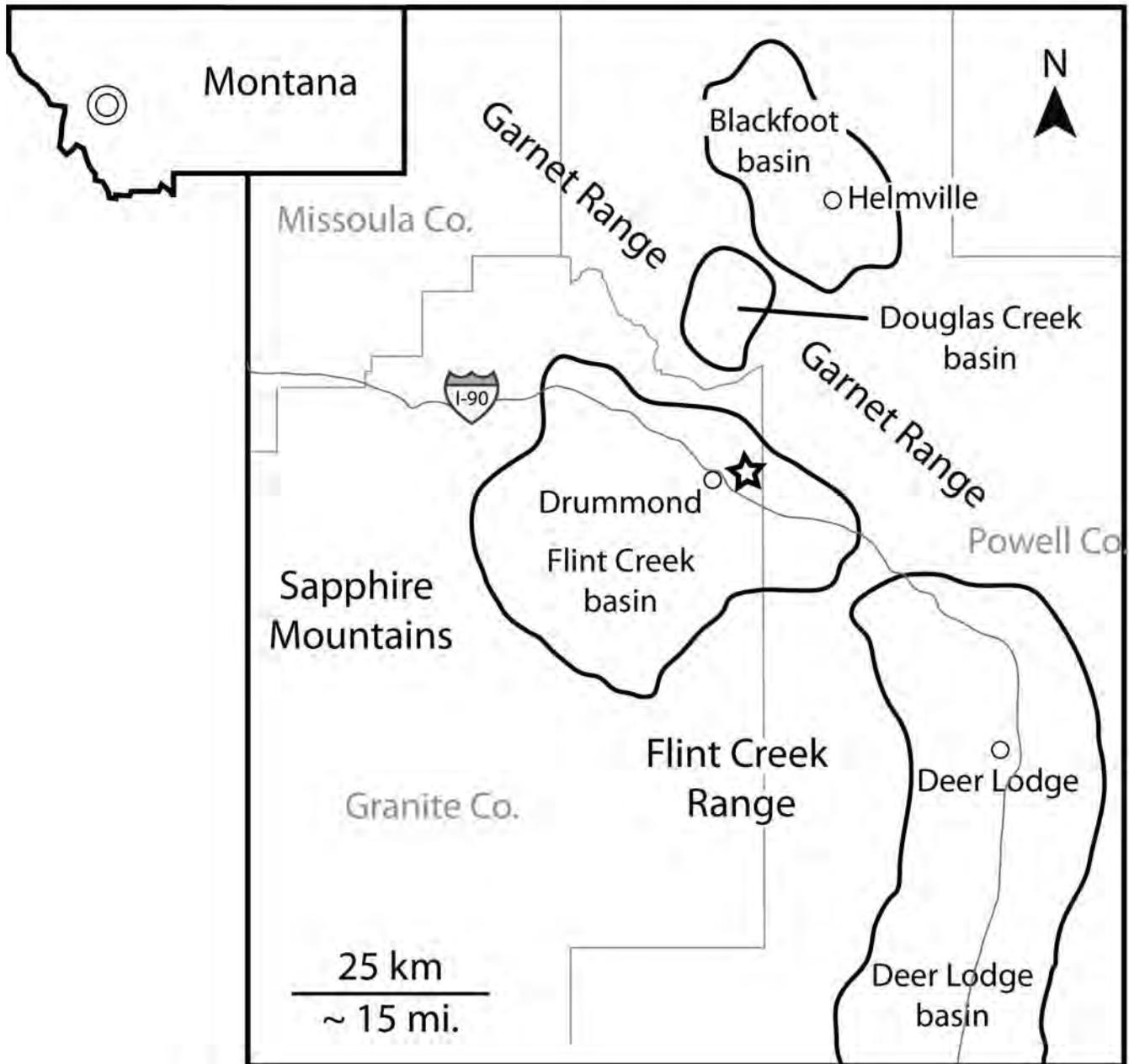
Figure 1. Regional context of the localities detailed in this guide. The circle on the map of Montana in the upper left corner denotes the location of the main section of the figure. The star shows the location of the details of figure 4. The fossiliferous Divide basin is not shown but lies directly south of the Deer Lodge basin.
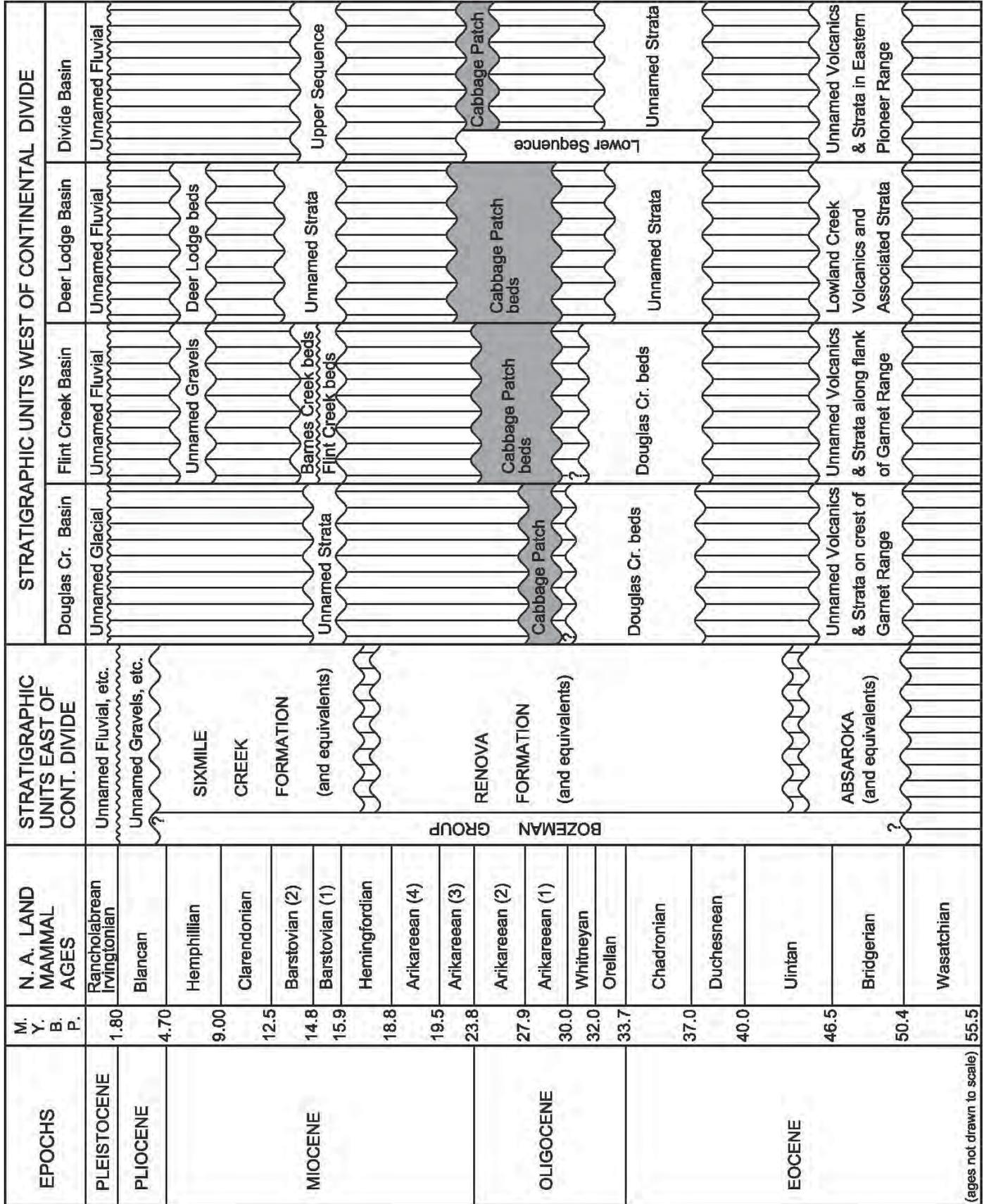
Figure 2. Distribution, stratigraphic position, and time relationship of the Cabbage Patch beds in four Cenozoic basins of central-western Montana (updated and modified from Rasmussen and Prothero, 2003). The age of the Douglas Creek beds is from Miller (1980).

wich, 1972; Monroe, 1976; Fields and others, 1985; Barnosky and Labar, 1989; Burbank and Barnosky, 1990; Fritz and Sears, 1993; Sears and Fritz, 1998; Sears and Ryan, 2003; Sears, 2010, 2013).

Unnamed late Cenozoic and Quaternary strata unconformably onlap the Cabbage Patch strata in parts of the Blackfoot, Douglas Creek, Deer Lodge, and Divide basins (in fig. 2 the overlying Cenozoic strata are equivalent to the Sixmile Creek Formation east of the Continental Divide). The upper contact of the Cabbage Patch strata is strictly erosional and, at good exposures, there does not appear to be significant weathering (with pedogenic clays) or an equivalent to the calcic paleosol reported at the upper boundary of "Sequence 3" east of the Continental Divide by Hanneman and Wideman (1991, 2006). Portner (2005) noted that "neither, a kaolinite group mineral [nor] a red lateritic horizon is observed below the mid-Miocene unconformity of the [Flint Creek basin]." In a stream bank southeast of the town of New Chicago, barite nodules from within a thin zone below the "middle Tertiary unconformity" (between the Barstovian Flint Creek beds and the Arikareean Cabbage Patch beds) mark the only known location of an unconformity paleosol in the Flint Creek basin (pointed out to Don Rasmussen by Ryan Portner in June 2003). All other contacts observed along the unconformity are sharp, as a consequence of erosion, and without paleosols; however, gravels (conglomerates) are not always present at the base of the overlying Flint Creek beds.

The Cabbage Patch strata are dominated by fresh volcaniclastics and montmorillonitic mudstones. These tuffaceous strata are usually poorly bedded because of deposition and re-working in fluvial environments and the subsequent intense bioturbation by plants and invertebrates. Lacustrine, lacustrine delta fill, and paludal deposits are well-bedded, contain thin ash beds, and locally may be highly fossiliferous with plants (Table 1), invertebrates (Table 1), and vertebrates (Table 2, see below). Conglomerates, arkose, and other coarse clastics are locally derived and occur as scattered lenses throughout the entire Cabbage Patch stratigraphic sequence; none appear to mark boundaries for finer parasequences.

Lacustrine strata in the Flint Creek basin and northern Deer Lodge basin (Gold Creek area) extend to the erosional limits of the Cabbage Patch strata in these areas, suggesting that some of the lakes in which the strata were deposited were large in size within the basin of deposition. However, the absence of even a single thick continuous section of lacustrine strata suggests that the lakes were ephemeral, perhaps lasting only a few thousand years at best. Lacustrine intervals within the Cabbage Patch strata are thin compared to fluvial intervals, and the oldest lacustrine strata recognized in the Flint Creek basin occur well above the base of the Cabbage Patch strata (fig. 3). Some lacustrine intervals can be traced for several kilometers, but individual beds within the intervals usually cannot be traced beyond a few hundred meters. From the aquatic mollusks and associated aquatic fauna and flora, Pierce (1993) concluded that the lakes were "shallow, sub-permanent to permanent (several thousand years maximum), [perhaps] soft bottomed and well vegetated, and experiencing seasonal desiccations". Studies of the Cabbage Patch strata indicate that streams were mostly aggrading, lakes were shallow and ephemeral, and swamps were very local with abundant plant material and occasional peat deposits (evidenced by lignites). Plant growth in some cases was coeval with deposition, leaving traces of their roots and debris, but in many cases subsequent intense growth of roots was through the sediment and soil after deposition and prior to lithification. Bedded gypsum and gypsum cement in lacustrine strata in the upper part of the Cabbage Patch beds indicate periods of dryness and the presence of playa lakes. Some Arikareean lakes in southwest Montana became saline enough to support marine foraminifera (Van Niewuwenhuise and He, 1986) that could have been brought to Montana by birds (a method suggested by Patterson and others, 1997).

Lateral and vertical variations in physical, chemical, and paleontological characters occur throughout the Cabbage Patch strata. Lateral changes indicate deposition was contemporaneous in different environments, and changes in an upward direction indicate that environments, at any given place, changed through time (Rasmussen, 1969, 1977, 1989; Rasmussen and Prothero, 2003). Physical, chemical, and paleontological characters of the lithological units from measured stratigraphic sections provide evidence for six basic types of depositional environments: fluvial channel, fluvial overbank, lacustrine, lacustrine delta fill, paludal, and aeolian (Rasmussen, 1969, 1977, 1989). Aeolian strata are composed of undisturbed

Table 1. Distribution of plants and invertebrates throughout the Cabbage Patch beds (modified and updated from Rasmussen and Prothero 2003). Abbreviations: L = lower, M = middle, U= upper.

Plants			L	M	U
Diatomophyceae (diatoms)	Centrales	*?Melosira*			X
	Pennales	several indet. forms	X	X	X
Algae (charophytes)	Characeae	several indet. Forms	X	X	X
Gymnospermae	Pinaceae	*Pinus* (pine)	X	X	X
	Taxodiaceae	*Sequoia* (redwood)	X	X	X
Angiospermae	Typhaceae	*Typha* (cattail)	X	X	X
	Fragaceae	*Quercus* (oak)	X	X	X
Invertebrates			L	M	U
Demospongea (fresh water sponges)	Monaxonida	Spongillidae indet.	X	X	X
Gastropoda (aquatic and terrestrial)	Oreohelicidae	*Oreohelix*	X	X	X
	Helminthoglyptidae	*?Monadenia*			X
	Valvatidae	*Valvata*	X	X	
	Viviparidae	*Viviparus*		X	
	Lymnaeidae	*Lymnaea*	X	X	X
	Planorbidae	*Planorbula*	X	X	
		Biomphalaria	X	X	X
	Pupillidae	*Gastrocopta*	X	X	X
		Vertigo	X	X	X
		Pupoides	X		X
		Columella			X
	Succineidae	*?Catinella*	X		X
	Valloniidae	*Vallonia*	X	X	X
	Zonitidae	*Nesovitrea*	X		
	Limacidae	*Deroceras* (slug)	X	X	X
	Punctidae	*Punctum*	X		
	Ammonitellidae	*Polygyroidea*	X	X	X
Pelecypoda (pelecypods)	Sphaeriidae	*Sphaerium* (pea clam)		X	
Crustacea (ostracodes)	Cyprididae	*Cypris*	X	X	
		Cyprinotus	X	X	X
		Candona	X	X	X
	Cyclosyprididae	*Cyclocypris*			X
		Cypria			X
	Ilyocyprididae	*Ilyocypris*	X	X	X

Table 2. Distribution of non-mammalian vertebrates throughout the Cabbage Patch beds (modified and updated from Rasmussen and Prothero 2003). Abbreviations: L = lower, M = middle, U= upper.

Non-mammalian vertebrates			L	M	U
Actinopterygii	Amiiformes	*Amia* (bowfin)	X	X	X
	Cypriniformes	*Gila* (minnow)	X	X	X
		Amyzon (sucker)	X	X	X
	Perciformes	*Lepomis* (sunfish)	X	X	X
		Sciaenidae gen. sp. indet. (drum)	X	X	X
Lissamphibia	Anura	?*Ascaphus* (tailed frog)	X	X	X
		?*Scaphiopus* (pelobatid toad)	X	X	X
		Tephrodytes (pelobatid toad)	X	X	X
		gen. sp. indet. (large frog)	X	X	X
	Caudata	*Taricha* (*Palaeotaricha*) (newt)		X	
		Plethodon (woodland salamander)		X	
		Aneides (climbing salamander)		X	
Reptilia	Chelonia	*Testudo* (tortoise)	X	X	X
		gen. sp. indet. (pond turtle)			X
Aves	Galliformes	*Palaeonossax* (cracid)		X	
	Charadriformes	gen. sp. indet. (large dowitcher)		X	
		gen. sp. indet. (sandpiper)	X		

ash falls. From the measured sections, Cabbage Patch strata are predominantly fluvio-lacustrine in origin with fluvial strata four-to-five times as abundant as lacustrine strata; whereas paludal and aeolian strata only account for approximately three percent of the total Cabbage Patch strata (Rasmussen, 1977). Lacustrine strata were mainly deposited in an area that includes parts of the present Flint Creek basin and northern Deer Lodge basin. They are unknown (either absent or eroded away) in the Divide, Douglas Creek, and Blackfoot basins.

The volume of overbank deposits in the Cabbage Patch beds in the Flint Creek basin is five times greater than that of channel deposits (Rasmussen, 1977). This suggests a high-suspended load capacity for the streams flowing into and through the basin of deposition. Poor sorting of the channel and overbank sediments indicates low-energy environments. Thus, the streams (rivers) flowing into and through the basin of deposition were likely small-to-medium in size, low in velocity, shallow, and mostly aggrading. Abandonment of channels (avulsion) may have occurred whenever the stream overflowed. This situation would account for the limited areal extent of the channels

and the rarity of multi-story channel deposits (a few thick sandstone sequences seen in a measured section in the Blackfoot basin may be considered multi-story; Rasmussen, 1977). Avulsion was also possibly more common during or immediately after periods of extensive aeolian ash fall deposition. Thus, streams that eroded and carried the newly deposited unconsolidated tuffaceous material would have become overloaded. Aggradational processes would have then overcome the streams' ability to maintain their channel. During avulsion, coarse sediments in the channel may not have been moved by the stream but buried at the bottom of the abandoned channel. With each new deposit of tuffaceous material on the floodplain, there was extensive reworking and bioturbation by vegetation and, to a lesser extent, by burrowing invertebrates and vertebrates. Occasionally, there was also the development and preservation of paleosols. With continued deposition, a new stream course would be established to replace the previously abandoned channel though not always in exactly the same position. Eventually each new stream would cut a new channel into the underlying deposits and coarser clastics (arkose and gravels) would once again be moved from the upland areas into the basin of deposition. Shallow lakes and
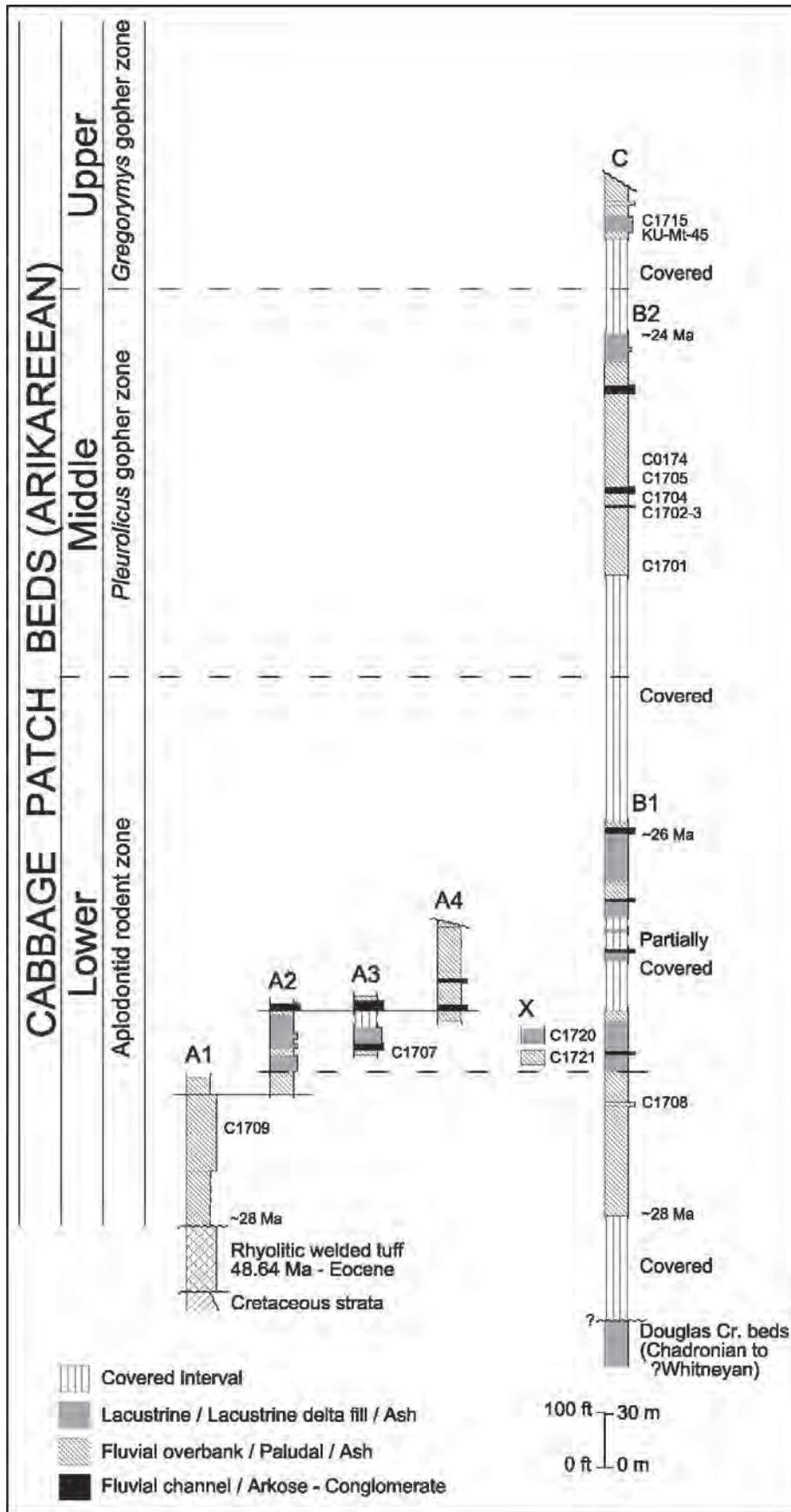
Figure 3. Stratigraphic context of the Cabbage Patch beds. Localities detailed in this guide are placed in the overall stratigraphic section of the Cabbage Patch beds through the northern Flint Creek basin (modified and updated from Rasmussen, 1977; Rasmussen and Prothero, 2003). The date for the rhyolitic welded tuff is from Portner and others (2011). The letters refer to the sections measured by Rasmussen (1977) except X (Calede, unpublished). The exact boundaries between the lower and middle units as well as middle and upper units of the Cabbage Patch beds are not exposed; they are within the covered intervals shown in this figure.

ponds developed on the low deposition plain between previous channels.

Paleosols are common throughout the Cabbage Patch beds. They are most obvious by the preservation of abundant root molds and casts. Though pervasive, the paleosols of the Cabbage Patch strata should not be considered stacked. They are also not dominated by calcite enough to be considered limestones. Rather, those with abundant calcite should be considered calcretes; they do not contain enough silica cement to be considered silcretes, and our observations indicate that they are not related to any unconformity surface (or parasequence boundary) within or at the top of the Cabbage Patch beds. Not to be confused with paleosols are "case-hardened" beds of a few centimeters to a meter in thickness that are sometimes found in groups of several meters in thickness in exposures of the Cabbage Patch strata in the Flint Creek basin. These case-hardened beds are common on sun-facing exposures where seasonal and storm-related wetting and drying has altered specific components of the beds. These case-hardened beds extend back into the outcrop for as little as a few centimeters but as much as a meter. They are usually composed of fine-grained silty and sandy strata, highly cemented with opal and/or chalcedony and calcite. The unaltered strata behind the hardened beds contain abundant glass shards, marl, and sometimes fossil shell debris. Several years of alternating wetting and drying of these strata have mobilized the silica from the glass shards and the calcite from the marl or shell debris to cement the stratum into something that appears much like a hard cherty or opalized limestone bed at first glance. Fossils that are common in the unaltered stratum are absent or highly replaced in the case-hardened stratum. They are sometimes only represented by hollow molds. Where numerous beds occur in the same exposure, they can be easily misidentified as a stacked sequence of lacustrine limestones or terrestrial paleosols despite different original environments of deposition.

The silt- to sand-sized glass shards of the Arikareean-aged Cabbage Patch beds are fresh. In the absence of vertebrate fossils, they can be used to differentiate isolated outcrops of Arikareean strata from nearby, similar-looking, older Cenozoic strata that contain only devitrified glass shards. Volcanic sources for this large amount of volcaniclastic debris have not been individually identified, but most material perhaps came from volcanoes far to the west (ancestral Cascade Mountains: Larson and Evanoff, 1998; Rasmussen, 2003) or the contemporaneous large calderas in the northern Great Basin, with less material from more local sources, such as Crater Mountain (Melson, 1971) and Helena Field areas (Chadwick, 1972, 1978, 1981, 1985). A rhyolitic welded tuff at the base of Cabbage Patch strata east of Drummond (fig. 3) is perhaps equivalent to the same welded tuff exposures directly across the Clark Fork River reported by Portner and others (2011), with a date of 46.64 Ma (Bridgerian, Eocene, see fig. 2). The welded tuff in figure 3 is no longer thought to be Arikareean in age (Rasmussen, 1977), an age based on a zircon fission track date. Strata just above the rhyolitic welded tuff once considered as lahar deposits are now thought to be a local channel deposit with cobbles of volcanic rocks.

The arkose found in channel sandstones was definitely derived from nearby Cretaceous batholiths. There is a clear decrease in pebbles and pebble size in the conglomerates to the west and northwest as seen in the northern Flint Creek basin and in the Blackfoot basin near Helmville. This indicates that streams flowed west and/or northwest from the Boulder and Philipsburg batholiths into the area of Cabbage Patch deposition, including the present Deer Lodge, Flint Creek, Douglas Creek, and Blackfoot basins. Portner (2005) pointed out that arkoses in the Cabbage Patch beds on the north flank of the Flint Creek range have two micas indicating a source in the erosion of the Cretaceous Philipsburg batholith (that has rock with muscovite and biotite). The outlet of the basin of deposition is still unknown, but was perhaps northward through the southern Rocky Mountain Trench in northwest Montana and eventually into a tributary of the ancestral Columbia River system or into a drainage system leading to Hudson Bay and the Labrador Sea in eastern Canada (see Seeland, 1985; Rasmussen and Prothero, 2003; Sears, 2013). There also might not have been an outlet as suggested by Pierce (1993) who concluded, from his analysis of western Montana fossil aquatic mollusks, that "western Montana had not been part of an integrated system of through-flowing rivers for some period of time prior to the deposition of the Cabbage Patch strata and, although local permanent water may have existed, these [basins must have been part of a basin of interior drainage]" (Pierce, 1993:988).

The diverse assemblages of fossils from the Cabbage Patch beds (Tables 1, 2, see below) are the result of mixing and transportation; however, few remains were moved very far (except perhaps for the plant material). Mollusks are usually broken and fragmentary, but locally abundant complete shells are very well preserved, evidence of little transportation (Pierce, 1992, 1993; Pierce and Rasmussen, 1992). Indeed, at a few localities, gastropods, including many complete shells, can be easily washed from weathered or poorly consolidated tuffaceous matrix. In some intervals, gastropod shells have sediment plugs in their apertures and the empty upper whorls point upward in the sedimentary matrix. Often, these sediment-free whorls contain loosely packed juvenile gastropods, ostracods, charophytes, diatoms and other fossil debris. Ostracods and other microfossils are abundant in the lacustrine strata, and have yet to be studied. Vertebrate fossils are usually fragmental and disassociated. Some may have been scavenged or ingested by carnivorous mammals or raptorial birds. Several partial skeletons have been recovered. A complete gopher skeleton was recovered from a mud-filled burrow, undisturbed by predators and insects prior to burial (Rasmussen, 1977, 1989). A partial toad skeleton was also found within what is likely an estivation burrow (Henrici, 1994). Small mammals are the most common vertebrate fossils recovered from the Cabbage Patch strata. In decreasing order of abundance, frogs and salamanders, large mammals, fish, turtles and tortoises, and birds are the other vertebrate fossils recovered from the beds (Rasmussen, 1977, 1989; Rasmussen and Prothero, 2003). The Cabbage Patch beds, with their rich mammalian fossil record placed in a stratigraphic context, offer a unique opportunity to track changes in mammalian biodiversity leading up to the Oligocene-Miocene boundary, the time period of the advent of many modern mammalian families and the decline of more archaic, and now extinct, taxa (Webb and Opdyke, 1995; Tedford and others, 2004; Woodburne, 2004). This period of faunal change was associated with drastic changes in global climate (Zachos and others, 2008) as well as vegetational changes in North America (Strömberg, 2005). The localities visited as part of this field trip are a glimpse into the unique mammalian fauna, as well as the rich molluscan assemblages, of the Cabbage Patch beds, their environment, and depositional setting.

Institutional abbreviations: KUVP, University of

Kansas Vertebrate Paleontology collections, Lawrence, Kansas, USA; UMPC, University of Montana Paleontology Center, Missoula, Montana, USA; UWBM, University of Washington Burke Museum, Seattle, Washington, USA.

Locality abbreviations: KU-Mt-, University of Kansas; UMV-, University of Montana; UWBM C-, University of Washington.

Anatomical abbreviations: c, lower canine; i, lower incisor; p, lower premolar; m, lower molar; P, upper premolar; M, upper molar.

FIELD GUIDE TO THE CABBAGE PATCH BEDS IN THE FLINT CREEK BASIN

The location of the field stops are shown on figure 4. A summary of locality names is provided in table 3.

Original discovery area

STOP 1   UWBM C1709

The Big One (Lower Cabbage Patch beds): [= UMV6203 (Cabbage Patch 1); = KU-Mt-31 (Cabbage Patch 11).] View of outcrop from frontage road along Interstate 90 east of Drummond (figs. 4, 5).

C1709 is the outcrop of the Cabbage Patch beds where fossil vertebrates were first collected. Douglas (1903) reported the presence of "*Mesocyon drummondensis*" (a dog now synonymized with *Cynodesmus thooides*, Wang 1994), "*Leptomeryx transmontanus*" (a deer-like ruminant; now *Pronodens transmontanus*) and an oreodont identified as "*Promerycochoerus minor*" (both *Eporeodon* sp. and *Promerychochoerus superbus* are now identified from this locality). The Oligocene-aged Cabbage Patch beds exposed at C1709 unconformably overlie an Eocene-aged rhyolitic welded tuff dated to 48.64 ±0.17 million years ago based on samples from a nearby outcrop of the same tuff (Portner and others, 2011). The deposits at C1709 are the thickest continuous exposure of lower Cabbage Patch strata exposed in the Flint Creek basin (figs. 3, 5). Over 80 m of mudstones and siltstones preserve the greatest number of large mammals found in a single locality of the Cabbage Patch beds; mostly oreodonts (Riel, 1964; Rasmussen, 1969, 1977). The skull of the largest mammal from the Cabbage Patch beds, the type and only specimen of *Kukusepasutanka*

Table 3. Summary of locality data. Abbreviations: Loc. = locality, # = number.

UWBM Loc. #	Loc. name	UMPC Loc. #	KUVP Loc. #	Biostratigraphic unit
C1715	On Edge	MV6552	KU-Mt-16	Upper
NA	NA	MV6552-1	KU-Mt-45	Upper
C0174	Cabbage 13	MV6547	KU-Mt-46	Middle
C1705	Horse Locality	MV6504-5	KU-Mt-9	Middle
C1704	Strawberry Quarry	MV6504-4	KU-Mt-12	Middle
C1703	Rabbit Locality	MV6504-3	NA	Middle
C1702	Gopher Locality	MV6504-2	NA	Middle
C1701	Rhino Quarry	MV6504-1	NA	Middle
C1707	Grizzly Den	MV6554	KU-Mt-17	Lower
C1721	Hops Garden	MV6621	KU-Mt-70	Lower
C1720	Maze in Creek	MV6620	KU-Mt-69	Lower
C1709	The Big One	MV6203	KU-Mt-31	Lower
C1708	Sharp Claw Butte	MV6558-2	KU-Mt-25	Lower
NA	NA	MV6501	NA	Lower
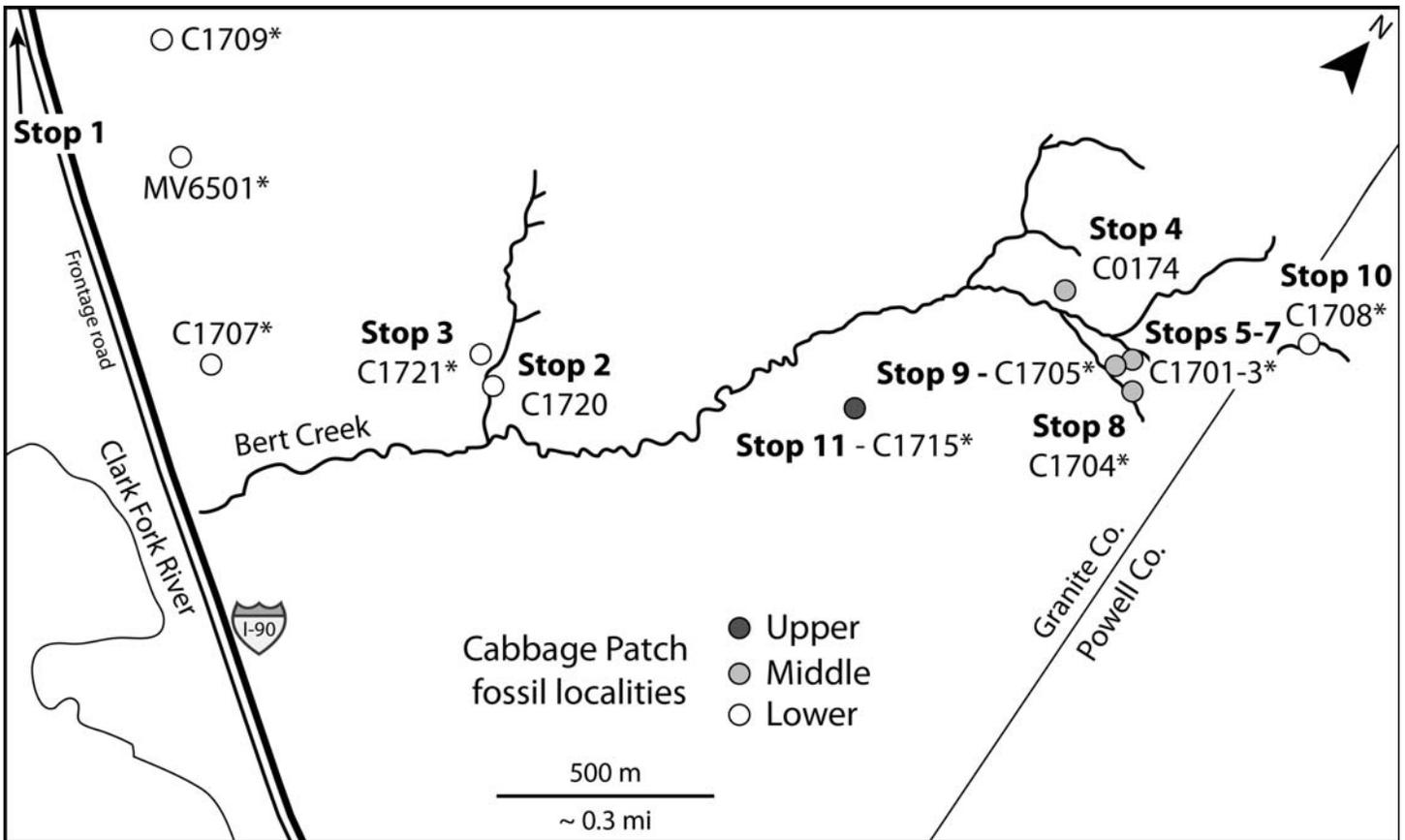
Figure 4. Map of the localities discussed in this paper focusing on the Bert Creek area (Table 1). The location of this area is shown by a star in figure 1. * denotes localities where stratigraphic sections were measured (see fig. 3).

Figure 5. View of the outcrop at C1709 (lower Cabbage Patch beds). These outcrops are almost certainly where Earl Douglass (1903) and others collected vertebrate fossils from the Cabbage Patch beds prior to the late 1950s.

schultzi (Macdonald, 1956), an antracothere (extinct relatives of hippos, Geisler and others, 2007; Lihoreau and Ducrocq, 2007), was also found at C1709. Only two small mammal taxa, both aplodontids, have been found at C1709: a new species of *Downsimus* and a new species of *Niglarodon*.

Bert Creek area

STOP 2 | **UWBM C1720**

Maze in Creek (Lower Cabbage Patch beds): [= UMV6620 (Bert Creek 14), = KU-Mt-69 (Cabbage Patch 14).] Access is by dirt road through two locked gates. Stop is in gulch on west side of Bert Creek (fig. 6).

The deposits at C1720 are a series of interbedded mudstones and siltstones from the lower Cabbage Patch beds, interpreted to represent interbedded lacustrine, lacustrine delta fill, and fluvial overbank depos-

its. They are stratigraphically located above the beds at C1721 and are equivalent to the middle of the section measured by Rasmussen (1977) at C1707 (figs. 3, 6). Note the presence of abundant volcanic glass shards (sparkle in the sun). Silicification occurs in the upper part of the outcrop where the volcanic glass shards in the mudstone matrix have been altered by weathering and the freed silica was re-deposited as opal or chalcedony cement. Fossils found at C1720 include land and freshwater snails, fish bones, frog bones, ostracods, sponge spicules, diatoms, and charophytes (Rasmussen, 1969; Calede, unpublished data).

Only three mammalian taxa have been identified to the species level from C1720 (Table 4), including one new species of *Niglarodon*, two specimens of *Mystipterus*, and an isolated lower molar of a new sicistine rodent better known from the middle Cabbage Patch beds. Both rodent species have also been identified from the underlying beds at C1721.

Table 4. Mammalian fauna from C1720 and C1721.

| Locality	Order	Family	Genus	Species
C1720	Eulipotyphla	Talpidae	*Mystipterus*	sp.
	Rodentia	Aplodontidae	*Niglarodon*	new species B
		Dipodidae	new genus	new species
C1721	Artiodactyla	Leptomerycidae	*Pronodens*	*transmontanus*
		Merycoidodontidae	*Eporeodon*	sp.
	Carnivora	Canidae	*Archaeocyon*	*leptodus*
	Didelphimorphia	Herpetotheriidae	*Herpetotherium*	sp.
	Eulipotyphla	Proscalopidae	*Proscalops*	sp.
		Soricidae	*Domnina*	new species
	Lagomorpha	Leporidae	*Megalagus*	sp.
	Rodentia	Aplodontidae	*Allomys*	cf. *A. cavatus*
			Downsimus	new species
			Niglarodon	new species A
				new species B
			Rudiomys?	new species
		Castoridae	*Agnotocastor*	sp.
			new Anchitheriomyinae	new species A
				new species C
		Cricetidae	*Leidymys*	new species
		Dipodidae	new genus	new species
			Plesiosminthus	species A
		Sciuridae	*Miosciurus*	cf. *M. ballovianus*
			Petauristodon?	sp.
			Sciurion	cf. *S. campestre*

Figure 6. View of the outcrop at C1720 (lower Cabbage Patch beds) with geologist for scale. Light-colored rocks are rich in fresh volcanic glass shards.

STOP 3   UWBM C1721

Hops Garden (Lower Cabbage Patch beds): [= UMV6621 (Bert Creek 15); = KU-Mt-70 (Cabbage Patch 15).] Walk to outcrops further up gulch from C1720 on west side of Bert Creek (fig. 8).

C1721 is a very productive outcrop of the lower Cabbage Patch beds. The main fossiliferous horizon is a ~1.5 m thick unit of moderately sorted massive mudstone with reworked ash lenses that may be as thick as 15 cm (figs. 7, 8). Strata at this site are stratigraphically equivalent to the basal units measured at C1707 (fig. 3: A3). The fossils include isolated and disarticulated fragments and elements dispersed throughout the unit. The overlying aeolian ash is currently being dated using ^{40}Ar/^{39}Ar. The fossils include root traces and plant fragments scattered throughout the unit as well as some molds and debris of land and freshwater snails. Mammal and frog remains, including bones and teeth, are common throughout the unit. No fish have been discovered at this locality yet. This deposit is interpreted as fluvial overbank.
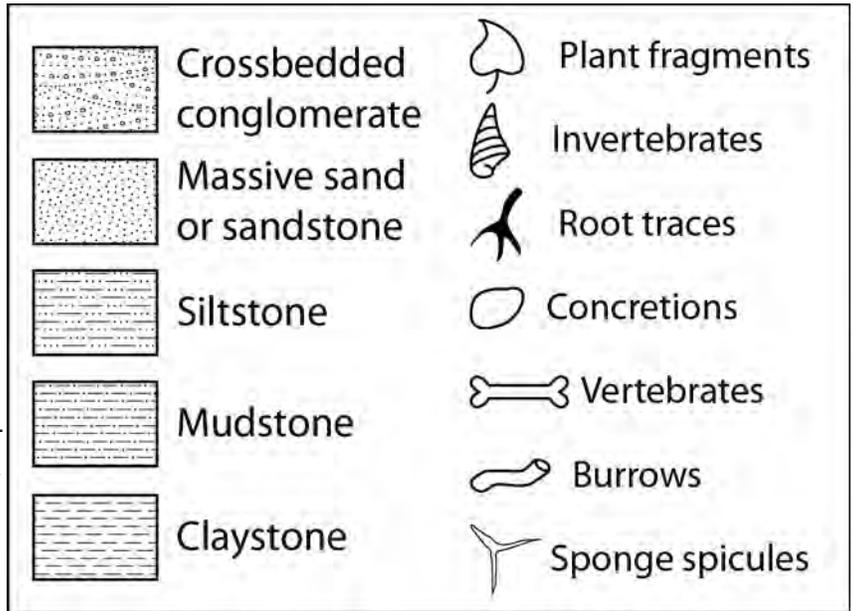
Figure 7. Legend of symbols used in the stratigraphic sections of Cabbage Patch deposits.

The fauna of C1721 includes at least 21 different species of mammals (Table 4, fig. 9). The most abundant taxon by far is the leptomerycid *Pronodens transmontanus*, a small deer-like hornless ruminant. It represents about 15% of the fauna, more than at any other assemblage of the lower Cabbage Patch beds. Aplodontids, relative of the modern sewellel (*Aplodontia rufa*), are also very common in this assemblage. No gopher has been recovered from this outcrop or

Figure 8. Geology of C1721 (lower Cabbage Patch beds). A: View of the outcrop with geologist for scale, B: Stratigraphic section. The approximate location on the outcrop of the lower and upper units are marked with circles.
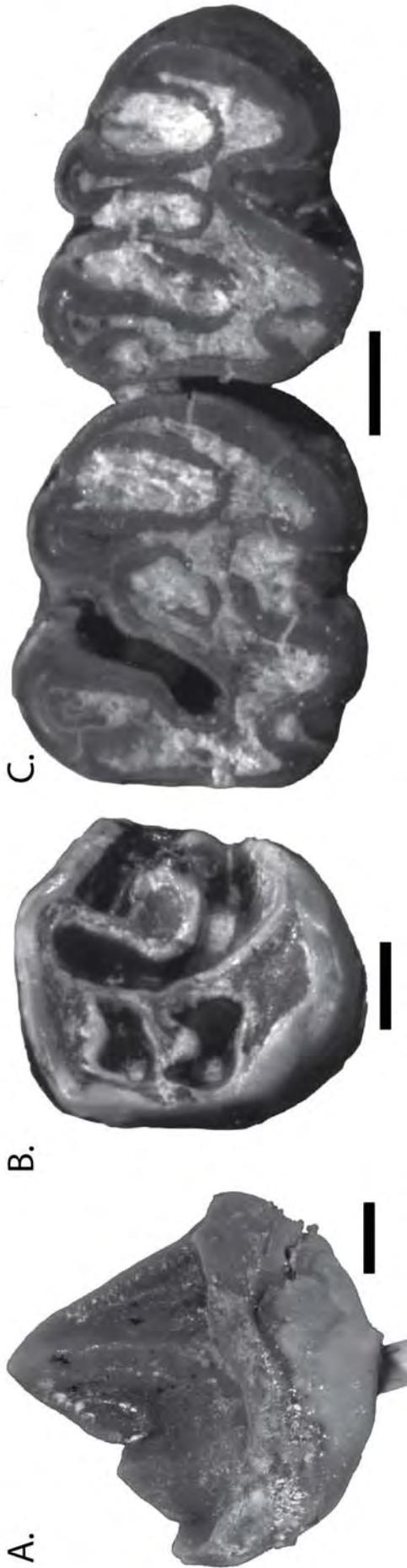
Figure 9. Select mammalian specimens from C1721. A: P3 of *Archaeocyon leptodus* (dog, UWBM 97341), scale equals 1 mm, B: M3 of *Rudiomys?* new species (aplodontid, UWBM 108093), scale equals 0.5 mm, C: m2-3 of *Leidymys* new species (mouse, UWBM 101298), scale equals 0.5 mm.

any other locality of the lower Cabbage Patch beds. The greatest number of sciurid species (squirrels) in the beds is also found at this locality. Along with the presence of shrews (*Domnina*) and proscalopid moles (*Proscalops*), these animals suggest a closed, more forested environment, with the moles indicating soft moist soils. Some rare members of the fauna, like the mixed-feeding oreodont *Eporeodon* and a likely salta-torial sicistine rodent (birch mouse), support a mosaic habitat with some openings in a wooded environment.

STOP 4 | UWBM C0174

Cabbage 13 (Middle Cabbage Patch beds): [= UMV6547 (Bert Creek 3); = KU-Mt-46 (Cabbage Patch 13).] Stop is on north side of east tributary of Bert Creek northwest of the ruins of a long hog shed along creek (fig.10). Depending on road conditions, access to other stops might be by hiking (total less than 1 mile, 1.6 km).

Cabbage 13 is a locality of the upper part of the middle Cabbage Patch beds. The unit is a 14 m thick massive silty mudstone (fig. 10). Mammalian remains, including teeth and partial bones, are isolated and scattered throughout the outcrop but most abundant in the middle of the unit. The largest specimen recovered from the locality is an in-situ *Diceratherium radt-kei* dentary (fig. 10; Konizeski and Donohoe, 1958; Prothero and Rasmussen, 2008). No fish have been recovered from this horizon but invertebrates are very abundant. Freshwater snails (including *Valvata paula*, *Viviparus nanus*, *Planorbula powelli*, *Biomphalaria haydeni*, *Lymnaea vetusta*, and *Lymnaea tumere*) are the most abundant macrofossils in the horizon where complete shells are very commonly recovered in addi-tion to molds and debris (Pierce, 1993). This locality is the type locality for the freshwater snail *Lymnaea tu-mere* (Pierce, 1993). Land snails, including *Oreohelix brandi* (Pierce, 1992), are also present, though rarer. This biodiversity of freshwater mollusks has been in-terpreted as indicative of the "most permanent aquatic environment [..] studied [in the Cabbage Patch beds]" (Pierce, 1993, brackets denote edits of the original by ourselves). Diatoms are rare but plant fragments and root traces, some very large, are both very abundant. The deposit is interpreted as interbedded ephemeral lacustrine, lacustrine delta fill, and fluvial overbank.

Fourteen different species of mammals are cur-

171
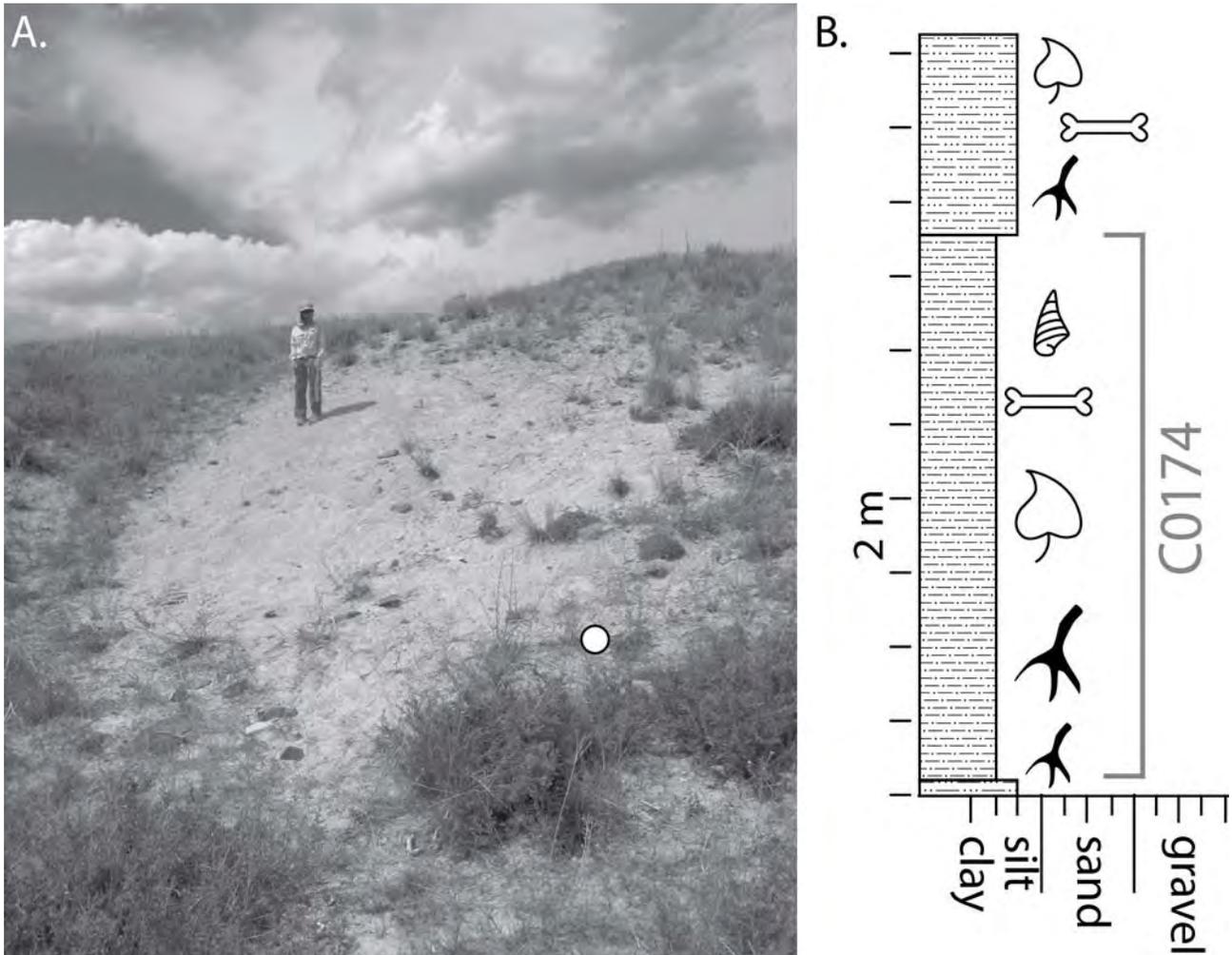
Figure 10. Geology of C0174 (middle Cabbage Patch beds). A: View of the outcrop with student for scale, the circle indicates the location of the Diceratherium lower jaw mentioned in the text, B: Stratigraphic section (modified and updated from Rasmussen, 1977). C0174 is correlated to the main section. The units above and below the fossil producing horizon are measured in the main section.

Table 5. Mammalian fauna from C0174.

Order	Family	Genus	Species
Carnivora	Canidae	genus indet.	species indet.
Didelphimorphia	Herpetotheriidae	*Herpetotherium*	species B
Eulipotyphla	Erinaceidae	*Stenoechinus*	*tantalus*
Lagomorpha	Leporidae	*Archaeolagus*	species indet. B
Perissodactyla	Equidae	*Miohippus*	sp.
	Rhinocerotidae	*Diceratherium*	*radtkei*
Rodentia	Aplodontidae	*Meniscomys*	new species A
	Castoridae	new Anchitheriomyinae	sp.
		Neatocastor	cf. *N. hesperus*
	Cricetidae	*Leidymys*	*alicae*
	Dipodidae	new genus	new species
	Geomyidae	*Pleurolicus*	new species C
			new species B
	Sciuridae	*Sciurion*	cf. *S. campestre*
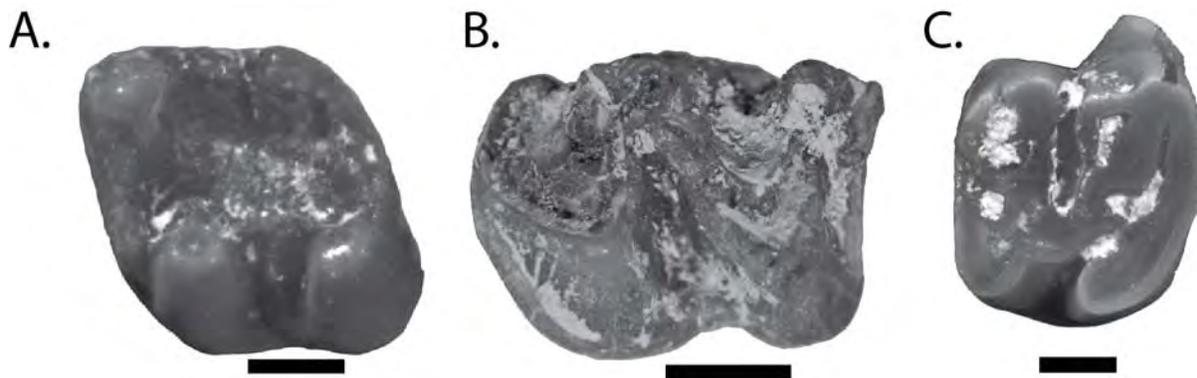
Figure 11. Select mammalian specimens from C0174. A: p4 of Sciurion cf. S. campestre (squirrel, UWBM 98877), scale equals 0.5 mm, B: lower molar of Miohippus sp. (horse, UWBM 98603), scale equals 5 mm, C: M1 of Neatocastor cf. N. hesperus (beaver, UWBM 97507), scale equals 1 mm.

rently recognized in Cabbage 13 from just over 50 specimens (Table 5, fig. 11). The mammalian fauna at C0174 is characteristic of the middle Cabbage Patch beds. In addition to sharing taxa with both the lower and upper Cabbage Patch, Cabbage 13 includes three taxa only found in the middle Cabbage Patch beds: two species of the fossorial entoptychine gopher genus *Pleurolicus*, and the rabbit *Archaeolagus*. These two genera, and others like the horse *Miohippus*, likely reflect a more-open environment in the middle Cabbage Patch beds. Nevertheless, some taxa found at Cabbage 13 but already present in the lower Cabbage Patch beds, such as the squirrel *Sciurion*, suggest that the habitat remained partially wooded.

STOP 5 | UWBM C1701

Rhino Quarry (Middle Cabbage Patch beds): [= UMV6504-1 (Bert Creek 2-1, Rhino Quarry).] Walk to site from parking area or from C0174 (fig. 12).

C1701 is the basal-most fossil locality of the middle Cabbage Patch beds (fig. 3). The 9 m thick mudstone hosts few mammalian fossils, mostly in the top 1.2 m of the horizon (fig. 12). Numerous root traces can be seen in the outcrop as well as invertebrate (likely insect) burrows, diatoms and sponge spicules (Rasmussen, 1977, 1989). Fragments of freshwater snails are rare. No fish or amphibians have been recovered from this outcrop. The locality is interpreted as a mud hole in a fluvial overbank deposit.

Figure 12. Geology of C1701-C1703 (middle Cabbage Patch beds). A: View of the outcrops with field vehicle for scale, B: Stratigraphic section (modified and updated from Rasmussen, 1977). The locations on the outcrop of the units are marked with circles.

Only six fossil specimens identifiable to the species level have been recovered from C1701. Rasmussen (1977) described the discovery of the remains of the type of a large rhinocerotid *Diceratherium radtkei* (described in Prothero and Rasmussen, 2008), the oreodont *Promerycochoerus*, and the oldest occurrence of the gopher *Pleurolicus* in the Cabbage Patch beds (fig. 13C). Two specimens of a new, large species of the aplodontid *Allomys* have recently been collected from this locality (Table 6).

STOP 6 | UWBM C1702

Gopher Locality (Middle Cabbage Patch beds): [= UMV6504-2 (Bert Creek 2-2, Gopher Locality).] Walk up section to site from C1701 (fig. 12).

C1702 is located towards the middle of a 30 m thick series of interbedded mudstones and siltstones (figs. 4, 12; Rasmussen, 1977). This unit includes root traces, rare diatoms, locally abundant land and freshwater snails, and few frog and mammal bones. The deposits of this unit indicate a fluvial overbank environment at C1702 and C1703 (see below).

Fifteen specimens of fossil mammals identifi-

able to the species level have been recovered from C1702. They represent at least eight species (Table 6) including the oldest *Miohippus* (horse) material from Cabbage Patch and the only known specimen of *Parvericius montanus* (hedgehog) from the beds (Rich and Rasmussen, 1973). The mammalian fauna from C1702, including the genera *Miohippus* (horse), *Pleurolicus* (gopher), and *Archaeolagus* (rabbit), suggests an open environment in the lower part of the middle Cabbage Patch beds.

STOP 7 | UWBM C1703

Rabbit Locality (Middle Cabbage Patch beds) [= UMV6504-3 (Bert Creek 2-3, Rabbit Locality).] Walk up section to site from C1702 (fig. 12).

C1703 is located towards the top of the 30 m thick series of interbedded mudstones and siltstones that also hosts the fossils from C1702 (figs. 4, 12; Rasmussen, 1977).

Very few fossil mammal specimens identifiable to the species level have been recovered from C1703 (Table 6). The fossils at C1703 include an exceptional specimen of *Archaeolagus* cf. *A. macrocephalus* (a
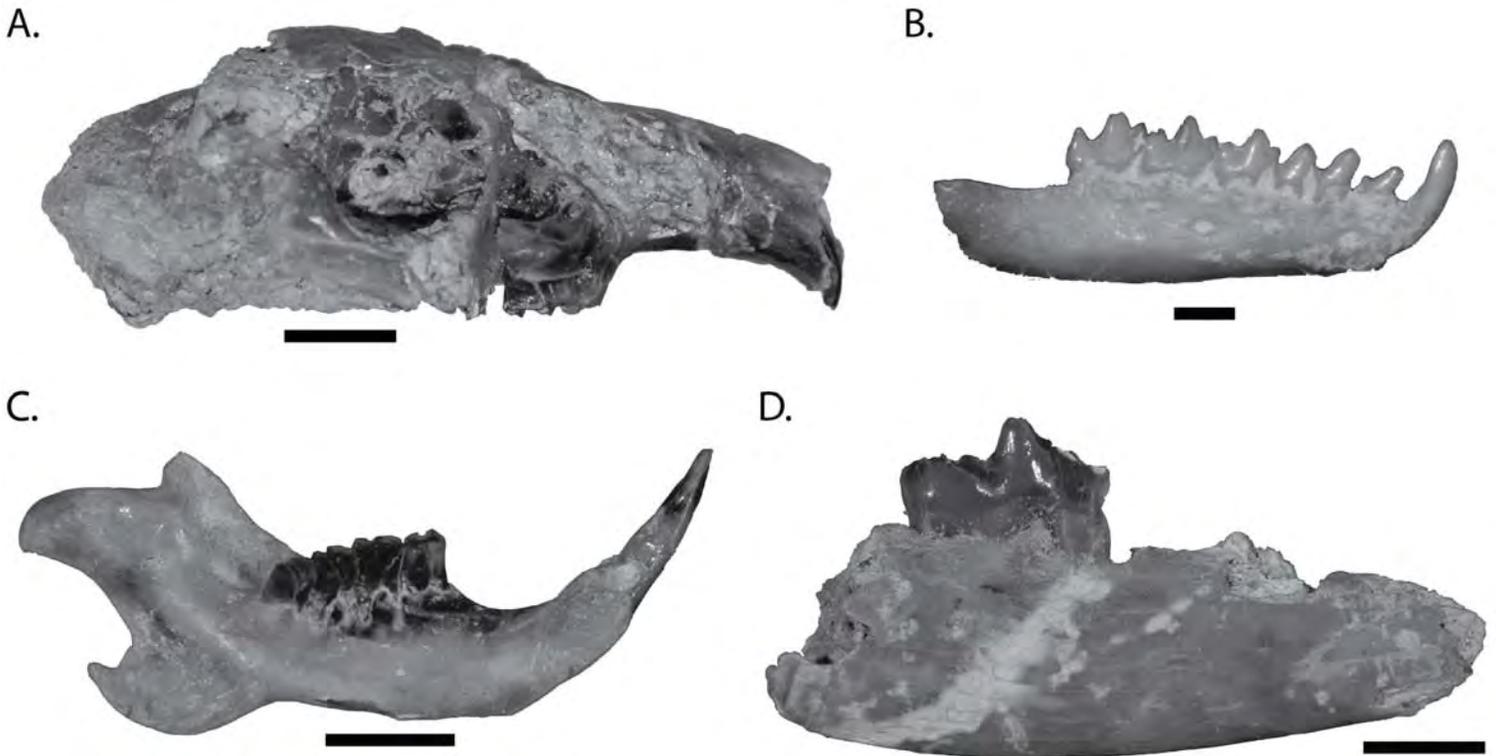

Figure 13. Select mammalian specimens from C1701-1703, C1705. A: partial skull of Archaeolagus cf. A. macrocephalus (rabbit, UMPC 1393) from C1703, scale equals 1 cm, B: partial dentary with c, p1-m3 of Nanodelphys species B (marsupial, KUVP 18164) from C1705, scale equals 1 mm, C: partial dentary with i, p4-m3 of Pleurolicus new species A (gopher, UMPC 2046) from C1701, scale equals 5 mm, D: partial lower jaw and m1 of Archaeocyon leptodus (dog, UMPC 13979) from C1703, scale equals 5 mm.

Table 6. Mammalian fauna from C1701-C1703, C1705.

Locality	Order	Family	Genus	Species
C1701	Artiodactyla	Merycoidodontidae	*Promerycochoerus*	*superbus*
	Perissodactyla	Rhinocerotidae	*Diceratherium*	*radtkei*
	Rodentia	Aplodontidae	*Allomys*	new species
		Geomyidae	*Pleurolicus*	new species A
C1702	Artiodactyla	Merycoidodontidae	genus indet.	species indet.
	Didelphimorphia	Herpetotheriidae	*Herpetotherium*	species B
	Eulipotyphla	Erinaceidae	*Parvericius*	*montanus*
	Lagomorpha	Leporidae	*Archaeolagus*	sp.
	Perissodactyla	Equidae	*Miohippus*	sp.
	Rodentia	Cricetidae	*Leidymys*	new species
		Geomyidae	*Pleurolicus*	new species A
				new species B
C1703	Carnivora	Canidae	*Archaeocyon*	*leptodus*
	Lagomorpha	Leporidae	*Archaeolagus*	cf. *A. macrocephalus*
	Rodentia	Geomyidae	*Pleurolicus*	new species B
C1705	Didelphimorphia	Herpetotheriidae	*Nanodelphys*	species B
	Eulipotyphla	Erinaceidae	*Amphechinus*	*horncloudi*

rabbit) that includes a mostly complete skull, dentaries, and a partial skeleton (fig. 13A). The youngest specimen of *Archaeocyon* (a dog) from the Cabbage Patch beds was also found at C1703 (fig. 13D).

STOP 8   UWBM C1704

Strawberry Quarry (Middle Cabbage Patch beds): [= UMV6504-4 (Bert Creek 2-4, Strawberry Quarry); = KU-Mt-12 (Cabbage Patch 4).] Walk up section to site from C1703 (fig. 14). Thick fluvial channel sandstones and conglomerates are present at this site. Other channel sandstones to the east can be seen from this site.

Strawberry Quarry has yielded a large assemblage of fossils from the middle Cabbage Patch beds (fig. 3). The unit is an almost 7 m thick mudstone dominated by clay and ash-derived silt sandwiched between fluvial channel deposits. Fossils are concentrated in the middle 60 cm of the horizon (fig. 14). Burrow casts of insects can be found in situ. The fossils recovered from C1704 include rare diatoms (Rasmussen, 1977) and common plant fragments. Root casts are very common and can be quite large, suggesting the sediment was heavily vegetated after deposition.

Ostracods are rare. A few molds and fragments of freshwater and land snails have also been found. Large slug shells (including the type for *Deroceras secures*; Pierce, 1992, 1993) are present and sometimes abundant. Fish bones are very rare, but both frog and salamander bones have been recovered from this horizon (including the type and reference material for *Taricha miocenica*, Tihen 1974; *Plethodon* sp. and *Aneides* sp., Tihen and Wake 1981; and additional specimens of Salamandridae, Calede pers. obs.). Mammal bones and teeth are common both in surface deposits and in situ where they are isolated and scattered.

Twenty three mammalian species have been identified from over 170 specimens identified to the species level (Table 7, fig. 15). The taxa present include mammals characteristic of the middle Cabbage Patch beds that are indicative of an open environment: the gopher *Pleurolicus* and the rabbit *Archaeolagus*. Alike other deposits from the middle Cabbage Patch beds, the assemblage at C1704 also includes taxa shared with the upper (e.g., *Neatocastor* and *Leidymys alicae*) and the lower Cabbage Patch beds (e.g., *Eutypomys*, *Ocajila*, and *Diceratherium*). Recently, several specimens of the canid *Cynodesmus thooides* were recovered by quarrying the deposits at C1704, thereby extending
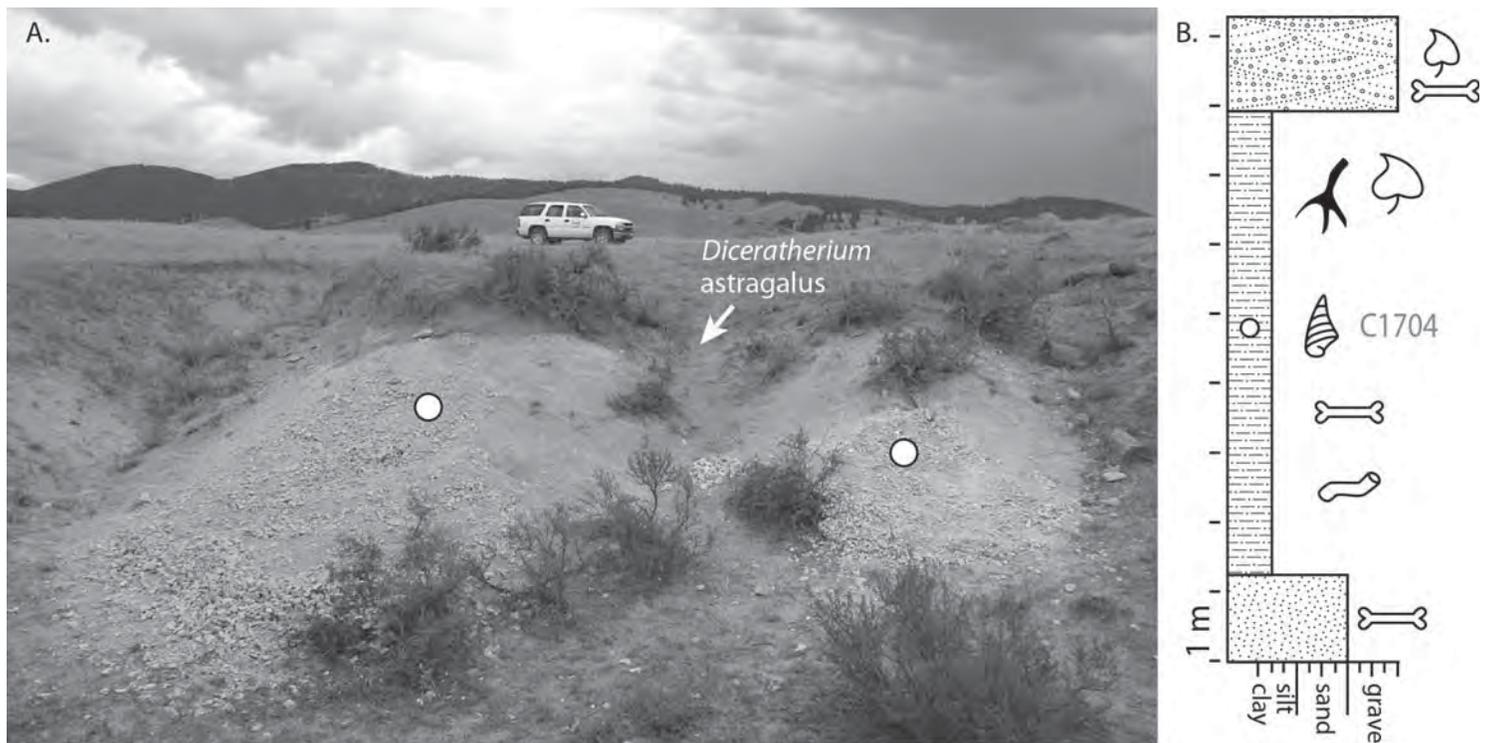
Figure 14. Geology of C1704 (middle Cabbage Patch beds). A: View of the outcrop with field vehicle for scale, B: Stratigraphic section (modified and updated from Rasmussen, 1977). The location on the outcrop of the productive fossil horizon is marked in the stratigraphic section with circles. The arrow shows the location where a Diceratherium armatum astragalus (UMPC 1462) eroded out at C1704 (Prothero and Rasmussen, 2003).

Table 7. Mammalian fauna from C1704.

Order	Family	Genus	Species
Carnivora	Canidae	*Cynodesmus*	*thooides*
Didelphimorphia	Herpetotheriidae	*Herpetotherium*	species B
			species D
		Nanodelphys	species B
Eulipotyphla	Erinaceidae	*Ocajila*	cf. O. makpiyahe
	Proscalopidae	*Proscalops*	species A
	Talpidae	*Mystipterus*	sp.
Lagomorpha	Leporidae	*Archaeolagus*	cf. *A. macrocephalus*
Perissodactyla	Rhinocerotidae	*Diceratherium*	*armatum*
Rodentia	Aplodontidae	new Allomyinae?	new species
		Allomys	new species A
		Meniscomys	new species A
		Niglarodon	new species A
	Castoridae	*Neatocastor*	cf. *N. hesperus*
	Cricetidae	*Leidymys*	*alicae*
	Dipodidae	new genus	new species
		Plesiosminthus	species D
	Eomyidae	*Leptodontomys*	species B
	Eutypomyidae	*Eutypomys*	sp.
	Geomyidae	*Pleurolicus*	new species C
			new species B
	Sciuridae	genus indet.	species indet.
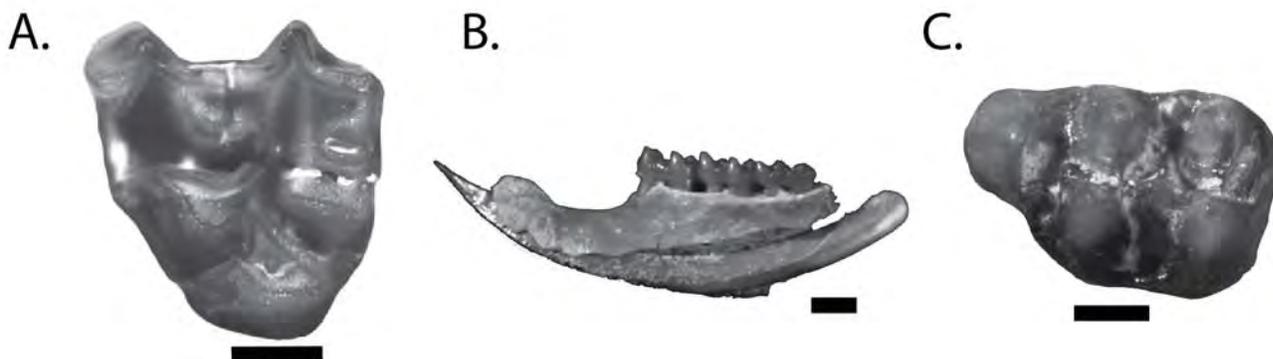
Figure 15. Select mammalian specimens from C1704. A: P4 of Niglarodon new species A: (aplodontid, UMPC 1823), scale equals 1 mm., B: partial lower jaw with i, m1-3 of a new genus and species of Dipodidae (birch mouse, UWBM 97393), scale equals 1 mm., C: M1 of Leidymys alicae (mouse, UWBM 98615), scale equals 0.5 mm.

the stratigraphic range of this taxon previously only known from the lower Cabbage Patch beds (Douglas, 1903; Wang 1994) into the middle Cabbage Patch beds.

STOP 9   UWBM C1705

Horse Locality (Middle Cabbage Patch beds) [= UMV6504-5 (Bert Creek 2-5, Horse Locality), = KU-Mt-09 (Cabbage Patch 2).] Walk up section to site at top of ridge from C1704 (fig. 16). From here we will walk through the gulch below C1705 to look at the strata and the interbedded fluvial channel sandstones.

This outcrop is located near C1701-1704 but is stratigraphically higher (fig. 3). The fossil-bearing unit is a massive 2.5 m thick mudstone that contains mostly clay with only minor amounts of ash-derived silt (fig. 16). Fossil mammals are concentrated in the upper half of the unit (Rasmussen, 1977). Common root traces and rare diatoms can be found throughout the unit. No amphibians or fish have been recovered from this unit but a tortoise scute has been found along with some unidentified mammal bones and teeth.

Few specimens of fossil mammals have been discovered at C1705 (fig. 13B, Table 6). Only two species can be conclusively identified from this locality based on dental material: the herpetotheriid marsupial *Nanodelphys* and the hedgehog *Amphechinus*. This latter taxon is only found in the middle and upper Cabbage Patch beds (Rich and Rasmussen, 1973). *Amphechinus* has been suggested to be a taxon tolerant of arid conditions (Klietman and others, 2015), further support for a more open environment in the middle and upper units of the Cabbage Patch beds. The toothless anterior part of the fused lower jaws and some postcranial

elements likely belonging to the horse *Miohippus* have also been recovered from this site (Rasmussen, 1977).

STOP 10   UWBM C1708

Sharp Claw Butte (Lower Cabbage Patch beds) [= UMV6558-2 (Bert Creek 12-2), = KU-Mt-25 (Cabbage Patch 10).] We will walk to this site from the Rhino Quarry (C1701). Short hike will be up a narrow gulch with sparse outcrops. Main exposure is across the fence (fig. 17).

C1708 is the most productive assemblage of the lower Cabbage Patch beds. This locality is located near the base of the Cabbage Patch beds above an uncertain unconformity with the older, underlying late Eocene to early Oligocene Douglas Creek beds (fig. 3). The unit is a ~8.5 m thick ash-derived siltstone (fig. 17) that contains some clay and little very fine sand. Fossil vertebrates are concentrated approximately 1 to 2 m below the top of the massive unit. Fossils found within this unit include root traces and plant fragments, a few molds and debris of land and freshwater snails, a few molds of ostracods, and very abundant vertebrate remains. Fish bones, scales and partial jaws are abundant at this locality, more so than in any other assemblage of the Bert Creek area. Amphibians are also common and sometimes articulated. Henrici (1994), in particular, described an articulated skeleton of an anuran (a burrowing toad which may have died in its estivation burrow), the type of *Tephrodytes brassicarvalis*, from this assemblage (see also Henrici and others, 2013). Mammal remains, including partial dentaries and bone fragments, are commonly found isolated and scattered. More complete material, including a few partial skulls, have also been recovered. Phytoliths recovered from the matrix surrounding

Figure 16. View of the outcrop at C1705 (middle Cabbage Patch beds). The productive zone of the outcrop, where remains of Amphechinus (hedgehog) and ?Miohippus (horse) were discovered, is the area circled in the foreground with field vehicle for scale. The arrow shows the location of C0174 (fig. 10) in the distance.
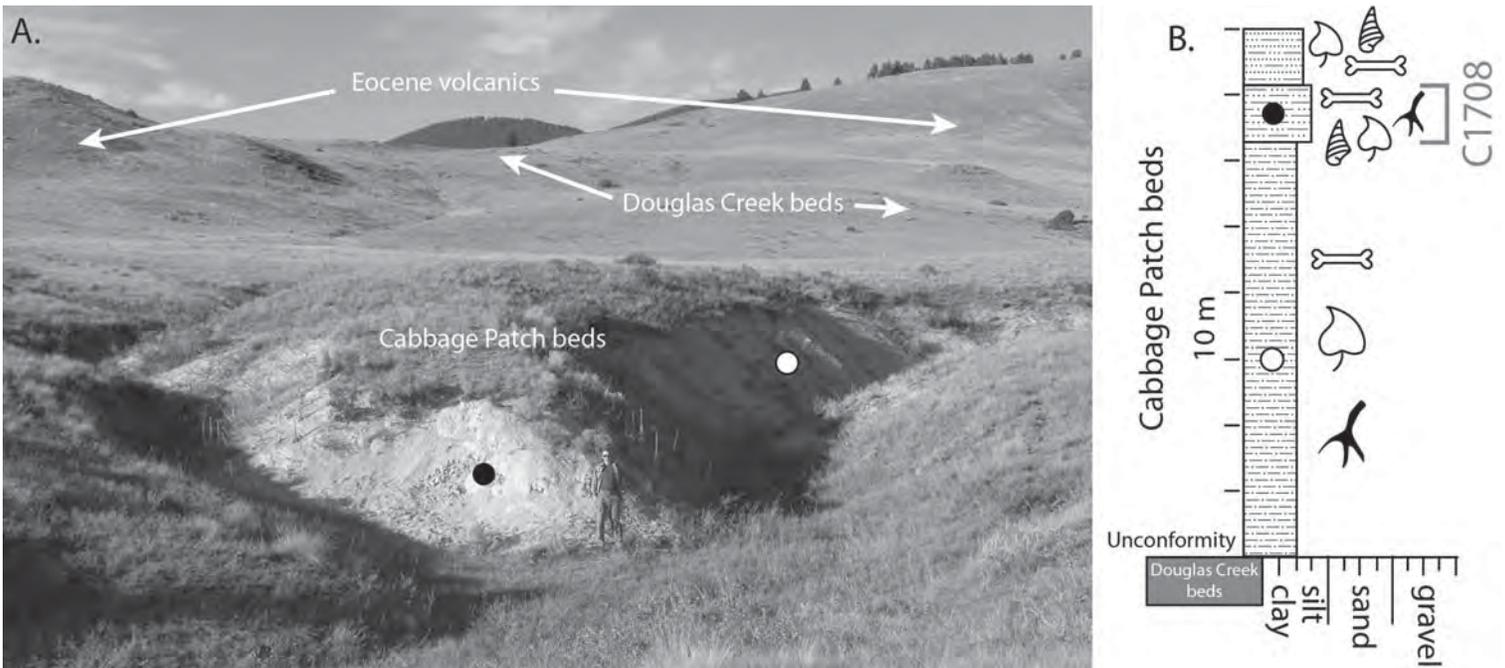
Figure 17. Geology of C1708 (lower Cabbage Patch beds). A: View of the outcrop with student for scale, B: Stratigraphic section (modified and updated from Rasmussen, 1977). The location on the outcrop of the lower-most two units of the Cabbage Patch beds are marked with circles.

a rhinoceros tooth indicate the presence of wetland plants (e.g. sedges), palms, and various grasses at or near the site (Strömberg, 2005). Deposition was in a fluvial environment with slow moving water and periods of dryness. Some fragmented bones and partial jaws show evidence for predator damage and digestion. Although tortoise remains are absent from this site, tortoise shell fragments have been found in the underlying clay-rich mudstone strata.

Over 190 specimens of fossil mammals from C1708 have been identified to the species level. The mammalian fauna from this locality is notable for its very high proportion of eomyid rodents (*Leptodontomys*, ~ 16%) and herpetotheriid marsupials (~ 23%). Twenty-two different species have been identified (Table 8, fig. 18), including the rabbit *Palaeolagus* and the rhinoceroses *Diceratherium annectens* and *Skinneroceras manningi* (described in Prothero and Rasmussen, 2008), all three of which are absent from any other locality. The mammalian fauna is otherwise similar to other assemblages of the lower Cabbage Patch beds in the presence of *Pronodens*, *Miosciurus*, *Agnotocastor*, and a new aplodontid taxon perhaps belonging to the genus *Rudiomys*. The mammalian assemblage at C108 also shares genera with the middle Cabbage Patch beds (e.g., *Diceratherium, Mystipterus*). The presence of the forest-dwelling eomyids, *Proscalops, Pronodens,* and *Miosciurus* suggests a closed-habitat for C1708.

STOP 11   UWBM C1715

On Edge (Upper Cabbage Patch beds) [= UMV6552 (Bert Creek 6), = KU-Mt-16 (Cabbage Patch 8).] Walk to site from dirt road near old ranch buildings (fig. 19).

The extensive exposures at this locality span close to 30 m of measured section covering nine successive depositional environments (fig. 19; Rasmussen, 1977; Rasmussen and Fields, 1980). The top of the section is unconformably overlain by the late Miocene-aged Flint Creek beds. The lowermost beds have been interpreted as fluvial overbank deposits; however, up section, thick deposits of alternating fluvial, lacustrine, and paludal sediments are represented. Organic-rich shale and lignite are present in the paludal environment deposits, with the lignites very rich in sponge spicules. The lacustrine deposits are associated with ledge-forming, sometimes laminated, beds that display occasional fibrous gypsum cement that may be over 3 cm thick. The gypsum-cemented beds are sometimes directly above lacustrine strata with extensive well-developed mud cracks, thereby suggesting periods of aridity with evaporation when the lake (playa) slowly dried up. Abundant plant fossils in the form of plant fragments and leaf imprints are found throughout most of the horizons exposed. Sponge spicules and diatoms are locally abundant. Freshwater snails are also com-

Table 8. Mammalian fauna from C1708.

Order	Family	Genus	Species
Artiodactyla	Leptomerycidae	*Pronodens*	*transmontanus*
Carnivora	Canidae	*Archaeocyon*	*leptodus*
Didelphimorphia	Herpetotheriidae	*Herpetotherium*	species A
			species C
		Nanodelphys	species A
Eulipotyphla	Erinaceidae	*Ocajila*	*makpiyahe*
	Proscalopidae	*Proscalops*	sp.
	Soricidae	*Domnina*	new species
	Talpidae	*Mystipterus*	sp.
Lagomorpha	Leporidae	*Paleolagus*	*hypsodus?*
Perissodactyla	Rhinocerotidae	*Diceratherium*	*annectens*
		Skinneroceras	*manningi*
Rodentia	Aplodontidae	*Rudiomys?*	new species
	Castoridae	new Anchitheriomyinae	new species A
		Agnotocastor	sp.
	Cricetidae	*Leidymys*	new species
	Dipodidae	new genus	new species
	Eomyidae	*Leptodontomys*	*cf. L. douglassi*
			species A
			species B
			species C
	Sciuridae	*Miosciurus*	*cf. M. ballovianus*
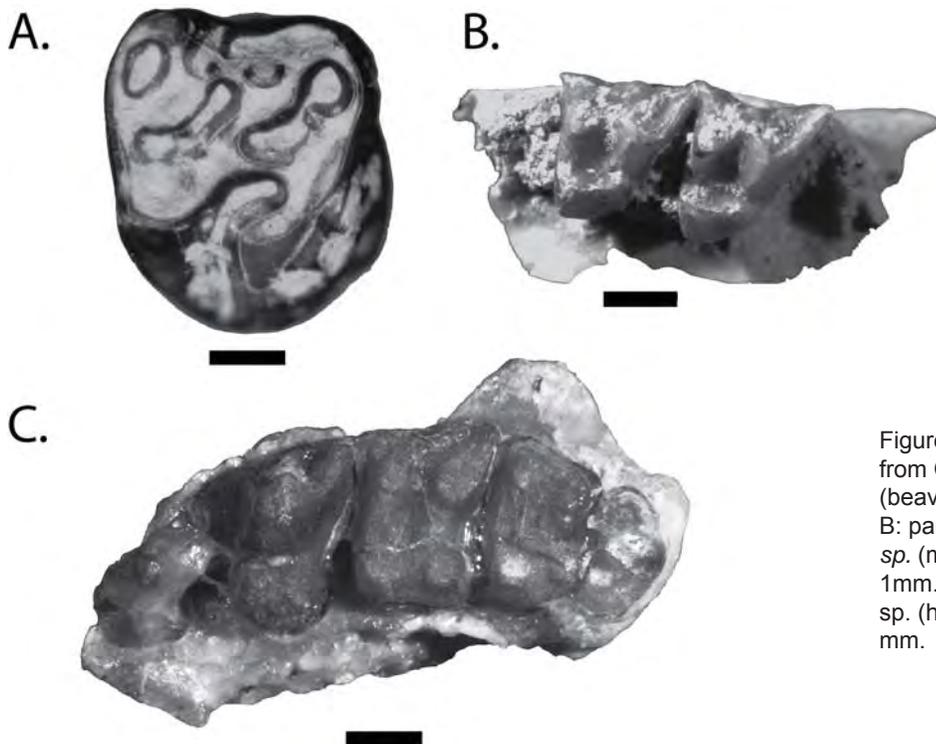
Figure 18. Select mammalian specimens from C1708. A: M1 or M2 of Agnotocastor sp. (beaver, KUVP 18176), scale equals 1 mm, B: partial maxilla with M1-2 of *Herpetotherium sp.* (marsupial, UWBM 98761), scale equals 1mm., C: partial maxilla with P3-M3 of Ocajila sp. (hedgehog, KUVP 18155), scale equals 1 mm.
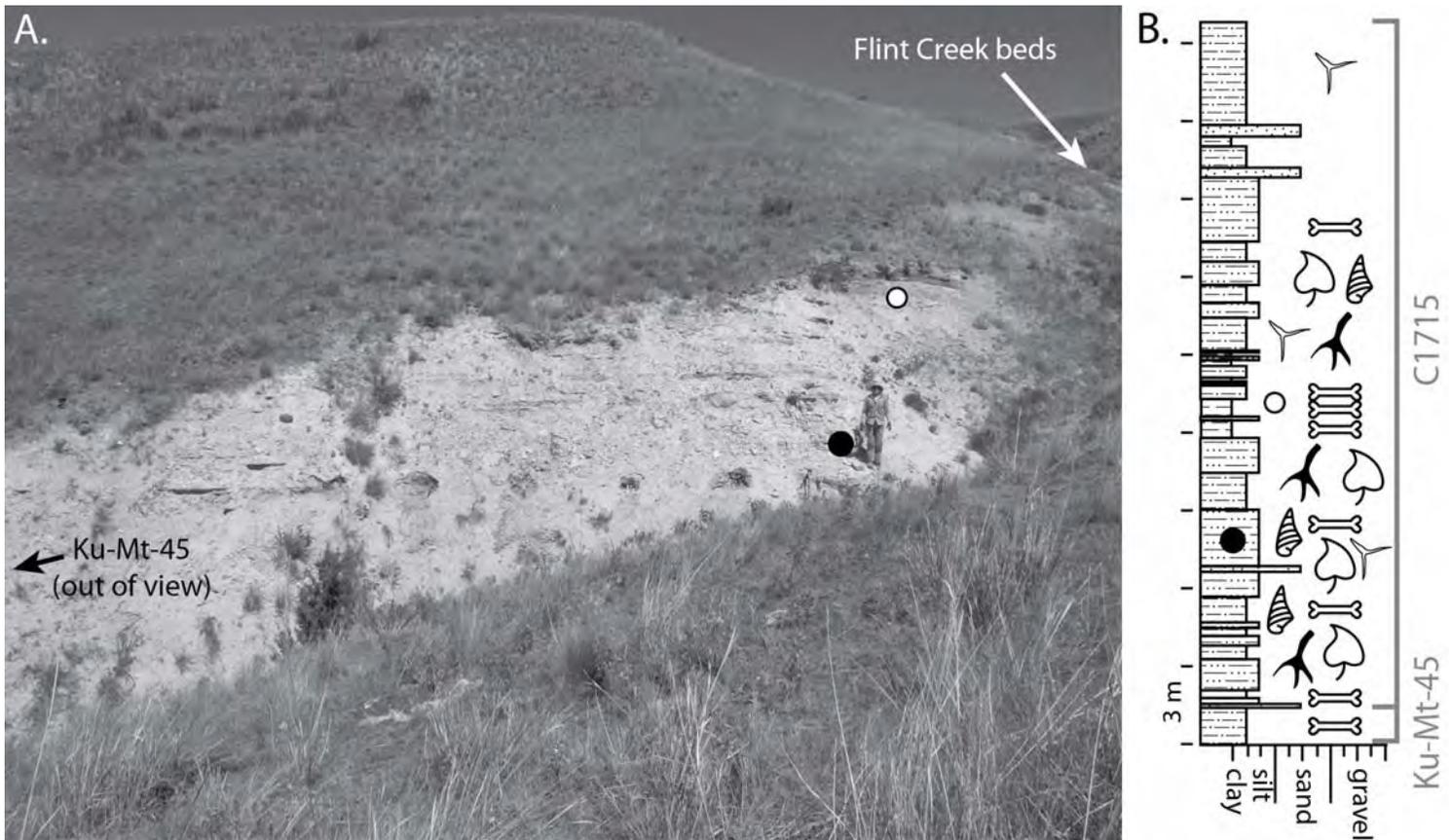
Figure 19. Geology of C1715 (upper Cabbage Patch beds). A: View of the outcrop with student for scale. Light-colored strata are from the abundance of fresh volcanic glass shards. Dark beds above the upper circle are lignites, B: Stratigraphic section (modified and updated from Rasmussen, 1977, 1989). The location on the outcrop of select horizons is marked in the stratigraphic section with circles.

mon in the lacustrine strata, and root traces suggest periods of dryness and subaerial exposure. Pea clams (Sphaeriidae) are very rare and only partial specimens have been found. Fossil vertebrates are rare. Fossil mammals and frog bones have only been recovered from the very base of the large outcrop exposed in this area. Fish bones and even articulated partial skeletons of fish have been recovered in the middle lacustrine deposits.

The only identifiable mammalian specimen, an isolated tooth of the entoptychine gopher *Gregorymys* cf. *G. douglassi*, was recovered from the lowest part of the outcrop (Ku-Mt-45; fig. 3; Rasmussen, 1977). This taxon helps constrain the location of the beds at this locality to the upper unit of the Cabbage Patch beds. Ongoing work dating the Cabbage Patch beds using $^{40}Ar/^{39}Ar$ will provide radiometric estimates of the age of the lower most units of this outcrop.

CONCLUSIONS

The mammalian fossil record of the Cabbage Patch beds is evidence of a well-sampled and species-rich series of assemblages through time. The stratigraphic context of the fossils in the Flint Creek basin (fig. 3) allows the tracking of mammalian and molluscan taxa through time. The pattern of mammalian and molluscan taxonomic replacement that emerges out of this work supports the division of the Cabbage Patch beds in three biostratigraphic units (fig. 20; Rasmussen, 1977; Pierce, 1993; Rasmussen and Prothero, 2003). The faunal transitions between these units suggest changes in the ecomorphological composition of mammalian communities throughout the beds. Indeed, the composition of the mammalian assemblages of the middle and upper Cabbage Patch beds appears to support a greater biodiversity of taxa adapted to more open-environments in the younger units of the beds and a relative decline in the closed-habitat mammals abundant in the lower Cabbage Patch beds. Ongoing work on the paleoecological affinities of the Cabbage Patch mammals and the vegetational history of the beds will help shed light on the role of environmental change in mammalian evolution during the Oligocene. The location in western Montana of the Cabbage Patch beds, geographically intermediate between coeval deposits from the Great Plains (Arikaree Group) and
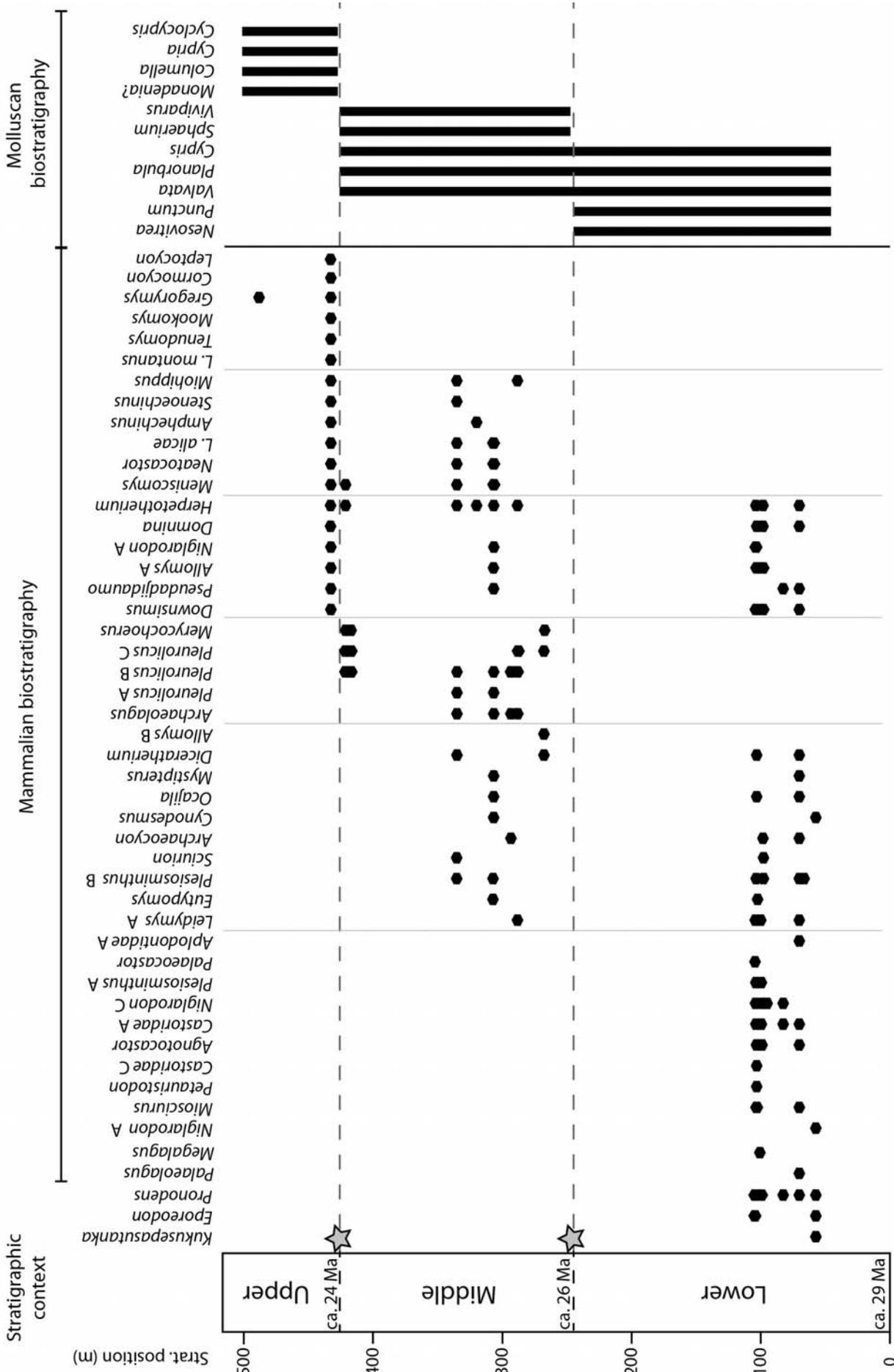
Figure 20. Summary of the biostratigraphy of mammalian and molluscan taxa in the Cabbage Patch beds (stratigraphic context modified and updated from Rasmussen, 1977 and Rasmussen and Prothero, 2003; molluscan data from Rasmussen and Prothero, 2003; Pierce, 1993). The presence of mammalian taxa throughout the section is indicated by black dots. Species names are indicated only when several species from the same genus are present. The presence of select molluscan taxa within each unit is indicated by black bars. Stars indicate faunal turnover events. They correspond to the boundaries between the lower, middle, and upper Cabbage Patch units.

Oregon (John Day Formation), is a unique opportunity to also assess the biogeographic affinities of the mammalian fauna of the Cabbage Patch beds. Preliminary results of this work suggest that the Rocky Mountains may have been a faunal mixing zone during the Arikareean with some taxa shared with the assemblages from the Arikaree Group and others found in the John Day Formation.

ACKNOWLEDGMENTS

REFERENCES

Barnosky, A.D. and Labar, W.J., 1989, Mid-Miocene (Barstovian) environmental and tectonic setting near Yellowstone Park, Wyoming and Montana: Geological Society of America Bulletin, v. 101, p. 1448-1456.

Burbank, D.W. and Barnosky, A.D., 1990, The magnetochronology of Barstovian mammals in southwestern Montana and implications for the initiation of Neogene crustal extension in the northern Rocky Mountains: Geological Society of America Bulletin, v. 102, p. 1093-1104.

Chadwick, R.A., 1972, Volcanism in Montana: Northwest Geology, 1, p. 1-20.

Chadwick, R.A., 1978, Geochronology of post-Eocene rhyolitic and basaltic volcanism in southwestern Montana: Isochron/West, no. 22, p. 25-28.

Chadwick, R.A., 1981, Chronology and structural setting of volcanism in southwestern and central Montana: *in* Thomas, T.E., ed., Montana Geological Society Field Conference and Symposium, Guidebook to southwest Montana: Montana Geological Society, p. 301-310.

Chadwick, R.A., 1985, Overview of Cenozoic volcanism in the West Central United States: *in* Flores, R.M. and Kaplan, S.S. eds., Rocky Mountain Paleogeography Symposium 3, Cenozoic Paleogeography of the West-Central United States: Rocky Mountain Section, Society of Economic Paleontologists and Mineralogists, Denver, Colorado, p. 359-382.

Douglass, E. 1899, The Neocene lake beds of western Montana and descriptions of some new vertebrates from the Loup Fork: Univ. Montana M.S. thesis, p. 1-27: *in* R.W. Fields, ed., 1958, Western Montana, Guidebook Eighth Field Conference, Society of Vertebrate Paleontology, Appendix.

Douglass, E. 1901, Fossil Mammalia of the White River beds of Montana: Transactions American Philosophical Society, v. 20, p. 237-279.

Douglass, E., 1903, New vertebrates from the Montana Tertiary: Annals of the Carnegie Museum, v. 2, p. 141-199.

Douglass, E., 1909, A geological reconnaissance in North Dakota, Montana, and Idaho; with notes on Mesozoic and Cenozoic Geology: Carnegie Museum Annals 5, p. 211-288.

Fields, R.W., Rasmussen, D.L., Tabrum, A.R., and Nichols, R., 1985, Cenozoic rocks of the intermontane basins of western Montana and eastern Idaho: A summary: *in* Flores, R.M. and Kaplan, S.S. eds., Rocky Mountain Paleogeography Symposium 3, Cenozoic Paleogeography of the West-Central United States: Rocky Mountain Section, SEPM, p. 9-36.

Fritz, W.J. and Sears, J.W., 1993, Tectonics of the Yellowstone hotspot wake in southwestern Montana: Geology, v. 21, p. 427-430.

Geisler, J.H., Theodor, J.M., Uhen, M.D., Foss, S.E., 2007, Phylogenetic relationships of cetaceans to terrestrial artiodactyls: *in* Prothero, D.R., and Foss, S.E., eds., The evolution of artiodactyls. Baltimore: Johns Hopkins University Press, p. 19-31.

Gwinn, V.E., 1960, Cretaceous and Tertiary stratigraphy and structural geology of the Drummond area, western Montana [Ph.D. dissertation]: Princeton, Princeton University, 153 p.

Gwinn, V.E., 1961, Geology of the Drummond area, central-western Montana: Montana Bureau of Mines and Geology Special Publication 21, map 4.

Hanneman, D.L. and Wideman, C.J., 1991, Sequence stratigraphy of Cenozoic continental rocks, southwestern Montana: Geological Society of America Bulletin v. 103, p. 1335-1345.

Hanneman, D.L. and Wideman, C.J., 2006, Calcic pedocomplexes – Regional sequence boundary indicators in Tertiary deposits of the Great Plains and western United States: *in* Alonso-Zarza, A.M., and Tanner, L.H., eds., Paleoenvironmental record and applications of calcretes and palustrine carbonates: Geological Society of America Special Paper 416, p. 1-15.

Hanneman, D.L., Cheney, E.S., and C.J. Wideman, 2003, Cenozoic sequence stratigraphy of Northwestern USA: *in* Flores, R.M. and Raynolds, R.G. eds., Cenozoic Systems of the Rocky Mountain Region: Rocky Mountain Section, SEPM, p. 135-155.

Henrici, A.C., 1994, *Tephrodytes brassicarvalis*, new genus and species (Anura: Pelodytidae), from the Arikareean Cabbage Patch beds of Montana, US, and pelodytid-pelobatid relationships: Annals of the Carnegie Museum, v. 63, p. 155-183.

Henrici, A.C., Baez, A.M., and Grande, L., 2013, *Aerugoamnis paulus*, new genus and species (Anura: Anomocoela): First reported anuran from the Early Eocene (Wasatchian) Fossil Butte Member of the Green River Formation, Wyoming: Annals of the Carnegie Museum, v. 81, p. 295-309.

Klietman, J., van den Hoek Ostende, L.W., Nagel, D., and Rummel, M., 2015, Insectivore palaeoecology. A case study of a Miocene fissure filling in Germany: Palaeogeography, Palaeoclimatology, Palaeoecology, v. 418, p. 278-289.

Konizeski, R.L., 1957, Paleoecology of the medial Pliocene Deer Lodge local fauna, western Montana: Geological Society of America Bulletin, v. 68, p. 131-150.

Konizeski, R.L., 1965, Tertiary deposits in basins marginal to the Flint Creek Range: *in* R.W. Fields and W. Shepard, eds., Geology of the Flint Creek Range, Montana: 16th Annual Field Conference, Billings Geological Society, p. 10-18.

Konizeski, R.L., and Donohoe, J.C., 1958, Faunal and stratigraphic relationships of the Cabbage Patch beds, Granite County, Montana: *in* Fields, R.W. ed. Society of Vertebrate Paleontology, 8th Annual Field Conference Guidebook, p. 45-49.

Kuenzi, W.D., 1966, Tertiary stratigraphy in the Jefferson River basin, Montana: Unpublished Ph.D. dissertation, University of Montana, Missoula, 293 p.

Kuenzi, W.D. and Richard, B.H., 1969, Middle Tertiary unconformity, North Boulder and Jefferson basins, southwestern Montana: Geological Society of America Bulletin v. 80, p. 115-120.

Kuenzi, W.D. and Fields, R.W., 1971, Tertiary stratigraphy, structure and geologic history, Jefferson basin, Montana: Geological Society of America Bulletin, v. 82, p. 3374-3394.

Larson, E.E. and Evanoff, E., 1998, Tephrostratigraphy and source of the tuffs of the White River sequence: *in* Terry, D.O., LaGarry, H.E., and Hunt, R.M., Jr., Depositional environments, lithostratigraphy, and biostratigraphy of the White River and Arikaree Groups (late Eocene to early Miocene, North America): Geological Society America Special Paper 325, p. 1-14.

Lihoreau, F., and Ducrocq, S., 2007, Family Anthracotheriidae *in* Prothero, D.R., and Foss, S.E., eds., The evolution of artiodactyls: Baltimore, Johns Hopkins University Press, p. 89-105.

Loen, J.S., 1986, Origin of gold placers in the Pioneer District, Powell County, Montana: Unpublished M.S. thesis, Colorado State University, Fort Collins, 164 p.

Macdonald, J.R., 1956, The North American Anthra-

cotheres: Journal of Paleontology, v. 30, p. 613-645.

McLeod, P.J., 1987, The depositional history of the Deer Lodge basin, western Montana: Unpublished M.S. thesis, University of Montana, Missoula, 61 p.

McCune, J.G., 2008, Cenozoic sedimentary evolution of the Helmville basin, west-central Montana: Unpublished M.S. thesis, University of Montana, Missoula, 58 p.

McCune, J.G. and Hendrix, M.S., 2009, Geologic map of the Helmville basin, west-central Montana: Montana Bureau of Mines and Geology Open File Report MBMG 574, 10 p.

Melson, W.G., 1971, Geology of the Lincoln area, Lewis and Clark County, Montana: Smithsonian Contributions in Earth Sciences, v. 7, p. 1-29.

Miller, C.N., Jr., 1980, Road Log No. 2, Missoula to florule locales near Drummond and Lincoln, *in* Miller, M.R., ed., Guidebook of the Drummond-Elkhorn areas, west-central Montana: Montana Bureau of Mines and Geology Special Publication82, p. 11-16.

Monroe, S., 1976, Vertebrate paleontology, stratigraphy and sedimentation of the Upper Ruby River basin, Madison County, Montana: Unpublished Ph.D. dissertation, University of Montana, Missoula, 301p.

Patterson, R.T., McKillop, W.B, Kroker, S, Nielsen, E, and Reinhardt, E.G., 1997, Evidence for rapid avian-mediated foraminiferal colonization of Lake Winnipegosis, Manitoba, during the Holocene hypsithermal: Journal of Paleolimnology, v. 18, p. 131-143.

Petkewich, R.M., 1972, Tertiary geology and paleontology of the northeastern Beaverhead and lower Ruby River basins, southwestern Montana: Unpublished Ph.D. dissertation, University of Montana, Missoula, 365 p.

Pierce, H.G., 1992, The nonmarine mollusks of the late Oligocene-early Miocene Cabbage Patch fauna of western Montana. II. Terrestrial gastropod families other than Pupillidae (Pulmonata: Stylommatophora): Journal of Paleontology, v. 66, p. 610-620.

Pierce, H.G., 1993, The nonmarine mollusks of the late Oligocene-early Miocene Cabbage Patch fauna of western Montana III. Aquatic mollusks and conclusions: Journal of Paleontology, v. 67, p. 980-993.

Pierce, H.G. and Rasmussen, D.L. 1989, New land snails (Archaeogastropoda, Helicinidae) from the Miocene (early Barstovian) Flint Creek beds of western Montana: Journal of Paleontology, v. 63, p. 846-851.

Pierce, H.G. and Rasmussen, D.L. 1992, The nonmarine mollusks of the late Oligocene-early Miocene Cabbage Patch fauna of western Montana. I. Geologic setting and the family Pupillidae (Pulmonata: Stylommatophora): Journal of Paleontology, v. 66, p. 39-52.

Portner, R.A., 2005, Sedimentary and tectonic evolution of the Flint Creek basin, west-central Montana: Unpublished M.A. thesis, University of Montana, Missoula, 160 p.

Portner, R. and Hendrix, M., 2005, Preliminary Geologic Map of the Eastern Flint Creek basin west-central Montana: Montana Bureau of Mines and Geology Open File Report MBMG 521.

Portner, R.A., Hendrix, M.S., Stalker, J.C., Miggins, D.P., and Sheriff, S.D., 2011, Sedimentary response to orogenic exhumation in the northern Rocky Mountain Basin and Range Province, Flint Creek basin, west-central Montana: Canadian Journal of Earth Sciences, v. 48, p. 1131-1153.

Prothero, D.R., and Rasmussen, D.L., 2008, New giant rhinoceros from the Arikareean (Oligocene-Miocene) of Montana, South Dakota, and Wyoming *in* Lucas, S.G., Morgan, G.S., Spielmann, J.A., and Prothero, D.R., eds., Neogene mammals. New Mexico Museum History and Science Bulletin, v. 44, p. 323-330.

Rasmussen, D.L., 1969, Late Cenozoic geology of the Cabbage Patch area, Granite and Powell Counties, Montana: Unpublished M.A. thesis, University of Montana, Missoula, 188 p.

Rasmussen, D.L., 1973, Extension of the middle Tertiary unconformity into western Montana: Northwest Geology, v. 2, p. 27-35.

Rasmussen, D.L., 1977, Geology and mammalian paleontology of the Oligocene-Miocene Cabbage Patch Formation, central-western Montana: Unpublished Ph.D. dissertation, University of Kansas, Lawrence, 794 p.

Rasmussen, D.L., 1989, Depositional environments, paleoecology, and biostratigraphy of Arikareean Bozeman Group strata west of the Continental Divide in Montana: *in* French, D.E. and Grabb, R.F., eds., Geological Resources of Montana v. 1, Montana Geological Society, Montana Centennial Edition, 1989 Field Conference, Guidebook, p. 205-215.

Rasmussen, D.L., 2003, Tertiary history of western Montana and east-central Idaho: A synopsis: *in* Flores, R.M. and Raynolds, R.G. eds., Cenozoic Systems of the Rocky Mountain Region: Rocky Mountain Section, SEPM, p. 459-477.

Rasmussen, D.L., and Fields, R.W., 1980, Road Log No. 1, Missoula to Flint Creek via Upper Clark Fork Valley and Drummond, *in* Miller, M.R., ed., Guidebook of the Drummond-Elkhorn areas, west-central Montana: Montana Bureau of Mines and Geology Special Publication 82, p. 1-9.

Rasmussen, D.L., and Prothero, D.R., 2003, Lithostratigraphy, biostratigraphy, and magnetostratigraphy of the Arikareean strata west of the Continental Divide in Montana *in* Raynolds, R.G., and Flores, R.M., eds., Cenozoic Systems of the Rocky Mountain Region: Rocky Mountain Section SEPM. p. 479-499.

Rich, T.H.V., and Rasmussen, D.L., 1973. New North American Erinaceinae hedgehogs (Mammalia: Insectivora): Occasional papers of the Museum of Natural History, the University of Kansas, no. 21, p. 1-54.

Riel, S.J., 1964, A new oreodont from the Cabbage Patch Local Fauna, western Montana: Postilla, v. 85, p. 1-10.

Robinson, G.D., 1960, Middle Tertiary unconformity in southwestern Montana: U.S. Geological Survey Professional Paper 400-B, p. 227-228.

Robinson, G.D., 1963, Geology of the Three Forks Quadrangle, Montana: U.S. Geological Survey Professional Paper 370, 143 p.

Robinson, G.D., 1967, Geologic map of the Toston Quadrangle, southwestern Montana: U.S. Geological Survey Miscellaneous Geological Investigations Map 1486.

Sears, J.W., 2010, Lost lakes and re-arranged rivers: Neotectonic disruption of the Middle Miocene Big Hole River basin, SW Montana: Northwest Geology v. 39, p. 113-122.

Sears, J.W., 2013, Late Oligocene-early Miocene Grand Canyon: A Canadian connection?:Geological Society of America Today, v. 23, p. 4-10.

Sears, J.W., and Fritz, W.J., 1998, Cenozoic tilt domains in southwestern Montana: Interference among three generations of extensional fault systems: *in* Faulds, J.E. and Stewart, J.H., eds., Accommodation zones and Transfer zones: The regional segmentation of the Basin and Range Province: Geological Society of America Special Paper 323, p. 241-247.

Sears, J.W., Hendrix, M., Waddell, A., Webb, B., Nixon, B., King, T., Roberts, E. and Lerman, R., 2000, Structural and stratigraphic evolution of the Rocky Mountain foreland basin in central-western Montana: *in* Roberts, S. and Winston, D., eds., Geologic field trips, western Montana and adjacent areas: Rocky Mountain Section of the Geological Society of America, University of Montana, p. 131-155.

Sears, J.W. and Ryan, P., 2003, Cenozoic evolution of the Montana Cordillera: Evidence from paleovalleys: *in* Flores, R.M. and Raynolds, R.G. eds., Cenozoic Systems of the Rocky Mountain Region: Rocky Mountain Section, SEPM, p. 289-301.

Seeland, D., 1985, Oligocene paleogeography of the Northern Great Plains: *in* Flores, R.M. and Kaplan, S.S. eds., Rocky Mountain Paleogeography Symposium 3, Cenozoic Paleogeography of the West-Central United States: Rocky Mountain Section, SEPM, p. 187-205.

Strömberg, C.A.E., 2005, Decoupled taxonomic radiation and ecological expansion of open-habitat grasses in the Cenozoic of North America: Proceedings of the National Academy of Sciences, v. 102, p. 11980-11984.

Tedford, R.H., Albright, B. III, Barnosky, A.D., Ferrusquia-Villafranca, I., Hunt, R.M. Jr., Storer, J.E., Swisher, C.C. III, Voorhies, M.R., Webb, S.D., and Whistler, D.P., 2004, Mammalian biochronology of the Arikareean through Hemphillian interval (Late Oligocene through Early Pliocene Epochs) *in* Woodburne, M.O. ed., Late Cretaceous and Cenozoic Mammals of North America: Biostratigraphy and geochronology. Columbia University Press. p. 315-343.

Tihen, J.A., 1974, Two new North American Miocene salamandrids: Journal of Herpetology, v. 8, p. 219-229.

Tihen, J.A., and Wake, D.B., 1981, Vertebrae of plethodontid salamanders from the Lower Miocene of Montana: Journal of Herpetology, v. 15, p. 35-40.

Van Nieuwenhuise, D.S., and He, J., 1986, Implications of Arikareean (Oligocene-Miocene) ostracodal and foraminiferal assemblages from lacustrine deposits in southwestern Montana: Proceedings North American Paleontological Convention v. 4, p. A47.

Vuke, S.M., 2004, Geologic map of the Divide area, southwestern Montana: Montana Bureau of Mines and Geology Open File Report MBMG 502, 36 p.

Wang, X., Tedford, R.H., and Taylor, B.E., 1999, Phylogenetic systematics of the Borophaginae (Carnivora, Canidae): Bulletin of the American Museum of Natural History, v. 243, p. 1-391.

Webb, S.D., and Opdyke, N.D., 1995, Global climatic influence on Cenozoic land mammal faunas, *in* Stanley, S.M., Knoll, A.H., and Kennett, J.P. eds., Effects of past global change on life: Washington, D.C., National Academies Press, p. 184-208.

Woodburne, M.O., 2004, Global events and the North American mammalian biochronology: *in* Woodburne, M.O., ed., Late Cretaceous and Cenozoic Mammals of North America: Biostratigraphy and geochronology: Columbia University Press, p. 315-343.

Zachos, J.C., Dickens, G.R., and Zeebe, R.E., 2008, An early Cenozoic perspective on greenhouse warming and carbon-cycle dynamics: Nature, v. 451, p. 279-283.

GEOLOGIC FIELD GUIDE TO THE CHERRY CREEK FAULT, A POSSIBLE PROTEROZOIC FAULT NEAR HELENA, MONTANA

Jeff Lonn

Montana Bureau of Mines and Geology, 1300 W. Park St, Butte, MT 59701, jlonn@mtech.edu

INTRODUCTION

On this all-day hike through the foothills northwest of Helena, we will examine Proterozoic Belt Supergroup (Belt) strata preserved on both sides of the Cherry Creek fault, interpreted to have a Proterozoic ancestry. The hike is about 4 miles long on game and cow trails through scattered forest and open rangeland and includes about 1,000 feet of elevation gain. The land surface elevation averages about 5,000 feet, and air temperatures will likely be hot in early August. No water is available. The route crosses Bureau of Land Management and private land. Access to the privately owned land requires prior permission from the Prickly Pear Simmental Ranch.

GEOLOGIC SETTING

The sedimentary rocks of the Proterozoic Belt Supergroup of western Montana and northern Idaho are most often interpreted to have been deposited in a vast, shallow, and possibly intracratonic, sea. The Belt's immense thickness (more than 14 km; 8 miles) required significant basin subsidence during sedimentation. Based on abrupt stratigraphic thickness changes, Winston (1986) proposed a tectonic setting for the Belt basin that included a number of major growth faults (fig. 1). This field trip examines an area near the Garnet Line, one of the postulated east-west striking growth faults. South of the Garnet Line, a thin Belt stratigraphic succession is reported (Winston, 1986).
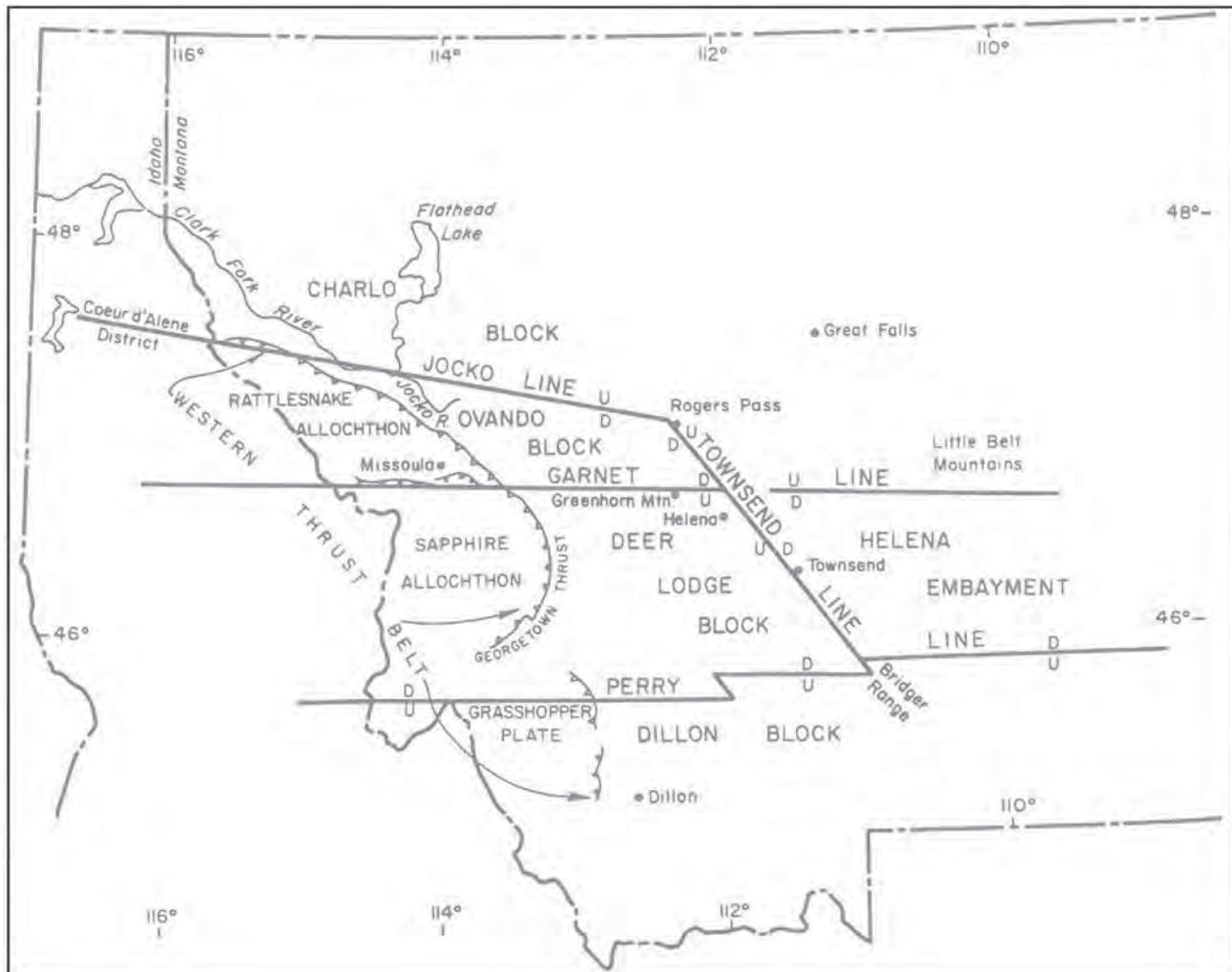

Figure 1. Location of the field trip with respect to Winston's (1986) hypothetical Belt basin growth faults. The Cherry Creek fault is near the proposed Garnet Line. (from fig. 11, p. 103, Winston, 1986).

North of the line, a thick stratigraphic section suggests that the Garnet Line was a down-to-the-north growth fault (see fig. 13, p. 105, in Winston, 1986). Faulting is postulated to have continued into Neoproterozoic time because the Cambrian Flathead Formation unconformably overlies lower Missoula Group formations south of the line, but overlies upper Missoula Group formations north of the line.

Recent 1:24,000-scale mapping of the Austin 7.5′ quadrangle (Berg and Lonn, 2011) revealed a fault, named the Cherry Creek fault, that results in significant offset of the Belt units, but only minor offset of the overlying Cambrian Flathead Formation (figs. 2, 3). North of the fault, the Flathead overlies the Mount Shields Formation, member 3 (Mt Shields 3), but south of the fault the Flathead overlies the lowermost Shepard and uppermost Snowslip Formations. On the
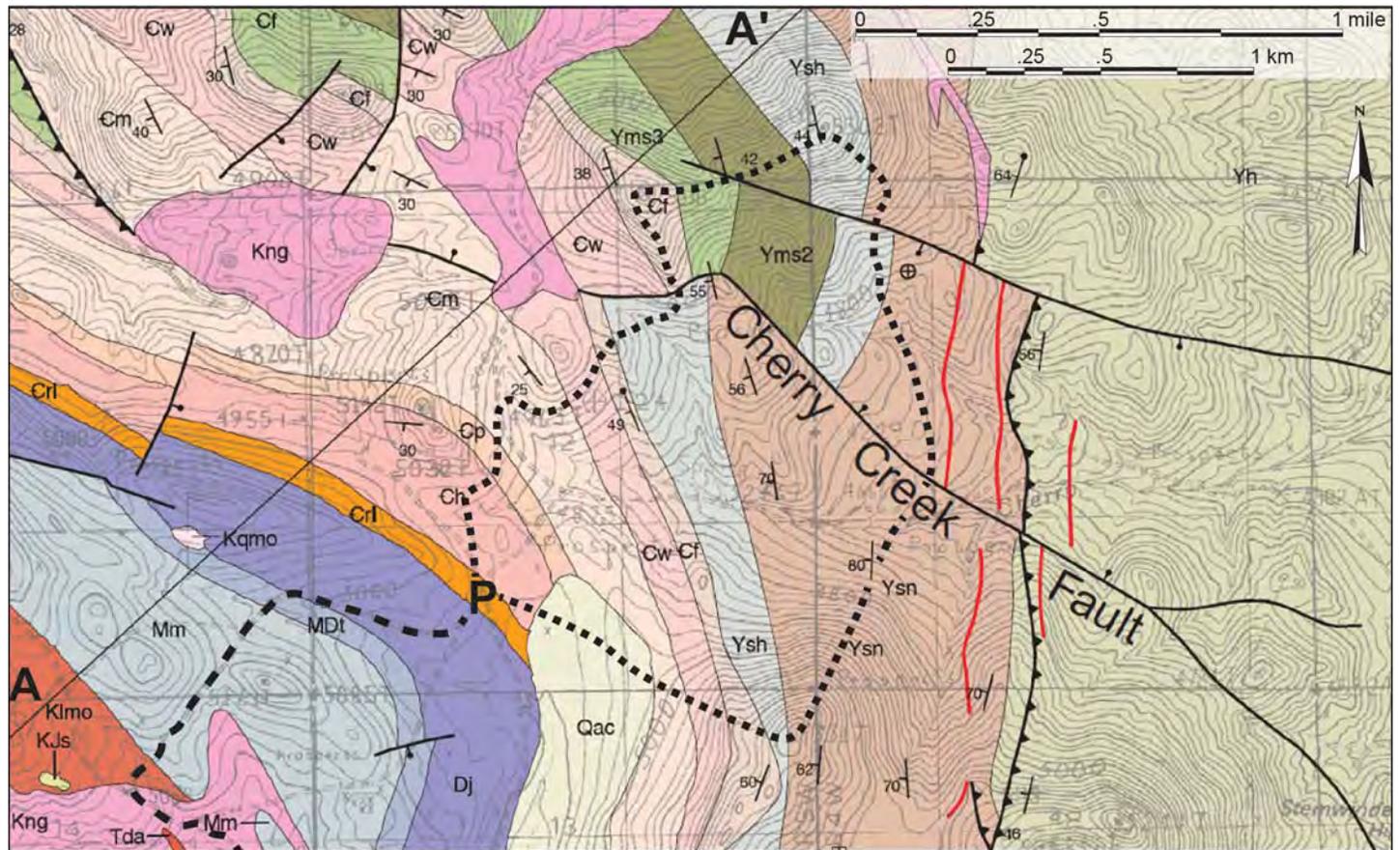
Mesozoic

Tda	Dacite
Klmo	Priest Pass leucomonzonite
Kqmo	Quartz monzonite
Kdgp	Porphyritic granodiorite
Kng	Non porphyritic granodiorite
KJs	Sedimentary rocks, undivided

Normal fault

Thrust or reverse fault

Field trip route

Paleozoic

Mm	Madison Group, undivided
MDt	Three Forks Formation
Dj	Jefferson Formation
Crl	Red Lion Formation
Ch	Hasmark Dolomite
Cp	Park Shale
Cm	Meagher Formation
Cw	Wolsey Shale
Cf	Flathead Formation

Mesoproterozoic (Belt Supergroup)

Yms3	Mount Shields Formation, third member
Yms2	Mount Shields Formation, second member
Ysh	Shepard Formation
Ysn	Snowslip Formation
Yh	Helena Formation
Ye	Empire Formation
Ys	Spokane Formation

Figure 2. Geologic map and stratigraphic column for the field trip area. Blue Cloud access road marked by dashed line, parking area marked "P", and hiking route shown by dotted lines. Field guide follows the hiking route in a counterclockwise direction. Scale approximately 1:24,000. (modified from Berg and Lonn, 2011).
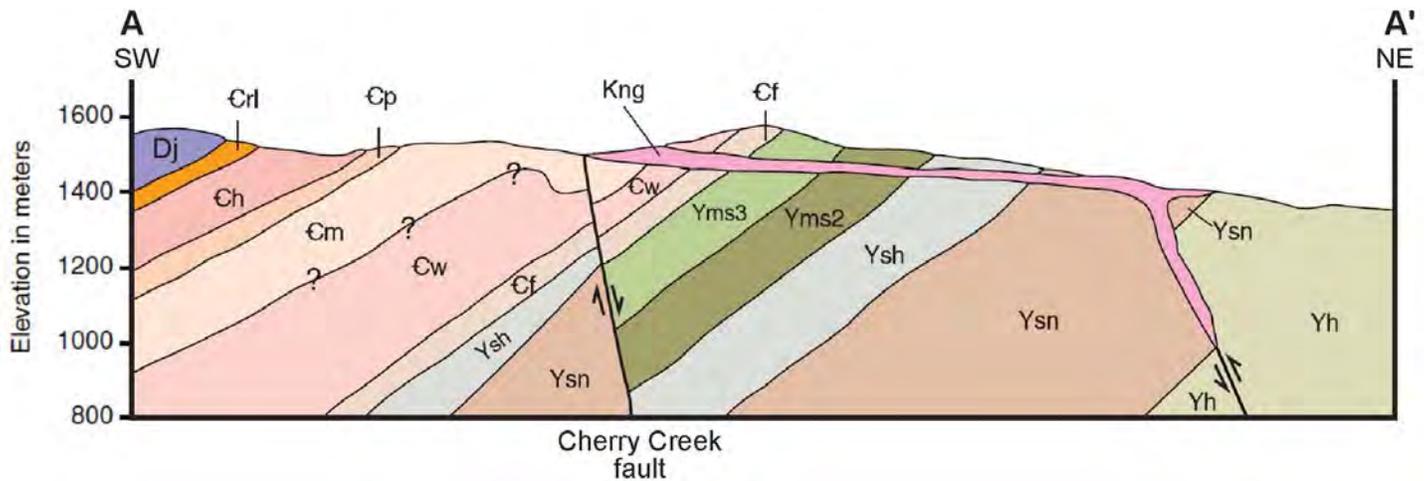
Figure 3. Part of cross section drawn near the field trip route showing the Cherry Creek fault and contrasting Belt stratigraphic sections preserved on both sides. (modified from Berg and Lonn, 2011).

south side, at least 650 m (2,100 ft) of Belt strata are missing and were presumably eroded prior to deposition of the Cambrian Flathead Formation (Berg and Lonn, 2011). This observation confirms Winston's (1986) hypothesis of Late Proterozoic or early Cambrian faulting along the Garnet Line. However, the Flathead Formation cuts gradually down section eastward (fig. 4) north and south of the fault (Wallace, 1987; Lewis, 1998; Reynolds and Brandt, 2005; Berg and Lonn, 2011; McDonald and others, in prep), suggesting that regional westward tilting occurred prior to faulting and erosion. Therefore the Proterozoic fault could have had dip-slip, down-to-the-north movement, or strike-slip, south-side-to-the-west movement. The Phanerozoic fault history shows similar, but less significant, apparent right-lateral offset of the Cambrian Flathead Formation, again indicating either down-to-the-north, or south-side-to-the-west displacement.

Immediately north of the Cherry Creek fault, Belt units from Shepard through the Mount Shields 3 are preserved, but appear to be much thinner (650 m; Berg and Lonn, 2011) than their counterparts farther northwest (1,335 m; Lonn, unpublished mapping, 2011-2012). The thickening to the northwest appears to confirm Winston's (1986) hypothesis that Belt units south of the Garnet Line are relatively thin. However, local Phanerozoic structure is complex, and unrecognized faults could account for some of the thinning.

On this field trip, we will examine the Belt section beneath the Flathead Formation on the

south side of the Cherry Creek fault, then cross the fault to compare it with the Belt section on the north side. We will also scrutinize the unusually thin Shepard-to-Mount Shields 3 stratigraphic section north of the fault and discuss whether it is a primary sedimentary feature resulting from its location on the upthrown side of a Mesoproterozoic growth fault, or whether it results from disruption of a more typical Belt section by Cretaceous and Tertiary faults.
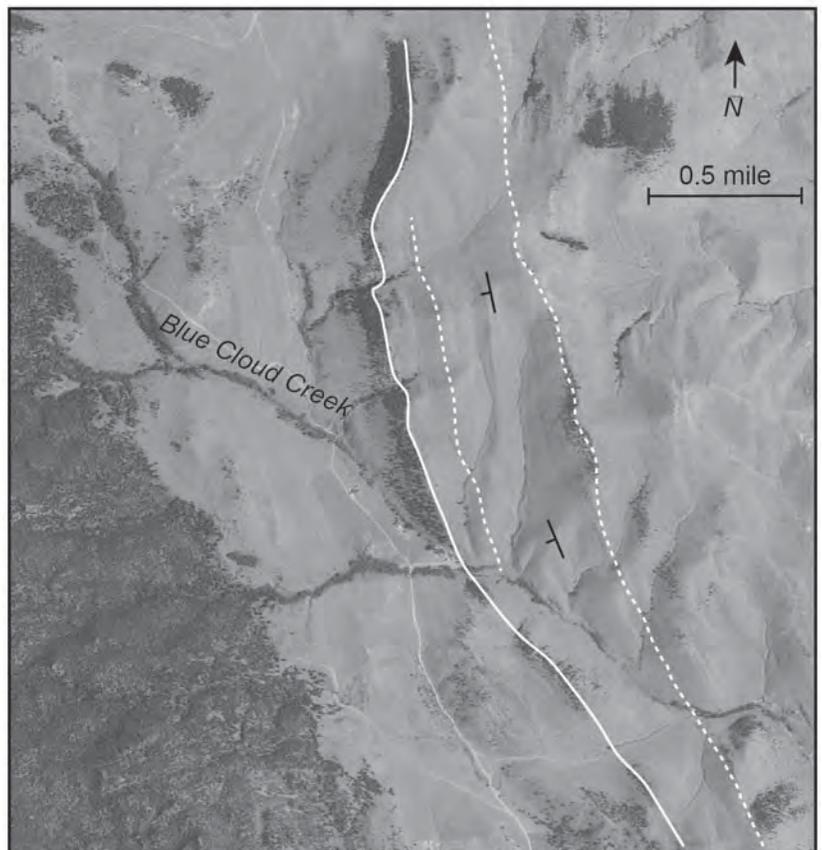

Figure 4. Aerial image from south of the field trip area, showing that the base of the Flathead Fm (solid white line) cuts across Belt strata (beds shown by dotted lines) at an acute angle. All units dip west, so Flathead overlies progressively lower Belt strata eastward.

ROAD LOG

Drive north about 5 miles from the Sunshine Camp to Highway 12, turn right (east) and proceed 15 miles towards Helena. Look for the Baxendale fire station on the left. Turn left (north) just beyond the Baxendale station on the Blue Cloud Road (fig. 5). Drive approximately 5 miles on the ungated road to a major road intersection marked "P" on figures 2 and 5. Park here.

THE HIKE

Follow the route marked by the dotted line (fig. 2) in a counterclockwise direction. First, head southeast to the prominent tree-covered hogback and ascend to its highest point. This hogback is formed by hard quartz-rich sandstone of the Cambrian Flathead Formation. The sandstone's massive bedding makes it difficult to get a bedding attitude here, but figure 4 shows that the Flathead dips slightly less steeply west than the underlying Belt units; thus, it cuts down section eastward.

Descend the northeast side of this hill down section through the bottom of the Shepard Formation—marked by a thin, discontinuous quartzite interval—into the underlying Snowslip Formation. Exposure is poor, but the Snowslip is characterized by interbedded intervals of red quartzite-argillite couplets and dark green siltite to light green argillite couplets and microcouplets. Desiccation cracks and mud rip-up clasts are common. Many argillite beds are colored a distinctive rosy red. The Snowslip also contains beds and lenses of clean white quartzite of well-sorted, well-rounded, coarse, frosted quartz grains. Just to the east of the route, the contact between the Snowslip and the underlying Helena Formation—which contains abundant limestone—is a north-striking, west-directed, reverse fault that is probably Cretaceous in age because it is only slightly offset by the Cherry Creek fault.

Descend to the bottom of the drainage, perhaps encountering a Cretaceous (?) porphyritic granodiorite dike.
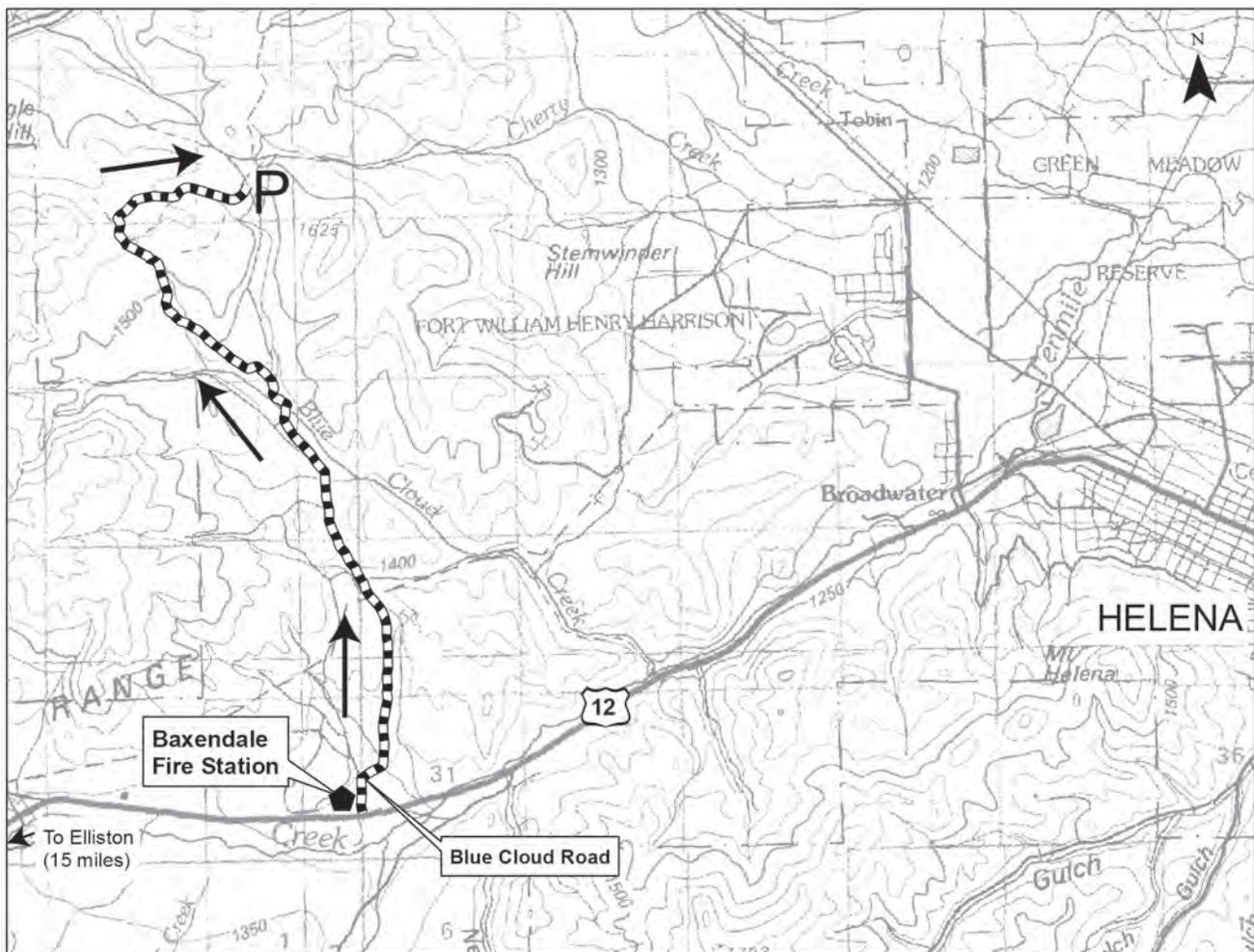

Figure 5. Route to the field trip area is shown by arrows. Park vehicles at location marked by "P". Access requires prior permission from the Prickly Pear Simmental Ranch.

From the Cherry Creek drainage bottom, walk north up the gentle slope towards the eastern high point of the ridge. As you proceed upward, you cross the poorly exposed Cherry Creek fault that has Snowslip Formation on both sides.

The eastern high point of the ridge has been mapped as westward dipping Shepard Formation. The Shepard is characterized by dolomitic and non-dolomitic, dark green siltite and light green argillite in microcouplets and couplets, and lenticular couplets of white quartzite and green siltite. It is poorly exposed, but the Shepard weathers into thin plates that often have a characteristic dolomitic orange-brown weathering rind. Ripples and load casts are common, but mud cracks are rare. Here the Shepard is estimated to be approximately 250 m (800 ft) thick, but just 8 km (5 miles) to the northwest the Shepard is estimated to be 830 m (2,700 ft) thick. Is this the thickening the result of Mesoproterozoic down-to-the-north growth faulting along the Garnet Line, or are there unmapped structures that omit section?

Proceed westward and up section along the ridgetop. Within a few hundred feet, there is a thick interval of light red to gray, flat-laminated to cross bedded, fine- to medium-grained quartzite interpreted to be the Mount Shields Formation, member 2 (Mt Shields 2). At this location it is 180 m (580 ft) in contrast to 460 m (1,500 ft) thick in the Avon area 25 km (15 miles) northwest (Lonn, unpublished mapping, 2011-12). The difference could be attributed to growth faulting along the Garnet Line. Alternatively, we may be observing a quartzite interval within the Shepard Formation, as commonly occurs in the thick Shepard section to the northwest. However, this interpretation would require that there be a fault between this quartzite and the overlying Mount Shields 3.

Continue west along the ridgetop and descend to a saddle. Does the saddle mark a fault? Berg and Lonn (2011) thought so, but did not think it significant. But if it were significant, it could change the stratigraphic interpretation and allow the quartzite mapped as Mount Shields 2 to instead be included in the Shepard Formation.

Beyond the saddle, the rock is comprised of red quartzite-argillite couples and couplets, with abundant mudcracks, mudchips, and well-formed cubic salt

casts. The salt casts are indicative of Mount Shields 3. Therefore, we have either come up section from the Mount Shields 2 into the Mount Shields 3, or we have crossed a fault separating a quartzite interval within the Shepard from the Mount Shields 3. The first alternative, shown on fig. 2, supports the interpretation of Winston (1986) that the Belt section south of the Garnet Line is depositionally thin. The second alternative suggests that an originally thick section may have been thinned by Phanerozoic structures.

Continue westward, up section, to a prominent hogback of Flathead Formation. The exposed thickness of the Mount Shields 3 is estimated to be 220 m (700 ft), but the top is missing due to pre-Flathead erosion. Regardless of which interpretation is used to explain the thin Shepard to Mount Shields 3 stratigraphic section, the Flathead here rests on a different stratigraphic level of the Belt Supergroup than just to the south, across the Cherry Creek valley and fault.

This Flathead hogback can be traced for 25 km northwest to the Avon Valley, and on its way the Flathead gradually ascends through the Belt section; it rests on the Mt. Shields 3 here; the Bonner near Greenhorn Mountain; and the McNamara near Avon (Schmidt and others, 1994; Lewis, 1998; Lonn, unpublished mapping 2011-12; McDonald and others, in prep). The angularity of the unconformity is demonstrated on the regional geologic maps, but is too slight to be observed at the outcrop scale.

Descend south along the spine of the Flathead hogback to its end against the Cherry Creek fault. Turn right (west) and proceed to the obvious Flathead outcrop on the south side of the fault. Here the Flathead overlies the Shepard Formation. The offset in the Flathead, like that in the Belt strata, demonstrates right-lateral, south-side-west movement, or down-to-the-north dip-slip movement. Therefore, there were at least two episodes of movement along the Cherry Creek fault; one in the Proterozoic and one in the Phanerozoic. Each episode had the same sense of movement.

Return to the cars by walking on contour generally southwestward until the flat parking area is reached. We will cross two drainages and outcrops of the Cambrian Wolsey, Meagher, Park, Hasmark, and Red Lion Formations.

REFERENCES

Berg, R.B., and Lonn, J.D., 2011, Geologic map of the Austin 7.5′ quadrangle, central Montana: Montana Bureau of Mines and Geology Open-File Report 603, scale 1:24,000, 1 sheet, 9 p.

Lewis, R.S., 1998, Geologic map of the Butte 1º x 2º quadrangle, southwestern Montana: Montana Bureau of Mines and Geology Open-File Report 363, 16 p., 1 sheet, scale 1:250,000.

McDonald, C., Mosolf, J.G, Vuke, S.M , and Lonn, J.D., in preparation, Geologic map of the Elliston 30′ x 60′ quadrangle, western Montana: Montana Bureau of Mines and Geology Open-File Report, scale 1:100,000.

Reynolds, M.W., and Brandt, T.R., 2005, Geologic map of the Canyon Ferry Dam 30' x 60' quadrangle, west-central Montana: United States Geological Survey Scientific Investigations 2860, 32 p., 3 sheets, scale 1:100,000.

Schmidt, R.G., Loen, J.S., Wallace, C.A., and Mehnert, H.H., 1994, Geology of the Elliston region, Powell, and Lewis and Clark Counties, Montana: U.S. Geological Survey Bulletin 245, 25 p., map scale 1:62,500.

Wallace, C.A., 1987, Generalized geologic map of the Butte 1 x 2 quadrangle, Montana: United States Geological Survey USGS Mineral Investigations Field Study Maps 1925, 1 sheet, scale 1:250,000.

Winston, Don, 1986, Sedimentation and tectonics of the Middle Proterozoic Belt Basin, and their influence on Phanerozoic compression and extension in western Montana and northern Idaho, *in* Peterson, J.A., ed., Paleotectonics and Sedimentation in the Rocky Mountain Region, United States: American Association of Petroleum Geologists Memoir 41, p. 87-118.

THE FINN MINING DISTRICT

Robin McCulloch

Mining Engineer / Consultant, Elk Park, Montana

INTRODUCTION

The field trip will explore the Finn mining district located in the northwest corner of the Avon Valley (fig. 1). The Finn district was historically known as a placer gold producer with a few scattered lode deposits. The source of the gold in the placers was roof-pendant skarns (now mostly eroded) and high-grade quartz feeder veins located in the upper ends of the major drainages. Many of the district's lode prospects contain high grade, low tonnage deposits that are poorly defined through workings and are difficult to follow in outcrop because of deep soil and vegetative cover.

GEOLOGY

The Finn district is underlain by Mesoproterozoic Belt metasedimentary rocks, Cretaceous intrusives, Tertiary volcanics, and Tertiary and Quaternary valley-fill deposits (Lewis, 1998). The predominate structural feature is a range-front fault along the east side of the Avon Valley that separates the Mesoproterozic bedrock from the Tertiary valley fill.

The oldest rock units exposed in the district are the Snowslip, Shepard, and Mount Shields formations of the Mesoproterozoic Missoula Group (upper Belt). The rock consists of quartzite, siltite, argillite, and silty dolomite and limestone. The Belt units underlie the mountains along the north and east side of the district east of the range-front fault, and are the host rock for most of the lode deposits.

The Belt rock was intruded by the Late Cretaceous Dalton Mountain Stock (granodiorite) that forms the north boundary of the district. Small gabbro intrusions (McDonald and others, in prep) border Washington Creek and are associated with local skarns. Smaller intrusions (mostly unmapped or known only from exploration drilling) occur throughout the district. Near the contact with the intrusions, the carbonate-rich Shepard Formation is metamorphosed to a hornfels; other Belt units show fewers effects from the intrusions.

Along the western and northwest boundary of the Finn district, Tertiary volcanic rocks (Eocene and Oligocene) unconformably overlie the Belt rock. The volcanic rock is predominantly dacite, porphyritic dacite, basalt, and minor lithic tuff. Tertiary, fine-grained, valley-fill deposits of the Eocene Renova Formation underlie the southern part of the district. Tertiary alluvial fan and debris-flow deposits overlie the Renova Formation, primarily adjacent to the range-front fault. These deposits host the placer gold. The youngest units in the district are Quaternary surficial deposits.

MINING HISTORY

Placer production in the Finn district was estimated at over $1.5 million (at $20.67/troy ounce) between the discovery in 1865 and 1870 (Raymond, 1870). An additional $294,495 of gold was produced between 1902 and 1968 (McClernan, 1976). Production from Washington Gulch in the 1980s and American Gulch in 2004 is unknown. Production from the lode deposits was not reported.

Early production utilized ground sluicing, as did some of the miners in the 1930s. Dragline and mobile wash plants were used in Buffalo Gulch, Jefferson Creek, and Washington Creek. The middle segment of Washington Creek was reworked in the 1980s utilizing scrapers and hydraulic excavators.

Current operations are confined to a stationary plant at the mouth of American Gulch and at Nevada Creek, near where it enters the Avon Valley. Both sites are near the range-front fault zone but the mining is in Tertiary debris flow deposits.

TERTIARY PLACER DEPOSITS

Tertiary sediments that form most of the placer deposits consist of boulders two to three feet long (1-5%), cobbles three to six inches in diameter (50-60%), and sand, silt and clay. The coarser sediments are
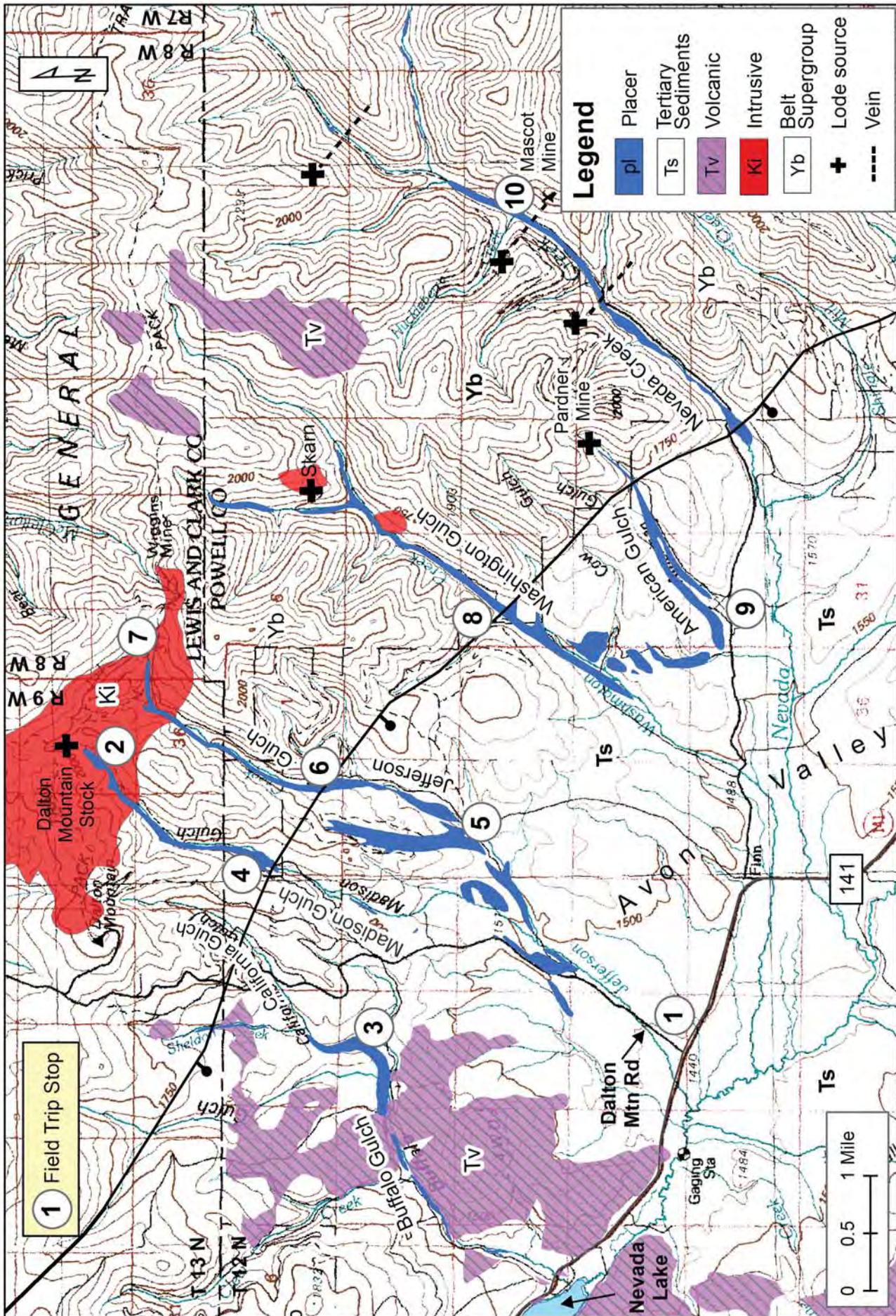
Figure 1. Generalized geology of the Finn Mining District. Field trip stops are shown in circles on the map.

sub- to well-rounded and poorly sorted. The cobbles and boulders are mostly Belt, with some intrusive and volcanic cobbles. The sediments become finer grained with distance from the range-front fault. Large cobble and boulder zones with limonitic clay coatings indicate high energy, braided stream channels (paleo-channels) typical of alluvial fan deposits. These zones are discontinuous, isolated segments on the surface. On a regional scale, the deposits appear to be over-lapping alluvial fans that formed during an extended sheet wash, mass wasting event. Modern streams have reworked and cut through some of the Tertiary depos-its, eroding the surface of some of the fans by about 600 feet.

The placer gold occurs as flakes and nuggets. The flakes are probably from precipitation in fractures and along bedding planes in the shale or carbonate rocks. Some nuggets in American Gulch exhibited crystalline gold while many of the others tended to be massive and somewhat plain. The purity of the gold (fineness) ranges from 875 to 932. This suggests the source is a skarn deposit associated with intrusions into the Meso-proterozoic carbonate rocks. The main intrusion in the district is the Dalton Mountain Stock.

LODE DEPOSITS

Some small lode mines, such as the Pardner Mine in American Gulch and the Humdinger Mine in Madi-son Gulch, are located on these small, discontinuous lodes. They are driven in incompetent rock and are impossible to access in most cases. The upper third of the west-flanking range exhibits roof pendant miner-alization in the Belt carbonate rocks alone the contact with the 2-3 intrusive bodies.

The range-front fault appears to be a minor source of the placer gold although it hasn't been explored for lode targets. The strike length of this potential min-eralization is 7½ miles. The placers indicate that the mineralization in this lode is discontinuous. .

ROAD LOG

The Finn district is located about 25 miles north-west of Elliston. From Elliston, head west 8 miles on Highway 12 to the intersection with Highway 141 at Avon.. Turn north (right) onto Highway 141 and pro-ceed approximately 15.4 miles to the turnoff to Dalton Mountain Road. Turnoff is on the right side (east) and

is marked by a small, brown USFS sign. Pull off road and park for Stop 1.

| STOP 1 | **Finn District/Geology Overview** |

Stop 1 will be a quick geologic summary and field trip overview. Figure 1 shows the location of the plac-er deposits, general geology, and field trip stops. Parts of this field trip are on private property and required prior permission.

| STOP 2 | **Deer Lodge Lode, Madison Gulch** |

The extensive placer deposit in this area extends from the scarn to just below the Deer Lodge lode. The Deer Lodge lode is collared in a feeder vein in the granodiorite of the Dalton Mountain Stock.

| STOP 3 | **Buffalo Gulch** |

Little of the gulch has been worked. Near the mouth of the Clear Creek drainage (lower Buffalo Gulch), handwork and ground sluicing were carried out next to hay ground in an area of less than an acre. Upstream, less than a mile away, a cable shovel with a mobile wash plant processed gravel in the bend of the creek in 1938. A total of 35,967 cubic yards was washed yielding 230 ounces of refined gold. At today's price, it would have yielded $2.68 per cubic yard. The workings do not indicate that the operation stripped the waste before washing. Extensive ground sluicing occurred on the toe of the ridge near where the Clear Creek/Buffalo Creek road leaves the creek bottom to access the Dalton Mountain road. The workings indicate a substantial paleo-channel that was worked where water was available. The hand workings and boulders on the hillside indicate the pay zone is likely perched on the hillside more than 100 feet north of the present stream. There is no indication that either the present drainage or paleo-channel has been tested in more recent times.

| STOP 4 | **Humdinger Mine, Madison Gulch** |

At the Humdinger Mine, the placer occurs in a paleo-channel deposit on a bench on the east side of the creek and continues up the drainage to the north. Downstream from the mine, near the range-front fault, the paleo-channel exists on the west side between the creek and the road. The paleo-channel, where ex-posed, is about 30-40 feet wide and 6-9 feet deep. Few

resources appear to remain where it is exposed but excavation may discover enough for a small operation. The stream bottom is unworked.

Continuing downstream, no obvious evidence of mining exists until near the divide between Jefferson and Madison creeks where a small portion of a paleo-channel has been worked. Near where the Dalton Mountain and Jefferson Creek roads split, a portion of the braided stream environment has been worked. East and west of the Dalton Mountain road, for the first half mile above where the two roads fork, an old channel was worked by ground sluicing. Below that, 10-12 acres were stripped with horse slips and about a third of the area was worked but none to bedrock. Clay coloration and cobble size indicate a channel exists but the workings show everything was processed regardless of value.

Farther down (south) on Jefferson Creek, a dragline processed gravel through a plant until the paleo-channel was crossed and the gold ran out. The dragline was then moved farther up Jefferson Creek where mining resumed. Sizable resources may still exist in this area but will require substantial testing to identify the economic gravels.

STOP 5 | Middle Jefferson Gulch

The middle part of Jefferson Gulch was heavily worked with a dragline. The lower end of this area is hay fields and likely has limited gold resources as it consists of silts and clays and may be beyond the transport distance of the gold. Most of the stream-reworked ground has been mined in this area. Hillside gravels have been ground sluiced but no machine work is in evidence. Consequently, a large volume of gravel exists but must be tested to determine if the grade is adequate for a profitable operation.

STOP 6 | Range-front fault, Jefferson Gulch

The range-front fault has been exposed in a 90-foot deep pit along Jefferson Creek. The vertical offset of the gravel on either side of the fault is about 95 feet. Rocks removed from the excavation show brecciation with cinnabar, gold and native mercury. Northeast of the fault, for about two mile,s are indications of tensional en echelon faults. Through the placer exca-

vation and lode exploration, it is apparent that two or three of these faults exist. Some faults created a fissure that was filled with quartz; in others, the porosity created allowed hydrothermal alteration of the country rock that resulted in limonite and manganese flooding of adjacent areas. Much of the drainage above the fault has been ground sluiced and some pay- gravel remains. It is likely that high-grade pockets remain below some of the fault zones. It is also probable that much of the remaining gravel is low grade and would need to be tested prior to mining to ensure profitability.

STOP 7 | Upper Jefferson Gulch

Placer mining extended to near the headwaters of Jefferson Gulch. Some areas are still being worked. Near the headwaters of Jefferson Creek, the contact between the Dalton Mountain Stock and carbonates of the Shepard Formation of the Belt Supergroup is exposed. The nearby Wiggins Mine is developed along the contact.

STOP 8 | Washington Gulch

The lower part of Washington Creek was heavily worked with a dragline and plant in the 1930s. The middle part was worked with a dragline and wash plant, then again with scrapers and finally excavators. Resources are indicated on the southeast side of the creek and extend about 600 feet up the hillside. Some of this was worked by hand but little has been tested.

Along the range front fault, a dry drainage extends northwest from the creek for about 1 mile. This drainage was ground sluiced. To the south and southwest, including part of Cow Gulch, the area was worked by shallow (5-8 ft deep) ground sluicing wherever sufficient water was available. Extensive, untested gravel deposits remain in this area. Excavations have shown intermittent paleo-placers interfingering with volcanics that contain gold, similar to the lower Gold Creek/Pioneer District placer deposits in Powell County.

In the upper part of Washington Gulch, the creek splits into two drainages. Workings extend up both drainages for at least ½ mile. The source of the gold in these drainages appears to be a skarn in the Belt carbonate. In the lower third of the left fork, the pay channel is on the right side of the creek. Farther up, it is on the left side. A landslide buried the placer mid-

way up the drainage. Above the landslide, most of the mining was done by hand. Along the right fork, current operations are mining the remaining resource. The resource appears to be 10-15 feet wide and about as thick and is confined to the left (north) side of the creek.

STOP 9 | American Gulch

The placer deposits in American Gulch were primarily mined by ground sluicing. Many of the workings continue well up the south hillside to the edge of the old ditch that brought water for the sluicing operations. These spots are 100 to 200 feet above the creek bottom. Placer resources continue up the drainage to the Pardner Mine but the volume produced is limited on the east side of the range-front fault.

Placer mining in this drainage is-and has been-limited by a shortage of water. Additional testing is critical to understanding the economics of this deposit. Drilling has identified multiple intrusive bodies but limited lode resources.

STOP 10 | Nevada Creek

Like the rest of the district, placer mining activity decreases rapidly once you cross to the east side of the range-front fault. The most significant lode source was the quartz gold deposit found at the Mascot Mine located on the south side of the lower portion of the deposit. Production was early in the last century through a gravity mill. A paleo-placer exists on the south fork of the drainage east of the USFS cabin, on the east side of the creek. It contains a small amount of yardage and no indication of mineralization exists above that point.

Gold is easily panned along the creek below the fault. There are significant volumes of gravel but ranching has limited development of placer reserves. Most of the area is untested. The fault continues to the southeast but the mineralization does not appear to continue much past Nevada Creek.

REFERENCES

Lewis, R.S., 1998, Geologic Map of the Butte 1°x2° quadrangle, southwestern Montana: Montana Bureau of Mines and Geology Open File Report MBMG 363, 16 p., scale 1:250,000.

McClernan, H.G., 1983, Metallic mineral deposits of Lewis and Clark County, Montana: Montana Bureau of Mines and Geology Memoir 52, 73 p., 1 sheet.

McDonald, C., Mosolf, J.G., Vuke, S.M., and Lonn, J.D., in preparation, Geologic map of the Elliston 30′ x 60′ quadrangle, west-central Montana: Montana Bureau of Mines and Geology Open-File Report, 1 sheet, scale 1:100,000.

Raymond, R.W. (compiler), 1870, Statistics of mines and mining in the states and territories west of the Rocky Mountains. [for 1869], 2nd report: United States Treasury Department, Government Printing Office, Washington, D.C., 805 p.

ORIGIN OF EOCENE VOLCANIC ROCKS AT THE SOUTH END OF THE DEER LODGE VALLEY, MONTANA

Kaleb C. Scarberry,[1] Stanley L. Korzeb,[1] and M. Garrett Smith[2]

[1]Montana Bureau of Mines and Geology, Butte, Montana; [2]Montana Department of Environmental Quality, Helena, Montana

ABSTRACT

This road log describes Eocene volcanic rocks northwest of Butte, Montana. Outcrops of tuff, lava, and breccia cross Interstate 90 (I-90) and exhibit a wide range in texture and composition. The composite section of volcanic rocks is 800 m thick and is the remnant of two ignimbrite sheets. A 12-km2 rhyodacite vent complex north of I-90 erupted most of these deposits at ~ 52 Ma. A 6-km2 andesite-dacite lava dome formed south of I-90 at ~ 50 Ma. Mineral deposits formed in association with extensional block faults, volcanic vents, and fissures. We present a model that ties these deposits to upper crustal magmatism in an extensional environment.

INTRODUCTION

The Sevier fold and thrust belt hosts Late Cretaceous – Eocene igneous rocks west of where it bends, and intersects the Great Falls Tectonic Zone and the Lewis and Clark Line (fig. 1, inset map) (see Vuke and others, 2007). The igneous rocks, in part, represent the Late Cretaceous volcanic arc in southwestern Montana. Extension of the arc began between 62 and 53 Ma. Block faults cut ca. 62 m.y. old Cu – Mo mineralization at Butte (Houston and Dilles, 2013). East of Butte, block uplift began at ~ 55 Ma at Bull Mountain, north of the Golden Sunlight (DeWitt and others, 1996). Southeast of Butte the Absaroka volcanic field near Yellowstone National Park (fig. 1), formed during extension c.a. 55 – 52 m.y. ago (summary in Feeley and others, 2002). Northeast of Butte, extension began prior to 53 Ma near the Montana Tunnels mine (Sillitoe and others, 1985). West of Butte, detachment faulting accompanied volcanism at 53 Ma near Anaconda (summary in Lonn and Elliott, 2010).

The Lowland Creek volcanic field (fig. 1) contains two ignimbrite sheets (fig. 2) that erupted between 53 - 49 Ma (Smedes, 1962; Smedes and Thomas, 1965; $^{40}Ar/^{39}Ar$ ages from Dudas and others, 2010)

that record caldera-forming eruptions (Foster, 1987). The basal ignimbrite is lithic-rich rhyolite (70.1 -72.9 wt. % SiO2; fig. 3) deposited at 53 Ma (Table 1, fig. 3; ^{40}Ar-^{39}Ar age from Dudas and others, 2010). The upper ignimbrite is a porphyry rhyodacite (65.0 -73.3 wt. % SiO2). The ignimbrites are capped by andesite - dacite lavas (61.6 wt. % SiO_2) and intruded by rhyolite dikes (72.2 wt. % SiO2) (fig. 2, Table 1). Periods of limited volcanic activity from 52.5 to 50.0 Ma separate the pyroclastic eruptions.

ROAD LOG

There are seven stops on this field trip. Stop 1 provides a structural overview of the southern Deer Lodge Valley. Stop 2 looks at an Au- and Ag-bearing rhyolite breccia at the Tuxedo Mine, and stops 3-7 examine vent proximal volcanic deposits.

This field trip begins at Elliston, Montana and ends east of Butte, Montana. From Elliston, drive west on U.S. Highway 12 21.5 miles to where it joins I-90 at Garrison Junction. Take southbound I-90 for 36.3 miles and take exit 211 (Fairmont Road). Turn right at the stop sign. Follow Fairmont road for 2.8 miles, passing the Fairmont resort. Turn left on to Shirley Way and drive for 1.1 miles. Turn right on to the dirt road and follow for 0.3 miles to a water tower.

STOP 1 | Geologic overview of the southern Deer Lodge Valley

Stop 1 is near the contact between the Late Cretaceous Boulder Batholith and the Eocene Lowland Creek volcanic field (fig. 1). Northeast-striking block faults controls the contact between Late Cretaceous and Eocene rocks. The contact lies within the Great Falls Tectonic Zone (O'Neill and Lopez, 1985) (fig. 1). We are standing on Late Cretaceous granite in the footwall block of a northeast-striking, north-dipping, normal fault. Over a km of Eocene volcanic deposits and sediment (Konizeski and others, 1968) cover
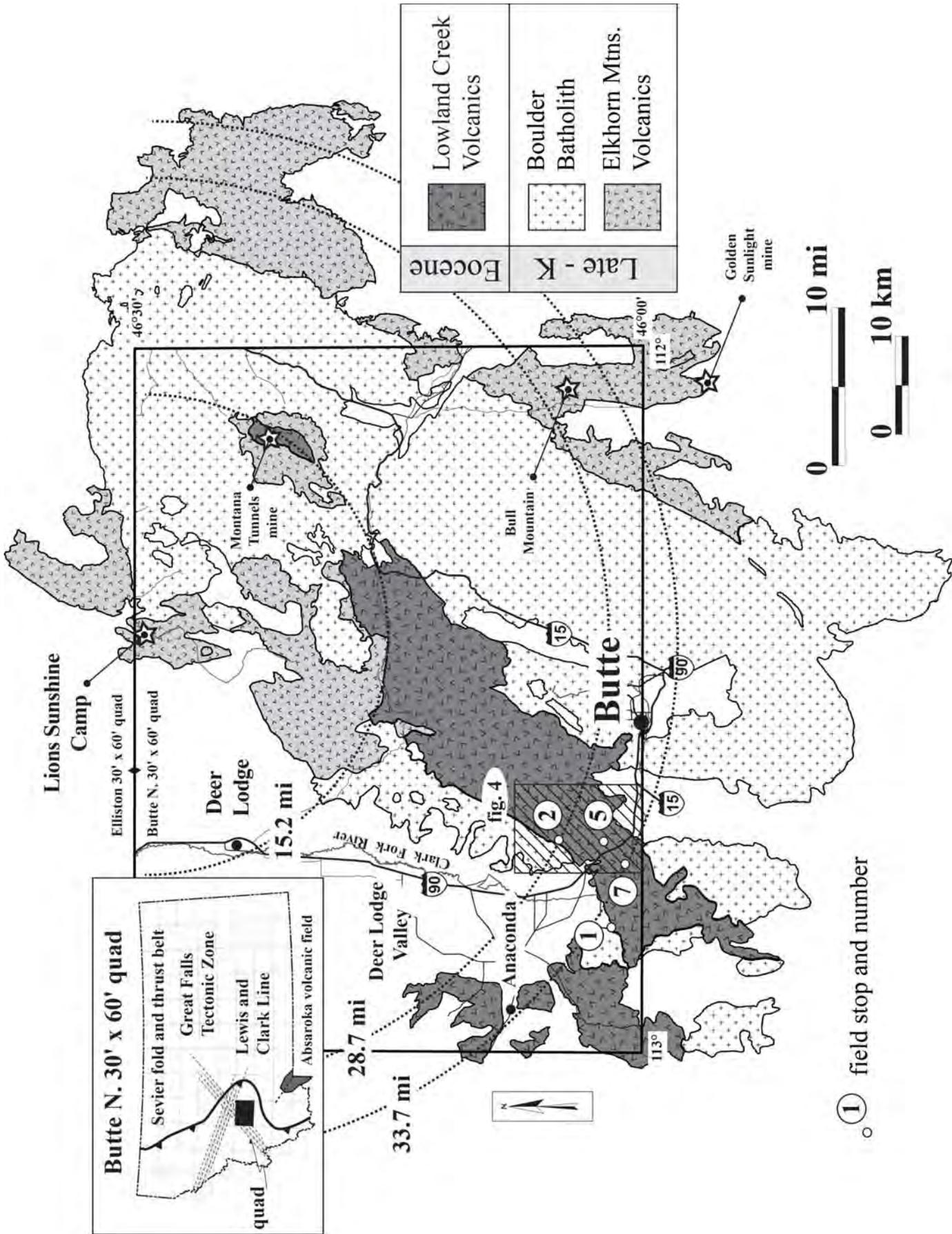
Figure 1. Late Cretaceous – Eocene igneous geology near Butte, MT. Also shown are the location of selected field trip stops, mineral deposits, and mountain blocks discussed in the text. See Figure 4 (inset) for detailed locations of stops 2 through 7. Geology modified from Vuke and others (2007).
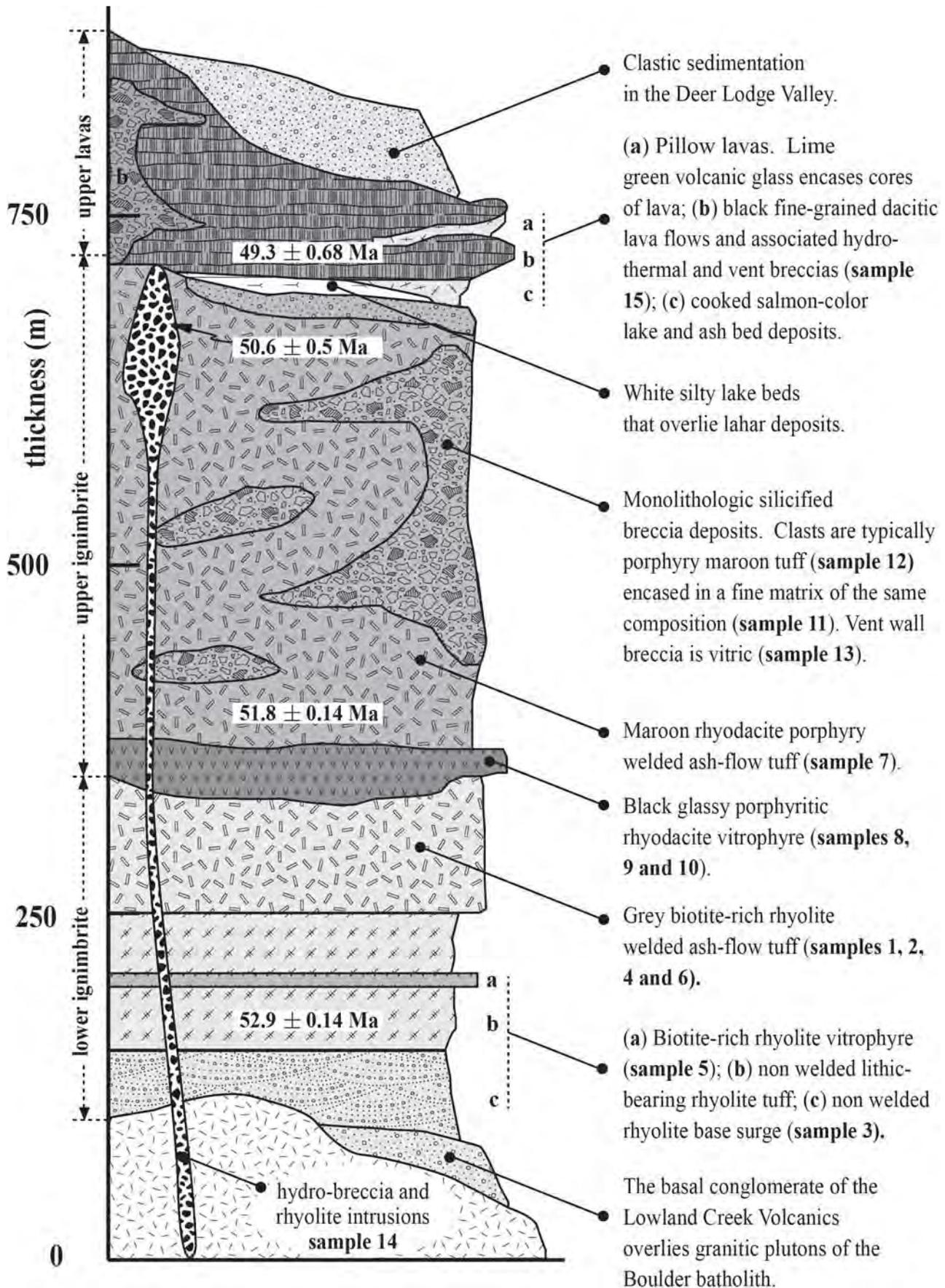
Figure 2. Composite section of Eocene volcanic rocks exposed west of Butte. Rock type data, and sample locations are shown on figures 3 and 4. Three eruptive cycles, the basal ignimbrite, upper ignimbrite, and upper lavas, occur in the section. The preferred age of ignimbrites and upper lavas are the ^{40}Ar-^{39}Ar ages of Dudas and others (2010). A preliminary U-Pb age of 50.6 ± 0.5 Ma is assigned to a rhyolite dike that cut the ignimbrites (sample 14, fig. 4).

the hanging wall block of the fault in the valley. North-striking Miocene Basin and Range faults (e.g., Reynolds, 1979) cut northeast-striking block faults. This fault intersection controlled basin formation and sedimentation in the southern Deer Lodge Valley.

To our south and west are hills formed from the basal ignimbrite of the Eocene volcanic field (fig. 2). To the northeast, across the southern end of the Deer Lodge Valley, you can see hills underlain by the upper ignimbrite of the 800 m thick volcanic package. The entire volcanic field is buttressed onto the Boulder Batholith (figs. 1 and 2).

The volcanic pile is compositionally zoned, from rhyolite at the base, to rhyodacite and to dacite-andesite lavas at its top (figs. 2 and 3). Together the rocks form a calc-alkaline igneous suite (fig. 3B). Breccia deposits are abundant and in most cases formed near vents (figs. 4 and 5).

Immediately to our northeast is Fairmont (Gregson) hot springs. Hot spring water is 71° C at the resort and around 129° C in its subsurface reservoir (Metesh, 2000). The location of the geothermal resource is controlled by the local fault geometry. Intersecting northeast- and north-striking fault zones allow for deep (4.3 km), and slow, groundwater circulation, if we assume a regional geothermal gradient of 30° C/km (Sonderegger, 1984).

STOP 2   The Tuxedo Mine

From stop 1, drive north on Shirley Way to where it intersects Fairmont road. Turn right on Fairmont road. Drive east on Fairmont road for 2.8 miles and cross over I-90. At the stop sign, turn northwest onto Bossard Road and drive for 0.2 miles to where the road splits. At the split, take the east road and drive for 0.9 miles. Turn north onto the dirt road, drive past a house on the left, and continue for less than 0.2 miles to a gate. Go through the gate and close it behind you. Continue northeast along the well-worn dirt road for 1.6 miles to a locked gate. Turn hard right and drive 0.4 miles uphill to the south on a less-worn road. Park near the old mine yard. Note: Stop 2 is on private property, and access requires landowner permission.

The Tuxedo Mine is at the Late Cretaceous Boulder Batholith – Eocene Lowland Creek volcanics

contact (fig. 1) where Au and Ag occur in silicified rhyolite breccia (fig. 4, Table 1: samples 16a and b). Mining occurred from 1920 to the 1950's. At the height of activity, operations consisted of a 30 m shaft and head frame intersected by two adits (both now caved). The Porter Tunnel in the hillside below the shaft collar, yielded Au values of 6 oz./ton. Company logs describe native gold occurrences and the property was of interest to mineral exploration companies as recently as the 1980's. Silver minerals include ruby silver (proustite and pyargyrite), and argentite, and occur in onionskin-textured chalcedony bands.

The deposit formed during fumarole activity along an Eocene fissure. Several generations of quartz indicate that repeated cycles of crack and seal occurred along the structure. Hydrothermal circulation resulted in silicification and chalcedonization of permeable clay zones. The principal ore is hydrothermal breccia set in a microcrystalline blue-gray quartz matrix. High-grade ore occurs in a 1 m zone that widens outward to 120 m, and decreases in grade. An estimated 6 million tons of mineralized rock follows the northeast-trending ridgeline (fig. 4).

STOP 3   Basal ignimbrite

From stop 2, turn around and follow the dirt road downhill, to the northeast, for 0.4 miles. Stay left, and continue to follow the road downhill for 1.5 miles to the gate. Go through the gate and close it behind you. Continue for 0.3 miles, past the house on your right, to a T in the road. Turn right and drive west on Craddock road for 1.1 miles and exit onto southbound I-90, towards Butte. Drive for 5 miles and take exit 216 (Ramsay). Turn left, at the stop sign and cross over I-90. Driving northwest, the road bends sharply to the northeast after 0.6 miles. Continue on this road for 1.6 miles, where it T's. Turn right at the T, and follow the winding gravel road north for 1.7 miles. Park along the side of the road, and hike ~ 0.1 miles northeast to our lunch spot. Note: Stop 7 is on private property, and access requires landowner permission.

Stop 3 provides exposures of semi- to completely welded ash-flow tuff that forms the top of the basal ignimbrite (Figure 2). The welded ash-flow tuff is rhyolite (fig. 3, Table 1: samples 1, 2, 4, and 6), and contains abundant quartz and biotite phenocrysts. It's exposed over 10 km2, and forms the southwestern wall of an Eocene vent complex (fig. 4).
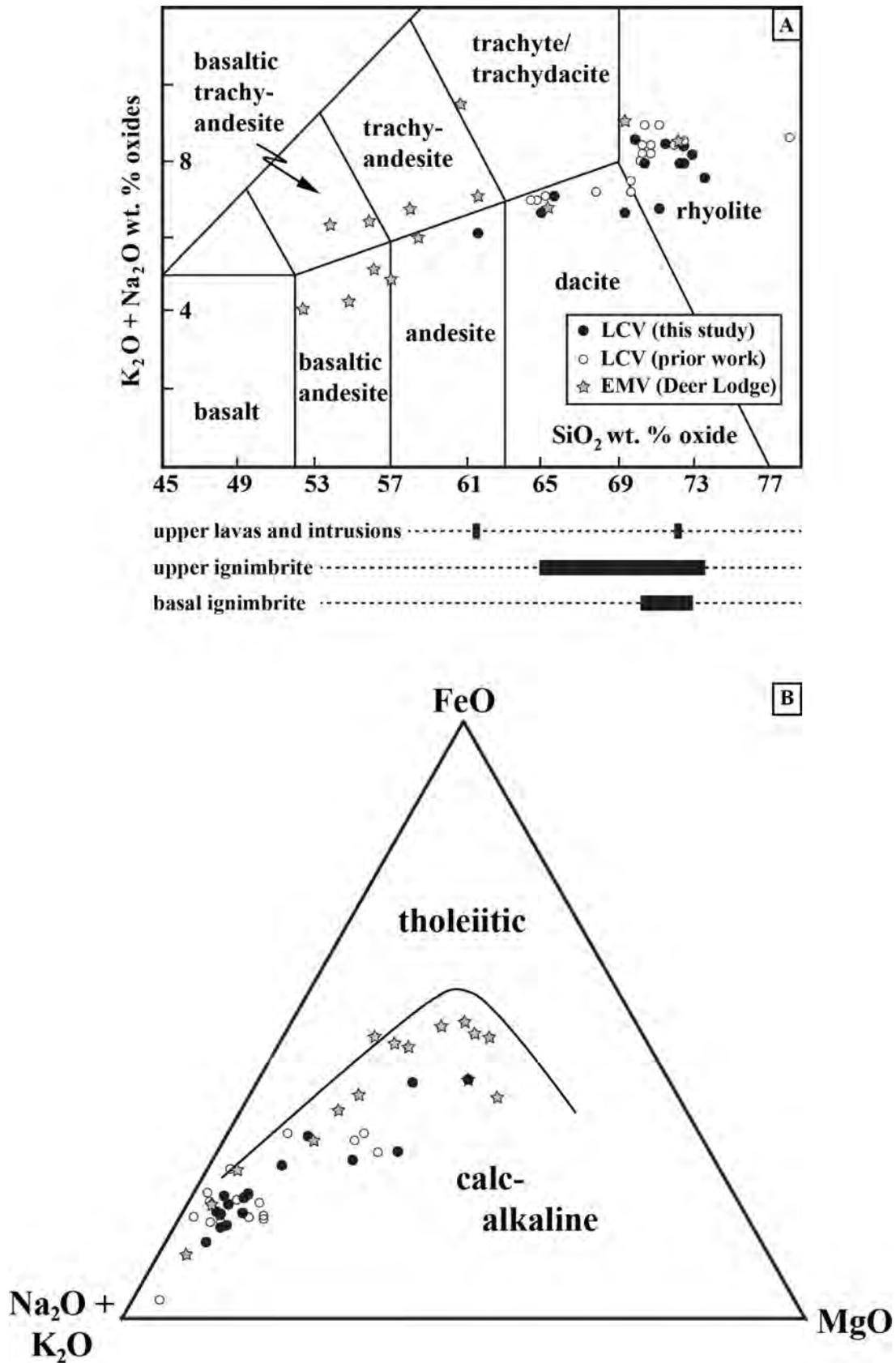
Figure 3. (A) Volcanic rock types after Le Maitre and others (1989). Compositional variability among Eocene eruptive cycles (Figure 2) is highlighted (t = time). (B) Ternary major oxide plot shows the boundary between the calc-alkaline and tholeiitic fields, after Irvine and Baragar (1971). Source of data - (LCV) Lowland Creek Volcanics: Derkey and Bartholomew (1988) and Dudas and others (2010). (EMV) Elkhorn Mountains Volcanics: Scarberry, in preparation.
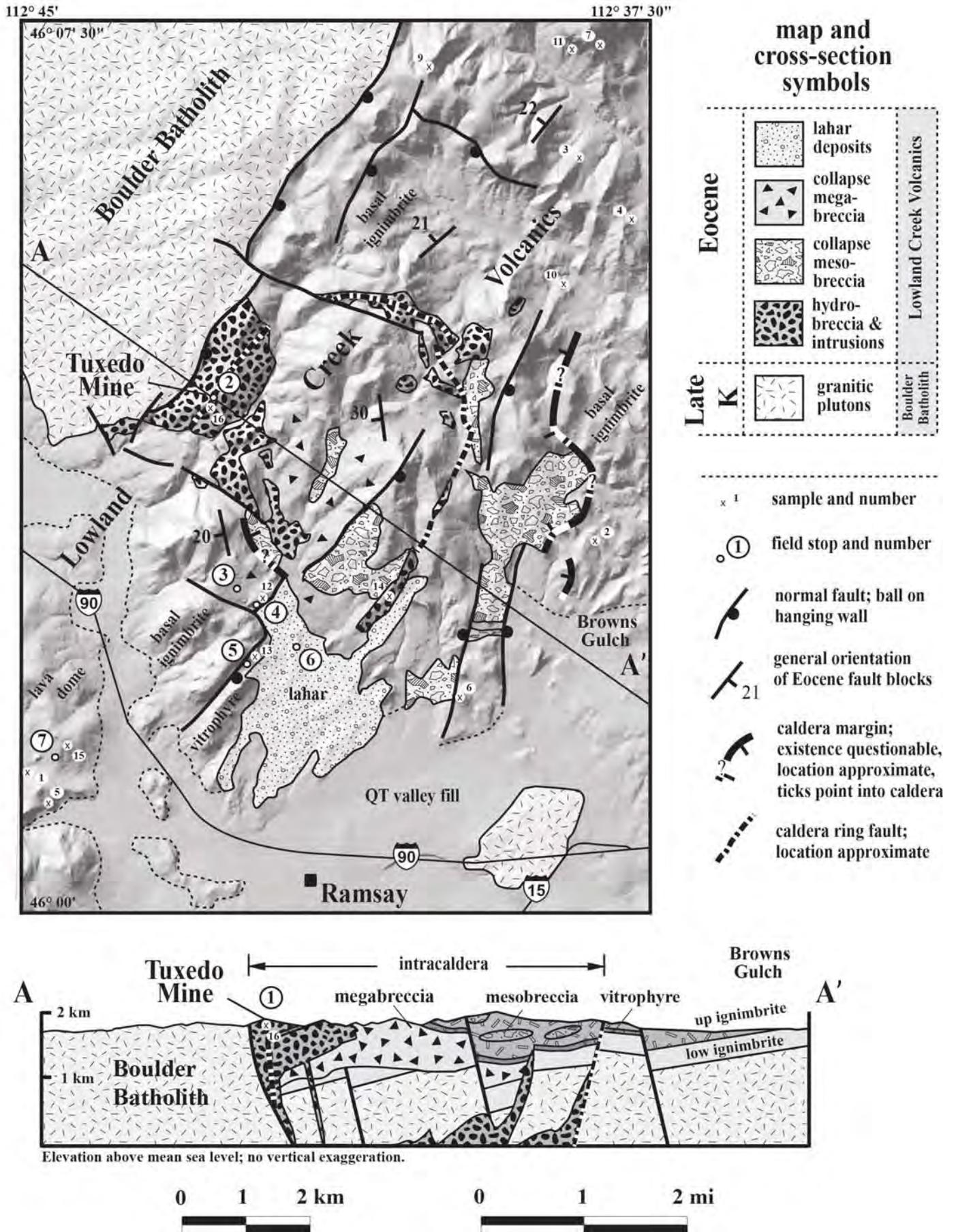
Figure 4. Geologic map and cross-section for an Eocene vent complex exposed in the Ramsay 7.5′ quadrangle.
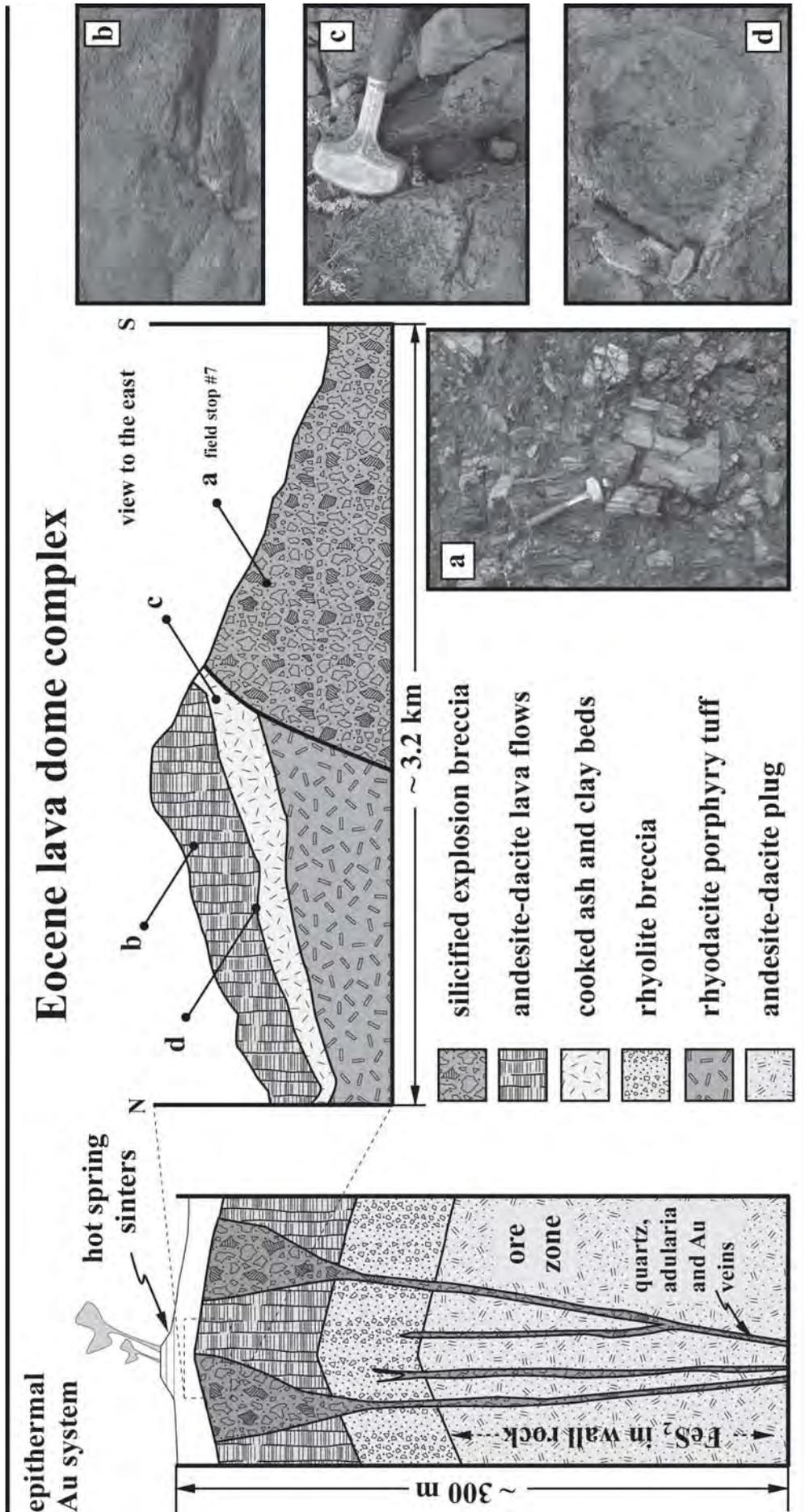
Figure 5. Schematic cross-section of an Eocene lava dome exposed south of I-90 in the Ramsay 7.5' quadrangle (stop 7, see fig. 4 for location). Description of photographs: (a) silicified explosion breccia, (b) vesicular lava flows, (c) cooked ash and clay beds with egg-shaped quartz bubble, and (d) pillow lava with core of vesicular lava mantled by rim of glass. Schematic cross-section of epithermal Au system is after Silberman (1982).

*sample #	1	2	3	4	5	6	7	8	9	10	11	12
strat (fig.2)	bas ignimbrite	bas ignimbrite	bas ignimbrite	bas ignimbrite	bas ignimbrite	bas ignimbrite	up ignimbrite	up ignimbrite	up ignimbrite	up ignimbrite	up ignimbrite	up ignimbrite
rock type	welded tuff	welded tuff	surge deposit	breccia	vitrophyre	welded tuff	welded tuff	vitrophyre	vitrophyre	vitrophyre	breccia matrix	breccia clast
lat.	46.01824	46.05260	46.11133	46.10036	46.01292	46.03030	46.12350	46.10271	46.11941	46.09067	46.12284	46.04192
long.	-112.75096	-112.64037	-112.64425	-112.63442	-112.74387	-112.66019	-112.63789	-112.69122	-112.66928	-112.64260	-112.64181	-112.70344
XRF (wt. %)												
SiO_2	71.15	72.70	72.92	72.50	70.09	71.23	70.56	65.59	69.63	64.96	70.73	73.30
TiO_2	0.41	0.31	0.30	0.35	0.37	0.37	0.35	0.53	0.48	0.52	0.34	0.29
Al_2O_3	15.10	14.54	14.62	15.01	15.47	15.19	15.64	16.18	15.75	16.04	15.72	14.54
**FeO_T	2.65	1.57	1.26	1.59	2.08	2.05	2.23	3.48	2.29	3.86	1.89	1.53
MnO	0.02	0.02	0.03	0.01	0.03	0.02	0.02	0.05	0.04	0.07	0.02	0.01
MgO	1.11	0.75	0.66	0.77	1.04	0.71	0.89	2.81	0.90	3.73	0.90	0.73
CaO	2.91	1.82	1.88	1.77	2.25	1.96	2.28	4.18	2.50	4.29	2.41	2.03
Na_2O	3.63	3.97	3.78	3.82	3.75	3.98	4.22	4.03	3.73	3.90	4.29	3.94
K_2O	2.91	4.24	4.41	4.06	4.79	4.37	3.69	3.00	4.46	2.50	3.58	3.56
P_2O_5	0.12	0.09	0.14	0.11	0.11	0.11	0.12	0.14	0.22	0.13	0.11	0.07
LOI	2.66	0.62	0.74	1.45	2.06	1.04	1.08	1.56	2.64	2.45	1.10	1.14
a.t.	97.04	99.04	98.56	97.39	96.95	98.19	97.95	98.03	96.11	97.14	98.21	98.64
Trace elements (ppm) (XRF)												
Ni	28	7	4	8	15	6	15	39	3	61	13	10
Cr	67	19	7	23	32	21	30	93	7	123	33	22
Sc	7	3	4	3	4	3	4	9	5	9	5	3
V	38	23	21	28	33	29	29	65	37	64	30	28
Ba	932	1102	1073	1146	1326	1189	1232	1144	2180	1014	1221	1161
Rb	74	160	198	148	145	160	108	84	121	84	104	112
Sr	632	386	423	396	505	419	569	677	756	646	612	576
Zr	119	151	149	168	193	192	140	149	184	141	140	124
Y	9	7	11	8	8	10	8	11	10	11	7	9
Nb	7	12	12	14	19	12	9	8	10	8	10	8
Ga	19	23	19	22	22	23	23	21	19	20	22	20
Cu	11	8	6	5	5	6	8	16	5	7	8	7
Zn	65	58	45	43	59	65	57	61	65	63	50	45
Pb	18	28	32	25	28	25	28	20	24	21	28	24
La	23	40	47	44	54	58	36	26	55	25	29	31
Ce	38	63	76	73	85	79	60	48	103	46	49	47
Th	6	19	23	21	24	23	11	7	17	7	11	10
Nd	19	21	30	25	29	33	22	18	38	17	18	19
U	1	5	9	5	4	4	3	3	4	3	3	2

*sample #	13	14	15	***error
strat (fig.2)	up lava	cuts up ignim	up lava	%
rock type	breccia clast	dike	lava flow	
lat.	46.035258	46.04545	46.021801	
long.	-112.702	-112.6752	-112.7418	
XRF (wt. %)				
SiO_2	69.39	72.15	61.60	0.64
TiO_2	0.50	0.37	0.90	0.54
Al_2O_3	14.99	14.59	16.09	0.37
FeO_T	3.51	2.06	6.23	2.09
MnO	0.03	0.02	0.07	0.22
MgO	1.38	0.67	3.61	0.71
CaO	3.47	2.11	5.26	0.71
Na_2O	3.72	4.00	3.53	0.75
K_2O	2.88	3.92	2.51	0.59
P_2O_5	0.13	0.12	0.20	0.90
LOI	2.84	1.65	1.95	0.04
a.t.	95.74	98.12	97.52	0.65
Trace elements (ppm) (XRF)				
Ni	81	14	73	0.6
Cr	156	32	108	1.4
Sc	10	6	11	13.7
V	50	25	91	1.9
Ba	935	1017	1026	1.0
Rb	79	164	63	0.3
Sr	549	386	598	0.4
Zr	127	179	181	0.6
Y	11	7	23	1.9
Nb	8	18	11	7.1
Ga	19	21	20	1.0
Cu	19	12	35	2.2
Zn	60	70	99	3.2
Pb	19	29	13	1.7
La	25	43	55	5.8
Ce	43	70	75	0.5
Th	7	22	9	17.3
Nd	20	24	40	9.6
U	4	4	2	51.2

	16a	16b
TUXEDO MINE	cuts up ignim. red breccia	cuts up ignim. yellow breccia
ICP-AES (ppm)		
Au	0.247	0.765
Ag	2	254
As	1030	401
Ba	12.6	31.5
Bi	0.075	0.162
Cu	76.7	49.5
Hg	1.62	0.44
Mo	4.2	7.7
Pb	8.2	20.7
Sb	39.4	18.6
Sr	4.00	11.9
Te	0.04	0.01
Zn	49.4	10.5

Analytical notes:

LOI = Loss on ignition

a.t. = analytical total

Samples 1–15 analyzed by X-ray fluorescence (XRF) at the Peter Hooper Geoanalytical Laboratory at WSU. Samples 16a and b analyzed by inductively coupled plasma atomic emission spectroscopy (ICP-AES) at ALS Global Corporation.

*Refer to figures 2 and 4 for additional sample details.
**All Fe expressed as Fe^{2+}
***Error (%) calculated from duplicate sample runs.

STOP 4 | Vent wall breccia

From stop 3, turn around, and head southeast along the gravel road. Pull off after 0.4 miles and hike ~200 feet northwest to a breccia outcrop.

Stop 4 provides views of the wall of an Eocene vent complex (fig. 4). The outcrop consists of silicified breccia. Clasts in the breccia are the basal ignimbrite (fig. 2 and 3; sample 12 in Table 1). The monolithologic breccia formed in place, and at the wall of the vent. To the southeast, a normal fault truncates the basal ignimbrite, and a lahar deposit covers the vent wall (Figure 4).

STOP 5 | Vent wall unconformity

From stop 4, continue southeast on the road for 0.1 miles and turn west onto Tenderfoot Trail. Follow the road west for 0.5 miles and park. Hike 200-300 feet south to a high point on the ridgeline where you have a view to the north and the south.

This stop is at the contact between the basal and upper ignimbrites (fig. 2). The contact is a vent wall exposed by post-volcanic, northeast-striking and down to the south, block faults. The top of the basal ignimbrite, exposed north of the road, is fractured, and brecciated. Vitrophyre of the upper rhyodacite ignimbrite is exposed south of the road and appears to be unusually thick. Both ignimbrite deposits have a steeply dipping cleavage. Vent collapse and an ensuing caldera eruption explain deformation cleavage in the ignimbrites, and intense welding of the upper ignimbrite (vitrophyre), at this stop.

A rhyolite dike is visible ~ 1 km northeast of stop 5 (fig. 4). The dike cuts the upper ignimbrite (Figure 2), and indicates that the vent observed at stops 2, 4, and 5 (fig. 4) formed prior to the 50.6 ± 0.5 Ma (preliminary U-Pb age) dike rock.

STOP 6 | Lahar

From stop 5, turn around, and follow Tenderfoot Trail to the northeast for 0.5 miles. Turn right when the road T's and drive east for 0.7 miles. We are driving into a lahar deposit that formed on a flank of the Eocene vent (fig. 4). Look at the deposits along the roadside.

At this stop moderate- to weakly-cemented volcanic debris overlies the upper rhyodacite ignimbrite (fig. 2). Lapilli, mud, and ash encase subangular to subrounded volcanic clasts. The clasts include black vitrophyre, maroon porphyry rhyodacite tuff, and gray biotite-rich porphyry tuff. These lithologies underlie the upper lavas in the volcanic section (fig. 2). Clasts of rhyolite are absent in the lahar, meaning that it formed between ~ 51.8 and 50.6 Ma.

The deposit could be interpreted as a hanging-wall landslide breccia. It is nested against the faulted vent wall observed at stops 4 and 5 (fig. 4). A landslide origin seems unlikely due to the subrounded nature of many of the clasts.

STOP 7 | Andesite-dacite lava dome

From stop 6, continue south and turn left onto a gravel road after 0.3 miles. Note: there are several poorly traveled dirt roads along the route that you should ignore. Follow the gravel road for 2.1 miles and cross over I-90, towards Ramsay. Turn west onto the frontage road (Miles Crossing) and continue for 2.1 miles. Follow the road to the right for 0.4 miles and turn west onto Canyon road. Follow Canyon road for 0.8 miles and turn right into a driveway. It's a short hike to the outcrop. Note: Stop 7 is on private property, and access requires landowner permission.

This stop is in silicified explosion breccia of a 49.3±0.68 Ma lava dome complex (^{40}Ar-^{39}Ar age from Dudas and others, 2010). The lava dome formed during the final phase of Eocene volcanic activity (figs. 1 and 2). Massive silicified explosion breccia formed at shallow depth in a hot spring system (fig. 5). Breccia clasts are aphanitic to porphyritic andesite - dacite lavas (fig. 5, photo a). Shallow intrusions transition up to lavas towards the crest of the dome complex. Lavas exhibit vesicular texture (fig. 5, photo b) and erupted into, and oxidized, water-saturated ash and clay beds (fig. 5, photo c). Pillow lavas are evidence of standing water at the time of eruption (fig. 5, photo d).

DISCUSSION AND CONCLUSIONS

The Eocene Lowland Creek volcanic field overlies Late Cretaceous igneous rocks at the south end of the Deer Lodge Valley (figs. 1 and 2). Eocene volcanic rocks are restricted in SiO2, K2O, and Na2O wt. %

relative to Late Cretaceous volcanic deposits (fig. 3A), and both are calc-alkaline suites (fig. 3b).

The Lowland Creek volcanic field overlaps the age with the Absaroka Volcanic field (fig. 1, inset map). Calc-alkaline, basaltic andesite - dacite of the Absaroka volcanic field likely formed in an active back-arc rift environment (see Feeley and others, 2002; Lindsay and Feeley, 2003). Rhyodacite of the Lowland Creek volcanic field (fig. 3A) may represent an end-stage of an Absaroka-like crustal magma system. The mineralogy (plagioclase > quartz > biotite) and porphyry texture of the ignimbrites (fig. 2) reflects extensive crystallization at shallow crustal depth. Early rhyolite deposits trend towards later mafic compositions (less wt. % SiO2) with time and may reflect inversion of a zoned crustal magma chamber.

Eocene vents

At stops 2 – 6 we examined vent-proximal deposits of a ~ 51.5 Ma caldera-forming eruption. The distribution of breccia, vitrophyre, and dikes north of Ramsay locates a 12-km2 cauldron, or deformed caldera vent (fig. 4). Hydrothermal breccia and rhyolite intrusions track the ring fault of the vent. Wildly irregular flow foliation in the basal ignimbrite is due to vent collapse. The megabreccia blocks are so large (100's of m) that they are generally not recognized as breccia in outcrop. Hydrothermal breccia and rhyolite dikes cut the ignimbrites (figs. 2 and 4). Mineralized breccia at the Tuxedo mine is characteristic of an epithermal Au-system, and may record tumescence of the caldera floor.

Stop 7 gives an overview of a lava dome exposed southwest of I-90 (figs. 4 and 5). Lavas and shallow intrusions erupted into a still, water-saturated, depression at ~ 50 Ma. The dome aligns with northeast-striking normal faults found north of the interstate (fig. 4), and may relate to a larger, unrecognized, Eocene vent that exists in the southern Deer Lodge Valley.

Structural setting of Eocene volcanism

Eocene magmatism records a transition from tectonic compression to extension in southwestern Montana. Block faults guided hydrothermal ore fluids into the extending crust (Berger and others, 2011). Extension at the latitude of Butte and within the Great Falls Tectonic Zone (fig. 1) occurred after 62 Ma and well

past 53 Ma. The orientation of lithic-bearing zones in the basal ignimbrite (fig. 2) indicates that 20 - 30° of west – northwest tilting occurred after 53 Ma (fig. 4).

The fissure system that erupted calc-alkaline andesite of the 55 – 52 Ma Absaroka volcanic field trends northwest towards Butte (Chadwick, 1970) (fig. 1, inset map), where it loses its exposure, and may be cut by the Great Falls Tectonic Zone. We propose that ca. 53 – 49 m.y.-old Lowland Creek Volcanics north and west of Butte (figs. 1 and 2) formed in an Absaroka-like andesite field. The pull apart of the andesite field, by the Great Falls Tectonic Zone, allowed an upper crustal magma reservoir to form. In this setting, ignimbrites erupted into northeast-trending structural basins, and epithermal systems developed near vents and fissures located at basin margins (figs. 4 and 5).

REFERENCES

Berger, B.R., Hildenbrand, T.G., and O'Neill, J.M., 2011, Control of Precambrian basement deformation zones on emplacement of the Laramide Boulder Batholith and Butte Mining District, Montana, United States: U.S. Geological Survey Scientific Investigations Report SI 2011-5016, 29 p.

Chadwick, R.A., 1970, Belts of eruptive centers in the Absaroka – Gallatin Volcanic Province, Wyoming – Montana: Geological Society of America Bulletin, v. 81, p. 267 -274.

Derkey, P.D., and Bartholomew, M.J., 1988, Geologic map of the Ramsay quadrangle, Montana: Montana Bureau of Mines and Geology Geological Map Series, GM 47, 1:24,000 scale.

DeWitt, Ed, Foord, E.E., Zartman, R.E., Pearson, R.C., and Foster, Fess, 1996, Chronology of Late Cretaceous Igneous and hydrothermal events at the Golden Sunlight gold-silver breccia pipe, southwestern Montana, U.S. Geological Survey Bulletin 2155, 48 p.

Dudas, F.O., Ispolatov, V.O., Harlan, S.S., and Snee, L.W., 2010, $^{40}Ar/^{39}Ar$ geochronology and geochemical reconnaissance of the Eocene Lowland Creek volcanic field, west-central Montana: Journal of Geology, v. 118, no. 3, p. 295-304.

Feeley, T.C., Cosca, M.A., and Lindsay, C.R., 2002, Petrogenesis and implications of cryptic hybrid magmas from Washburn Volcano, Absaroka Volcanic Province, U.S.A: Journal of Petrology, v.

43, p. 663-703.

Houston, R.A., and Dilles, J.H., 2013, Structural Geologic Evolution of the Butte District, Montana: Economic Geology, v. 108, pp.1397-1424.

Irvine, T.N., and Baragar, W.R.A., 1971, A guide to the chemical classification of the common volcanic rocks: Canadian Journal of Earth Science, v. 8, p. 523-548.

Konizeski, R.L., McMurtrey, R.G., and Brietkrietz, Alex, 1968, Geology and groundwater resources of the Deer Lodge Valley Montana: U.S. Geological Survey Water-Supply Paper 1862, 55 p., 2 plates.

Le Maitre, R.W., Bateman, P., Dudek, A., Keller, J., Lameyre Le Bas, M.J., Sabine, P. A., Schmid, R., Sorensen, H., Streckeisen, A., Woolley, A.R., and Zanettin, B., Zanettin, B., 1989, A classification of igneous rocks and glossary of terms, Blackwell, Oxford.

Lindsay, C.R., and Feeley, T.C., 2003, Magmagenesis at the Eocene Electric Peak – Sepulcher Mountain complex, Absaroka Volcanic Province, USA: Lithos, v. 67, p. 53-76.

Lonn, Jeff and Elliott, Colleen, 2010, A walking tour of the Eocene Anaconda detachment fault on Stucky Ridge near Anaconda, Montana: Northwest Geology, v. 39, p. 81-90.

Metesh, John, 2000, Geothermal springs and wells in Montana: Montana Bureau of Mines and Geology Open-File Report 415, 29 p., 2 appendices and state map.

O'Neill, J.M., and Lopez, D.A., 1985, Character and regional significance of Great Falls Tectonic Zone, east-central Idaho and west-central Montana: American Association of Petroleum Geologists Bulletin, v. 69, no. 3, p. 437-447.

Reynolds, M.W., 1979, Character and extent of Basin-Range faulting, western Montana and east-central Idaho, in Newman, G.W., and Goode, H.D., eds., Rocky mountain Association of Geologists and Utah Geological Association Basin and Range Symposium, p. 185-193.

Scarberry, K.C., in preparation, Geologic Map of the Sugarloaf Mountain 7.5' quadrangle, Deer Lodge, Jefferson, and Powell Counties, MT: Montana Bureau of Mines and Geology Open-File Report, 1 sheet, 1:24,000-scale.

Silberman, M.L., Hot-spring type, large tonnage, low-grade gold deposits, in Erickson, R.L., ed., Characteristics of Mineral Deposit Occurrences: U.S. Geological Survey Open-File Report 82-795, p. 131-142.

Sillitoe, R.H., Grauberger, G.L., and Elliott, J.E., 1985, A diatreme-hosted gold deposit at Montana Tunnels, Montana: Economic Geology, v. 80, p. 1707-1721.

Smedes, H.W., 1962, Lowland creek volcanics, an Upper Oligocene formation near Butte, Montana: The Journal of Geology, v. 70, no. 2.

Smedes, H.W. and Thomas, H.H., 1965, Reassignment of the Lowland Creek Volcanics to Eocene age: Journal of Geology, v. 73, no. 3, p. 508-510.

Sonderegger, J.L., 1984, A summary of geothermal studies in Montana, 1980-1983: Montana Bureau of Mines and Geology Open-File Report 142, 45 p.

Tilling, R., Klepper, M., and Obradovich, J., 1968, K-Ar ages and time span of emplacement of the Boulder Batholith, Montana: American Journal of Science, v. 266, p. 671-689.

Vuke, S.M., Porter, K.W., Lonn, J.D., and Lopez, D.A., 2007, Geologic Map of Montana: Montana Bureau of Mines and Geology Map 62A, 1:500,000-scale.

GEOLOGIC FIELD GUIDE TO THE TERTIARY VOLCANIC ROCKS IN THE ELLISTON 30′ X 60′ QUADRANGLE, WEST-CENTRAL MONTANA

Jesse G. Mosolf

Montana Bureau of Mines and Geology, 1300 W. Park St, Butte, MT 59701, jmosolf@mtech.edu

INTRODUCTION

This field trip explores Tertiary volcanic rocks exposed throughout the Elliston quadrangle located in west-central Montana. Tertiary volcanic and volcaniclastic deposits in this region generally record eruptive activity during a transition period from regional Cretaceous-Paleocene crustal shortening to mid-Eocene transtensive faulting associated with the Lewis and Clark Line (Portner and others, 2011), and therefore provide an exceptional opportunity to investigate the relationship between magmatism and tectonism in this part of the North American Cordillera. Three volcanic complexes in the Elliston area are visited on this field trip including the Avon, Garnet Range, and Crater Mountain volcanic fields. The age, petrology, stratigraphic architecture, and structural setting of each volcanic field are documented and correlated, shedding light on patterns of volcanism and transtensive deformation in the Elliston area during the Tertiary.

The day-long trip begins in the town of Elliston and travels through the scenic Avon, Helmville, and Lincoln Valleys on Highways 12, 141, and 200, ultimately ending at the summit of Crater Mountain southeast of Lincoln. Most of the stops are along highways and roads; participants are urged to be cognizant of traffic. Two of the stops require driving on gravel roads for a cumulative distance of approximately 40 miles (round-trip). A high clearance vehicle is recommended but not crucial. The last stop entails a 3 mile (round-trip) moderate, off-trail hike ascending 600 vertical feet to the summit of Crater Mountain, with scenic views of the surrounding area including the Lincoln and Helena Valleys, and the high peaks forming the Scapegoat Wilderness boundary. Participants should bring food, water, hiking apparel, rock hammer, hand lens, and enthusiasm for volcanic rocks.

GEOLOGIC SETTING

Regional geologic setting

The Elliston area lies within the extensive Eocene Challis-Kamloops volcanic belt (CKVB) that spans over 10 degrees of latitude in the North American Cordillera (fig. 1). The CKVB is composed of several large volcanic fields including the Buck Creek, Kamloops, Penticton, Princeton, Colville, Clarno, Challis, Absaroka, and Montana alkali fields, most of which were erupted between ~40-52 Ma and have a wide range of silica concentrations and high-K calc-alkaline geochemical signatures (Schleiffarth and Larson, 2014). Volcanism recorded by the CKVB was most certainly linked to North America's active plate margin, but the petrogenesis and tectono-magmatic setting of these rocks are poorly understood. Eocene volcanic intervals composing the CKVB have been previously interpreted as intra-arc deposits formed during the subduction of the Farallon and Kula plates beneath North America (Moye and others, 1988). Eocene volcanism appears to be temporally and spatially tied to extensional structures and the development of metamorphic core complexes, however, and several studies have also linked volcanism in the CKVB to regional crustal extension (MacDonald and others, 1992; Morris and others, 2000; Dostal and others, 2003). Although there is no broadly accepted explanation for the petrogenesis of the CKVB, most models attempt to account for the calc-alkaline signature of these rocks and the extensional stress field prevalent in the North American Cordillera during the Eocene. Petrotectonic models for this brief flare-up of calc-alkaline volcanism include the passage of a slab window (Breitsprecher and others, 2003); shallow subduction followed by slab rollback (Vance, 1979); delamination of the Farallon plate (Humphreys, 1995; Feeley, 2003); and intra-arc rifting (Dostal and others, 2001).

Figure 1. Simplified tectono-volcanic map showing regional extent of Eocene extrusive volcanic rocks of the Challis-Kamloops volcanic belt and Eocene metamorphic core complexes recognized throughout the North American Cordillera. Major volcanic fields are labeled. The location of the Elliston 30′ x 60′ quadrangle (fig. 2) is shown by black box. Simplified geologic map was compiled from Case and others (2013), Lewis and others (2012), Massey and others (2005), Schuster (2005), Vuke and others (2007), and Walker and MacLeod (1991).
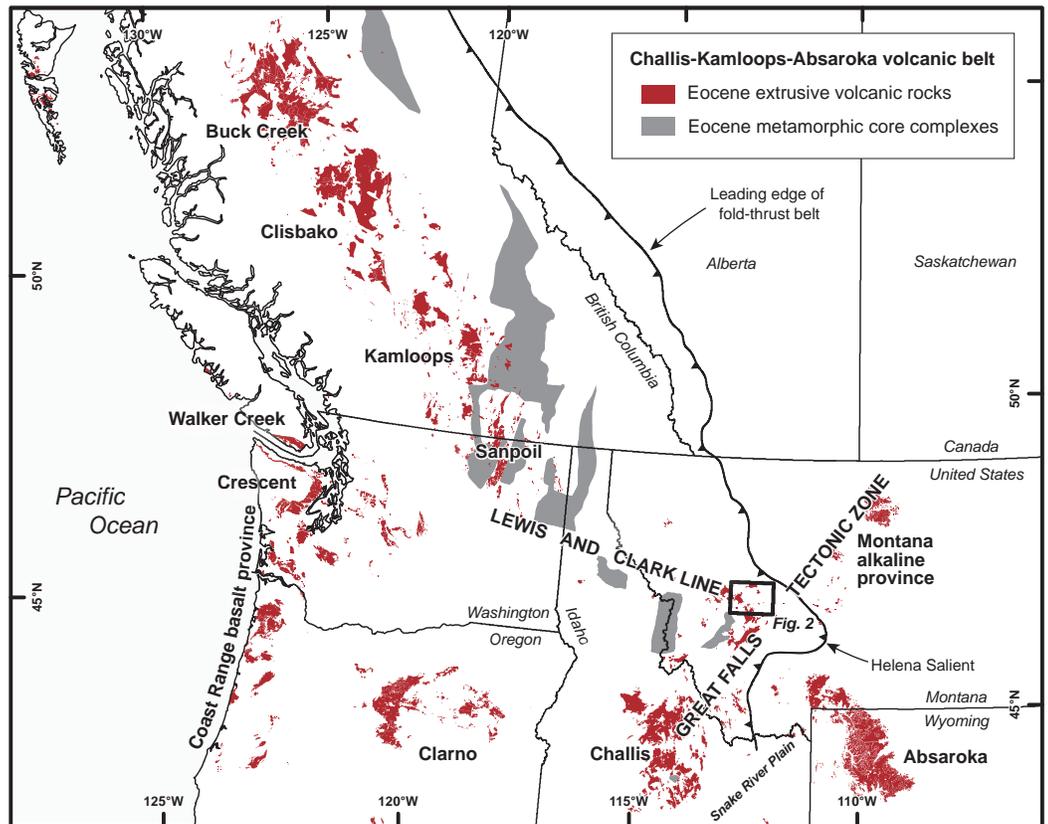
Local geologic setting of the Elliston quadrangle

The local geologic setting of the Elliston region is complex, located at the intersection of several tectonic elements including the Lewis and Clark Line, the Great Falls tectonic zone, the leading edge of Montana's fold-thrust belt, and the Basin and Range extensional corridor (fig. 1). These differing elements represent a composite tectonic history spanning the Mesoproterozoic to the present. Strike-slip faulting associated with the long-lived Lewis and Clark Line has culminated in the dominantly northwest-striking structural grain observed in the Elliston area (e.g. Sears and Hendrix, 2004).

Tertiary volcanic and sedimentary deposits rest on a regional unconformity that truncates northwest-trending transpressive structures deforming Mesoproterozoic through Late Cretaceous units (fig. 2). Transpressive structures presumably developed in a shear zone that accommodated differential rotation between the Lewis-Eldorado-Hoadley (LEH) thrust slab to the north and the Sapphire-Lombard thrust slab to the south during Late Cretaceous-Paleocene shortening (Sears and Hendrix, 2004; Mudge and Earhart, 1983).

Dominantly northwest- and northeast-striking transtensive faults overprint the older transpressive structures, and locally tilt and displace Tertiary volcanic and sedimentary rocks (fig. 2). Although the timing of transtensive deformation in the Elliston area is somewhat uncertain, faulting likely initiated during rapid exhumation of the nearby Anaconda metamorphic core complex (39-53 Ma; Foster and others, 2010) and the onset of mid-Eocene volcanism recorded by volcanogenic deposits in the Elliston quadrangle. Following the brief flare-up of mid-Eocene volcanism, a broad depositional basin with minor internal faulting developed in the Elliston region and accommodated fine-grained basin deposits of the Renova Formation that unconformably overlie the Eocene volcanic deposits, and are locally intercalated with basaltic lava flows. A regional mid-Miocene unconformity separating the Renova Formation from the overlying Sixmile Creek Formation marks the start of segmentation of the Renova basin into fault-bounded valleys including the Avon Valley traversed in this field trip. These valleys are interpreted as grabens created by pull-apart structures formed during Miocene and younger transtensive deformation (Reynolds, 1979).
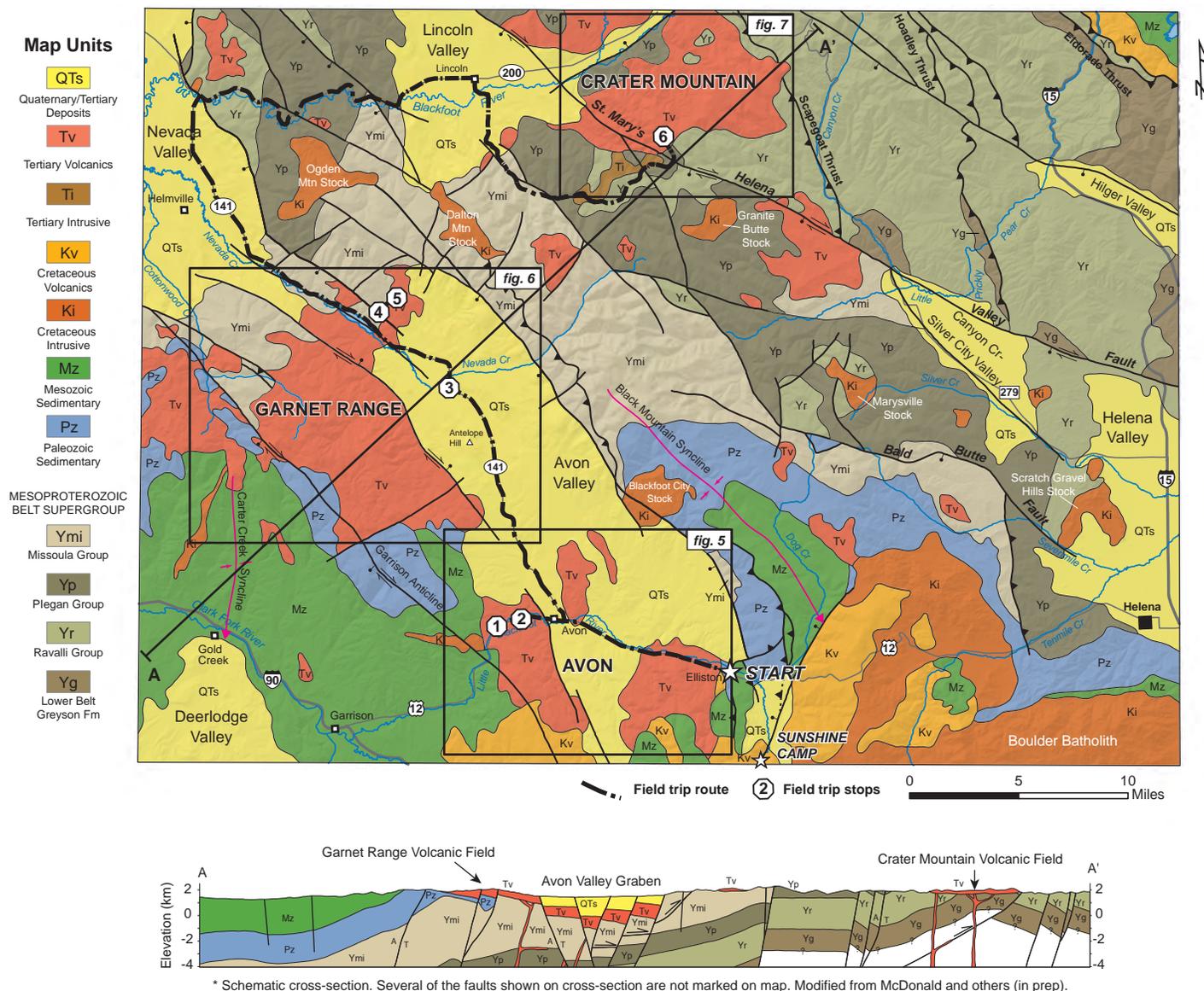
Figure 2. Simplified geologic map of the Elliston 30′ x 60′ quadrangle. The Avon, Garnet Range, and Crater Mountain volcanic complexes visited in this field guide are labeled. Boxes show the locations of figures 5, 7, & 9. Figure modified from McDonald and others (in prep).

Introduction to the geology of the Elliston region's Tertiary volcanic fields

The Avon, Garnet Range, and Crater Mountain volcanic fields were the focus of recent STATEMAP 1:24,000 scale geologic mapping within the Elliston 30' x 60' quadrangle (McDonald and others, in prep). One major goal of this project was to develop a map-pable stratigraphy for Tertiary volcanic and volcani-clastic deposits (fig. 3). Field observations and map-ping were aided by thin section analyses, U-Pb zircon geochronology (table 1), and whole-rock major and trace element analyses (fig. 4). Field and analytical results were compiled with existing data published in prior reports and student theses. The following sec-tions provide a brief geologic overview of each major

volcanic complex visited on this field trip. See Call-meyer (1984), Parker (1995), Trombetta (1987) for detailed descriptions of the Tertiary volcanic rocks in the Elliston region.

Avon volcanic field

The Avon volcanic field is located west of the Con-tinental Divide near the towns of Avon and Elliston in Powell County (fig. 5). This predominantly rhyolitic volcanic complex was previously considered part of the Eo-Oligocene Helena volcanic field (Chadwick, 1981; 1985), and was first mapped in detail by Trom-betta (1987) as part of a master's thesis.

The Avon complex consists of at least four map-pable volcanic units ranging from rhyolitic tuff de-
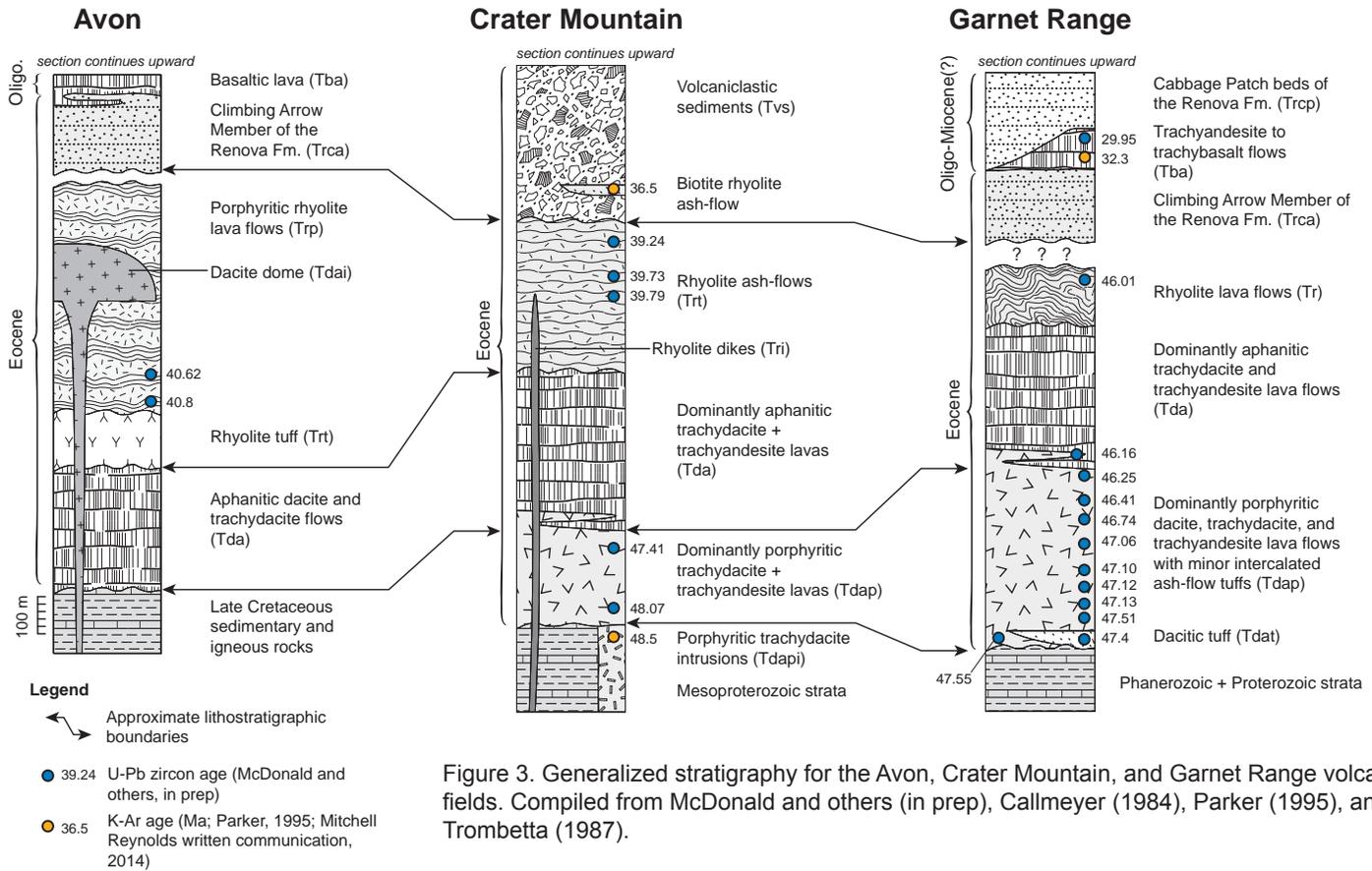
Figure 3. Generalized stratigraphy for the Avon, Crater Mountain, and Garnet Range volcanic fields. Compiled from McDonald and others (in prep), Callmeyer (1984), Parker (1995), and Trombetta (1987).

Table 1. New U-Pb zircon ages from the Elliston area (McDonald and others, in prep)

Sample	Map Unit	Volcanic Field	Lat	Long	Age	2σ
ES-26	Trp	Avon	46.59736317	-112.632849	40.62	0.16
ES-28	Trt	Avon	46.59517783	-112.578902	40.8	0.17
ES-46	Trt	Crater Mountain	46.93388517	-112.444502	39.24	0.16
ES-44	Trt	Crater Mountain	46.92759833	-112.509388	39.73	0.1
ES-43	Trt	Crater Mountain	46.9272425	-112.509045	39.79	0.12
ES-41	Tdap	Crater Mountain	46.9174195	-112.498173	47.41	0.22
ES-55	Tdap	Crater Mountain	46.97887817	-112.494779	48.07	0.18
ES-04	Tba	Garnet Range	46.65870559	-112.715109	29.95	0.17
ES-06	Tr	Garnet Range	46.70213132	-112.736969	46.01	0.23
ES-14	Tdap	Garnet Range	46.75128213	-112.782292	46.16	0.26
ES-47	Tdap	Garnet Range	46.70218683	-112.801876	46.25	0.27
ES-20	Tdap	Garnet Range	46.77179663	-112.839973	46.41	0.18
ES-07	Tdap	Garnet Range	46.70311819	-112.762471	46.74	0.27
ES-12	Tdap	Garnet Range	46.80671289	-112.758211	47.06	0.12
ES-61	Tdap	Garnet Range	46.720548	-112.787072	47.1	0.29
ES-40	Tdap	Garnet Range	46.70349183	-112.833733	47.12	0.19
ES-50	Tdap	Garnet Range	46.6840605	-112.808736	47.13	0.26
ES-05	Tdat	Garnet Range	46.66565741	-112.738676	47.4	0.19
ES-24	Tdap	Garnet Range	46.659745	-112.774804	47.51	0.21
ES-18	Tdap	Garnet Range	46.82876974	-112.7299	47.55	0.16

Zircon separates were prepared at the Montana Bureau of Mines and Geology and analyzed at the University of California - Santa Barbara. U-Pb ages were determined by calculating the weighted mean of 28+ spot analyses per sample. Uncertainties are ± 2σ.
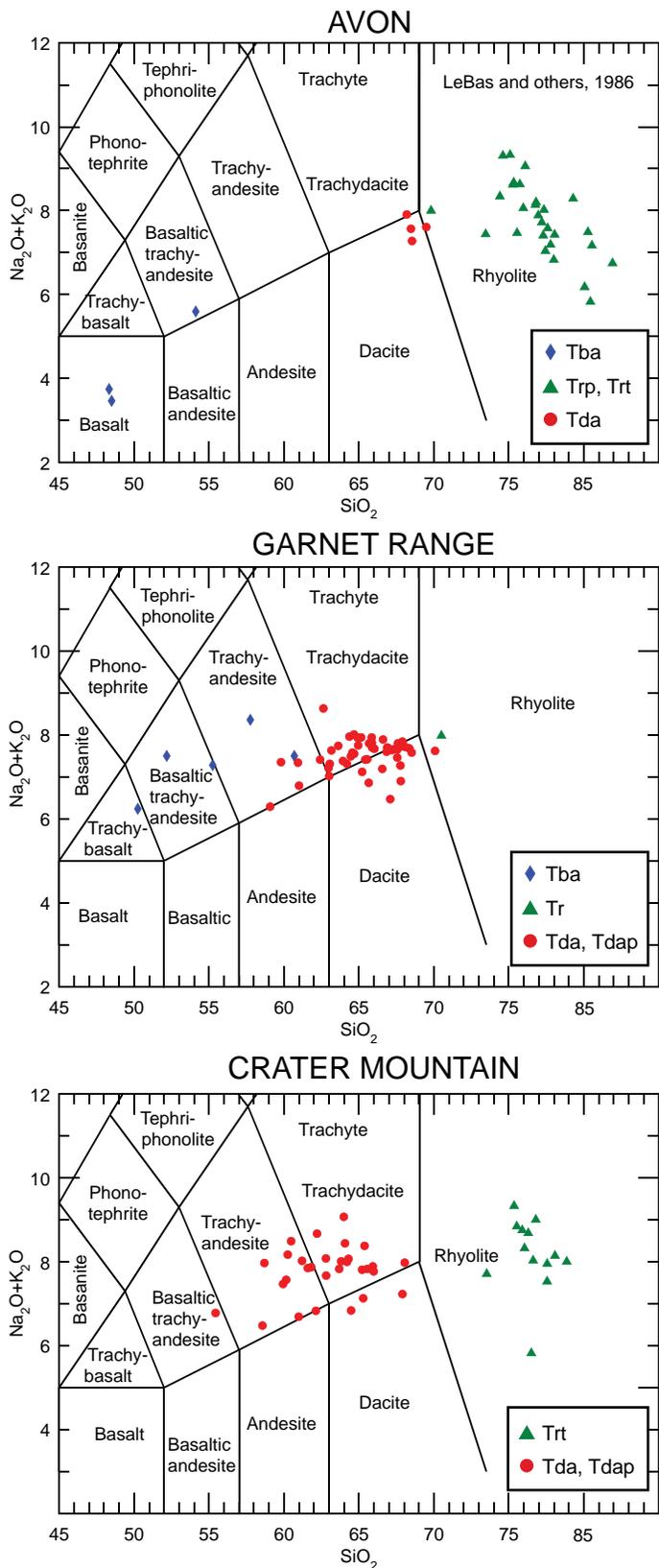
Figure 4. Whole-rock geochemical data from samples collected in the Avon, Garnet Range, and Crater Mountain volcanic fields. Data are grouped by map unit and plotted on a volcanic rock type diagram ($Na_2O + K_2O$ vs. SiO_2) after LeBas and others (1986). Data compiled from McDonald and others (in prep), Mahoney and others (this volume), Parker (1995), and Trombetta (1987). See Figures 5, 7, & 9 for sample locations and unit abbreviations.

posits to basaltic lavas (figs. 3, 5, & 6), all of which unconformably overlie Late Cretaceous sedimentary and igneous rocks. Aphanitic trachydacite and dacite lavas (Tda) are the oldest volcanic units exposed. The age of these flows has not been constrained by reliable radiometric age data, but they are likely correlative with aphanitic lavas mapped in the Garnet Range (Callmeyer, 1984; McDonald and others, in prep) that are constrained between 46.01 and 46.16 Ma (see following section). A series of conspicuously porphyritic rhyolite lavas (Trp) and subordinate rhyolite tuff (Trt) overly the dacitic lavas in the Avon area, and are intruded and intercalated with an exogenous dacite dome exposed along Highway 12. The porphyritic lava flows yielded two agreeable U-Pb zircon ages of 40.62±0.16 and 40.8±0.17 Ma (fig. 4) that firmly establish a middle Eocene age for this eruptive cycle. Basaltic andesite flows (Tba) locally overlie rhyolite flows, and are assumed to be the youngest extrusive volcanics exposed in the Avon field. No age data have been obtained for basaltic lavas in the Avon region, but they are likely correlative with Eo-Oligocene (29.95 to 37.3 Ma) basaltic lava flows exposed in the eastern Garnet range.

Garnet Range volcanic field

The Garnet Range volcanic field is located north of the Clark Fork River in parts of Powell, Granite, and Missoula Counties. The eastern Garnet Range has been the focus of several geologic studies dating back to the pioneering work of Joseph Pardee (1917). Despite numerous geologic investigations and historic mining in the Garnet Range dating back over a century, the volcanic rocks in this region were not mapped in full detail until somewhat recently (Callmeyer, 1984; McDonald and others, in prep).

Eocene volcanic rocks in the eastern Garnet Range unconformably overlie Mesoproterozoic through Mesozoic strata deformed by northwest-oriented transpressional folds and faults. The Garrison Anticline is the one of the largest, most notable of these structures and was originally mapped by Pardee (1917). The Garnet Range volcanic field is composed of at least five mappable volcanic units (figs. 3, 7, & 8). The oldest map unit (Tdap) is a stack of predominantly porphyritic trachydacite to trachyandesite lavas intercalated with minor dacitic tuff deposits (mapped locally as Tdat; fig. 7). U-Pb zircon ages span 46.16

to 47.55 Ma and firmly establish a mid-Eocene age for this map unit. A series of dominantly aphanitic trachydacite and trachydacite flows (Tda) overlie the porphyritic lavas. A single K-Ar age of 44±2.2 Ma was reported for this unit (Callmeyer, 1984) but the large associated error suggests this may not be a reliable age. Flow-banded rhyolite lava (Tr) overlies the aphanitic flows near the western margin of the Avon Valley (fig. 7). A flow from this unit yielded a single U-Pb zircon age of 46.01 Ma, suggesting the underlying aphanitic lavas are older than Callmeyer's reported K-Ar of 44.8 Ma. The youngest volcanic unit in the eastern Garnet Range is composed of basaltic lava flows (Tba) that locally overlie Mesoproterozoic bedrock and are intercalated with Tertiary sedimentary deposits of the Renova Formation. These flows yielded U-Pb zircon and K-Ar ages spanning 29.95 to 37.3 Ma (McDonald and others, in prep; Reynolds, written communication, 2014).

Crater Mountain volcanic field

The Crater Mountain volcanic field is located in Lewis and Clark County east-southeast of Lincoln. Volcanic deposits of the Crater Mountain volcanic field rest on an unconformity truncating metasedimentary rocks of the Belt Supergroup that are tilted and faulted. At least four volcanogenic units are observed in this area (figs. 3, 9, & 10), all of which can be correlated to map units in the Avon and Garnet Range volcanic fields. The oldest volcanic unit exposed is a stack of porphyritic trachydacite and trachyandesite lava flows (Tdap) that are remarkably similar to those in the eastern Garnet Range. Two U-Pb zircon ages of 47.41±0.22 and 48.07±0.18 Ma were obtained from this unit. A series of aphanitic trachydacite and trachyandesite lavas (Tda) overlie the porphyritic lavas. No reliable age data have been obtained from these flows, but they most likely are correlative with those in the Garnet Range and Avon fields. Expansive rhyolite ash flow tuff deposits (Trt) overlie aphanitic (Tda) and porphyritic (Tdap) lava flows locally (fig. 9), and are the main host of epithermal gold mineralization in the region, which includes the McDonald gold deposit north of the Blackfoot River (Bartlett and others, 1998). U-Pb zircon ages from rhyolite ash flows span 39.24 to 39.79 Ma, indicating this unit is slightly younger than the porphyritic rhyolite lavas (Trp) exposed in the Avon field.

ROAD LOG

This field trip begins in Elliston, MT. Field trip stops are referenced to GPS coordinates, and also to geographic locations, highway markers, and road/highway names. The mileage to or between stops is given in addition to points of interest in-between stops.

MILEAGE

STOP 0   0 mi (45.5612, -112.4303): beginning of road log in Elliston, MT.

Reset your car's trip odometer. Begin driving west on Highway 12 towards the town of Avon, following the Little Blackfoot river valley. Exposures of Eocene rhyolite lava overlain by fine-grained sediments of the Renova Formation occur north and south of the highway (fig. 5).

2.6   Dacite outcrop (Tdai) south of the highway with prominent columnar jointing and vertical igneous foliations. This unit was interpreted by Trombetta (1987) to be a dacite lava dome intruding and intercalated with porphyritic rhyolite lava flows and tuffs occurring in this area. The rock is typically gray to black and fine-grained with sparse phenocrysts of quartz, sanidine, oligoclase, hypersthene, and augite. No reliable age data have been obtained from this unit.

7.5   Roadcut of rhyolite porphyry south of the highway (east of the Avon Café) containing phenocrysts of quartz, plagioclase, biotite, hornblende in a waxy, maroon matrix. Abundant circular cavities in this rock are interpreted to be weathered/altered lithophysae. Black vitrophyre can be seen in the float. A rock sample from this outcrop yielded a U-Pb zircon age of 40.8±0.17 Ma. We will visit an outcrop of this unit at STOP 2.

Continue driving west on Highway 12 through the town of Avon and towards the Garrison Junction. The Little Blackfoot River valley narrows past Avon and is bordered to the north and south by Eocene volcanic rocks.
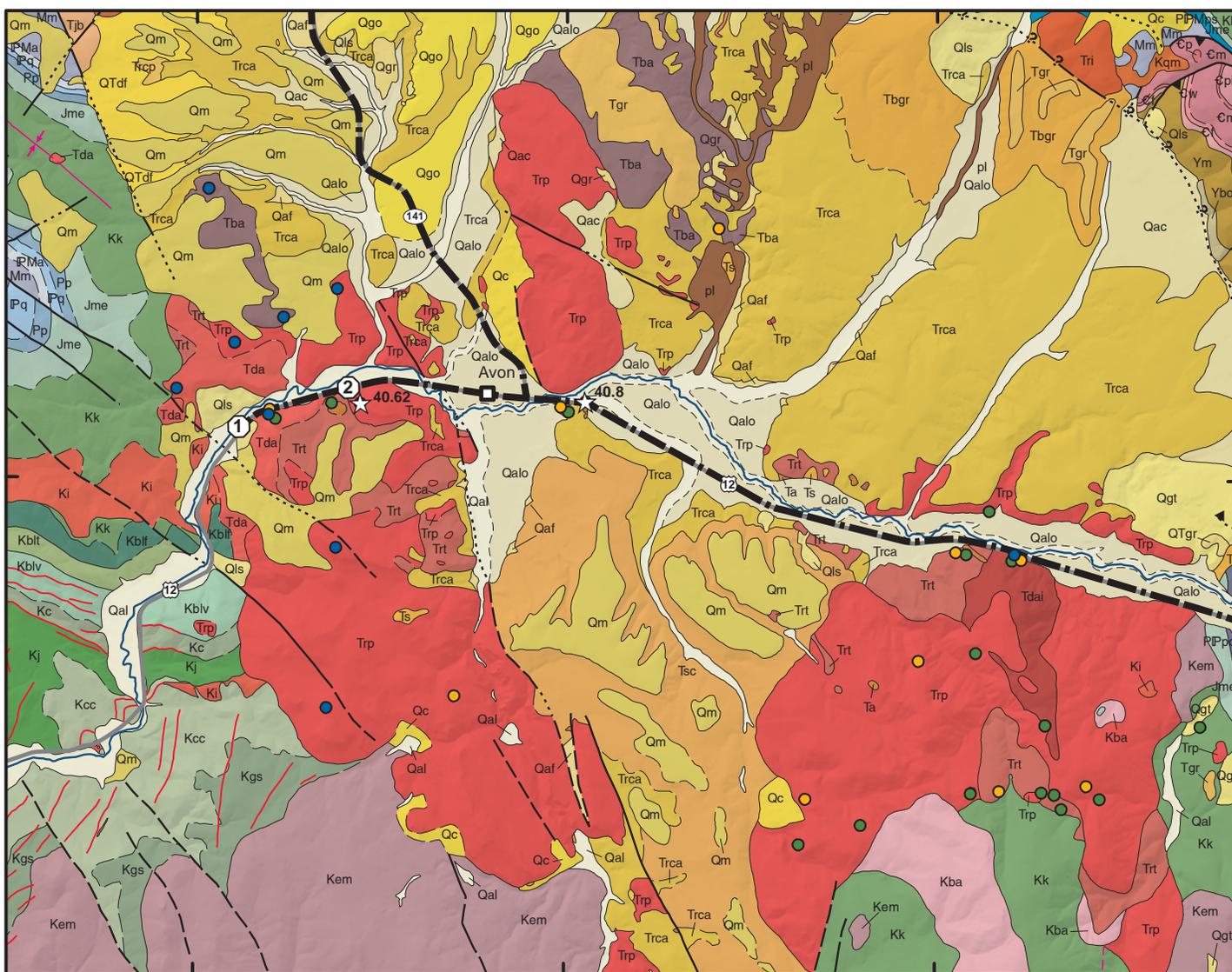
LEGEND

▰▰	Road log route
①	Field trip stops
☆ **40.8**	Zircon ages (Ma; McDonald and others; in prep)
pl	Placer
▬	Cretaceous dike or sill (Ki)

Certain, approximate, concealed contact

——— — ···········**?**

Certain, approximate, concealed fault

▲—▬— ··········**?**

Certain, approximate, concealed syncline

✚— — ·······**?**

Teritary volcanic units

Tba	Basaltic lava flows
Tri	Rhyolite intrusions
Tdai	Dacite dome
Trp	Rhyolite lava flows
Trt	Rhyolite tuff
Tda	Dacitic lava flows

Geochemical analysis

- 🔵 McDonald and others (in prep)
- 🟡 Trombetta, 1987
- 🟢 Mahoney and others (this volume)

Quaternary sedimentary deposits
Qal, Qaf, Qc, Qac, Qgr, Qm, Qls, Qalo, Qgo, Qgt

Quaternary-Tertiary sed. deposits
QTgr, QTdf, Tgr, Tbgr, Tsc

Tertiary sed. Renova Fm.
Trcp, Trca

Tertiary jasperoid
Tjb

Mz volcaniclastic, volcanic, and instrusive rocks
Kqm, Ki, Kem, Kba, Kgs

Mesozoic sed. rocks
Kcc, Kj, Kc, Kblv, Kblt, Kblf, Kk, Jme

Paleozoic sedimentary rocks
Pp, IPq, IPMa, PPpq, PIPMps, Mm, €pi, €p, €m, €w, €f

Mesoproterozoic metased. rocks
Ym, Ybo

5 kilometers

N

Figure 5. Simplified geologic map of the Avon volcanic field. Map unit descriptions in McDonald and others (in prep).

| STOP 1 | **11.3 (46.5912, -112.6568): Eocene aphanitic lava flows, Avon volcanic field.** |

Park in the broad gravel pullout with an interpretive sign immediately after a pronounced bend in the highway. Prominent cliffs of trachydacite lava flows (Tda) can be seen NNE of the highway. A large Quaternary landslide over a ¼-mile wide can be seen between the base of the cliffs and the river.

Aphanitic dacite and trachydacite lava flows compose the oldest volcanic unit exposed in the Avon volcanic field and rest unconformably on faulted and folded Mesozoic strata. In outcrop, the lava flows are typically brown to gray weathering and commonly have an aphanitic texture with sparse phenocrysts of plagioclase. Under the microscope, the rock consists mostly of plagioclase microlites with centimeter-scale flow foliations. Fractures preferentially developed along flow foliation planes give the rock a blocky to flaggy characteristic in outcrop. Monolithologic breccia is abundant throughout this unit and is interpreted to be autobreccia formed while the lava was flowing. Bulk rock geochemical data reveal these flows to be dacites (fig. 4). No reliable radiometric age data have been obtained from this unit, but it likely correlates to aphanitic lavas mapped in the eastern Garnet Range constrained between 46.01 and 46.16 Ma (fig. 7). These dacitic lava flows were likely effusive (i.e. non-violent) erupting from vents or fissures in the Avon area.

Cross the highway and walk approximately 0.36 miles northeast (towards Avon) to view an excellent outcrop of this unit. BE CAREFUL! Traffic moves fast on this highway and the crossing is near a blind corner. Abundant float of this unit can be seen along the road approaching the outcrop. Return to car and carefully execute a U-turn, heading eastward on Highway 12 back towards Avon.

| STOP 2 | **12.6 (46.5974, -112.6322): Eocene porphyritic rhyolite and tuff, Avon volcanic field.** |

Park in the large pullout on right side of the highway near mile marker 11. Prominent cliffs of porphyritic rhyolite lava (Trp) can be seen across the

river, north of the highway. These flows comprise the majority of rock exposed in the Avon volcanic complex. Walk approximately 200-300 feet westward to a roadcut of rhyolite porphyry on the south side of the highway. In outcrop, rhyolite lavas are commonly gray, white, tan, red and/or purple weathering. Centimeter- to meter-scale flow foliations typically give this unit a blocky characteristic in outcrop. Phenocrysts compose up to 28 percent of the rock and include quartz, sanidine, oligoclase, biotite, and amphibole in a matrix of glass, clay, and cryptocrystalline material. Devitrification of the matrix varies from none to complete. Lithophysae, up to 10 centimeters in diameter, are locally abundant and are eroded and partially filled with chalcedony. Discontinuous zones of vitrophyre and autobreccia separate individual flows. Bulk-rock major element analyses show the porphyritic flows to be exclusively rhyolite (fig. 4). A sample from this outcrop yielded an U-Pb zircon age of 40.62±0.16 Ma.

Continue to walk west for ~100 ft to a white weathering, poorly consolidated lapilli tuff underlying the rhyolite lava flow. This unit contains up to 10-15 percent lapilli-size fragments of rhyolite and sedimentary rock. Sparse crystals of quartz, sanidine, oligoclase, biotite, and amphibole are set in a matrix of glass shards, pumice fragments, and clay. The lapilli tuff in this outcrop is the upper part of a densely welded rhyolite ignimbrite with distinct black fiamme that occurs throughout the Avon area.

The volcanic setting of voluminous eruptions of rhyolite lava is somewhat enigmatic. Rhyolite lavas are scarce among rocks of highly silicic compositions because most silicic magmas erupt violently and fragment into pyroclasts. Rhyolite lavas are typically associated with calderas, however, and are emplaced after violent caldera forming eruptions. The lower, welded lapilli tuff (Trt) in the Avon complex likely erupted in a violent Plinian-type eruption followed by voluminous extrusion of rhyolite lava (Trp). This eruptive sequence is broadly consistent with caldera formation in the Avon region circa 40 Ma. Interestingly, extensive rhyolite ignimbrite sheets were emplaced near Lincoln around this same time. We will visit ignimbrite deposits in the Crater Mountain area later in the day (STOP 6).

Return to your vehicle and drive east towards the town of Avon. Turn left onto Highway 141 in the town of Avon and proceed north. The highway traverses
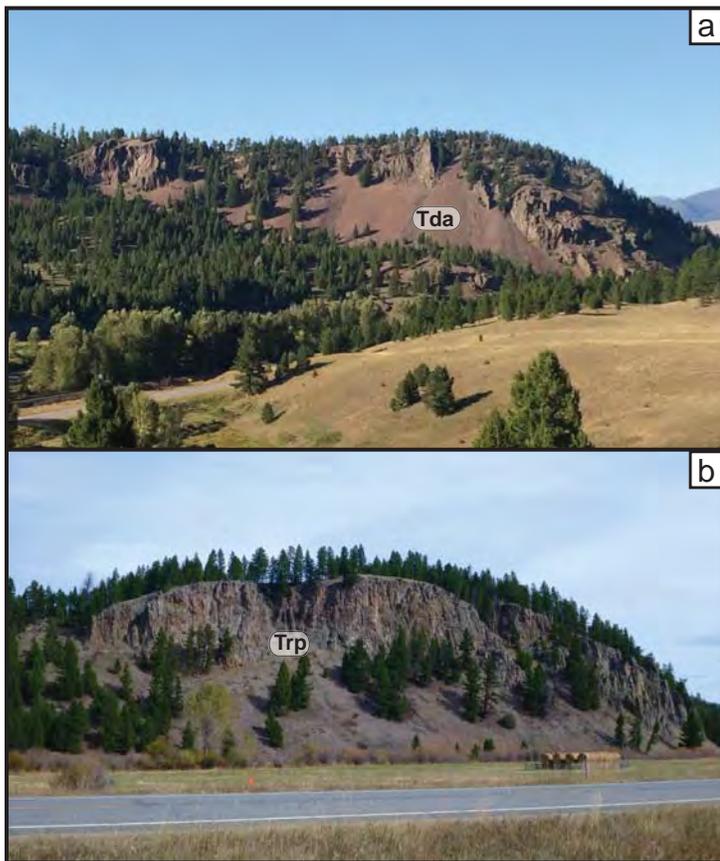
Figure 6. Field photographs from the Avon volcanic field. a) Red weathering aphanitic dacite lava flow (Tda) exposed along Highway 12 west of Avon. b) Prominent cliff of porphyritic rhyolite lava (Trp) exposed along Highway 12 west of Avon.

flows that yielded a U-Pb zircon date of 29.95±0.17 Ma (Mosolf and Vuke, in review). The carbonate beds on Antelope Hill are locally silicified to white-weathering, gray porcellanite and variegated chert that was quarried by native people for projectile points. The "Avon Chert" has a distinctive chemical signature and has been found as distant as Illinois (Roll and others, 2005).

| STOP 3 | 27.2 (46.7518, -112.704): overview of the Avon Valley graben and the eastern Garnet Range volcanic field. |

Park in the large gravel lot on the left side of the highway immediately after the Little Valley Ranch turnoff. Much of the eastern Garnet Range volcanic field is hard to access, requiring long drives on rough jeep roads. This stop offers good vistas of the eastern Garnet Range volcanic complex to the southwest, as well as faults bounding the Avon Valley graben. We will visit representative outcrops of the eastern Garnet Range volcanic complex at STOPS 4 & 5.

Systems of oblique-slip faults bound the southwestern and northeastern margins of the Avon Valley, and were synchronous with the high-angle, northeast-striking faults occurring in the area (fig. 2). The Avon Valley graben and associated faults are interpreted to be pull-apart structures formed by dextral strike-slip motions within the Lewis and Clark Line during the Cenozoic (Reynolds, 1979).

To the northeast, a major northwest-striking fault system clearly defines the Avon Valley's northeast margin where dramatic triangular facets are observed along the Nevada Mountains range front. This system of faults places Mesozoic through Mesoproterozoic rocks against poorly consolidated Quaternary-Tertiary sedimentary deposits that locally interfinger with lava flows.

To the southwest, the fault system bounding the southwest margin of the Avon Valley is less obvious with weakly developed or no triangular facets occurring along the eastern Garnet Range front. Despite poor geomorphic expression, numerous fault kinematic measurements made along the range front suggest that a system of NW-striking and steeply dipping oblique-slip faults with right-lateral offsets occur

the Avon Valley, a northwest-trending graben located between the Garnet Range to the west and the Nevada Mountains to the east. For the next several miles, fine-grained sedimentary deposits of the Renova Formation are visible in road cuts and low hills adjacent to road. This formation is prone to landslides.

21.9 Drainage divide between the Little Blackfoot River to the south and the Blackfoot River to the north. The divide is aligned with a gravity high (Hanna and others, 1994; Knatterud and others, this volume) that bisects the Avon Valley and is along the projected strike of a northeast-trending, high-angle fault mapped in the eastern Garnet Range (fig. 7). We suspect the gravity high marks an eastward continuation of this high-angle fault.

23.3 The timbered hill to the west is Antelope Butte, a northwest-trending syncline deforming the Renova Formation. The lower slopes are composed of the Eocene Climbing Arrow Member, whereas the upper slopes are the Oligo-Miocene Cabbage Patch beds. The Cabbage Patch beds locally overlie basaltic lava

Figure 7. Simplified geologic map of the eastern Garnet Range volcanic field. Map unit descriptions in McDonald and others (in prep).

along the Avon Valley's southwest margin.

To the south-southwest, the southern part of the Garnet Range is underlain by folded and faulted Mesozoic and Paleozoic rocks locally overlain by sparse Eocene volcanic deposits. A prominent northeast-striking, down to the northwest fault bisects the range, juxtaposing deformed Paleozoic-Mesozoic rocks to the south against Eocene volcanic rocks of the eastern Garnet Range volcanic field to the north. This northeast-trending fault is along strike of a gravity high bisecting the Avon Valley (Knatterud and others, this volume). The Eocene volcanic sequences north of this fault are primarily composed of aphanitic (Tda) and porphyritic (Tdap) trachydacite and trachyandesite lava flows with minor tuffaceous intercalations. Lava flows and ash deposits rest on an unconformity that truncates deformed Phanerozoic and Proterozoic strata. Volcanic strata appear to thicken eastward and dip gently towards the valley and were perhaps deposited in a broad, actively subsiding, extensional or transtensional basin.

Fine-grained sediments of the Renova Formation overlie the older Eocene lavas along the margins and within the Avon Valley. These deposits are locally intercalated with Eo-Oligocene basaltic lavas (Tba) and are generally confined to the valley. The Renova Formation and intercalated lavas are locally tilted and displaced by faults associated with the Avon graben.

To the northwest, the Avon Valley narrows dramatically near Nevada Lake, where a complex system of northwest- and northeast-striking faults displace Eocene volcanic rocks resting on Mesoproterozoic metasedimentary rocks of the Belt Supergroup.

Continue driving north on Highway 141 for 5 miles to the Clear Creek road turnoff on the right.

32.2   Turn right on to Clear Creek (gravel road) and drive for approximately 0.8 mi passing exposures of the Mount Shields Formation of the Belt Supergroup.

| STOP 4 | **33 (46.8000, -112.772): Eocene porphyritic lava flows, Garnet Range volcanic field.** |

Pull over onto the shoulder of the road near the outcrop of a porphyritic lava flow (fig. 7). Porphyritic

lava flows (latites) represent the oldest volcanic unit in the eastern Garnet Range volcanic complex. In outcrop, the lava flows commonly weather to gray, green, and red blocks and plates with some outcrops forming hoodoos and spires. Individual lava flows typically have a massive interior encompassed by carapaces of autobreccia several meters thick. Lava flows have a distinct porphyritic texture with subhedral to euhedral phenocrysts of plagioclase (up to ~5 mm) and minor amounts of amphibole, biotite, and quartz. Microscopically, the fine-grained groundmass typically has a trachytic texture and consists mainly of aligned microlites of plagioclase but also includes amphibole, biotite, and magnetite. Whole-rock major element data identify these lavas as dacites, trachydacites, and trachyandesites (fig. 4). U-Pb zircon ages span 46.16 to 47.55 Ma (fig. 3; table 1). The hills east of the road are underlain by porphyritic lavas (Tdap) that are overlain by aphanitic flows (Tda).

Porphyritic lavas were viscous, slow moving flows that did not travel far from their source vents, and likely formed lava domes locally. Volcanic centers are hard to identify in this area, but flows composing this geographically widespread unit likely erupted from several fissure-type vents throughout the eastern Garnet Range volcanic field. More explosive eruptions of dacitic tuff typically preceded the extrusion of porphyritic lava flows.

Return to vehicle and continue driving north on Clear Creek road passing through intermittent road cuts of the Mount Shields Formation and Quaternary landslide deposits.

33.1   Small quarry of the brecciated Mesoproterozoic Mount Shields 2 Formation.

33.5   Bear right at fork in the road.

34.0   Turn right on to Buffalo Gulch Road and continue driving for approximately 0.3 mi.

| STOP 5 | **34.3 (46.8104, -112.754): Eocene aphanitic lava flows, Garnet Range volcanic field.** |

Pull into the small roadside quarry or park on the shoulder of the road near the outcrop. The lava flow exposed in this outcrop is part of a stack of predomi-
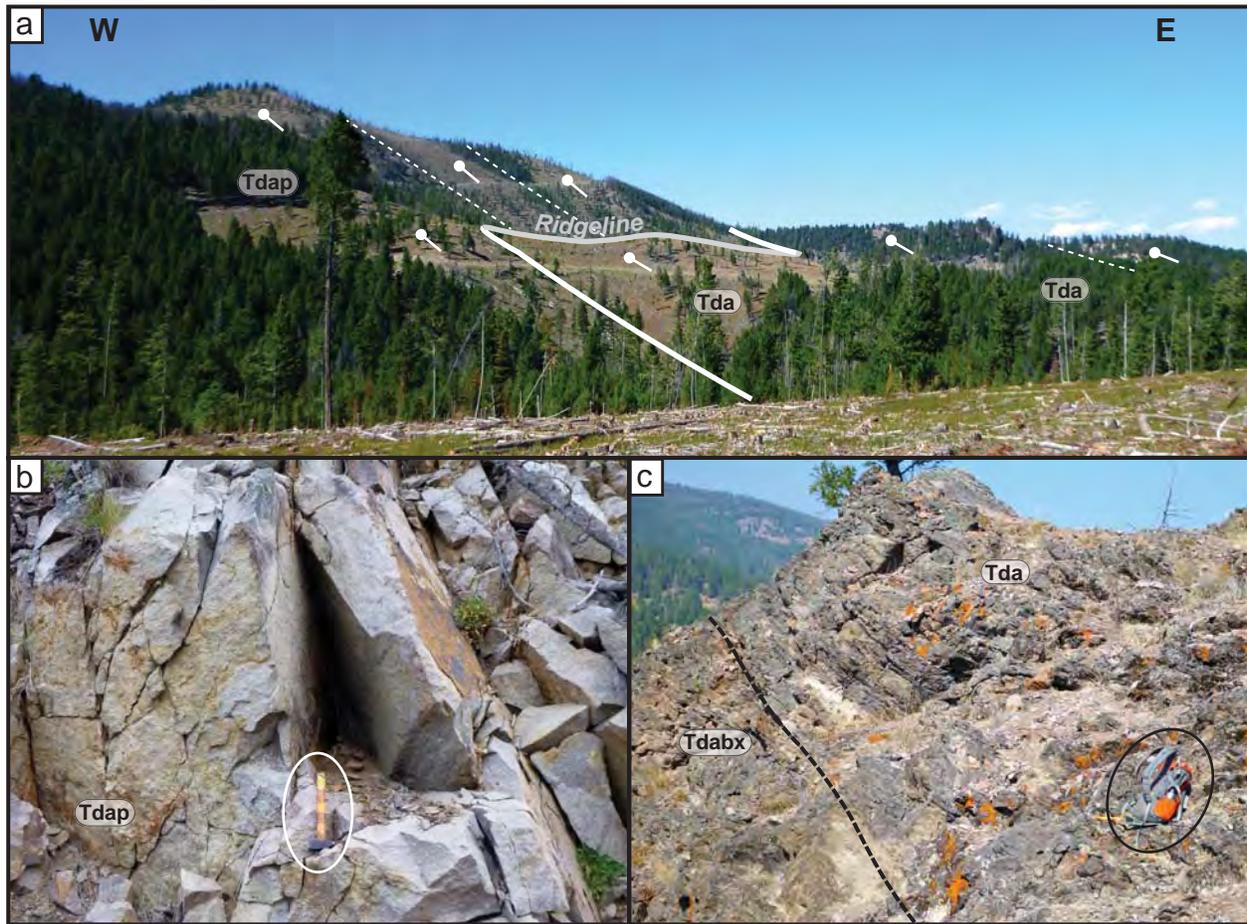
Figure 8. Field photographs from the eastern Garnet Range volcanic field. a) View looking north of Strickland Creek of the contact between a succession of porphyritic dacitic lavas (Tdap) and overlying aphanitic flows (Tda). Solid white line shows contact; solid grey line outlines ridge; dashed white lines are form lines, some of which are coincident with the boundaries of individual lava flows; ball-and-sticks show the apparent dip of paleohorizontal (inferred). Note that lava flows appear to be tilted eastward. b) Field photograph of the massive interior of a porphyritic dacitic lava flow (Tdap). Rock hammer for scale. c) Field photograph of a aphanitic lava flow (Tda) with a rubbly base and coherent interior. Dashed black line shows approximate boundary between the basal autobreccia (Tdabx) and the flow foliated interior of the lava flow. Backpack for scale.

nantly aphanitic lavas (Tda) overlying the porphyritic flows (Tdap) visited at STOP 4, and unconformably resting on Mesoproterozoic rocks locally. In outcrop, aphanitic lava flows typically weather gray and commonly exhibit a distinct flow banding that cleaves into flaggy, angular talus often with red iron staining on parting surfaces. Massive flows with rare columnar jointing are also observed. Aphanitic lavas exhibit a strong trachytic texture consisting mainly of plagioclase microcrystals, but also include minor amounts of pyroxene, magnetite, and volcanic glass. Porphyritic (<5-10% phenocrysts) flows contain subhedral to euhedral phenocrysts of plagioclase, amphibole, and minor amounts of biotite. Exposures throughout the Clear Creek drainage contain abundant amphibole laths that are flow-aligned and give the rock a well-defined parting cleavage. Whole-rock geochemical analysis identifies most of these lavas as trachydacites and trachyandesite (fig. 4); no age data have been reported but they are likely correlative to the aphanitic flows visited in the Avon volcanic field (STOP 1). Aphanitic flows composing this geographically expansive unit were likely effusive, erupting from multiple vents or fissures that are difficult to identify in the field.

Return to the vehicle and drive back out to the Highway 141. Turn right onto the highway and drive northwest passing Nevada Lake.

36.4 to 43   Rocks north and south of the highway are Eo-Oligocene volcanic rocks resting unconformably on strata of the Belt Supergroup. These rocks are deformed by a system of steeply dipping strike-slip faults interpreted to have formed in a dextral shear zone (McDonald and others, this volume).

43 to 51.3 Continue driving northward into the Nevada Valley towards the junction with Highway 200. Tertiary sediments of the Climbing Arrow Member of the Renova Formation, and overlying Sixmile Creek Formation underlie most of the Nevada Valley with a few remnants of Cabbage Patch beds. Quaternary glacial deposits cover the Tertiary sediments in the northern part of the valley. A suspected active fault bounds the valley's ENE margin, truncating the Snowslip, Helena, Empire, and Spokane Formations of the Belt Supergroup.

51.3 Turn right onto Highway 200 and drive east towards Lincoln traveling along the scenic Blackfoot River. Exposures of the Spokane, Empire, Helena, and Snowslip Formations occur north and south of the highway. These units are generally tilted to the east and displaced by high-angle, oblique-slip faults.

Continue driving east into the Lincoln Valley. The Lincoln Valley is mostly covered by Quaternary glacial outwash and till deposits obscuring the underlying geology. The trace of the St. Mary's-Helena Valley fault can clearly be seen along the northeastern margin of the Lincoln Valley. Continue driving east into the town of Lincoln.

67.1 Turn right onto Stemple Pass road at Lincoln's only stoplight and proceed southward towards Stemple Pass. The road traverses more Quaternary glacial deposits before entering the Nevada Mountains. Metasedimentary rocks of the Helena (typically yellow weathered) and Empire (gray-green argillite) Formations can be seen north and south of the road along Poorman Creek once in the mountains. These units are generally tilted and offset by steeply dipping faults and locally intruded by Eocene granodiorite (Tgd), including that of the Silver Bell Stock.

73.0 Mined placer gold deposits along Poorman Creek. Placer gold was likely derived from epithermal mineralization hosted in the Eocene volcanic rocks. These deposits were only worked for ten seasons between 1904 and 1945 (Lyden, 1948). The most productive year was 1910 when a total of 36 troy ounces of gold were recovered. McClellan Creek, a tributary of Poorman Creek, was much more productive yielding $7,000,000 in gold between 1864 and 1875.

80.7 Roadcut of the Silver Bell Stock. The Silver Bell Stock is an equigranular to porphyritic granodiorite composed of plagioclase, orthoclase, quartz, biotite, and hornblende. A single K-Ar age of 52.0 was reported for the Silver Bell Stock (Schmidt and others, 1994), but it is not clear where this sample was collected. Parker (1995) reported a K-Ar age of 48.5 Ma for a smaller porphyritic intrusion cropping out near Crater Mountain that we tentatively correlate with the larger Silver Bell Stock. These intrusions were emplaced just prior to the initiation of volcanism in the Crater Mountain volcanic field ca. ~48 Ma.

81.9 Stemple Pass. Turn left onto U.S. Forest Service road #1827. Continue straight on the main road through all intersecting jeep roads.

82.6 Turn left onto a small jeep road (#1825), drive 1.5 miles to a fork in the road and stop.

STOP 6	**84.1 (46.919, -112.498): Crater Mountain volcanic field.**

Park the vehicle near the fork in the road and begin walking along the west (left) fork of the road. Walk approximately 0.25 miles and then climb a small hill composed of porphyritic lava located immediately south (left) of the road.

STOP 6.1	**(46.9186, -112.503): Eocene porphyritic lava flows, Crater Mountain volcanic field.**

Porphyritic flows (Tdap) are the oldest units exposed in the Crater Mountain volcanic field and rest unconformably on metasedimentary rocks of the Belt Supergroup (fig. 9). Porphyritic flows typically form subdued outcrops and platy talus slopes along ridges. Individual flows are separated by intervals of autobreccia several meters thick and local thin paleosol intervals. Lava flows have a distinct porphyritic texture containing 20-30 percent white subhedral phenocrysts of plagioclase, 3-10 percent biotite books, and variable amounts of pyroxene and amphibole in a granular aphantitic groundmass. Intervals of moderately to densely welded pumice lapilli tuff are locally intercalated with porphyritic lavas. Whole-rock geochemical data show porphyritic lavas to be trachydacite and trachyandesite (fig. 4). Two U-Pb zircon ages of 47.41±0.22 and 48.07±0.18 Ma were obtained

Figure 9. Simplified geologic map of the Crater Mountain volcanic field. Map unit descriptions in McDonald and others (in prep).
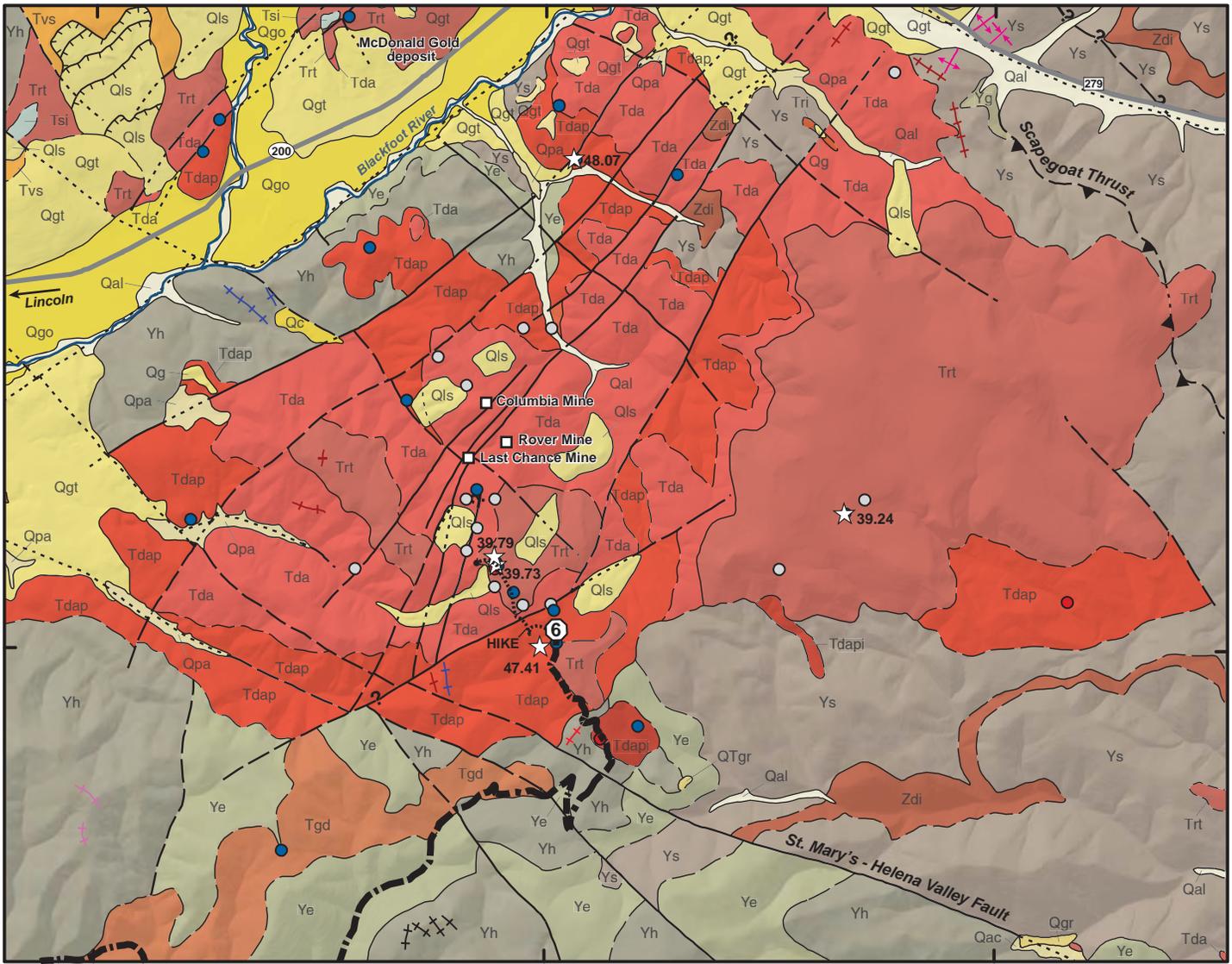
LEGEND

Road log route	
Hiking route	
①	Field trip stops
☆ 40.81	Zircon ages (Ma; McDonald and others, in prep)

Certain, approximate, concealed contact

Certain, approximate, concealed fault

Certain, approximate, concealed fold

Eocene rhyolite dikes and sills

Eocene(?) aphanitic shonkinite dikes and sills

Eocene(?) granodiorite intrusions

Middle Proterozoic meta-andesite and metadiorite sills and dikes

Geochemical analysis

● McDonald and others (in prep)

○ Parker (1995)

Tertiary volcanic units

Tvs	Volcaniclastic sediments
Trt	Rhyolite ash flows
Tda	Aphanitic dacite lava flows
Tdap	Porphyritic dacite lava flows

Tertiary intrusions

Tri	Rhyolite
Tdapi	Dacite porphyry
Tgd	Granodiorite

Units other than Tertiary igneous rocks

Quaternary sedimentary deposits: Qal, Qpa, Qc, Qac, Qgr, Qls, Qalo, Qg, Qgo, Qgt, QTgr

Tertiary sinter: Tsi

Mesoproterozoic metased. rocks: Yh, Ye, Ys, Yg

Mesoproterozoic dikes and sills: Zdi

from this unit. These lavas are remarkably similar but slightly older than porphyritic flows mapped in the eastern Garnet Range volcanic field (46.16 to 47.5 Ma; STOP 4), but were likely emplaced during the same magmatic event.

Begin ascending the relatively treeless south aspect of Crater Mountain, crossing the road and also a suspected fault juxtaposing porphyritic lava flows (Tdap) against aphanitic lava flows (Tda). Scattered outcrops of Tda occur on the south aspect of Crater Mountain.

STOP 6.2 (46.9208, -112.505): Eocene aphanitic lava flows, Crater Mountain volcanic field.

A series of aphanitic to slightly porphyritic lava flows (Tda) overlie the porphyritic lavas (Tdap) and are remarkably similar to those in the Avon and Garnet Range complexes. Aphanitic lavas commonly weather dark gray to brownish gray and form prominent cliffs and hogback ridges with blocky talus slopes. Lava flows commonly exhibit columnar joints and platy fractures developed along closely spaced flow bands. Zones of autobreccia and thin, brick-red paleosol intervals typically separate individual flows. Lava flows are mostly aphanitic, containing flow-aligned microlites of plagioclase and minor augite. Porphyritic flows (7-20% phenocrysts) contain black, subhedral phenocrysts of amphibole up to seven millimeters long that are flow-aligned, giving the rock a distinct trachytic texture. Whole-rock geochemical data indicate these flows are dominantly trachydacite and trachyandesite (fig. 4). No reliable age data have been obtained for this unit.

Porphyritic and aphanitic trachydacite and trachyandesite lavas host epithermal precious metals in the Seven Up Pete mining district adjacent to Crater Mountain. The mineralization is characterized by silicification, quartz veining, and associated argillic and propylitic alteration controlled by fault zones. Epithermal mineralization was likely associated with siliceous magmatism and emplacement of the overlying ash-flow tuff deposits (Trt).

Continue ascending to the summit ridge of Crater Mountain, crossing the contact between the aphanitic lavas (Tda) and rhyolitic ash-flow deposits (Trt).
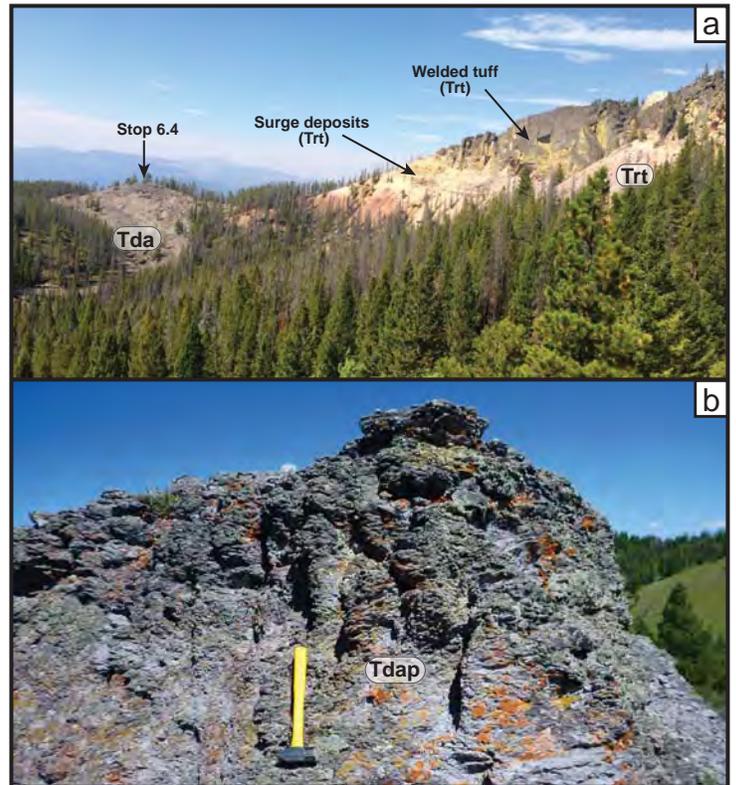

Figure 10. Field photographs from the Crater Mountain volcanic field. a) Rhyolite ash-flow tuff (Trt) of Crater Mountain overlying aphanitic dacitic lava flows (Tda; STOP 6.4). b) Flow-foliated interior of a porphyritic dacite lava flow (Tdap).

STOP 6.3 (46.9241, -112.506): Eocene rhyolite tuff, Crater Mountain volcanic field.

The summit ridge of Crater Mountain offers commanding 360-degree views of the surrounding geology. The hills and mountains immediately adjacent to Crater Mountain are underlain by tilted and faulted Mesoproterozoic rocks unconformably overlain by Eocene volcanic rocks and cut by Mesoproterozoic to Tertiary intrusions. The Helena Valley Fault, a regional strike-slip fault extending for over 100 km (Wallace and others, 1990), can be seen to the southeast where it bounds the northeast margin of the Helena Valley. The fault crosses the mountains southwest of Crater Mountain and continues to the northwest where it bounds the northeast margin of the Lincoln Valley. The high peaks defining the Scapegoat Wilderness boundary can be seen in the distance to the northwest including Red Mountain that dominates the skyline. A large Quaternary landslide can be seen in the upper reaches of the Humbug Creek drainage to the west, immediately below the Crater Mountain summit ridge. The scarp of this landslide provides an excellent cross-

sectional view of the rhyolite tuff underlying Crater Mountain.

Pyroclastic rocks composing Crater Mountain were originally interpreted to be a exogeneous dome or plug (Melson, 1964). Parker (1995) later mapped these rocks as a rootless body of crystal-lithic, rhyolite, lapilli tuff resting unconformably on dacitic lavas (Tda). The tuff of Crater Mountain is part of an extensive sheet of rhyolite ash-flow tuff deposits that form flat-crested, steep-sided plateaus supporting stunted stands of Lodgepole pine. Ash-flow tuff deposits typically contain 10 to 30 percent subangular lithic fragments that are mostly derived from the Belt Supergroup, but also include porphyritic and aphanitic fragments from the underlying Eocene volcanics. Pumice lapilli compose 10-25 percent of the rock and typically occur as fiamme in zones of dense welding. Tuff deposits typically contain subequal amounts of subhedral, smokey-gray quartz phenocrysts and euhedral sanidine phenocrysts. Quartz crystals are commonly broken and deeply embayed. Rare biotite books compose less than one percent of the rock. Ash-flow tuff deposits exhibit considerable local variation in the degree of welding. Unwelded ash and breccia intervals locally exhibit planar and low-angle cross-laminated beds and grading, and are interpreted to be pyroclastic surge deposits (Fisher and Schmincke, 1984; Cas and Wright, 1988; Parker, 1995). Devitrification of ash-flow deposits varies from incipient to complete, and locally abundant lithophysae are up 60 centimeters in diameter near the base of ash-flow deposits. Rhyolite ash-flow deposits do not contain major unconformities, air-fall deposits, or reworked bedded ash deposits, and therefore are considered to represent one, compound cooling unit composed of multiple ash-flows emplaced in rapid succession. Whole-rock geochemical data confirm a high-silica rhyolite composition for the ash-flow deposits (fig. 4). U-Pb zircon ages span 39.2 to 39.8 Ma, indicating the ash-flow deposits are slightly younger than rhyolite lava flows in the Avon volcanic field (40.6-40.8 Ma), discounting zircon residence time in the magma chamber.

The rhyolite ash-flow deposits are cut by a system of northeast-striking faults that dropped the fault block northwest of the Blackfoot River a minimum of 400 meters (Parker, 1995). A 360+ meter thick sequence of volcaniclastic conglomerate, sandstone and fine-grained sediments interbedded with a biotitic rhyolite tuff overlie the downthrown block. The older rhyolite ash-flow deposits (Trt) host epithermal precious mineral deposits forming the McDonald gold deposit (Bartlett and others, 1998).

Arcuate structures, dome complexes, or vent facies associated with a caldera-type volcanic setting are not readily identifiable in the Crater Mountain area; therefore, the source of the ash-flow deposits (Trt) is somewhat uncertain. These features may be buried by ash-flow and volcaniclastic deposits, and further obscured by transtensive faulting and Quaternary glacial deposits. Extensive volcaniclastic deposits occurring north of the Blackfoot River are dominated by detritus derived from the older ash-flow tuff (Trt), and likely accumulated in a basin formed either by caldera-type subsidence and/or transtensive faulting. The development of a geothermal system and associated mineralization (37-39 Ma; Bartlett and others, 1998) north of the Blackfoot River was closely tied to volcanism, possibly occurring along the margin of a caldera. Alternatively, the rhyolite tuff deposits in the Crater Mountain area could be outflow sheets sourced from a caldera in the Avon volcanic field.

Continue walking north along the Crater Mountain summit ridge examining welded and unwelded parts of the Crater Mountain tuff. Descend along the northwest spur ridge crossing the contact with the underlying aphanitic lavas.

STOP 6.4 (46.9275, -112.514): overview of the Crater Mountain tuff.

Standing on the small knob of aphanitic lava (Tda) provides an excellent cross-sectional view of the Crater Mountain tuff. At least two zones of welded tuff (dark colored) delineated by weakly to unwelded tuff intervals (light colored) can be seen from this vantage point. The Crater Mountain tuff exhibits well-developed flow foliations that mirror the contact with the underlying dacitic lavas (Tda), and steepens towards the southern end of the Crater Mountain. Parker (1995) interpreted the steepening of the flow foliation to be rheomorphic, formed by slumping and shearing of the ash-flow against a paleovalley wall when it was still hot and plastic.

Return to the vehicle by retracing the hike in, or by walking along the base of the ignimbrite and ascend-

ing the southwest spur ridge of Crater Mountain. Drive back to Elliston by retracing the road log route, or by traveling east from Stemple Pass to Highway 279 and returning to Elliston via Helena.

End Road Log

SUMMARY

Elliston's Tertiary volcanic fields share a strikingly similar volcanic stratigraphy that can be grouped into an upper and lower series. The lower series consists of aphanitic and porphyritic lava flows (46.16 to 48.07 Ma) of intermediate-composition with alkaline affinities. The lava flows are intercalated with subordinate ash flow tuffs of similar composition and rhyolite lava flows. The upper volcanic series consists of voluminous rhyolite lavas and ashflows (39.24 to 40.8 Ma) that were possibly erupted in caldera-type settings, and locally hosted epithermal mineralization. Rhyolitic sequences are locally overlain by Tertiary volcaniclastic and sedimentary deposits intercalated with basaltic lavas (29.95 to 37.3 Ma) and rhyolite tuff (36.5 Ma). The flare-up in Eocene magmatism was coeval with the development of the nearby Anaconda metamorphic core complex indicating volcanism in the Elliston region may have occurred in an extensional or transtensive tectonic setting. Volcanic deposits are tilted and displaced by a system oblique-slip faults bordering valley grabens. The grabens are interpreted to be pull-apart structures that initiated in the Miocene and have remained active to the present.

REFERENCES

Bartlett, M.W., Enders, M.S., Volberding, J.E., and Wilkinson, W.H., 1998, The geology of the McDonald gold deposit, Lewis and Clark County, Montana: Northwest Geology, v. 28, p. 27-52.

Breitsprecher, K., Thorkelson, D.J., and Dostal, J., 2003, Geochemical confirmation of the Kula-Farallon slab window beneath the Pacific Northwest in Eocene time: Geology, v. 31, no. 4, p. 351-354.

Callmeyer, T.J., 1984, The structural, volcanic, and hydrothermal geology of the Warm Springs Creek area, eastern Garnet Range, Powell County, Montana: Bozeman, Montana State University, M.S. thesis, 79 p., 2 sheets, scale: 1:41,700.

Cas, R.A.F. and Wright, J.V., 1988, Volcanic Successions Ancient and Modern: Unwin Hyman, London, Boston, Sydney, Wellington, 528 p.

Case, J.C., Arneson, C.S., and Hallberg, L.L., 2013: Surficial geologic map of Wyoming: Wyoming State Geological Survey: Geologic Map WSGS-1998-HSDM-1a, scale 1:500,000.

Chadwick, R.A., 1981, Chronology and structural setting of volcanism in southwestern and central Montana: Montana Geological Society, 1981 Field Conference Southwestern Montana, p. 301-310.

Chadwick, R.A., 1985, Overview of Cenozoic volcanism in the west-central United States, *in* Flores, R.M., and Kaplan, S.S. eds., Economic Paleontologists and Mineralogists, Rocky Mountain Section, Symposium 3, p. 359-381.

Dostal, J., Church, B.N., Reynolds, P.H., and Hopkinson, L., 2001, Eocene volcanism in the Buck Creek basin, central British Columbia (Canada): transition from arc to extensional volcanism: Journal of Volcanology and Geothermal Research, v. 107, p. 149-170.

Fisher, R.V. and Schmincke, H.U., 1984, Pyroclastic Rocks: Springer-Verlag, Berlin, Heidelberg, New York, Tokyo, 472 p.

Feeley, T.C., 2003, Origin and tectonic implications of across-strike geochemical variations in the Eocene Absaroka Volcanic Province, United States: The Journal of Geology, v. 111, p. 329-346.

Foster, D.A., Grice, W.C., and Kalakay, T.J., 2010, Extension of the Anaconda metamorphic core complex: ^{40}Ar/^{39}Ar thermochronology and implications for Eocene tectonics of the northern Rocky Mountains and the Boulder Batholith: Lithosphere, v. 2, no. 4, p. 232-246.

Hanna, W.F., Hassemer, J. H., Elliott, J.E., Wallace, C.A., and Snyder, S.L., 1994, Maps showing gravity and aeromagnetic anomalies in the Butte 1° x 2° quadrangle, Montana: U.S. Geological Survey Miscellaneous Investigations Series Map I-2050, 35 p., 2 sheets, scale 1:250,000.

Humphreys, E.D., 1995, Post-Laramide removal of the Farallon slab, western United States: Geology v. 23, p. 987-990.

Knatterud, L.K., Speece, M.A., Mosolf, J.G., and Zhou, X., 2015, Using gravity and seismic reflection profiling to decipher the structural setting of

the Avon Valley, west-central Montana: Northwest Geology, v. 44.

LeBas, M.J., LeMaitre, R.W., Streckeisen, A., and Zanettin, B., 1986, A chemical classification of volcanic rocks based on the total alkali silica diagram: Journal of Petrology, v. 27, p. 745-750.

Lewis R.S., Link, P.K., Stanford, L.R., and Long, S.P., 2012, Geologic map of Idaho: Idaho Geological Survey Geologic Map 9, scale 1:500,000.

Lyden, C.J., 1948, Gold placers of Montana (reprinted 1987): Montana Bureau of Mines and Geology Reprint Series 6, 120 p.

Massey, N.W.D., MacIntyre, D.G., Desjardins, P.J. and Cooney, R.T., 2005: Digital map of British Columbia: Whole Province, B.C. Ministry of Energy and Mines, GeoFile 2005-1, scale 1:250,000.

MacDonald, R., Upton, B.G., Collerson, K.D., Hearn, B.C. and James, D., 1992, Potassic mafic lavas of the Bearpaw Mountains, Montana: mineralogy chemistry and origin: Journal of Petrology, v. 33, p. 305-346.

Mahoney, J. B., Pignotta, G.S., Ihinger, P.D., Wittkop, C., Balgord, E.A., Potter, J.J., and Leistikow, A., 2015, Geologic Relationships in the Northern Helena Salient, Montana: Geology of the Elliston Region: Northwest Geology, v. 44.

McDonald, C., Lonn, J.D., Vuke, S.M., and Mosolf, J.G., Field trip to the Nevada Lake breccias, Powell County, Montana: Northwest Geology, v. 44.

McDonald, C., Mosolf, J.G., Vuke, S.M., and Lonn, J.D., in preparation, Geologic map of the Elliston 30′ x 60′ quadrangle, west-central Montana: Montana Bureau of Mines and Geology Open-File Report, 1 sheet, scale 1:100,000.

Melson, W.G., 1964, Geology of the Lincoln area, Montana and contact metamorphism of the impure carbonate rocks: Princeton, New Jersey, Princeton University, Ph.D. dissertation, 153 p., 4 pls., scale 1:31,680.

Morris, G.A., Larson, P.B., Hopper, P.R., 2000, "Subduction Style" magmatism in a non-subduction setting: the Colville igneous complex, NE Washington State, USA: Journal of Petrology, v. 41, p. 43-67.

Mosolf, J.G., and Vuke, S. M., (in review), Geologic map of the Gravely Mountain 7.5' quadrangle,

Lewis and Clark and Powell Counties, west-central Montana: Montana Bureau of Mines and Geology Open-File Report, 1 sheet, scale: 1:24,000.

Moye, F.J., Hackett, W.R., Blakley, J.D., and Snider, L.G., 1988, Regional geologic setting and volcanic stratigraphy of the Challis volcanic field, central Idaho: Idaho Geological Survey Bulletin, v. 27, p. 87-99.

Mudge, M.R., and Earhart, R.L., 1983, Bedrock geologic map of part of the northern Disturbed Belt, Lewis and Clark, Teton, Pondera, Glacier, Flathead, Cascade, and Powell Counties, Montana: U.S. Geological Survey Miscellaneous Investigations Map I-1375, 2 sheets, scale 1:250,000.

Pardee, J.T., 1917, The Garrison and Philipsburg phosphate fields, Montana: U.S. Geological Survey Bulletin 640-K, p. 195-228.

Parker, D.B., 1995, The geology, petrology, and volcanic history of the Crater Mountain Volcanic Complex, Lewis and Clark County Montana: Missoula, University of Montana, M.S. thesis, 240 p., 1 sheet, scale: 1:24,000.

Peterson, M.P., 1985, The geology of the southwest quarter of the Avon 15-minute quadrangle, Powell County, Montana: Butte, Montana College of Mineral Science and Technology, M.S. thesis, 78 p., 1 sheet, scale: 1:62,500.

Portner, R.A., Hendrix, M.S., Stalker, J.C., Miggins, D.P., and Sheriff, S.D., 2011, Sedimentary response to orogenic exhumation in the northern Rocky Mountain Basin and Range province, Flint Creek basin, west-central Montana: Canadian Journal of Earth Sciences, v. 48, p. 1131-1153.

Reynolds, M.W., 1979, Character and extent of basin-range faulting, western Montana and east-central Idaho, *in* Newman, G.W., and Goode, H.D., eds., Basin and Range Symposium: Rocky Mountain Association of Geologists, p. 185-193.

Roll, T.E., Neeley, M.P., Speakman, R.J., and Glascock, M.D., 2005, Characterization of Montana cherts by LA-ICP-MS, *in* Laser Ablation-ICP-MS in Archaeological Research, Speakman, R.J., and Heff, H., eds., University of New Mexico Press, Albuqueque, p. 58-76.

Schleiffarth, K. and Larson, P., 2014, Eocene magmatism across the Northern Cordillera: Northwest Geology, v. 43, p. 15-20.

Schmidt, R.G., Loen, J.S., Wallace, C.A., and Mehnert, H.H., 1994, Geology of the Elliston region, Powell and Lewis and Clark counties, Montana: U.S. Geological Survey Bulletin 2045, scale 1:62,500.

Schuster, J.E., 2005, Geologic map of Washington State: Washington Division of Geology and Earth Resources Geologic Map GM-53, scale 1:500,000.

Sears, J.W., and Hendrix, M., 2004, Lewis and Clark Line and the rotational origin of the Alberta and Helena Salients, North American Cordillera, *in* Sussman, A.J., and Weil, A.B., eds., Orogenic curvature: integrating paleomagnetic and structural analyses: Geological Society of America Special Paper 383, p. 173-186.

Trombetta, M.J., 1987, Evolution of the Eocene Avon Volcanic Complex, Powell County, Montana: Bozeman, Montana State University, M.S. thesis, 112 p., 2 sheets, scale: 1:24,000.

Vance, J.A., 1979, Early and middle Cenozoic magmatism and tectonics in Washington State: Geological Society of America Abstracts with Programs, v. 11, p. 132.

Vuke, S.M., Porter, K.W., Lonn, J.D., and Lopez, D.A., 2007, Geologic Map of Montana: Montana Bureau of Mines and Geology Geologic Map 62, 73 p., 2 sheets, scale 1:500,000.

Walker, G.W., and MacLeod, N.S., 1991, Geologic map of Oregon: U.S. Geological Survey, 2 sheets, scale 1:500,000.

Wallace, C.A., Lidke, D.J., and Schmidt, R.G., 1990, Faults of the central part of the Lewis and Clark Line and fragmentation of the Late Cretaceous foreland basin in west-central Montana: Geological Society of America Bulletin, v. 102, p. 1021-1037.
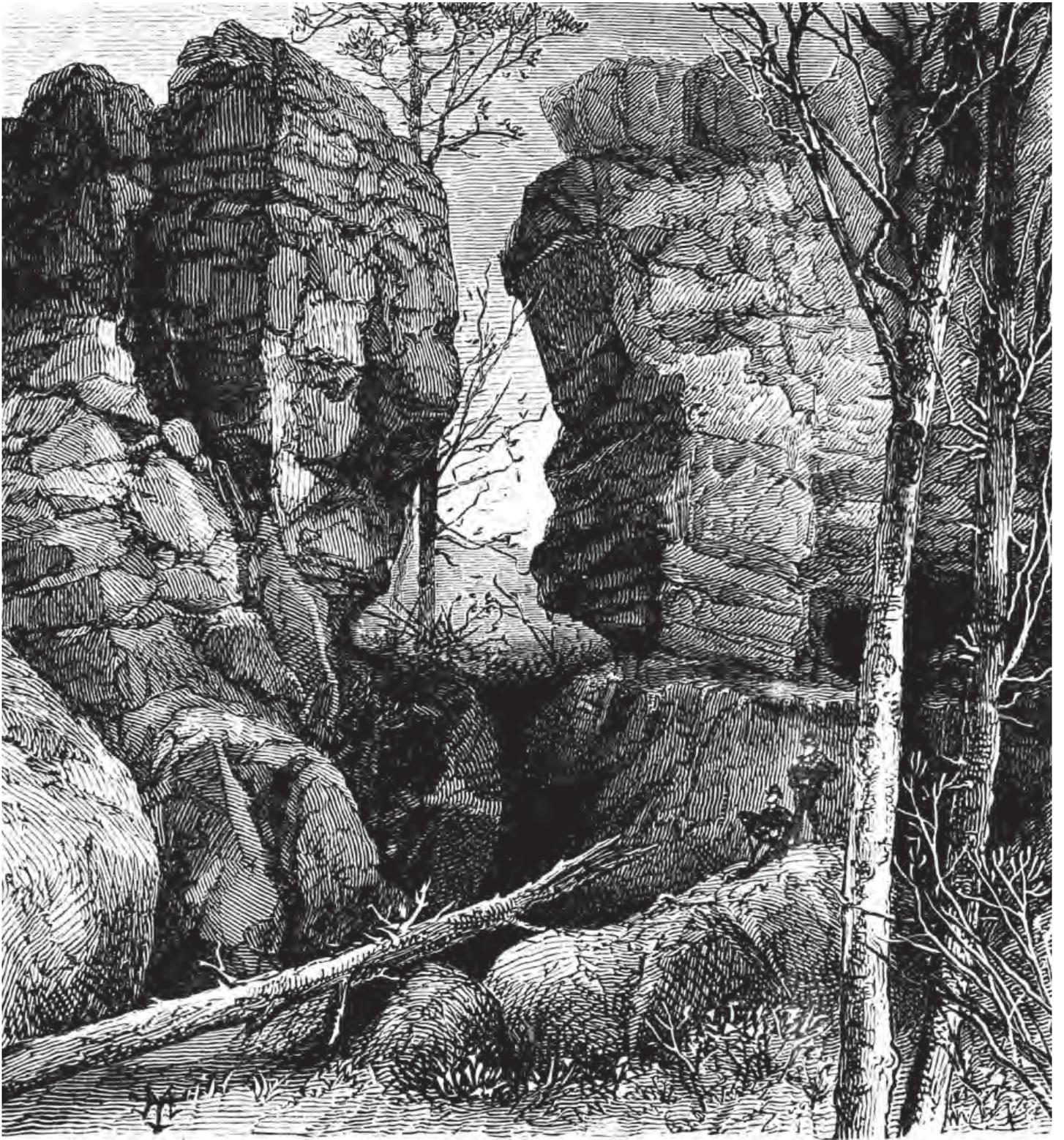
ROAD LOG: REGIONAL GEOLOGY AND GLACIAL GEOLOGY OF THE HELMVILLE TO LINCOLN AREA, POWELL AND LEWIS AND CLARK COUNTIES, MONTANA

L.N. Smith and Katie McDonald

Montana Bureau of Mines and Geology, Montana Tech of the University of Montana, Butte, MT 59701, lsmith@mtech.edu

INTRODUCTION

This road log is for a somewhat informal and scenic geologic field trip around and through the mountains northwest of Lincoln, Montana (fig. 1). The geology of the area was published on the Dearborn River (Vuke, 2015) and Elliston (McDonald and others, in prep.) 30 x 60-minute quadrangles.

Highlights of the trip are the scenic views from Coopers Lake and along the Huckleberry Pass road, from near Kleinschmidt Flat on the northwest to Lincoln on the southeast (fig. 2). Bedrock along the route is the Helena, Spokane, and Greyson Formations of the Mesoproterozoic Belt Supergroup. Tertiary sedimentary rocks of the Renova Formation locally overlie the Belt rocks. The southeastern portion of the Rocky Mountain ice cap (Locke, 1995) terminated near Lincoln and most of the glacial deposits in the area formed during several advances and subsequent melts of large glaciers during the :Pleistocene Bull Lake and Pinedale glaciations. Some of the mountains along the route were not glaciated during the last (Pinedale) glacial period that lasted from about 22 to 15ka (Young and others, 2011). The distribution of the last-glacial ice and glacial features are shown in Vineyard and others (this volume).

ROAD LOG

Leave Elliston and travel west on MT-12 to Avon, MT. Log begins at the intersection of MT-141 at MT-12.

Mileage

0.0 Avon MT, travel north on MT-141. We will travel through the Avon Valley, a northwest trending valley underlain by the Tertiary Renova Formation. The surrounding mountain and low hills are underlain by Mesoproterozoic through Mesozoic sedimentary rock, Cretaceous intrusive rock, and Tertiary volcanics.
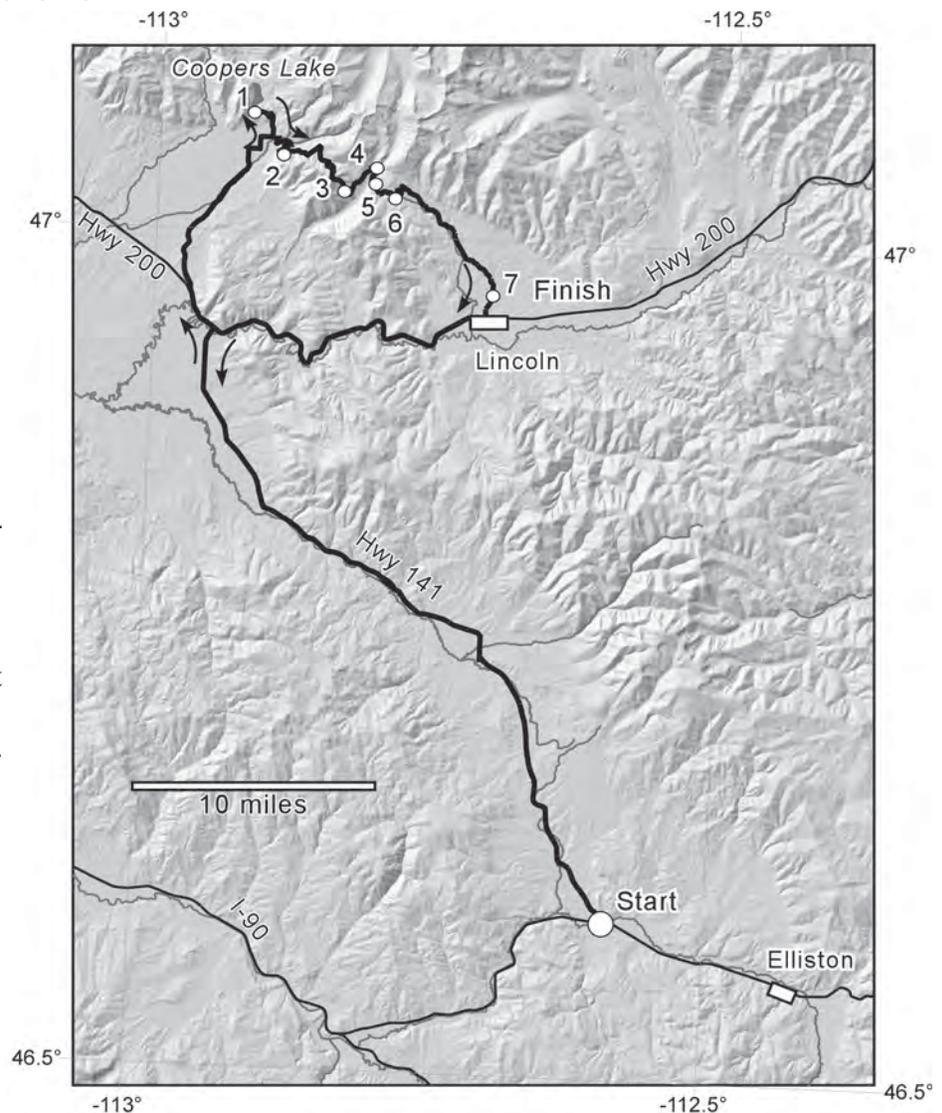

Figure 1. Location map of field trip route.
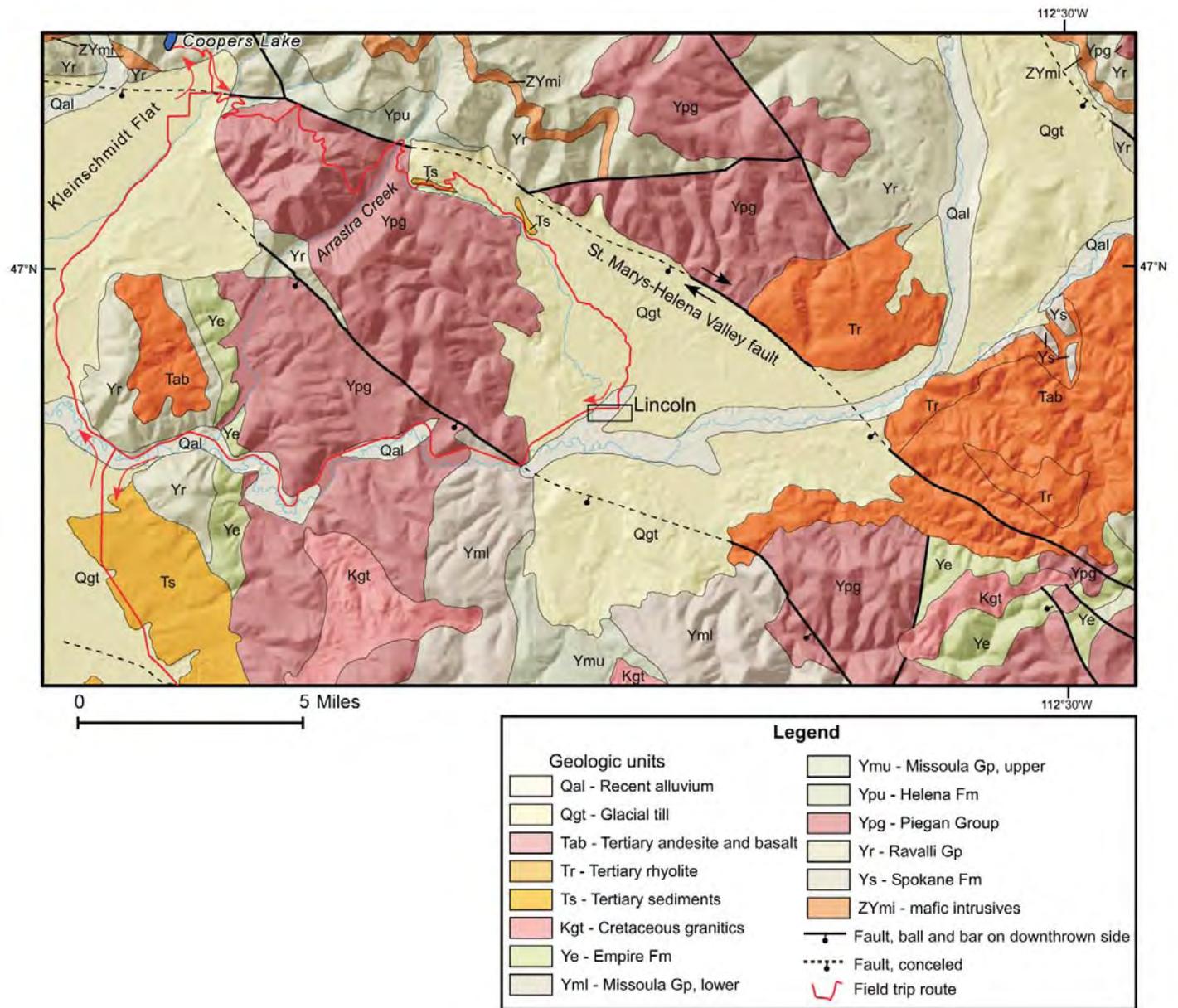
Figure 2. Generalized geological map of the field trip route (modified from Vuke and others, 2007; Vuke, 2014).

4.5   At 9:00 AM distinct rotational landslide in Tertiary Renova Formation of the Avon Valley.

18.1   Nevada Lake on left

27.5   Turnoff to Helmville on left, continue north. Helmville is located in the Nevada Creek Valley, another intermontane valley underlain by Tertiary sedimentary and volcanic rocks. The mountains to the east are underlain by metasediments of the Ravalli and Piegan Groups of the Mesoproterozoic Belt Supergroup.

32.5   Intersection with MT-200. Turn left (to northwest), watch for fast-moving traffic. The steep slope directly ahead is underlain by the Spokane

Formation (Ravalli Group).

35.2   Just past the left turn to Brown's Lake, turn right (northeast) on Cooper's Lake road. We are crossing ablation till of the McDermont Creek/North Fork of the Blackfoot glacier that extended ~3 miles southwest of here to beyond Browns Lake (fig. 1). The terrain is classic kame and kettle topography, highlighted by NE-SW trending, sinuous eskers.

36.4   Crest of prominent esker formed in an ablation till deposit.

37.5   Road follows boundary between outwash surface of Kleinschmidt Flat and kame and kettle topography. The southeastern edge of Kleinschmidt

Flat is nearly straight and Vuke (2014) shows this boundary as a NE-trending lineament. We speculate that it may be a fault.

40.7   Note along this road, we have been traveling in an underfit stream valley that developed upon incision of glacial outwash deposits on the southeastern edge of Kleinschmidt Flat, possibly in late-glacial or Holocene time.

41.8   Turn right to stay on main road

42.8   Turn right to stay on main road. The mountains straight ahead are the southern part of the Scapegoat Wilderness and are underlain by Belt Supergroup metasediments. The mountains are uplifted along the St. Marys-Helena Valley fault that parallels the range front (fig. 2). The fault extends from the Ovando Valley east to the Helena Valley and is one of the principal faults along the eastern Lewis and Clark line shear zone (Reynolds, 1979; Reynolds and Brandt, 2005; Wallace and others, 1990; Sears and others, 2004). The St. Marys-Helena Valley fault marks the northern boundary of the Lewis and Clark line in this area and has Cenozoic strike-slip and normal movement. We will cross this fault several times during the fieldtrip.

43.3   Turn left towards Coopers Lake

44.3   Pond to east is interpreted as a plunge pool at the base of a spillway over which glacial meltwater flowed

45.4 STOP 1

Rest stop and overlook of Coopers Lake from USFS Big Nelson Campground. Coopers Lake is a bedrock-bounded glacial lake along McDermott Creek. The Spokane Formation of the Belt Supergroup makes up the dam. Till was mapped near the campground and to the north (Vuke, 2014). We will discuss possible processes that formed the lake basin.

Back track along Coopers Lake road.

47.5   Turn left on Huckleberry Pass road and drive towards Lincoln, MT. We will be driving through till deposits from the Dry Creek glacier that merged with the glacier from McDermott Creek. The till overlies the Helena Formation. The Helena weathers a

characteristic yellowish brown and is visible in several of the road cuts along the route.

49.9 STOP 2

In this vicinity, we will stop at an overlook for nice views of Kleinschmidt Flat, the trace of the St. Marys-Helena Valley fault, and the southern end of the Scapegoat Wilderness. The St. Marys-Helena Valley fault is one of the major WNW trending faults of the Lewis and Clark Line-a complex zone of folds and fault that extends for about 800 km from western Idaho to west-central Montana.

51.2   Near top of lateral moraine in the Dry Creek glacier. Apparently Huckleberry Pass (to east) was not under ice in the most recent glaciation.

52.7   Grayish green argillite of the Mesoproterozoic Greyson Formation along the road. We have crossed into the footwall of the St. Marys-Helena Valley fault. The fault approximately parallels the road corridor (fig. 2) and juxtaposes the Helena Formation against the Greyson Formation; the Spokane and Empire Formations are missing. Movement on the fault is both strike slip and dip slip. There are rare striations in the outcrops along the road that may be tectonic or glacial.

53.9   Huckleberry Pass

55.6 STOP 3

At switchback overlooking Arrastra Creek valley. Till of the Arrastra Creek glacier overlies Helena Formation. The glacier flowed over the Arrastra Creek drainage divide from the Rocky Mountain Ice Cap to the north. Outcrop of Helena Formation is visible on the south side of the valley.

57.3 STOP 4

Walk up to nice exposures of the Greyson Formation north of the road along Arrastra Creek. The Greyson is grayish green argillite and siltite that dips gently north. We are again in the footwall of the St. Marys-Helena Valley fault.

58 STOP 5

Outcrops of the Helena Formation on the hanging wall of the St. Marys-Helena Valley fault. The Helena

Formation dips about 50 degrees into the fault, much steeper than the Greyson we observed at the previous stop.

58.4   Near Reservoir Lake

59.8 ⬚ **STOP 6**

Outcrops of Tertiary Renova Formation, Beaver Creek beds. The Renova Formation is exposed in several locations in the Beaver Creek area. It consists of laminated marlstone, oil shale, carbonaceous shale, limestone, conglomerate, and tuff. There are plant, insect, fish, frog, and salamander fossils (Miller, 1980; Jacobson, 1975, Fisher, 1984). These locations are laagerstatten deposits with outstanding preservation of tissues. The beds are Oligocene in age and equivalent to the Climbing Arrow Member of the Renova Formation. In 1978, the U.S. Geological Survey investigated these beds as a potential lithium resource but the grade and volume was too low to be economic (Brenner-Tourtelot and others, 1978). The beds at this location dip to the NE, into the St. Marys-Helena Valley fault.

63.7   Intersection with No. Beaver Creek road on left. We are traveling across till, likely due to ablation. A few lateral moraines were mapped to the east and west (Vineyard and others, this volume).

66.7   Smith Lake on right is a large kettle in the ablation moraine.

67.5 ⬚ **STOP 7**

Pull off road near two-track road on left (southeast). N. Beaver Creek road follows near a boundary of till (hummocky landscape on northwest) outwash plain, and recent alluvium. This area is near a recessional moraine from the Beaver Creek glacier that overrode the Lincoln area and abutted the mountains to the south.

68   Intersection of MT-200 and North Beaver Creek road.

End of log

REFERENCES

Brenner-Tourtelot, E.F., Meier, A.L., and Curtis, C.A., 1978, Lithium in rocks from the Lincoln, Helena, and Townsend areas, Montana: U.S. Geological Survey Open-File Report 78-430, 27 p.

Fisher, C., 1984, An Eocene palynoflora of the Renova Formation, Lincoln, Montana: Missoula, Montana University of Montana, unpublished B.S. thesis, 13 p.

Jacobsen, K.F., 1975, A fossil flora from the Beaver Creek area, west-central Montana: Missoula, Montana, University of Montana, unpublished B.S. thesis, 54 p.

Locke, W.W., 1995, Modelling of icecap glaciation of the northern Rocky Mountains of Montana, Geomorphology, v. 14, p. 123-130.

McDonald, C., Mosolf, J.G., Vuke, S.M., and Lonn, J.D., in prep, Preliminary geologic map of the Elliston 30' x 60' quadrangle, west-central Montana: Montana Bureau of Mines and Geology Open-File Report xxx, 1 sheet, scale 1:100,000.

Miller, C.N., 1980, Road Log No. 2, Missoula to florule locales near Drummond and Lincoln, in Guidebook of the Drummond-Elkhorn areas, west-central Montana: Montana Bureau of Mines and Geology Special Publication 82, p. 11-16.

Reynolds, M.W., 1979, Character and extent of basin-range faulting, western Montana and east-central Idaho, in Newman, G.W., and Goode, H.D., eds., RMAG and UGA 1979 Basin and Range Symposium: Denver, Colo., Rocky Mountain Association of Geologists, p. 185-193.

Reynolds, M.W., and Brandt, T.R., 2005, Geologic map of the Canyon Ferry Dam 30' x 60' quadrangle, west-central Montana: U.S. Geological Survey Scientific Investigations Map 2860, 32-p. pamphlet, 3 plates, scale 1:100,000.

Sears, J.W., and Hendrix, M.S., 2004, Lewis and Clark Line and the rotational origin of the Alberta and Helena salients, North American Cordillera, in Sussman, A.J., and Weil, A.B., eds., Orogenic Curvature: Integrating Paleomagnetic and Structural Analyses: Geological Society of America Special Paper 383, p. 173-186.

Vuke, S.M., 2014, Preliminary geologic map of the Dearborn River 30' x 60' quadrangle, west-central Montana: Montana Bureau of Mines and Geology Open-File Report 649, 9 p., 1 sheet, scale 1:100,000.

Vuke, S.M., Porter, K.W., Lonn, J.D., and Lopez, D.A., 2007, Geologic map of Montana: Montana

Bureau of Mines and Geology Geologic Map 62, 73 p., 2 sheets, scale 1:500,000.

Wallace, C.A., Lidke, D.J., and Schmidt, R.G., 1990, Faults of the central part of the Lewis and Clark line and fragmentation of the Late Cretaceous foreland basin in west-central Montana: Geological Society of American Bulletin, v. 102, p. 1021-1037.

Young, N.E., Briner, J.P., Leonard, E.M., Licciardi, J.M., and Lee, K., 2011, Assessing climatic and nonclimatic forcing of Pinedale glaciation and deglaciation in the western United States: Geology, v. 39, p. 171-174.
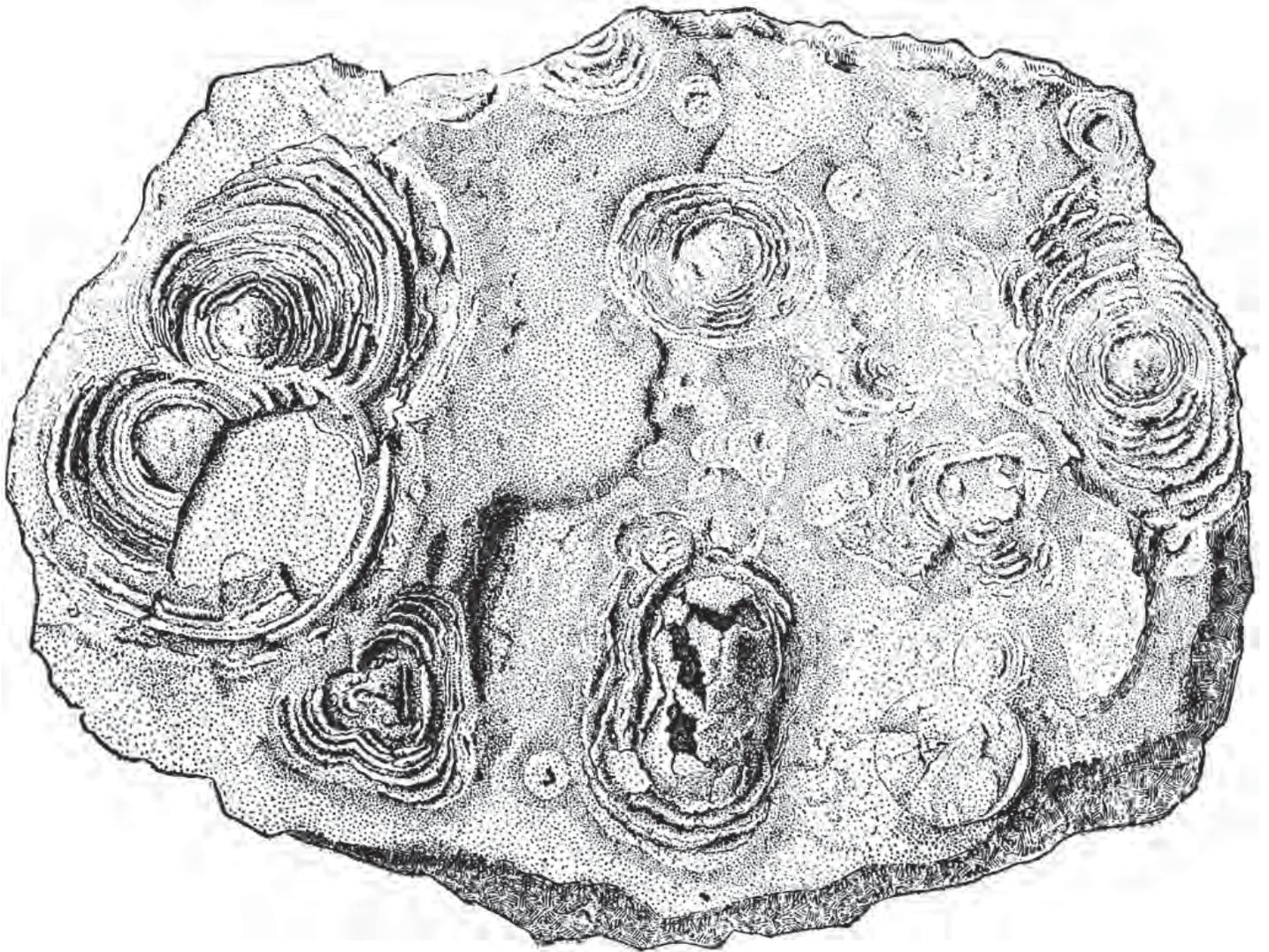
STRATIGRAPHIC AND STRUCTURAL CONTROLS OF MASS WASTING DEPOSITS IN THE SOUTHERN GARNET RANGE, MONTANA: POST-CONFERENCE FIELD TRIP

Bruce E. Cox

Geologist /Consultant—Missoula, Montana

INTRODUCTION

Recent geologic mapping in the southern Garnet Range (Cox, 2014) revealed numerous mass wasting deposits not previously documented including several large Quaternary landslides and an extensive system of Tertiary debris flow lobes and aprons. Three large landslides (Qls) each covering greater than 20 acres and several adjacent or isolated smaller landslides and slumps occur on the Bearmouth Ranch and Weaver Ranch between Drummond and Bonner. Mapping suggests that headwall detachment surfaces are aligned with a pattern of north and northwest-trending (shear) faults and fold axes directly north of the Bearmouth thrust.

Tertiary debris flow deposits (Tdf) are locally overlain by or conformable within Tertiary volcanic sequences. The Tdf surrounding Mount Baldy was deposited on incised topography underlain by the Amsden Formation and along rhyolite flow margins.

It is speculated that larger segments of the Tdf may be dismembered parts of a debris flow complex that extended southward from the crest of the Garnet Range parallel to the trend of the Bearmouth volcanic field.

ROAD LOG

The field trip will begin at Bearmouth (fig. 1). The trip will follow a counter-clockwise traverse (fig. 2) starting across Proterozoic rocks in the hanging wall
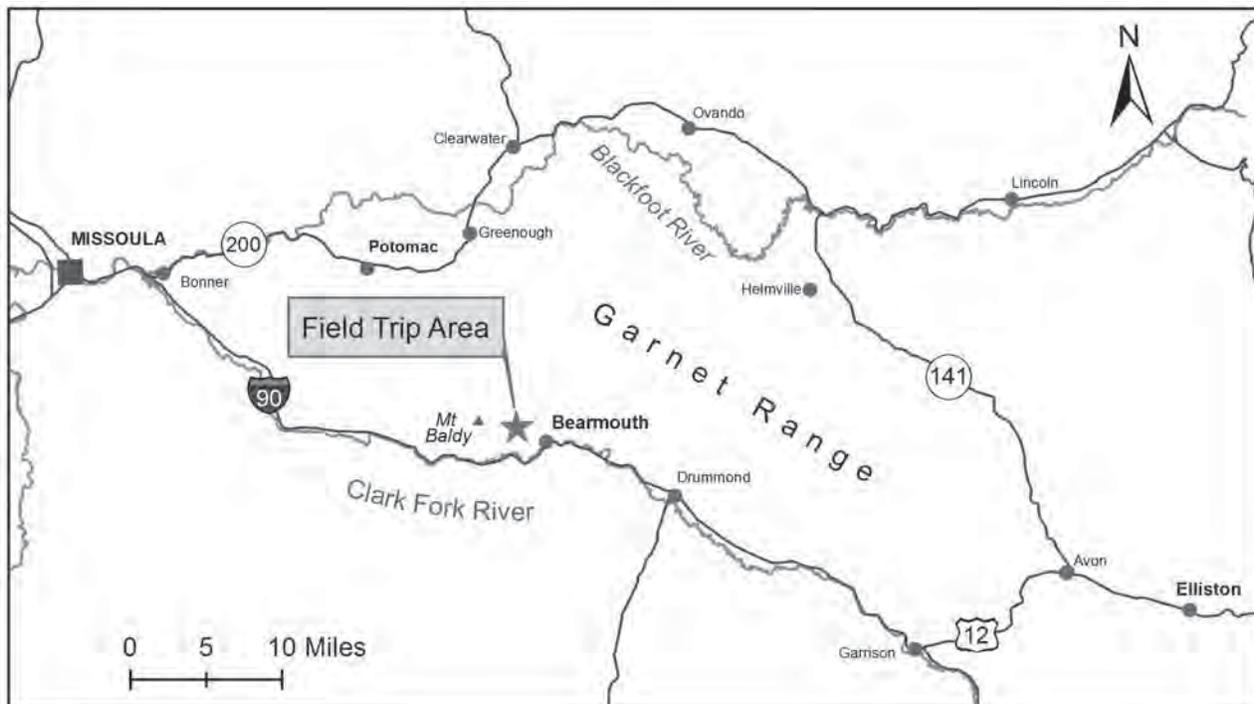

Figure 1. Field trip location map.

Northwest Geology, v. 44, 2015, p. 239–245
239
*The Journal of the Tobacco Root Geological Society*
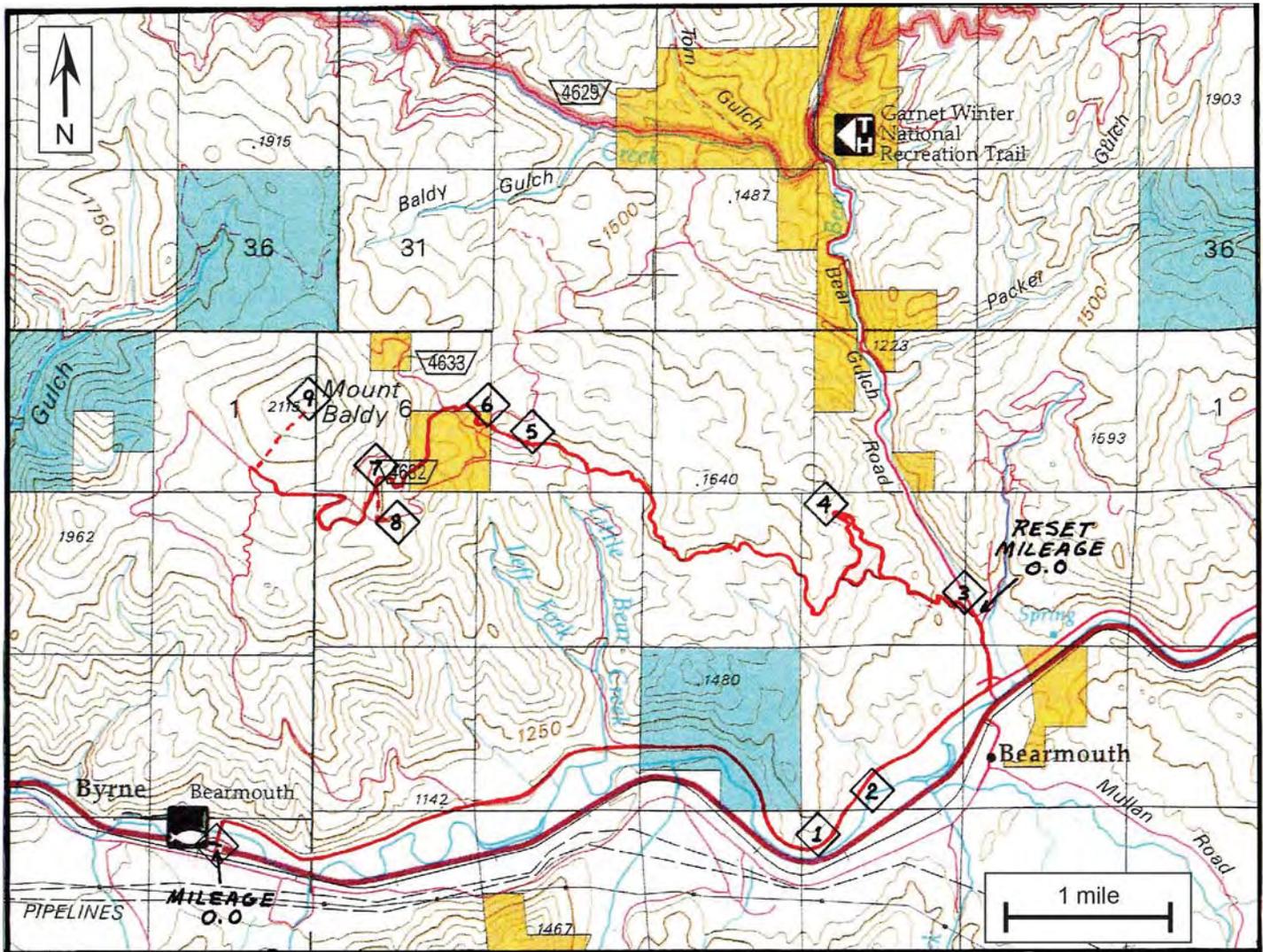
Figure 2. Map showing land ownership, field trip route, and stops in the Bearmouth area, Granite County, Montana. Numbered diamonds are field trip stops. Blue is State land, yellow is BLM, and white is privately owned land.

of the Bearmouth thrust, then climbing westward through the Bearmouth volcanics and ending in folded Paleozoic / Mesozoic strata.

MILEAGE

0.0   Turn off Interstate 90 at the Bearmouth Exit, set odometer to 0.0 and drive east on the Frontage Road following the Clark Fork River upstream (figs. 1 and 2).

2.4   Mine adit at base of mountainside (on left) was operated by Lawrence Shawbut and produced a small amount of shipping ore including some native copper. The adit was driven across one or more strands of the Bearmouth thrust (adit shown on fig. 4, which precedes fig. 3 in text at author's request).

4.5 | STOP 1 | **Tdf within Bearmouth volcanics (fig. 3)**

Park on the right shoulder and cross highway to the spur road which climbs to a private quarry in felsic tuff. The spur road cut exposes a debris flow which contains abundant cobbles of granodiorite for which there is no directly adjacent bedrock source. The debris flow is underlain by felsic tuff and overlain by basalt (fig. 5). Together these features suggest the debris flow may be a remnant of an extensive system of Tertiary deposits eroded from granitic terrain several mines to the north.

4.9 | STOP 2 | **Debris flows in highway through-cut**

Park on right shoulder at west end of through-cut and examine Tdf and deposit geometry with respect to

the lahar and basaltic andesite flows.

5.9   Turn left (north) onto Bear Gulch Road. The road is built on gold dredge tailings for several miles between the gulch's mouth and the Garnet ghost town at the crest of the Garnet Range.

6.7 $\boxed{\textbf{STOP 3}}$ **Bear Gulch gold dredge tailings**

Park on road shoulder.

Lithologies represented in tailings cobbles include: Proterozoic metasediments, Paleozoic sediments, Tertiary (?) granodioritic intrusives and Tertiary volcanics. Clusters of angular, mono-lithic cobbles and boulders indicate areas where the dredge digging ladder had reached deep enough to excavate bedrock. The dredge operated between 1936 and 1941 and recovered 13,996 ounces of fine gold (Lyden, 1987).

Return to vehicles, retrace the traverse 0.2 miles south and turn right off Bear Gulch Road onto Camp Bearmouth Road.

0.0   Reset mileage to 0.0 at the green gate. The road traverse between here and Stop 4 is underlain by flaggy grey-brown basaltic andesite and tan–to-pink rhyolite of the Tertiary Bearmouth volcanics.

0.8   Paved, 5-point intersection. Turn hard right (east) on graveled spur road.

1.5 $\boxed{\textbf{STOP 4}}$ **Quaternary landslide and Tertiary lamproite intrusive**

The Bear Gulch landslide occupies approximately 25 acres in the NW ¼ of Section 10 (fig. 3). The rock mass is entirely rhyolite which broke from a steep (faulted?) NW-trending slope and slid northeastward into and possibly across the Paleozoic limestone and dolomite cliffs which flank Bear Gulch. The hummocky surface in the core of the landslide contains large angular boulders, no soil, and supports few large trees; all suggesting the landform may be less than a few hundred years old.

Outcrops of a funnel-shaped lamproite intrusion are reached by a short walk northward from the spur road switchback. The lamproite has been the target

of diamond exploration programs since the 1980s. Irving and Kuehner (1998) report that border zone and interior micas yielded $^{40}Ar\,/\,^{39}Ar$ ages of 48.±0.1 and 48.4±0.1 Ma, respectively. The intrusion may be controlled by northwest-trending faults and folds that define the northeast margin of the Bearmouth volcanic field.

Return to vehicles and continue along the spur road (now trending southward). Shallow roadcuts expose rhyolite and a few outcrops of columnar basalt.

2.1   Rejoin main road, continue straight. The next three miles skirt the southwest margin of the Bearmouth volcanic field which overlays tightly folded Paleozoic and Mesozoic strata in the footwall of the Bearmouth thrust.

4.0   View to west of landslide and debris flow complex on east flank of Mount Baldy.

4.2   Cattle guard. Fenced area on the left is intended to re-establish aspen and other forage for a growing elk population.

4.6   Spur road on right; continue on main track which curves left around basalt knob.

4.65   Turn right and cross the North Fork of Little Bear Creek. Road climbs along the axis of a debris flow lobe for the next mile (fig. 4).

5.0 $\boxed{\textbf{STOP 5}}$ **Debris flow overlain by rhyolite tuff**

Lateral lobe of Tdf is overlain by a lithic tuff; both are flanked on the south by outcrop and talus of Quadrant Formation quartzite (Pq).

5.5 $\boxed{\textbf{STOP 6}}$ **Debris flow, medial lobe (at road switchback)**

Tdf here contains cobbles and boulders of brightly colored siliceous breccia. Note the character of this material for comparison with the jasperoid at Stop 9.

6.7 $\boxed{\textbf{STOP 7}}$ **Flank of landslide on south east face of Mount Baldy**

The steep slope to the northwest is a probable
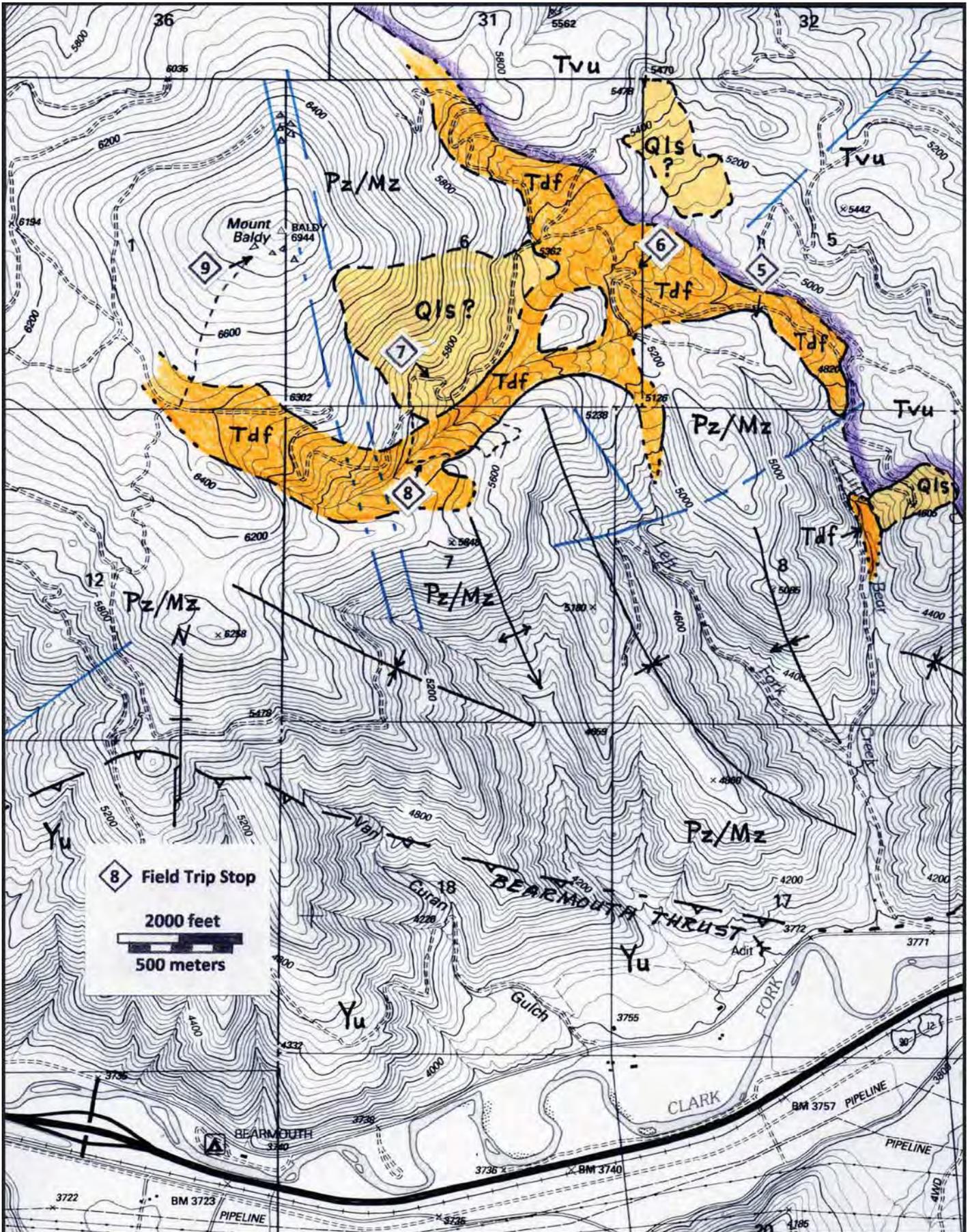
Figure 4. Generalized geologic map of the Mount Baldy area (adjoins Figure 2). Yu = upper Proterozoic sedimentary rock; Pz/Mz = Paleozoic and Mesozoic sedimentary rock, undivided: Tvu = Bearmouth volcanics, undivided; Tdf = debris flow deposit; Qls = landslide. Lineaments shown in blue; fold axes shown in black. Mapping is modified from Kauffman (1963) and Griffin (1989).
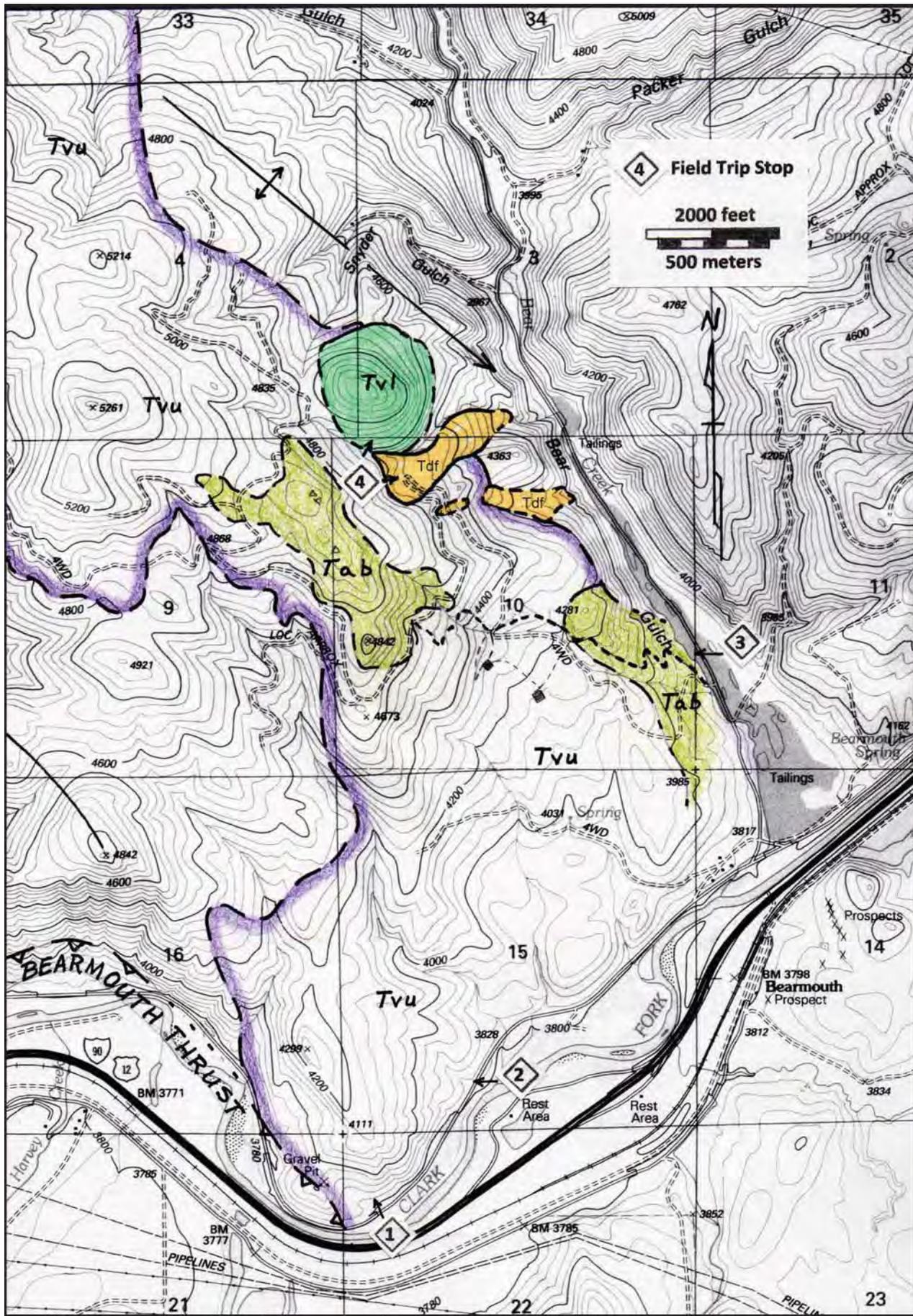
Figure 3. Generalized geologic map of the lower Bear Gulch – Clark Fork River area. Tvu = Bearmouth volcanics, undivided; Tab = andesitic basalt; Tvl = lamproite intrusive; Qls = landslide. Mapping is modified from Kauffman (1963).
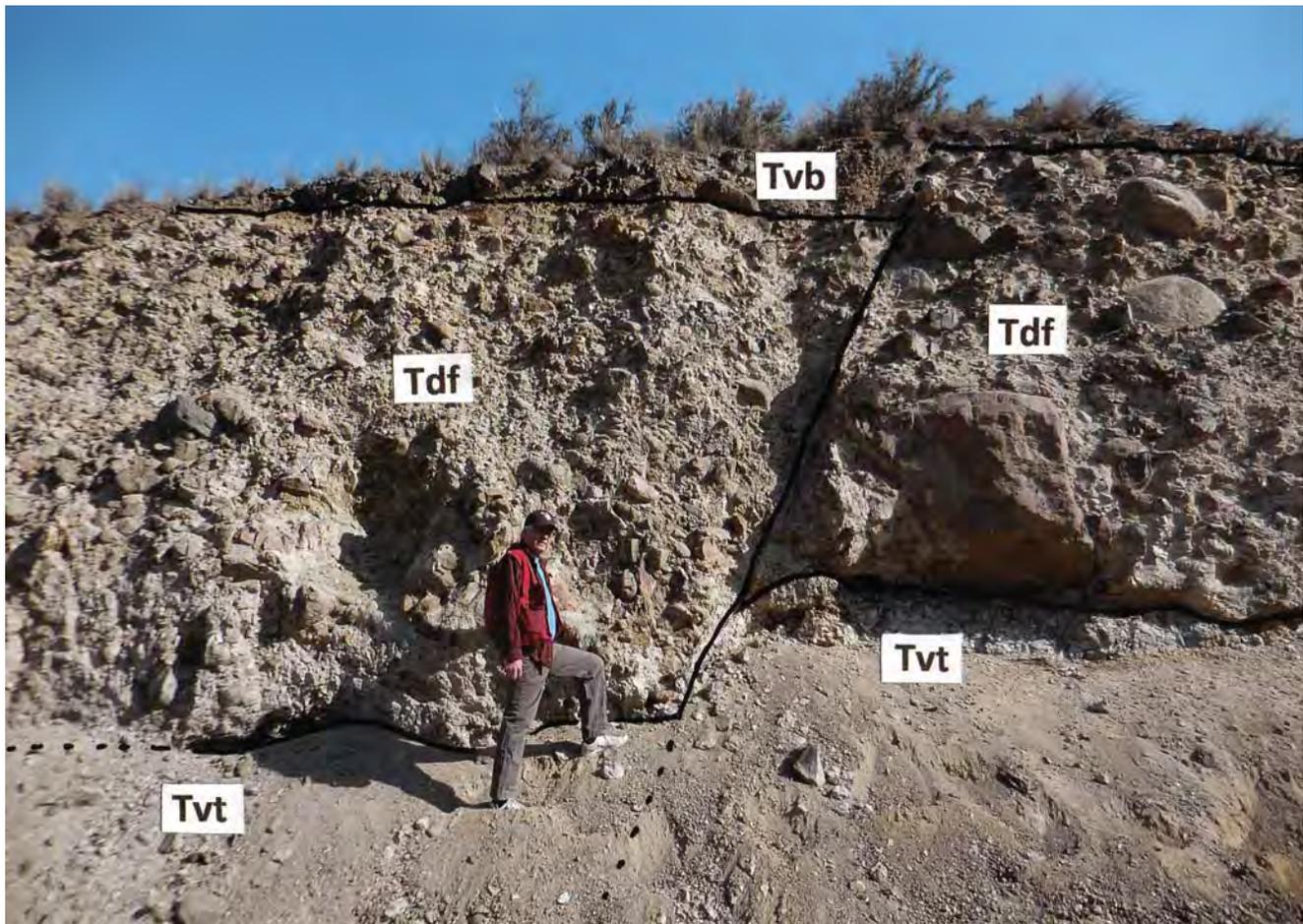
Figure 5. Photograph of spur road cut face at Stop 1. Tvt = pumiceous tuff; Tdf = debris flow; Tvb = basalt.

dipslope in the Madison limestone and suspect mass wasting detachment surface. Structural control at the head of this detachment is indicated by NNW-trending topographic lineaments that align with a rib of varicolored siliceous breccia along the north-plunging nose of Mount Baldy.

6.8 Turn left and head downhill (south) on spur road.

7.0 | STOP 8 | Grizzly Cabin

Park here and walk eastward for views of the Tdf channels and to examine roadcuts through debris flow lobes. Mapped bedrock stratigraphy and local reddish soil in Tdf suggest debris flows locally exploited older channels eroded into Amsdsen Formation between more resistant strata of the Madison limestone and Quadrant quartzite.

Return to vehicles and retrace traverse to main road (rejoin main road at mileage 7.2). Road climbs westward through Tdf complex and onto the south flank of Mount Baldy; knobs to the south are underlain

by Quadrant quartzite.

8.4 Turn right (north) on faint spur road to Mount Baldy summit.

8.6 Summit Chalet.

9.0 | STOP 9 | Baldy Park and paleolithic tool site

This site was first described in a master's thesis by Flint (1977). The artifacts she recorded were quarried here and probably at other sites on or near Mount Baldy where the jasperoid is suitable for toolmaking. The original indian name for the Clark Fork River was the "Arrowstone", probably so-named for its proximity to this quarry and the paleolithic quarries in the Flint Creek valley (Rich and others, 1950).

End of field trip. Return to Frontage Road via the same route.

REFERENCES

Cox, B.E., 2014, Geology of the Bearmouth Ranch, Granite County, Montana: Private Report for John Greytak, 7 pages plus maps.

Flint, P.A., 1977, Archaeology and ethnohistory of the Bearmouth area: Missoula, University of Montana, MS Thesis, 117 p.

Griffin, J.H., 1989, Structural style in a left-lateral thrust ramp zone, Bearmouth, Montana: Missoula, University of Montana, M.S. thesis, 68 p., map scale 1:24,000.

Irving, A.J., and Kuehner, S.M., 1998, Petrology and Geochemistry of the Ruby Slipper Lamproite, Western Montana: A Leucite-Bearing, Ultrapotassic Magma in an Eocene Continental Arc: extended abstract from 7th International Kimberlite Conference, Capetown, SA, p. 349-351.

Kauffman, M.E., and Earll, F.N., 1963, Geology of the Garnet-Bearmouth Area, Western Montana: Montana Bureau of Mines and Geology Memoir 39, 40 pages.

Lonn, J.D., McDonald, C., Sears, J.W., and Smith, L.N., 2010, Geologic map of the Missoula East 30' x 60' quadrangle, western Montana: Montana Bureau of Mines and Geology Open File Report 593, scale 1:100,000.

Lyden, C.J., 1987, Gold Placers of Montana: Montana Bureau of Mines and Geology Reprint 6, 120 pp.

Rich, E.E., Johnson, A.M., and B.B. Barker, 1950, Peter Skene Ogden's Snake Country Journals, 1824-25 and 1825-1826: Hudson's Bay Records Society, Kittson Map.

Stickney, Michael, 2014, Seismicity of the Bearmouth Region: unpublished map assembled from data in the files of the Montana Bureau of Mines and Geology.

Sylvester, A.G., 1988, Strike-Slip Faults: Geological Society of America Bulletin, volume 100, p.1666-1703.
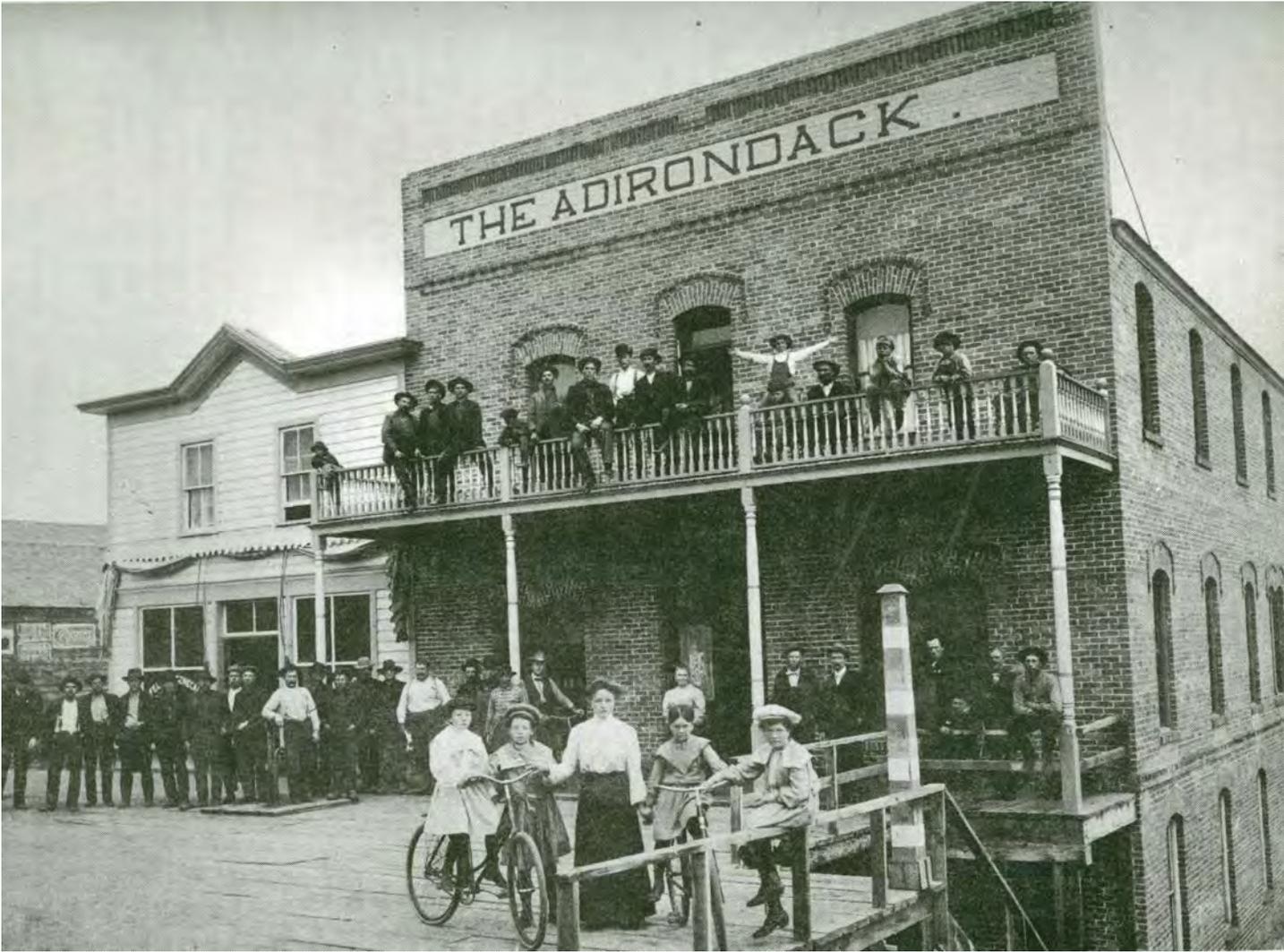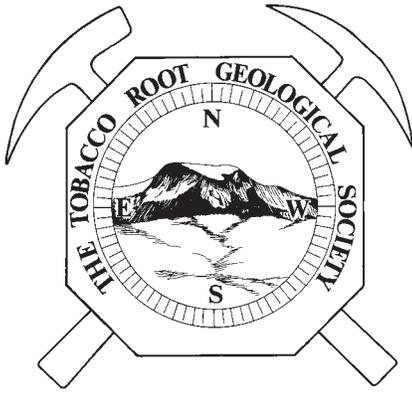
NORTHWEST GEOLOGY
The Journal of The Tobacco Root Geological Society

Requirements for Contributions
TEXT FORMAT: Word Doc (not docm), or plain text (TXT or RTF)
IMAGE FORMAT: JPG—do not embed in Word Docs
DO NOT SUBMIT TABLES OR IMAGES AS EXCEL SPREADSHEETS
FINAL DEADLINE FOR RECEIPT BY EDITORS: JUNE 1 (may be earlier; check website)

Generally, follow USGS style for writing. See COMPLETE REQUIREMENTS at trgs.org. YOU MUST READ AND FOLLOW.

Text should be submitted to the Editor(s) in MS Word-compatible (DOC) format (plain TXT or RTF is fine). **Please DO NOT provide formatting.** Do not assign page numbers, do not double space, do not use columns or backgrounds, **do not indent** anything. Especially, **PLEASE do not include images within Word documents** – they have to be removed, re-formatted, re-sized, and introduced into the publisher program. Word formats images in a way that makes files huge. Do not include large tables in text – make a separate file or image for tables. IMAGES PROVIDED AS WORD DOCUMENTS WILL BE RETURNED.

Photographs and other images should be submitted as JPG or PDF files, **separate** from text. Dimensions should be so that the full size of the image is approximately as it will be displayed – that is, if it will be 3 inches wide when printed, 3 inches wide when displayed on the computer monitor will be adequate. We can interpret most image formats; **this does not include Word or Excel, which are not image formats. ANYTHING SENT AS AN EXCEL SPREADSHEET WILL BE RETURNED.**

Scanned images and line drawings should be at NO MORE than 300 dots per inch resolution. The native size, as displayed on a computer screen should generally be no larger than the screen. If necessary, we can scan hard-copy drawings or photos for you – this is preferable to submitting images in unusual file formats. Figure captions should be submitted as a separate text file, or part of the text file.

Road Logs **must** be accompanied by (at a minimum) a location map of stops; ideally, a geologic map with stops would be included. Such maps should be provided separately from the text.

Please use the following bibliographic format. Note especially capitalization and use and position of commas and colons. For journals, do not abbreviate except J. for "journal" and U.S. in "U.S. Geological Survey."

Sears, J.W., and Hendrix, M., 2004, Lewis and Clark Line and the rotational origin of the Alberta and Helena Salients, North American Cordillera: *in* Sussman, A., and Weill, A., eds., Orogenic Curvature: Geological Society of America Special Paper 383, p.173-186.

Tikoff, B., and Teyssier, C., 1992, Crustal-scale, en-echelon P-shear tensional bridges: a possible solution to the batholithic room problem: Geology, v.20, p. 927-930.

Color images are accepted at our discretion, and will only be included if the color is critical to the understanding of the image (e.g., a complex geologic map). Images including photographs can be submitted in color, but expect that we will likely convert them to grayscale. Each color page adds about $200 to the cost of a normal press run of the guidebook.

Topics: In general, papers published in Northwest Geology do NOT need to be directly related to a particular TRGS Field Conference.

Abstracts: In general, we prefer to NOT publish stand-alone abstracts. Exceptions may be made, but we encourage you to create a short paper (which can be thought of as an expanded abstract) including at least one informative map, cross section, or image.

The Tobacco Root Geological Society, Inc.
P.O. Box 2734 • Missoula, Montana 59806
http://trgs.org